

PALEOZOIC SHALE-GAS RESOURCES OF THE COLORADO PLATEAU AND EASTERN GREAT BASIN, UTAH: MULTIPLE FRONTIER EXPLORATION OPPORTUNITIES

EDITED BY

Thomas C. Chidsey, Jr.



BULLETIN 136

UTAH GEOLOGICAL SURVEY
a division of
UTAH DEPARTMENT OF NATURAL RESOURCES

2016

PALEOZOIC SHALE-GAS RESOURCES OF THE COLORADO PLATEAU AND EASTERN GREAT BASIN, UTAH: MULTIPLE FRONTIER EXPLORATION OPPORTUNITIES

EDITED BY

Thomas C. Chidsey, Jr.

Cover photo: Outcrop of the Mississippian/Pennsylvanian Manning Canyon Shale in Soldier Canyon, Oquirrh Mountains, Tooele County, Utah; view to the west from the north side of the canyon. Utah Geological Survey staff are shown measuring, describing, and sampling the Manning Canyon stratigraphic section.

ISBN 978-1-55791-909-0



BULLETIN 136

UTAH GEOLOGICAL SURVEY
a division of
UTAH DEPARTMENT OF NATURAL RESOURCES

2016

STATE OF UTAH

Gary R. Herbert, Governor

DEPARTMENT OF NATURAL RESOURCES

Michael Styler, Executive Director

UTAH GEOLOGICAL SURVEY

Richard G. Allis, Director

PUBLICATIONS

contact

Natural Resources Map & Bookstore

1594 W. North Temple

Salt Lake City, UT 84114

telephone: 801-537-3320

toll-free: 1-888-UTAH MAP

website: mapstore.utah.gov

email: geostore@utah.gov

UTAH GEOLOGICAL SURVEY

contact

1594 W. North Temple, Suite 3110

Salt Lake City, UT 84114

telephone: 801-537-3300

website: geology.utah.gov

Although this product represents the work of professional scientists, the Utah Department of Natural Resources, Utah Geological Survey, makes no warranty, expressed or implied, regarding its suitability for a particular use. The Utah Department of Natural Resources, Utah Geological Survey, shall not be liable under any circumstances for any direct, indirect, special, incidental, or consequential damages with respect to claims by users of this product.

CONTENTS

LIST OF ACRONYMS AND ABBREVIATIONS.....	1
ABSTRACT <i>Thomas C. Chidsey, Jr.</i>	3
CHAPTER 1 Introduction <i>Thomas C. Chidsey, Jr., Steven Schamel, and S. Robert Bereskin</i>	5
CHAPTER 2 Geologic Setting <i>Thomas C. Chidsey, Jr., and Steven Schamel</i>	11
CHAPTER 3 Drilling Activity <i>Thomas C. Chidsey, Jr., and Steven Schamel</i>	27
CHAPTER 4 Data Compilation and Core Descriptions <i>S. Robert Bereskin, Stephanie Carney, Thomas C. Chidsey, Jr., and Steven Schamel</i>	33
CHAPTER 5 Petrographic Analysis <i>S. Robert Bereskin, Steven Schamel, Thomas C. Chidsey, Jr., Steve Herbst, and Chloe Skidmore</i>	43
CHAPTER 6 Geochemical Analysis <i>Steven Schamel, Jeffrey Quick, Stephanie Carney, Rebekah W. Stimpson, Thomas C. Chidsey, Jr., and S. Robert Bereskin</i>	85
CHAPTER 7 Petrophysics and Rock Mechanics <i>Thomas C. Chidsey, Jr., S. Robert Bereskin, and Steven Schamel</i>	115
CHAPTER 8 Regional Correlations and Outcrop Analogs <i>Craig D. Morgan, Stephanie Carney, Thomas C. Chidsey, Jr., Douglas A. Sprinkel, Steve Herbst, Gerald Waanders, David E. Eby, Steven Schamel, and Gary L. Gianniny</i>	145
CHAPTER 9 Regional Mapping and Burial Histories <i>Robert Resselar and Sonja Heuscher</i>	173
CHAPTER 10 Generalized Best Completion Practices for Developing Paleozoic Shale Gas Plays in Utah <i>Richard Curtice, Stephanie Carney, and Thomas C. Chidsey, Jr.</i>	199
CHAPTER 11 Conclusions and Play Area “Sweet Spots” <i>S. Robert Bereskin, Steven Schamel, and Thomas C. Chidsey, Jr.</i>	219
ACKNOWLEDGMENTS.....	225
REFERENCES.....	225
APPENDICES	
Appendix A Technology Transfer.....	on CD
Appendix B Bibliography of Published Stratigraphic Definition, Petrographic, Rock Mechanics, Geochemical, and Geochemical Analysis.....	on CD
Appendix C Well Database.....	on CD
Appendix D Coregraphs and Core Descriptions.....	on CD
Appendix E Core Photographs.....	on CD
Appendix F Core Thin Section Descriptions.....	on CD
Appendix G Scanning Electron Microscopy.....	on CD
Appendix H X-ray Diffraction Analysis.....	on CD
Appendix I Doughnut Lithology Logs and Close-up Core Photo Plates.....	on CD
Appendix J Paradox Formation Photo Close-up Plates.....	on CD
Appendix K Fracture Analysis.....	on CD
Appendix L Geochemical Analysis.....	on CD
Appendix M Tight Rock Analysis.....	on CD
Appendix N Triaxial Testing.....	on CD
Appendix O Palynology and Thermal Maturation Report.....	on CD
Appendix P Outcrop Petrography Report.....	on CD
Appendix Q Regional Correlations and Outcrop Analog Plates.....	on CD
Appendix R Stratigraphic Data Used for Regional Isopachs and Burial Histories Well Database.....	on CD
Appendix S Erosion Calculations.....	on CD
Appendix T Stratigraphic and Thermal Data Tables.....	on CD
Appendix U Burial and Maturation Models.....	on CD

LIST OF ACRONYMS AND ABBREVIATIONS

SEM – scanning electron microscopy	SWEPI – Shell Western Exploration & Production Inc.
XRD – X-ray diffraction	Eh – low oxygen-reduction potential
AU – assessment units	API – American Petroleum Institute
BCFG – billion cubic feet of gas	GR – gamma ray
BCMG – billion cubic meters of gas	RHOB – density log
MMCM – million cubic meters	NPHI – neutron porosity log
BPM – barrels per minute	DPHI – density porosity log
TOC – total organic carbon	GRI – Gas Research Institute
m – meter	Fe ⁺⁺ – Iron
kPa – kilopascal	CIA – Chemical Index of Alteration
km ² – kilometer squared	K – potassium
UGS – Utah Geological Survey	Th – thorium
DOGMM – Division of Oil, Gas, and Mining	U – uranium
RPSEA – Research Partnership to Secure Energy for America	HI – hydrogen index
Ma – million years ago	wt% – weight percent
m/kyr – meters per thousand years	dm – decimeter
BLM – Bureau of Land Management	mm – millimeters
SITLA – School and Institutional Trust Lands Administration	g/L – grams/liter
DST – drillstem test	R _o – vitrinite reflectance
MMCFGPD – million cubic feet of gas per day	mg HC/g – milligrams of hydrocarbons per gram
MCMGPD – thousand cubic meters of gas per day	CO ₂ – carbon dioxide
SLB&M – Salt Lake Base Line & Meridian	GP – genetic potential
ha – hectare	OI – oxygen index
IPF – initial potential flow	PI – production index
BW – barrels of water	CM – cubic meters
3-D – three-dimensional	TPS – total petroleum system
m ³ – meters squared	GPa – gigapascal
PSI – per square inch	ISRM – International Society for Rock Mechanics
cm – centimeter	σ ₃ – confining pressure
TD – total depth	Pp – pore pressure
TRA – tight rock analysis	E – Young’s Modulus (psi),
S1 – amount of free hydrocarbons	ν – Poisson’s ratio (dimensionless),
S2 – amount of hydrocarbons generated by pyrolytic degradation of the kerogen	C(σ ₃ ') – compressive strength (psi),
S3 – carbon dioxide generated by pyrolysis	σ1 – total axial stress (psi),
Tmax – the maximum temperature	σ ₁ ^{max} – maximum (peak) total axial stress (psi),
EDAX – energy dispersive X-ray spectroscopy	σ ₁ ^{max} – maximum (peak) effective axial stress (psi),
ICCD – International Center for Diffraction Data	εa – axial strain (inch/inch),
XRF – X-ray fluorescence	εr – radial strain (inch/inch), and
UCRC – Utah Core Research Center	Δ – change in the relevant quantity
	psig – per square inch gauge

μ D – microdarcy
mD – millidarcy
nD – nanodarcy
Kg – resulting permeability
g/cc – grams per cubic centimeter
ppm – parts per million
TAI – thermal alteration index
CAI – Conodont Alteration Index
MFS – maximum flooding surfaces
UTM – Universal Transverse Mercator
MCS – Manning Canyon Shale
ft./m.y. – feet per million year
ARCO – Atlantic Richfield Company
LL – Lawrence-Livermore National Laboratory
ELH – expandable liner hanger
ID – inside diameter
CST – capillary suction time
ULPTA – ultra-low-permeability testing apparatus
MRIL – magnetic resonance imaging log
CHI – cased hole interpretation
LWD – logging while drilling
CMPM – cubic meters per minute
DFIT – diagnostic fracture-injection test
kH – permeability thickness
APD – application for permit to drill
MD – measured depth
TVD – true vertical depth
HCl – hydrochloric acid
KCl – potassium chloride
L – liter
HRWF – high-rate water frack fluid
CMW – cubic meters of water
PZS – process-zone stress
FR – friction reducer
MCPM – meters cubed per minute

ABSTRACT

Paleozoic shales in Utah have tremendous untapped gas potential. These include the Mississippian/Pennsylvanian Manning Canyon Shale/Doughnut Formation and Pennsylvanian Paradox Formation of central and southeastern Utah, respectively. Shale beds within these formations are widespread, thick, buried deep enough to generate dry gas (or oil in some areas of the Paradox Basin), and sufficiently rich in organic material and fractures to hold significant recoverable gas reserves. This study provides a detailed evaluation of these potential shale-gas reservoirs including (1) identifying and mapping/correlating the major shale intervals, (2) determining the areas having the greatest gas potential ("sweet spots"), (3) characterizing the geologic, petrographic, geochemical, and petrophysical rock properties of those reservoirs, and (4) recommending the best completion practices.

Based on palynomorphs extracted from samples of the limited outcrops and from well cuttings, the Manning Canyon Shale is middle to late Chesterian (possibly as young as Morrowan) and restricted to the allochthonous rocks of the eastern Basin and Range Province. The Doughnut Formation is restricted to autochthonous rocks of central and eastern Utah. It is late Meramecian through late Chesterian, equivalent to the Manning Canyon and underlying Great Blue Limestone in the Basin and Range Province.

The greatest Manning Canyon Shale/Doughnut Formation potential is a 600-square-mile (1600 km²) area at the north end of the San Rafael Swell in central Utah. Gas tests and shows are reported from many of the exploration wells in this area. The Doughnut is 400 to 1200 feet (130–400 m) thick; the average depth to the top of the formation is 7470 feet (2280 m). Four major lithotypes are (1) carbonate, (2) fine-grained quartz sand and silt, (3) illite, smectite, and chlorite clays, and (4) organic matter composed dominantly of degraded fragments of terrestrial plants. The Manning Canyon/Doughnut may have been deposited in a shallow, restricted-marine, brackish, and freshwater setting not unlike the modern Everglades and Florida Bay. The organic matter has good to excellent richness distributed throughout the shale, limestone, and even siltstone. Vitrinite reflectance and burial history models indicate that kerogen-bearing shale beds are in the dry gas thermal maturity window. The pore systems in most of the shale consist of poorly interconnected micropores that contribute to very low permeability. Brittle silty shale beds could be conducive to hydraulic fracturing.

Within the Paradox Formation, the Chimney Rock, Gothic, and Hovenweep shales have the greatest shale-gas potential and are the principal targets of exploration. The Colorado part of the Paradox Basin has seen moderate success, particularly for the Gothic shale zone, using horizontal drilling. Two unconventional assessment units (AU) in the Paradox Formation defined by the U.S. Geological Survey include these shale zones; the deeper, more mature Gothic, Chimney Rock, Hovenweep Shale Gas AU (located in the Paradox fold and fault belt) assessed to contain 6490 billion cubic feet of gas (BCFG [184 BCMG]), and the Gothic, Chimney Rock, Hovenweep Shale Oil AU (in the Blanding sub-basin and Aneth platform) assessed to contain a mean of 256 million barrels of oil (40.7 MMCM) and 205 BCF (5.8 BCM) of associated gas. Individual shale units generally range in thickness between 25 and 50 feet (8 and 15 m) at depths of 5800 to 6500 feet (1900–2200 m). Cores reveal several important parameters: (1) most shales are organic mudstones containing significant amounts of silt, pyrite, and fossil debris, (2) total organic carbon values are modest (1.5 to 3%), (3) maturity values fall within the oil (or oil-gas) window based on pyrolysis and vitrinite reflectance, and (4) porosity (1 to 3%) and permeability values are low. The bounding and interbedded carbonate units are silty or muddy dolomite, in many cases possess modest amounts of intercrystalline and microvugular pore space. These dolomite beds, as well as some shale beds, also contain numerous subvertical fractures. Therefore, the gas production very likely is derived not only from the shale, but also from the associated carbonates. Thus, this shale play is likely an intermixed series of reservoir types, all of which could produce upon successful stimulation.

Although numerous wells penetrate the Manning Canyon Shale and the Chimney Rock, Gothic, and Hovenweep shales, there have been relatively few attempts to produce any of them in Utah. However, the following are some of the recommended general best completion practices (drilling, stimulation, and evaluation): (1) drill horizontal wellbores instead of vertical wellbores regardless of the thickness of the shale, (2) install swell packers with mechanical sliding sleeves to effectively isolate and treat fairly long horizontal sections, (3) treat slick water stimulation fluid with as few additives as possible, particular gelling agents, and very small proppant sizes, (4) start out on the larger end of the scale in terms of fluid volumes and then increase or decrease fluid volumes during the development state, and (5) conduct post-stimulation follow-up with radioactive tracers, microseismic mapping, and production logs.

CHAPTER 1: INTRODUCTION

BY

Thomas C. Chidsey, Jr., *Utah Geological Survey*;
Steven Schamel, *GeoX Consulting, Inc.*;
S. Robert Bereskin, *Bereskin and Associates, Inc.*

CONTENTS

GEOLOGIC OVERVIEW OF POTENTIAL PALEOZOIC SHALE-GAS RESERVOIRS	7
STUDY GOALS AND OBJECTIVES	8

FIGURES

Figure 1.1. Location of the Basin and Range, Colorado Plateau, and Cordilleran thrust belt.....	7
Figure 1.2. Potential Paleozoic shale-gas play areas and “sweet spots” for the Manning Canyon and Paradox Formations in Utah	8
Figure 1.3. Stratigraphic column of the Paleozoic section in the northern San Rafael Swell area, east-central Utah	8
Figure 1.4. Pennsylvanian stratigraphy in the Paradox Basin	9

CHAPTER 1: INTRODUCTION

GEOLOGIC OVERVIEW OF POTENTIAL PALEOZOIC SHALE-GAS RESERVOIRS

Shale-gas reservoirs in Utah have untapped frontier potential. Paleozoic shale in the Colorado Plateau and eastern Basin and Range Province (figure 1.1) have long been known for their potential as source rocks for hydrocarbons that have migrated into other formations, but have not been considered as in situ gas reservoirs. These include the Mississippian/Pennsylvanian Manning Canyon Shale (Doughnut Formation) and Pennsylvanian Paradox Formation of central and southeastern Utah, respectively (figure 1.2). Shale beds within these formations are widespread, thick, buried deep enough to generate oil, wet gas, or dry gas, and contain sufficient organic material and fractures to hold significant recoverable hydrocarbon reserves. Additional factors pointing to the substantial gas resources and development potential include observed gas during drilling, overpressure, numerous intercalated brittle lithologies for supporting fracture stimulation of the reservoir, reasonable operating depths, and proximity to gas transmission pipelines. Exploratory efforts are just beginning to target these potential frontier gas-shale reservoirs.

The Manning Canyon Shale (Doughnut Formation equivalent in east-central Utah; figure 1.3) is mainly claystone with interbeds of limestone, sandstone, siltstone, and mudstone, and has a maximum thickness of 2000 feet (600 m). Total organic carbon (TOC) varies from 1% to more than 8% with type III (?) kerogen. In north-central Utah, the Manning Canyon was deeply buried by sediments in the Pennsylvanian-Permian-aged Oquirrh basin and is therefore likely very thermally mature. The greatest Manning Canyon potential is a 600-square-mile (1600 km²) area at the north end of the San Rafael Swell. Gas tests and shows are reported from many of the exploration wells. In this region, the formation is 400 to 1200 feet (130–400 m) thick; the average depth to the top of the formation is 7470 feet (2280 m). Approximately two-thirds of the section is dark gray, organic-rich silty limestone and mudstone.

The Paradox Basin of southeastern Utah and southwestern Colorado has been known as a hydrocarbon producer for many decades. Most historical production originated from a series of carbonate intervals that occupy various positions within well-known geologic cycles typical of many Pennsylvanian-aged rocks, recognized almost worldwide. In Utah, these mostly oil-productive cycles belong to the Paradox Formation, and the cycles dealt within this study

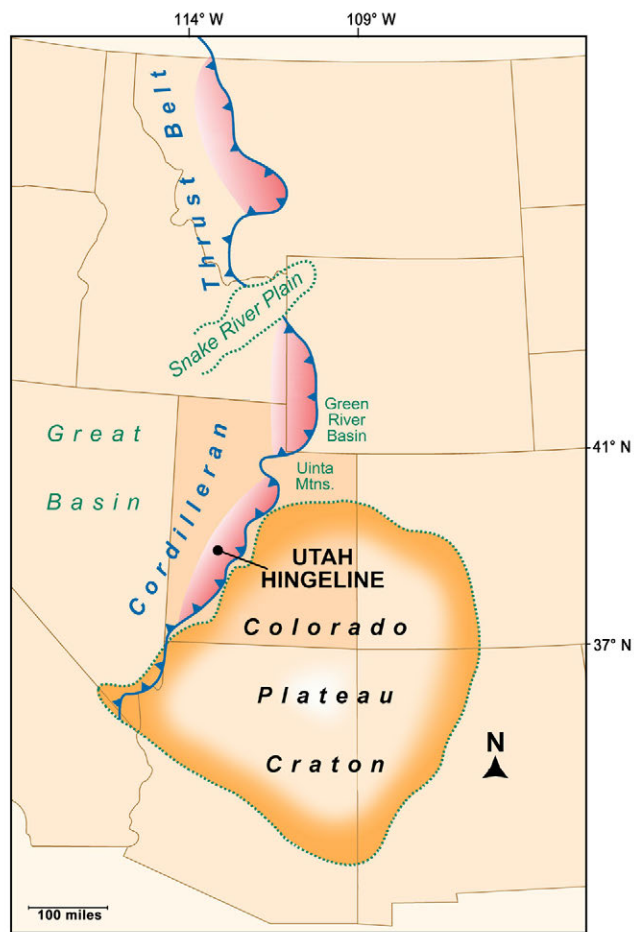


Figure 1.1. Location of the Basin and Range, Colorado Plateau, and Cordilleran thrust belt including the Utah “Hingeline,” (modified from Gibson, 1987).

conform to the Desert Creek, lower Ismay, and upper Ismay deposits, in ascending stratigraphic order. Stratigraphically interbedded with the known carbonate rocks are a series of very dark organic-rich shale zones that have been historically regarded as geochemical source rocks for the oil found in the stratigraphically proximal porous carbonate reservoirs of the basin. In 1991, however, liquid hydrocarbons were directly recovered from one of these naturally fractured shale deposits (Cane Creek cycle), stratigraphically below the cycles listed above (Grove and others, 1993). Since the 1990s, and especially from 2002 to the present-day, dark organic shales have been intense exploration objectives for mostly gas production rather than for oil. Recent vertical and horizontal drilling has successfully produced natural

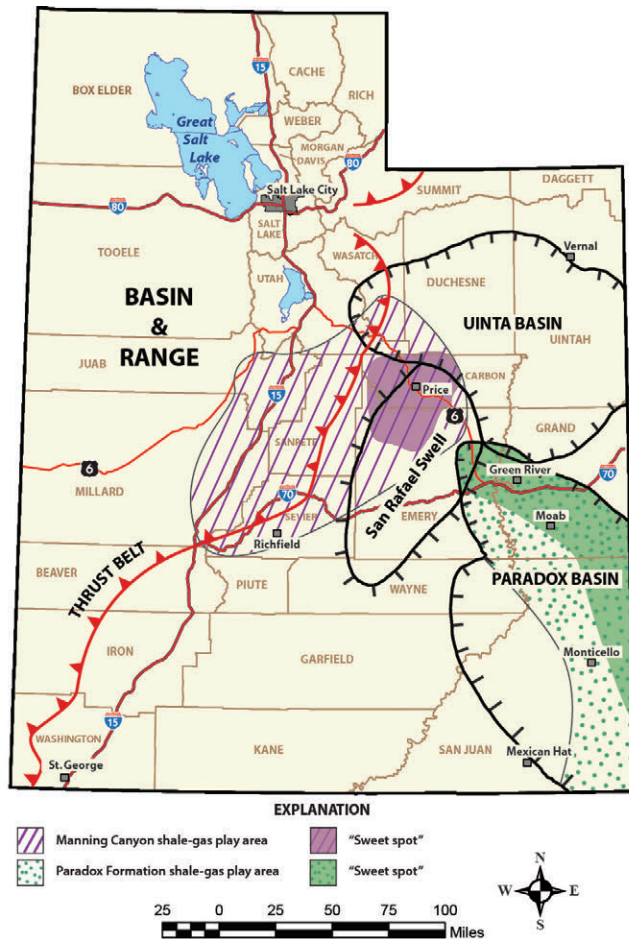


Figure 1.2. Potential Paleozoic shale-gas play areas and for the Manning Canyon and Paradox Formations in Utah, and the identified “sweet spots” for each play area.

gas emanating from the shales themselves. This natural-gas interest has occurred because of the normally limited liquid permeability of these very fine grained clastics.

The cyclic dark-shale units in the Paradox Formation consist of thinly interbedded, black, organic-rich, marine shale; dolomitic siltstone; dolomite; and anhydrite. Of these dark-shale units, three offer the greatest shale-gas potential and are the principal targets of exploration: the Chimney Rock (Desert Creek cycle), Gothic (lower Ismay cycle), and Hovenweep (upper Ismay cycle) shales (figure 1.4). Individual shale units generally range in thickness between 25 and 50 feet (8 and 15 m); the cumulative shale thickness is typically 100 to 200 feet (30–60 m). The average depths to these units range from 5800 to 6500 feet (1900–2200 m). These units contain TOC as high as 15% with type III and mixed type II-III kerogen, are naturally fractured (usually on the crest of anticlinal closures), and are often overpressured. The Colorado part of the basin has seen success, particularly for the Gothic shale zone, using slant tests/horizontal drilling. The purpose of this study is to assess pertinent geological attributes of these somewhat younger black shales

AGE	FORMATION	THICKNESS	LITH
PERM	Black Box Dolomite	170	T-1 UNCONFORMITY
	White Rim Sandstone	500-700	
	Pakoon Dolomite	650-800	
IP	Callville Limestone	250-300	
MISS	Doughnut Formation (Manning Canyon Shale)	600-700	
	Humberg Formation	400-500	
	Redwall Dolomite	750-970	
D	Pinyon Peak Limestone	20	
	Ouray Formation	110-130	
€	Cambrian dolomite	350	
	Ophir Shale	200	
	Tintic Quartzite	210	

Figure 1.3. Stratigraphic column of part of the Paleozoic section determined from measured outcrop sections and subsurface well data in the San Rafael Swell, Carbon and Emery Counties, Utah (modified from Hintze and Kowallis, 2009).

and to evaluate which attributes favor the production of liquid and/or gaseous hydrocarbons.

STUDY GOALS AND OBJECTIVES

Although the organic content of some of these Paleozoic shales is partially known, the reservoir quality and the basic rock-mechanics data so important to successful completions are poorly known. In addition, the distribution and thickness of these rocks are poorly mapped and the vertical succession and regional correlation of the Manning Canyon, in particular, have not been interpreted. The burial history of the Manning Canyon appears complex and probably varies widely from deep burial in the Permian Oquirrh basin (>10,000 feet [3000 m] of overlying Pennsylvanian and Permian strata) to shallower burial along the Paleozoic shelf of central Utah. There are no published studies of the best completion practices for the Manning Canyon and Paradox shales.

The overall goals of this study are to (1) identify and map the major trends for target Paleozoic shale reservoirs and identify areas having the greatest gas potential, (2) characterize the geologic, geochemical, and petrophysical rock properties of target reservoirs, (3) reduce exploration costs and drilling risk, especially in environmentally sensitive areas, and (4) recommend the best practices to complete and stimulate these frontier Paleozoic gas shales to reduce development costs and maximize gas recovery. The study therefore developed techniques and methods for exploration and production for emerging frontier basins where these

CHAPTER 2: GEOLOGIC SETTING

BY

Thomas C. Chidsey, Jr., *Utah Geological Survey*;
Steven Schamel, *GeoX Consulting, Inc.*

CONTENTS

CENTRAL UTAH	13
Thrust Belt	13
Colorado Plateau and the San Rafael Swell	16
Mississippian Stratigraphy.....	17
Regional Distribution	19
Discussion	21
PARADOX BASIN.....	22
General Basin Structure and Geologic History	22
Paradox Formation.....	24

FIGURES

Figure 2.1. Location of oil fields, uplifts, and selected thrust systems in the central Utah thrust belt province	13
Figure 2.2. Balanced structural cross sections through the central Utah thrust belt	14
Figure 2.3. Tectono-stratigraphic columns for the Canyon Range-Pahvant-Paxton and Aurora-Salina thrust sheets	15
Figure 2.4. Generalized geologic map of the San Rafael Swell	18
Figure 2.5. Diagrammatic cross section across the San Rafael Swell	19
Figure 2.6. Location of the San Rafael Swell and surrounding physiographic features and Wilderness Study Areas.....	19
Figure 2.7. Stratigraphic position of the Manning Canyon Shale relative to the Mississippian-Pennsylvanian stratigraphy of Utah	20
Figure 2.8. Regional occurrence of Manning Canyon Shale and age-equivalent rocks in Utah	20
Figure 2.9. Spatial distribution and reported thickness of the Manning Canyon Shale in the northern San Rafael Swell area of north-central Utah	21
Figure 2.10. Oil and gas fields in the Paradox Basin.....	22
Figure 2.11. Generalized map of Paradox Formation facies with clastic wedge, evaporite salt basin, and carbonate shelf.....	23
Figure 2.12. Generalized cross section across the Paradox Basin	23
Figure 2.13. Typical gamma ray-compensated neutron/litho density log for the Hovenweep, Gothic, and Chimney Rock shales in the Blanding sub-basin, Cherokee field	24
Figure 2.14. Typical gamma ray-compensated neutron/density log for the Gothic and Chimney Rock shales in the Aneth platform, Greater Aneth field.....	25

CHAPTER 2: GEOLOGIC SETTING

CENTRAL UTAH

The shale-gas potential of the Mississippian/Pennsylvanian Manning Canyon Shale and organic-rich stratigraphic equivalent formations is greatest in two geologically diverse areas within central Utah: the thrust belt and the San Rafael Swell on the Colorado Plateau. The central Utah thrust belt is structurally varied and complex. The San Rafael Swell represents classic Colorado Plateau geology and is relatively simple structurally.

Thrust Belt

The central Utah thrust belt (sometimes referred to as the “Hingeline”) is more than 100 miles (160 km) wide and is part of the Sevier thrust belt, which extends through the entire state (figure 1.1). It is loosely defined as the portion of the thrust belt south of the Uinta Mountains of northeastern Utah, trending through central Utah to the Marysvale-Wah Wah volcanic complex of south-central Utah. Classic papers describing and interpreting the geology of the Hingeline region include Eardley (1939), Kay (1951), Armstrong (1968), Stokes (1976), and, most recently, Schelling and others (2007). Throughout this area’s geologic history, the Hingeline has marked a pronounced boundary between different geologic terranes and processes. From Late Proterozoic to Triassic time, it represented the boundary between a very thick succession of sediments deposited in western Utah and a thin succession deposited in eastern Utah. These sediments include the Mississippian/Pennsylvanian Manning Canyon Shale and its correlative formations. During Cretaceous and early Tertiary time, the Hingeline coincided with and influenced thrusts at the eastern edge of the Sevier orogenic belt. At present it forms the general boundary in central Utah between the Basin and Range and Colorado Plateau physiographic provinces: Sevier orogenic thrust faults, basement-cored Late Cretaceous–Oligocene Laramide uplifts (plateaus and the Wasatch monocline), and Miocene to Holocene normal faults.

Paleozoic carbonate rocks thicken westward across the Hingeline area (which represented a passive continental margin during the Paleozoic) from thin eastern cratonic deposits. The Upper Cretaceous section in the Hingeline area includes thick synorogenic deposits reflecting proximity of the Sevier orogenic belt to the west. Several depositional environments during the Mississippian through Permian produced organ-

ic-rich deposits capable of generating and storing hydrocarbons, such as the Manning Canyon Shale.

In central Utah, large-scale thrust sheets were emplaced during latest Jurassic through early Tertiary time by compression of the actively evolving foreland basin (Schelling and others, 2005, 2007; DeCelles and Coogan, 2006). Major thrust faults in central Utah (from west to east) include the Canyon Range thrust, Leamington fault, Pahvant thrust, Paxton thrust (Royse, 1993), Charleston-Nebo thrust system, Gunnison detachment, and Salina thrust (Villien and Kligfield, 1986; Schelling and others, 2007) (figures 2.1 through 2.3). These thrust faults represent detached, thin-skinned, compressional styles of deformation, with eastward combined movement of greater than 90

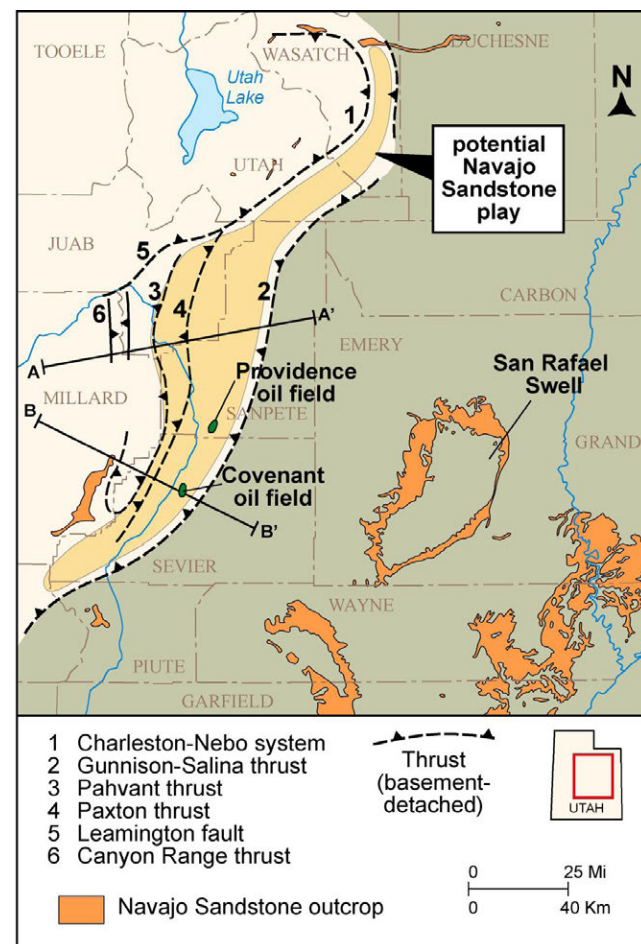


Figure 2.1. Location of oil fields, uplifts, and selected thrust systems in the central Utah thrust belt province. Numbers and sawteeth are on the hanging wall of the corresponding thrust system. Modified from Hintze (1980), Sprinkel and Chidsey (1993), and Peterson (2001). Cross sections A–A’ and B–B’ are shown on figure 2.2.

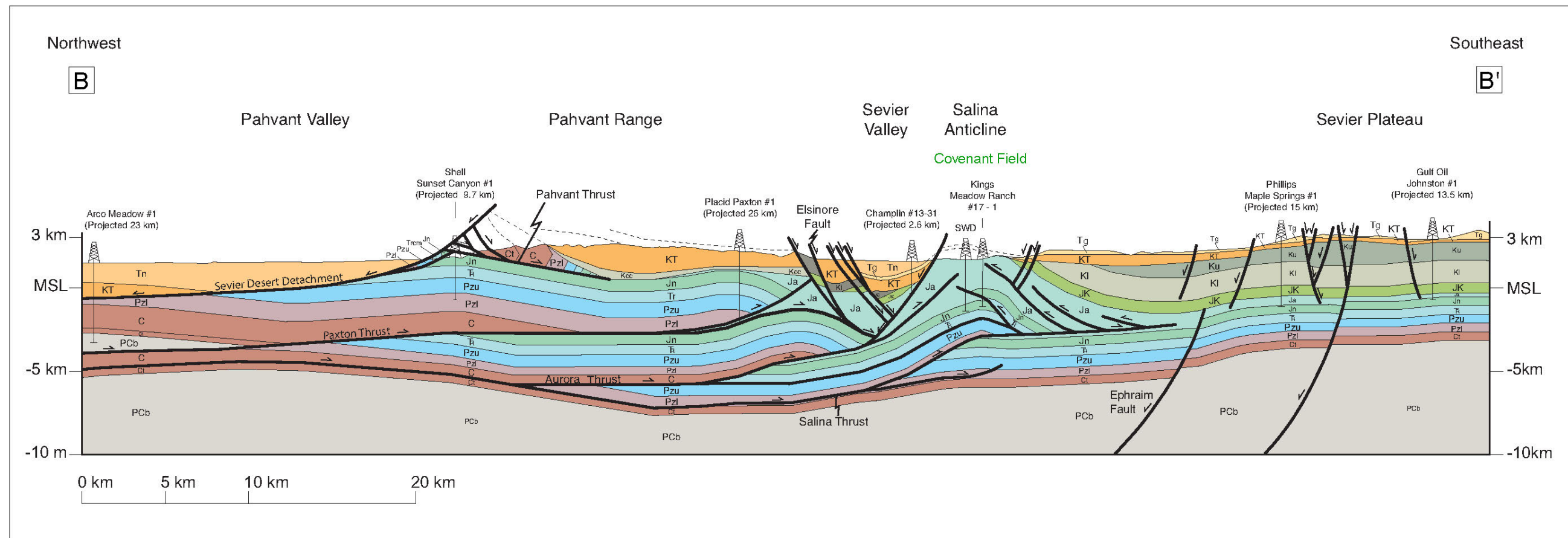
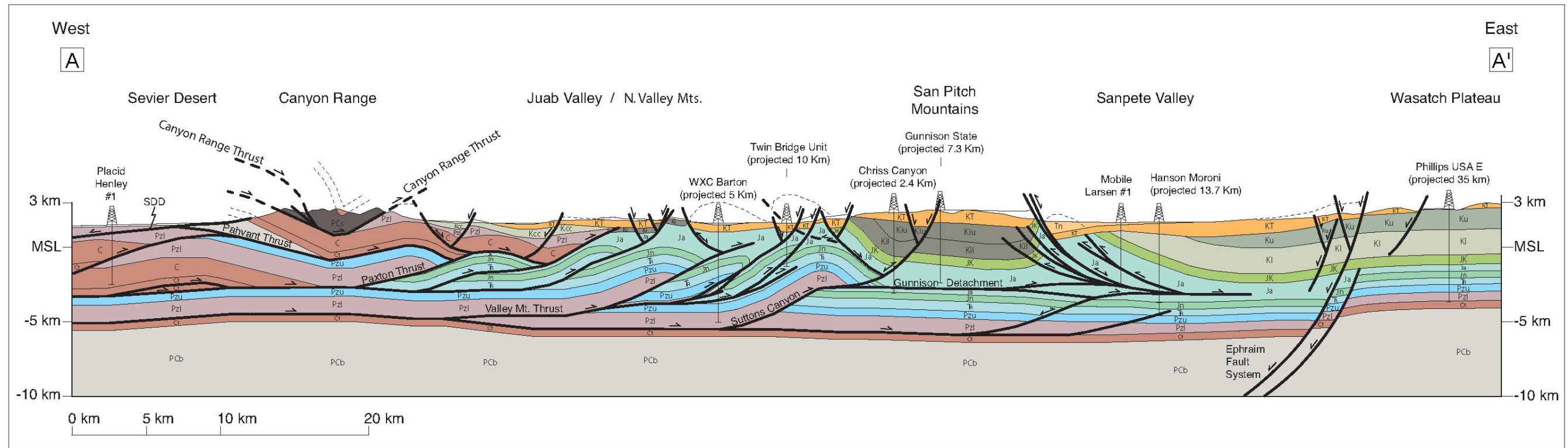


Figure 2.2. Balanced structural cross sections through the central Utah thrust belt. **A.** Southern Canyon Range to the Wasatch Plateau. **B.** Pahvant Valley through Covenant oil field to the Sevier Plateau. Location of cross sections shown on figure 2.1; stratigraphic labels are shown on figure 2.3. After Schelling and others, 2007.

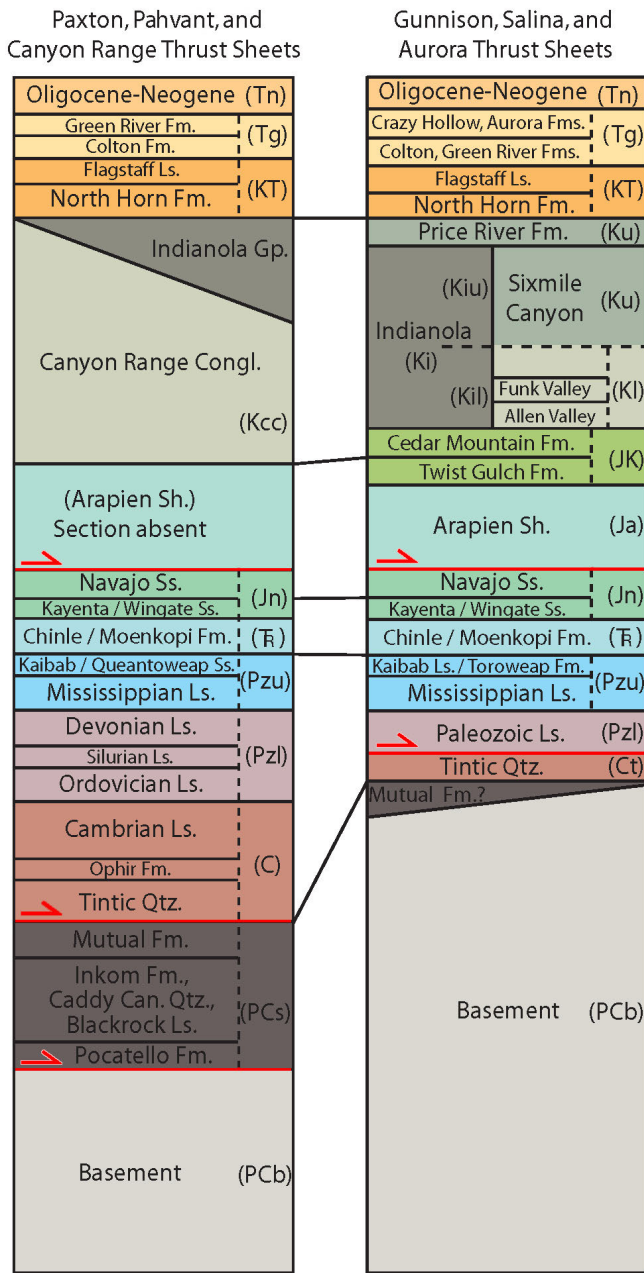


Figure 2.3. Tectono-stratigraphic columns for the Canyon Range-Pahvant-Paxton and Aurora-Salina thrust sheets. Stratigraphic labels used on structural cross sections (figures 2.2A and 2.2B) are included; arrows indicate significant detachments within or at the base of the thrust sheets. After Schelling and others, 2007.

miles (>140 km) for the Canyon Range and Pahvant thrusts (DeCelles and Coogan, 2006). Eastern thrust systems moved less than western thrust systems and are generally younger—the Canyon Range thrust was emplaced during latest Jurassic-Early Cretaceous time, the Pahvant thrust was emplaced in the Albian, the Paxton thrust was emplaced in the Santonian, and the Gunnison detachment-Salina thrust was active from late Campanian through early Paleocene time (DeCelles and Coogan, 2006).

Surface traces of the thrust faults generally trend in a north-northeast direction. Some of the thrust faults do not extend to the surface, and the term “blind” thrust is applied to buried faults like the Gunnison detachment-Salina thrust. The Pahvant, Paxton, and Gunnison detachment-Salina thrust systems contain Lower Cambrian through Cretaceous strata. Jurassic shale, mudstone, and evaporite beds serve as the main glide planes along the hanging-wall flats of these thrust systems.

The leading edges of the thrust faults are listric in form and structurally complex (figure 2.2). They include numerous thrust splays, back thrusts, duplex systems (particularly in eastern thrusts), fault-propagation folds, and ramp anticlines (fault-bend folds) such as the huge fold that makes up most of Mount Nebo (near the town of Nephi) along the Charleston-Nebo thrust system where overturned upper Paleozoic and attenuated Triassic and Jurassic rocks are spectacularly displayed. The duplex systems are similar to those found in the Alberta Foothills in the eastern Canadian Rocky Mountains (Dahlstrom, 1970); these types of features are not present in the Utah-Wyoming-Idaho salient of the thrust belt to the north.

Central Utah thrust plates, like the Canyon Range thrust plate, are up to 36,000 feet (12,000 m) thick (DeCelles and Coogan, 2006), although eastern plates tend to be thinner. The eastern plates also deformed into smaller-amplitude fault-propagation folds and ramp anticlines than western plates (Willis, 1999). Basement-involved, high-angle extensional faults in the region, such as the Middle Jurassic “ancient” Ephraim fault (Moulton, 1976), determined the position of these ramp anticlines and associated duplexes along thrust systems by acting as buttresses to plate movement (Schelling and others, 2005, 2007). However, a blind, low-angle thrust fault continues east of the Ephraim fault within the Jurassic Arapien Shale-Carmel Formation under the Wasatch Plateau (Neuhauser, 1988). Smaller imbricate faults from the décollement form fault-propagation and fault-bend folds, creating some of the hydrocarbon-producing anticlines on the Wasatch Plateau.

Deformation related to compression continued to about 41 Ma in central Utah and was quickly followed by pre-Basin and Range extension (Judge, 2007). It was during this early extension period (middle to late Eocene) that the Wasatch monocline and associated structures formed, likely as a result of relaxation (reversed movement) along the back thrust system on the east side of the San Pitch Mountains (Weiss and Sprinkel, 2002; Cline and Bartley, 2007; Judge, 2007; Judge and others, 2011). Continued extension in the Neogene likely reactivated movement along some thrust ramps, splays, and associated back thrusts, which formed listric normal faults. Other normal faults related to Basin and Range extension dissected thrust plates into additional, compartmentalized blocks (Schelling and others, 2005, 2007). Some local, tectonically driven ductile deformation of Jurassic evaporites further com-

plicated the structural picture of the region (Witkind, 1982; Schelling and others, 2007).

Internal deformation within large-scale thrust plates includes frontal and lateral duplex zones. The deformation front along the leading edge of these major thrusts, particularly the Paxton and Gunnison detachment-Salina thrusts, includes complex back thrusting, tectonic-wedge formation, triangle zones, fault-propagation and fault-bend folds, and passive-roof duplexing (figure 2.2) (Schelling and others, 2005, 2007). Low-amplitude, fault-bend anticlines in the hanging walls of thrusts associated with these features form multiple structural traps for hydrocarbons—the targets of the Covenant and Providence oil discoveries of 2004 and 2008, respectively, the only fields in the central Utah thrust belt. These features are obscured by complex surface geology that includes (1) major folds, (2) angular unconformities, (3) Oligocene volcanic rocks, (4) pre-Basin and Range (middle to late Eocene) to Basin and Range (Miocene-Holocene) listric(?) normal faulting, and (5) local diapirism. The most likely hydrocarbon source for Covenant and Providence fields are upper Paleozoic rocks with the thrust sheets, including the Manning Canyon Shale (Chidsey and others, 2007, 2011; Wavrek and others, 2005, 2007, 2010).

Colorado Plateau and the San Rafael Swell

The Colorado Plateau is a major physiographic province covering almost the eastern half of Utah, northern Arizona, western Colorado, and northwest New Mexico (figure 1.1). In comparison to the central Utah thrust belt, the Colorado Plateau is relatively undeformed. The plateau is characterized by a thick section (10,000 feet plus [3000+ m]) of colorful, relatively horizontal, upper Paleozoic and Mesozoic rocks carved by the Colorado River and its tributaries into the spectacular canyons, cuestas, high plateaus, mesas, and buttes that make the region so scenic. A wide variety of environments are recognized in the sedimentary rocks exposed on the Colorado Plateau: eolian, lacustrine, alluvial, flood plain, fluvial, deltaic, paludal, tidal flat, and shallow marine. The climate is arid which has a major impact on the topography and rock colors.

Structural basins, such as the Uinta and San Juan Basins in Utah and New Mexico, respectively, are developed throughout the Colorado Plateau and many contain significant hydrocarbon accumulations. Other structures include large-scale, elongate monoclines and broad anticlinal uplifts cored by basement-involved reverse faults at depth. These basins and uplifts formed in response to Laramide orogenic compressional forces between latest Cretaceous time (about 70 Ma) and the Eocene (about 40 Ma) (Hintze and Kowallis, 2009). Regional extension beginning during the Miocene (about 17 Ma) (Hintze and Kowallis, 2009) produced major high-angle normal faults, such as the Sevier and Paunsaugunt faults east and west of Bryce Canyon, respectively. These faults often

bound high plateaus and earlier Laramide features in the western part of the Colorado Plateau.

Oligocene-age pyroclastic rocks (mainly ash-flow tuff) cap many of the high plateaus whereas igneous intrusive bodies (laccoliths such as the Henry and La Sal Mountains in southeast Utah) disrupt the plateau topography. Neogene to Pleistocene basalts are found in several areas of the Colorado Plateau as well. Lava flows affected drainage patterns creating inverted topography and lake deposits behind now-eroded lava dams.

The compression associated with the Laramide orogeny may also be responsible for the Colorado Plateau and most of the western U.S. to rise. Some workers believe that as the hot, young, Farallon oceanic plate slid beneath the North American continental plate (underplating), the crust was forced to rise in compensation (Burchfiel and others, 1992; Anderson and others, 2010; Grant C. Willis, UGS, written communication, 2011). Most of the uplift occurred in the early Tertiary, but some uplift, in part isostatic, continued throughout the remainder of the Cenozoic to the present (Hunt, 1956; Lucchitta, 1979; Graf and others, 1987; Fleming, 1994; Young and Spamer, 2001). By middle Tertiary time, parts of the Colorado Plateau stood as a broad high plain (Anderson and others, 2010; Grant C. Willis, UGS, written communication, 2011).

The uplifting of the Colorado Plateau turned the region from one of deposition to one of massive erosion by running water, mass wasting, and wind (Doelling and others, 2010). Burial history models for the area near Green River, Utah, estimate the removal of 8000 feet (2400 m), equating to a long-term average vertical erosion rate of 0.2 foot per thousand years (0.06 m/kyr) (Nuccio and Condon, 1996a; Nuccio and Roberts, 2003; Williams and others, 2007). Other estimates of the stream incision rates on the Colorado Plateau range from 0.6 foot per thousand years (0.2 m/kyr) over the last one million years (Willis and Biek, 2001; Pederson and others, 2002), up to 1.3 to 1.6 feet per thousand years (0.4–0.5 m/kyr) over the past several hundred thousand years (Davis and others, 2001; Hanks and others, 2001; Marchetti and Cerling, 2001).

Most of the eroded material from the Colorado Plateau has been carried to the sea by the Colorado River system. During the early Tertiary, the regional drainages in the Colorado Plateau flowed north from central Arizona toward the Uinta Basin and other lacustrine basins (Dickinson and others, 1989; Potochnik and Faulds, 1998; Young and Spamer, 2001). About 5.5 million years ago, southwest-flowing drainages in the southern Nevada, which had been lowered by structural collapse of the Basin and Range Province between 10 and 15 million years ago, succeeded in cutting headward into the higher Colorado Plateau to the east (Grant C. Willis, UGS, written communication, 2011). Eventually, headward erosion managed to capture and integrate the drainages of the Colorado Plateau, reversing flow directions. As a result, the modern

Colorado River was formed. Due to the great topographic relief between the southern Nevada area and the higher Colorado Plateau, the Colorado River and its tributaries had tremendous erosional energy and rapidly cut the Grand Canyon over a few million years (Luchitta, 1989; Grant C. Willis, UGS, written communication, 2011). The new drainage system quickly eroded the soft Mesozoic strata of the Colorado Plateau, creating wide valleys, narrow canyons, and entrenched meanders.

The San Rafael Swell in east-central Utah is a classic example of a large Laramide uplift on the Colorado Plateau (figures 2.4 and 2.5). The structure is a broad, asymmetric, northeast-trending anticline about 70 miles (113 km) long and 30 miles (50 km) wide. Strata on the west flank form a cuesta dipping 2 to 6 degrees west-northwest. Strata on the east flank form a steep monocline, known as the San Rafael Reef, dipping 45 to 85 degrees east-southeast (Witkind, 1991). The structural nose plunges to the north. The uplift is likely underlain by a high-angle, basement-involved reverse fault (figure 2.5). Two styles of faulting have been identified, particularly in the northern part of the San Rafael Swell: (1) west-directed reverse faults on the east flank within the Permian and older section related to the Pennsylvanian Uncompahgre uplift (Ancestral Rockies) (Witkind, 1991; Morgan, 2007), and (2) Sevier ramp-style thrusting that is the termination of a west-to-east decollement in the Jurassic Carmel Formation (Neuhauser, 1988; Morgan, 2007). Several small subsidiary structures are found along the flanks of the San Rafael uplift such as Woodside Dome on the east flank and Farnham Dome near the structural nose.

The oldest rocks exposed on the structural axis of the San Rafael Swell are Permian in age (figures 2.4 and 2.5): Pakoon Dolomite, White Rim Sandstone (Cedar Mountain Formation), and Kaibab Limestone (Black Box Dolomite). The shale, mudstone, and siltstone beds in the Triassic Moenkopi and Chinle Formations cover a major portion of the topographic crest of the structure (figure 2.4). The cliffs of the San Rafael Reef and the gentle west-northwest-dipping flank are composed of non-marine sandstones in the Triassic-Jurassic Glen Canyon Group (Wingate, Kayenta, and Navajo Formations). Marine and non-marine limestone, shale, conglomerate, sandstone, and siltstone ranging in age from Middle Jurassic through Early Cretaceous overlie the Glen Canyon. The gray marine shale forming the strike valleys that surround the San Rafael Swell is the Upper Cretaceous Mancos Shale (a shale-gas target in the Uinta Basin to the north and northeast). The deltaic sandstone and coal beds of the Upper Cretaceous Mesaverde Group make up the Book Cliffs and Wasatch Plateau that rim the San Rafael Swell (figure 2.6).

The majority of the lands within the San Rafael Swell are public and controlled by the U.S. Bureau of Land Management (BLM). Within each township (36 square miles [36 sections]), generally, are four sections owned by the State of Utah School and Trust Lands Administration (SITLA). However,

significant parts of the central San Rafael Swell have been designated as Wilderness Study Areas (figure 2.6). It is highly unlikely that these areas will ever be available for oil and gas exploration.

The subsidiary structures on the flanks and the structural nose of the San Rafael Swell have been targets for hydrocarbon exploration. Woodside Dome and Farnham Dome have yielded nitrogen and carbon dioxide from Permian and Jurassic rocks, respectively. Ferron field on the west flank has produced nearly 13 billion cubic feet of gas from the Cretaceous Ferron Sandstone, and Grassy Trail field on the east flank has produced over 673,000 barrels of oil from the Triassic Moenkopi Formation (Utah Division of Oil, Gas, and Mining, 2016a).

Mississippian Stratigraphy

Across broad areas of northern and west-central Utah, the Upper Mississippian is represented by two formations that have an interbedded relationship, the Manning Canyon Shale and the Great Blue Limestone (figure 2.7). The first is dominated by siliciclastics with secondary carbonates and the other by carbonates with secondary silt and clay. Both share most of the same sedimentologic components. Together the two formations occupy the space between the Humbug Formation below and the Oquirrh Group or the Round Valley/Morgan Formations above. There are conformable relationships with the bounding formations. The Manning Canyon and Great Blue both are Chesterian in age. However, the Manning Canyon extends upward slightly into the lowermost Morrowan and the lower member of the Great Blue Limestone is uppermost Meramecian in age. Thus, the formations taken together span a time just slightly longer than the 15 million year duration of the Chesterian, 333 to 318 million years ago (Ma) (Gradstein and others, 2004).

In the Middle Mississippian, the sea was withdrawing from the broad carbonate shelf that had been developed across much of western North America, leaving an extensive karst plain from the Four Corners area north through eastern Utah, Colorado, and Wyoming, and into Montana (De Voto, 1988; Sando, 1988). In northeast Utah an embayment remained on the shelf in which carbonate and sandstone deposition (Humbug Formation) continued (Welsh, 1979; Sandberg and others, 1982). To the west in central Nevada, the foredeep basin to the Antler orogenic belt had advanced eastward onto the edge of the carbonate shelf, burying it under terrigenous sediments derived from the thrust belt, the proximal Diamond Peak Conglomerate and the distal Chainman Shale (Sandberg and others, 1982). It was into this setting (figure 2.8) that the Manning Canyon Shale and interbedded Great Blue Limestone were deposited. It was also at this time that the Oquirrh basin and its shelfal extension, the Oquirrh sag (Stokes, 1979), began to take shape. Both may be expressions of an early onset of Ancestral Rockies uplift of the Uncompahgre uplift, or some other tectonic process. Regionally, isopach and facies

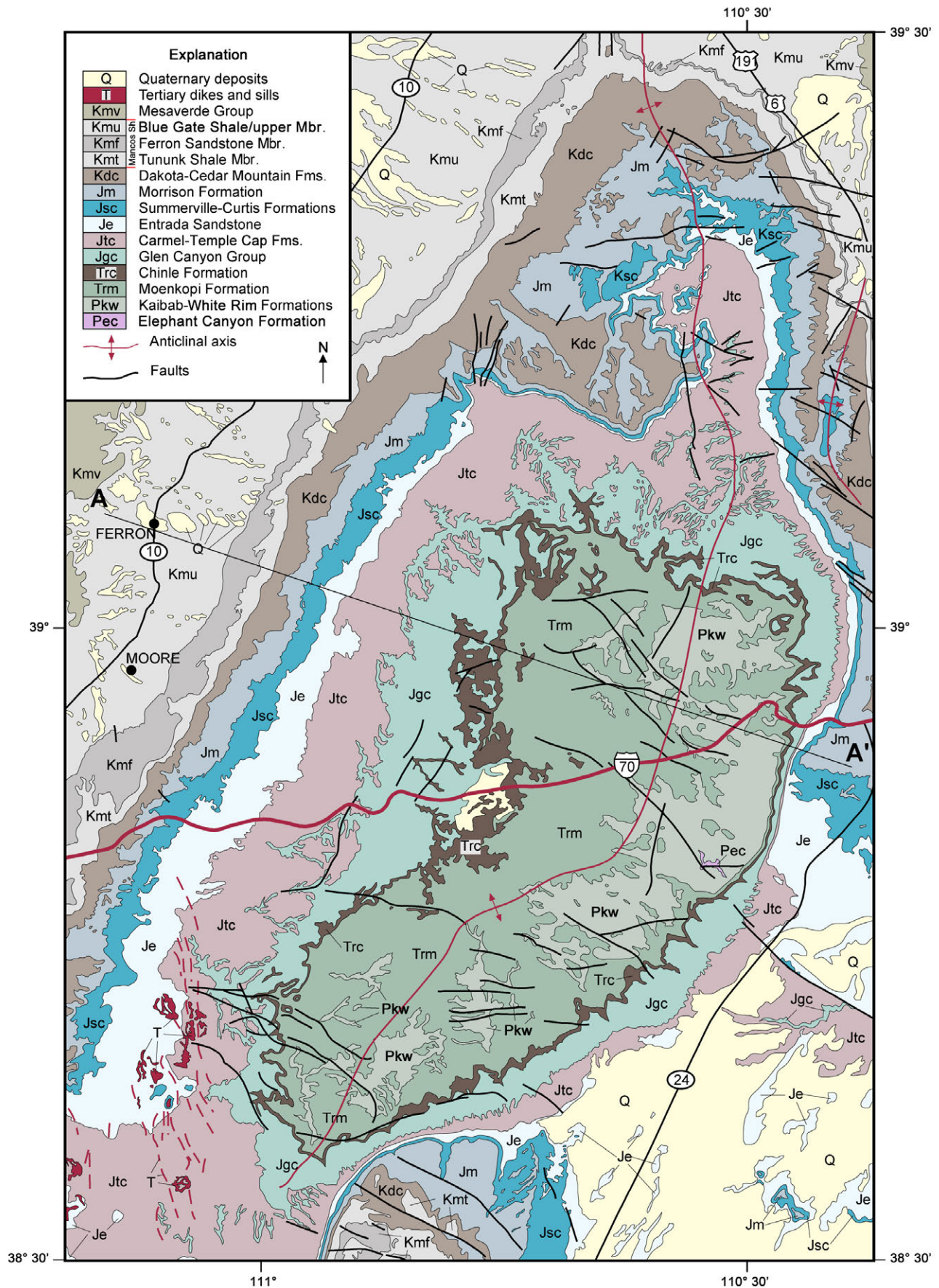


Figure 2.4. Generalized geologic map of the San Rafael Swell. Cross section A–A' shown on figure 2.5. After Doelling and Hylland, 2002.

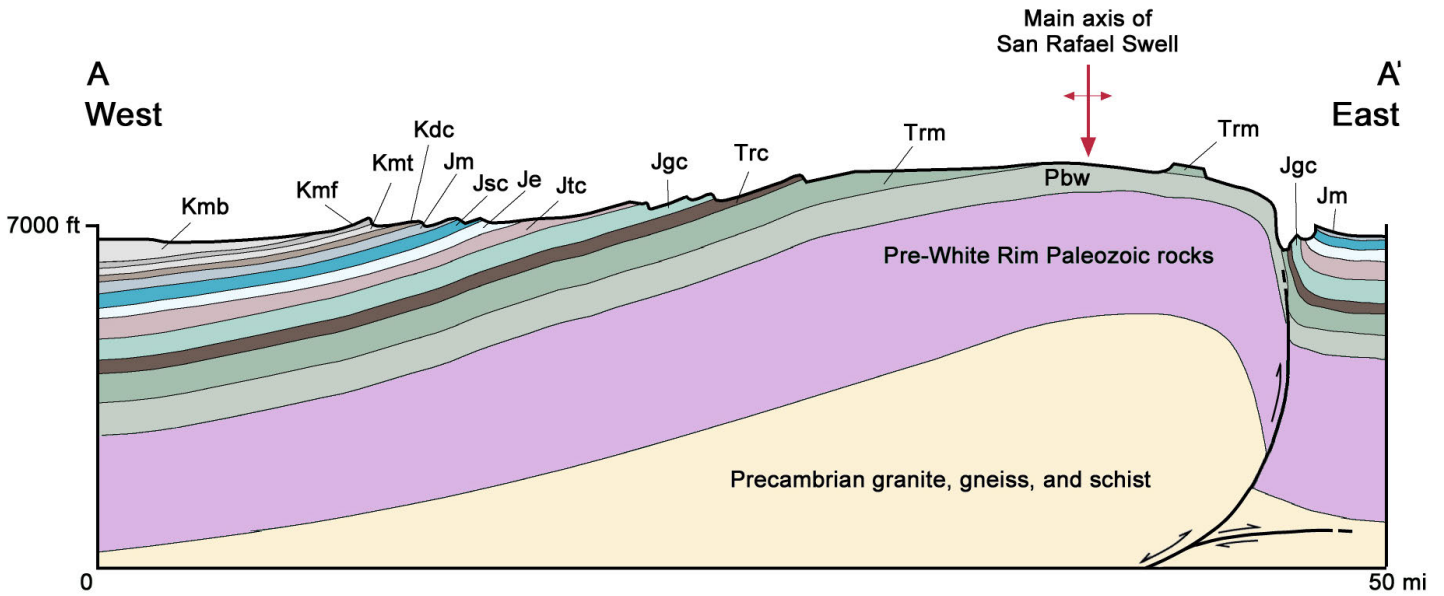


Figure 2.5. Diagrammatic cross section across the middle of the San Rafael Swell. The cross section is not drawn to scale, but the vertical dimension is exaggerated about eight times relative to the horizontal; the horizontal length of the cross section covers about 50 miles (80 km). Symbols and colors of geologic formations correspond to those shown on figure 2.4; location of cross section also shown on figure 2.4. Modified from Doelling and Hylland, 2002.

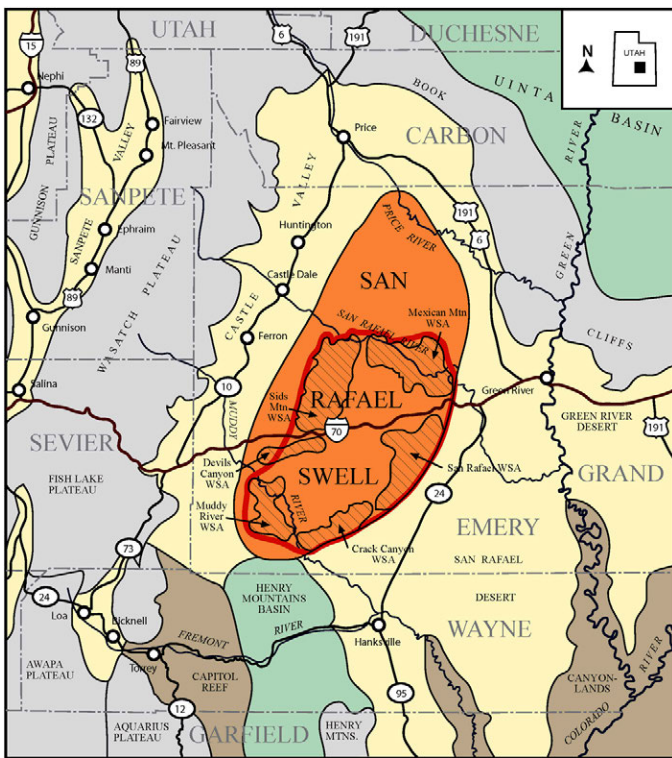


Figure 2.6. Location of the San Rafael Swell and surrounding physiographic features and existing Wilderness Study Areas (WSAs). Valleys and desert areas are shown in yellow, plateaus and mountains in gray, canyonlands in brown, and basins in green. From Doelling and Hylland, 2002.

maps indicate an Early Pennsylvanian initiation of this tectonic episode (Johnson and others, 1992; Blakey, 2009). The Manning Canyon is distributed across a broad area in western and northeast Utah (figure 2.8). To the west, it overlies the Great Blue and is restricted in age; to the east where it is called the Doughnut Formation, it rests on the Humbug and spans the entire Chesterian-lowermost Morrowan.

Regional Distribution

The Manning Canyon Shale normally is very poorly exposed. The unit is inherently mechanically weak, subject to deep erosion, and prone to landslides. Outcrops, especially of the shale intervals, are few and far between. The type section of the Manning Canyon Shale is in the southern Oquirrh Mountains (see chapter 8 for detailed description and appendix Q for regional correlations and measured section). The name was assigned by Gilluly (1932) for the 1560-foot-thick (475 m) succession of dark gray carbonaceous shale with interbeds of argillaceous limestone and siltstone-sandstone situated conformably between the Great Blue Limestone and the younger West Canyon Limestone of the Oquirrh Group (Moyle, 1958, 1959; Prince, 1964; Hintze and Kowallis, 2009). Previously this unit had been referred to as the “upper shale of the Great Blue Limestone” (Gordon and others, 2000).

The 3450- to 3600-foot-thick (1050–1100 m) Great Blue Limestone is represented in the southern Oquirrh Mountains by three members (Bissell and Barker, 1977; Gordon and

		OQUIRRH BASIN	OQUIRRH SAG	N. PARADOX BASIN
Pennsylvanian	299	Oquirrh Group Wallsburg Ridge Formation Shingle Mill Ls. Bear Canyon Fm. Bridal Veil Ls.	Oquirrh Formation (undivided) or Weber Sandstone Morgan Formation Round Valley Limestone	Elephant Canyon Fm.
	304			Honaker Trail Formation
	309			Paradox Fm.
	312			Pinkerton Trail Fm.
	318			Molas Formation <i>regolith on limestone and/or a regional hiatus</i>
Mississippian	318	Manning Canyon Shale	Doughnut Formation	
	326	Great Blue Limestone Long Trail Shale		
		Great Blue Limestone Humbug Sandstone	Humbug Sandstone	
		Deseret Limestone	Deseret Limestone	
		Gardison Limestone	Redwall Dolomite	
		upper Fitchville Formation		
				Leadville (Redwall) Limestone

Figure 2.7. Stratigraphic position of the Manning Canyon Shale and Doughnut Formation relative to the Mississippian-Pennsylvanian stratigraphy of Utah.

others, 2000). The lower limestone (or Silveropolis) member is dark gray, medium-bedded limestone with minor intercalations of sandstone and argillaceous limestone about 850 feet (260 m) thick. Corals date the member as latest Meramecian. With a gradual increase in terrigenous components, this lower member grades upward into the Long Trail Shale, a 110-foot-thick (33 m) interval of dark gray silty shale with interbeds of limestone and siltstone (Gilluly, 1932). The upper limestone member is a dark blue-gray, argillaceous, micritic limestone with interbedded black and dark gray shale and very fine grained sandstone. The limestone is thin laminated to thin bedded and is rich in silt- to clay-sized quartz. The upper member contains three unnamed, but mappable, shale intervals (Bissell and Barker, 1977). The middle and upper members are Chesterian in age. The passage from Great Blue Limestone into the overlying Manning Canyon Shale is gradual over an interval of 200 to 300 feet (60–90 m) as the argillaceous limestone interbeds thin and the calcareous shale intervals thicken.

Across most of the Oquirrh basin the Manning Canyon Shale has thicknesses exceeding 1000 feet (300 m), but in western Utah the thicknesses are variable. The mechanical weakness of the formation and slumped contacts makes accurate measurement difficult. In northeast Utah, in the “Humbug embayment,” the unit is rarely more than a few hundred feet thick (figure 2.8). Here, too, structural deformation and poor exposures inhibit accurate measurements. The exception is in the Oquirrh sag south of the Uncompahgre uplift, the northern San Rafael Swell area, where thicknesses occasionally exceeding 1000 feet (300 m) are reported from exploration wells (figure 2.9).

For “mapping convenience” in the Cottonwood arch area, Crittenden and others (1952) assigned the name “Doughnut

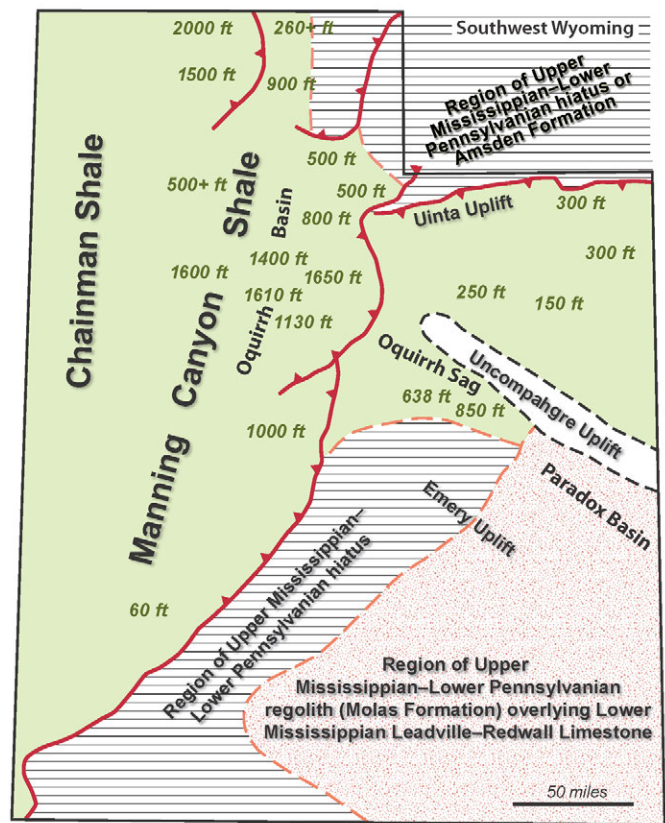


Figure 2.8. Regional occurrence of Manning Canyon Shale and age-equivalent rocks in Utah. Major Sevier-Laramide thrust faults shown in red.

Formation” to the dark, poorly resistant shales overlying the “blue limestone” of the upper Humbug Formation. This shale interval was well known on the flanks of the Uinta Mountains, where it was known simply as the “Black Shale” unit (McDougald, 1953). Sadlick (1955a, 1955b, 1956) recognized the unit to have the same stratigraphic characteristics and age as the Manning Canyon Shale in the southern Oquirrh Mountains, and consequently used that established name for this unit east of the Wasatch fault. Crittenden (1959) justified the utility of the name Doughnut by arguing that it was possible to map this black shale unit from the Cottonwood arch south to the American Fork area, thickening from 400 to 1300 feet (120–400 m), where it was overridden by the Charleston-Nebo thrust sheet which carried a slightly thicker Manning Canyon Shale (1650 feet [500 m] in Provo Canyon; Baer and Rigby, 1980). Going further with this line of argument, Welsh (1979) and Welsh and Bissell (1979) maintained that the Doughnut has had no physical connection to the Manning Canyon and, therefore, it is a separate formation. The Doughnut was deposited only on the central Utah shelf in the “Doughnut trough,” whereas the Manning Canyon is restricted to the Oquirrh basin to the west of the shelf. For additional discussion concerning the regional correlations of the Doughnut and Manning Canyon, refer to chapter 8 and appendix Q.

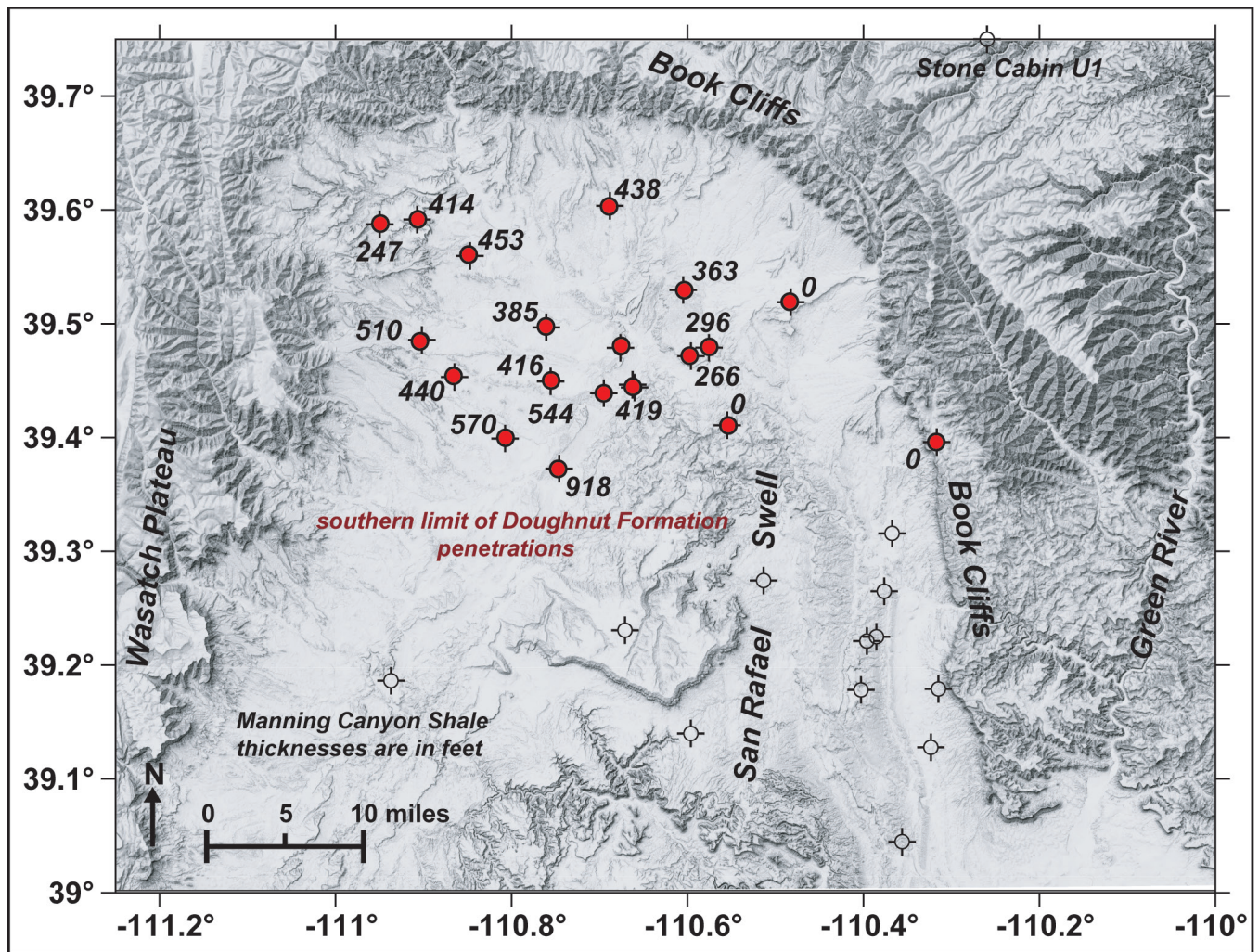


Figure 2.9. Spatial distribution and reported thickness (in feet) of the Doughnut Formation (Manning Canyon Shale) in the northern San Rafael Swell area of north-central Utah.

Discussion

The Manning Canyon Shale and the Chainman Shale are metamorphosed across a large portion of northwest Utah and adjacent Idaho and Nevada (Henderson, 1970; Christensen, 1975). In the Oquirrh and Lake Mountains and the Wasatch Range, within the Charleston-Nebo thrust sheet, the Manning Canyon has a mineral paragenesis characteristic of lower greenschist facies: quartz, illite, chlorite, pyrophyllite, rectorite, kaolinite, paragonite-phengite, albite, calcite, dolomite, goethite, pyrite, and carbonaceous material (Christensen, 1975).

In the vicinity of Morgan, Utah, in the Round Valley area, the Great Blue Limestone occupies a conformable stratigraphic position between the Humbug Formation and the Round Valley Formation. The Great Blue is about 900 feet (300 m) of dark gray to bluish-gray limestone that includes an 85-foot-thick (26 m) dark gray shale interval in its mid-section. The formation has thin black shale beds in its upper section. Nohara (1966) has identified 40 species of Ostracoda having close affinities to

Chesterian-age ostracodes of the Illinois basin. The fauna is a marine, benthonic assemblage deposited in littoral to shallow neritic settings.

To the south of the Oquirrh sag and to the north of the Uinta Mountains are large parts of the shelf where the Late Mississippian-earliest Pennsylvanian is absent, represented only by a stratigraphic hiatus (figure 2.8), areas of presumed karst plains. To the south of Price, in central Utah, is the well-documented Emery uplift that persisted as an area of non-deposition well into the Middle Pennsylvanian. However, to the southeast of the Oquirrh sag, in the part of the shelf that would evolve in the Middle Pennsylvanian into the Paradox Basin, the paleokarst that developed on the Mississippian Leadville Limestone and older carbonate units (De Voto, 1988) was acting as a dust trap for loess blown onto the surface. The loess infiltrated into the paleokarst or was eroded, transported, and redeposited farther downwind (Evans and Reed, 2007). Remobilization and redeposition of the loess, which is largely sorted, angular, and medium- to coarse-grained quartz silt (Pye, 1987), was halted only

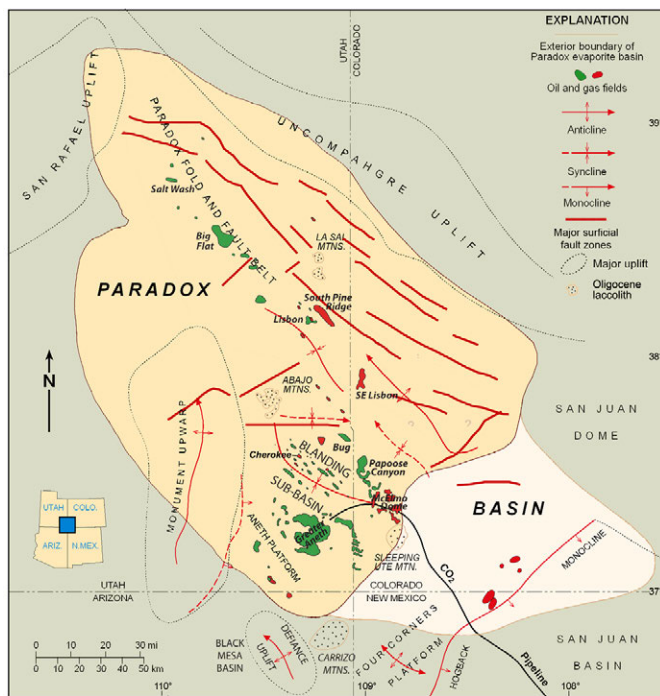


Figure 2.10. Oil and gas fields in the Paradox Basin of Utah, Colorado, and Arizona (modified from Harr, 1996). Play area colored light orange.

by sea-level rise that stabilized the eolian deposits and resulted in the accumulation of the maroon-colored Molas Formation (figure 2.7). Marginal-marine epeiric seas are ideal sinks for eolian dust (Soreghan, 1992). In the area of the Paradox Basin this process began in the latest Chesterian or Morrowan (Evans and Reed, 2007), although some authors (Merritt and Winar, 1958) have assigned an earlier time for the base of the formation. The silty mudstones of the Molas contain clays from the regolith developed on the Leadville karst plain (Power, 1969).

To the north and northeast, in west and central Wyoming, the Late Mississippian is represented by the three members of the Amsden Formation that record a gradual west-to-east marine transgression across a very low-relief karst surface developed on the Madison Limestone (Mallory, 1967; Sando and others 1975). The Darwin Sandstone Member is deposited unconformably on the karst plain and is middle Meramecian on the extreme west and Chesterian in central Wyoming. This 60- to 100-foot-thick (18–30 m) non-marine quartz arenite deposit was deposited in an eolian dune and sabkha complex (Houlik, 1973; Kirschbaum and others, 2007). Conformably overlying the Darwin Sandstone is the Horseshoe Shale Member, a varicolored succession of siltstone, shale, and mudstone with thin beds of silty or sandy argillaceous limestone. The siliclastic beds commonly contain plant remains and locally they are black and carbonaceous (Sando and others, 1975). The limestone beds contain shelly marine fauna. The Horseshoe Shale is thought to be a reworked regolith derived from chemical weathering of the Madison (Gorman, 1962) that was deposited in a tidal flat, lagoon, and estuarine environment

just outboard of the Darwin coastal sand erg. This shaly unit grades upward into the carbonate-rich Ranchester Limestone Member, a heterogeneous largely marine sequence of interbedded cherty dolomite and limestone, sandstone similar to the Darwin, and varicolored shale similar to the Horseshoe. This 100- to 250-foot-thick (30–80 m) member in western to central Wyoming is late Chesterian to Atokan (late Early-early Middle Pennsylvanian) in age. It is overlain conformably by the widespread, thick, eolian sandstone of the Tensleep Formation. During the Late Mississippian, central Wyoming was a karst plain gradually being covered by a sand erg. Not until the end of the Chesterian did the sea begin to encroach on the region.

PARADOX BASIN

General Basin Structure and Geologic History

The Paradox Basin is located mainly in southeastern Utah and southwestern Colorado with small portions in northeastern Arizona and the northwestern corner of New Mexico (figure 2.10). The Paradox Basin is an elongate, northwest-southeast-trending, evaporitic basin that predominately developed during the Pennsylvanian, about 330 to 310 Ma. The most obvious structural features in the basin are the spectacular anticlines that extend for miles in the northwesterly trending fold and fault belt. The events that caused these and many other structural features to form began in the Proterozoic, when movement initiated on high-angle basement faults and fractures 1700 to 1600 Ma (Stevenson and Baars, 1986, 1987). During Cambrian through Mississippian time, this region, as well as most of eastern Utah, was the site of thin, marine deposition on the craton while thick deposits accumulated in the miogeocline to the west (Hintze and Kowallis, 2009). However, major changes began in the Pennsylvanian when a pattern of basins and fault-bounded uplifts developed from Utah to Oklahoma as a consequence of the collision of South America, Africa, and southeastern North America (Kluth and Coney, 1981; Kluth, 1986), or from a smaller-scale collision of a microcontinent with south-central North America (Harry and Mickus, 1998). One result of this tectonic event was the uplift of the Ancestral Rockies in the western United States. The Uncompahgre highlands (uplift) in eastern Utah and western Colorado initially formed as the westernmost range of the Ancestral Rockies during this ancient mountain-building period.

The Uncompahgre highlands are bounded along their southwestern flank by a large basement-involved, high-angle, reverse fault identified from seismic surveys and exploration drilling (Frahme and Vaughn, 1983). As the highlands rose, an accompanying depression, or foreland basin, formed to the southwest—the Paradox Basin. The form of the Paradox Basin was strongly influenced by rejuvenation of pre-existing (late Precambrian), northwesterly trending structures (Baars and Stevenson, 1981). Rapid basin subsidence, particularly during the Pennsylvanian and continuing into the Permian, accommodated large volumes of evaporitic and marine sediments that intertongue with

non-marine arkosic material shed from the highland area to the northeast (figures 2.11 and 2.12) (Hintze and Kowallis, 2009). Deposition in the basin produced a thick cyclical sequence of carbonates, evaporites, and organic-rich shale (Peterson and Hite, 1969; Hite and others, 1984; Rasmussen, 2010). The Paradox Basin is defined for the purposes of this study by the maximum extent of anhydrite beds in the Paradox Formation.

The present Paradox Basin includes or is surrounded by other uplifts that formed during the Late Cretaceous-early Tertiary Laramide orogeny, such as the Monument upwarp in the west-southwest, and the Uncompahgre uplift, corresponding to the earlier Uncompahgre highlands, forming the northeast boundary (figure 2.10). Oligocene laccolithic intrusions form the La Sal and Abajo Mountains in the north and central parts of the basin in Utah, whereas the Carrizo Mountains in Arizona and the Ute, La Plata, and San Miguel Mountains in Colorado were intruded along the southeastern boundary of the basin (figure 2.10).

The Paradox Basin can generally be divided into three areas: the Paradox fold and fault belt in the north, the Blanding sub-basin in the south-southwest, and the Aneth platform in the southernmost part in Utah (figure 2.10). The area now occupied by the Paradox fold and fault belt was also the site of greatest Pennsylvanian/Permian subsidence and salt deposition. Folding in the Paradox fold and fault belt began as early as the Late Pennsylvanian as sediments were laid down thinly over, and thickly in areas between, rising salt (Doelling, 2003). The Paradox fold and fault belt was created during the Late Cretaceous through Quaternary by a combination of (1) reactivation of basement normal faults, (2) additional salt flowage followed by dissolution and collapse, and (3) regional uplift (Doelling, 2003). Trudgill and Paz (2009) suggest that salt movement initiated during the Late Pennsylvanian/Early Permian due to sediment loading. The relatively undeformed Blanding sub-basin and Aneth platform de-

veloped on a subsiding shallow-marine shelf. Each area contains oil and gas fields with structural, stratigraphic, or combination traps formed on discrete, often seismically defined, closures. The Blanding sub-basin and Aneth platform areas were the focus of our evaluation of potential gas-shale reservoirs in the Paradox Basin.

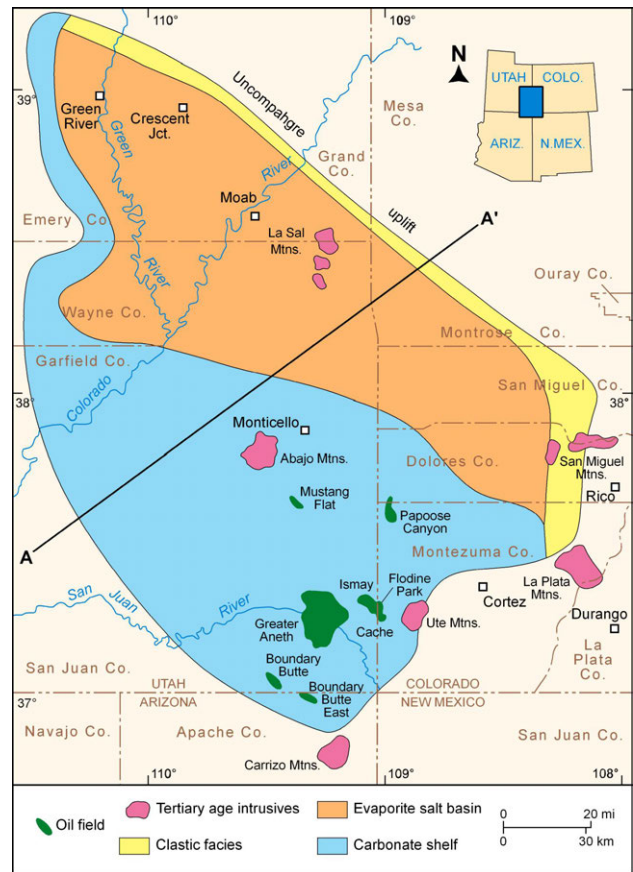


Figure 2.11. Generalized map of Paradox Formation facies with clastic wedge, evaporite salt basin, and carbonate shelf (modified from Wilson, 1975). Cross section A-A' shown on figure 2.12.

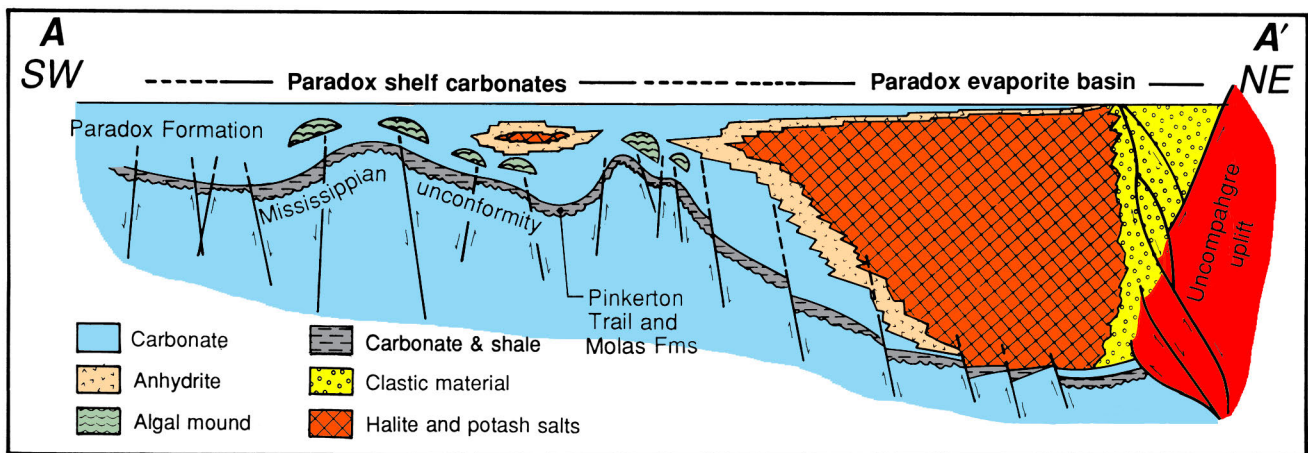


Figure 2.12. Generalized cross section across the Paradox Basin with gross facies relations between Middle Pennsylvanian shelf carbonates, restricted basin evaporites, and coarse clastics proximal to the Uncompahgre uplift (modified from Baars and Stevenson, 1981). Maximum extent of anhydrite beds in the Paradox Formation that define the basin is not shown. Location of cross section shown on figure 2.11.

Paradox Formation

The Paradox Formation is part of the Pennsylvanian Hermosa Group (Baker and others, 1933) (figure 1.4). The 500- to 5000-foot-thick (150–1500 m) Paradox is overlain by the Honaker Trail Formation and underlain by the Pinkerton Trail Formation (Wengerd and Matheny, 1958; Hintze and Kowallis, 2009). The Paradox is divided into (1) a lower member consisting of interbedded black shale, siltstone, dolomite, and anhydrite, (2) a middle (saline) member consisting of thick halite interbedded with dolomite, dolomitic siltstone and shale, and anhydrite, and (3) an upper member of interbedded dolomite, anhydrite, and dolomitic shale. Rasmussen (2010) divided the middle (saline) member of the Paradox Formation in the evaporite basin into as many as 35 salt cycles that onlap onto the basin shelf to the west and southwest. Each cycle consists of a clastic interval/salt couplet. The clastic intervals are typically interbedded dolomite, dolomitic siltstone, anhydrite, and organic-rich shale—the focus of this study. The clastic intervals typically range in thickness from 10 to 200 feet (3–60 m) and are generally overlain by 200 to 400 feet (60–120 m) of halite. In the interior of the basin, a typical cycle consists of a black shale facies overlain almost entirely by salt, whereas on the shelf, a cycle consists of a black shale facies overlain primarily by carbonates. The regionally extensive black shale facies allows correlation of salt cycles in the interior of the basin with carbonate cycles on the shelf. Hite and Cater (1972) and Reid and Berghorn (1981) divided the Paradox Formation into informal zones, in ascending order: Alkali Gulch, Barker Creek, Akah, Desert Creek, and Ismay (figure 1.4). This usage is currently the most common in the literature, as well as in completion and production reports.

In the Blanding sub-basin the Desert Creek and Ismay zones are relatively easy to correlate because they are bounded by persistent and targeted potential shale gas units (i.e., the Hovenweep, Gothic, and Chimney Rock) that have distinctive geophysical log responses (figure 2.13). The Desert Creek zone is typically dolomite, while the Ismay is mainly limestone with some dolomite units. The average thickness of the Desert Creek zone is 85 feet (24 m). It is overlain by the Gothic shale and underlain by the Chimney Rock shale, both informal units of the Paradox Formation (figure 2.13). The average depth to the Gothic and Chimney Rock shales in Blanding sub-basin fields is 5900 feet (1800 m) and 6000 feet (2000 m), respectively. The average thickness of the Ismay zone is 230 feet (70 m). It is overlain by the Honaker Trail Formation and underlain by the Gothic shale (figure 2.13). The Ismay zone is subdivided into an upper interval and a lower interval separated by the 30- to 45-foot-thick (10–15 m) Hovenweep shale, also an informal unit (figure 2.13). The average depth to the Hovenweep in Blanding sub-basin fields is 5780 feet (1930 m).

On the Aneth platform (figure 2.10), the Desert Creek and Ismay zones are predominately limestone, with local dolomitic units, and are the major producers in the area. Like in the Blanding sub-basin, the Desert Creek is again overlain by the Gothic

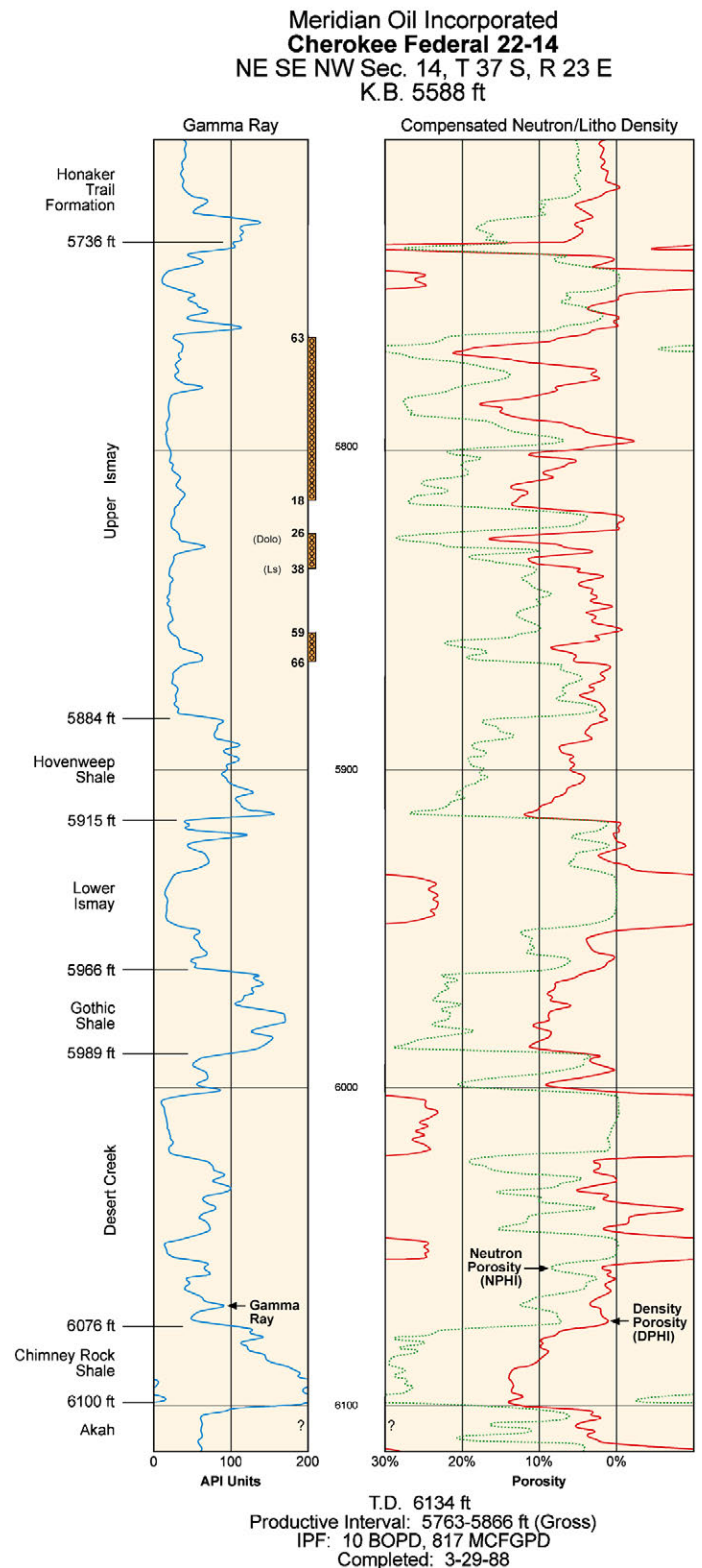


Figure 2.13. Typical gamma ray-compensated neutron/litho-density log for the Ismay and Desert Creek zones including the Hovenweep, Gothic, and Chimney Rock shales of the Paradox Formation in the Blanding sub-basin, from the Cherokee Federal 22-14 well (section 14, T. 37 S., R. 23 E., SLBL&M), Cherokee field, San Juan County, Utah. Producing (perforated) interval between depths of 5763 and 5866 feet. See figure 2.10 for location of Cherokee field.

shale and underlain by the Chimney Rock shale. The geophysical log response has variations that correspond to changes in lithofacies representing shallow-marine shoal, peritidal, phylloid-algal buildups, low-energy marine, etc. (figure 2.14). Thickness of the Desert Creek zone averages 140 feet (45 m). The average depths to the Gothic and Chimney Rock shales in Aneth platform fields are 5510 feet (1840 m) and 5670 feet (1890 m), respectively. The Ismay zone is again overlain by the Honaker Trail Formation and underlain by the Gothic shale. The Ismay geophysical log response also has variations that correspond to lithofacies similar to that of the Desert Creek zone; however, the Hovenweep shale is thin in this part of the Paradox Basin (figure 2.14). Thickness of the Ismay zone averages 160 feet (50 m).

Most Paradox Formation petroleum production comes from stratigraphic traps in the Blanding sub-basin and Aneth platform that locally contain phylloid algal-mound and other carbonate lithofacies buildups. The sources of the petroleum are the black, organic-rich shales (including the Hovenweep, Gothic, and Chimney Rock, figures 1.4 and 2.13) within the Paradox Formation (Hite and others, 1984; Nuccio and Condon, 1996a, 1996b).

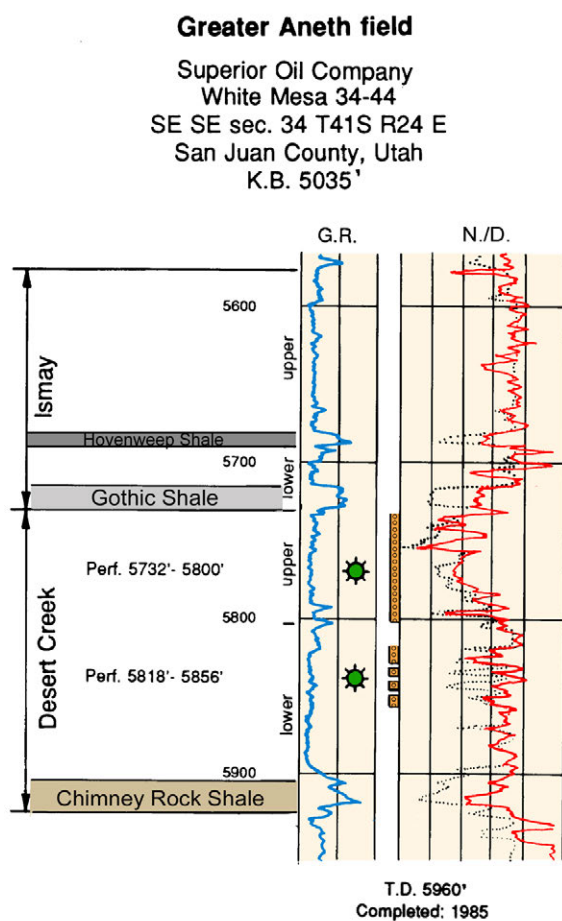


Figure 2.14. Typical gamma ray-compensated neutron/density log for the Desert Creek zone bounded by the Gothic and Chimney Rock shales of the Paradox Formation in the Aneth platform, from the White Mesa 34-44 well (section 34, T. 41 S., R. 24 E., SLBL&M), Greater Aneth field, San Juan County, Utah. Producing (perforated) interval between depths of 5732 and 5856 feet. See figure 2.10 for location of Greater Aneth field.

CHAPTER 3: DRILLING ACTIVITY

BY

Thomas C. Chidsey, Jr., *Utah Geological Survey*;
Steven Schamel, *GeoX Consulting, Inc.*

CONTENTS

MANNING CANYON SHALE/DOUGHNUT FORMATION	29
PARADOX FORMATION	30

FIGURES

Figure 3.1. Locations of exploration wells fully penetrating the Manning Canyon Shale in the northern San Rafael Swell area of north-central Utah.....	29
Figure 3.2. Location of recently drilled wells targeting the Mississippian/Pennsylvanian Manning Canyon Shale, northern San Rafael Swell	30
Figure 3.3. Location of recently drilled wells targeting the shales in the Pennsylvanian Paradox Formation in Utah part of the Paradox Basin.....	31

CHAPTER 3: DRILLING ACTIVITY

MANNING CANYON SHALE/ DOUGHNUT FORMATION

The Manning Canyon Shale (Doughnut Formation) was a specific exploration target for many wells drilled in the northern San Rafael Swell area (figure 3.1) during the late 1950s through 1980s as documented in various well and hearing files of the Utah Division of Oil, Gas, and Mining. Operators were attracted by potential limestone and sandstone reservoir targets embedded in this organic carbon-rich shale source rock. In May 1958, the North Springs Federal 1 well (section 27, T. 15 S., 9 E., Salt Lake Base Line and Meridian [SLB&M], Carbon County) (figure 3.1) drill-stem tested (DST) the Doughnut in the interval 10,589 to 10,730 feet (3227–3270 m). Over a 2.5-hour period, a maximum gas rate of 2.6 million cubic feet of gas per day (MMCFGPD [73.6 MCMGPD]) stabilizing to 1.8

MMCFGPD (50.9 MCMGPD) was reported, plus one quart of 52° API straw-colored condensate. In December 1964, the well was reworked. A production test within the same part of the Doughnut as the 1958 DST had an initial potential flow (IPF) of 865 thousand cubic feet of gas per day (MCFGPD [24.5 MCMGPD]), but after 24 hours the rate had dropped to 695 MCFGPD (19.7 MCMGPD) and after 48 hours it was just 555 MCFGPD (15.7 MCMGPD). The well was then shut-in. The Federal Mounds 11-1 well (section 34, T. 14 S., R. 9 E., SLB&M, Carbon County) (figure 3.1) tested 759 MCFGPD (21.5 MCMGPD) from “stray sands.” The Utah D-6 well (figure 3.1) has recorded natural gas flow rates of 34 to 78 MCFGPD (1–2.2 MCMGPD). Other wells, such as the Skyline-Spjut 16.1, Mounds 1, State 1-16, Drunkards Wash 31-1, and Washboard Wash USA 1-A (figure 3.1), encountered natural gas in small volumes in DSTs, and in cuttings and core.

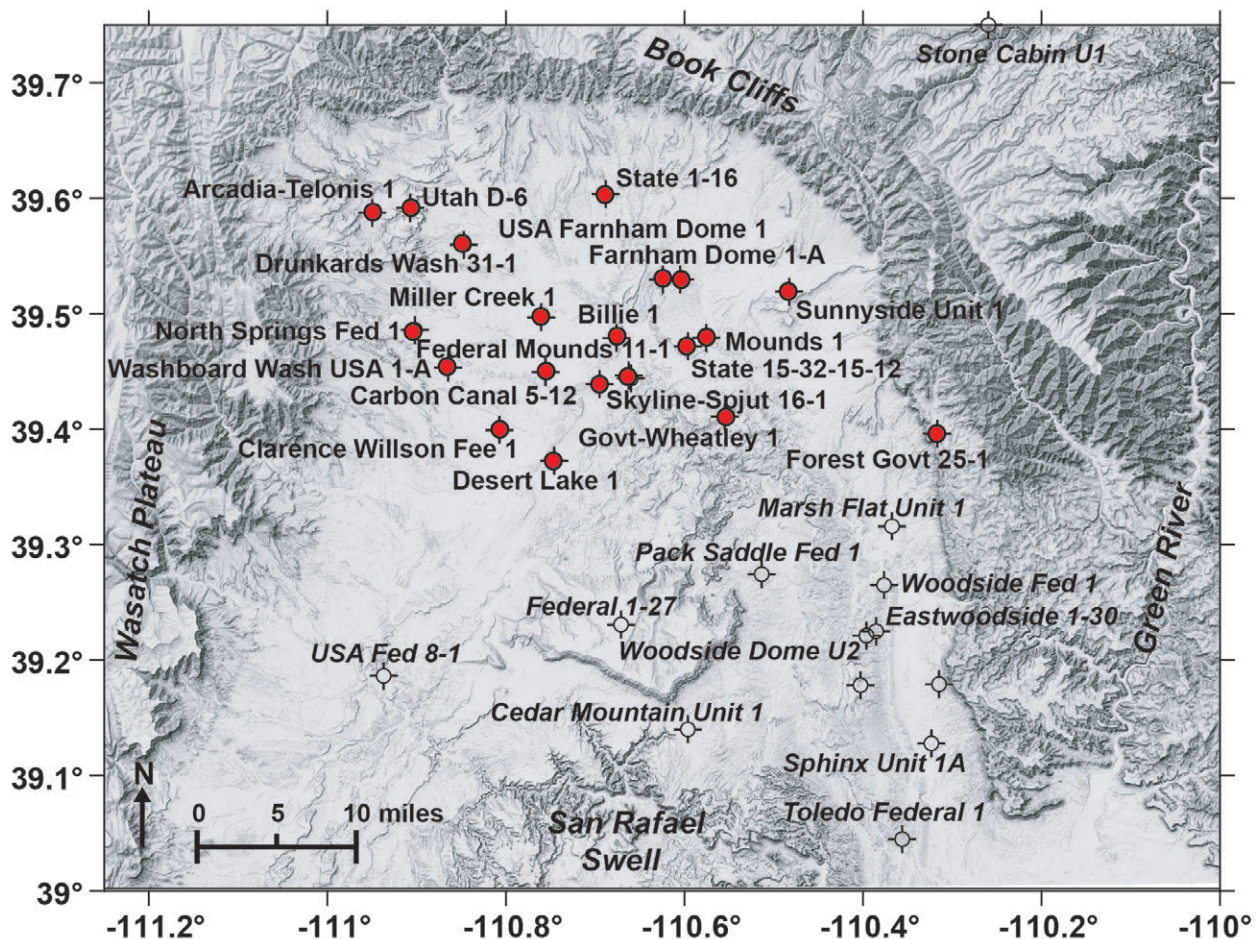


Figure 3.1. Locations of exploration wells fully penetrating the Doughnut Formation (red fill) in the northern San Rafael Swell area of east-central Utah.

After a two-decade hiatus the petroleum industry returned to the Doughnut Formation shale play in the northern San Rafael Swell. Bill Barrett Corporation and its partner ConocoPhillips acquired leasehold acreage in a 58,000-acre (23,500 ha) area named “Hook prospect.” In 2008, Barrett (50% working interest with ConocoPhillips) drilled the State 15-32-15-12 well (section 32, T. 15 S., R. 12 E., SLB&M, Carbon County; figure 3.2) to a total depth 8550 feet (2606 m) in the Hook prospect targeting the Doughnut Formation. The Doughnut consisted of 589 feet (180 m) of shale over a total formation thickness of 816 feet (249 m), 422 feet (129 m) of which was cored for gas content and reservoir analysis. The well analysis indicated good gas shows and high gas contents from core samples, but the well was completed as a dry hole. In October 2009, the company completed a horizontal well with a 3700-foot (1130 m) horizontal lateral offsetting the vertical well in the same section. The State 16H-32-15-12 well (figure 3.2) had a subcommercial IPF of 275 MCFGPD [7.79 MCMGPD] and 235 barrels of water (BW [37.4 m³]) on an 18/64-inch choke through a hydraulically fractured gross interval from 8252 to 10,436 feet (2515–3181 m). This horizontal production well is shut-in, but the vertical test well is merely “suspended.” Barrett presented plans to the Utah Division of Oil, Gas, and Mining (DOG M) to drill two more wells in section 32 (a request was made to permit one of the wells) with longer horizontal lengths and using improved completion techniques based on the information acquired from their first horizontal well. In addition, Barrett received DOGM approval to stake two additional Doughnut wells 3 miles (5 km) east in section 35, T. 15 S., R. 12 E., SLB&M, Carbon County, within its Hook prospect area. The company had also planned to conduct a three-dimensional (3-D) seismic program in the area covering 142 square miles (368 km²). However, all these exploration plans were dropped due to falling gas prices and other issues; no drilling or seismic surveys in the area are projected by Barrett in the near future.

Chief Oil & Gas International Petroleum LLC announced plans to drill a 7287-foot (2221 m) test of the Mississippian (section 3, T. 16 S., R. 12 E., SLB&M, Emery County), 1.5 miles (2.4 km) southeast of the Barrett State 15-32-15-12 well. The drill site was just west of Grassy Trail Creek field, which produces oil and gas from the Triassic Moenkopi Formation. Within Grassy Trail Creek, Genesis Petroleum U.S. announced plans to reenter a former Moenkopi producer and drill 7200 feet (2200 m) to the Precambrian. The 2-43X State well (section 2, T. 16 S., R. 12 E., SLB&M, Emery County) was to evaluate the Doughnut Formation and other Mississippian units. However, although these wells were approved by DOGM, the drilling plans were dropped by both operators.

West of the Hook area, Shell Western Exploration & Production, Inc. drilled and cored the Doughnut Formation in the 5-12 Carbon Canal well (section 12, T. 16 S., R. 10 E., SLB&M, Emery County; figure 3.2). The Doughnut was 975 feet (297 m) thick, of which 531 feet (162 m) was cored for gas content and reservoir analysis. The well was completed in 2008 as a gas discovery with an IPF of 468 MCFGPD (13.3 MCMGPD) and 1750 BW (278 m³). The natural gas produced has an energy value of 1052 Btu/Mcf. Production is from three hydraulically fractured Doughnut intervals. Flow was gauged through chokes ranging from 16/64 inch to 64/64 inch. Flowing casing pressure ranged up to 5200 pounds per square inch (psi) (36,000 kPa). The well is currently shut-in. Shell intended to drill two additional 9400-foot (2900 m) wells to test potential Paleozoic shale-gas reservoirs, 3.5 miles (5.6 km) southwest and 6 miles (10 km) west-northwest in Emery and Carbon Counties, respectively. However, like the area in the east, these drilling activities were dropped when gas prices fell.

PARADOX FORMATION

In early 2007, CrownQuest Operating LLC began an ambitious exploration program to drill new wells and conduct workovers in former dry holes to evaluate the Hovenweep, Gothic, and Chimney Rock shale zones of the Paradox Formation in the Utah part of the Paradox Basin. They reported the completion of the 1-21X Anteatr State well (section 21, T. 34 S., R. 26 E., SLB&M, San Juan County; figure 3.3) with an IPF of 329 MCFGPD (9.3 MCMGPD) from the Paradox. Cumulative production as of January 1, 2012, was 10.9 million cubic feet of gas (MMCFG [0.31 MMCMG]) (Utah Division of Oil, Gas, and Mining, 2012); the well is currently shut-in. CrownQuest also confirmed the discovery of Horsehead Point field with the completion of the 1-32 Chanticleer State well (section 32, T. 34 S., R. 26 E., SLB&M, San Juan County; figure 3.3) from the Paradox. Cumulative production from Horsehead Point field as of January 1, 2016, was 544.8 MMCFG (15.4 MMCMG) (Utah Division of

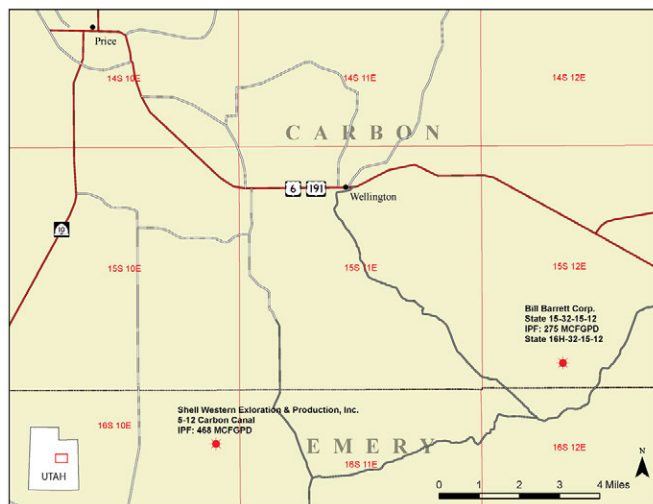


Figure 3.2. Location of recently drilled wells targeting the Mississippian/Pennsylvanian Doughnut Formation in the northern San Rafael Swell.

Oil, Gas, and Mining, 2016a). CrownQuest also drilled the Raider 1-17 Fee well (section 17, T. 33 S., R. 25 E., SLB&M, San Juan County; figure 3.3), completing it for an IPF of 450 MCFGPD (12.7 MCMGPD) from several Paradox zones; the well is also currently shut-in. Finally, CrownQuest reported completion of the 1-16 Explorer State well (section 16, T. 34 S., R. 25 E., SLB&M, San Juan County; figure 3.3) as another gas discovery in the Paradox with an IPF of 136 MCFGPD (3.9 MCMGPD); cumulative production as of January 1, 2016, was 69.7 MMCFG (2.0 MMCMG) (Utah Division of Oil, Gas, and Mining, 2016b). Few details have been released on these wells. In addition, Cabot Oil & Gas, Baytex, Fidelity E&P, and Babcock & Brown also staked wells targeting Paradox shale in the basin. Little information is available on these wells and low gas prices have also likely curtailed drilling activities.

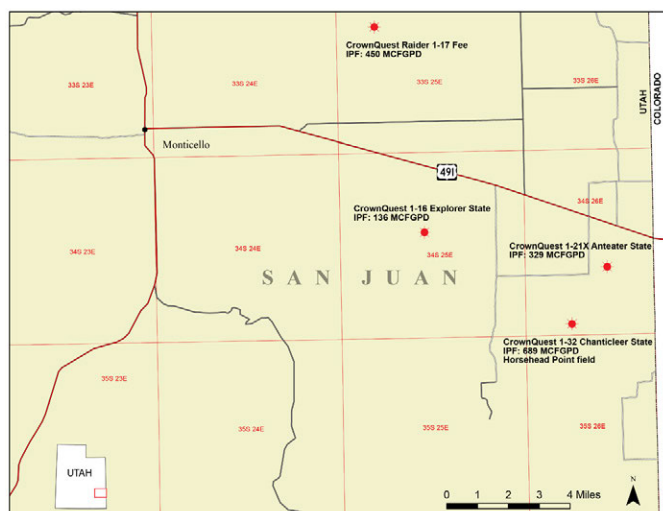


Figure 3.3. Location of recently drilled wells targeting the Hovenweep and Gothic shales and other zones in the Pennsylvanian Paradox Formation in the Utah part of the Paradox Basin.

In the northwestern part of the Paradox Basin, Delta Petroleum evaluated clastic zones in the Paradox Formation, which likely include shale. Delta's 28-11 Samson Federal well, 2008 Greentown field discovery (section 28, T. 22 S., R. 17 E., SLB&M, Grand County, Utah) initially flowed at a rate of 1700 MCFGPD (48,000 MCMGPD) from the "O" zone clastic interval within the Paradox cyclic salt section. As of January 1, 2016, Greentown field has produced 255 MMCFG (7.2 MMCMG); three wells are shut-in (Utah Division of Oil, Gas, and Mining, 2016a).

On the Colorado side of the Paradox Basin, Bill Barrett Corporation conducted an extensive, moderately successful horizontal drilling exploration and development program for the Gothic and Hovenweep shales in what the company named the "Yellow Jacket" and "Green Jacket" areas, respectively. Bill Barrett Corporation estimated gross in-place reserves are 50 BCFG/section (1.4 BCM/section). The Yellow Jacket area covers 1850 square miles (4800 km²), where the company had about 140,000 net undeveloped acres (57,000 ha). Within the play area, the target Gothic shale is 80 to 150 feet (24–46 m) thick and is found at depths between 5500 and 7500 feet (1700–2300 m). Bill Barrett Corporation, the operator and a 55% leasehold owner, with its partner, Williams Production RMT Company, drilled and completed four vertical wells and 10 horizontal wells to test in the play in 2009–10. Three wells are on production totaling 3.0 MMCFGPD (85 MCMGPD). Davis Petroleum Corporation also staked Gothic wells in the Yellow Jacket area. The Green Jacket area, which extends into Utah, covers 1300 square miles (3400 km²), where the company had about 150,000 net undeveloped acres (61,000 ha) (Peter G. Moreland, formerly with Bill Barrett Corporation, verbal communication, June 15, 2010).

CHAPTER 4: DATA COMPILATION AND CORE DESCRIPTIONS

BY

S. Robert Bereskin, *Bereskin and Associates, Inc.*;
Stephanie Carney and Thomas C. Chidsey, Jr.,
Utah Geological Survey;
Steven Schamel, *GeoX Consulting, Inc.*

CONTENTS

DATA COLLECTION AND COMPILATION	35
CORE DESCRIPTIONS.....	35
Gothic Shale Example	39
General Results	39
Manning Canyon Shale/Doughnut Formation	39
Paradox Formation	40

FIGURES

Figure 4.1. Location of cores described in this study from the Mississippian/Pennsylvanian Manning Canyon Shale in the northern San Rafael Swell	35
Figure 4.2. Location of cores described in this study from the Hovenweep, Gothic, and Chimney Rock shales, Paradox Basin	36
Figure 4.3. Interpreted geophysical well log and core description, Aneth Unit H-117 well	37
Figure 4.4. Typical examples of core from the Hovenweep, Gothic, and Chimney Rock shales, Paradox Basin	38

TABLE

Table 4.1. List of well conventional slabbed core examined and described from potential Paleozoic shale gas reservoirs, Utah	36
------------------------------------------------------------------------------------------------------------------------------------	----

CHAPTER 4:

DATA COMPILATION AND CORE DESCRIPTIONS

DATA COLLECTION AND COMPILATION

Although no single, previous study of the Utah Paleozoic shale gas potential has been conducted, numerous useful and important papers describe various attributes of these rocks. Cumulatively, these papers provide a significant wealth of information and background for an evaluation or study of Paleozoic shale gas resources in Utah. Therefore, a comprehensive bibliography of these publications was compiled for this study and for subsequent use by others investigating Utah's potential Paleozoic shale gas resources. The bibliography (appendix B) consists of three sections: (1) general references for the Mississippian and Pennsylvanian Systems mainly in the mountain west, (2) Pennsylvanian-age-specific references for the Gothic, Chimney Rock, and Cane Creek shale zones of the Paradox Formation, and (3) Mississippian-age-specific references for the Manning Canyon Shale, Delle Phosphatic Member of the Deseret Limestone/Chainman Shale, and Doughnut Formation. Within these sections are papers dealing with stratigraphic definitions, petrography, rock mechanics, geochemistry, and geochronology.

A well database was also compiled for this study to provide a source of critical subsurface information that would aid in evaluating the resource potential of Paleozoic shale gas reservoirs of Utah. The well database (appendix C) includes the following:

1. operators and locations of wells of interest (having penetrated targeted Paleozoic shales, i.e., Manning Canyon Shale, Doughnut Formation, or the Hovenweep, Gothic, or Chimney Rock shales of the Paradox Formation) from the eastern Basin and Range Province, central Utah thrust belt, San Rafael Swell, and the Paradox Basin,
2. available cores and cuttings, formation and zone, sample interval, repository, and geophysical well logs,
3. completion data such as date of completion and current status, producing formation, targeted formation(s), and total depth (TD) and age of the formation at TD,
4. test-treatment data—formation tested, test type, test interval, IPF, pressures, choke size, and treatment type, and
5. geochemical analysis, from both published sources and acquired as part of this study—formation/zone, sample source and type, total organic carbon, programmed pyrolysis (RockEval) results (S1, S2, S3, Tmax), petroleum index, oxygen index, hydrogen index, vitrinite reflectance (R_o), and thermal alteration index.

CORE DESCRIPTIONS

All available conventional cores through the Manning Canyon Shale (Doughnut Formation) from the northern San Rafael Swell and the Hovenweep, Gothic, or Chimney Rock shales in the Paradox Basin (figures 4.1 and 4.2, table 4.1) were examined and utilized for a variety of geological and geochemical purposes. The cores were described and digitally photographed (figure 4.3, appendix D—Coreographs and Core Descriptions [on compact disc] and figure 4.4, appendix E—Core Photographs [on compact disc]). Many cores were in a whole-core state and required slabbing for more accurate megascopic inspection.

A survey of drilling records in the study regions revealed that only three cores were taken from the Manning Canyon Shale (Doughnut Formation), all from wells drilled with the Manning Canyon as the primary objective. One of the three, State 15-32-15-12 well (section 32, T. 15 S., R. 12 E., SLB&M, Carbon County; figure 3.1), is confidential, is still being evaluated by the operator Bill Barrett Corporation, and was not available for this study. Wells in the Paradox Basin typically target the productive carbonate reservoirs in the Ismay and Desert Creek zones of the Paradox Formation (figure 1.4). Any cores of the

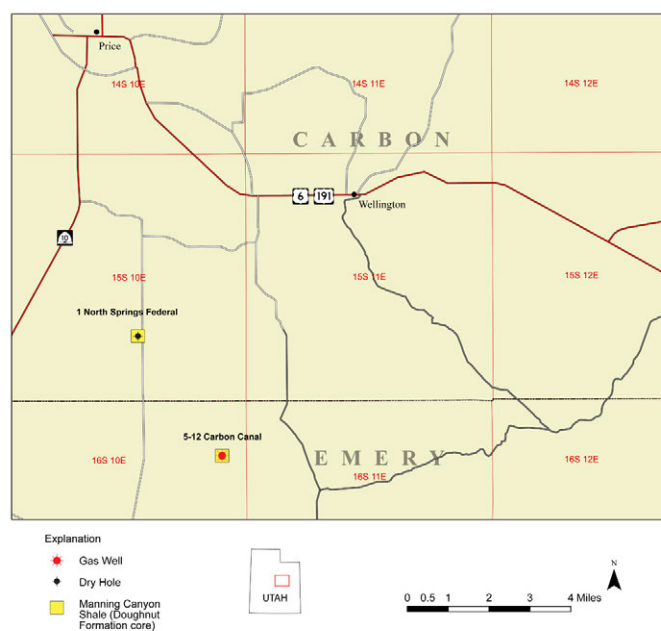


Figure 4.1. Location of cores described in this study from the Mississippian/Pennsylvanian Manning Canyon Shale (Doughnut Formation) in the northern San Rafael Swell.

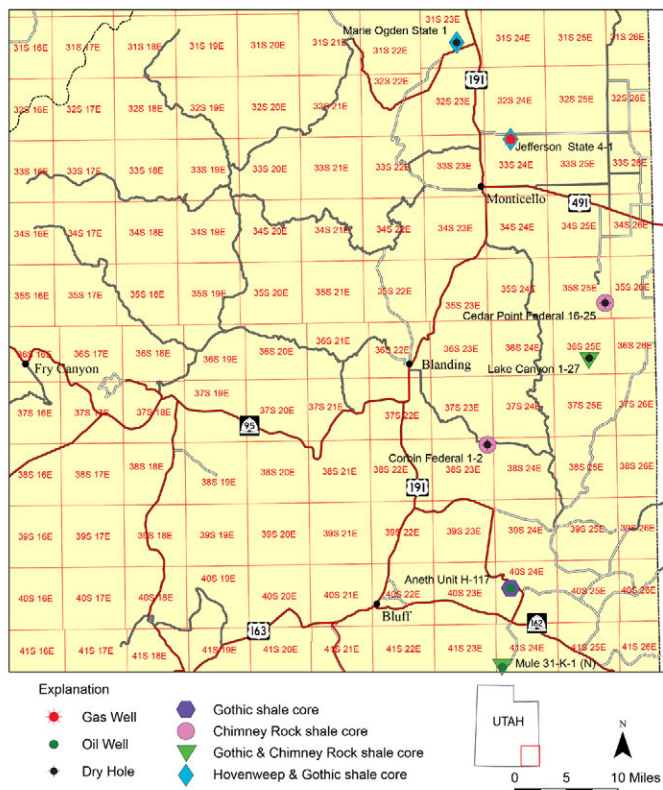


Figure 4.2. Location of cores described in this study from the Hovenweep, Gothic, and Chimney Rock shales in the Pennsylvanian Paradox Formation in the Utah part of the Paradox Basin.

Hovenweep, Gothic, and Chimney Rock shales are likely the result of a missed core point. Therefore, very few cores of these shales exist and most shale beds represent only part of the section. However, the cores usually include a contact with the bounding carbonate zone, which, as we discovered in the course of this study, can be very significant in terms of potential gas resources. In terms of the coregraphs, the end sections of the graphs show parts of adjacent zones.

For this study, all materials were used for the following procedures: (1) a foot-by-foot inspection of slabbed surfaces for megascopic geological assessment (figure 4.3), (2) geochemical analyses, mostly involving assessment of total organic carbon content and overall level of maturation (programmed pyrolysis [RockEval™]), (3) preparation and examination of selected thin sections for examination on a microscopic scale, (4) preparation and scanning electron microscopy (SEM) examination of samples for determination of porosity abundance and void morphology, (5) performance of recently-developed tight rock analysis (TRA) for quantitative measurements of shale porosity and permeability as well as routine core analysis for the associated carbonates, and (6) X-ray diffraction (XRD) for semi-quantitative compositional evaluation. In the TRA process above (5), accurate fluid saturations are also an objective of this procedure, but the archived, partially dehydrated core would prohibit any correct quantitative assessment of oil, gas, or water saturations.

Table 4.1. List of wells with conventional slabbed core examined and described from potential Paleozoic shale gas reservoirs, Utah.

Well	API Number	Location	County	Core Interval (feet)	Formation/Zone	Appendix D Plate No.
1 North Springs Fed.*	43-007-10791	SE SW 27, T. 15 S., R. 10 E.	Carbon	10,739–10,757	Manning Canyon	D1
Carbon Canal 5-12	43-015-30709	SW NW 12, T. 16 S., R. 10 E.	Emery	8805–9351	Manning Canyon	D2–D9
Marie Ogden 1 State	43-037-31825	SE NW 22, T. 31 S., R. 23 E.	San Juan	5183–5232	Hovenweep	D10
Marie Ogden 1 State	43-037-31825	SE NW 22, T. 31 S., R. 23 E.	San Juan	5318–5335	Gothic	D11
Jefferson State 4-1	43-037-31832	SW NW 4, T. 33 S., R. 24 E.	San Juan	5899–5944	Hovenweep	D12
Jefferson State 4-1	43-037-31825	SW NW 4, T. 33 S., R. 24 E.	San Juan	6003–6041.5	Gothic	D13
Cedar Point Federal 16-25	43-037-30786	NE SE 25, T. 35 S., R. 25 E.	San Juan	6403–6413	Chimney Rock	D14
Lake Canyon 1-27	43-037-30692	NW NW 27, T. 36 S., R. 25 E.	San Juan	5746–5775	Gothic	D15
Lake Canyon 1-27	43-037-30692	NW NW 27, T. 36 S., R. 25 E.	San Juan	5865–5888	Chimney Rock	D16
Corbin Federal 1-2	43-037-30927	NW SE 1, T. 38 S., R. 23 E.	San Juan	6088–6097	Chimney Rock	D17
Aneth Unit H-117	43-037-30153	NE NE 17, T. 40 S., R. 24 E.	San Juan	5376–5395	Gothic	D18
Mule 31-K-1 (N)	43-037-31617	SE SW 31, T. 41 S., R. 24 E.	San Juan	5900–5926	Gothic	D19
Mule 31-K-1 (N)	43-037-31617	SE SW 31, T. 41 S., R. 24 E.	San Juan	6095–6118	Chimney Rock	D20

*Repository: Texas Bureau of Economic Geology; all other cores stored at the Utah Core Research Center.

Aneth Unit H-117
 NE NE Sec. 17, T. 40 S., R. 24 E.,
 San Juan County, Utah
 KB 4553 ft
 Cumulative Production =
 479,197 BO, 296,878 MCFG, 1,871,016 BW

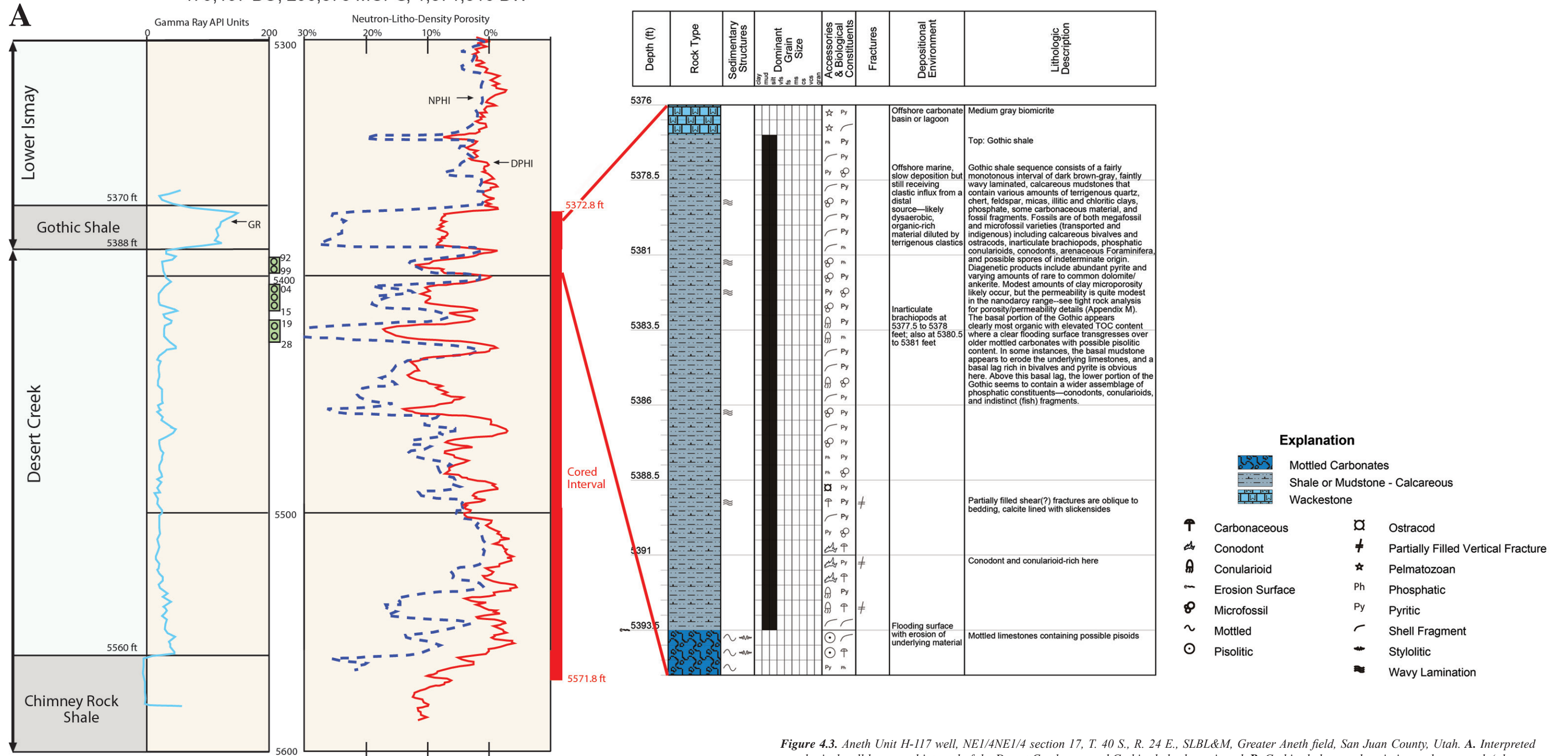


Figure 4.3. Aneth Unit H-117 well, NE1/4NE1/4 section 17, T. 40 S., R. 24 E., SLBL&M, Greater Aneth field, San Juan County, Utah. A. Interpreted geophysical well log; cored interval of the Desert Creek zone and Gothic shale shown in red. B. Gothic shale core description and coregraph (also see plate D18 in appendix D).

A



B



C



D



Figure 4.4. Typical examples of core from the Doughnut Formation (A), Chimney Rock (B), Gothic (C), and Hovenweep (D) shales.

The coregraphs and core descriptions follow the guidelines of Bebout and Loucks (1984), which include the following parameters: (1) basic porosity types, (2) mineral composition in percentage, (3) nature of contacts, (4) sedimentary structures, (5) textures in percentage (in carbonate beds), (6) carbonate fabrics, (7) grain size, (8) fractures, (9) color, (10) fossils, (11) cement, and (12) depositional environment. Carbonate fabrics were determined according to Dunham's (1962) and Embry and Klovan's (1971) classification schemes. A subsequent digital column or coregraph was generated (figure 4.3; appendix D, plates D-1 through D-20). Similarly, the presence of any natural fractures was documented in the foot-by-foot inspection. Fracture morphologic features also documented included orientation (e.g., vertical, subvertical, or horizontal), length, mineral infilling, aperture width, shape (e.g., curvilinear, planar), and presence or absence of oil stain. As most shale operators know, the presence of "open" fractures will greatly influence the hydrocarbon productivity for both vertical and horizontal wellbores, and even filled fractures are particularly important to hydraulic fracturing procedures.

The description of the cores helped characterize the potential reservoir lithofacies and provided the basis for sample selection used in petrographic, petrophysical, geochemical, and geomechanical analysis. Descriptions can also be used to produce cross sections, strip logs, lithofacies maps, various graphs, and other types of presentations. The typical vertical sequence through the shale sections, as determined from conventional core, was tied to its corresponding log response (figure 4.3; appendix D, plates D-1 through D-20).

Gothic Shale Example

Core from the Aneth Unit H-117 well (table 4.1) in Greater Aneth field of the Paradox Basin (figure 2.7) contains nearly a complete (16 feet [4.9 m]), unslabbed section of Gothic shale (figure 4.3A). Therefore, this core was ideal for detailed representative analysis of the Gothic for the southern part of the basin. In the Gothic shale, seemingly subtle variations in mineralogical character, cementation, or depositional environment may result in important changes in reservoir capacity or cause mechanical boundaries. These subtle differences may in turn control fracture spacing, distribution, orientation, and conductivity.

The Gothic shale strata in the Aneth Unit H-117 core consist of a fairly monotonous interval of dark brown to gray, faintly wavy laminated, calcareous mudstone (see figure 4.3B for detailed core description). The strata contain various amounts of terrigenous quartz, chert, feldspar, micas, illitic and chloritic clays, phosphate, some carbonaceous material, and fossil fragments. Both megafossils and microfossils are present (transported and indigenous), including calcareous bivalves and ostracods, inarticulate brachiopods, phosphatic conularioids, conodonts, arenaceous foraminifera, and possible spores of indeterminate origin. Diagenetic products include

abundant pyrite and varying amounts of rare to common dolomite/ankerite. Modest amounts of clay microporosity likely occur, but the permeability is in the nanodarcy range. The basal portion of the Gothic appears clearly most organic with elevated total organic content (TOC) where a clear flooding surface transgressed over older mottled carbonates with possible pisolitic content. In some instances, the basal mudstone appears to erode the underlying limestones, and a basal lag rich in bivalves and pyrite is obvious there. Above this basal lag, the lower portion of the Gothic seems to contain a wider assemblage of phosphatic constituents—conodonts, conularioids, and indistinct (fish) fragments.

The Gothic depositional environment represented by the Aneth Unit H-117 core was offshore marine. The slow deposition still received clastic influx from a distal source. This source was likely dysaerobic, organic-rich material diluted by terrigenous clastics.

General Results

Manning Canyon Shale/Doughnut Formation

Based on core from the Manning Canyon Shale/Doughnut Formation, the lithotypes within this heterogeneous formation consist of mixtures of four components: (1) calcite microbio-clasts and shelly debris, largely thin-shelled brachiopods and thick-shelled pelecypods, (2) eolian coarse silt to fine-grained quartz sand, (3) an assemblage of mature clays (illite, smectite-illite, kaolinite, and chlorite) derived from an intensely leached regolith on adjacent Mississippian-age limestone, and (4) degraded fragments of terrestrial plants occurring as disseminated micron-size grains or as discrete plant parts. These four components combine to form a range of carbonate fabrics and lithologies: organic-rich or organic-poor, silty or non-silty packstone, wackestone, and dark gray or varicolored, calcareous or non-calcareous mudstone; siltstone and fine-grained sandstone; black shale; and coal. The several lithotypes are interbedded at a scale of feet to at most a few tens of feet.

The continuous core exhibits a weak vertical cyclicity indicating possible flooding surfaces and parasequences, but stratal cyclicity was not detected in well logs. In the gas-play area, the unit was deposited in a broad structural depression adjacent to the nascent Uncompahgre uplift.

The freshwater marshes of the Everglades together with the shallow water brackish to marine carbonate factory of Florida Bay may serve as a conceptual model for the depositional setting of the Manning Canyon Shale/Doughnut Formation as interpreted from cores. Hummocks and marshes formed on the carbonate mud mounds in the bay are an additional source of terrestrial and algal organic matter. A robust stratigraphic model is essential for effective future exploitation of this gas resource.

Paradox Formation

Cores from the Paradox Formation reveal several important parameters: (1) most shale beds are organic mudstone containing significant amounts of silt, pyrite, and fossil debris, (2) organic content appears modest, and (3) enough silt is present to create brittleness. The bounding and interbedded carbonate units are silty or muddy dolomite beds, in many cases possessing modest amounts of conventional intercrystalline and microvugular pore space. This porosity has largely been unrecognized or minimized because most open-hole density logs are run on a 2.71 g/cm^3 matrix density based on the assumption that the rocks are limestone. However, because they are dolomitic density logs should be run on a matrix density between 2.78 and 2.83 g/cm^3 and therefore porosity will more likely be detected.

The dolomite beds, as well as some shale, are also beset by numerous subvertical fractures, both filled and partially filled, mainly by calcite. Therefore, the gas production very likely is derived not only from the shale, but also from the associated carbonates and from the natural fractures. Thus, this shale play is likely an intermixed series of reservoir types, all of which could produce upon successful slant and/or directional drilling and optimized stimulation programs.

CHAPTER 5: PETROGRAPHIC ANALYSIS

BY

S. Robert Bereskin, *Bereskin and Associates, Inc.*;
Steven Schamel, *GeoX Consulting, Inc.*;
Thomas C. Chidsey, Jr., Steve Herbst, and Chloe Skidmore,
Utah Geological Survey

CONTENTS

INTRODUCTION	47
METHODS	47
Basic Thin Section Petrographic Analysis.....	47
Scanning Electron Microscopy.....	47
X-Ray Diffraction.....	47
X-Ray Fluorescence.....	48
DOUGHNUT FORMATION.....	48
Scope of Investigation	48
Petrography and Stratigraphy	49
Information from Well Cuttings and Geophysical Logs.....	50
Carbon Canal 5-12 Core	53
Lithologies.....	56
Mineral Composition.....	57
Chemical Composition of Shale.....	60
Spectral Gamma Ray.....	62
Fractures.....	63
Cyclicity and Parasequences	63
North Springs Federal 1 Core.....	64
State 1-16 Core	66
Discussion of Depositional Setting.....	66
PARADOX FORMATION	69
Core Descriptions	69
Microscopic Observations Through Petrography.....	70
Microscopic Observations Through Scanning Electron Microscopy (SEM).....	71
Microscopic Observations of Natural Fractures Through Petrography.....	73
Mineral Analysis Through X-Ray Diffraction (XRD).....	76
Examples of the Gothic Shale, Aneth H-117 Well, Greater Aneth Oil Field.....	76
Argillaceous Shale.....	76
Argillaceous Mudstone.....	80
Silty Calcareous/Argillaceous Mudstone	80
Phosphatic Argillaceous Mudstone	80

FIGURES

Figure 5.1. Common Doughnut Formation lithologies composed of principal sedimentary components.....	50
Figure 5.2. Lithology log for Spjut 16.1 well	51
Figure 5.3. Doughnut Formation lithologies in well cuttings.....	52
Figure 5.4. Geophysical logs for the Desert Lake Unit 1 well	52
Figure 5.5. Geophysical logs for the State 1-16 well.....	53
Figure 5.6. Doughnut Formation comparative caliper and gamma-ray log profiles.....	54
Figure 5.7. Lithology log for the Carbon Canal 5-12 core	55
Figure 5.8. Key to the lithology and color panels in the Carbon Canal 5-12 lithology log.....	56
Figure 5.9. Photographs of the principal Doughnut Formation lithotypes described in the Carbon Canal 5-12 core.....	56
Figure 5.10. The relative occurrence of lithologies in the Carbon Canal 5-12 core as a percent of net feet of the lithology ...	57
Figure 5.11. Vertical distribution of lithologies in the Carbon Canal 5-12 core expressed as cumulative thickness versus core depth	57
Figure 5.12. Mineral composition and spectral gamma-ray logs for the Carbon Canal 5-12 core interval	58
Figure 5.13. Ternary plot of the major mineral compositions of Doughnut Formation and the overlying Round Valley Limestone from XRD analyses	59
Figure 5.14. Ternary plot of the carbonate mineral compositions of Doughnut Formation and the overlying Round Valley Limestone from XRD analyses	59
Figure 5.15. Photomicrographs of rocks associated with possible condensed intervals or hardgrounds within the Carbon Canal 5-12 core.....	60
Figure 5.16. Photographs of possible stratigraphic boundaries in the Carbon Canal 5-12 core.....	64
Figure 5.17. Possible stratigraphic cycle boundaries in the Carbon Canal 5-12 core	65
Figure 5.18. Satellite images of southern Florida	67

Figure 5.19. Mud mounds and lagoons in the eastern part of Florida Bay	68
Figure 5.20. Fossil conulariid from the Gothic shale.....	69
Figure 5.21. Slickensides in an oblique to bedding fracture in the Gothic shale.....	70
Figure 5.22. Photomicrograph of silty mudstone from the Hovenweep shale typical of all three black mudstone zones from the Paradox Formation	70
Figure 5.23. Photomicrograph at very base of Upper Ismay cycle immediately above the Hovenweep contact.....	71
Figure 5.24. Photomicrographs from flooding surface found at the contact between the underlying Gothic shale and the overlying Lower Ismay carbonate sequence	71
Figure 5.25. Photomicrograph of a series of induced subhorizontal microfractures and mineral fluorescence	72
Figure 5.26. SEM photomicrographs from the Chimney Rock shale of stacked and crenulated clay flakes	72
Figure 5.27. SEM photomicrographs from the Chimney Rock shale of dolomite	73
Figure 5.28. SEM photomicrographs from the Gothic shale of an argillaceous mudstone and kerogen coating clay minerals	73
Figure 5.29. SEM photomicrographs from the Hovenweep shale of dolomitic mudstone and intercrystalline pores	74
Figure 5.30. Photomicrographs showing examples of type 2 microfractures from the Lower Ismay cycle near the subjacent Gothic shale	75
Figure 5.31. Photomicrographs showing examples of type 4 cracks completely occluded by calcite	75
Figure 5.32. Pie charts showing the average mineral assemblages based on X-ray diffraction analysis of the Hovenweep, Gothic, and Chimney Rock shale zones	77
Figure 5.33. Graphs depicting the weight percent of quartz based on X-ray diffraction analysis of the Hovenweep, Gothic, and Chimney Rock shale zones.....	78
Figure 5.34. Graphs depicting the weight percent of the sum of illite and chlorite based on X-ray diffraction analysis of the Hovenweep, Gothic, and Chimney Rock shale zones.....	79
Figure 5.35. Photomicrographs of argillaceous shale lithotype in Gothic shale.....	80
Figure 5.36. Photomicrographs and SEM images of argillaceous mudstone in Gothic shale	81
Figure 5.37. Photomicrographs and SEM images of silty calcareous/argillaceous mudstone in Gothic shale	82
Figure 5.38. Photomicrographs and SEM images of phosphatic argillaceous mudstone in Gothic shale.....	83

TABLES

Table 5.1. Exploration wells in the northern San Rafael Swell area that penetrate the Doughnut Formation	48
Table 5.2. Exploration wells the northern San Rafael Swell area that penetrate the Carboniferous section, but that do not encounter the Doughnut Formation.....	49
Table 5.3. Summary of the mineralogy of the Doughnut Formation and the Round Valley Limestone as determined by X-ray diffraction analysis of samples from the Carbon Canal 5-12 core.....	58
Table 5.4. Chemical compositions of whole rock shale, claystone, or mudstone samples from the Carbon Canal 5-12 and State 1-16 cores as determined by X-ray fluorescence.....	61
Table 5.5. Summary of spectral gamma-ray data for the Carbon Canal 5-12 well.....	62

CHAPTER 5:

PETROGRAPHIC ANALYSIS

INTRODUCTION

The rock fabrics, porosity types, and mineral composition found in various hydrocarbon-bearing shale beds can be indicators of reservoir flow capacity, brittleness, storage capacity, and untested reservoir potential. Concurrent with the megascopic core inspection, we collected samples for (1) basic traditional thin section petrographic descriptions, (2) scanning electron microscope (SEM) analysis, and (3) X-ray diffraction. Sampling bias was based on original lithofacies classification obtained through the macroscopic examination. Although a depositional history was formulated for these shales based on the macroscopic core examination, details and confirmation of such a history were determined through the petrographic studies.

METHODS

Basic Thin Section Petrographic Analysis

Thin section analyses of shale samples are used for petrological description of the lithofacies and to establish a baseline correlation of petrophysical properties related to the geologic/petrologic descriptions. They are used as a screening tool for important reservoir parameter investigations such as diagenetic alteration, cementation, and fracture fill. To determine the shale characteristics listed above, we selected thin sections of representative samples from the conventional cores listed in table 4.1 (none from the Corbin Federal 1-2 due to the poor quality of the core) for petrographic description. Bounding carbonate fabrics were determined according to Dunham's (1962) and Embry and Klovan's (1971) classification schemes. Pores and pore systems were described using Choquette and Pray's (1970) classification. Each thin section was described and photographed to show the occurrence of (1) basic mineral components, (2) typical preserved primary and secondary pore types, (3) cements, (4) sedimentary structures, and (5) where present, fractures (appendix F).

Our photomicroscopic work on thin sections emphasized a series of plane and cross-polarized views implementing a traditional petrographic transmitted light source. In addition, we produced several views from an ultraviolet reflected light source using a blue-violet filter. The former transmitted light views allow identification of minerals, their grain size (to some degree for mudrocks), and compaction/cementation (diagenetic) effects upon the original sedimentary materials. In some cases, magenta epoxy can be seen in pores of some

magnitude. The latter epifluorescent or reflected light views are qualitative estimates of porosity-only images, where pores usually are represented by light yellow green (mesopores) and orange (micropores) hues. In some cases, mineral fluorescence, especially from dolomites (also yellow-green), can make porosity detection difficult.

Scanning Electron Microscopy

To further determine the mineralogy and pore systems of the shale (and bounding carbonates in some examples), we selected additional samples from the thin section blanks for SEM analysis. The SEM was used to photograph (1) clays and other mineral constituents, (2) typical preserved primary and secondary pore types and pore throats, (3) kerogen location, (4) cements, (5) sedimentary structures, (6) fractures, and (7) possible pore-plugging anhydrite and halite. For the complete descriptions and SEM images refer to appendix G.

In addition, because of the potential confusion regarding mineral fluorescence versus porosity fluorescence, we used SEM techniques to verify the presence or absence of void space. In some samples, energy-dispersive X-ray spectroscopy (EDAX), as explained in the SEM photomicrograph materials (appendix G), can be used to detect major atomic elements, thus allowing modest mineralogy detection for specific grains. Most certainly, SEM work was instrumental in determining void space, particularly for the mudrocks (shales). However, SEM samples are extremely small and may not completely represent overall reservoir characteristics.

X-Ray Diffraction

X-ray powder diffraction (XRD) was employed to identify the mineral constituents of important reservoir intervals and facies. We performed XRD analysis on bulk samples using a Rigaku MiniFlex II instrument, which has a copper target. Due to small sample size requirements, a mortar and pestle were used to crush the samples, with all precautions taken to limit sample contamination. A USA standard test sieve number 325 was used to process samples to achieve a grain size of less than 45 microns required for optimal analysis. Measurement conditions included sampling from 2.0° to 90.0°, with a sampling width of 0.02° and a continuous scan speed of 2.0° per minute. We used International Center for Diffraction Data (ICDD) software for interpretive analysis. For the complete XRD data compilations refer to appendix H.

X-Ray Fluorescence

We employed X-ray fluorescence (XRF) to conduct elemental analysis and determine bulk elemental components for each sample. XRF analysis of pressed pellets was conducted using a Rigaku ZSX Mini instrument. Bulk samples were crushed using a ring-and-puck mill. Silica sand was used to clean the mill between each sample to limit sample contamination. Powdered samples were measured and mixed with wax using a 9:1 ratio, for a total of 5 grams. Each sample was run for approximately 60 minutes. The resulting data were processed qualitatively to establish mass percent of constituent elemental oxides.

DOUGHNUT FORMATION

At the north-plunging terminus of the San Rafael Swell in a 24-township (864-square-mile [2240 km²]) area encompassing

T. 14 S. through T. 17 S. and R. 9 E. through R. 14 E., SL-BL&M, there are 21 exploration wells (figure 3.1) that fully or partially penetrate the Doughnut Formation and an additional two wells that enter at least the upper part of the unit (table 5.1). These wells offer a unique opportunity to characterize the stratigraphic character and hydrocarbon potential of this carbonaceous formation. This area and these wells are the main focus of this investigation.

Scope of Investigation

The well completion reports and additional information are available from the DOGM for all but two of the wells in the northern San Rafael Swell region: the State 15-32-15-12, which remains confidential three years after operations were suspended, and the Billie 1, for which a completion report was never submitted (figure 3.1). Formation tops are available for all wells. Additionally, eight well records include detailed sam-

Table 5.1. Exploration wells in central Utah in the northern San Rafael Swell area that penetrate the Doughnut Formation (DF). Data from the Utah Division of Oil, Gas, and Mining online record system.

API number	Well name	Twp	Rng	Section	TD (ft)	DF top (ft)	DF base (ft)	DF thick (ft)	Overlain	Underlain
43-007-30093	Arcadia-Telonis 1 (D2)	14S	09E	19 SESE	13,013	11,836	12,376	540	Oquirrh	Humberg
43-007-30100	Utah D-6	14S	09E	34 SWSW	13,915	11,454	11,851	397	Oquirrh	Deseret
43-007-30040	Drunkards Wash 31-1 (D-1)	14S	10E	31 SESW	13,500	11,620	12,850	1230	Oquirrh	Humberg
43-007-30071	State 1-16	14S	11E	16 SWSE	12,153	10,100	10,990	890	N/A	N/A
43-007-10791	North Springs Fed 1	15S	09E	27 SESW	12,737	10,475	10,928	453	Oquirrh	Humberg
43-007-11029	Miller Creek 1	15S	10E	26 NENE	10,852	8170	8950	780	Oquirrh	Humberg
43-007-30149	Billie 1	15S	11E	34 SENW	7424	6890	N/A	N/A	N/A	N/A
43-007-10356	Mounds 1	15S	12E	33 SWSE	9360	6860	8040	1180	Oquirrh	Humberg(?)
43-007-10819	USA Farnham Dome 1	15S	12E	7 SWSW	8509	5882	7042	1160	N/A	N/A
43-007-15395	Farnham Dome 1-A	15S	12E	08 SWSW	9174	7257	7546	289	Oquirrh	Humberg
43-007-31366	State 15-32-15-12	15S	12E	32 SWSE	8600	7585	8401	816	Oquirrh	Humberg
43-007-31482	State 16H-32-15-12	15S	12E	32 SESE	10,565	7839	N/A	N/A	Pennsylv.	N/A
43-007-30012	Sunnyside Unit 1	15S	13E	17 NWSE	9158	7480	7880	400	Hermosa	Deseret
43-007-11330	Washboard Wash USA 1-A	16S	09E	12 NENW	11,675	9030	9470	440	Oquirrh	Humberg
43-015-30067	Skyline-Spjut 16-1	16S	09E	16 NENW	8872	7003	8080	1077	Oquirrh	Humberg
43-015-20190	Clarence Willson Fee 1	16S	10E	28 SESW	10,000	8506	9350	844	Oquirrh(?)	Humberg
43-015-30709	Carbon Canal 5-12	16S	10E	12 SWNW	9731	8910	9548	638	Oquirrh	Humberg
43-015-10825	Federal Mounds 1	16S	11E	11 NWSW	9425	6545	7661	1116	Oquirrh	Humberg
43-015-30077	Federal Mounds 11-1	16S	11E	11 SESW	7750	6545	7661	1116	Oquirrh	Humberg
43-015-10500	Govt-Wheatley 1	16S	12E	27 NWNE	7132	4830	6340	1510	Hermosa	Humberg
43-015-10374	Forest Govt 25-1 Arnold	16S	14E	25 SWSW	12,602	11,342	11,618	276	Hermosa	Humberg
43-015-11328	Desert Lake Unit 1	17S	10E	01 NWSE	10,915	8252	9130	878	Oquirrh	Humberg
43-015-10928	Marsh Flat Unit 1	17S	14E	29 SWNE	8507	7265	8160	895	Paradox	Madison

TD = total depth

N/A = not applicable

ple logs of the rocks penetrated. For nearly all wells some type of geophysical well log is available as a raster file. Gamma-ray logs exist for virtually all wells, but otherwise the log suites are sparse and of varied quality. The Utah Core Research Center (UCRC) has cuttings for eight of the wells, although in several instances there are gaps in the collection within the Doughnut interval. For this study, Shell Western Exploration & Production Inc. (SWEPI) donated a split of the 544-foot (166 m) Carbon Canal 5-12 core with analytical data to the UGS. An 18-foot (5.5 m) core from the North Springs Federal 1 well was loaned to the UGS by the Texas Bureau of Economic Geology, and core photographs for a 27-foot (8.2 m) segment of the State 1-16 well was obtained from the U.S. Geological Survey Core Depository (Denver, Colorado). For this interval in the State 1-16 well, the UCRC had rock fragments of the core in its collection. For core descriptions and photographs see appendices D and E, respectively.

In the 18 townships to the south of the Doughnut Formation penetrations (figure 3.1), encompassing T. 18 S. through T. 20 S. and R. 9 E. through R. 14 E., SLBL&M, 11 exploration wells penetrated the Upper Mississippian-Lower Pennsylvanian stratigraphic interval, but did not encounter any reported Doughnut (table 5.2). This group of wells document rocks of the Hermosa Group and Molas Formation resting unconformably on Leadville Limestone. The only other well in the area (figure 3.1) sufficiently deep to have possibly penetrated Doughnut, the Stone Cabin U1 well, is on the Uncompahgre uplift where Permian-age Elephant Canyon Formation rests unconformably on reported Leadville Limestone.

Petrography and Stratigraphy

The petrography and stratigraphy of the Doughnut Formation (listed as Manning Canyon Shale in many reports and pub-

lications) in north-central Utah is known broadly from well cuttings and well reports, a few short cores in the public domain, and geophysical logs of variable quality and vintages. A considerably more comprehensive view of the formation is available from core and wireline logs of a single well, the Carbon Canal 5-12 (figures 3.1, 3.2, and 4.1).

The stratigraphic units overlying and underlying the Doughnut Formation—the Round Valley Limestone (or Oquirrh Group) and the Humbug Formation, respectively—are characterized by interbedded carbonate and sandstone beds. The Doughnut is distinguished by the presence of substantial clay, silt, and organic matter punctuating an otherwise continuous open-marine carbonate shelf succession. Nearly all of the rocks belonging to this unit that were examined in thin section contain variable proportions of five lithic components:

- Carbonate – in skeletal debris, microbiodolites and/or lime mud.
- Clay – commonly admixed with the lime mud or within distinct laminae.
- Quartz grains – either angular silt-size to very fine grained sand or as siliceous sponge spicules.
- Organic matter – commonly recognizable plant parts, but also as very fine grained particles dispersed within the lime mud-clay rock matrix.
- Pyrite and other diagenetic minerals – indicative of a low oxygen-reduction potential (Eh) environment in the sedimentary column and low-rank greenschist metamorphic phases.

Table 5.2. Exploration wells in central Utah in the San Rafael Swell area that penetrated the Carboniferous section, but that did not encounter the Doughnut Formation. Data from the Utah Division of Oil, Gas, and Mining online record system.

API number	Well name	Twsp	Rng	Section	TD (ft)	Comment
43-015-20091	Federal 1-27	18S	11E	27 SWNE	6861	TD in Lynch Dolo after Hermosa Gr(?) + Leadville Ls(?) penetration
43-015-10350	Pack Saddle Fed 1	18S	12E	12 SENE	6806	TD in basement after Penn. + Miss. Strata
43-015-10506	Woodside Dome U2	18S	14E	30 SWSW	7084	TD in Leadville Ls after full Hermosa(?) + Molas Fm(?) penetration
43-015-10658	Woodside Fed 1	18S	14E	08 SWSW	7920	TD in Leadville Ls after full Hermosa + Molas Fm penetration
43-015-30086	Eastwoodside 1-30	18S	14E	30 NWSE	7400	TD in Leadville Ls after full penetration of Paradox Fm
43-015-10969	Cedar Mountain Unit 1	19S	12E	29 NESW	6031	TD in Ophir Sh; penetrates Penn. (1241') + Miss. (816')
43-015-30701	Woodside 1	19S	13E	12 SESE	6370	TD in Cane Creek sh near base Paradox Fm
43-015-30001	Barrier Bank 1	19S	14E	11 SWSE	8795	TD in upper Paradox Fm salt
43-015-10504	Sphinx Unit 1A	19S	14E	35 SWNW	8737	TD in Leadville Ls after full penetration of Paradox Fm
43-015-30039	USA Fed 8-1	19S	9E	8 SENW	6215	TD in Leadville Ls; overlying units not specified
43-015-30003	Toledo Federal 1	20S	14E	33 NENW	7558	TD in Leadville Ls after full Hermosa Gr + Molas Fm penetration

TD = total depth

These lithic components occur in a variety of recognizable lithologies (figure 5.1), such as carbonate wackestone, laminated silty carbonaceous shale, interlaminated carbonaceous shale and silty carbonate packstone, and laminated carbonaceous, calcareous siltstone.

Information from Well Cuttings and Geophysical Logs

Collections of well cuttings were available for just eight of the 23 wells penetrating the Doughnut Formation in north-central Utah. Several of these wells also had detailed geologic reports and/or mud logs from which lithology logs could be constructed (for example, figure 5.2; appendix I, plate I-1). The cuttings were examined to characterize the range of lithologies, gather samples for geochemical analysis, and confirm the accuracy of the existing well reports.

The lithologies recognized in cuttings (figure 5.3) consist of the following:

- Carbonates – described in the reports as both limestone and dolomite. Colors range from dark gray to very light gray. The dark gray limestones are normally carbonaceous.
- Shale – silty, calcareous and/or carbonaceous, black to medium gray, in blocky to paper-thin fragments.
- Sandstone and siltstone – light to medium gray quartz arenite. Sandstone is common only in the Sunnyside Unit 1 cuttings. In other wells siltstone is present, but sparse in cuttings.
- Coal – common in association with the dark gray carbonaceous shale as distinct blocky fragments or streaks within shale fragments.

Other fragments prevalent in the cuttings are shell fragments of both thick-walled and thin-walled brachiopods, identified from shell ornamentation, and maroon-colored silty mudstone (appendix I, plate I-1, the Miller Creek 1 well). In cuttings, fragments identified as dolomite might actually be limestone, a microbiodolomite packstone that breaks with a cryptocrystalline texture common in dolomite.

The lithology log of the Spjut 16.1 well (figure 5.2) is characteristic of others for the Doughnut Formation interval (appendix I, plate I-1). The operator assigned the formation top and bottom at 7003 feet and 8080 feet (2134 m and 2463 m), respectively. The interval that is dominantly carbonaceous, very dark gray to black shale with interspersed limestone and sandstone-siltstone is from the major part of the formation, 7300 to 8020 feet (2225–2444 m). Within this interval coal fragments are found in cuttings. The interval dominated by shale coincided with elevated background values of gamma ray (60 to 100 API units) and many, but not all, of the gamma

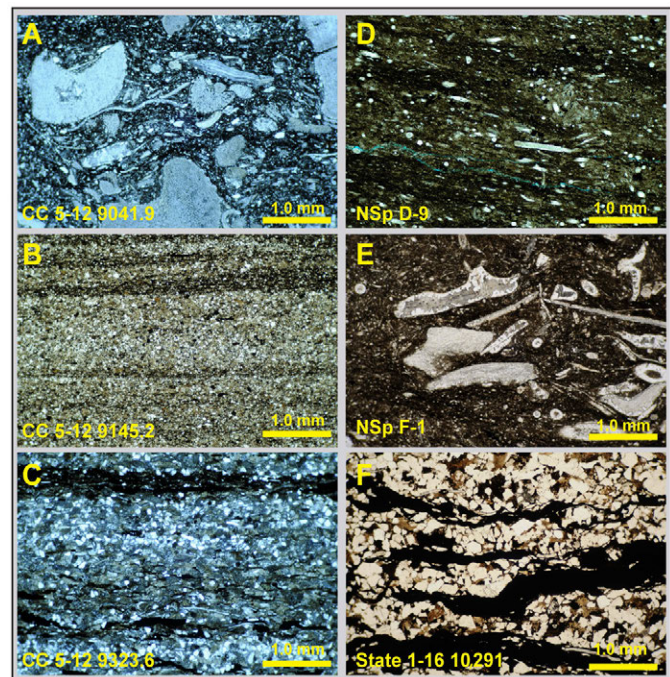


Figure 5.1. Common Doughnut Formation lithologies composed of principal sedimentary components. **A.** Very dark gray wackestone rich in skeletal material, including fragmented bryozoans, crinoids, and thin-walled pelcyopods. Lime mud rip-up clasts. Carbon Canal 5-12 well, 9041.9 feet. **B.** Finely laminated silty shale with minor microbiodolomite. Carbon Canal 5-12 well, 9145.2 feet. **C.** Interlaminated calcareous siltstone and organic-rich black shale. The thicker siltstone laminae contain a mix of quartz silt, silt-sized microbiodolomite, and plant fragments. Carbon Canal 5-12 well, 9323.6 feet. **D.** Carbonaceous, calcareous shale containing abundant siliceous sponge spicules. North Springs Federal 1 well, D-9. **E.** Carbonaceous, argillaceous wackestone with skeletal debris, including thick-walled brachiopod shells and spines and siliceous spicules. Secondary feldspar overgrowths rim shell fragments. North Springs Federal 1 well, F-1. **F.** Interlaminated carbonaceous, calcareous siltstone, and opaques composed of organic matter and pyrite. The siltstone contains silt-size microbiodolomite and thin flakes of white mica up to 1.5 mm in size. State 1-16 well, 10,291 feet. See figure 3.1 for well locations.

ray spikes with values up to 400 API units. Maroon-colored shale (mudstone) is observed below the base of the Doughnut, as picked by the operator, and in a single bed in the upper part of the formation. Inspection of the cuttings shows that most of the shale beds are calcareous, not just the mudstone interval shown in the log. Also, the sandstone is actually composed of very fine grained sand and silt that would be more accurately described as a siltstone.

Examination of four additional lithology logs (appendix I, plate I-1) shows the difficulty of picking the stratigraphic limits of the Doughnut Formation from cuttings alone. Whereas each log has a thick, dominantly dark gray to black shale interval within the designated formation limits, the part that is recognized as carbonaceous and/or has coal fragments is limited. On the other hand, dark shale and limestone, some iden-

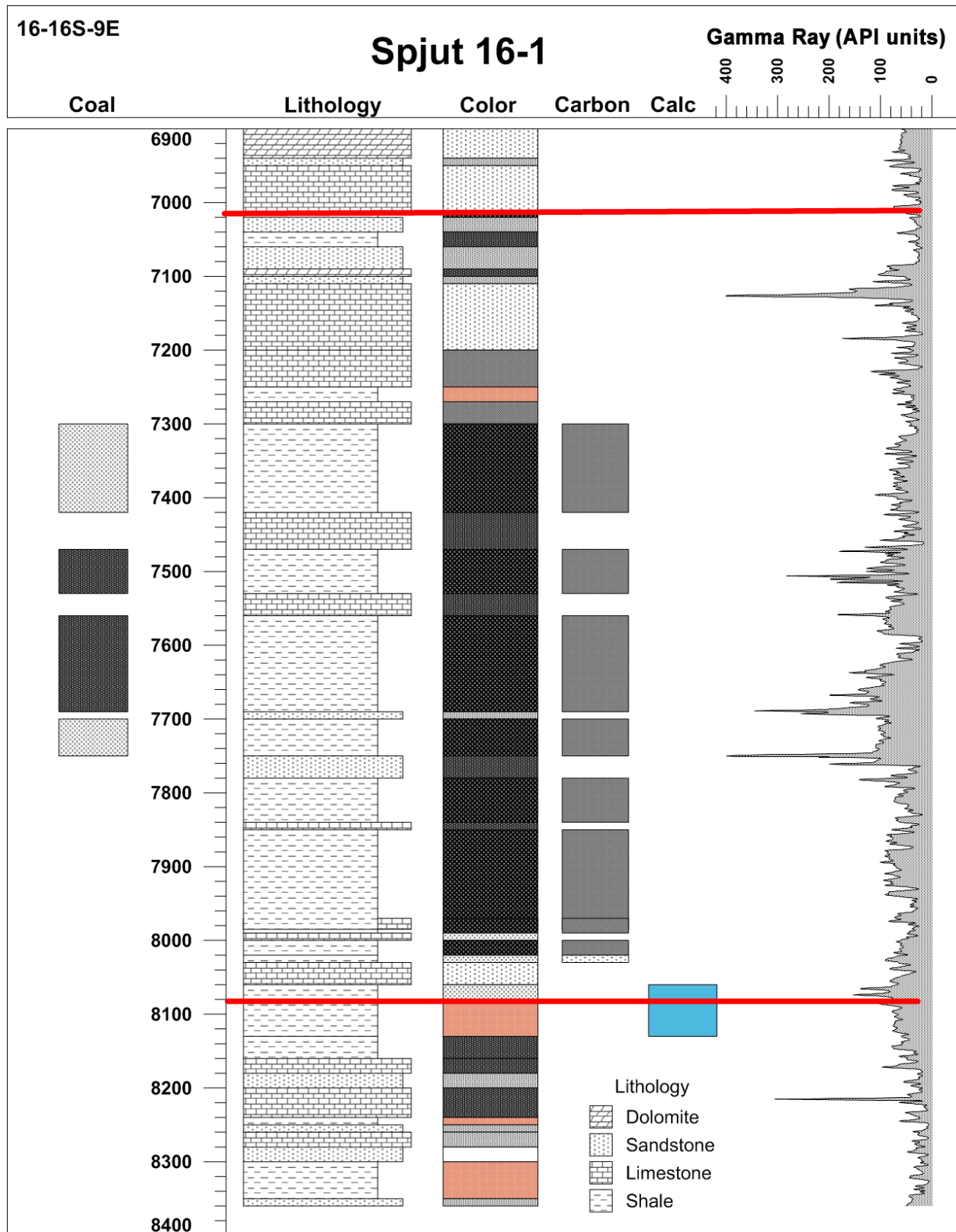


Figure 5.2. Lithology log for Spjut 16-1 well. See figure 3.1 for well location. The log is constructed from the well report as described from cuttings. Intervals described as carbonaceous (Carbon), calcareous (Calc), and coal-bearing are shown. Coal is indicated as abundant to sparse by gray shade intensity. The horizontal red lines show the operator picks for top and bottom of the Doughnut Formation.



Figure 5.3. Doughnut Formation lithologies in well cuttings.

tified as argillaceous, extend outside of the carbonaceous intervals. In some wells, the maroon-colored mudstone is within the formation, but in others it is outside. Chert fragments are outside of the formation in the Miller Creek 1 and Washboard Wash 1-A wells, but within the designated Doughnut in the North Springs Federal 1 well (appendix I, plate I-1).

The geophysical log response appears to be a more effective tool for consistently setting the limits of the Doughnut Formation. Consistently, in well after well, this shale-rich formation stands out in wireline log suites. The characteristic log response is higher background gamma ray (GR) with numerous GR spikes, a higher than normal interval transit time (lower seismic velocity), density and neutron log response indicative of high shale content, and major and pervasive borehole washout evidenced in expanded caliper log width. Logs for a 4500-foot (1370 m) section of the Desert Lake Unit 1 well have the characteristic features of the Doughnut interval (figure 5.4). The formation top and bottom picks on the figure are those reported in the 1961 well completion report. This well has a detailed cuttings sample log, so it is reasonable that the stratigraphic tops are based on observed lithologies, and not on the log response alone. The 100-foot (30 m) interval between the Humbug Formation and Doughnut described in the well report as “regolith” contains reddish mudstone and shale. It could be a true soil zone or regolith developed on the Humbug, or the transitional section observed in many wells (appendix I, plate I-1) containing maroon-colored mudstone. The log response is characteristic of the overlying Doughnut. This well is near the southern

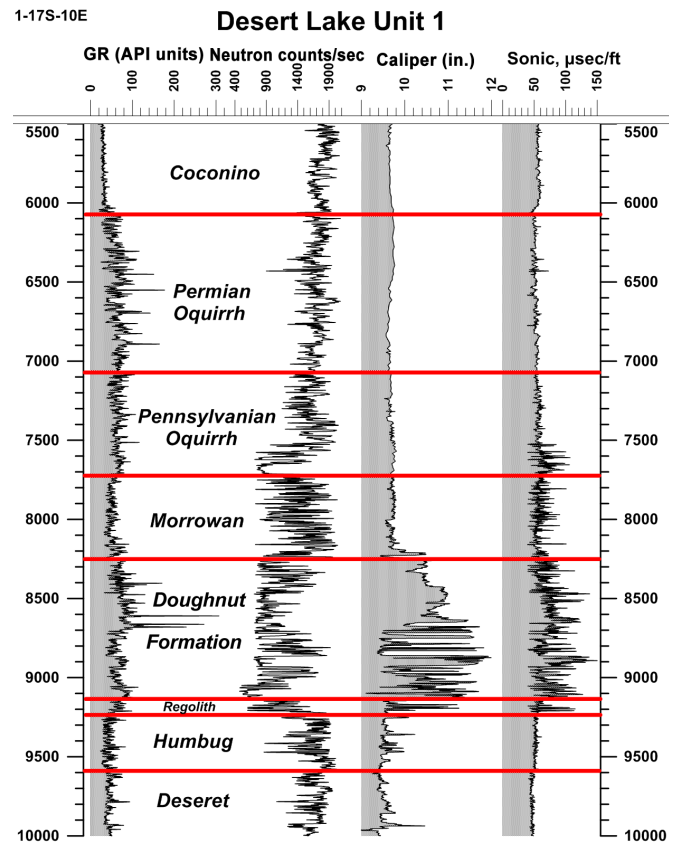


Figure 5.4. Geophysical logs for the Desert Lake Unit 1 well. See figure 3.1 for well location.

limit of the formation in the northern San Rafael Swell area (figure 2.9).

The well with the most complete log suite is Spjut State 1-16, completed in April 1982 (figure 5.5). The log characteristics for the Doughnut section are similar to those observed in other wells. Borehole washout is observed through most of the section and is extreme over broad intervals, up to 22 inches (56 cm) in the 10.5-inch (26.7 cm) borehole. The washouts may be a reliable indicator of the dominantly shale-rich intervals. Conversely, the intact sections reasonably indicate the mechanically stable limestone and siltstone-sandstone intervals. The 18-foot (5.5 m) siltstone core described in this report is from near the top of the formation (10,263 to 10,291 feet [3128–3137 m]) in an interval with relatively high density, background values of GR and interval transit time, and no appreciable washout. Therefore, the caliper logs can aid in identifying possible lithology and, thus, are a useful tool in well-to-well stratigraphic correlations.

The washouts clearly have had some effect on the values of the sonic and density logs, but in directions that enhance the already strong shale response. Both sets of tools are sensitive to washouts (Asquith and Krygowski, 2004; Ellis and Singer, 2008). In a washed-out borehole, the neutron porosity increases just 1% for each inch of added well radius (Rider, 1996).

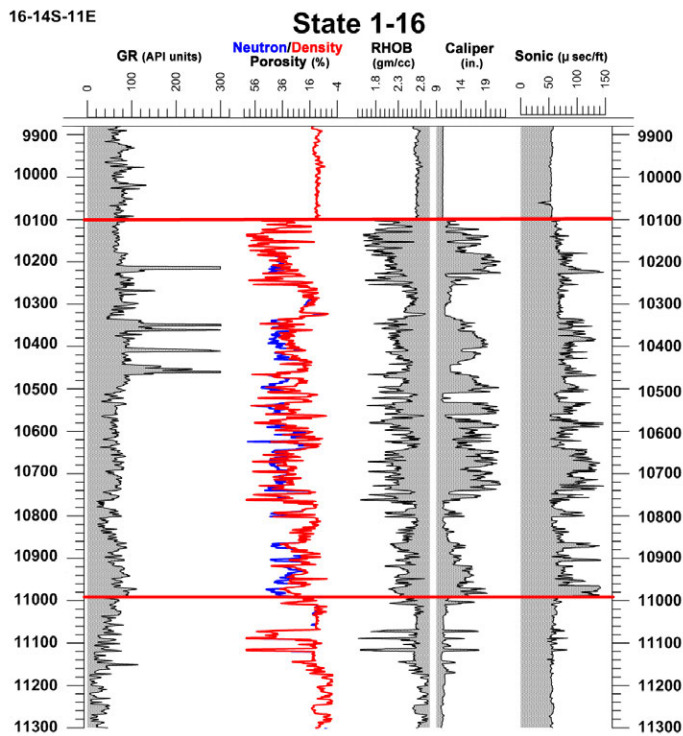


Figure 5.5. Geophysical logs for the State 1-16 well. Red lines = top and bottom Doughnut picks. See figure 3.1 for well location.

The density log (RHOB) values less than 2.0 and density/neutron porosity greater than 30% must be indicative of fractured shale. Through most of the section neutron porosity (NPHI) tracks density porosity (DPHI). However, in a few short intervals neutron porosity is slightly higher. When clays are part of the formation matrix, neutron porosity is greater than the actual formation porosity due to the hydrogen in the clay structure and in “bound water” (Ellis and Singer, 2008). Gas saturation would have the opposite shift, resulting in logs in which density porosity is too high and neutron porosity is too low. Note that in the Spjut State 1-16 well the GR spikes are clustered in the upper part of the Doughnut Formation.

Within the group of geophysical log suites available, only GR and caliper logs were common enough and of suitable quality and depth range to attempt a well-to-well correlation. The four best log pairs, and GR only for the two most recent wells (figure 5.6), show the difficulty in identifying stratigraphic intervals in the Doughnut Formation that can be tied across the northern San Rafael Swell area. Caliper logs have not been publicly released for the Carbon Canal 5-12 and State 15-32-15-12 wells. The wells shown on figure 5.6 are just 10 miles (16 km) or less apart, and each has distinctive Doughnut log signatures. Yet neither the intervals of washouts nor GR patterns are similar from well to adjacent well. This suggests the lack of stratigraphic correlations within the Doughnut, at least in this area with the available well log control.

The two easternmost wells, Sunnyside Unit 1 and Forest Govt 25-1, stand apart from all others in their lack of thick intervals of black shale and a distinctive Doughnut Formation wireline log character. Yet, both have operator-identified Doughnut intervals and lithologies in cuttings that are associated with the formation. In Sunnyside Unit 1, between 7480 and 7880 feet (2280 and 2402 m), the cuttings are red and brown siltstone identical to the “maroon” siltstone observed in limited intervals in most of the other wells, and light- to medium-gray fine- to coarse-grained sandstone. Also observed in cuttings and described in the driller’s report are small fragments of dark gray to black, fissile shale. Some fragments are clearly carbonaceous. In the reported Doughnut interval in the Forest Govt 25-1 well between 11,342 and 11,618 feet (3457 and 3541 m) similar siltstone and sandstone fragments are observed, but more common is medium to dark gray limestone. In the interval from 11,500 to 11,540 feet (3505–3517 m), the cuttings are dominantly dark gray to black, fissile and carbonaceous shale together with smaller amounts of the other lithologies. Neither well has a characteristic shale GR log response, but the caliper log for the Forest Govt 25-1 well has several washout intervals that are more than 5 inches (13 cm) greater than the well bore. From the geographic position of these wells (figure 3.3), we could be seeing a basin-margin facies in the Doughnut.

Carbon Canal 5-12 Core

The reported top and bottom of the Doughnut Formation in the Carbon Canal 5-12 well are at depths of 8573 and 9548 feet (2613 and 2910 m), respectively (Grover, 2008). Just the middle 544.4 feet (165.9 m) of this total 975-foot (297 m) interval was cored. Of the cored interval, the net thickness of rock available for examination is 422.1 feet (128.6 m). The core (figure 5.7, appendix D, plates D-2 to D-9), appendix E, and appendix I, plate I-2) has many gaps representing 1-foot (0.3 m) lengths taken for gas desorption measurements, companion gas desorption samples generally shorter than 1 foot (0.3 m) that are sealed in gas-impermeable Mylar pouches, and even shorter samples (many marked GRI) removed for analysis.

All of the lithologies represented in the cored interval are available for observation in the core boxes. However, the samples removed for analysis or preserved in sealed pouches are disproportionately the more organic-rich lithologies or they are thin beds that are highly unique.

After examining the core it became clear that the upper 101.4 feet (30.9 m) lacked the carbonaceous black shale and limestone that characterize the Doughnut Formation. This interval has been assigned to the lowermost Oquirrh Group (Bridal Veil Limestone) or the lower Round Valley Limestone (figure 5.7). The upper 16.5 feet (5.03 m) of the underlying Doughnut was sampled for gas desorption measurements. Below this gap in the core, carbonaceous rocks dominate the section.

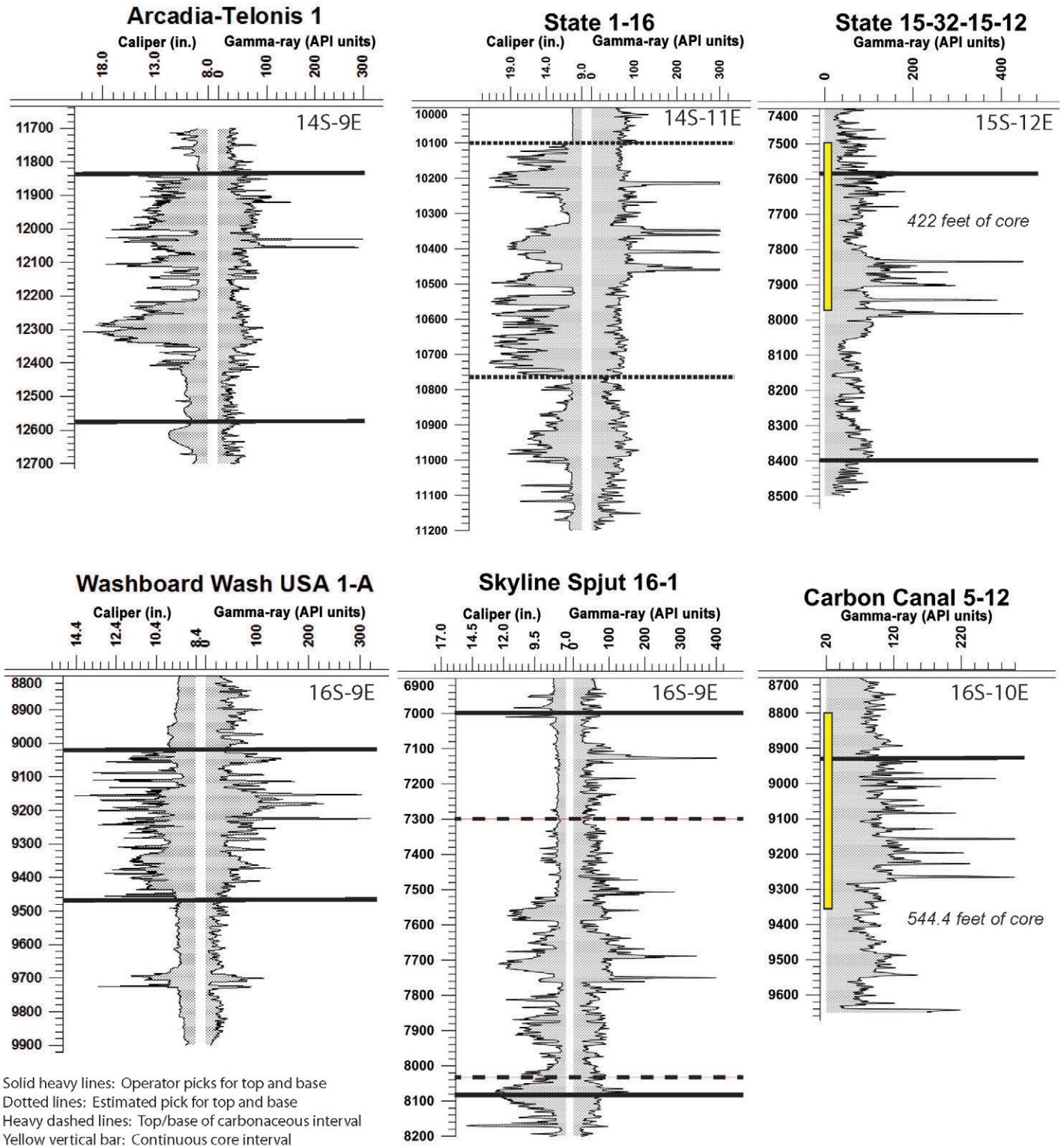


Figure 5.6. Doughnut Formation comparative caliper and gamma-ray log profiles.

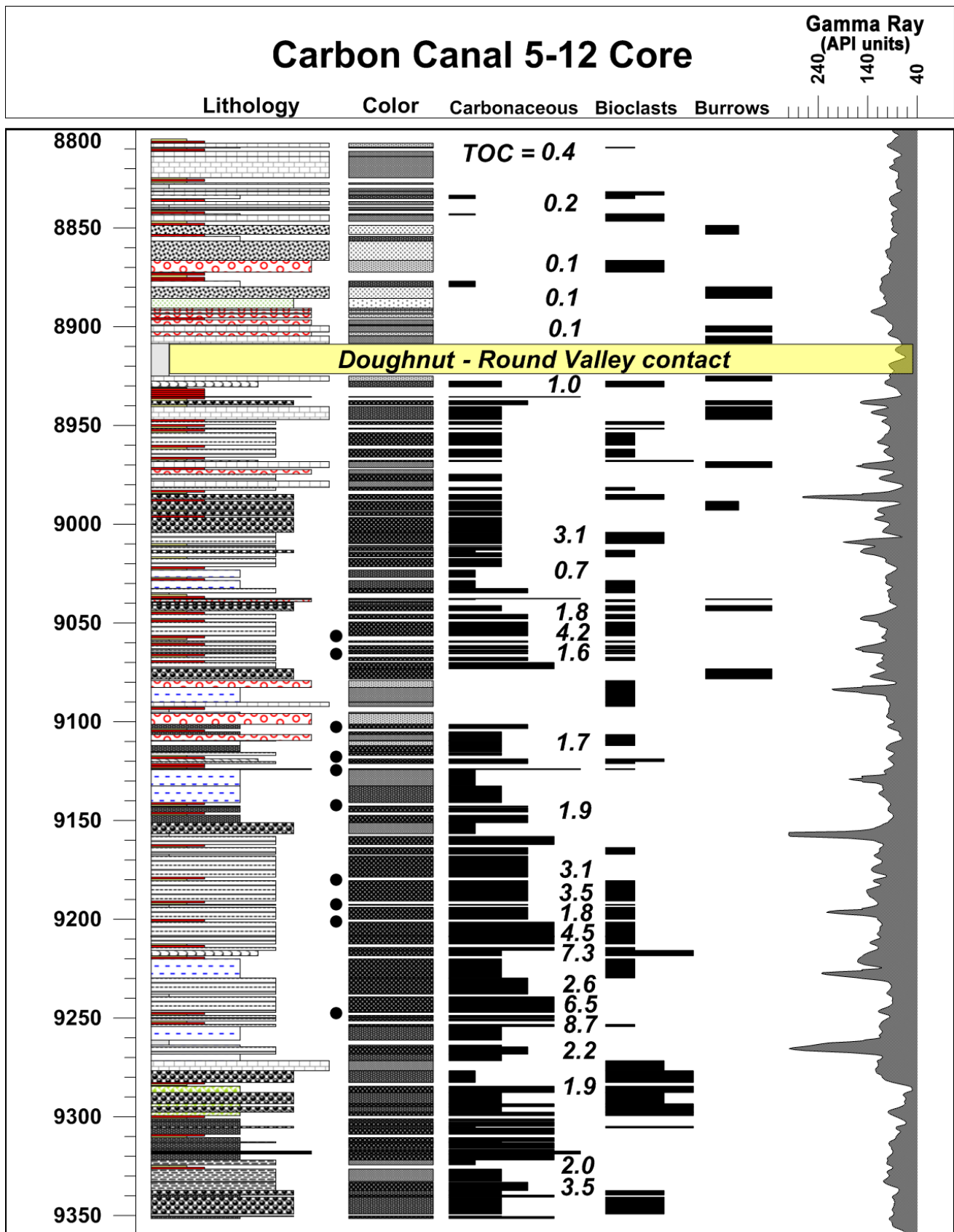


Figure 5.7. Lithology log for the Carbon Canal 5-12 core. Short red bars = gas desorption test; short yellow bars = sample removed. Locations of the inflated sealed pouches are indicated as black dots. See figures 3.1 and 4.1 for well location; also refer to figure 5.8 for key lithology log symbols.

Core to wireline log correlation by Grover (2008) indicates that the core is shifted downward with respect to the logs. Above the proposed top of the Doughnut Formation, the downward shift is 8 feet (2.4 m). That is, the top of the unit in the core at 8910 feet (2716 m) depth is equivalent to a depth of 8902 feet (2713 m) in the wireline logs. Below 8925 feet (2720 m) in the core the shift is 10 feet (3 m), and below 9095 feet (2772 m) in the core the shift is 12 feet (3.7 m). The key markers used by Grover (2008) may be core segments that were removed for testing and analysis. Initially, the reported shift could not be confirmed, so the displays in this report do not have a depth shift.

Lithologies

The lithologies observed in the core are described by lithotype, color, the relative abundance of organic matter and skeletal debris (shell fragments), and the relative intensity of burrowing (figure 5.7). In the entire core, 10 lithotypes are distinguished, all but one of which (no. 3 – sandstone) are found in the Doughnut interval. The lithotypes are displayed in the “Lithology” log on figure 5.7 and in appendix I, plate I-2; refer to figure 5.8 for the keys to lithotype and rock color. The lithotypes are illustrated and described with photos on figure 5.9 and in appendix I, plate I-3; thin-section photomicrographs are displayed and described on plate I-4.

The Doughnut Formation lithologies fall into two groups, those that are carbonaceous and those that are not. The lithotypes can be simplified as follows:

- 1 Limestone, micritic – limy mudstone (figure 5.9) that is dark gray to medium dark gray (N3-N4), but has little or no organic carbon. The rock can be irregularly bedded, or structureless.
- 1A Limestone, carbonaceous micritic – poorly bedded, dark gray (N3) to grayish black (N2), organic-rich, limy mudstone (figure 5.9). Distin-

- 2 Limestone, nodular – irregularly bedded to nodular limy mudstone (figure 5.9) commonly containing skeletal debris, but has little or no organic carbon.
- 4 Siltstone – characterized by thin-laminated alternations of medium gray (N5) siltstone and dark gray (N3) carbonaceous shale (figure 5.9). The silt layers are a mix of angular quartz and microbioclast grains (figure 5.1C).
- 5 Mudstone – poorly bedded or structureless, non fossiliferous, calcareous to slightly calcareous, has little or no organic carbon, medium light gray (N6) (figure 5.9).
- 6 and 7 Shale, carbonaceous laminar – thin-laminated calcareous shale to weakly laminated argillaceous wackestone and microbioclast packstone (figure 5.9). These lithotypes contain an abundance of disseminated, fine-grained to coarse coaly plant fragments. The color is variably grayish black (N2) to dark gray (N3), but organic matter-poor laminae are lighter colored

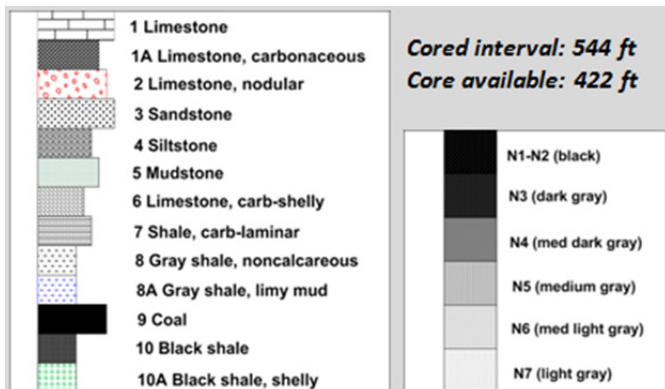


Figure 5.8. Key to the lithology and color panels in the Carbon Canal 5-12 lithology log (see figure 5.7 and appendix I, plate 2).

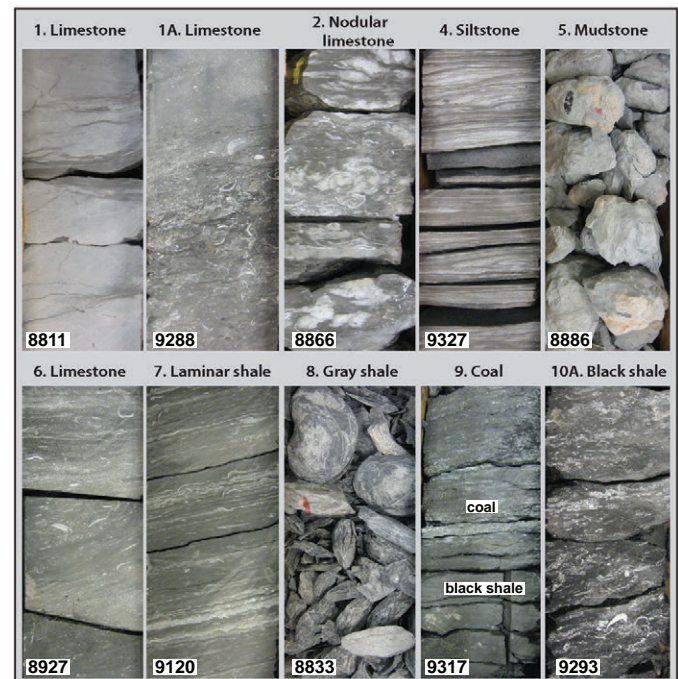


Figure 5.9. Photographs of the principal Doughnut Formation lithotypes described in the Carbon Canal 5-12 core.

(N4-N5). The laminated shale may enclose thin-shelled pelecypod or brachiopod fragments strongly aligned with bedding. The weakly laminated limestone variant is normally rich in thin- and thick-shell whole and fragmental skeletal material.

8 and 8A Gray shale – structureless to weakly laminated, carbonaceous shale that is grayish black to dark gray (N2-N3) in color. The rock is a “paper shale” where very organic rich (lithotype 8A), but breaks into convex chips (figure 5.9, lithotype 8) when less so. The rock is weakly to non-calcareous and normally free of skeletal debris.

9 Coal – faintly bedded on millimeter scale, or unbedded and structureless. Fracture surfaces are conchoidal and highly luminous. One of the four coal beds contains a 0.3-inch-thick (0.8 cm) bed of microfossils and thin-shelled brachiopod fragments in a black shale matrix. The deepest coal bed (9317.3 to 9318.3 feet [2839.8–2840.1 m]; figure 5.9) contains thin laminae rich in clay and pyrite.

10 and 10A Black shale – laminar, carbonaceous, grayish black to black (N2-N1) shale, normally rich in thick- and thin-walled shell fragments. Lithotypes 10 and 10A (figure 5.9) are shell-free and shell-rich, respectively. The shale is commonly silty (figure 5.1B) and may interfinger with siltstone.

Figure 5.10 is a pie chart showing the relative proportions of each of the lithologies in the core. Each wedge represents the percentage of net feet of the lithology in the core relative to the 422 feet (129 m) of core available for the study.

In the Carbon Canal 5-12 core the various lithologies tend to group themselves in distinct intervals, as can be seen on figure 5.11. The interval from the base of the core to core depth 9284.5 feet (2829.8 m) is mainly black shale with interbeds of siltstone and carbonaceous micritic limestone. This is overlain by a section (9151.1 to 9284.5 feet [2789.1–2829.8 m]) that is dominantly carbonaceous laminar shale and limestone with minor interbeds of carbonaceous micritic limestone and carbonaceous gray shale. From core depth 9101.3 to 9151.1 feet (2773.9–2789.1 m), black shale with associated carbonaceous gray shale dominates the section. The interval from core depth 9101.3 feet (2773.9 m) to the top of the Doughnut Formation is dominantly carbonaceous laminar shale and limestone with minor carbonaceous gray shale. The non-carbonaceous micritic and nodular limestone lithotypes are observed only in this upper interval of the formation. This also is the exclusive interval having prominent burrows.

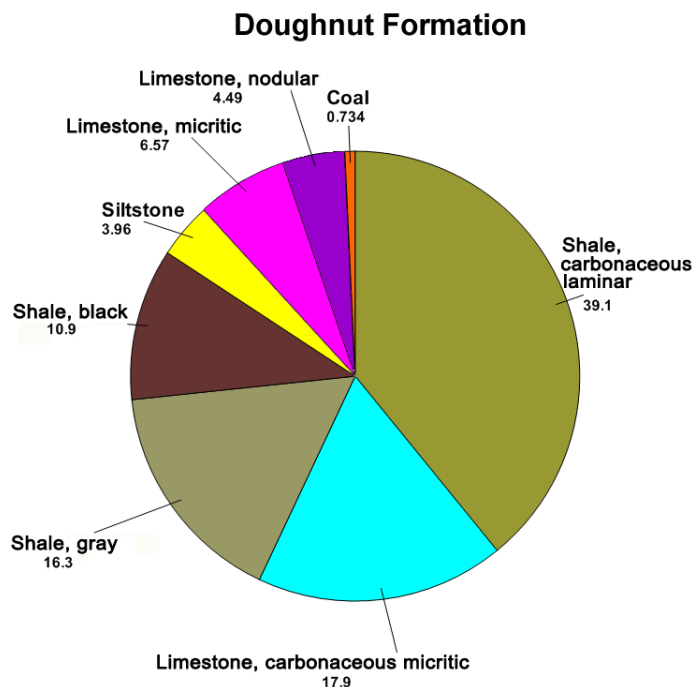


Figure 5.10. The relative occurrence of lithologies in the Carbon Canal 5-12 core as a percentage of net feet of the lithology.

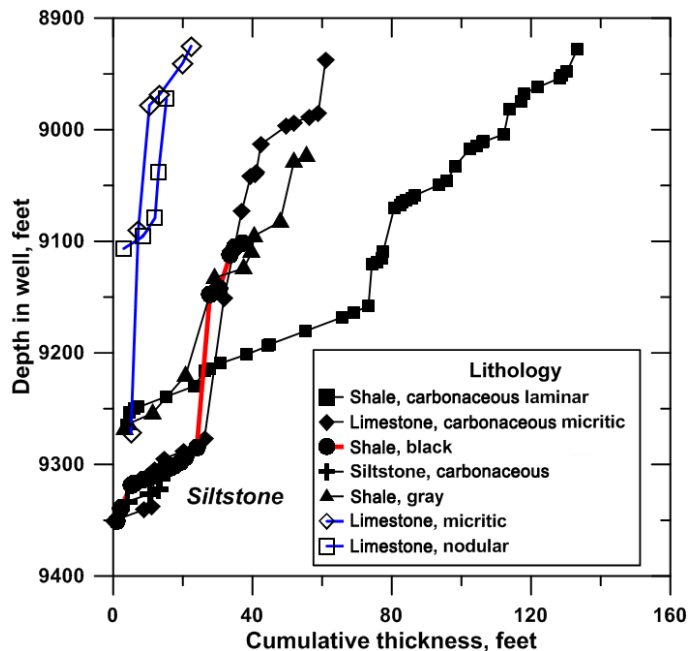


Figure 5.11. Vertical distribution of lithologies in the Carbon Canal 5-12 core expressed as cumulative thickness versus core depth.

Mineral Composition

The inorganic mineral composition for 48 whole-rock samples from the Carbon Canal 5-12 core was determined by Core Laboratories (Grover, 2008) using XRD analysis. Thirty-five of the samples are from the Doughnut Formation part of the core and 13 samples are from the part assigned to the Round Valley Limestone. The mineral compositions are tab-

ulated in appendix H, summarized in table 5.3, and displayed as both total minerals and as the relative percent of just the clay species on figure 5.12 and plate I-2 of appendix I. The samples selected for analysis are distributed throughout the core with an average spacing of 12.1 ± 9.5 feet (3.7 ± 2.9 m). The sampled lithologies have approximately the same relative proportions as their occurrence in the core (figure 5.10). The carbonaceous laminar shale and limestone, 39% of the core, constitute just over half of the XRD samples. The carbonaceous micritic limestone, 18% of the core, constitutes 17% of the XRD samples. The remaining XRD samples are distributed through most of the remaining core lithologies.

Table 5.3. Summary of the mineralogy of the Doughnut Formation and the Round Valley Limestone as determined by x-ray diffraction (XRD) analysis of rock samples from the Carbon Canal 5-12 core. Thirty-five samples from the Doughnut interval and 13 from the overlying Round Valley were run. The table shows the average and standard deviation of the percent of each mineral phase recognized by XRD, as well as the median, maximum and minimum percentages of the minerals, and the number of samples in which the mineral was detected. A total clay value is shown, as well as the breakdown by clay species.

Mineral	Average	StDev	Median	Max	Min	No.
Doughnut Formation						
Quartz	25.4	8.7	25.0	45.0	8.0	35
K-spar	0.3	0.6	0.0	2.0	0.0	7
Plagioclase	3.4	2.4	3.0	9.0	0.0	33
Calcite	31.3	20.6	29.0	81.0	1.0	35
Dolomite	10.3	14.2	6.0	60.0	0.0	34
Apatite	0.4	1.6	0.0	9.0	0.0	5
Siderite	1.9	7.9	0.0	40.0	0.0	3
Pyrite	4.4	3.3	4.0	14.0	0.0	32
Total carbonate	43.5	19.8	39.0	81.0	11.0	35
Clay total	23.3	12.0	24.0	50.0	3.0	35
Illite/Smectite	51.0	12.6	55.0	70.0	0.0	34
Illite	19.7	8.8	18.0	63.0	8.0	35
Kaolinite	15.1	7.1	15.0	31.0	0.0	33
Chlorite	14.3	9.1	11.0	37.0	4.0	35
Round Valley Limestone						
Quartz	28.9	22.6	22.0	84.0	2.0	13
K-spar	0.5	0.5	0.0	1.0	0.0	6
Plagioclase	1.7	1.5	2.0	5.0	0.0	9
Calcite	49.5	26.5	50.0	94.0	2.0	13
Dolomite	8.2	14.2	2.0	42.0	0.0	9
Apatite	0.0	0.0	0.0	0.0	0.0	0
Siderite	0.0	0.0	0.0	0.0	0.0	0
Pyrite	0.4	0.8	0.0	2.0	0.0	3
Total carbonate	57.7	25.6	63.0	94.0	2.0	13
Clay total	11.2	7.6	10.0	31.0	4.0	13
Illite/Smectite	45.6	13.9	51.0	62.0	12.0	13
Illite	29.4	13.1	31.0	48.0	5.0	13
Kaolinite	5.8	9.3	0.0	29.0	0.0	5
Chlorite	19.5	12.6	18.0	55.0	0.0	12

Figure 5.12 shows the relative proportion of all mineral phases when arranged in two groups: (1) the terrigenous minerals and those formed by diagenesis or anchimetamorphism of terrigenous components (iron oxides and clays) on the left-hand side of the “Mineral%” panel and (2) the carbonates formed by biogenic processes within the basin on the right-hand side. The distinction is between those components (silicates and iron oxide) transported into the basin and those generated within the basin. Due to the removal of core material at the critical boundary, the top of the Doughnut Formation falls within the interval indicated by the gray box. The overlying unit is either Round Valley Limestone, or possibly the Oquirrh Group.

The Doughnut Formation has three main mineral constituents: quartz (average $25.4 \pm 8.7\%$), clays ($23.3 \pm 12.0\%$), and calcite ($31.3 \pm 20.6\%$). Except in limited portions of the core, other carbonate minerals are relatively sparse or absent: dolomite and ferroan dolomite (average $10.3 \pm 14.2\%$) and siderite ($1.9 \pm 7.9\%$). Total carbonate averages $43.5 \pm 19.8\%$.

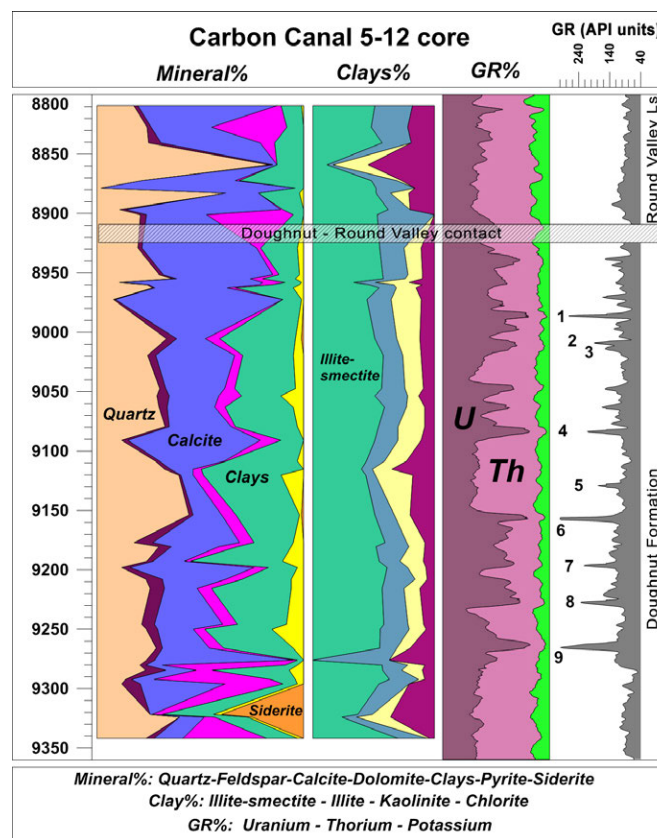


Figure 5.12. Mineral composition and spectral gamma-ray logs for the Carbon Canal 5-12 core interval. The mineral composition determined for 43 rock samples by XRD analysis was performed by Core Laboratories and reported in Grover (2008). The spectral log is displayed as percentage of element expressed as API units. The width of each of the three percentage logs in color is 100%. The data for the numbered gamma-ray spikes is shown in table 5.5. The top of the Doughnut Formation falls within the light gray striped bar (core material was removed from this interval).

Below core depth 8280 feet (2524 m), dolomite or siderite are the dominant carbonate species, constituting a full quarter to more than half of the rock (refer to appendix H).

The overlying Round Valley Limestone is even richer in total carbonate ($57.7 \pm 25.6\%$). Calcite averages $49.5 \pm 26.5\%$ and dolomite averages $8.2 \pm 14.2\%$. Quartz content is similar to the Doughnut by both average and median values (table 5.3), but the values are somewhat distorted by the presence of two sandstone samples. Clay content is considerably lower, averaging $11.2 \pm 7.6\%$.

All of the core samples are admixtures of quartz, carbonates, and clay, as shown on a ternary plot of these three end members (figure 5.13). On this plot the Doughnut Formation samples form a continuum between silty calcareous shale and silty argillaceous limestone. The Round Valley Limestone samples, except for the two sandstones, cluster with the silty argillaceous limestone. With respect to the three carbonate species (figure 5.14), the rocks cluster near the carbonate end-members in silty sideritic shale, dolowackestone, and the considerably more common argillaceous limestone and calcareous shale. The dolomite- and siderite-rich rocks are segregated into limited intervals of the core as shown by sample core depths on figure 5.14 (refer also to figure 5.12).

The XRD analyses show four clay species (figure 5.12; table 5.3). Their average relative proportions in the Doughnut Formation are: illite-smectite ($51.0 \pm 12.6\%$), illite ($19.7 \pm 8.8\%$), kaolinite ($15.1 \pm 7.1\%$), and chlorite ($14.3 \pm 9.1\%$). Core Laboratories reports that the illite-smectite contains 15 to 25% smectite layers (Grover, 2008). Unusually high val-

ues of chlorite and kaolinite are associated with the siderite-rich black shales between core depths 9321.7 and 9324.0 feet (2841 and 2842 m). There are other chlorite-rich spikes in the section (figure 5.12) that could relate to the presence of iron enrichment in these intervals. Except for the absence of kaolinite in all but five of the 13 samples and higher relative abundance of chlorite ($19.5 \pm 12.6\%$), the clay suite in the Round Valley Limestone is similar to that of the underlying rocks (figure 5.12).

Pyrite is a common component in the Doughnut Formation (average $4.4 \pm 3.3\%$), but it is nearly absent in the Round Valley Limestone. The interval from core depth 9053.5 to 9266 feet (2759–2824 m) is particularly rich in pyrite, with values exceeding 10%. This coincides with the particularly organic carbon-rich part of the core. Pyrite is virtually absent in the siderite-rich part of the core (figure 5.12). The siderite forms distinct nodules observed in core, but may be a component in the rock matrix as well. In addition to the siderite-rich samples at 9321.7 feet and 9324.0 feet (2841 m and 2842 m), a trace of siderite is detected in samples at 9005.5 feet and 9153.8 feet (2745 m and 2790 m) (appendix H). Siderite is absent in Round Valley samples (appendix H). Siderite formation requires reducing conditions to mobilize Fe^{2+} and low sulfide concentrations (Berner, 1971, 1981). It is common in anoxic freshwater lake, swamp, and marsh deposits (Stonicepher, 1999). Where sulfide concentrations are higher, such as in marine settings, the Fe^{2+} precipitates as pyrite or other iron sulfate phases (Berner, 1971).

Three mineral phases occur as porphyroblasts and may be anchimetamorphic in origin. A white mica is present in some organic-rich laminae as round to elliptical flakes up to 1.0 mm in

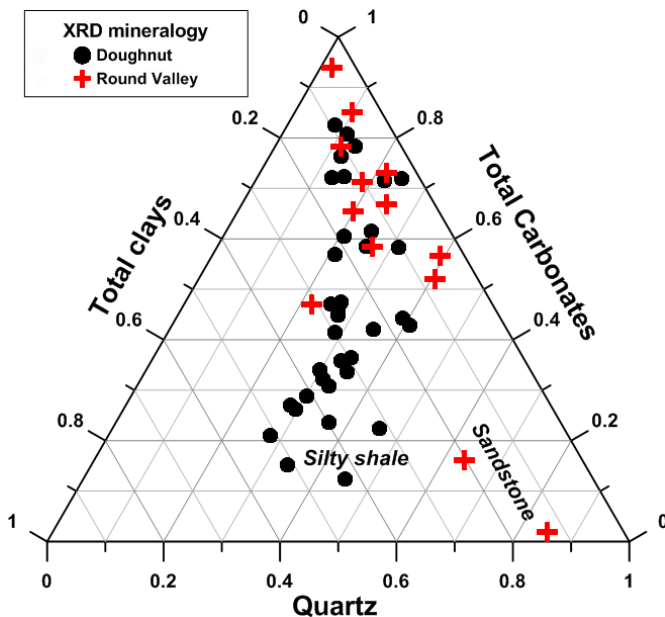


Figure 5.13. Ternary plot of the major mineral compositions of the Doughnut Formation and the overlying Round Valley Limestone from XRD analyses shown on figure 5.12.

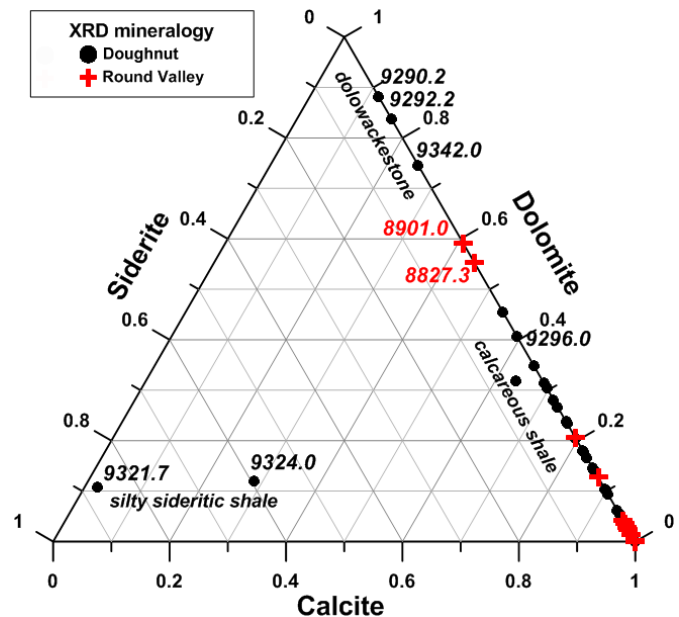


Figure 5.14. Ternary plot of the carbonate mineral compositions of the Doughnut Formation and the overlying Round Valley Limestone (core depths [feet] indicated) from XRD analyses shown on figure 5.12.

diameter. They are very thin and nearly always have an interface with organic matter. They are much too fragile and well formed to be detrital mica. Very commonly thick shell clasts are rimmed by euhedral tabular crystals that replace the shell material (figure 5.1E) and grow perpendicular to the shell edge. Grover (2008) identified these as quartz overgrowths, yet they have a tabular habit, lacking pyramidal truncations characteristic of quartz, and in thick thin sections where quartz has first-order birefringence colors, these overgrowths are gray to white. In this study the overgrowths are identified as plagioclase, probably calcium-rich, a mineral that averages $3.4\% \pm 2.4\%$ and has a maximum of 9.0% in XRD analyses (table 5.3; appendix H). Also, many of the rocks contain white rhombs of dolomite up to 0.5 mm in size which are euhedral overgrowths in the lime mud and bioclast matrix.

Apatite is detected in five of the Doughnut Formation XRD samples; in each instance the sample coincides with phosphatic intervals observed in core and in thin section. Phosphatic material is common throughout the Doughnut. In places through the core, distinct phosphate-rich rocks are observed (figure 5.15). These zones are recognized by the presence of pellet-like components that in thin section are brown-red to amber, spherical grains of polycrystalline apatite. These in-

tervals are frequently rich in skeletal debris and in pyrite as separate grains or replacing skeletal fragments (figure 5.15). These intervals are provisionally identified as condensed intervals, “abrasion flats,” or “hardgrounds.” Phosphate-rich rocks commonly are associated with coastal upwelling events (Sheldon, 1964; Parrish, 1982), but in the Doughnut, these intervals could be merely sediment-poor flooding surfaces or condensed zones. The XRD sample intervals with apatite are 9177 to 9180.5 feet (2797–2798.1 m) (figure 5.15B) and 9249.5 to 9250.0 feet (2819.1–2819.3 m) (figure 5.15D). Where observed in core and thin sections, the phosphate-rich zones are considerably thicker and more widely distributed than the intervals with XRD analyses.

Chemical Composition of Shale

The origin of the terrigenous components of the sediments should be reflected in the elemental composition of the least carbonate-rich shale and mudstone (Potter and others, 2005). If, as proposed earlier, the non-carbonate fractions are derived from erosion of lateritic soils developed on the broad karst plains in central and southern Utah, the shale should be rich in quartz and oxides of titanium, iron, aluminum, and manganese, elements enriched by intense chemical weathering.

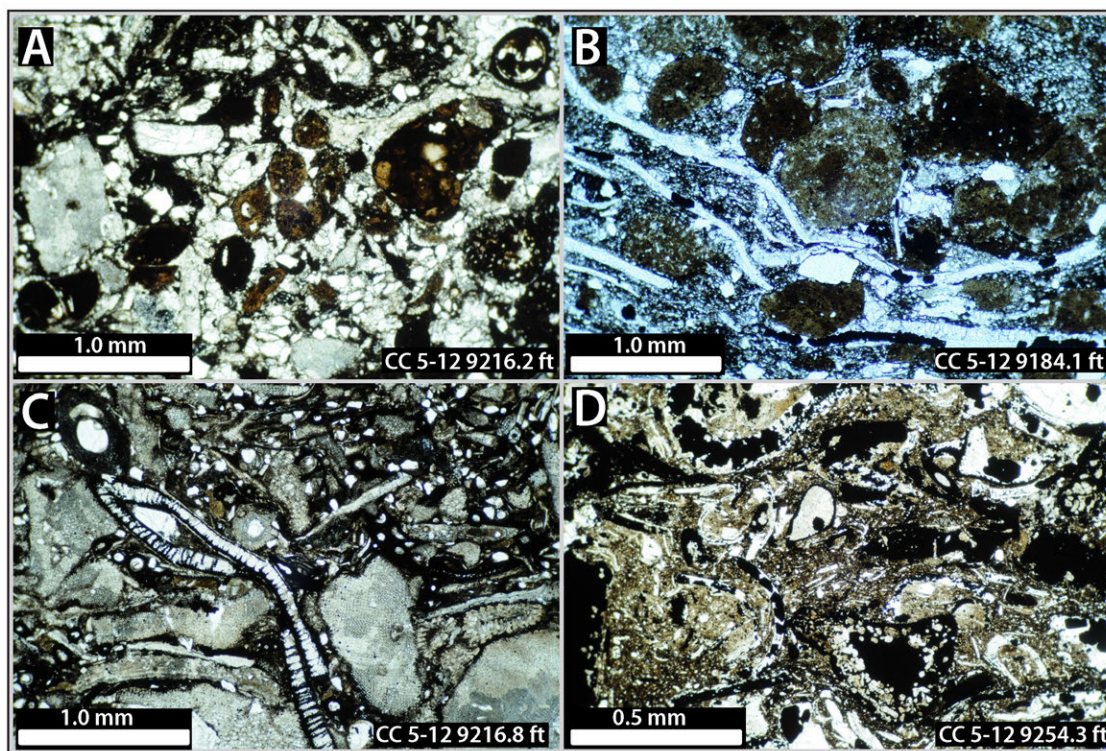


Figure 5.15. Photomicrographs of rocks associated with possible condensed intervals or hardgrounds within the Carbon Canal 5-12 core. **A.** Spherical reddish-brown phosphate grains within a partially recrystallized packstone matrix. Highly abraded clasts of shells debris and crinoid fragments. Many white euhedral grains of dolomite. **B.** Spherical grains or pellets of greenish glauconite (?) and reddish brown phosphate with thin-walled shell fragments in a fine-grained, partially recrystallized grainstone. **C.** Skeletal wackestone with partially recrystallized, highly abraded crinoid and shell fragments, small reddish-brown grains of phosphate, and subhedral dolomite grains. Pyrite replaces many of the shell fragments and is widely disseminated in the rock matrix. **D.** Skeletal wackestone rich in pyrite and reddish-brown phosphate grains. Euhedral pyrite is replacing many of the large shell fragments.

Likewise, they would be relatively low in the soluble alkali elements. The Chemical Index of Alteration (CIA) uses the molar values of aluminum to alkalis as a measure of the degree of chemical weathering (Nesbitt and Young, 1982; Potter and others, 2005; Bahlburg and Dobrzinski, 2009; Goldberg and Humayun, 2010; Li and Yang, 2010). See the footnote in table 5.4 for the equation used to calculate CIA. Average shale has CIA values of 70 to 75, shale resulting from glacial abrasion and little to no chemical weathering has CIA values of 50 to 70, and shale resulting from tropical weathering (laterite) has CIA values in the range 80 to 100.

Table 5.4 shows the elemental composition of 10 shale or mudstone beds from the Carbon Canal 5-12 core and three argillaceous siltstones from the State 1-16 core fragments determined at the UGS using XRF analysis. Table 5.4 also shows elemental compositions of a variety of standard composite or “averaged” shale beds compiled by Gromet and others (1984).

Silica compositions are relatively wide ranging due to the variable admixture of silt- and clay-size quartz detritus in the

shale and mudstone beds. Inexplicably, alumina also is compositionally variable, ranging from a high of 23 weight percent (wt%) to a very low 3.4 wt%. On the whole, the Doughnut shale beds are slightly lower in alumina than the composite shale. Titanium and phosphorous are greatly enriched and iron and manganese are slightly enriched relative to the composite shale. The alkalis, sodium and potassium, are depleted compared to normal shale. An average Doughnut Formation CIA (molar) of 78.7 approaches the range of values typical of laterite, and individual samples are well within the laterite range. Overall, the Doughnut shale compositions suggest a temperate to subtropical setting for the origin of the terrigenous sediments. However, this assumes that the terrigenous components are first-cycle, derived from weathering of crystalline rocks. Stratigraphic evidence from the Molas Formation and underlying karst suggests a more complex origin for the terrigenous sediments, whereby they are partly derived from primary soils and partly a residuum from dissolution of the Leadville Limestone and other carbonate rocks (Power, 1969; Evans and Reed, 2007).

Table 5.4. Whole rock chemical compositions (in oxide weight percent) of shale, claystone, or mudstone samples from the Carbon Canal 5-12 (CC) and State 1-16 (St 1-16) cores as determined by x-ray fluorescence. The samples are: (1) gray shale, (2) claystone, (3) mudstone, (4) gray shale, (5) claystone from beneath coal bed, (6) black shale, (7) through (9) gray shale, (10) black shale, (11) black siltstone, (12) black coaly shale, and (13) gray silty mudstone. The comparative reference composite or averaged shales are the North American Composite Shale (NACS) 1 and 2, Clark (1924) average shale composition, North American (NA) Paleozoic composite shale, North American Mesozoic/Cenozoic (NA Mesa/Ceno) composite shale, and Canadian composite shale.

Well_Sample Depth (ft)	Lithology	SiO ₂	TiO ₂	Al ₂ O ₃	Fe ₂ O ₃	MnO	MgO	CaO	Na ₂ O	K ₂ O	P ₂ O ₅	SO ₃	CIA (molar)†
CC_8877.5	1	46.90	1.60	11.10	8.18	0.06	2.01	26.40	0.40	2.73	0.32	0.10	75.5
CC_8879.0	2	69.70	2.21	21.10	2.43		1.02	0.39	0.78	1.74	0.06	0.17	87.0
CC_8889.4	3	72.50	1.54	13.80	3.94		1.46	0.58	0.72	4.15		1.05	70.9
CC_9028.6	4	44.50	1.28	11.20	7.23	0.09	1.53	29.70	0.69	1.29	0.13	2.01	81.6
CC_9119.3	5	65.00	1.65	16.90	8.20		1.03	0.43	1.54	2.33	0.03	2.65	77.0
CC_9121.2	6	59.10	1.21	14.60	14.70	0.12	1.46	1.21	1.08	2.74	0.22	3.23	75.5
CC_9125.5	7	71.60	2.09	18.40	3.90		0.60	0.49	0.85	0.68	0.03	1.09	89.6
CC_9130.0	8	60.70	2.19	19.50	7.40		1.19	4.61	0.81	2.65	0.45	0.14	82.3
CC_9134.0	9	59.70	2.15	23.00	7.47		1.33	1.16	0.87	3.49	0.35	0.09	81.5
CC_9258.0	10	64.50	2.07	21.40	5.79		1.58	0.69	1.32	1.35	0.05	0.87	85.5
St 1-16_10,268	11	69.90	1.24	12.10	9.31	0.07	0.87	1.30	0.41	2.86	0.49	1.25	76.3
St 1-16_10,270	12	57.00	2.87	21.40	7.45		0.87	1.18	0.65	5.27	0.49	2.15	76.0
St 1-16_10,295	13	83.30	0.36	3.41	5.20	0.09	0.92	4.43	0.65	0.71	0.46	0.38	65.1
Average		63.42	1.73	15.99	7.02	0.09	1.22	5.58	0.83	2.46	0.25	1.17	78.7
Max		83.30	2.87	23.00	14.70	0.12	2.01	29.70	1.54	5.27	0.49	3.23	89.6
Min		44.50	0.36	3.41	2.43	0.06	0.60	0.39	0.40	0.68	0.03	0.09	65.1
NACS 1		64.80	0.70	16.90	6.29	0.06	2.86	3.63	1.14	3.97	0.13		73.2
NACS 2		64.82	0.80	17.05	6.33	0.25	2.83	3.51	1.13	3.97	0.15		73.5
Clark, 1924		64.21	0.72	17.02	7.46	0.50	2.70	3.44	1.44	3.58	0.19		73.2
NA Paleozoic		59.75	0.98	17.79	6.21		4.02	6.10	0.72	4.82	0.12		73.5
NA Meso/Ceno		67.78	0.70	16.59	4.57		3.38	3.91	0.98	2.44	0.10		79.6
Canadian		66.90	0.78	16.67	6.52	0.06	2.59	0.53	1.50	4.97	0.14		68.0

† CIA (chemical index of alteration) is a unitless ratio of moles of Al to total moles of Al+Ca+Na+K based on the equation $CIA = [Al_2O_3 / (Al_2O_3 + CaO^* + Na_2O + K_2O)] \times 100$ (Nesbitt and Young, 1982).

Spectral Gamma Ray

There are three principal sources of natural radioactivity in rocks: potassium (^{40}K), thorium (^{232}Th), and uranium (^{238}U). The spectral GR tool measures the relative contribution of the three radioisotopes. From comparison with a known spectra, the chemical concentration of each element is determined quantitatively. Under ideal conditions and when the spectral tool is centered in the borehole, the vertical resolution is about 16 inches (40 cm). Thorium is relatively insoluble and is retained by the clay-size fraction produced by weathering of acidic to intermediate rocks. It is a widely and generally uniformly distributed component in sediments that can be used reliably as a “shale indicator.” Typical shale has an average value of 12.0 ppm (8 to 18 ppm) thorium contributing 40 to 50% to the total GR signal (Rider, 1996). In contrast to thorium, uranium is very soluble. It enters sediments from solution in seawater by adsorption on organic matter (“hot shale”) or by syngenetic chemical reaction in phosphorites, where it substitutes for calcium in carbonate-fluorapatite. Consequently, uranium is less uniformly distributed in sediments. It is commonly associated with condensed sequences, hardgrounds, and breaks in sedimentation. In shale, the uranium average is 4 ppm (2 to 6 ppm), resulting in about 30% contribution to the total GR observed (Rider, 1996). Potassium normally is carried in clays produced from rock weathering, particularly illite, or in detrital potash feldspar.

A spectral GR wireline log for the Doughnut Formation interval in the Carbon Canal 5-12 well was available for this study. The total GR curve and the relative contributions of uranium (U), thorium (Th), and potassium (K) to the total GR signal are shown on figure 5.12 and in appendix I, plate I-2. The relative contributions of each radioisotope are calculated from the following equivalents of Rider (1996): 1.0 ppm U = 8.09 API units, 1.0 ppm Th = 3.93 API units, and 1.0% K = 16.32 API units.

Through the full 646-foot-thick (197 m) Doughnut Formation (8902 to 9548 feet [2713–2910 m]) uranium and thorium contribute nearly equally to the average GR value, 36 and 34 API units (4.41 ppm and 8.60 ppm), respectively (table 5.5A). The average values for uranium and thorium in the overlying Round Valley Limestone (8800 to 8902 feet [2682–2713 m], table 5.5B) are less for both elements, 19 and 28 API units (2.37 and 7.11 ppm), respectively, reflecting the lower content of organic matter and clays (figures 5.7 and 5.12). However, the concentrations of uranium and thorium are variable through the cored portion of the Doughnut. In two intervals, 8010 to 9090 feet (2441–2770 m) and 9150 to 9280 feet (2789–2828 m), uranium is higher than the average value for the Doughnut (table 5.5B; figure 5.12). In part, this is the result of GR spikes being concentrated in these two intervals. In the 9150 to 9280 feet (2789–2828 m) interval, the background total GR values are higher due to higher than normal uranium and thorium. The variation in background GR and the relative contribution of uranium and

Table 5.5. Summary of spectral gamma-ray (GR) data for the Carbon Canal 5-12 well. A: Average spectral GR values for the entire Doughnut Formation. B: Average spectral GR values for specific intervals in the core. C: Spectral GR values at the principal GR spikes (refer to figure 5.12).

	Log Picks (ft)		Core (ft)	U (ppm)	Th (ppm)	K (%)
	From	To				
A:	8902.0	9548.0	8910.0	4.41	8.60	0.50
B:	8800.0	8901.5	8808.0	2.37	7.11	0.50
	8902.0	9089.5	8910.0	4.77	6.72	0.40
	9090.0	9149.5	9100.0	2.74	10.75	0.50
	9150.0	9279.5	9162.0	8.21	9.56	0.60
	9280.0	9548.0	9292.0	2.69	8.96	0.50
	Peak	Log Picks (ft)	Core (ft)	U (ppm)	Th (ppm)	K (%)
C:	1	8986	8976	29.96	14.37	0.70
	2	9009	8999	6.14	4.86	0.30
	3	9014	9004	10.74	11.72	0.50
	4	9084	9074	20.42	8.76	0.50
	5	9129	9117	3.08	13.15	0.40
	6	9157	9145	48.00	22.20	1.30
	7	9196	9184	17.30	14.65	0.90
	8	9226	9214	22.41	14.16	0.80
	9	9265	9253	30.12	13.73	1.00

thorium can be related to variations in Doughnut lithologies as follows:

8910 to 9100 feet (2757–2774 m): Interval of high uranium concentration and moderate thorium associated with a dominance of carbonaceous laminated shale (lithotype 7) and carbonaceous limestone (lithotype 1A); sub-equal amounts of quartz silt, carbonate, and clays; average total organic carbon (TOC) of 2.3 wt% and presence of two thin coals, yet the low average hydrogen index (HI) of 7.3 suggests aerobic bottom waters.

9100 to 9162 feet (2774–2792 m): Interval of low uranium concentration and high thorium dominated by black and gray shale (lithotypes 10 and 8A); very high quartz silt and clay content and low carbonate; the interval is less carbonaceous than adjacent intervals.

9162 to 9292 feet (2792–2832 m): Interval of very high uranium and thorium marked by a dominance of carbonaceous laminated shale (lithotype 7) and minor black and gray shale (lithotypes 10 and 8A) beds; heavily sampled for TOC which averages 3.86 wt% with normal average HI of 47; an interval rich in both organic matter and clays.

9292 to 9350 feet (2832–2850 m): Interval of very low uranium and high thorium that is dominated by interbedded black shale (lithotype 10) and siltstone (lithotype 4); the interval is carbonaceous with one coal bed, average

TOC of 2.7 wt% and HI of 50; the very low uranium concentration could relate to deposition in fresh to brackish water as supported by the presence of siderite.

The contribution from potassium to the total GR values is uniformly low throughout the core. It is not known why the spectral GR concentration of potassium is much lower than that determined by XRF (table 5.4) through the same rock section.

As noted earlier, the most prominent feature of the GR curves is the presence of sharp spikes where the total GR values exceed 150 to 200 API units (figure 5.12). The spectral value of the nine most prominent GR spikes with their log depths is presented in table 5.5C. In large measure the GR spikes are due to much higher than background uranium values. The peaks at 9009 and 9129 log feet (2746 and 2782 m) are the only exceptions. Throughout, however, the GR peaks are associated with elevated values of the thorium and potassium spectral values (table 5.5C). This implies that there is a large shale or clay component to the GR spikes. Peak 5 is related to a higher than normal thorium component, but a low uranium component. The largest peak, number 6, has large components of uranium, thorium, and potassium.

To understand the relationship between the GR peaks and the lithologies responsible for them, the sections of the core were examined at the depths determined from the log-to-core shift specified by Grover (2008). This involved a downward shift of the core relative to the GR log on the order of 8 to 12 feet (2.4–3.7 m). At the GR peak core depths there were many gaps in the core where samples had been removed, but most of the gaps were on the order of a foot or less. Generally, there were no abnormalities in the lithologies that could explain the elevated GR values. This was true also when the core depths were assumed equal to the log depths. However, at the core depths resulting from an upward shift of the core relative to the log of the magnitudes specified by Grover (2008), a plausible explanation for the GR peaks was apparent. These are the core depths shown in table 5.5. Six of the GR spikes are associated with intervals of core that contain phosphate as nodules or altered shell fragments. Peaks 7 to 9 are in intervals identified as possible condensed sections (refer to photomicrographs in figure 5.15). The high values (1 to 9 wt%) of fluorapatite observed in the core are correlated with peak 9 at the 9253-foot (2820 m) core depth. Peak 6 is associated with a phosphatic, organic-rich black shale. Peak 5, with low uranium spectral value and high thorium, corresponds to a silty shale interval with 50% clay fraction. Peak 4 corresponds to a proposed flooding surface identified at a core depth of 9073.2 feet (2765.4 m).

If the correlations are correct, there is apparently no single origin for the GR spikes. Rather, each spike is due to a variable combination of clay and uranium-rich organic matter and/or clay, organic matter, and phosphate.

Fractures

A variety of fracture types and orientations are found in the Carbon Canal 5-12 core (see appendix K for the complete fracture report, data, and graphical analysis). Fractures are most commonly found in competent, thin, interbedded limestone units. Most fractures in limestone are straight, high angle, and cement filled with a combination of calcite and minor dolomite and anhydrite. The calcite-filled fracture sets have northwest or north-northeast strikes. Fractures in shale beds are low angle, closed, and sometimes cemented with calcite with a slickenside texture on the face. Most of the slickenside surfaces indicate normal displacement. These fractures have a similar orientation to the calcite-filled fractures. Some poorly indurated shale beds have a small outside layer of the core that has spalled off. These features are termed ring fractures and result from gas expansion within the shale as the core is pulled to the surface. Finally, fractures in sandstone and siltstone units are high angle and tend to have a north-south strike and dip to the east (Grover, 2008).

Grover (2008) proposed that well-indurated, organic-rich shale with fractures having abundant slickenside surfaces make the best candidates for fracture stimulation. These units are, or have been, under differential stress regimes based on their various orientations. Partially open fractures with slickenside surfaces may accept fracture fluid which would “grease” the fracture plane, partially ease the vertical pressure, and may cause the slickenside fracture to reactivate.

Cyclicality and Parasequences

The Carbon Canal 5-12 core exhibits two types of stratigraphic cyclicality. The most obvious cycling relates to the secular variation in the proportions of siliciclastics versus carbonates as observed in the XRD mineral compositions (figure 5.12). There are five relatively thick intervals dominated by siliciclastics separated by thin carbonate-dominant intervals. The cycle boundaries, as defined by core depths of XRD samples having exceptionally large carbonate contents, are at 8900 feet (2713 m), 8972 feet (2735 m), 9091 feet (2771 m), 9198 feet (2803 m), 9296 feet (2833 m), and 9342 feet (2847 m) or deeper (figure 5.12). Given that the Oquirrh basin and Oquirrh sag were inherently carbonate environments of deposition into which siliciclastics were deposited, probably transported by wind, the cycles are recording times at which the influx of silt, clay, and iron oxides are especially high.

The second type of cyclicality is more subtle and is tied to alternations in the lithotypes described above. Packets of gray shale (lithotype 8) and/or micritic limestone (lithotypes 1, 1A, or 6) alternate with intervals of carbonaceous, laminar shale (lithotype 7). Most of the boundaries between lithotypes are gradational and do not imply sudden changes in depositional setting. However, one reoccurring pattern involves a black or very dark gray carbonaceous lithotype passing gradually upward into a medium gray, less carbonaceous or non-carbo-

naceous lithotype. With either a sharp contact or a transition over a few centimeters, the black or dark gray carbonaceous lithotype returns (figure 5.16). The surfaces clearly mark an upward change from aerobic or dysaerobic to anoxic or anoxic-dysaerobic sediments (Rhoads and Morse, 1971; Wenger and Baker, 1986; Wignall, 1994). From this single core it is not clear if such surfaces can be designated as flooding surfaces or parasequence boundaries. They appear to mark the tops of shoaling-upward packets, but the lateral extent of the succession and its continuity across large parts of the basin are unknown. Alternatively, the packets could indicate merely the upward freshening of bottom waters, as within poorly ventilated lagoons becoming better ventilated.

The surfaces marking the tops of these possible shoaling- or freshening-upward successions are indicated in red on figure 5.17. The four coal beds each fall at or very near a cycle boundary, and seven of the nine larger GR spikes discussed above coincide with a cycle boundary. Above a core depth of 9185 feet (2800 m) the tops of the cycles are bioturbated (figure 5.17). Below that depth burrowing is not observed. Just 14 surfaces are identified with confidence in the 420-foot (128 m) Doughnut section of the core. It is likely that there are others, perhaps where samples have been removed from the core. It is also likely that the sampled sections have special features, such as condensed intervals with phosphate, thin coals, or especially carbonaceous shales.

Within the resolution of the XRD sampling, the boundaries of the siliciclastic cycles and corresponding occurrences of abundant and sparse phosphorite indicated by the large and small blue arrows, respectively, on figure 5.17, coincide with the tops of the lithotype cycles shown by the heavy red lines. The siliciclastic cycle boundaries at 8900 feet (2713 m), 8972 feet (2735 m), 9091 feet (2771 m), and 9296 feet (2833 m) are represented by micritic limestone, the 1, 1A, or 2 lithotypes (figure 5.9; appendix I, plate I-3). The boundary at 9198 feet (2803 m) falls within a thick and relatively uniform succession of laminated carbonaceous shale/limestone (lithotype 7). However, the sample that marks the boundary is a 1-foot-thick (0.3 m) limestone bed (9197.8 to 9198.8 feet [2803.4–2803.7 m]) composed of skeletal debris with rip-up clasts and pellets suggestive of a condensed zone. The XRD mineralogy of this bed lacks apatite and has only 3% pyrite. Within each of the siliciclastic cycles are several of the lithotype cycles (figure 5.17). The coal beds are at or near lithotype cycle boundaries near the midpoints of the siliciclastic cycles.

North Springs Federal 1 Core

The North Springs Federal 1 well is located on the west flank of the San Rafael Swell near the edge of the Wasatch Plateau and within the general area of the Drunkards Wash coalbed gas field. The well is 8 miles (13 km) west-northwest of the Carbon Canal 5-12 well (figures 3.1 and 4.1). North Springs Federal 1 well was drilled in 1964 and tested natural gas from

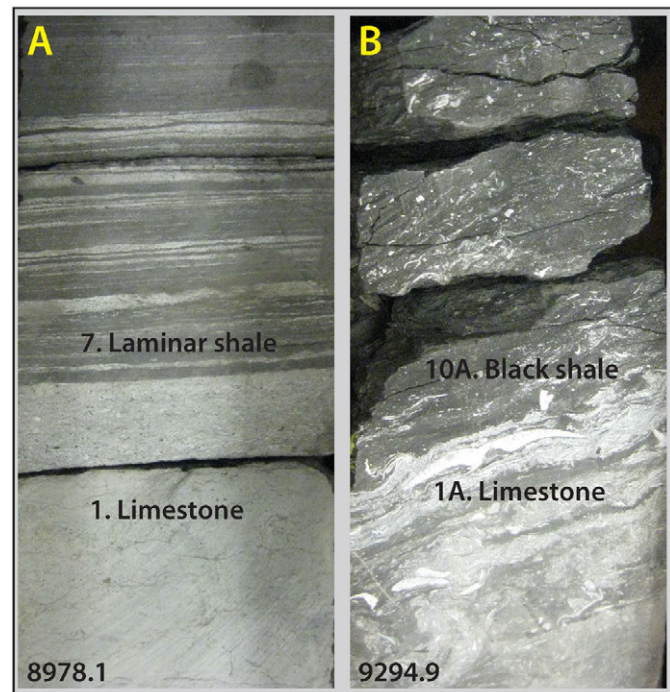


Figure 5.16. Photographs of possible stratigraphic boundaries in the Carbon Canal 5-12 core. **A.** Sharp contact between light gray limestone and dark gray to black laminar shale. **B.** Transitional contact between light gray limestone and dark gray to black shell-bearing shale.

the Doughnut Formation, but it was shut-in shortly after testing. A core was recovered from the interval that was tested, of which an 18-foot (5.5 m) segment (10,739 to 10,757 feet [3273–3279 m]) was preserved. The core is located near the center of the formation within a thick carbonaceous shale section containing interbedded limestone beds (appendices D, plate D-1, E, and I, plate I-5).

This core was loaned to the UGS by the Texas Bureau of Economic Geology for this study. Unfortunately, the core was poorly packed for shipment and it arrived with the rock segments badly jumbled. There was no original core photograph to assist reassembly. The attempt to replace the pieces in their proper order left an uncertainty as to original order. For that reason, the core pieces are identified separately, as shown in the core photographs in appendix I, plate I-5, not by core depth. The photomicrographs are tied to the core using this identification, rather than core depth.

Interbedded on a 0.5- to 4-inch (cm to dm) scale are carbonaceous calcareous shale and argillaceous limestone with a few thin laminae of calcareous siltstone. The shale beds are grayish black to dark gray (N2 to N3) and the limestones are dark to medium gray (N3 to N4). All rocks contain some coaly organic matter. The average TOC content of the 13 samples analyzed is 1.65 wt% with a range of values 0.67 to 3.74 wt%. The TOC values are shown on the core photograph (appendix I, plate I-5) in red text. Many beds are burrowed (letters-numbers refer to plate I-5; A-6, B-1, C-8), whereas a few are thinly

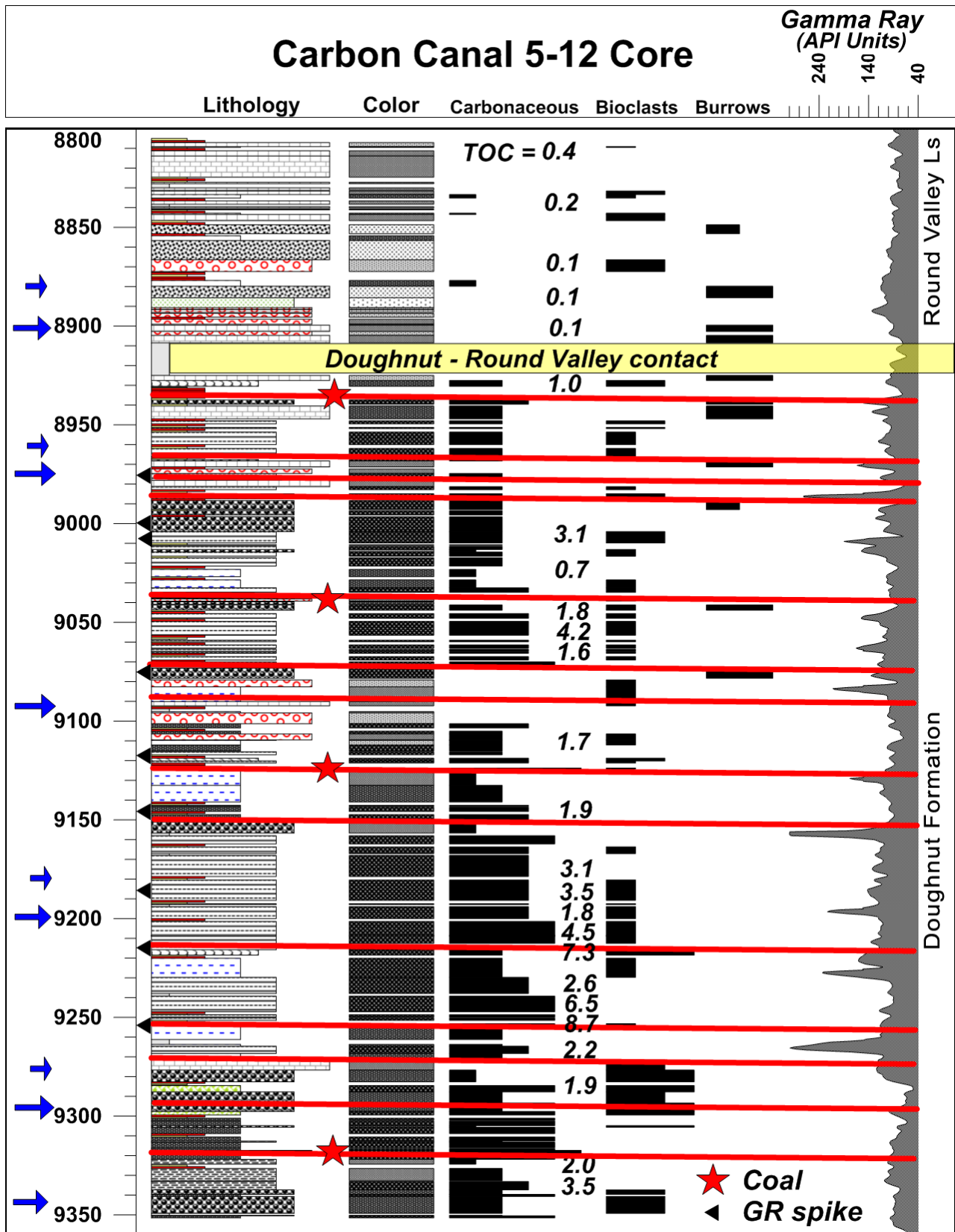


Figure 5.17. Possible stratigraphic cycle boundaries in the Carbon Canal 5-12 core. The interpreted parasequence boundaries are shown by the horizontal red lines. Occurrences of abundant and sparse phosphorite are indicated by large and small blue arrows, respectively. The relative abundance of carbonaceous matter, bioclasts, and burrows is indicated by the length of the bar. Due to the removal of core material at the critical boundary, the top of the Doughnut Formation falls within the interval indicated by the yellow bar. The overlying unit is either Round Valley Limestone or possibly the Oquirrh Group.

laminated (C-8). The limestones range from lime mudstone, to wackestone with an abundance of skeletal fragments and whole fossils, to packstone. The skeletal fragments are of thick- and thin-shelled brachiopods and pelecypods, brachiopod spines, and bryozoa (B-1, C-4, C-6, C-8, F-1). Siliceous sponge spicules are common throughout; they are a major lithic component in the lime mudstone, wackestone, and shale (A-5, A-6, D-9). Angular grains of coarse quartz silt to very fine grained sand are present in all rocks, and it is the principal component in the siltstone laminae (C-8). Many of the thick-walled shell fragments are replaced along their edges by euhedral feldspar crystals (B-2, F-1).

State 1-16 Core

The State 1-16 well is the northernmost of the wells penetrating the Doughnut Formation. As a consequence of its position on the north-plunging nose of the San Rafael Swell, the top of the Doughnut is deeper than 10,000 feet (3050 m). The well is 11 miles (18 km) north-northeast of the Carbon Canal 5-12 well (figure 3.1). Operator picks for the formation top and base are lacking from public well records, but, for this study, the top has been placed at 10,100 feet (3078 m) and the base at 10,900 feet (3222 m) based on interpretation of geophysical logs (figure 5.5). A 27-foot (8.2 m) core was taken from the interval 10,263 to 10,290 feet (3128–3137 m). This core is housed at the U.S. Geological Survey Core Laboratory in Denver, Colorado, and was not borrowed for this study. Rather, high-resolution core photographs were obtained from the U.S. Geological Survey that were adequate to describe this short interval. The UCRC had cuttings for this well that included fragments of the core large enough to examine visually and in thin section. Images of the core and photomicrographs of core segments are displayed in appendix I, plate I-6.

The core is quite uniform in character through its 27-foot (8.2 m) length. With just slight vertical variation, the rock is thinly laminated, medium-gray calcareous siltstone. At a scale of 0.1 to 1 inch (mm to cm) lighter gray quartz silt together with silt-size microbioclasts alternate with darker gray carbonaceous shale or argillaceous lime mudstone (appendix I, plate I-6; figure 5.1F). The dark laminae are very rich in coaly plant fragments, some large enough to see vascular plant structures. The plant parts are particularly well displayed on bedding surfaces. They are also visible in some thin sections (refer to photomicrographs at 10,273-foot [3132 m] and 10,291-foot [3138 m] depths on plate I-6, appendix I). The coaly bedding surfaces also have a scattering of large (0.2 to 0.04 inch [0.5–1.0 mm]), white mica grains that are seen also in thin section (refer to photomicrograph at 10,289-foot [3137 m] depth on plate I-6, appendix I). These thin, nearly circular grains are considered to be too delicate and well formed (un-abraded) to be detrital in origin. They normally occur against organic matter as if growing on this organic substrate. This mica phase tentatively is considered to be anchimetamorphic.

The rock has planar, flaser, and herringbone cross-bedding. Some intervals, such as the core segment at 10,279 feet (3133 m), have small-scale, bidirectional cross-bed sets characteristic of tidalites.

The core occupies a position on the well log between shale washout and high GR zones (figure 5.5). Above the cored interval, the cuttings are dark gray carbonaceous shale with coaly plant fragments. The same is true for a sampling of cuttings below the cored interval to nearly the base of the formation. Cuttings in the interval 10,960 to 10,970 feet (3340–3343 m) include carbonaceous shale, dark gray limestone, and fragments of brachiopods and bryozoa.

Discussion of Depositional Setting

All of the Doughnut Formation (Manning Canyon Shale) rocks examined for this study, described above and illustrated in the figures and plates referenced, contain some amount of carbonate material. This is present as a lime mud, microbioclasts and/or skeletal debris, or whole fossils. When dolomite or siderite is present in the rock, textural evidence indicates that its presence is the consequence of diagenetic alteration of the lime mud matrix of the rock or some other biogenetic component. Siliceous sponge spicules are an additional common biogenic component of the lime mud, although they are detected by XRD measurements as quartz, indistinguishable from the siliciclastic rock elements.

The fauna observed in rock and thin sections consists dominantly of thick- and thin-shelled brachiopods and thin-shelled pelecypods. When skeletal material is present, the shelly zones within the laminar carbonaceous shale/limestone (lithotype 7) are almost entirely thin-shelled, inoceramid-like pelecypods (paper pectins; Wignall, 1994), either a dysaerobic benthic or a pseudoplanktonic fauna. The less-carbonaceous limestone beds commonly have a larger faunal assemblage that also includes bryozoans, crinoids, ostracods, and, more rarely, cephalopods. Striking in their absence are foraminifera and/or fusulinids. Also absent from the allochems are oolites or pisolites.

The carbonate particles observed in the Doughnut Formation/Manning Canyon Shale, and indeed also the greater part of the Great Blue Limestone (Butkus, 1975), comprise a heterozoan assemblage (James, 1997) characteristic of subtropical and cool-water settings. This is a curious observation in that the region lay very near the mid-Carboniferous paleoequator (Butts, 2005) and should have a warm-water tropical or photozoan assemblage, one rich in foraminifera, fusulinids, green algae, and oolites. Shoore and Ritter (2007) also observed a heterozoan assemblage in the Bridal Veil Limestone of the Oquirrh Group, which lies immediately above the Manning Canyon Shale in Provo Canyon. They attribute the anomalous cool-water carbonate particle assemblage in an equatorial setting to low-light conditions in murky waters, the result of the nearly continuous influx of terrigenous dust. The Bridal

Veil Limestone and the Manning Canyon Shale are similar in terms of their petrography.

Whereas the fauna in the Doughnut Formation/Manning Canyon Shale indicates a marine to possibly brackish depositional setting, the flora is distinctly terrestrial, indicative of a swamp or marsh (paludal) environment. The palynology of Carbon Canal 5-12 core samples (described in chapter 8 and appendix O) revealed only spores of terrestrial plants and no marine taxa. The dominant spores are *Lycospora sp.* and *Densosporites sp.*, both associated with arborescent (tree-like) lycopsids, the giants of coal-age or Carboniferous forests, and *Punctatisporites sp.*, a tree fern spore (Willard, 1989). All are commonly found in coal swamps or sediments deposited in brackish to freshwater lagoons in proximity to land. In the upper Manning Canyon Shale west of Utah Lake, Tidwell (1966, 1998) identified 36 genera (68 species) of terrestrial plant fossils, a variety of pteridosperms, ferns, lycopsids, and calamites. In the same strata are fossils of insects (Nelson and Tidwell, 1987), fish (Mickle, 2009), and early reptiles (Gillette, 1999).

There are many instances in Ancestral Rockies basins of loess constituting a significant contribution to the Carboniferous-Permian sedimentary section. These include the Pennsylvanian Molas Formation of the Paradox Basin (Evans and Reed, 2007), the Pennsylvanian Maroon Formation in the Eagle basin of west-central Colorado (Johnson, 1989), the Pennsylvanian-Permian silty strata in the northern Pedregosa basin of southeast Arizona (Soreghan, 1992), and the silty Meade Peak Member of the Permian Phosphoria Formation in southwest Wyoming and adjacent Idaho and Utah (Carroll and others, 1998). The abundance of eolian dust in upper Paleozoic strata is causally linked to the late Paleozoic icehouse (Soreghan and Soreghan, 2002). Although there had been short, localized glaciations starting in the Late Devonian, the main late Paleozoic glaciations of Gondwana got underway in the Late Mississippian (Fielding and others, 2008). The mass extinction event occurring in the Late Mississippian, the seventh largest of the Phanerozoic Era, coincided with the onset of the glaciation (Powell, 2008; Bonelli and Patzkowsky, 2011).

Loess accumulation occurred in the Loess Plateau of northern China principally during late Cenozoic glacial and stadial periods when climates were drier (Porter, 2007). Wind erosion rates in the semi-arid western Qaidam basin (central Asia), the source of some of the Loess Plateau dust, are on the order of 0.5 inch (1.2 cm)/kyr, but can be greater than 39 inches (1.0 m)/ky off of tectonically rising topographic highs (Kapp and others, 2011). Late Cenozoic desert dust accumulation rates of 4 to 6 inches (10–16 cm)/kyr have been measured in the southern Arabian Peninsula (Nettleton and Chadwick, 1996). At these rates, 330 to 525 feet (100–160 m) of loess would be deposited in just a million years. In the Oquirrh basin the rates of dust accumulation need not have been so great.

Investigation of the Carbon Canal 5-12 core led Grover (2008) to identify an assemblage of depositional settings: restricted lagoon and algal flat, shoreface, upper to distal shoal, storm deposit or washover fan, shallow marine bay and shelf, and restricted marine bay. Most, but not all, of these environments are consistent with observations made in this study. It is clear that the Doughnut/Manning Canyon Shale was deposited in a marine to brackish environment that in part included or was in proximity to coastal swamps and marshes. Furthermore, the apparent absence of lateral continuity of stratigraphic markers within the formation suggests a heterogeneous setting in which environments varied over short distances, not just through time.

The freshwater marshes of the Everglades and the shallow, brackish to marine carbonate factory of Florida Bay (figure 5.18) might serve as a conceptual model for the depositional setting of the Doughnut Formation/Manning Canyon Shale. Furthermore, the adjacent West Florida Shelf could be a modern analog for the depositional setting of the Great Blue Limestone.

Florida Bay extends along the south side of the Everglades for a distance of about 45 miles (73 km). The widest part facing the West Florida Shelf is 25 miles (40 km) north-south. The waters of the bay are brackish to hypersaline and can vary seasonally and due to storms. The salinity in the interior of the

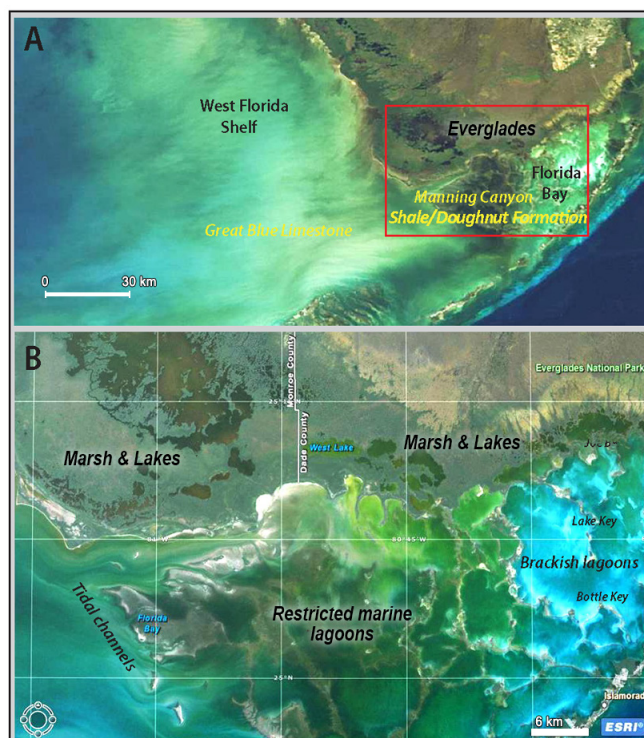
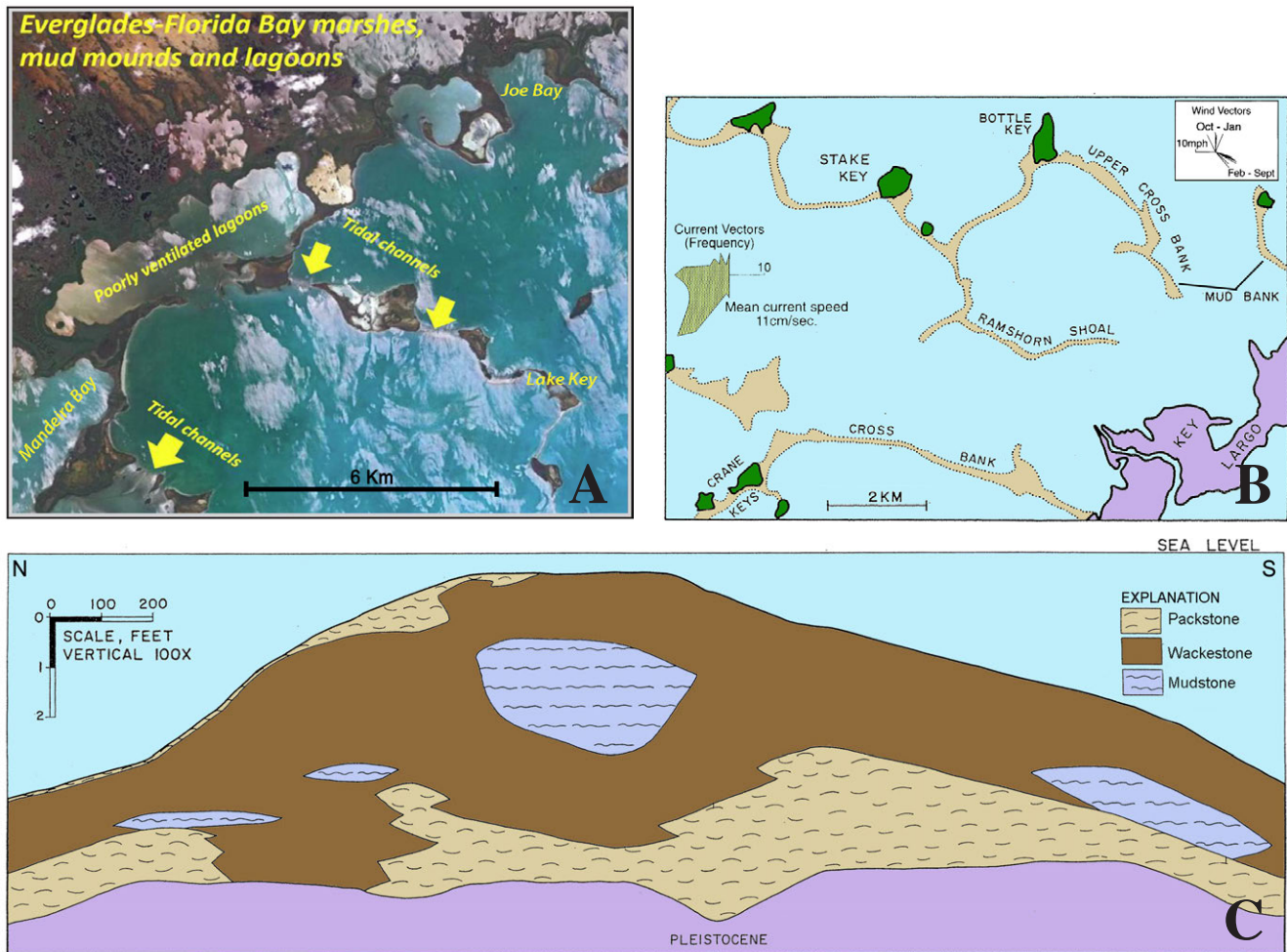


Figure 5.18. Satellite images of southern Florida, possible modern analogs for the depositional setting of the Manning Canyon Shale/Doughnut Formation and Great Blue Limestone. **A.** Locations of Florida Bay, the Everglades, and the West Florida Shelf. The area shown in panel **B** is marked by the red rectangle. **B.** ESRI ArcGIS Explorer image of Florida Bay and adjacent Everglades showing the web of carbonate mud mounds, keys (islands), and lagoons.



bay ranges from 2.0 to 11 ounces/gallon (15–80 g/L) (Swart and Kramer, 1997); normal seawater averages 4.7 ounces/gallon (35 g/L). The unconsolidated sediments in the bay consist almost entirely of aragonite and calcite (95%) with minor silica (detrital quartz and opaline silica), clays, and organic matter. Skeletal and non-skeletal lime muds are the most common sediment type, but skeletal sands dominate in higher-energy settings. Wind and tidal-driven currents are the main transport mechanisms in the bay. Storms, especially hurricanes, have a major impact on sediment transport. The small rivers entering the bay from the Everglades bring nutrients and organic matter, but only minor siliciclastics. The most prominent sedimentary features of Florida Bay are the mud mounds (mudbanks and mud islands) that form a web of shoals and keys enclosing shallow lagoons (figures 5.18 and 5.19). The mounds are built of bioturbated or laminar lime mud and skeletal sand that have strongly lenticular geometries and vary vertically on a scale of feet (Wanless and Tagett, 1989; Wanless and others, 1995). The coarser sediments (“packstone” and “grainstone”) tend to build up on the steep windward side of the mounds

and the muds form broad flats on the lee side (figure 5.19). Over time, the mounds migrate leeward due to winter storms (Swart and Kramer, 1997). The mud islands stand less than a few feet (1 m) above sea level, yet nevertheless have distinct flora zonation (and successions) of (a) algal mats and salt-tolerant mangrove and halophytic marshes, (b) brackish-water vegetation, and (c) grasses, palms, and hardwoods. Many of the keys (islands in and bordering Florida Bay) contain freshwater lakes. Geochemical proxies in the surface sediment of the lagoons indicate a change across the bay in the source of organic matter from dominantly mangroves in the near-shore northeast to seagrass off-shore along with contributions from bacteria and cyanobacteria in mats of the central and southwest bay (Xu and others, 2006). The natural input of phosphorous into the bay is from marine water entering from the Gulf of Mexico, whereas iron is transported dissolved in fresh water draining from the Everglades (Zhang and others, 2004).

The West Florida Shelf is a ramp or “unrimmed shelf” that slopes gently westward from Florida Bay for about 100

miles (160 km) before the shelf/slope boundary is reached at the 300-foot (100 m) isobath. The sediments are a complex, mixed siliciclastic and carbonate system (Beck, 2010). A latitudinal transition from warm temperate to subtropical water is reflected in the increase in carbonates having a high mud content southward to offshore of Florida Bay. The higher content of TOC in the shelf sediments adjacent to Florida Bay is attributed to influx of nutrients from the Everglades (Schwing, 2010). Sediment distribution on the shelf is controlled by waves, tides, and storms. Especially on the inner shelf, there are sediment ridges created by currents (Finkl and others, 2007).

Imagine that across a similar shallow unrimmed shelf and near-shore marine to brackish-paludal environment there was a virtually constant rain of dust during the Late Mississippian and Early Pennsylvanian. This was a time of both exposure of large areas of the shelf in western North America, the source of dust, and entry into global icehouse-produced climates that were drier with likely stronger winds. What distinguishes the Doughnut Formation/Manning Canyon Shale from the Great Blue Limestone is the relative amount of silt and clay, as well as terrestrial organic matter. The rocks identified as Great Blue Limestone were those on the carbonate shelf more distant from land, the source of the dust, and the plant debris. Deposition of the Manning Canyon/Doughnut “facies” began when large quantities of dust were made available by icehouse-driven climate change across an extensive exposed land surface and ended when large portions of this land surface were flooded by shallow epeiric seas in the Early Pennsylvanian.

PARADOX FORMATION

In any examination of the three pertinent Paradox Formation shale units—from youngest to oldest, the Hovenweep, Gothic, and Chimney Rock—it is important to remember that these shales are stratigraphically separated from one another by a cyclical sequence of mostly carbonate/evaporite lithologies with subordinate amounts of terrigenous clastics, all lithologies belonging to the well-known Upper Ismay, Lower Ismay, and Desert Creek cycles (in descending stratigraphic order). In terms of the well locations used in this study, the archived core material was available for wells that were fairly well spread out within the Utah portion of the Paradox Basin. These wells, their locations, and corresponding cored shale units are listed in table 4.1.

Core Descriptions

The basic lithology of all three shales is fairly consistent, as seen both megascopically and microscopically. From a megascopic perspective, all shales are mostly dark brown-gray, wavy to planar laminated, calcareous mudstones. The rocks are very organic looking because of the dark hues. The

lowest unit studied, the Chimney Rock shale, is adequately represented in the Mule 31-K (N) well and in some sidewall cores from the Jefferson State 4-1 well (figure 4.2). This unit contains various percentages of dolomite, including beds or intervals of a medium brown color that represent relatively pure dolomite, and, in fact, the Chimney Rock grades upward into dolomite of the Desert Creek cycle. The next highest mudrock, the Gothic shale, is consistently a dark brown to gray, calcareous mudstone for most of its stratigraphic extent. Some interbedded dolomite is subordinately present. The Gothic is naturally fractured, especially in the Jefferson State 4-1 core. The stratigraphically highest shale, the Hovenweep shale, is also consistent in its calcareous mudstone content.

Refer to appendix D for megascopic core graphs of each of the wells listed in table 4.1. Also, one can consult the close-up core photographs in appendix J. These foot-by-foot assessments, although found in some detail on the coregraphs, can also be more succinctly summarized through the following major conclusions:

1. All three mudstone sequences are composed largely of dark brown-gray, organic, calcareous mudstones with significant compositional dilution by terrigenous clastics related to erosion of the near-concurrent and proximal Uncompahgre uplift. Some overprinting by diagenetic cryptocrystalline and finely crystalline dolomite also is prevalent. Composition is fairly consistent and predictable in most shale intervals among the different wells. Some significant stratigraphic variation is seen in organic content and in the occurrence of dolomite interbeds.
2. Fossils include articulate (calcareous) and inarticulate (phosphatic) brachiopod fragments, ostracods, microfossils (including both locally abundant arenaceous foraminifera) and plant(?) spores, sponge spicules, conodonts, and conulariids (figure 5.20), among other taxa—some fossils



Figure 5.20. Fossil conulariid from the Gothic shale. These somewhat rare fossils are accompanied by brachiopods (inarticulate and articulate), ostracods, conodonts, and agglutinated foraminifera.

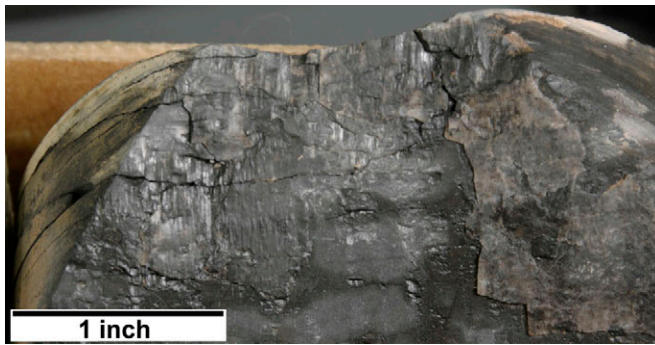


Figure 5.21. An oblique to bedding ($\sim 45^\circ$) fracture with a veneer of calcite in the Gothic shale. Slickensides (lineations) are evident. Hydraulic fracturing may increase shear and reactivate the planes of tensile fractures.

are clearly transported, and some are indigenous to what was likely a dysaerobic environment. Trace fossils are rare, and most bioturbation is consistently near the upper and lower contacts (more aerobic[?] environments) of the shales.

3. Compositional variation recognized through downhole logs mainly results from fluctuations in TOC content, in carbonaceous material, in dolomite/calcite content, and in phosphate remains. Most shale intervals initiated as flooding surfaces over subjacent carbonates, and organic content seems highest in the lowermost or basal beds of each shale.
4. Equally important is the occurrence of silty dolomite occasionally interbedded within the shale; both dolomite and limestone occur above and below the dark mudrocks as conveyed earlier.
5. Natural fractures occur within the cored intervals. Most fractures are subvertical and are partially to completely infilled, primarily with calcite. Other fractures are horizontal and calcite mineralized; the origin of these horizontal filled fractures is conjectural at this point, although some cracks may simply be mineralized sheared and slickensided surfaces as seen on figure 5.21. Fractures are more common in the brittle dolomite and limestone, some of which are interbedded with the mudstone; additional fractures lie both above and below the organic mudstone sequences. However, fractures also occur within the comparatively ductile (but unusually strong in a mechanical sense) mudstone units themselves, although mechanical stratigraphy contrasts usually favor crack generation in the more brittle carbonate materials. We did not quantify fracture orientations, but such determinations would be important for horizontal drilling and/or stimulation protocol. In any case, even healed fractures would likely reopen during any stimulation procedure, resulting in improved permeability.

Inclined shear fracture zones, possible permeability pathways, are undulant and contain multiple fracture surfaces; overall dip ranges from 30° to 44° (Chidsey and others, 2009; Heath and

others, 2009). Slickensides rake obliquely across the dip of the shear planes, and are probably parallel on successive planes. They suggest significant horizontal tectonic compression at some point during the geologic history of the strata. These sub-horizontal shear planes were observed in both the Gothic shale and upper Desert Creek zone. The inference is that these shear planes may be zones of incipient or limited detachment (Chidsey and others, 2009; Heath and others, 2009).

Microscopic Observations Through Petrography

Details of our microscopic observations through petrography can be found in the extensive set of photomicrographs (with descriptions) in appendix F. Basic conclusions are summarized as follows:

1. Dark, organic mudrock or shale can be simply classified as calcareous silty mudstone (figure 5.22) in almost all cases, irrespective of the stratigraphic interval (Hovenweep, Gothic, or Chimney Rock). Organic material seems to vary in terms of affecting the dark coloration, and while most accessories are fairly consistent in their abundance (fossils, pyrite, phosphate, muscovite flakes, carbonaceous material) amounts of diagenetic dolomite, clay, and terrigenous clastics are somewhat variable (also see phosphate comment under [3] below).
2. The interbedded and mudstone-bounding dolomites normally contain modest amounts of terrigenous clastic material as well as illitic clays (figure 5.23). When little quartz or feldspar occurs in these carbonates, the dolomite is occasionally bimodal where one size mode of the dolomite

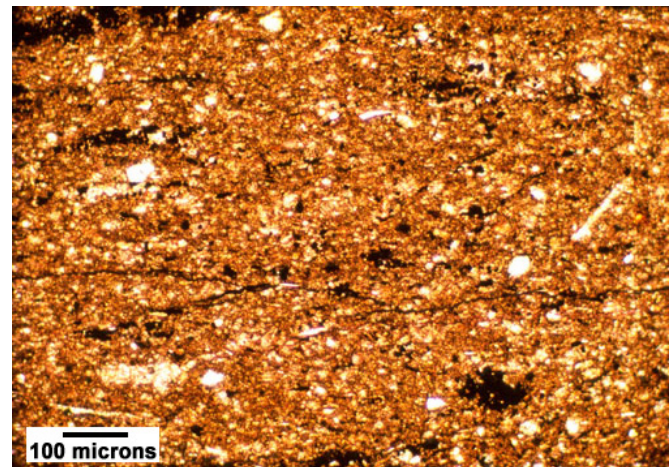


Figure 5.22. Representative photomicrograph (plane-polarized light, 100x) of silty mudstone from the Hovenweep shale typical of all three black mudstone zones from the Paradox Formation investigated for this study. The rock contains a certain percentage of terrigenous clastics as well as finely fragmented fossil debris (white in this view). In addition, both carbonaceous material and pyrite are recognized by the brown-black hues, and the organic clay (mostly illite) represents the dominant matrix material. Marie Ogden 1 well (figure 4.2), depth = 5213.1 feet.

crystals corresponds to the siliciclastic grain size as the latter are selectively replaced by perhaps a separate dolomitization event. The other mode is cryptocrystalline dolomite, likely an alteration of original lime mud.

- Besides abundant dolomite content, other important accessories include (a) common diagenetic pyrite, (b) calcite as fossil material, as diagenetic patches, and as fracture fill, (c) carbonaceous matter, (d) anhydrite infilling and replacement, and (e) phosphate (shell material and recycled lumps; figure 5.24). Some phosphate is concentrated at the base of the flooding surfaces over underlying carbonates. If this phosphate presence is considerable, a locally higher gamma-ray signature can result.
- Porosity in the mudstones can be seen in many of the thin sections as clay-associated microporosity (figure 5.25). The pore space in the dolomites can be seen more readily, but accurate reservoir quality in terms of porosity/permeability values can be better found in the routine core analysis for the carbonates and in the tight rock analysis (TRA) for the organic mudstones (chapter 7). Finally, scanning electron images remain a powerful visual tool that helps immensely with the determination of reservoir quality.

Microscopic Observations Through Scanning Electron Microscopy (SEM)

The observations using SEM fall into two general categories of (1) dolomite and (2) mudstone, and all images and descrip-

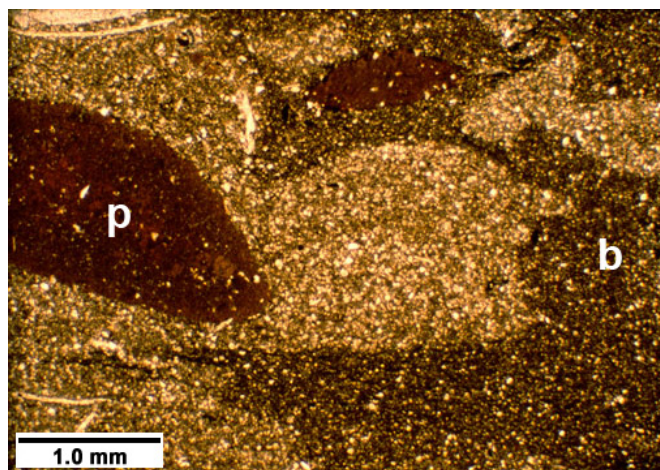


Figure 5.23. Photomicrograph (plane-polarized light, 20x) at very base of upper Ismay cycle immediately above the Hovenweep contact where muddy dolomite here contains an array of distinct elements: (1) phosphate clasts (p), (2) bioturbation features (b), (3) terrigenous quartz, (4) small green grains of glauconite (not visible in this image), and (5) skeletal debris. Dolomite is bimodal as seen previously, and this rock marks an important demarcation between dysaerobic deeper conditions below and an aerobic shallower setting in the superjacent strata. Marie Ogden State 1 well (figure 4.2), depth = 5191 feet.

tions can be found in appendix G. In summary, the mudstones are described in terms of their obvious texture (size, shape, and composition) and likely fabric (laminated). The porosity appears visually low as verified by other methods (TRA), and the permeability is also modest by shale standards as evidenced by the relatively isolated nature of the voids. The dolomites are variable in terms of their reservoir quality; some possess high porosities and correspondingly elevated permeabilities due to euhedral crystal shape, loose packing, and modest occlusion by other minerals. When the crystals are more subhedral or anhedral, tightly packed, and occluded by other minerals (including clays and other authigenic materials), reservoir quality appreciably decreases. Our SEM photos and

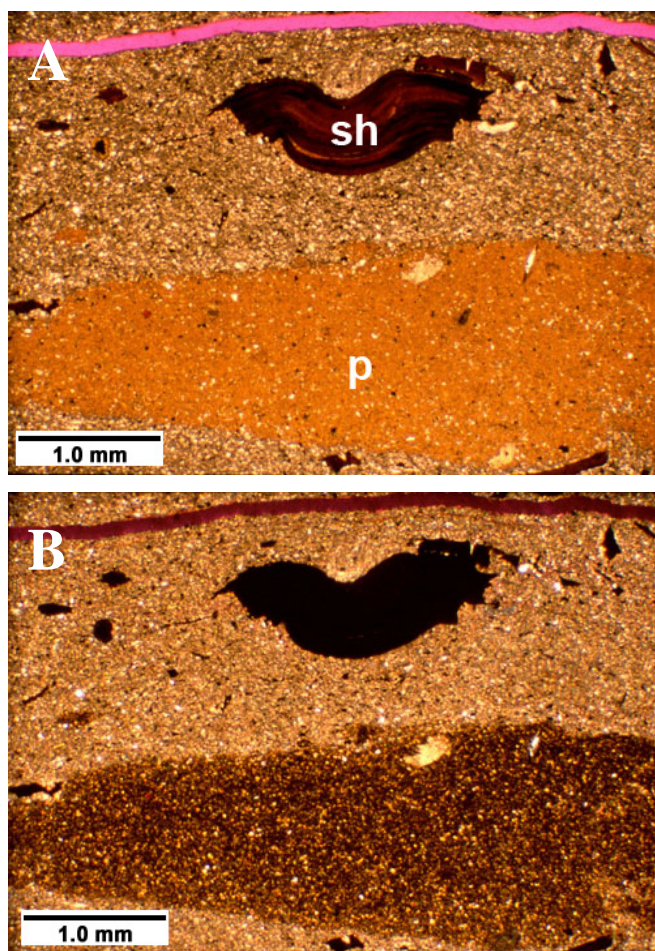


Figure 5.24. Photomicrographs from flooding surface found at the contact between the underlying Gothic shale and the overlying Lower Ismay carbonate sequence. **A.** At this position, several reworked fragments are common, including in this view a medium brown phosphatic clast (p) strung out subparallel to bedding and a dark orange-brown phosphatic shell fragment (sh) from perhaps from one of the conularioids (plane-polarized light, 20x). Black material is a combination of carbonaceous material that has been partially pyritized. Linear magenta feature at right margin is an induced fracture, probably produced during thin section preparation. **B.** Cross-polarized view of A reveals certain phosphatic composition through isotropic optical behavior—dark brown to black upon extinction. Aneth Unit H-117 well (figure 4.2), depth = 5376.5 feet.

overall semi-quantitative conclusions are commonly verified by routine core analysis, or by thin section photomicrographs.

The Chimney Rock shale texture generally exhibits weakly developed laminae composed of stacked and crenulated clay flakes (figure 5.26A). The matrix composition is often a mixed illite, illite/smectite, and chlorite. Where little or no silt or sand-sized material is observed, the sample is shale rather than mudstone and exhibits a blocky, crumbly, and soft texture with moderate lamination. Carbonaceous particles align parallel to bedding and discrete organic particles are sparsely distributed throughout the Chimney Rock samples. Crenulated shapes of clay flakes, irregularities introduced by diagenetic cement crystals, and admixed organic particles all create open micropores in the heterogeneous shale matrix. Natural intercrystalline micropores (< 1 micron) as well as more linear, stress-release or dehydration fractures are common (figure 5.26B). Quartz and feldspar silt grains, where present, prop open voids between clay flakes. These micropores average 1 to 2 microns in size. Calcareous and dolomitic cements admixed with laminated

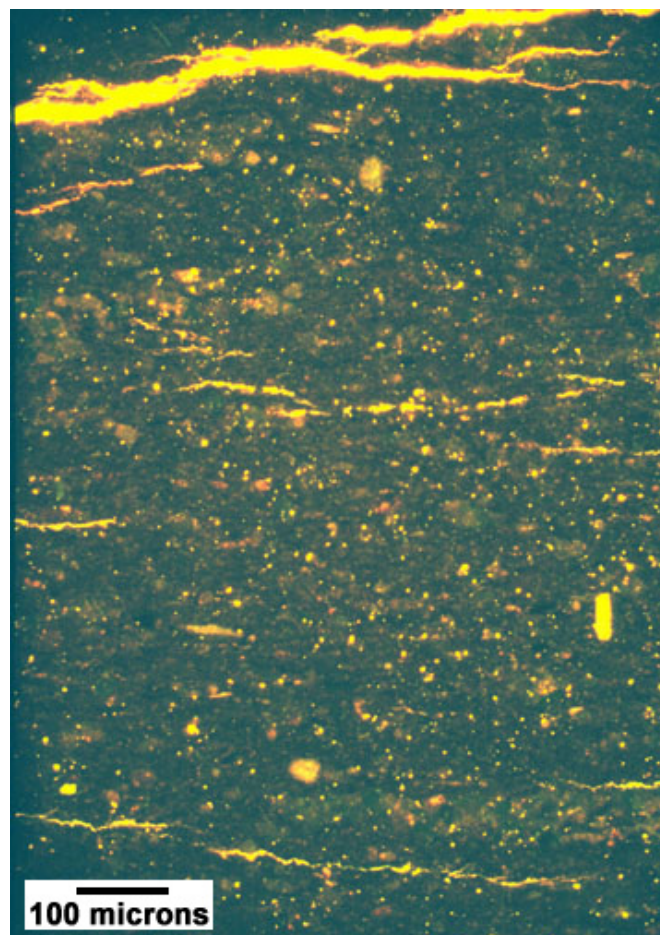


Figure 5.25. Photomicrograph (reflected ultraviolet light with blue-violet filter, 100x) of the Gothic shale demonstrates in bright yellow a series of induced subhorizontal microfractures and some mineral fluorescence. The orange shades, however, likely represent areas of modest clay microporosity. Lake Canyon 1-27 well (figure 4.2), depth = 5773.3 feet

clay minerals reduce primary porosity that mainly includes flattened intercrystalline micropores between clay minerals. The general texture of Chimney Rock dolomite is characterized by euhedral dolomite crystals that are about 10 microns wide (figure 5.27A); silt is sparse. Visible porosity in the dolomite is significantly reduced by authigenic cements, such as silica and flaky clay minerals including chlorite, that fill most intercrystalline micropores between euhedral dolomite (figure 5.27B).

The Gothic shale is typically argillaceous mudstone with microlamination defined by wavy clay flakes (figure 5.28A). Argillaceous shale, silty calcareous/argillaceous mudstone, and phosphatic argillaceous mudstone are also common (see later

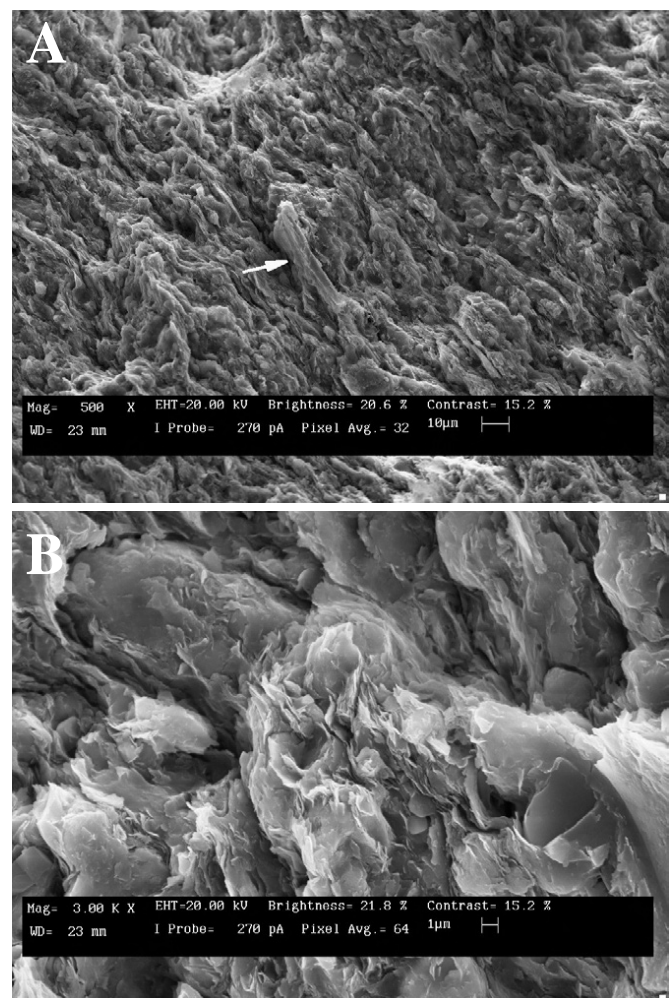


Figure 5.26. Scanning electron microscope photomicrographs from the Chimney Rock shale, Jefferson State 4-1 well (figure 4.2), depth = 6195.5 feet. **A.** Overview of shale texture exhibiting weakly developed laminae composed of stacked and crenulated clay flakes. A matrix composition of mixed illite, illite/smectite, and chlorite is probable. The flake at center (arrow) is most likely a degraded mica. Scale bar = 10 microns. **B.** Higher magnification of whorled habit in clay flakes. Natural intercrystalline micropores (< 1 micron) as well as more linear, stress-release or dehydration fractures are visible in this image. A mixed composition of illite and either magnesium smectite or chlorite is inferred. Scale bar = 1 micron.

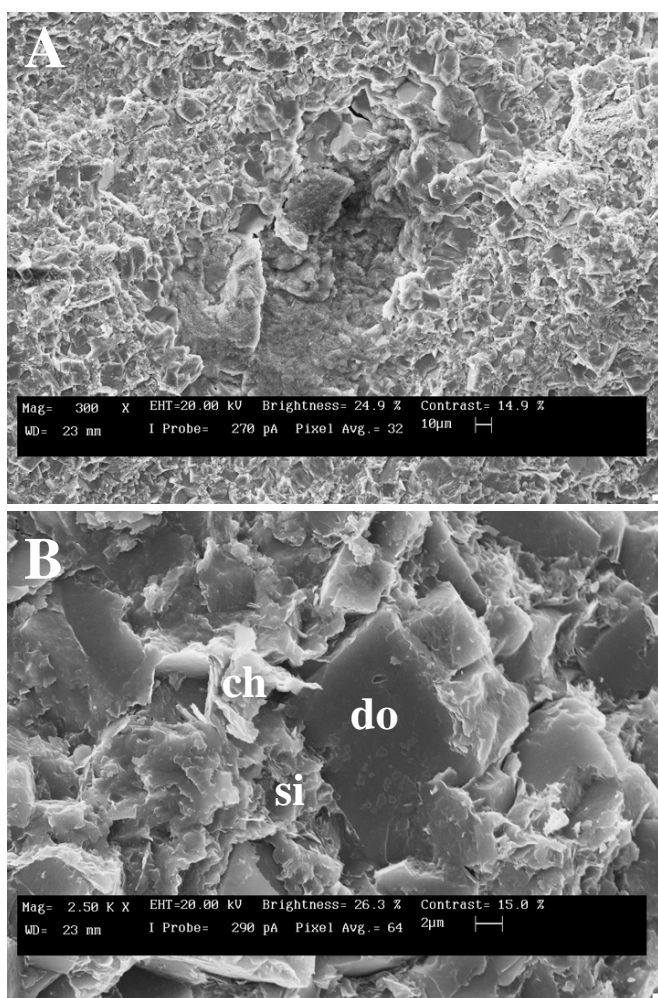


Figure 5.27. Scanning electron microscope photomicrographs from the Chimney Rock shale, Mule 31-K-1 (N) well (figure 4.2), depth = 6099 feet. **A.** General texture overview of a dolomite characterized by euhedral dolomite crystals that are about 10 microns wide and sparse silt. A calcareous microfossil is shown in the middle of the image. Scale bar = 10 microns. **B.** A closer view showing authigenic cements such as silica (si) and flaky minerals including chlorite (ch) filling intercrystalline cavities between dolomite rhombs (do). Scale bar = 2 microns.

detailed discussion of the Gothic). Silt-sized calcite and non-ferroan dolomite grain replacements often populate the matrix of wavy and crenulated clay flakes. Degraded, nanoporous kerogen contains a high surface area per unit volume, creating numerous gas adsorption sites (figure 5.28B). The most common pores are intercrystalline micropores between clay flakes. Pyrite (framboids) and rectangular dolomite are relatively common in the Gothic. In mudstone textures dominated by interlocking, subhedral dolomite crystals, porosity is generally minimal. In addition, packets of clays sandwiched between dolomite crystals leave little visible microporosity in the tightly crystalline fabrics.

The Hovenweep shale is typically a dolomitic mudstone containing a mixture of carbonate minerals and matrix clays (figure 5.29A). Detrital quartz and feldspar silt are dispersed; pyrite is also common. Discrete organic particles are embedded

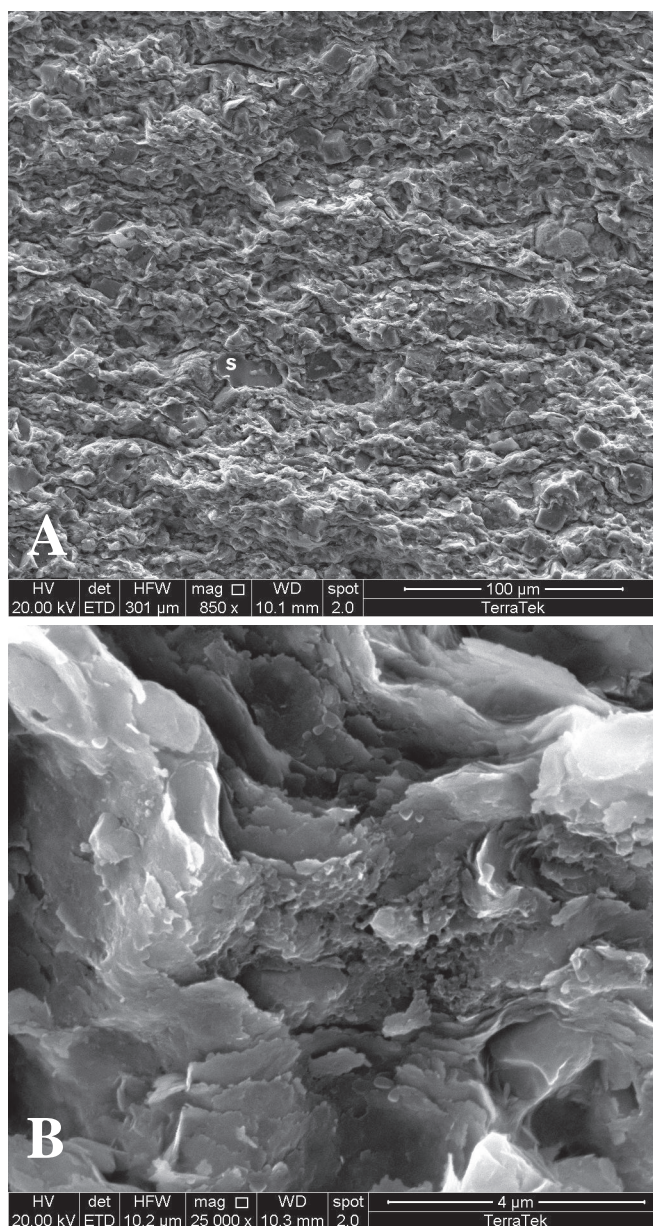


Figure 5.28. Scanning electron microscope photomicrographs from the Gothic shale, Lake Canyon 1-27 well (figure 4.2), depth = 5774.8 feet. **A.** An argillaceous mudstone with microlamination defined by wavy clay flakes. Detrital silt (s) and authigenic minerals are randomly dispersed. Scale bar = 100 microns. **B.** High-magnification image of the stippled texture indicative of kerogen coating clay minerals. Scale bar = 4 microns.

in matrix clays. The most common pore type is intercrystalline with pores found between clays, authigenic dolomite, and pyrite (figure 5.29B). Clay minerals are compacted, leading to elongate pores. Intergranular porosity is observed between quartz silts and the surrounding matrix clays.

Microscopic Observations of Natural Fractures Through Petrography

Fracture analysis includes the evaluation of natural and induced fracture systems, fracture orientation, and mineral com-

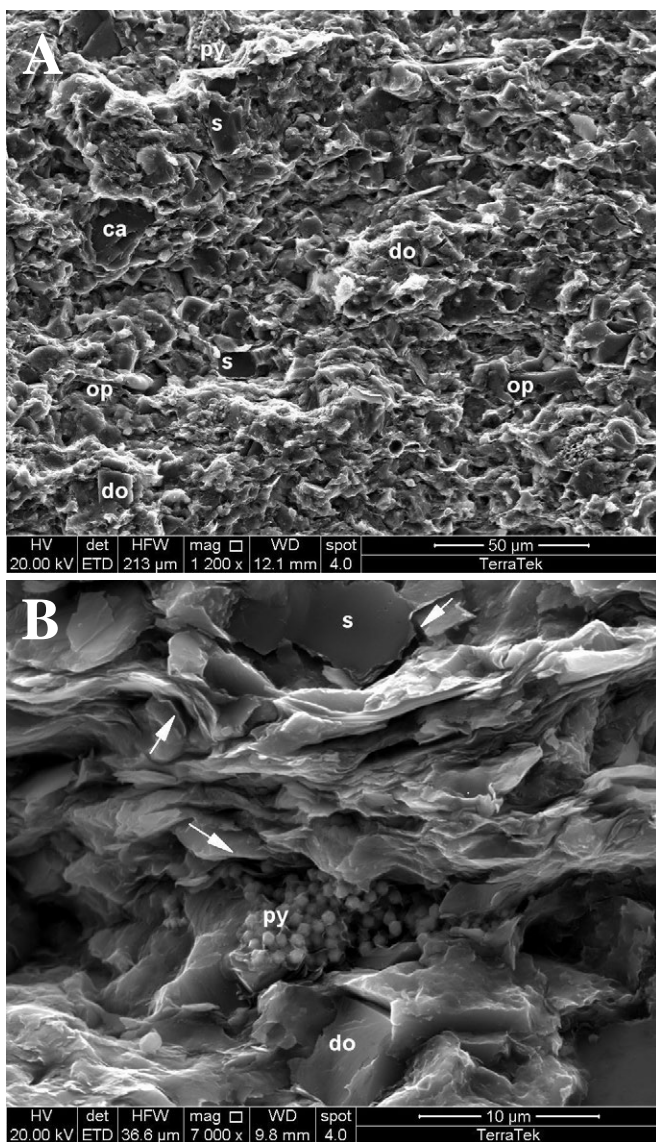


Figure 5.29. Scanning electron microscope photomicrographs from the Hovenweep shale, Marie Ogden State 1 well (figure 4.2), depth = 5196.3 feet. **A.** Low-magnification image reveals an irregular texture due to a mixture of carbonate minerals (*ca* = calcite, *do* = dolomite) and matrix clays in this dolomitic mudstone. Detrital quartz and feldspar silt (*s*) is dispersed. A few discrete organic particles (*op*) and pyrite (*py*) are observed. Scale bar = 50 microns. **B.** High-magnification image of the matrix microfabric shows the relationship between clay flakes, authigenic minerals, and detrital grains. Intergranular porosity is observed between quartz silt (*s*) and the surrounding matrix clays. The most common pore type, however, is intercrystalline pores (arrows) found between clays, authigenic dolomite (*do*), and pyrite (*py*). Scale bar = 10 microns.

position of fracture fill. Typical tabulated data from the fracture analysis includes general fracture type, fracture dip orientation, type of mineral fill, type of oil stain, apparent fracture dip, fracture porosity, fracture spacing, and fracture intensity. Natural fractures include inclined shear fractures or fracture zones and horizontal shear fractures. Fractures are slickensided and partially mineralized. Five generic types (or “classes”) of natural

fractures occur in the Chimney Rock, Gothic, and Hovenweep shales:

1. short fractures of a vertical nature but sinuous along their length,
2. microfractures (particularly developed in a carbonate facies of the Ismay cycle) where rigid allochems are preferentially cracked,
3. filled and partially open, mostly subvertical fractures commonly located in the mechanically strong carbonates stratigraphically proximal to the more ductile calcareous organic mudstones,
4. filled and partially filled subvertical to horizontal cracks common to the mudstones themselves, some of which are proximal to carbonates and others which have no clear development attributable to contrasting mechanical properties, and
5. tension gash development associated with stylolitization.

For example, the Jefferson State 4-1 well (figure 4.2) has fractures on several scales (appendix K). The short and sinuous fractures (type 1) likely comprise syneresis cracks related to dewatering of soupy muds which later were occupied by solid mineral infill, mostly calcite and/or pyrite. The best examples occur in the Mule 31-K-1 (N) well (figure 4.2) at 5923.5 to 5925 feet (1805.4–1805.9 m) (core depth). The microfractures (type 2)—related to perhaps differential compaction of allochems—occur in the oil-stained subjacent carbonates in the Jefferson State 4-1 well between 6010.5 and 6016 feet (1831.9–1833.6 m) (appendix K) and in the Marie Ogden State 1 well at 3 feet (1 m) above the Gothic shale (figure 5.30). These examples provide additional evidence for overall reservoir quality enhancement from the (mostly) carbonate strata bounding any stimulated black shale. This statement is theoretically true depending on rock mechanics properties and on the stimulation protocol itself. The third type of carbonate cracking (type 3) is most impressive in Mule 31-K-1 (N) dolomite or silty dolomite very near the underlying calcareous mudstone of the Chimney Rock shale (6097.5 to 6101.5 feet [1858.4–1859.6 m]). The most impressive fractures in the mudstone themselves (type 4) occur in the Gothic and Chimney Rock shales (appendix K). These cracks are partially to completely occluded by calcite (figure 5.31), and their origin remains problematic. The origin of these horizontal cracks is certainly conjectural, but identical features are commonly seen in other black shales of North America. These cracks could have formed during bedding-plane shearing (a process particularly common to mudrocks), or even as a result of hydrocarbon expulsion phenomena. However, these cracks may simply be related to structural flexing. Type 5 development appears minor, and a good example of such cracks is situated in the Mule 31-K-1 (N) well at around 6097.5 feet (1858.4 m) in the carbonates above Chimney Rock mudstone.

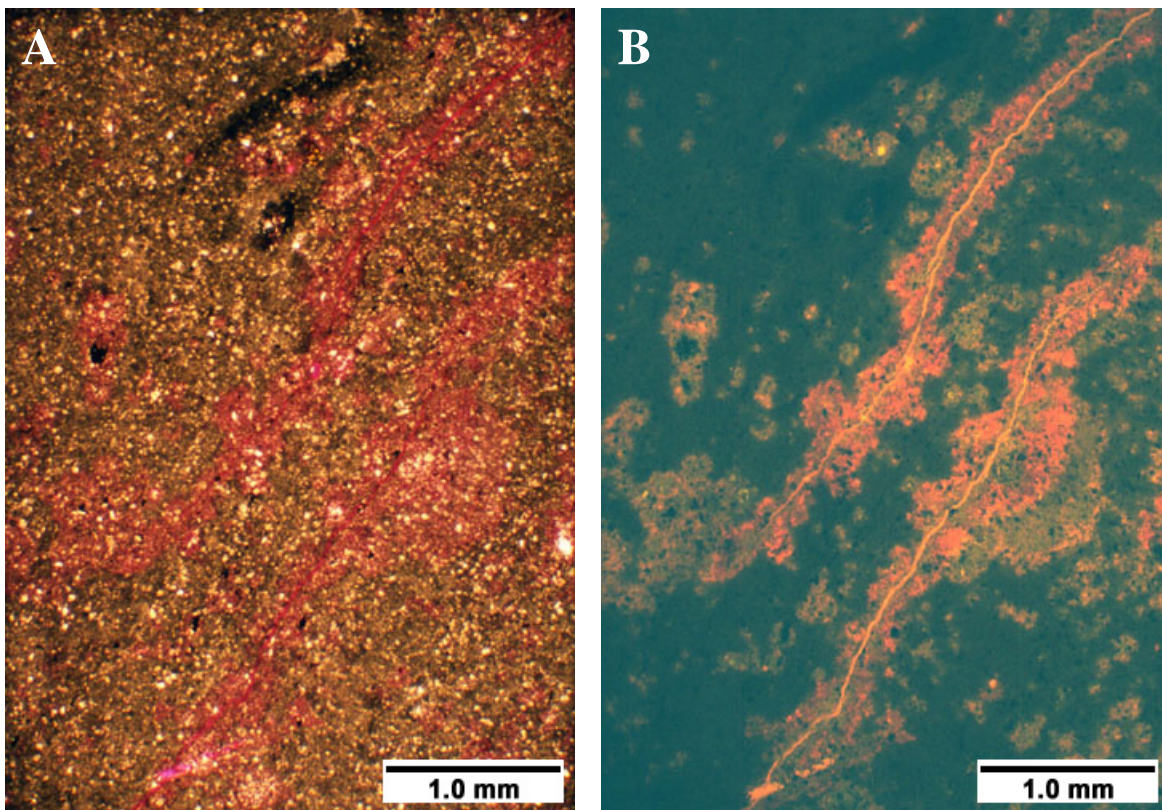


Figure 5.30. Photomicrographs showing examples of type 2 microfractures in the lower Ismay cycle 3 feet away from the subjacent Gothic shale. **A.** Finely crystalline dolomite beset by a series of natural microfractures, trending from upper right to lower left (plane-polarized light, 20x). The cracks themselves seem quite diffuse and not strictly linear. Other patches of magenta indicate additional amounts of matrix porosity. **B.** Epifluorescent view (reflected ultraviolet light with blue-violet filter; 20x) of **A** is quite revealing in that the “linear nature of the cracks is better outlined; however, the orange fluorescence surrounding these linears indicates that some additional dissolution of the matrix also occurred to modest degrees, augmenting the strictly defined fracture porosity/permeability. Other isolated patches represented by orange hues may also reflect this dissolution phase. Marie Ogden State 1, depth = 5320.6 feet.

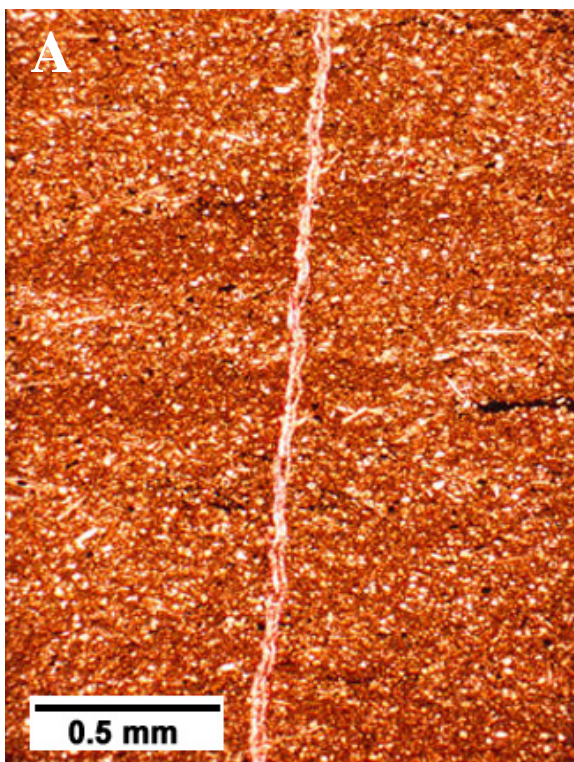
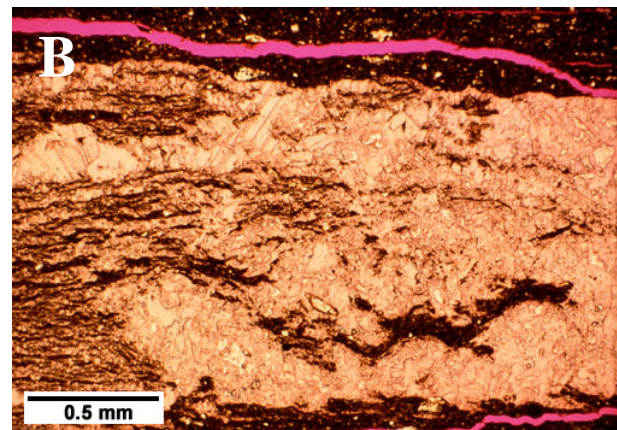


Figure 5.31. Photomicrographs (plane-polarized light, 40x) showing examples of type 4 cracks completely occluded by calcite. **A.** Gothic shale composed of terrigenous material, fossils, and clays. Mottled appearance may be related to some bioturbation. In this well, the Gothic is decidedly fractured, and in this view a subvertical fracture is composed of red-stained calcite. Not all fractures in this interval are completely occluded by diagenetic minerals—see appendix K. Jefferson State 4-1 well (figure 4.2), depth = 6036.6 feet. **B.** In this Chimney Rock sample, a subhorizontal fracture in typical organic mudstone is also infilled by red-stained calcite. Lake Canyon 1-27, depth = 5877.7 feet.



Mineral Analysis Through X-Ray Diffraction (XRD)

Six cores from the Paradox Formation were sampled and analyzed using XRD. Figure 4.2 shows the well locations and table 4.1 lists depths and stratigraphic units. However, samples from the Aneth Unit H-117 core were not analyzed in this project, so data are presented only as a diagram in Chidsey and others, 2009, and in appendix H. The cores contained samples from the Hovenweep, Gothic, and Chimney Rock shale zones (see appendix H). The basic petrography is similar among the cores, and the predominant minerals are calcite, quartz, illite, dolomite, and ankerite, with smaller amounts of other carbonates, clays, and micas (figure 5.32). Specific attention was paid to the variations of quartz, carbonates, and clays at depth since these are indicators of the siltiness, brittleness, permeability, and other telling features of the rock that could indicate its candidacy for accessible hydrocarbons.

The Marie Ogden State 1 core captures both the Hovenweep and Gothic shales (table 4.1). The average wt% of quartz is similar in each of the shale zones, but slightly increases with depth and is therefore somewhat higher in the Gothic (figures 5.32 and 5.33). Both calcite and dolomite are present in each shale zone; however, the Hovenweep has predominantly calcite while Gothic has a significant portion of dolomite. Illite is the most abundant clay mineral and does not follow a distinctive pattern although its highest concentration is at 5224.8 to 5224.9 feet (1592.4–1592.5 m). Chlorite is another distinctive clay mineral, but again does not follow any observable trends (figure 5.34).

The Lake Canyon 1-27 core is made up of the Gothic and Chimney Rock shales. The clay content notably increases with depth in this core and the Chimney Rock has higher concentrations of both chlorite and illite (figure 5.34). The quartz does not show as a distinctive pattern, but is more abundant in the top part of the Gothic (figure 5.33). The Gothic also contains slightly more dolomite than the Chimney Rock.

The Mule 31-K-1 (N) core was taken from the Gothic and Chimney Rock shales. The mineralogy of the XRD samples is therefore very similar to the Lake Canyon core; however, these samples contained a higher percentage of dolomite and ankerite but less calcite (figure 5.32). Neither quartz nor clay shows a distinctive pattern and the concentrations of these minerals are similar between both shale zones (figures 5.33 and 5.34).

The Jefferson State 4-1 includes the Hovenweep and Gothic shale zones. The Gothic shale in this core contains more ankerite than the Gothic in previously mentioned cores. Quartz is in highest concentration at a depth of 5913.3 to 5913.6 feet (1802.3–1803.4 m), but otherwise does not show a distinctive pattern throughout the core. Chlorite and

illite increase toward the bottom of the Hovenweep and decrease toward the bottom of the Gothic (figure 5.34).

The Corbin Federal 1-2 core consists of only the Chimney Rock shale. It is the only core analyzed that contains greater wt% quartz than calcite (figure 5.33). The shale also contains higher concentrations of muscovite than other cores (figure 5.32). Only 5 feet (1.5 m) of this core was sampled, which makes it difficult to distinguish any variations of the minerals at depth.

The Cedar Point Federal 16.25 core also consists of only Chimney Rock shale. In this core, the shale contains similar minerals as in other places (calcite, quartz, illite, and dolomite), but also has distinctively high concentrations of muscovite and orthoclase (figure 5.32). The core sampled here also only spans about 5 feet (1.5 m), making vertical variations difficult to observe.

Limited XRD is probably typical of the two key lithologies involved (shale and silty dolomite), irrespective of the particular mudstone cycle. Undoubtedly, some mineralogic variation can be expected, but based on the extensive thin section examination, the basic mineralogic ingredients should be fairly consistent throughout the region.

Examples of the Gothic Shale, Aneth H-117 Well, Greater Aneth Oil Field

The nearly complete core of the Gothic shale from the Aneth Unit H-117 well (figure 4.3) in Greater Aneth oil field was not only ideal for a detailed description (appendix D), but also for a representative petrographic analysis. Thin section and SEM analyses were fundamental to the petrological description (appendices F and G). Thin section analyses of the selected Gothic shale samples are also used for petrological description of the lithofacies and to establish a baseline correlation of petrophysical properties to the petrology. They provide a screening tool for important shale parameters such as diagenetic alteration, cementation, and fracture fills. SEM analyses involved imaging of small, representative reservoir samples to identify clay morphology, kerogen location, and pore types.

The Gothic shale contains abundant carbonates and clays. Four basic lithotypes were identified from petrographic and SEM analyses of the Gothic: argillaceous shale, argillaceous mudstone, silty calcareous/argillaceous mudstone, and phosphatic argillaceous mudstone.

Argillaceous Shale

Argillaceous shale lithotypes in the Gothic shale show a clay matrix supporting a few elongate chert stringers (figure 5.35A). These likely represent microfossils, scattered pyrite, and silt, as well as silt-sized calcite crystals. Pyrite

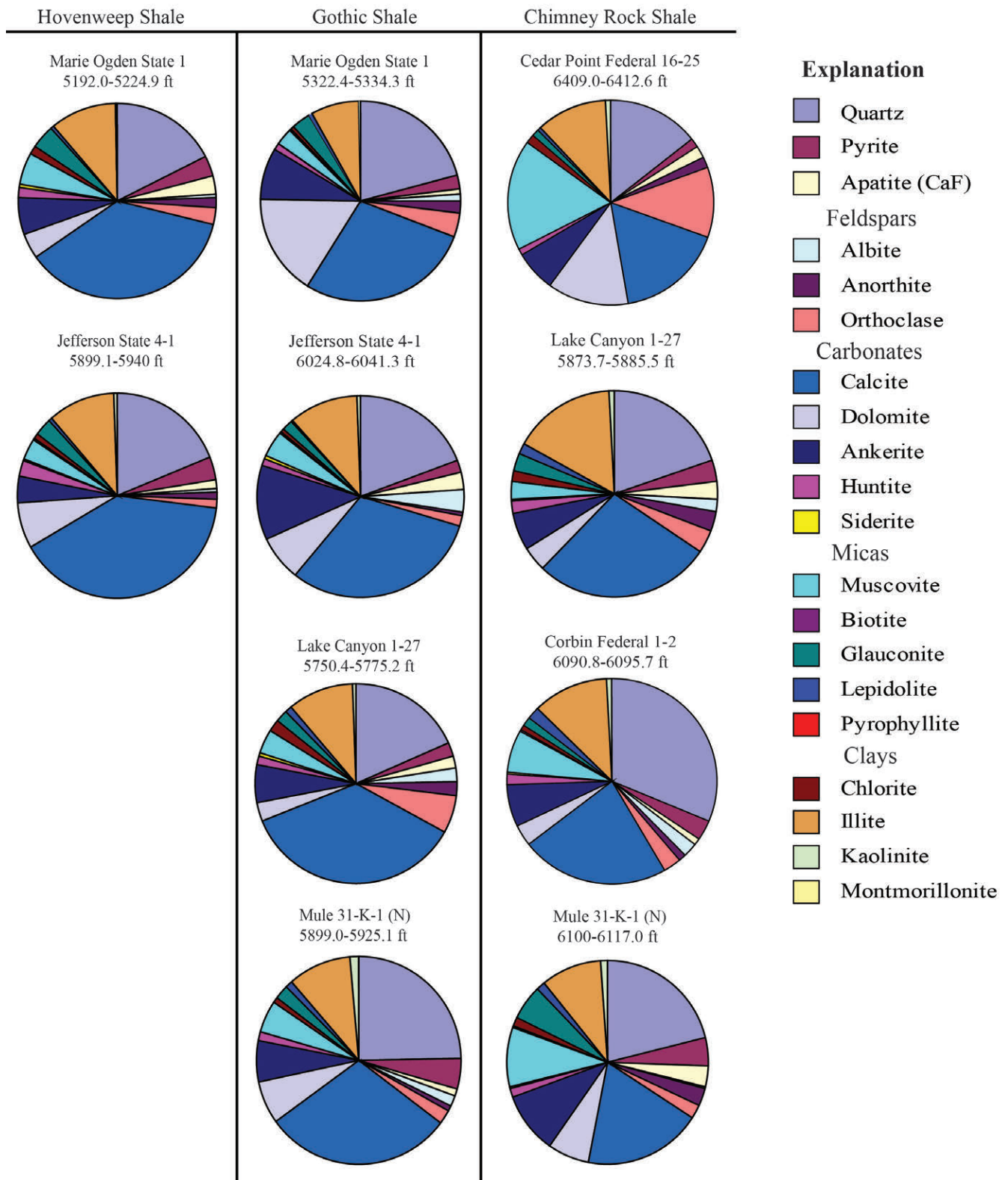


Figure 5.32. Pie charts showing the average mineral assemblages based on XRD of the Hovenweep, Gothic, and Chimney Rock shale zones taken from cores in the Paradox Formation. For detailed mineralogy see appendix H.

Quartz

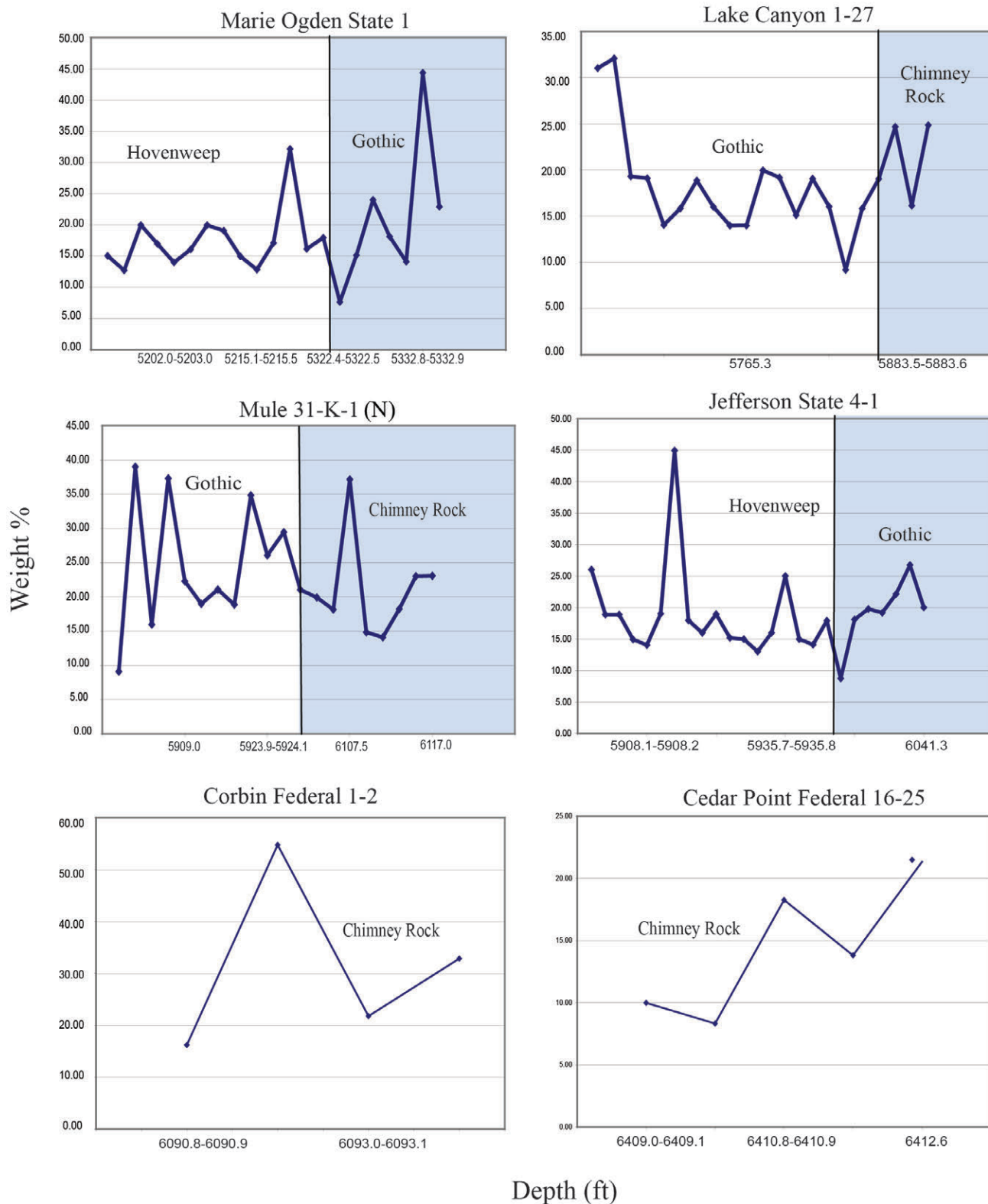


Figure 5.33. Weight percent of quartz in each core. Each point shows the wt % at a sampled depth. The blue shaded boundaries represent different shale zones found within a single core.

Illite + Chlorite

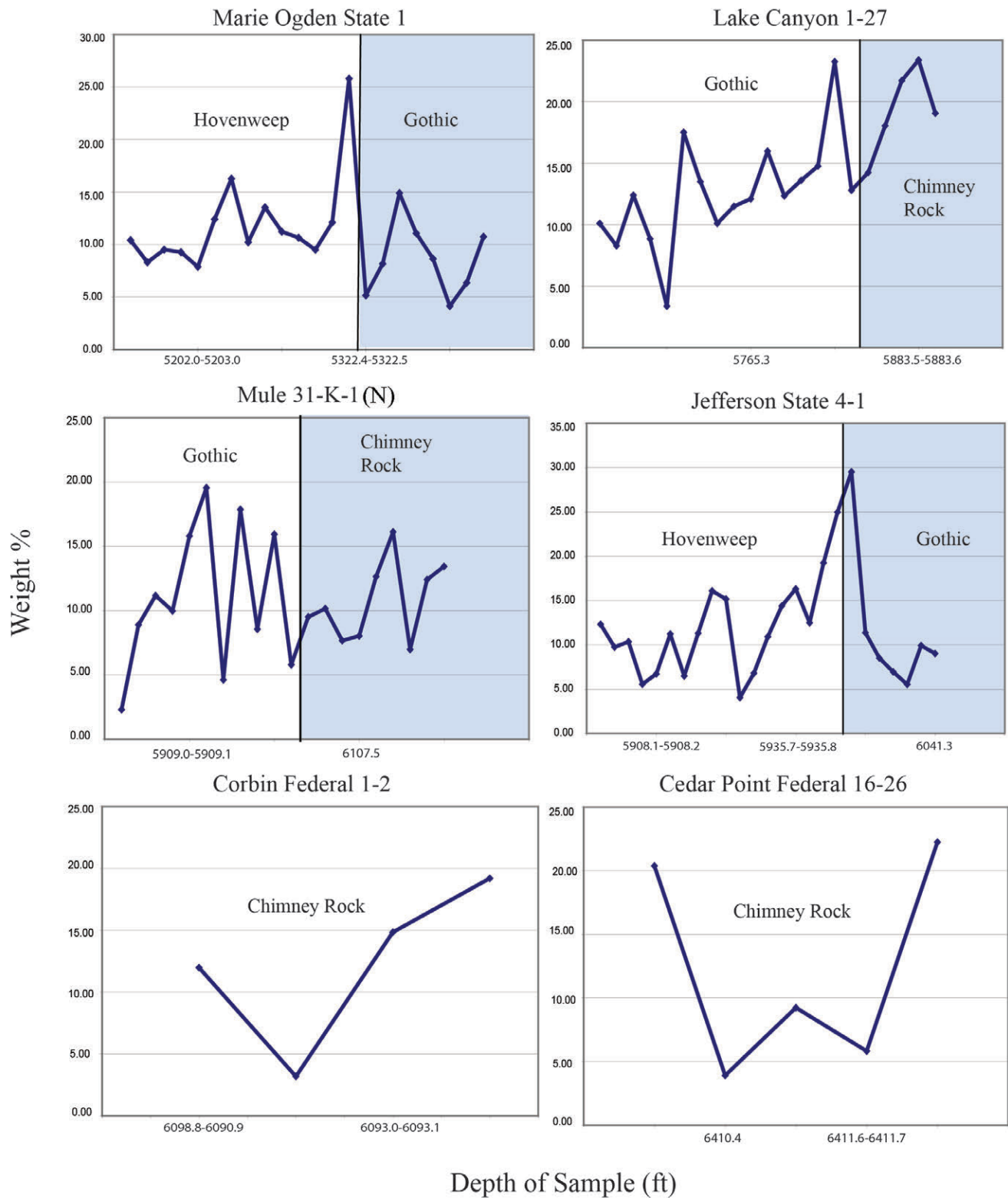


Figure 5.34. Weight percent of the sum of illite and chlorite in each core at a sampled depth. The blue shaded boundaries represent different shale zones found within a single core.

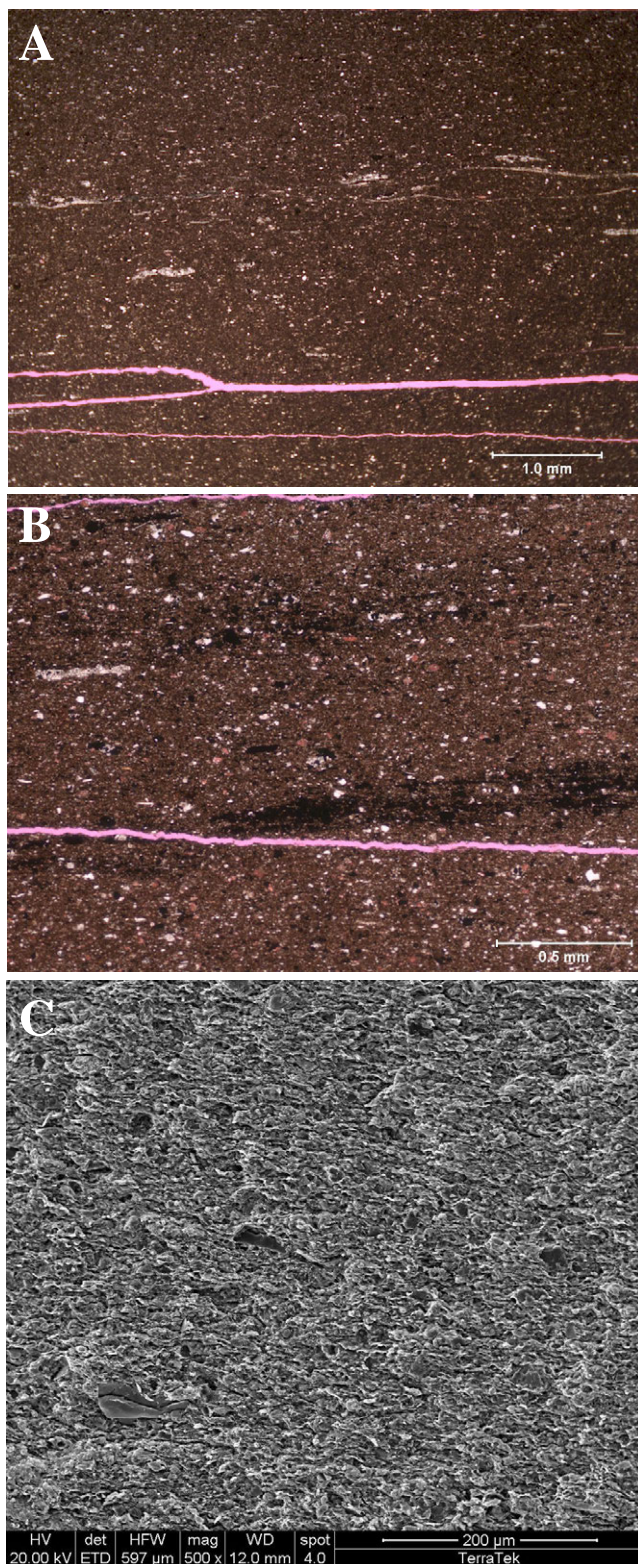


Figure 5.35. Argillaceous shale lithotype in Gothic shale from 5379.4 feet, Aneth Unit H-117 well. **A.** Photomicrograph of argillaceous shale lithotype in Gothic shale shown at low magnification. The magenta lines at the bottom of the image are induced stress-release fractures. **B.** Same image as 5.35A at slightly higher magnification. Black streaks are pyrite concentrated parallel to bedding. **C.** SEM overview of texture in uniform, laminated argillaceous shale.

is concentrated parallel to bedding (figure 5.35B). The SEM overview of this texture shows uniform, laminated argillaceous shale (figure 5.35C). A few siliceous and calcareous fragments float in a matrix of crenulated clays.

Argillaceous Mudstone

Argillaceous mudstone in the Gothic shale shows weak laminations defined by micas and compacted cherty microfossils (figure 5.36A). Mudstone contains silt-sized calcite particles. The argillaceous matrix also supports dispersed silt grains and compacted cherty microfossils in argillaceous mudstone matrix. Such forms are characteristic throughout this interval of Gothic shale, and commonly indicate microcrystalline quartz as a matrix cement. Reflected UV light displays swarms of intercrystalline micropores (figure 5.36B). SEM images of argillaceous mudstone display distinct grain orientation (figure 5.36C). Compacted packets of clays are the main textural feature, separated by planar parting surfaces. The clay-rich matrix hosts numerous micropores; authigenic pyrite is ubiquitous. Mudstone matrix has wavy parting planes between clay packets (figure 5.36D). Replaced microfossils are lined with kerogen residue. Matrix clays are likely illite and/or mixed layer illite-smectite. The matrix also shows unaltered and altered carbonaceous material (figure 5.36D).

Silty Calcareous/Argillaceous Mudstone

Silty calcareous/argillaceous mudstone consists of finely disseminated carbonaceous material and abundant silt grains (figure 5.37A). The dominant textural components in the matrix are quartz silt, silt-sized calcite, mica flakes, and authigenic pyrite that float in a predominantly clay matrix (figure 5.37B). SEM images of calcareous argillaceous mudstone confirm the presence of many calcite particles and quartz silt grains. Cement-coated clay flakes preserve the microporous structure (figure 5.37C). Elongate pores are parallel to parting planes and the micropore network consisting of flattened voids with sizes from 2 to 10 microns. Carbonaceous material is often preserved and commonly associated with pyrite (figure 5.37D). Intercrystalline porosity developed through alteration of organics.

Phosphatic Argillaceous Mudstone

Phosphatic argillaceous mudstone is a common component of the Gothic shale. It contains flattened, amalgamated pellets that are phosphatic in composition (figure 5.38A). Phosphatic argillaceous mudstone also includes compacted chert, siliceous fossils, micas, and flattened fecal pellets in a mixed siliceous/argillaceous matrix with a siliceous cement component (figure 5.38B). Micropores appear under UV light (figure 5.38B). SEM images of phosphatic argillaceous mudstone show the clay packets that make up the matrix are separated along parting surfaces, contributing to an unusual carbonate fissile texture (figure 5.38C). Flattened phosphatic/organic pods have granular internal textures along horizontal parting planes (figure 5.38D).

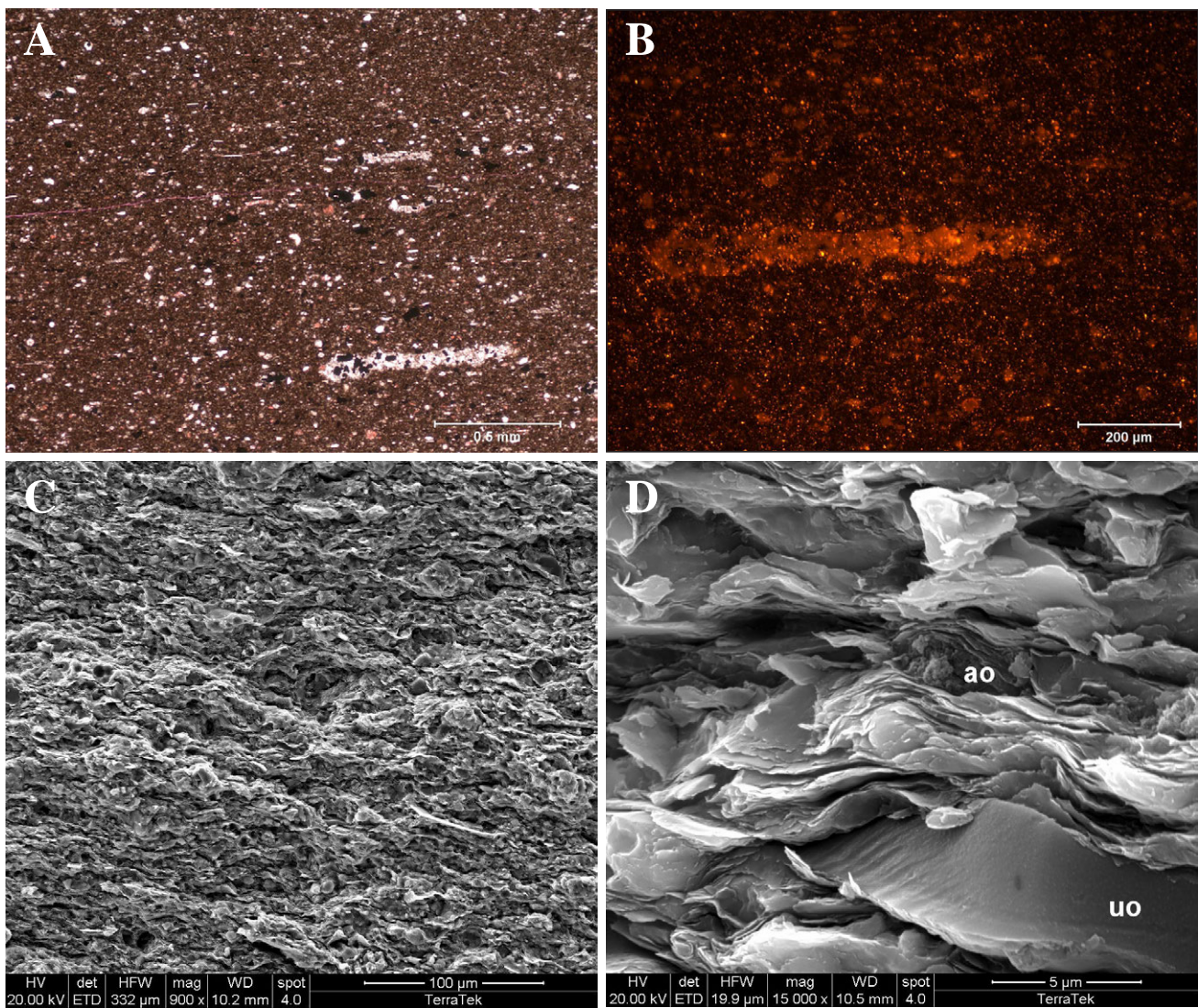


Figure 5.36. Argillaceous mudstone in Gothic shale from 5382.8 feet, Aneth Unit H-117 well. **A.** Photomicrograph of argillaceous mudstone showing weak lamination defined by micas and compacted cherty microfossils (white, lower right). Pink specks in the matrix are stained, silt-sized calcite particles. **B.** Reflected UV light with rhodamine filter showing a compacted cherty microfossil (grain at center) in the argillaceous mudstone matrix and swarms of orange pinpoints that indicate intercrystalline micropores. Brighter fluorescence inside a microfossil is attributed to mineral fluorescence. **C.** SEM overview of argillaceous mudstone highlighting distinct grain orientation. **D.** SEM matrix detail showing unaltered and altered carbonaceous material. The smooth particle at lower right (uo) represents a discrete carbonaceous grain with little alteration. At top center, a particle representing a different class of organics, embedded between clay flakes (ao), displays fuzzy, rough texture.

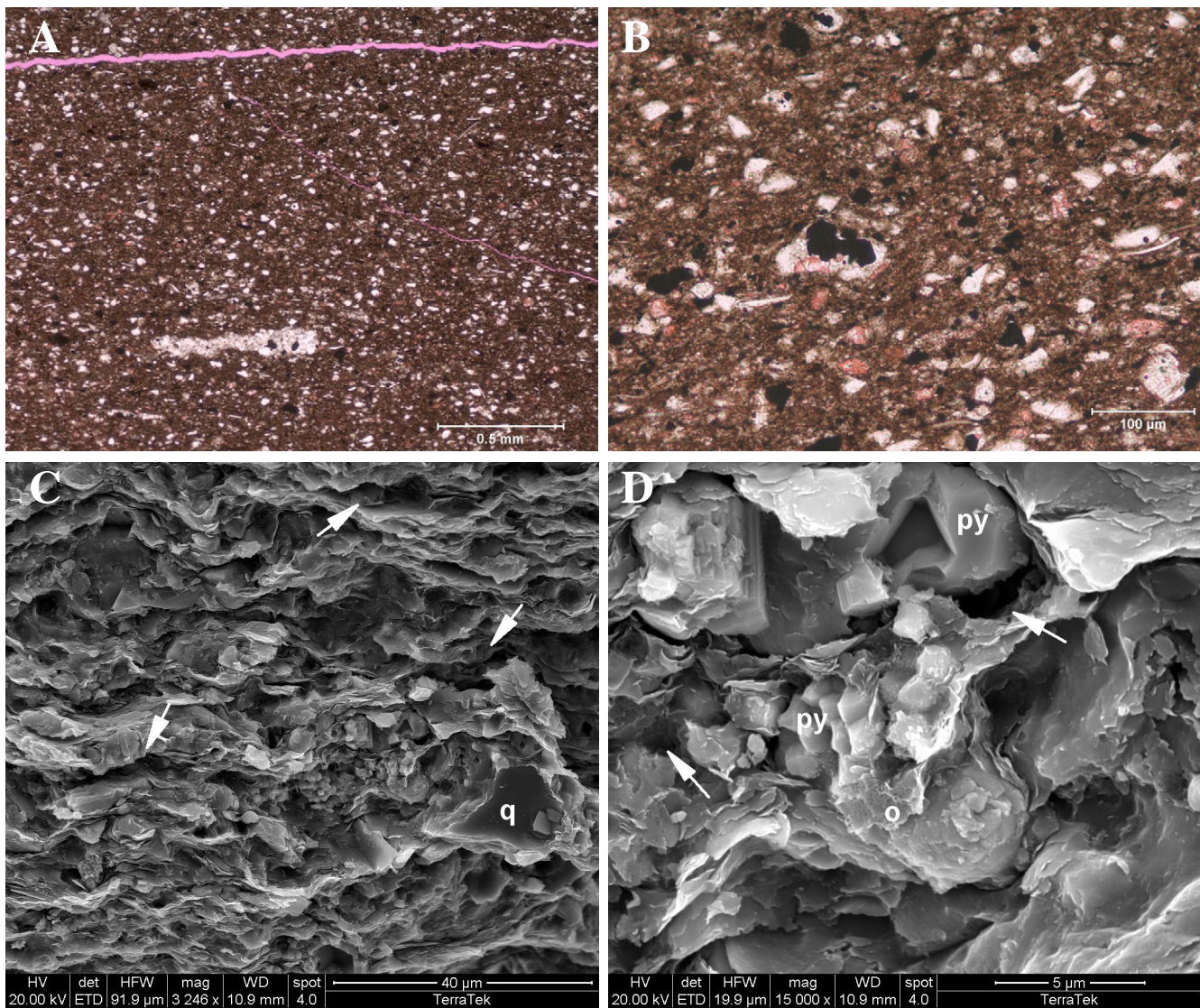


Figure 5.37. Silty calcareous/argillaceous mudstone in Gothic shale from 5386.9 feet, Aneth Unit H-117 well. **A.** Photomicrograph of silty calcareous/argillaceous mudstone with induced fracture at the top of the image (magenta). Finely disseminated carbonaceous material is visible in the matrix, as are abundant silt grains, calcite crystals (pink), and pyrite. Note cherty microfossil at bottom of image. **B.** Photomicrograph showing matrix detail highlighting dominant textural components. Quartz silt, silt-sized calcite (red), mica flakes, and authigenic pyrite float in a predominantly clay matrix. **C.** This medium-magnification SEM view of the matrix shows elongate pores parallel to parting planes (arrows). The micropore network is also visible, consisting of voids with sizes from 2 to 10 microns, and flattened in shape. The irregular grain at right is quartz (q). **D.** Image illustrates a common association of pyrite with carbonaceous material. The perforated flakes of organics (o) surround pyrite crystals (py). Intercrystalline porosity (arrows) is believed to have developed through alteration of organics.

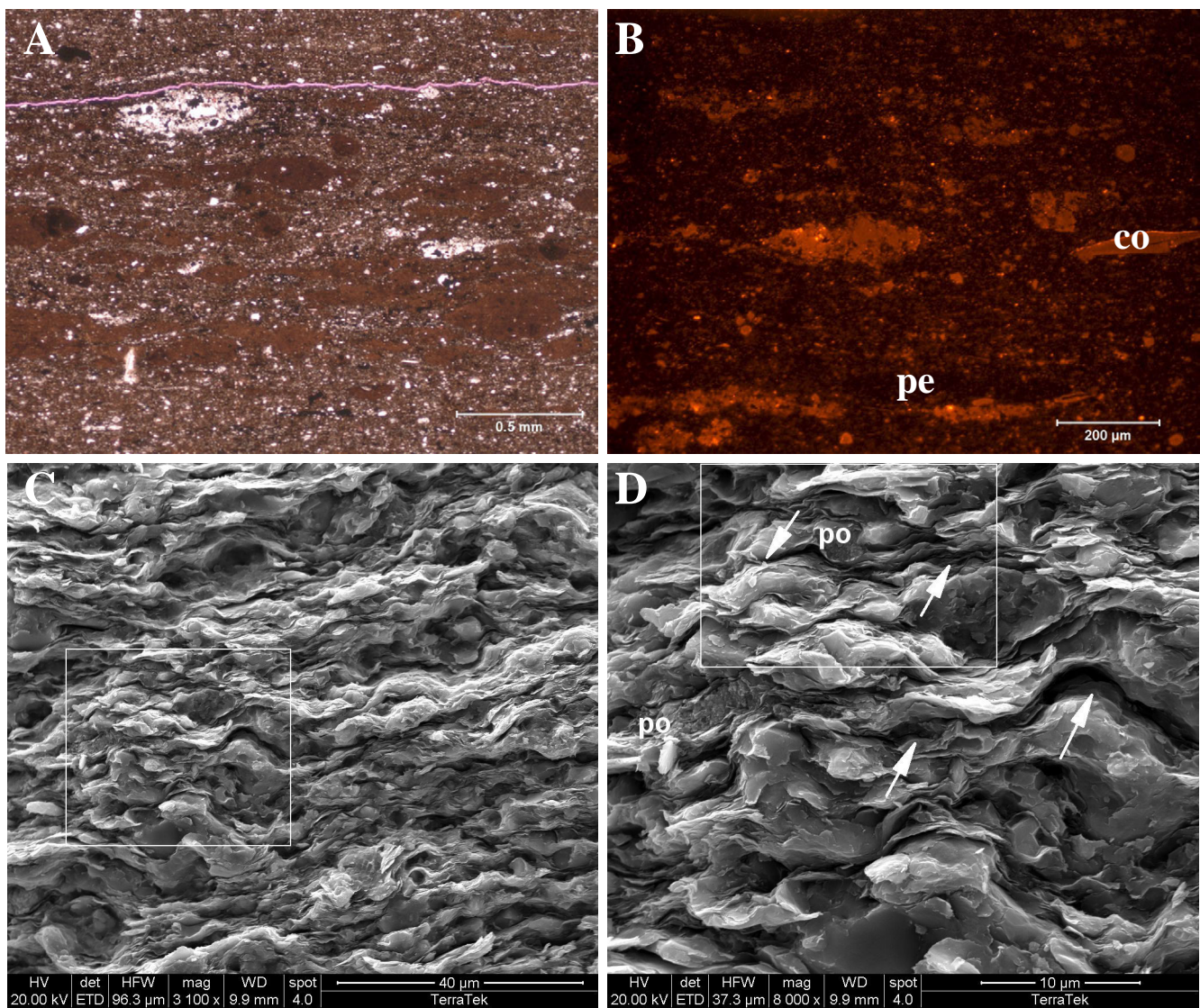


Figure 5.38. Phosphatic argillaceous mudstone in Gothic shale from 5390.8 feet, Aneth Unit H-117 well. **A.** Photomicrograph of overview showing flattened, amalgamated pellets (lighter brown), which SEM shows to be phosphatic in composition. The matrix overview highlights compacted siliceous forms (white) composed of chert, and flattened fecal pellets in a mixed siliceous/argillaceous matrix. The lighter brown matrix color and abundance of siliceous fossils, as well as phosphatic pellets suggest a siliceous matrix cement component. **B.** Closer view showing microfossils, micas, a fecal pellet (pe), and a conodont (co) supported by argillaceous matrix under reflected UV light. Note the matrix micropores appearing as bright orange dots. Dull orange is mineral fluorescence. (Reflected UV light with rhodamine filter.) **C.** Medium-magnification SEM view of phosphatic, argillaceous mudstone. Clay packets that make up the matrix are separated along parting surfaces, contributing to a fissile texture. The sample splits easily along closely spaced (<1 mm), brittle, wavy partings. The boxed area is enlarged in the image 5.38D. **D.** SEM detail of part of the image 5.38C highlighting two flattened phosphatic/organic pods (po) with granular internal texture arranged along horizontal parting planes (arrows). Inset represents close up of boxed area.

CHAPTER 6: GEOCHEMICAL ANALYSIS

BY

Steven Schamel, *GeoX Consulting, Inc.*;
Jeffrey Quick, Stephanie Carney, Rebekah W. Stimpson,
and Thomas C. Chidsey, Jr., *Utah Geological Survey*;
S. Robert Bereskin, *Bereskin and Associates, Inc.*

CONTENTS

INTRODUCTION	89
INTERPRETATIONS, MAPS, AND GRAPHS	89
Data Generation	89
Methods	89
MANNING CANYON SHALE/DOUGHNUT FORMATION	90
Organic Petrography	91
Thermal Maturity	93
Total Organic Carbon and Programmed Pyrolysis Geochemistry	95
Occurrences of Natural Gas	95
Interpretation of Regional Geochemical Data	98
PARADOX FORMATION	99
Thermal Maturity	101
Total Organic Carbon and Programmed Pyrolysis Geochemistry	103
Occurrences of Natural Gas	104
Interpretation of Regional Geochemical Data	106
Chimney Rock Shale	106
Gothic Shale	107
Hovenweep Shale	108

FIGURES

Figure 6.1. Photomicrographs of organic matter in the Doughnut Formation.....	90
Figure 6.2. Organic petrography of Doughnut Formation coal and dispersed organic matter relative to the siliciclastics cycles, Carbon Canal 5-12 core.....	91
Figure 6.3. Relative distribution of inertinite and vitrinite in coal and organic-rich shale, Carbon Canal 5-12 and Farnham Dome 1A wells	93
Figure 6.4. A first-order maturity trend of the Doughnut Formation.....	94
Figure 6.5. Vitrinite reflectance values for samples from the Carbon Canal 5-12 core.....	94
Figure 6.6. Vitrinite reflectance measurements in the Doughnut Formation plotted as a function of depth in wells from the northern San Rafael Swell area	94
Figure 6.7. Doughnut Formation total organic carbon and genetic potential in wells from the northern San Rafael Swell area.....	98
Figure 6.8. Total organic carbon and the programmed pyrolysis values plotted as a function of depth to show hydrocarbon potential, Carbon Canal 5-12 core.....	98
Figure 6.9. Doughnut Formation hydrogen and oxygen indices in wells from the northern San Rafael Swell area	98
Figure 6.10. Measured, calculated, and average vitrinite reflectance values from eight wells show the maturity of the Doughnut Formation is not correlated with present-day burial depth	98
Figure 6.11. Averaged maximum temperatures for wells penetrating the Doughnut Formation shale, northern San Rafael Swell area	99
Figure 6.12. Averaged total organic carbon for wells penetrating the Doughnut Formation shale, northern San Rafael Swell area	99
Figure 6.13. Averaged production index for wells penetrating the Doughnut Formation shale, northern San Rafael Swell area.....	99
Figure 6.14. Averaged vitrinite reflectance for wells penetrating the Doughnut Formation shale, northern San Rafael Swell area	100
Figure 6.15. Plot comparing the averaged hydrogen index and amount of total organic carbon for wells through the Doughnut Formation shale, northern San Rafael Swell area	100
Figure 6.16. Pseudo-van Krevelen plot of wells with hydrogen and oxygen index values for the Doughnut Formation shale, northern San Rafael Swell area	100
Figure 6.17. Logarithmic cross plot comparing amount of total organic carbon with the amount of generated hydrocarbons from the decomposition of kerogen, Doughnut Formation shale, northern San Rafael Swell area	100
Figure 6.18. Thermal maturity map of the Paradox Basin through the Ismay–Desert Creek interval, Paradox Formation.....	102
Figure 6.19. Location of the Gothic, Chimney Rock, Hovenweep Shale Oil and Gas assessments units in the Paradox Basin	103
Figure 6.20. Modified van Krevelen plot from the Ismay–Desert Creek interval	103

Figure 6.21. Pseudo-van Krevelen plots with hydrogen and oxygen index values for the Paradox Formation, Paradox Basin	105
Figure 6.22. Averaged maximum temperature for wells penetrating the Chimney Rock shale	106
Figure 6.23. Averaged total organic carbon in wells penetrating the Chimney Rock shale	106
Figure 6.24. Averaged production index for wells penetrating the Chimney Rock shale.....	106
Figure 6.25. Averaged calculated vitrinite reflectance for wells penetrating the Chimney Rock shale.....	107
Figure 6.26. Plot comparing the average hydrogen index and amount of total organic carbon for wells through the Chimney Rock shale	107
Figure 6.27. Pseudo-van Krevelen plot with hydrogen and oxygen index values for wells through the Chimney Rock shale	107
Figure 6.28. Logarithmic cross plot comparing amount of total organic carbon with the amount of generated hydrocarbons from the decomposition of kerogen, Chimney Rock shale	108
Figure 6.29. Averaged production index for wells penetrating the Gothic shale.....	108
Figure 6.30. Averaged maximum temperatures for wells penetrating the Gothic shale	108
Figure 6.31. Averaged vitrinite reflectance for wells penetrating the Gothic shale.....	109
Figure 6.32. Averaged total organic carbon for wells penetrating the Gothic shale	109
Figure 6.33. Pseudo-van Krevelen plot of wells through the Gothic shale	109
Figure 6.34. Plot comparing the average hydrogen index and amount of total organic carbon for wells through the Gothic shale	110
Figure 6.35. Logarithmic cross plot comparing amount of total organic carbon with the amount of generated hydrocarbons from the decomposition of kerogen, Gothic shale.....	110
Figure 6.36. Averaged production index for wells penetrating the Hovenweep shale.....	110
Figure 6.37. Averaged maximum temperatures for wells penetrating the Hovenweep shale.....	110
Figure 6.38. Averaged total organic carbon for wells penetrating the Hovenweep shale.....	111
Figure 6.39. Averaged vitrinite reflectance for wells penetrating the Hovenweep shale.....	111
Figure 6.40. Pseudo-van Krevelen plot of wells through the Hovenweep shale	111
Figure 6.41. Plot comparing the average hydrogen index and amount of total organic carbon for wells through the Hovenweep shale.....	112
Figure 6.42. Logarithmic cross plot comparing amount of total organic carbon with the amount of generated hydrocarbons from the decomposition of kerogen, Hovenweep shale	112

TABLES

Table 6.1. Petrographic descriptions from the Doughnut Formation, Carbon Canal 5-12 core	91
Table 6.2. Measured vitrinite reflectance values from carbonaceous to coaly cuttings and core samples from seven wells, northern San Rafael Swell area	92
Table 6.3. Pyrolysis analyses of cuttings and core samples from six wells, northern San Rafael Swell area	96
Table 6.4. Pyrolysis analyses of core samples from five wells in the Paradox Formation, Paradox Basin	101

CHAPTER 6:

GEOCHEMICAL ANALYSIS

INTRODUCTION

The two factors that are essential for successful development of potential shale gas reservoirs in Utah are gas content and gas deliverability (Schamel, 2005, 2006). Initial gas content of shale is determined primarily by the combination of organic richness, maturity (kerogen rank), and migration from the shale. These factors influence the storage of free, adsorbed, and dissolved gas in the shale beds as well as gas deliverability. The required gas content and deliverability characteristics of potential Utah shale-gas reservoirs should exist over areas several tens of square miles for exploration and development.

Although some geochemical data were already available at the beginning of this study, additional analyses of selected core and cuttings material helped fill the gaps in the existing data package, including TOC and R_o . For this project, we compiled programmed pyrolysis (RockEval™), TOC, and R_o data from 49 individual well core and cutting analyses to evaluate the potential of the Mississippian/Pennsylvanian Manning Canyon Shale/Doughnut Formation and the Chimney Rock, Gothic, and Hovenweep shales of the Pennsylvanian Paradox Formation. We present the data using bubble maps, scatter graphs, and pseudo-van Krevelen plots. These data were sourced from industry reports, public literature, and new analyses from cores at the Utah Core Research Center (appendices C and L).

INTERPRETATIONS, MAPS, AND GRAPHS

Data Generation

The data for various geochemical interpretations, maps, and graphs were generated from programmed pyrolysis—an important tool used to assess the hydrocarbon potential and thermal maturity of organic-carbon-rich rocks. Programmed heating of the rock samples results in volatile release of residual hydrocarbons. Data derived from programmed pyrolysis of a rock sample, explained below, includes: TOC; S1, S2, and S3; genetic potential; Tmax; the hydrogen, oxygen, and production indices; and R_o . Pyrolysis and TOC are also used to determine kerogen type. Types I and II kerogen will generate oil; type III gas; and type IV little or no hydrocarbon.

The TOC, measured in wt%, is the amount of remaining organic material within a rock sample derived from decaying vegetation, bacterial growth, and metabolic activities of organisms. S1 (S1 peak) is the amount of free hydrocarbons (HC,

oil or gas) available in the rock (measured in mg HC/g rock) as the sample is heated. At still higher temperatures hydrocarbons are generated by thermal decomposition (cracking) of kerogen, producing the S2 peak. Thus, S2 is the amount of hydrocarbons (mg HC/g rock) generated by pyrolytic degradation of the kerogen. The sum of the two hydrocarbon peaks in mg HC/g dry rock serves as a measure of the remaining source potential or the genetic potential (GP). The amount of carbon dioxide (CO₂) generated by pyrolysis is the S3 value (mg CO₂/g rock). The maximum temperature (Tmax) (°C) is the temperature at which the maximum release of hydrocarbons from thermal cracking of kerogen during pyrolysis occurs (the top of the S2 peak) (appendix L).

The hydrogen index (HI) is the quantity of hydrocarbons from kerogen cracking relative to the TOC in the sample ($HI = [100 \times S2]/TOC$). It is used to determine the origin of the organic matter. For example, marine organisms and algae are generally composed of lipid- and protein-rich organic matter. The ratio of hydrogen to carbon is higher than in the carbohydrate-rich organic matter from land plants. The oxygen index (OI) is the amount of carbon dioxide relative to the TOC, and the production index (PI) is the ratio of S1/(S1+S2). The OI correlates with the ratio of oxygen to carbon ($OI = [100 \times S3]/TOC$). It is high for polysaccharide-rich remains of land plants and residual organic matter encountered as background in marine sediments. The production (PI) shows the amount of hydrocarbons generated versus the total capable of being generated by the thermal breakdown of kerogen. It is used to characterize the evolution level of the organic matter (appendix L).

Vitrinite reflectance of the sample can be calculated using Tmax. The R_o gives a good indication of whether a sample is in the oil or gas window, immature, or overmature.

Methods

Of the 49 oil and gas wells with programmed pyrolysis, TOC, or R_o data, 8 wells had a full suite of data for the Manning Canyon Shale/Doughnut Formation and 2 wells had only measured R_o values, 17 wells for the Chimney Rock shale, 28 wells for the Gothic shale, and 16 wells for the Hovenweep shale. Multiple wells had data for all three Paradox Formation shales. Because programmed pyrolysis data was obtained for samples at multiple depths in each well core, we averaged the pyrolysis data for each well. These averaged data points, combined with averaged TOC and R_o values from other wells, were used to create bubble maps and plots.

Bubble maps for each shale unit were made to show the average TOC, R_o , Tmax, and PI of each well with data for that unit. The bubble maps were created in ArcGIS™ and are superimposed on topography via a digital elevation model to show well locations relative to physiographic provinces within Utah.

Each shale has three plots comparing the programmed pyrolysis data: (1) Pseudo-van Krevelen plots (OI versus HI), (2) HI versus TOC, and (3) TOC versus S2. Pseudo-van Krevelen plots show whether the shales are currently in the oil or gas window or if they are thermally mature and not likely to produce hydrocarbons. The HI versus TOC plots show the kerogen quality of the sample (oil prone versus gas prone). The TOC versus S2 plot is used to determine the amount of hydrogen associated with organic matter.

MANNING CANYON SHALE/ DOUGHNUT FORMATION

Organic matter is ubiquitous and sometimes abundant in the Manning Canyon Shale/Doughnut Formation. Many of the shale and argillaceous limestone beds are clearly carbonaceous, or even “sooty” or “coaly” in appearance. Organic matter occurs in a wide variety of petrographic expressions. Most commonly, the organics are finely disseminated grains (figure 6.1A) segregated in darker laminae together with clays and pyrite, or uniformly scattered through the rock matrix. In many instances, the organic matter is recognizable as discrete plant tissue fragments (figures 6.1B and 6.1C). Where organics are concentrated in laminations, plant parts can be seen on the bedding surfaces broken on the laminations. Leaf veining and striations on coaly fragments make the plant fragments easy to identify (figure 6.1B). In other instances, much less common in the thin sections examined, enough of the plant

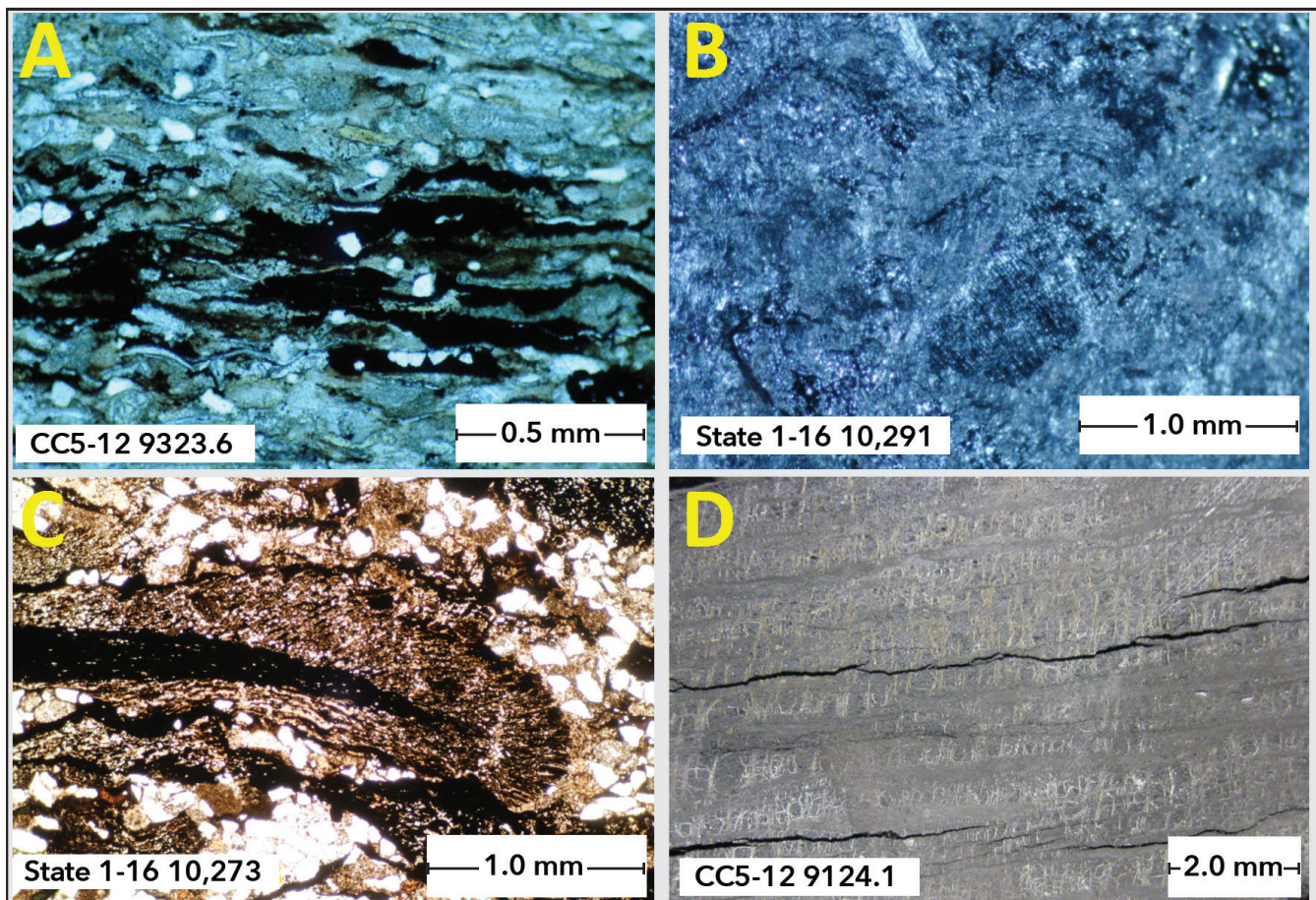


Figure 6.1. Photomicrograph of organic matter in the Doughnut Formation. **A.** Dispersed coaly terrestrial plant fragments in a silty carbonate packstone. The organic matter is segregated in a very dark gray lamination. Carbon Canal 5-12 well, 9323.6 feet. **B.** Discrete terrestrial plant fragments on the bedding surface within thinly laminated siltstone. Note the surface veining preserved on many of the leaf particles and the black, fractured coaly fragments. State 1-16 well, 10,291 feet. **C.** Discrete segment of a fern-like frond, possibly of the genus *Crossopteris* (Tidwell, 1998). The fragment is part of a dark lamination siltstone (also see appendix I, plate 6). State 1-16 well, 10,273 feet. **D.** Coal bed expressed as sub-millimeter laminae separated by even thinner clay- and pyrite-rich laminae. The coal is recognized by the subvertical network of hairline calcite-filled fractures. Carbon Canal 5-12 well, 9224.1 feet.

fragment is preserved to recognize the plant vadose structures (figure 6.1C). The Carbon Canal 5-12 (figure 3.2) core sampled four thin coal beds (figure 5.17). A common characteristic of these coal beds is distinct laminar bedding (figure 6.1D), even with thin laminations rich in shell fragments (appendix I, plate I-3). Many of the coals grade into carbonaceous shale, or are interbedded with carbonaceous shale on a scale of millimeters. In several of the wells examined only in cuttings, most notably Farnham Dome 1-A (figures 3.1 and 5.3), intervals were encountered dominated by coaly fragments, possibly from several net feet of distinct coal beds.

Organic Petrography

In investigating the palynology of the Manning Canyon Shale/Doughnut Formation (chapter 8 and appendix O), concentrates of the organic matter were prepared by acid reduction of the rock samples. This preparation liberates the organic matter (kerogen), which can then be examined using a transmitted light microscope. In 14 samples from the Doughnut Formation in the Carbon Canal 5-12 core, amorphous kerogen averaged 70%, ranging between 5% and 90% of the sample. Woody and inert kerogen averaged 15% (ranging from 5 to 40%) and cuticular kerogen averaged 10% (ranging from 5 to 30%). The 14 samples were dominantly carbonaceous laminar shale and limestone (lithotypes 7 and 6) and black shale (lithotype 10) (figure 5.9).

For organic petrography, core fragments and cuttings rich in coaly material were mounted in epoxy plugs and polished for examination in reflected light. Whereas transmitted light analyses of organic matter isolated with acid generally show relatively abundant amorphous kerogen, reflected light analysis

of whole rock specimens showed variable amounts of inertinite, vitrinite, and solid bitumen. Consistent with the relatively high maturity of these rocks, liptinite group macerals were not observed. Table 6.1 and figure 6.2 show petrographic observations for samples from the Carbon Canal core. Table 6.2 lists some petrographic observations made during vitrinite reflectance analyses.

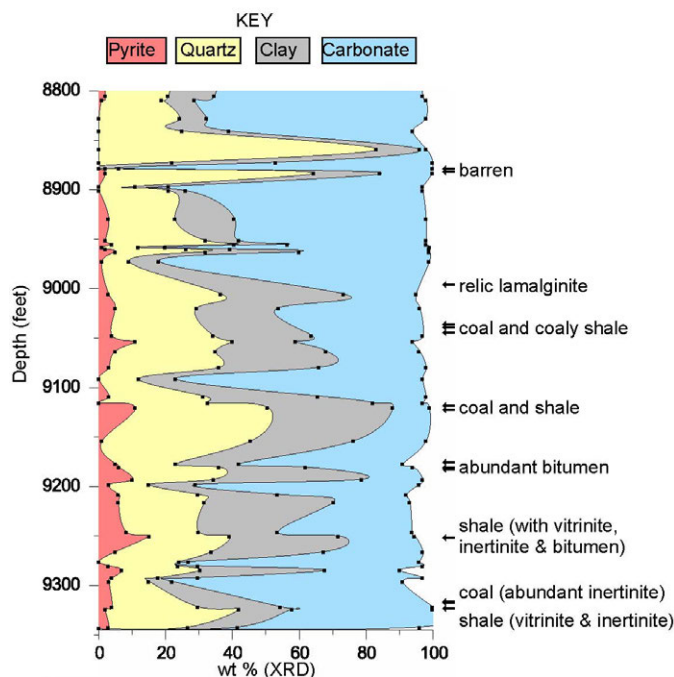


Figure 6.2. Organic petrography of Doughnut Formation coal and dispersed organic matter relative to the siliciclastics cycles in the Carbon Canal 5-12 core.

Table 6.1. Petrographic descriptions of polished specimens from the Doughnut Formation in the Carbon Canal 5-12 core examined with the reflected light microscope.

ID	Depth (ft)	Description
L6	8881	barren, abundant quartz, rare pyrite
L7	8884	barren, abundant quartz, rare pyrite
M2	8998	abundant lamalginites in carbonate matrix, rare vitrinite and inertinite, rare pyrite
CC1	9038	coal , 20% inertinite, massive pyrite
L8	9041	sparse, small organic fragments in calcareous shale, abundant pyrite, a few oolites, relic colonial algae mineral structures(?)
L9	9046	sparse, small organic fragments in calcareous shale, abundant pyrite, a few oolites, relic colonial algae mineral structures(?)
L11	9120	small vitrinite and inertinite fragments in shale, homogeneous bitumen between quartz grains
CC2	9124	coal , 10% inertinite, abundant clay & pyrite
L4	9177	sparse, small vitrinite and inertinite fragments in shale, rare granular bitumen, abundant pyrite
L5	9182	abundant inertinite, abundant granular bitumen, abundant pyrite
L10	9184	abundant granular bitumen dispersed in shale matrix, some vitrinite and inertinite, abundant pyrite
M7	9253	shale with carbonate in fractures, small vitrinite and inertinite fragments, likely bitumen, some pyrite
CC3	9317	coal with shale, shale contains abundant inertinite , abundant pyrite
CC4	9318	coal, 90% inertinite , abundant framboids
L1	9324	shale, abundant inertinite , abundant pyrite
L2	9324	shale, vitrinite and inertinite present, abundant pyrite

Table 6.2. Measured vitrinite reflectance values from carbonaceous to coaly cuttings and core samples from seven wells in the northern San Rafael Swell area. References (Ref) to source of the data: A = analysis for this study by the UGS; B = analyses by Core Laboratory as reported in Grover (2008). Of the 49 analyses are reported, 29 are on core samples and the remainder on well cuttings. See figure 3.1 for well locations.

Well name/location	Depth (ft)	Ref	R _o % measured	number of measurements	notes
Arcadia-Telonis 1 19 - 14S - 9E	12,025	A	1.42	12	cuttings
	12,055	A	1.39	21	cuttings
	12,285	A	1.36	16	cuttings
	12,355	A	1.45	10	cuttings
Carbon Canal 5-12 12 - 16S - 10E	9038	A	1.49	53	core, coal, 20% inertinite, framboid & massive pyrite in core
	9124	A	1.40	50	core, coal, 10% inertinite, abnt clay & sulfides
	9318	A	1.48	49	core, coal with shale, 30% inertinite, abnt small sulfides
	9319	A	1.59	25	shaly, 90% inertinite, abnt framboids
	8929	B	1.20		core
	9006	B	1.19		core
	9019	B	1.23		core
	9048	B	1.23		core
	9054	B	1.22		core
	9063	B	1.20		core
	9115	B	1.25		core
	9177	B	1.26		core
	9181	B	1.26		core
	9193	B	1.28		core
	9208	B	1.26		core
	9215	B	1.26		core
	9250	B	1.59		core
	9266	B	1.59		core
9285	B	1.62		core	
9322	B	1.64		core	
9333	B	1.80		core	
Farnham Dome 1-A 8 - 15S - 12E	7343	A	1.69	44	cuttings, coal with shale, 70% inertinite, minor sulfides
	7368	A	1.72	39	cuttings, coal with shale, 60% inertinite, minor sulfides
	7403	A	1.69	23	cuttings, coal with shale, 80% inertinite, minor sulfides
Fed Mounds 1 11 - 16S - 11E	7065	A	1.42	19	cuttings
	7205	A	1.43	22	cuttings
	7305	A	1.44	24	cuttings
	7345	A	1.40	25	cuttings
Miller Creek 1 26 - 15S - 10E	8365	A	1.28	27	cuttings, abnt coal particles
	8415	A	1.38	17	cuttings
	8705	A	1.33	19	cuttings
	8785	A	1.32	18	cuttings, small organic fragments
North Springs 1 27 - 15S - 9E	10,740	A	1.69	67	cuttings, sparse pyrite, low confidence
State 1-16 16 - 14S - 11E	10,291	A	1.67	52	cuttings, abnt inertinite
	10,365	A	1.75	18	cuttings
	10,435	A	1.71	19	cuttings
	10,685	A	1.77	15	cuttings, good vitrinite population

The inertinite content of some samples is unusually high (near 90%), especially in the carbonaceous shales, as opposed to the coals (figure 6.3). Inertinite in the Doughnut Formation likely originated as the charred remnants of partially burned woody plants or peat. Large, thick-walled inertinite fragments observed in some of the coals are consistent with subsurface peat fires and/or subaerial oxidation (smoldering) of decomposed wood. Inertinite fragments dispersed in shale were uniformly small and thin-walled, consistent with eolian transport and sorting of charred plant material from distant, upland fires.

Given the identification of abundant terrestrial plant parts and the observation that only spores from terrestrial flora are present in the formation, it is understandable that inertinite is common. Diessel (2010) observed that the increasing abundance of inertinite in coal during the mid- and late-Paleozoic correlates with increasing atmospheric oxygen during this time. Indeed, using inertinite (charcoal) abundance as a proxy for wildfires, Scott and Glasspool (2006) had earlier proposed that fires became increasingly widespread and common through the Carboniferous and were especially significant during the Permian, when the modeled atmospheric O_2 approached 30%. During the Late Mississippian modeled atmospheric O_2 was about 25%, which is higher than the present-day concentration (~21%). Accordingly, the sometimes abundant inertinite in the Doughnut Formation/Manning Canyon Shale can be considered an early record of globally significant wildfire.

Thermal Maturity

Samples selected for measurement of R_o are from cuttings and core from wells on the crest and broad western flank of the northern San Rafael Swell (table 6.2). Of the 41 R_o measurements, about half are from core samples and the remainder are from cuttings. The vitrinite reflectance values vary from about 1.2 to 1.8% R_o (figure 6.4 and table 6.2), which is within the dry gas generative window (figure 6.4). The selected wells represent a wide range of present-day depths of burial, from 7000 feet (2100 m) (Federal Mounds 1) on the crest of the anticline to over 12,000 feet (4000 m) (Arcadia-Telonis 1) on the edge of the Wasatch Plateau (figure 3.1).

Reflectance analyses undertaken at the Utah Geological Survey (Lab A, figure 6.5) for four coal samples from the Carbon Canal 5-12 core varied from 1.4 to 1.6% R_o . Vitrinite reflectance values reported by a commercial lab (Lab B, figure 6.5) for 17 samples collected from this core exhibited more variation, ranging from 1.2 to 1.8% R_o over a 404-foot (123 m) interval. This range of variation is unlikely.

Several factors likely contributed to the different results from these labs. Above about 1% R_o , vitrinite reflectance

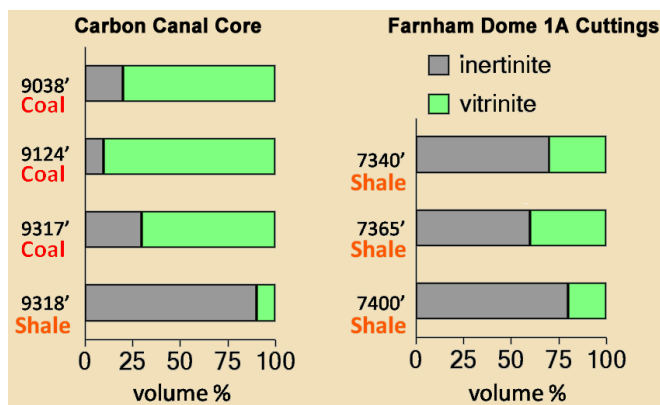


Figure 6.3. Relative abundance of inertinite and vitrinite in coal and organic-rich shale in the Carbon Canal 5-12 and Farnham Dome 1A wells. Note that the coal samples are enriched in vitrinite, whereas the shale samples are enriched in inertinite.

increasingly varies with particle orientation; higher reflectance values are obtained from bedding plane surfaces whereas lower reflectance values are obtained from surfaces that are perpendicular to the bedding plane. The commercial lab specimens were likely cutoff blanks produced during preparation of thin sections used for transmitted light analyses; these specimens would cut the bedding plane at 90° and show lower reflectance values than the UGS coal specimens, which were made from crushed and randomly oriented particles. Whereas low reflectance values might be attributed to particle orientation and optical anisotropy, high reflectance values can be attributed to maceral identification and sample lithology. Although it is easy to identify vitrinite in coal, it is more difficult to identify vitrinite that is dispersed in mineral-rich rocks. This difficulty increases where vitrinite is rare but inertinite is abundant. In these instances inertinite can be mistaken for vitrinite, resulting in erroneously high reflectance values. Indeed, the abundance of inertinite in the Doughnut Formation shale was not fully appreciated until examination of the Carbon Canal 5-12 coal sample at 9318 feet (2840 m) revealed a remarkable 90% inertinite content. The inertinite in this sample was dominated by thin-walled inertinite particles with a classic bogen (star) structure. This key observation improved recognition of similar inertinite particles in other specimens from Doughnut shale. Finally, estimated reflectance values calculated from RockEval Tmax values (where S2 values were >1 mg HC/g) are consistent with measured reflectance values near 1.4% R_o .

Figure 6.6 shows that R_o is not correlated with depth of the Doughnut Formation, as would be expected if the basin had been tectonically stable following the time of peak thermal maturity. Indeed, the deepest samples have the same R_o values as the shallowest, even across a depth difference of 5000 feet (1500 m). The absence of a depth- R_o relationship indicates that the peak of maturity was reached prior to uplift of the San Rafael Swell.

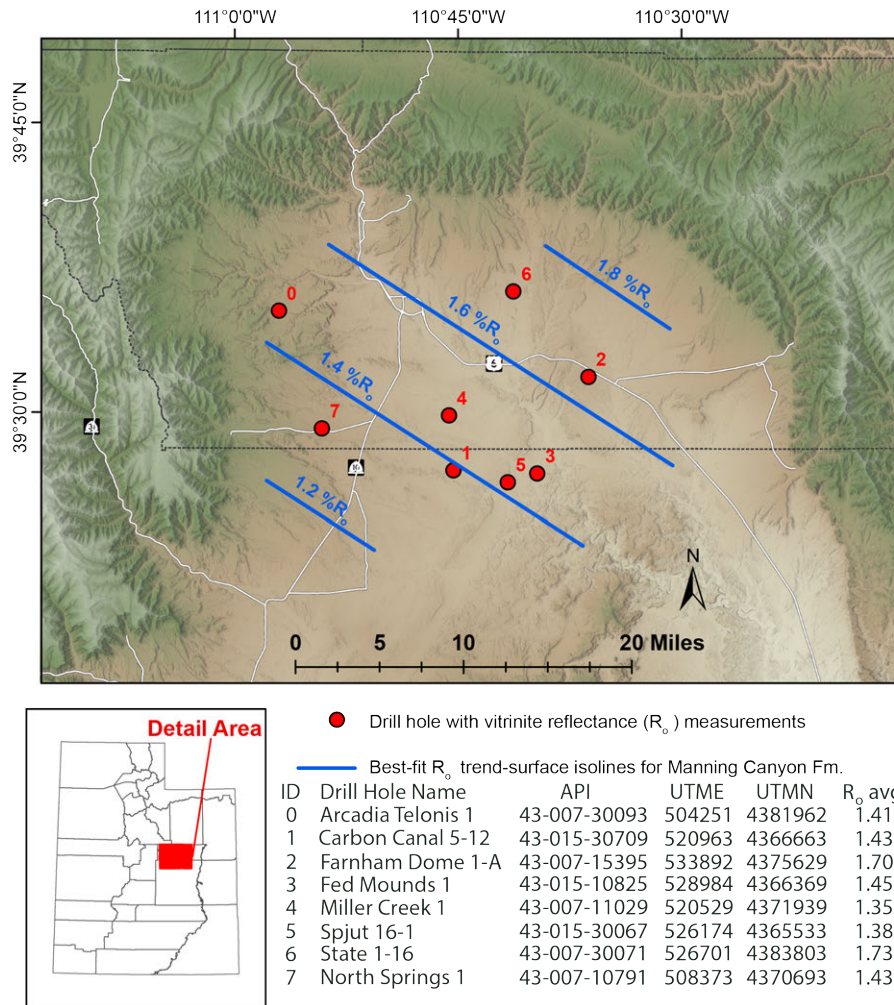


Figure 6.4. A first-order trend surface shows increasing maturity of the Doughnut Formation towards the northeast. The equation: $R_o = -9.739E^{-6} UTME + 1.4918E^{-5} UTMN - 68.83$, had an adjusted R^2 of 0.68, and a standard error of 0.08, where UTME and UTMN are the Universal Transverse Mercator easting (E) and northing (N) geographic coordinates (North American Datum, 1983). Basemap source: ArcMap Bing hybrid basemap. R_o values (R_o avg) used to create the trend surface were calculated using UGS measured R_o values (table 6.2) and R_o values derived from RockEval™ assays (table 6.3).

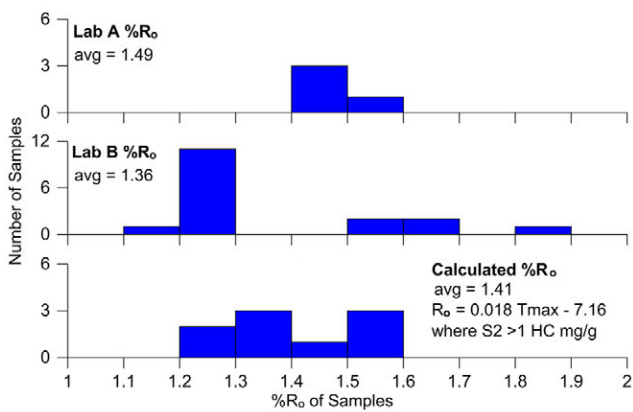


Figure 6.5. Relatively uniform vitrinite reflectance values were reported by Lab A (UGS) for four coal samples from this core, as were vitrinite reflectance values calculated from programmed pyrolysis analyses. Vitrinite reflectance values reported by Lab B (Grover, 2008) for 17 samples from a several-hundred-foot interval of the Carbon Canal 5-12 core show a large and unlikely range of variation.

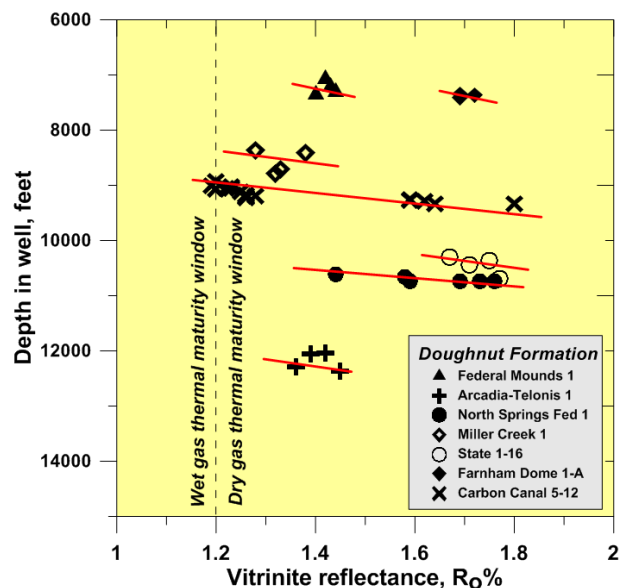


Figure 6.6. Vitrinite reflectance measurements in the Doughnut Formation plotted as a function of depth in wells from the northern San Rafael Swell area.

Stratigraphic evidence (Molenaar and Cobban, 1991) suggests that uplift began possibly in the Turonian (94–89 Ma). It continued at least through the youngest members of the Eocene Green River Formation deformed in the Bruin Point-Mount Bartles flexure (Covington and Young, 1985) near Sunnyside on the northeast flank of the San Rafael arch. Major uplift ended by the close of the early Eocene (48.6 Ma). Peak thermal maturity can be no younger than this time, and it may have been earlier. A burial history model for the Carbon Canal 5-12 well discussed in chapter 9 estimates the time for entry of the base of the Doughnut Formation into the dry gas window (1.35% R_o) at 46 Ma and the maximum R_o reached as 1.45%. In a burial history analysis of the deep Paradox Basin, Rasmussen and Rasmussen (2009) modeled a well to the southeast of the Oquirrh sag, the Norris Federal 1 in section 8, T. 18 S., R. 16 E., SLBL&M, east of the Woodside Federal 1 well (figure 3.1). The Cane Creek shale (Pennsylvanian Paradox Formation), misidentified as Manning Canyon Shale in the driller's report, has an estimated present-day R_o of 0.88% and reached peak thermal maturity at 82.2 Ma.

Total Organic Carbon and Programmed Pyrolysis Geochemistry

A total of 71 TOC and programmed pyrolysis (RockEvalTM) analyses for samples of Doughnut Formation from 8 wells have been compiled for this study (table 6.3). Two additional wells had only R_o and were not included in table 6.3. Thirty-three of the analyses were performed on core material; the other 38 are on cleaned cuttings. The analyses are from three service companies: TerraTek Schlumberger performed analyses for this study, Core Laboratories performed analyses on the Carbon Canal 5-12 core samples and are reported in Grover (2008), and Humble Geochemical Services performed analyses found in UGS in-house files. The source of the data and the type of sample are identified in table 6.3 (all geochemical data can be found in appendix L).

The TOC measured in the Doughnut Formation for this study (table 6.3) averages 4.11 ± 8.17 wt% ranging from a low of 0.09 wt% in a silty limestone (Drunkards Wash 31-1, D-1 on plate I-5, appendix I) to a high of 61.7 wt% in coal-rich cuttings (Farnham Dome 1-A). From the standpoint of TOC these appear to be good to excellent source rocks. However, TOC describes only the quantity of organic carbon, not its quality, i.e., its potential for generating hydrocarbons (Peters and Cassa, 1994).

In rocks within the dry gas generative window, both the residual hydrocarbons and the remaining kerogen have been converted to natural gas, which is not detected by programmed pyrolysis analysis. Therefore, it is not surprising that the GP of the Doughnut Formation samples tends to be low relative to their TOC (figure 6.7). The average GP

is just 2.44 ± 3.90 mg HC/g dry rock. The average S1 and S2 values are 0.60 ± 0.52 and 1.84 ± 3.56 , respectively. As a source rock, the formation is largely spent. An exception may be a short interval in the Carbon Canal 5-12 core where the TOC and genetic potential (S1 + S2) are exceptionally high (figure 6.8).

The HI ranges between 1 and 79 (figure 6.9) and has a median value of 39, which is very near the average value of 37 ± 18 (table 6.3). The OI ranges between 2 and 100 (figure 6.9) and has a median value of 11, which is lower than the average value 18 ± 19 . Hydrogen index values less than 50 characterize type 4 kerogen, “dead carbon,” dominated by inertinite macerals or “spent” organic carbon in the dry gas generative window that is no longer capable of generating hydrocarbons.

The thermal maturity of the rocks can be inferred from the temperature at the peak of the S2 curve, the Tmax parameter (table 6.3). Tmax is most reliable when the S2 peak is large enough for the peak to be resolved on the pyrogram. Where the S2 peak is greater than 1 mg HC/g, the Tmax averages 891°F (477°C), corresponding to a calculated vitrinite reflectance of 1.42 % R_o . Indeed, with rare exception, the calculated R_o values (table 6.3) are similar to the measured values described above (figure 6.10). Moreover, combining both the measured and calculated R_o data allowed calculation of the average maturity of the Doughnut Formation in eight wells. A first-order trend surface for these wells showed a significant trend of increasing maturity to the northeast (figure 6.4).

Occurrences of Natural Gas

Markers in the Carbon Canal 5-12 core boxes indicate that 42 samples 1 foot (0.3 m) in length were removed from the Doughnut Formation for gas desorption analyses. Eleven such samples were removed from the overlying Round Valley Limestone portion of the core. In many instances, multiple gas desorption samples were taken from single intervals. Commonly, a core sample generally slightly less than a foot in length was sealed in a Mylar pouch and left in the core box. Down to the depth of 9057.5 feet (2760.6 m) these pouches show no evidence of inflation caused by gas release from the core. However, the sealed pouches between 9057.5 and 9248.1 feet (2760.6–2818.7 m) are clearly inflated indicating gas expulsion. The pouch at 9141.9 feet (2786.3 m) is inflated to near bursting. Locations of the inflated sealed pouches are indicated in figure 5.7 as black dots. The actual gas desorption measurements were not made available to the UGS for this study.

The Carbon Canal 5-12 well was production tested shortly after the well was completed as described in chapter 3. The flow rate over a 63-hour period from the interval from 9030 to 9350 feet (2752–2850 m) was 178 MCF/DPD (5.0

Table 6.3. Programmed pyrolysis (RockEval™) analyses of cuttings and core samples from 8 wells in the northern San Rafael Swell area. Seventy-one analyses are reported, 33 of which are on core samples and 38 on well cuttings. See figure 3.1 for well locations.

Well name/location	Depth ¹ (ft)	TOC ²	S1 ³	S2 ⁴	S3 ⁵	Tmax ⁶	R _o % calc ⁷	HI ⁸	OI ⁹	PI ¹⁰	GP ¹¹	Ref ¹²
Carbon Canal 5-12 12 - 16S - 10E	8929	1.01	0.03	0.01	0.60	407	NA	1	60	0.74	0.04	B
	9006	3.14	0.01	0.03	0.42	256	NA	1	13	0.24	0.04	B
	9019	0.74	0.01	0.01	0.38	230	NA	1	52	0.50	0.02	B
	9048	1.80	0.24	0.30	0.49	416	NA	17	27	0.45	0.54	B
	9054	4.22	0.01	0.03	0.23	282	NA	1	5	0.25	0.04	B
	9063	1.58	0.49	0.36	0.50	399	NA	23	32	0.58	0.85	B
	9115	1.69	0.37	0.48	0.51	418	NA	28	30	0.43	0.85	B
	9145	1.90	0.17	0.87	0.19	500	NA	46	10	0.16	1.04	A
	9177	3.13	0.93	1.55	0.41	467	1.25	50	13	0.38	2.48	B
	9181	3.48	0.71	1.16	0.41	469	1.28	33	12	0.38	1.87	B
	9193	1.79	0.62	0.71	0.38	462	1.16	40	21	0.46	1.33	B
	9208	4.48	1.77	3.54	0.49	474	1.37	79	11	0.33	5.31	B
	9215	7.33	1.58	3.79	0.46	478	1.44	52	6	0.29	5.37	B
	9216	7.33	1.12	3.22	0.15	486	1.59	44	2	0.26	4.34	A
	9247	2.61	0.38	0.94	0.16	465	1.21	36	6	0.29	1.32	A
	9250	6.47	1.29	3.63	0.51	471	1.32	56	8	0.26	4.92	B
	9253	8.68	1.22	4.62	0.18	472	1.34	53	14	0.21	5.84	A
	9266	2.17	0.19	0.61	0.26	483	1.53	28	12	0.24	0.80	B
9285	1.93	0.53	0.74	0.37	476	1.41	38	19	0.42	1.27	B	
9322	1.95	0.45	1.07	1.16	485	1.57	55	60	0.29	1.52	B	
9333	3.51	0.26	1.57	0.21	483	1.53	45	6	0.14	1.83	B	
Farnham Dome 1-A 8 - 15S - 12E	7343	31.50	1.29	11.14	1.30	485	1.57	35	4	0.10	12.43	A
	7368	61.74	1.93	25.06	3.85	497	1.79	41	6	0.07	26.99	A
	7403	9.12	0.41	2.88	0.54	495	1.75	32	6	0.13	3.29	A
Fed Mounds 1 11 - 16S - 11E	7050	17.12	1.49	12.98	0.52	477	1.43	76	3	0.10	14.47	C
	7150	4.34	1.47	2.14	0.41	476	1.41	49	9	0.41	3.61	C
	7250	5.68	1.82	2.92	0.46	488	1.26	51	8	0.33	4.74	C
Miller Creek 1 26 - 15S - 10E	8325	3.24	0.44	1.45	0.28	476	1.41	46	9	0.23	1.89	C
	8375	2.42	0.49	1.02	0.30	475	1.39	42	12	0.32	1.51	C
	8425	3.75	1.15	2.19	0.38	470	1.30	58	10	0.34	3.34	C
	8475	3.75	1.67	2.06	0.43	468	1.26	55	11	0.45	3.73	C
	8575	3.60	0.63	0.93	0.34	465	1.21	26	9	0.40	1.56	C
	8625	2.49	0.49	1.17	0.30	481	1.50	47	12	0.30	1.66	C
	8675	3.43	0.77	1.56	0.32	472	1.34	45	9	0.33	2.33	C
	8725	2.67	0.58	0.95	0.25	488	1.26	36	9	0.35	1.53	C
	8775	2.63	0.35	0.83	0.26	476	1.41	32	10	0.30	1.18	C
	8825	2.42	0.62	1.02	0.19	473	1.35	42	5	0.38	1.64	C
North Springs 1 27 - 15S - 9E	10,577	2.65	0.46	1.52	0.23	468	1.26	57	9	0.23	1.98	C
	10,650	3.66	0.56	2.07	0.26	478	1.44	57	7	0.21	2.63	C
	10,715	3.74	0.93	2.05	0.31	476	1.41	55	8	0.31	2.98	C
	A-4	1.31	0.10	0.36	0.17	497	NA	28	13	0.21	0.46	A
	A-6	1.76	0.07	0.43	1.15	505	NA	24	65	0.14	0.50	A
	A-8	2.04	0.11	0.56	1.67	493	NA	27	82	0.16	0.67	A
	B-5	2.01	0.12	0.37	0.27	476	NA	18	13	0.24	0.49	A

Table 6.3. Continued.

Well name/location	Depth ¹ (ft)	TOC ²	S1 ³	S2 ⁴	S3 ⁵	Tmax ⁶	R _o % calc ⁷	HI ⁸	OI ⁹	PI ¹⁰	GP ¹¹	Ref ¹²
North Springs 1 27 - 15S - 9E	C-2	1.09	0.07	0.12	0.11	444	NA	11	10	0.37	0.19	A
	C-6	1.36	0.10	0.22	0.58	452	NA	16	43	0.31	0.32	A
	D-1	0.93	0.12	0.21	0.45	444	NA	23	48	0.37	0.33	A
	D-6	0.84	0.07	0.13	0.27	372	NA	16	32	0.35	0.20	A
	D-10	1.78	0.15	0.40	0.15	476	NA	23	8	0.28	0.55	A
	G-4	0.67	0.09	0.13	0.19	422	NA	19	28	0.42	0.22	A
	H-2	0.79	0.11	0.15	0.11	354	NA	19	14	0.43	0.26	A
	H-5	0.64	0.08	0.10	0.13	333	NA	16	20	0.46	0.18	A
	10,785	1.84	0.26	0.65	0.35	467	1.25	35	19	0.29	0.91	C
	10,792	1.06	0.15	0.17	0.21	476	NA	16	20	0.47	0.32	C
	10,828	1.44	0.23	0.42	0.21	479	NA	29	15	0.35	0.65	C
10,875	1.65	0.16	0.38	0.19	483	NA	23	12	0.30	0.54	C	
Spjut 16-1 16 - 16S - 11E	7620	3.42	0.77	1.92	0.30	480	1.48	56	9	0.29	2.69	C
	7675	2.53	0.70	1.13	0.25	471	1.32	45	10	0.39	1.83	C
	7725	3.22	0.96	1.58	0.29	475	1.38	49	9	0.38	2.54	C
	7775	3.27	0.65	1.70	0.25	471	1.32	52	8	0.28	2.35	C
	7825	1.87	0.58	0.65	0.35	473	1.35	35	19	0.47	1.23	C
	7875	3.67	1.10	2.06	0.21	468	1.26	56	6	0.35	3.16	C
	7925	3.45	1.07	1.52	0.21	474	1.37	44	6	0.41	2.59	C
	7975	3.08	1.00	1.33	0.21	471	1.32	43	7	0.43	2.33	C
	8025	3.43	0.81	1.47	0.23	481	1.50	43	7	0.36	2.28	C
8070	2.57	0.73	1.07	0.25	477	1.43	42	10	0.41	1.80	C	
Drunkards Wash 31-1 (D-1) 31 - 14S - 10E	11,625	0.09	NA	NA	NA	NA	NA	NA	NA	NA	NA	D
	11,705	0.33	NA	NA	NA	NA	NA	NA	NA	NA	NA	D
	11,985	0.56	0.27	0.37	0.56	453	NA	66	100	0.42	1	D
Wa Drew Gov 1 (Utah D-6) 31 - 14S - 9E	11,487	0.26	NA	NA	NA	NA	NA	NA	NA	NA	NA	D
	11,685	0.76	0.07	0.12	0.29	456	NA	16	38	0.37	NA	D
		TOC	S1	S2	S3	Tmax	R_o% calc	HI	OI	PI	GP	
	Average	4.11	0.60	1.84	0.43	455	1.39	37	18	0.33	2.44	
	StDev	8.17	0.52	3.56	0.50	54	0.25	18	19	0.12	3.90	
	Median	2.51	0.49	0.99	0.30	473	1.37	39	11	0.34	1.53	
	Max	61.74	1.93	25.06	3.85	505	1.79	79	82	0.74	26.99	
	Min	0.09	0.01	0.01	0.11	230	1.21	1	2	0.07	0.02	

¹ Alpha-numeric code (A-4, A-6, etc) refers to selected samples where exact depths are unsure; see plate 5, appendix I.

² TOC = total organic carbon (%)

³ S1 = amount of free hydrocarbons in the sample (mg HC/g rock)

⁴ S2 = amount of hydrocarbons generated by pyrolytic degradation of kerogen (mg HC/g rock)

⁵ S3 = amount of CO₂ (mg CO₂/g rock) produced during pyrolysis of kerogen

⁶ Tmax = temperature (°C) of maximum release of hydrocarbons from cracking of kerogen during pyrolysis

⁷ R_o = vitrinite reflectance (%)

⁸ HI = hydrogen index

⁹ OI = oxygen index

¹⁰ PI = production index

¹¹ GP = genetic potential

¹² Ref = references to the source of data: A = analyses for this study by UGS/TerraTek Schlumberger; B = analyses by Core Laboratories as reported in Grover (2008); C = analyses by Humble Geochemical Services, data from UGS files; D = analyses by Petroleum Systems International, data from UGS files

NA = not available

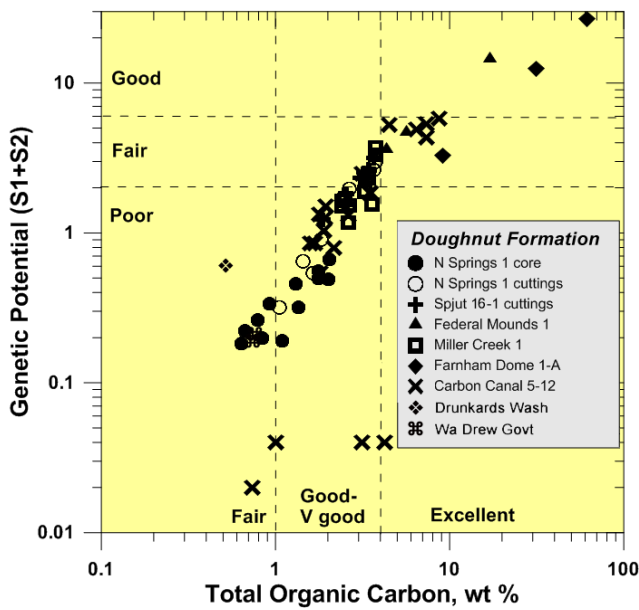


Figure 6.7. Doughnut Formation total organic carbon (TOC wt%) and genetic potential (GP, S1 + S2) in wells from the northern San Rafael Swell area.

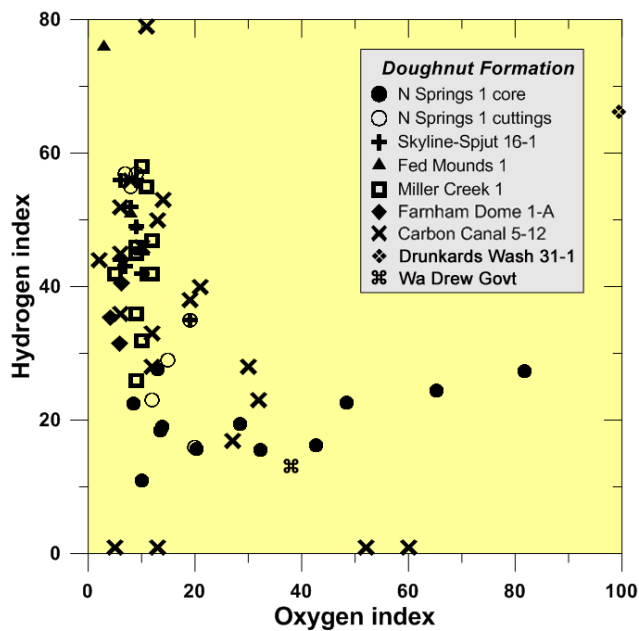


Figure 6.9. Doughnut Formation hydrogen and oxygen indices in wells from the northern San Rafael Swell area.

MCMGPD) with 667 BW (106 CM). Fiber optics showed that most of the fluid flow was from the interval 9124 to 9350 feet (2781–2850 m), the middle to the bottom of the core. The gas produced has a heating value of 1052 Btu and a composition of 93% methane, 4% ethane, 1.4 % nitrogen, and 0.5% carbon dioxide.

Interpretation of Regional Geochemical Data

Ten wells have programmed pyrolysis, TOC, or R_o data for the Doughnut Formation in the northern San Rafael Swell area. Bubble maps for these wells show average

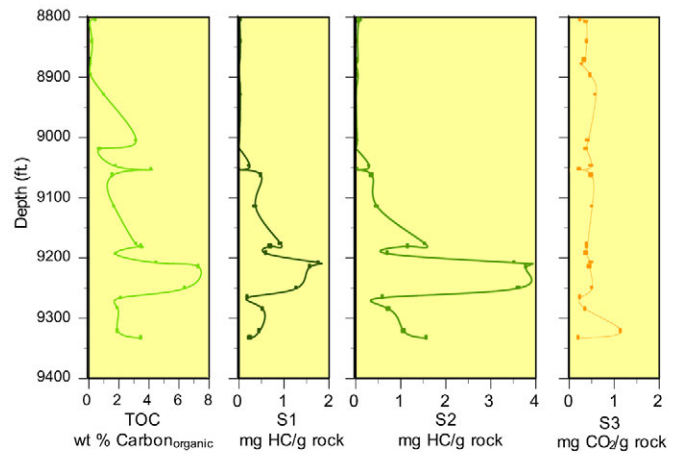


Figure 6.8. Total organic carbon (TOC) and the programmed pyrolysis S1, S2, and S3 values plotted as a function of depth to show the interval of greater hydrocarbon potential at 9208 to 9253 foot depths in the Carbon Canal 5-12 core.

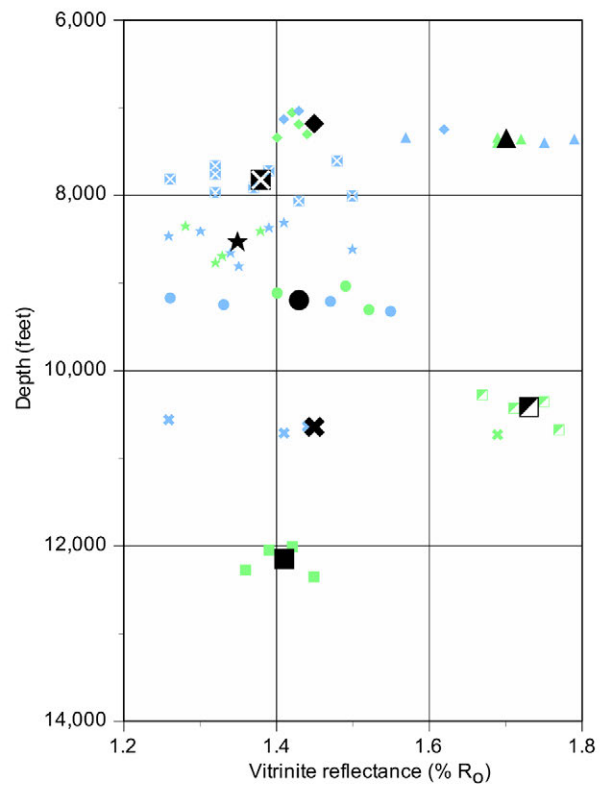


Figure 6.10. Measured, calculated, and average vitrinite reflectance values from eight wells show the maturity of the Doughnut Formation is not correlated with present-day burial depth. Note: only wells with S2 analysis greater than 0.50 (as required to calculate R_o) are included on the graph.

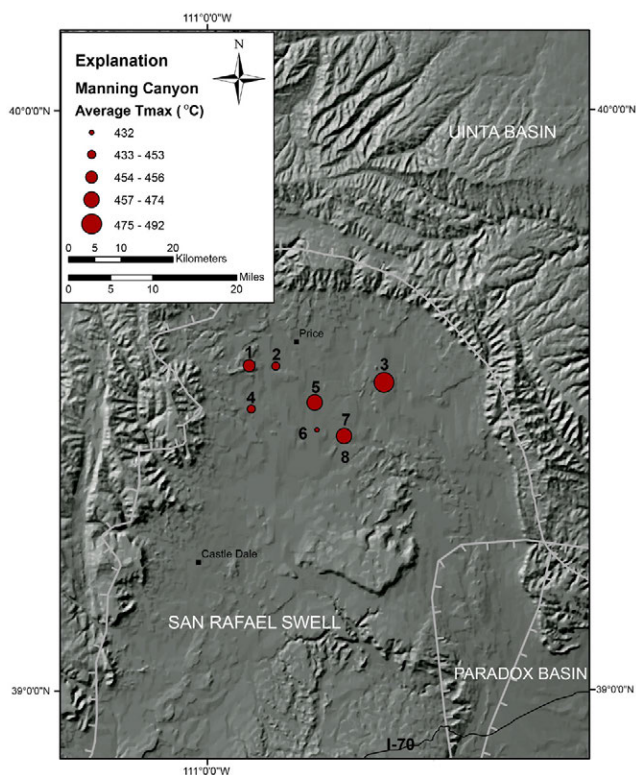


Figure 6.11. Averaged T_{max} for wells penetrating the Doughnut Formation shale, northern San Rafael Swell area. See table 6.3 for source of data. Well names: 1 = Wa Drew Govt 1 (Utah D-6), 2 = Drunkards Wash 31-1, 3 = Farnham Dome 1-A, 4 = North Springs 1, 5 = Miller Creek 1, 6 = Carbon Canal 5-12, 7 = Spjut 16-1, 8 = Federal Mounds 1.

T_{max} values ranging from 809 to 917°F (432–492°C) (figure 6.11) and generally low TOC values ranging from 0.33 to 34.12% (figure 6.12). The map of PI shows ratios varying from 0.10 to 0.42 (figure 6.13), which are generally low ratios and indicate rocks near thermal maturity. R_o values (figure 6.14) indicate that the shale is likely in the dry gas to overmature window. The plot of HI versus TOC indicates that the samples are all in the gas-prone to thermally mature window (figure 6.15). The pseudo-van Krevelen plot shows that the Doughnut falls in the type III and IV kerogen window, is very close to thermally mature, and not likely to produce (figure 6.16). The TOC versus S2 plot suggests the amount of hydrogen is poor, while organic matter level ranges from poor to excellent (figure 6.17).

PARADOX FORMATION

Unlike the Manning Canyon/Doughnut Formation of central Utah, the geochemistry of potential shale-gas reservoirs (Chimney Rock, Gothic, and Hovenweep shales) in the Paradox Formation has been studied and published fairly extensively (for example, Hite and others, 1984; Nuccio and Condon, 1996a, 1996b). These studies focused on the Paradox shale zones as the source of the oil produced in

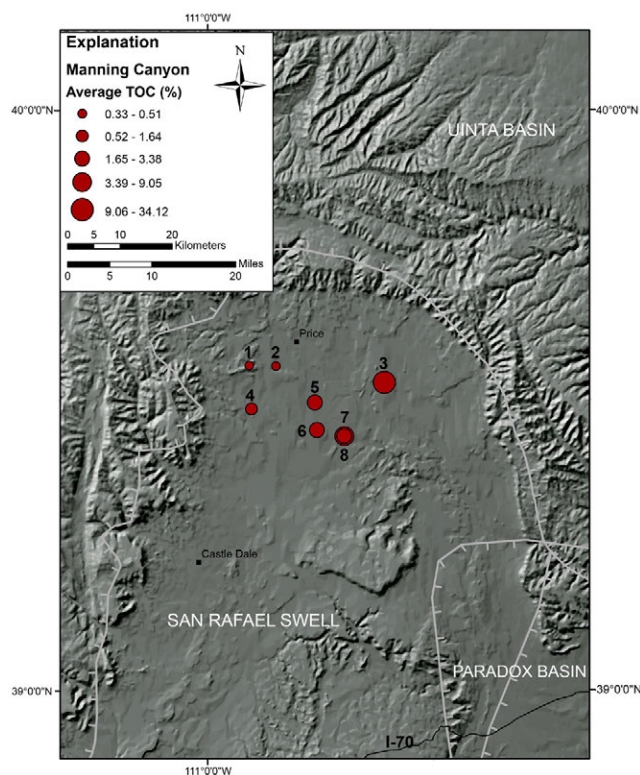


Figure 6.12. Averaged total organic carbon for wells penetrating the Doughnut Formation shale, northern San Rafael Swell area. See table 6.3 for source of data; wells are listed on figure 6.11.

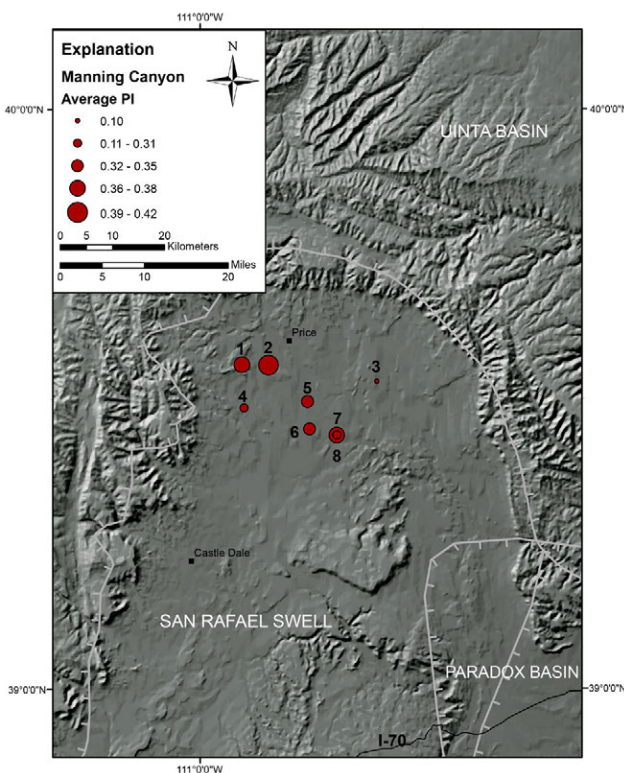


Figure 6.13. Averaged production index for wells penetrating the Doughnut Formation shale, northern San Rafael Swell area. See table 6.3 for source of data; wells are listed on figure 6.11.

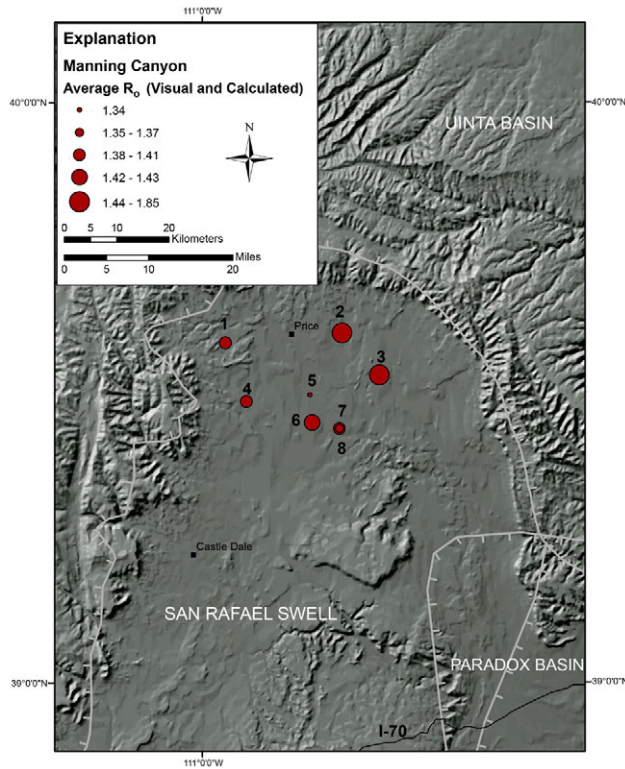


Figure 6.14. Averaged visual and calculated vitrinite reflectance values for wells penetrating the Doughnut Formation shale, northern San Rafael Swell area. See tables 6.2 and 6.3 for source of data. Well names: 1 = Arcadia-Telonis 1, 2 = State 1-16, 3 = Farnham Dome 1-A, 4 = North Springs 1, 5 = Miller Creek 1, 6 = Carbon Canal 5-12, 7 = Spjut 16-1, 8 = Federal Mounds 1.

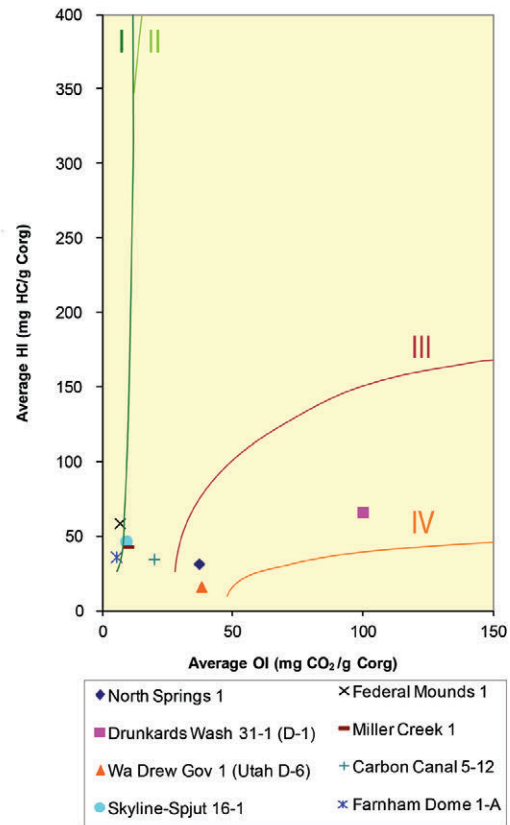


Figure 6.16. Pseudo-van Krevelen plot of wells with hydrogen and oxygen index values for the Doughnut Formation shale, northern San Rafael Swell area. Most of the wells are in the type III immature kerogen window.

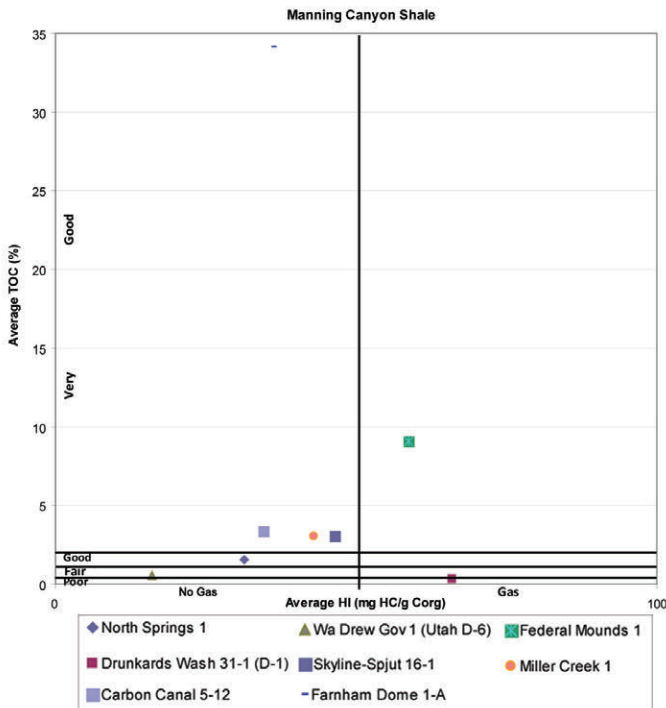


Figure 6.15. Plot comparing the average hydrogen index and amount of total organic carbon for wells through the Doughnut Formation shale, northern San Rafael Swell area.

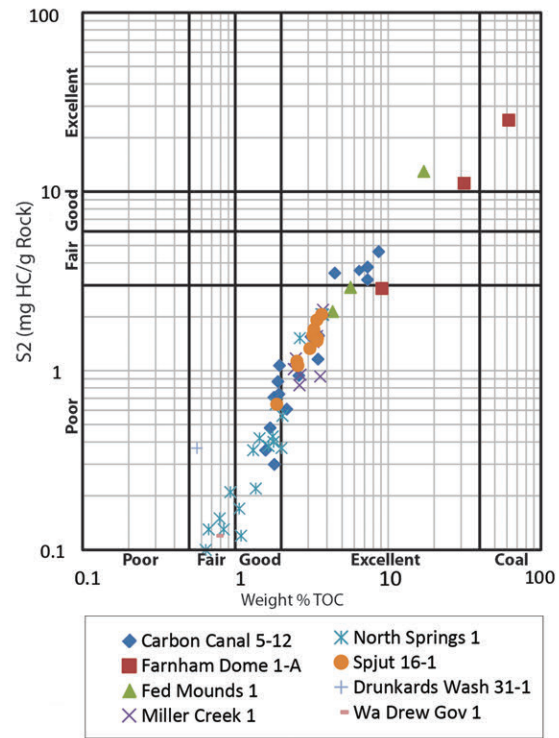


Figure 6.17. Logarithmic cross plot comparing amount of total organic carbon (TOC) with the amount of generated hydrocarbons from the decomposition of kerogen (S_2) for the Doughnut Formation shale, northern San Rafael Swell area.

the basin, primarily from carbonate buildups in the adjacent Desert Creek and Ismay zones (figure 1.4) and, in the case of the Cane Creek shale (not included in this study), as a self-sourcing oil reservoir. In the Colorado part of the Paradox Basin, the Gothic and Hovenweep shales produce gas. In Utah, however, oil with associated gas dominates current production.

In the following sections, we summarize some of the major findings by Hite and others (1984), Nuccio and Condon (1996a, 1996b), Schamel (2005, 2006), and Bereskin and McLennan (2008). The results of new geochemical analy-

sis conducted as part of this study on recent wells or newly acquired cores are also presented and listed in table 6.4.

Thermal Maturity

Nuccio and Condon (1996b) offer a somewhat unconventional view of thermal maturity in a map (figure 6.18), contouring production index (PI) values derived from pyrolysis data. For oil-prone source rocks, values in the range 0.1 to 0.5 are attributed to the oil-generative window (values less than 0.1 are considered immature), and values greater than 0.5 are placed in the gas-generative window. Given that the

Table 6.4. Programmed pyrolysis (RockEval™) analyses of core samples from five wells in the Paradox Formation, Paradox Basin.

Zone	Depth (ft)	TOC ¹	S1 ²	S2 ³	S3 ⁴	Tmax ⁵	HI ⁶	OI ⁷	S ¹ /TOC	PI ⁸	GP ⁹	Calc R _o % ¹⁰	Ref ¹¹
Marie Ogden State 1													
Hovenweep	5191.9	1.48	1.78	4.10	0.47	438	277	32	120	0.30	5.88	0.72	A
	5193.5	2.21	2.82	5.98	0.53	441	271	24	128	0.32	8.8	0.78	A
	5195.1	2.17	2.98	6.01	0.58	437	277	27	137	0.33	8.99	0.71	A
	5196.8	1.36	1.72	2.97	0.40	438	218	29	127	0.37	4.69	0.72	A
	5198.6	1.57	2.04	3.60	0.39	441	229	25	130	0.36	5.64	0.78	A
	5200.5	2.13	3.47	6.20	0.55	440	291	26	163	0.36	9.67	0.76	A
	5202	1.45	1.72	2.72	0.46	440	188	32	118	0.39	4.44	0.76	A
	5203.9	1.68	2.16	4.26	0.36	442	254	21	129	0.34	6.42	0.80	A
	5205.7	2.28	3.74	6.70	0.46	440	294	20	164	0.36	10.44	0.76	A
	5208	2.50	3.07	7.82	0.55	444	313	22	123	0.28	10.89	0.83	A
	5210.5	1.25	1.32	2.36	0.39	440	189	31	105	0.36	3.68	0.76	A
	5212.3	1.76	2.27	4.28	0.41	441	243	23	129	0.35	6.55	0.78	A
	5214.9	1.94	3.23	5.64	0.55	439	291	28	167	0.36	8.87	0.74	A
	5217.8	2.01	3.20	5.58	0.55	442	278	27	159	0.36	8.78	0.80	A
	5220.1	2.17	3.48	6.61	0.55	441	305	25	160	0.34	10.09	0.78	A
5222.5	2.42	3.83	8.55	0.62	440	353	26	158	0.31	12.38	0.76	A	
5224.5	6.52	6.75	25.37	0.60	440	389	9	104	0.21	32.12	0.76	A	
Gothic	5324.1	2.59	0.76	11.17	0.28	438	431	11	29	0.06	11.93	0.72	A
	5325	1.84	0.51	5.70	0.36	438	310	20	28	0.08	6.21	0.72	A
	5326.8	1.54	0.73	5.54	0.33	442	360	21	47	0.12	6.27	0.80	A
	5331.2	1.55	1.89	4.19	0.56	437	270	36	122	0.31	6.08	0.71	A
	5332.9	1.62	1.97	4.59	0.57	437	283	35	122	0.30	6.56	0.71	A
5334.1	1.53	2.11	4.28	0.55	438	280	36	138	0.33	6.39	0.72	A	
Jefferson State 4-1													
Upper Ismay	5876.4	1.17	0.49	1.07	0.30	461	92	26	42	0.31	1.56	1.14	B
Hovenweep	5903.3	1.77	1.90	2.50	0.45	444	141	25	108	0.43	4.4	0.83	B
	5930.4	1.39	1.49	2.12	0.56	442	152	40	107	0.41	3.61	0.80	B
Lower Ismay	6009.3	0.46	0.79	0.44	0.63	397	95	138	172	0.64	1.23	N/A	B
	6017.5	0.05	0.03	0.10	0.23	473	193	453	60	0.24	0.13	N/A	B
Gothic	6030.4	1.32	0.84	1.52	0.48	445	115	37	63	0.36	2.36	0.85	B
	6036.6	0.78	0.97	0.74	0.52	432	95	67	124	0.57	1.71	0.62	B
Cedar Point Federal 16-25													
Chimney Rock	6410.4	1.70	0.79	1.16	2.01	442	68	118	47	0.41	1.95	0.80	C
	6412.6	2.81	0.98	1.34	0.31	463	48	11	35	0.42	2.32	1.17	C

Table 6.4. Continued.

Zone	Depth (ft)	TOC ¹	S1 ²	S2 ³	S3 ⁴	Tmax ⁵	HI ⁶	OI ⁷	S ¹ /TOC	PI ⁸	GP ⁹	Calc R _o % ¹⁰	Ref ¹¹
Lake Canyon 1-27													
Gothic	5755.2	1.46	0.79	0.74	1.05	436	51	72	54	0.52	1.53	0.69	C
	5765.2	1.51	0.80	0.74	1.51	446	49	100	53	0.52	1.54	0.87	C
	5767.3	1.85	1.62	1.59	0.51	442	86	28	88	0.50	3.21	0.80	C
	5774.1	4.10	3.34	4.51	0.78	453	110	19	82	0.43	7.85	0.99	C
Aneth Unit H-117													
Gothic	5379.4	2.89	2.09	6.45	0.73	445	224	25	72	0.24	8.54	0.85	C
	5382.8	2.81	2.16	5.97	0.64	451	213	23	77	0.27	8.13	0.96	C
	5386.9	2.23	1.93	5.15	0.84	444	231	38	87	0.27	7.08	0.83	C
	5390.8	4.42	2.39	9.46	0.76	449	214	17	54	0.20	11.85	0.92	C

¹TOC = total organic carbon (%)

²S1 = amount of free hydrocarbons in the sample (mg HC/g rock)

³S2 = amount of hydrocarbons generated by pyrolytic degradation of kerogen (mg HC/g rock)

⁴S3 = amount of CO₂ (mg CO₂/g rock) produced during pyrolysis of kerogen

⁵Tmax = temperature (°C) of maximum release of hydrocarbons from cracking of kerogen during pyrolysis

⁶HI = hydrogen index

⁷OI = oxygen index

⁸PI = production index

⁹GP = genetic potential

¹⁰R_o = vitrinite reflectance (%)

N/A = not applicable

¹¹Ref = references to the source of data: A = Baseline DGS Analytical Laboratories; B = Bereskin and McLennan (2008); C = UGS/TerraTek Schlumberger

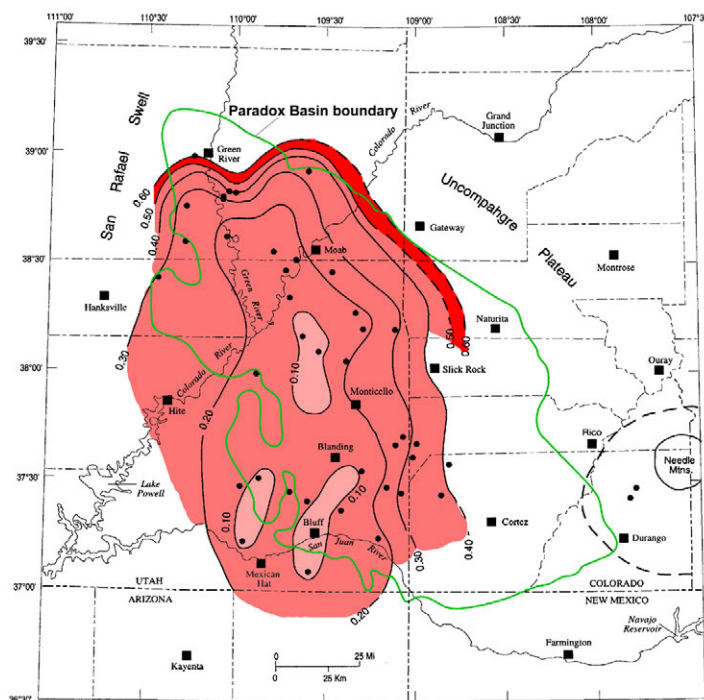


Figure 6.18. Thermal maturity map of the Paradox Basin through the Ismay–Desert Creek interval, Paradox Formation, which includes the Hovenweep, Gothic, and Chimney Rock shales (after Nuccio and Condon, 1996a). Contoured are production indices (PI); contour interval = 0.10. Light pink (PI ≤ 0.10) represents thermally immature areas while medium pink (PI between 0.10 and 0.50) indicates the region of the basin thermally mature enough to generate petroleum; the red area (PI > 0.50) is overmature and more likely gas prone.

kerogen is dominantly humic, the gas threshold might better be set at a PI of 0.2, in which case a large volume of the organic-rich shale in the Paradox fold and fault belt (figure 2.10) would have been, or now is, generating natural gas (Schamel, 2005, 2006).

To investigate the maturity and kerogen type further, two samples were selected for R_o and visual kerogen analyses from Hovenweep (5208.0 feet [1587.3 m] and Gothic 5324.1 feet [1622.7 m] shales in the Marie Ogden State 1 well (appendix L) located basically on the boundary between the Blanding sub-basin and the Paradox fold and fault belt (figures 2.10 and 4.2; appendix L). Kerogens in both samples consist primarily of unstructured lipids (85%) with massive texture, inertinite (5%), and vitrinite (5%). This suggests these samples contain oil-prone kerogen. Vitrinite reflectance values ranged between 0.74 and 0.78%. Maturity is estimated to be in the middle of the oil-generation window.

The U.S. Geological Survey recently published (2012) a geology-based, total petroleum system (TPS) assessment of the undiscovered gas and oil resources in the Paradox Basin, which extends into parts of Colorado, New Mexico, and Arizona. The TPS includes source rocks (hydrocarbon maturation, generation, and migration), reservoir descriptions, and trapping mechanisms (type, timing of formation, and seal). Two unconventional assessments units (AU) in the Paradox Formation TPS were defined that consist of the potential shale gas zones described in our study (figure 6.19): the Gothic, Chimney Rock,

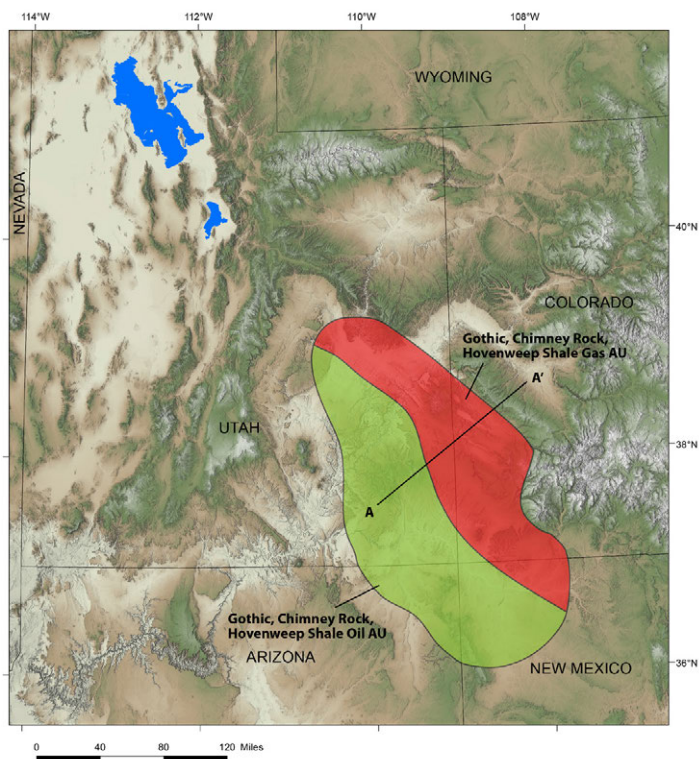


Figure 6.19. Location of the Gothic, Chimney Rock, Hovenweep Shale Oil and Gas assessments units (AUs) in the Paradox Basin (modified from U.S. Geological Survey, 2012). Cross section A–A' shown on figure 2.12.

Hovenweep Shale Gas AU and the Gothic, Chimney Rock, Hovenweep Shale Oil AU (U.S. Geological Survey, 2012). The shale zones in these AUs are considered continuous reservoirs with diffuse boundaries and lacking clear traps. The oil and gas AUs are separated by a maturation boundary of $R_o = 1.1\%$, where the more mature gas-prone shale zones are located in the deeper northeast part of the basin parallel to the Uncompahgre uplift (figures 2.11 and 2.12) (U.S. Geological Survey, 2012).

The boundaries of U.S. Geological Survey's Gothic, Chimney Rock, Hovenweep Shale Oil and Gas AUs fit into the findings of our study. We too determined that the shale zones in the Paradox Formation of the Blanding sub-basin and the Aneth platform tend to be oil prone, whereas in the deeper part of the basin, the Paradox fold and fault belt (figures 2.10 through 2.12), they should be more gas prone.

Total Organic Carbon and Programmed Pyrolysis Geochemistry

A compilation of TOC data for 39 wells scattered across the Paradox Basin provides a more comprehensive assessment of organic richness from various stratigraphic intervals in the Paradox Formation (Schamel, 2005). The data set is from Nuccio and Condon (1996a) and (Hite and others, 1984). The median and maximum TOC values for the Ismay–Desert Creek interval (Chimney Rock, Gothic, and Hovenweep shales) are 1.93 and

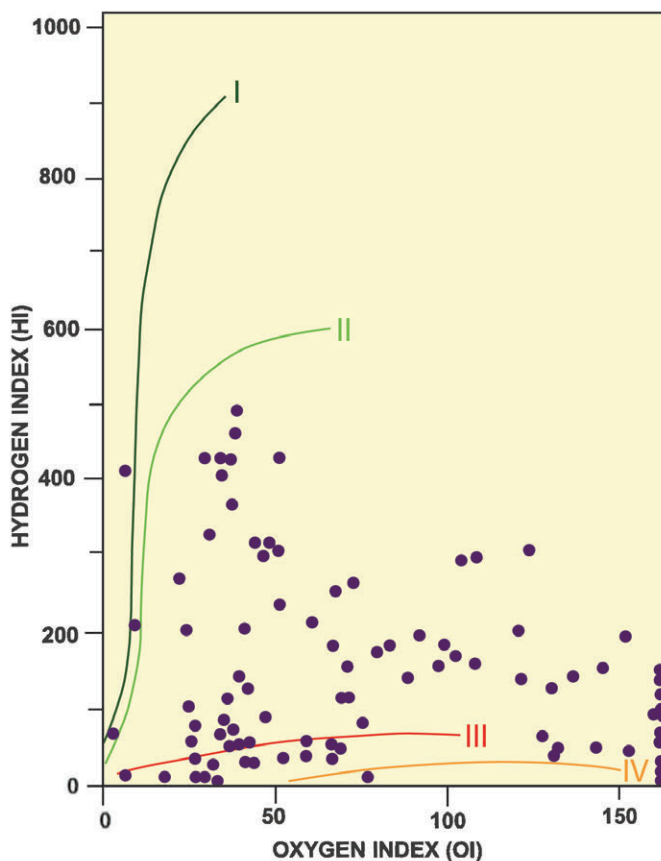


Figure 6.20. Modified van Krevelen plot of samples from the Ismay–Desert Creek interval showing that the kerogen is mainly types II and III (after Nuccio and Condon, 1996a).

10.98%. The kerogen is largely types II and III (figure 6.20), capable of generating both oil and gas (Nuccio and Condon, 1996b). Nuccio and Condon (1996a) showed the organic matter is both marine and terrestrial separated by a transition zone, and samples in the eastern part of the basin are more gas prone (terrestrial in origin), now confirmed by recent gas discoveries in the Gothic and Hovenweep shales in Colorado.

As part of our study, samples from cores were analyzed from five wells (see appendix D for core descriptions and appendix L for complete geochemical reports), north to south across the basin. The results and interpretations are summarized below.

- Gothic and Hovenweep samples from the Marie Ogden State 1 core, representing the northernmost well and that is closest to the Paradox fold and fault belt (figures 2.10 and 4.2; table 6.4) contain between 1.3 and 2.6% TOC (with one exception) and S₂ yields between 2.4 and 8.6 mg HC/g (with two exceptions). T_{max} values are between 819 and 828°F (437 and 442°C) and the calculated HI ranges between 190 and 430. From these data we conclude all of the samples have some hydrocarbon source potential and the T_{max} values suggest these intervals have reached peak oil generation. The TOC and pyrolysis data of the Gothic and

Hovenweep samples show the kerogens are oil generating types I and II (figure 6.21A).

- Gothic and Hovenweep samples from the Jefferson State 4-1 core (figure 4.2 and table 6.4) contain modest values of TOC, between 0.78 and 1.8% with S2 yields between 0.7 and 2.5 mg HC/g. Tmax values are between 810 and 833°F (432 and 445°C) and the calculated HI ranges between 95 and 152. The maturation stage is well within the oil window. The kerogen is largely types I and II (figure 6.21B), capable of generating oil; there are some gas-prone type III samples as well. Both the Gothic and Hovenweep shales gave off significant shows of gas while being cored (Bereskin and McLennan, 2008).
- The Chimney Rock and Gothic shales were sampled from the Cedar Point 16-25 and Lake Canyon cores, respectively, in the center of the Blanding sub-basin (figures 2.10 and 4.2; table 6.4). They contain between 1.5 and 4.1% TOC with S2 yields between 0.7 and 4.5 mg HC/g. Tmax values are between 819 and 865°F (436 and 463°C) and the calculated HI ranges between 48 and 110. The kerogen types I through III (figure 6.21C), capable of generating both oil and gas.
- Gothic samples from the Aneth Unit H-117 core, representing the southernmost well located on the Aneth platform (figures 2.10 and 4.2; table 6.4), have a TOC between 2.8 and 4.4%. S1 in the Gothic ranges from 1.9 to 2.4 mg HC/g, S2 ranges from 5.2 to 9.5 mg HC/g, and S3 ranges from 0.6 to 0.8 mg/g. Tmax values show little variation ranging between 831 and 844°F (444 and 451°C). Similarly, the calculated HI also yield a narrow but high value range between 213 and 231. Kerogen type determination from TOC and pyrolysis data shows the Gothic contains type II and mixed type II-III kerogen (figure 6.21D) while kerogen quality suggests it to be gas prone.

The Chimney Rock, Gothic, and Hovenweep shales look organic rich because of the dark hues, and TOC measurements overall reflect a modest but significant degree of organic richness. Higher TOC values would be evident if not for the dilution attributable to significant amounts of terrigenous silt, various clays, pyrite, and phosphate and variable quantities of diagenetic dolomite. Presumably, any calcite would not dilute the TOC measurements due to selective removal of this mineral prior to TOC testing. Pyrolysis in particular points to a maturation stage well within the oil window, less than 880°F (470°C) (Bereskin and McLennan, 2008).

Because of the mineralogical and/or fossil “contaminants” described above, acceptable TOC values can be comparatively low (1.5 to 3.0%) but not in every instance. Pyrolysis clearly points to rocks in the oil or oil/gas windows; existing gas production is therefore anomalous in terms of simple geochemical analysis—at least in Utah portions of the Paradox. Produced

natural gas might be the product of solution gas drive or of a more complicated pressure-volume-temperature relationship.

Occurrences of Natural Gas

The Gothic, Chimney Rock, Hovenweep Shale Gas AU was estimated to contain a mean of 6490 BCFG (184 BCMG); the Gothic, Chimney Rock, Hovenweep Shale Oil AU was assessed to contain a mean of 256 million barrels of oil (40.7 MMCM) and 205 BCF (5.8 BCM) of associated gas (U.S. Geological Survey, 2012). However, the shale zones in the Paradox fold and fault belt, specifically the deeper Cane Creek shale (figure 1.4), are enigmatic. The Cane Creek contains mixed type II to III kerogen that should favor gas generation (Schamel, 2005, 2006), yet oil with associated gas dominates current production in six active oil fields and two new discoveries in the area; currently there is no production from the Chimney Rock, Gothic, or Hovenweep shales in the Paradox fold and fault belt. The Cane Creek is encased in excellent sealing rocks: salts and anhydrite that retard gas leakage, even by diffusion.

Geochemical analysis was conducted on 23 core samples from Hovenweep and Gothic shales in the Marie Ogden State 1 well (table 6.4 and appendix L). Seventeen samples were taken between 5191.9 and 5224.5 feet (1582.4–1592.3 m) through the Hovenweep. Six samples were collected between 5324.1 and 5334.1 feet (1622.7–1625.8 m) representing the upper 10 feet (3 m) of the generally 40-foot-thick (12 m) Gothic. The sections represented by these samples contain significant concentrations of oil-prone, rather than gas-prone, organic matter that has reached the middle of the oil window. However, they have generated and expelled 20% of the original oil source potential.

Structurally, the Paradox fold and fault belt is dominated by large fault-bounded salt walls and salt-cored anticlines where shale beds can be complexly deformed. Salt movement began during the Pennsylvanian as evidenced by thinning of the Paradox Formation and younger strata towards and over the salt structures (Doelling, 1988). The influence of early salt movement on stratal thickness and depositional patterns is known from other salt basins (Schamel and others, 1995; Schamel, 2005, 2006). Most exploratory wells have targeted structural highs and samples have therefore been recovered from “cooler” parts of the basin perhaps skewing the geochemical analysis towards oil-prone shale. In the structurally low areas beyond the salt walls or synclines parallel to the anticlines, one can expect less deformation, thicker deposits, and shale zones possibly in the gas-generative window and retained natural gas (Schamel, 2005, 2006). The Cane Creek and other shale zones are also overpressured (Montgomery, 1992; Morgan, 1992), which suggests hydrocarbon generation currently ongoing or occurred in the recent past. Thus, structural low or synclinal areas remain untested over a significant part of the Paradox fold and fault belt. These areas have potential for shale gas reservoirs despite the greater required drilling depths.

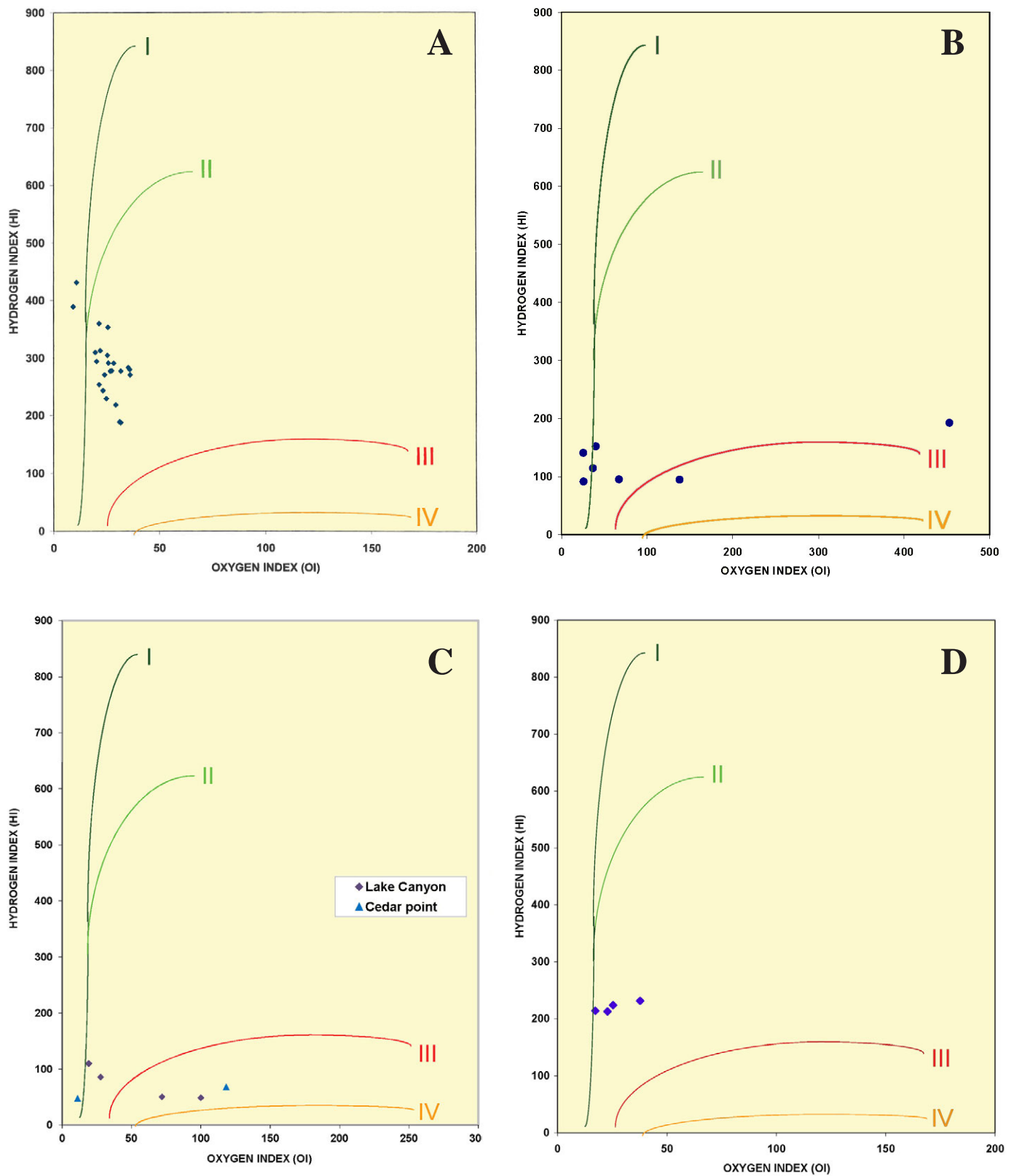


Figure 6.21. Pseudo-van Krevelen plots with hydrogen and oxygen index values for the Paradox Formation, Paradox Basin. **A.** Gothic and Hovenweep shales from the Marie Ogden State 1: most samples are type I and II kerogen. **B.** Gothic and Hovenweep shales and Ismay carbonates from the Jefferson State 4-1: most samples are type I and II kerogen with some type III. **C.** Chimney Rock and Gothic shales from the Cedar Point Federal 16-25 and Lake Canyon 1-27, respectively: samples are types I, II, and III kerogen. **D.** Gothic shale from the Aneth Unit H-117: samples are type II and mixed type II-III kerogen.

Interpretation of Regional Geochemical Data

Chimney Rock Shale

The 17 wells with programmed pyrolysis, TOC, and R_o data for the Chimney Rock shale are located in the northwestern and southeastern regions of the Utah part of Paradox Basin. Bubble maps for these wells show T_{max} values ranging from 779 to 867°F (415–464°C) (figure 6.22) and TOC values ranging from 0.66 to 4.97% (figure 6.23). The map of PI shows ratios varying from 0.09 to 0.61 (figure 6.24); 13 of the wells are within the oil maturation level and eight are near peak oil. Vitrinite reflectance values range from 0.3 to 1.19% (figure 6.25). If the shale has oil-prone generation, 12 wells are in the peak oil stage. If the shale has gas-prone generation, no wells are in the peak gas stage, but 13 wells are in the early gas stage. The plot of HI versus TOC suggests several samples have potential for oil or gas (figure 6.26). The pseudo-van Krevelen plot records Chimney Rock wells in the type II, III, and IV kerogen windows (figure 6.27). The TOC versus S_2 plot shows several wells contain encouraging amounts of hydrogen and organic matter (figure 6.28).

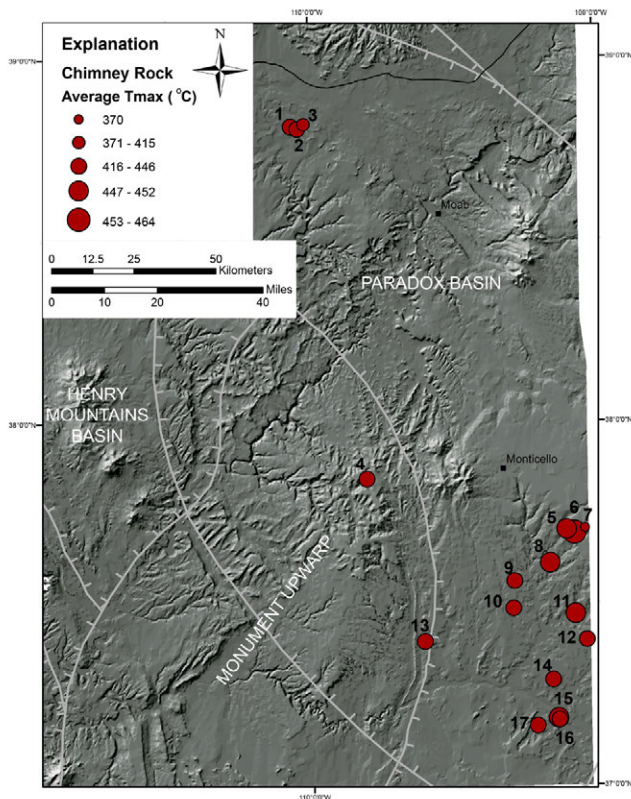


Figure 6.22. Averaged T_{max} for wells penetrating the Chimney Rock shale of the Paradox Formation, Paradox Basin, Utah. See appendix C for source of data. Well names: 1 = Government Smoot 1; 2 = Salt Wash Unit 1; 3 = Floy Unit 1; 4 = Elk Ridge Unit 1; 5 = Cedar Point Federal 1-25; 6 = UCOLO 1-32; 7 = Jones 27-11; 8 = Pickett Federal 33-1; 9 = Deadman Canyon Unit 1; 10 = Alkali Point 17-22; 11 = Federal 20-2; 12 = Federal G-G1; 13 = State 1-16; 14 = McElmo Creek Unit T-04; 15 = Navajo Tribal 34-31; 16 = Navajo Tribal 34-42; 17 = Lone Mountain Canyon 1-33.

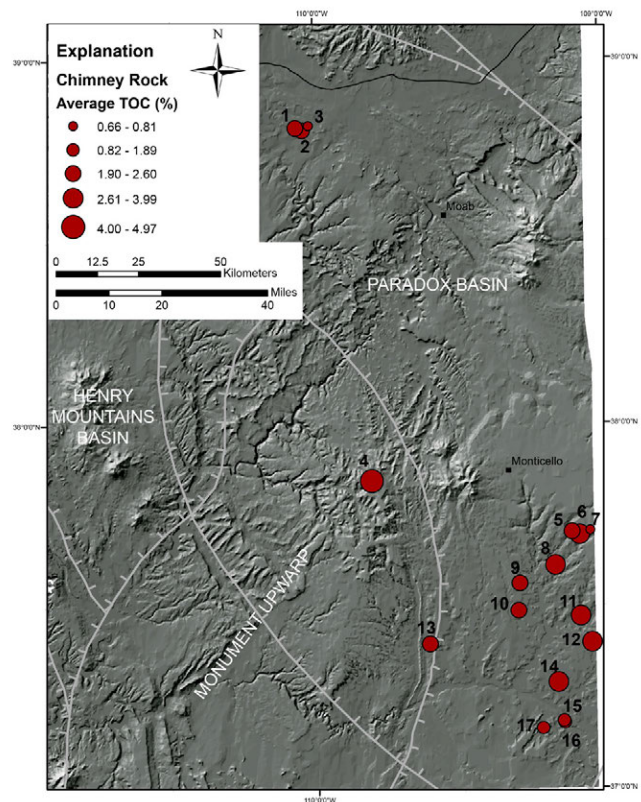


Figure 6.23. Averaged total organic carbon in wells penetrating the Chimney Rock shale of the Paradox Formation, Paradox Basin, Utah. See appendix C for source of data; wells are listed on figure 6.22.

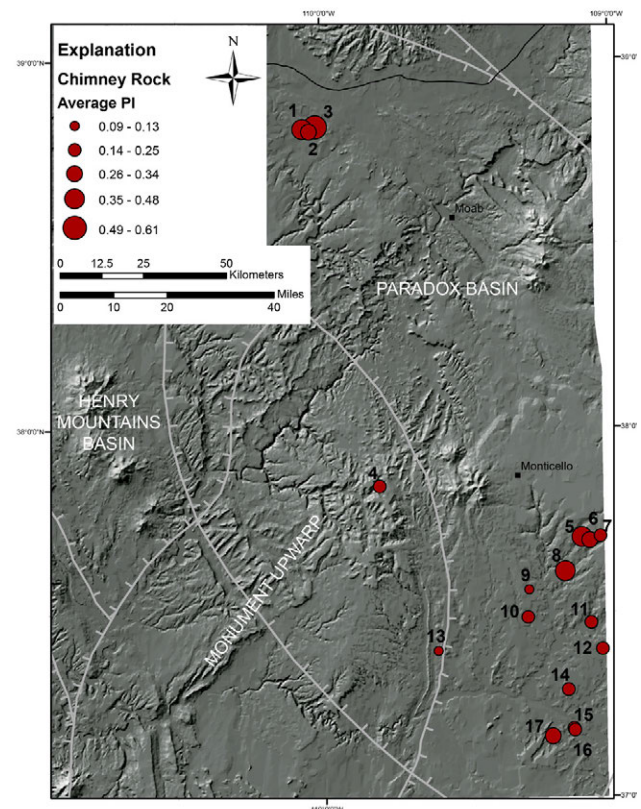


Figure 6.24. Averaged production index for wells penetrating the Chimney Rock shale of the Paradox Formation, Paradox Basin, Utah. See appendix C for source of data; wells are listed on figure 6.22.

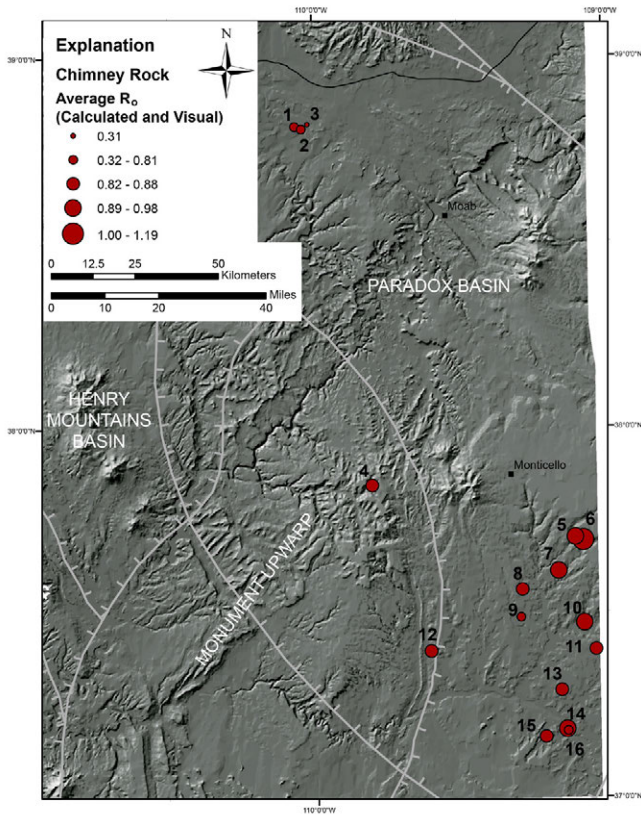


Figure 6.25. Averaged calculated vitrinite reflectance for wells generating the Chimney Rock shale of the Paradox Formation, Paradox Basin, Utah. See appendix C for source of data. Well names: 1 = Government Smoot 1; 2 = Salt Wash Unit 1; 3 = Floy Unit 1; 4 = Elk Ridge Unit 1; 5 = Cedar Point Federal 1-25; 6 = UCOLO 1-32; 7 = Pickett Federal 33-1; 8 = Deadman Canyon Unit 1; 9 = Alkali Point 17-22; 10 = Federal 20-2; 11 = Federal G-G1; 12 = State 1-16; 13 = McElmo Creek Unit T-04; 14 = Navajo Tribal 34-31; 15 = Lone Mountain Canyon 1-33; 16 = Navajo Tribal 34-42.

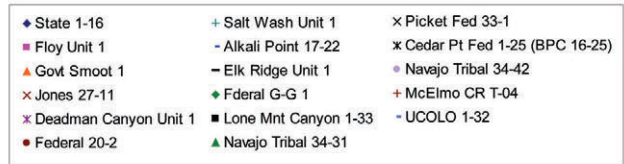
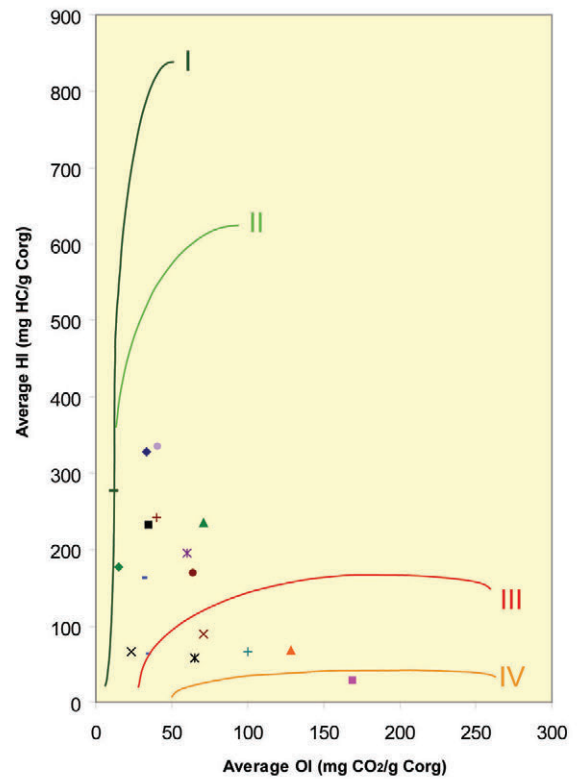


Figure 6.27. Pseudo-van Krevelen plot with hydrogen and oxygen index values for wells through the Chimney Rock shale, Paradox Formation, Utah. Most of the wells are in the type II gas-prone window, with some in the immature type III, and one well in the type IV “dead carbon” window.

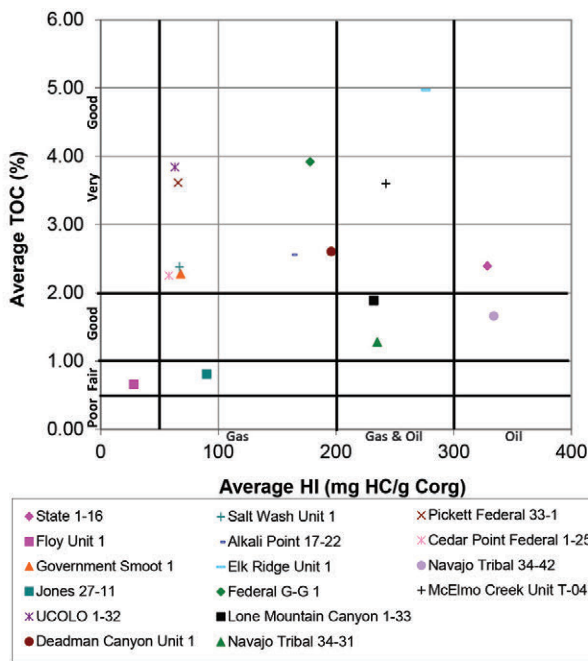


Figure 6.26. Plot comparing the average hydrogen index and amount of total organic carbon for wells through the Chimney Rock shale, Paradox Formation, Utah.

Gothic Shale

Twenty-eight wells throughout the Utah part of the Paradox Basin contain information for the Gothic shale. The PI values are 0.10 to 1.00 (figure 6.29); 17 of the wells are in the oil maturation level. Maximum temperatures range from 784 to 849°F (418–454°C) (figure 6.30) and nine wells are in the peak oil window based on their average temperatures. Average calculated and visual vitrinite reflectance values are 0.36 to 1.01% (figure 6.31) with 14 wells in the peak oil generation stage if the unit is oil prone and 15 wells in the early gas generation stage if the unit is gas-prone. The TOC varies from 0.45 to 3.94% (figure 6.32), and 23 of the wells have good to very good source rock generative potential. The pseudo-van Krevelen diagram shows several wells between the oil- and gas-prone pathways (figure 6.33). Wells plotted comparing HI with TOC show where there is potential to generate gas and oil (figure 6.34). The chart of TOC versus S2 shows six wells with good to excellent amounts of hydrogen and organic matter (figure 6.35).

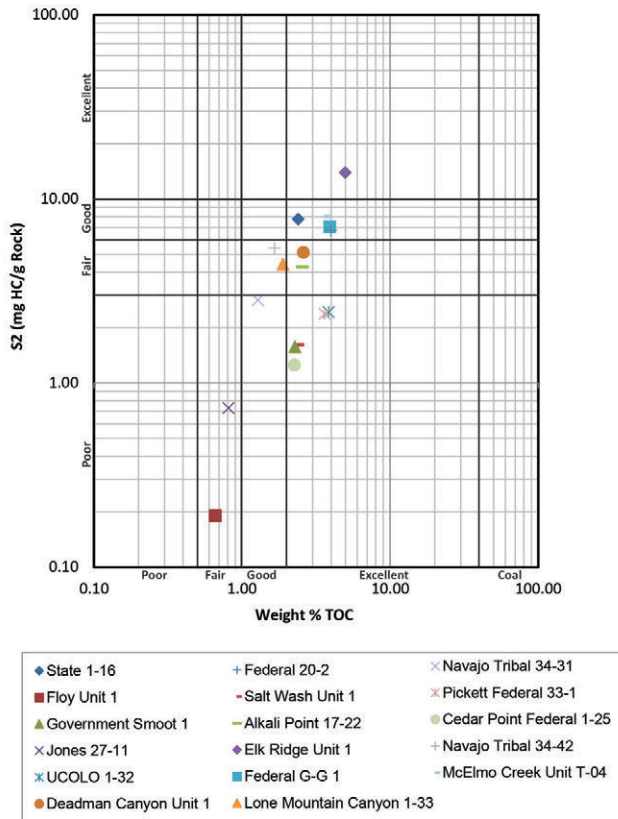


Figure 6.28. Logarithmic cross plot comparing amount of total organic carbon (TOC) with the amount of generated hydrocarbons from the decomposition of kerogen (S2) for the Chimney Rock shale, Paradox Formation, Utah.

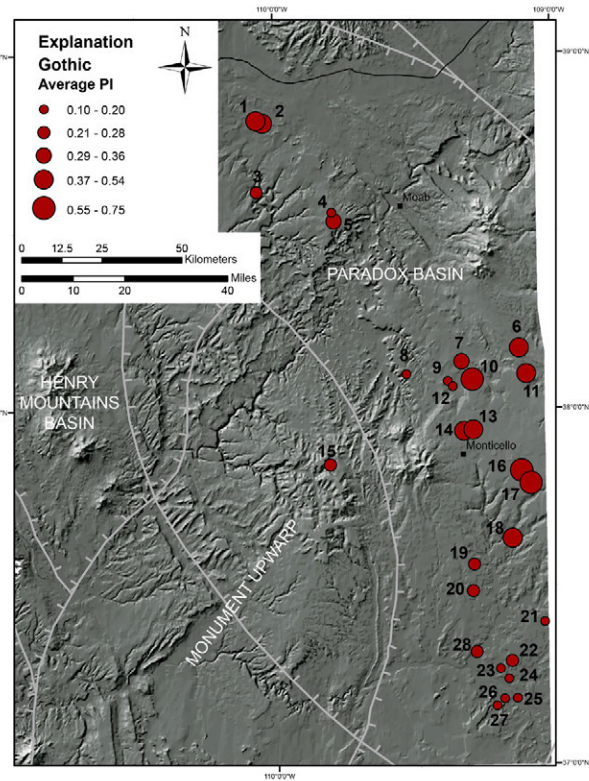


Figure 6.29. Averaged production index for wells penetrating the Gothic shale of the Paradox Formation, Paradox Basin, Utah. See appendix C for source of data. Well names: 1 = Government Smoot 1; 2 = Salt Wash Unit 1; 3 = Bowknot Unit 43-20; 4 = Tidewater Oil Co 74-11; 5 = Big Flat Unit 3; 6 = Big Indian 6; 7 = Federal 1-31; 8 = Hart Point Federal 1; 9 = Marie Ogden State 1; 10 = Winchester 21-1H; 11 = Utah Federal A-1; 12 = Church Rock Unit 1; 13 = Jefferson 4-1; 14 = Morris Nelson 6-11; 15 = Elk Ridge Unit 1; 16 = Utah A-1; 17 = S.P. Meyer 1; 18 = Lake Canyon Federal 1-27; 19 = Deadman Canyon Unit 1; 20 = Alkali Point 17-22; 21 = Federal G-G1; 22 = McElmo Creek Unit T-04; 23 = Aneth Unit K-231; 24 = McElmo Creek Unit R-18; 25 = Navajo Tribal 34-31; 26 = Clay Canyon 32-11; 27 = Lone Mountain Canyon 1-33; 28 = Aneth Unit H-117.

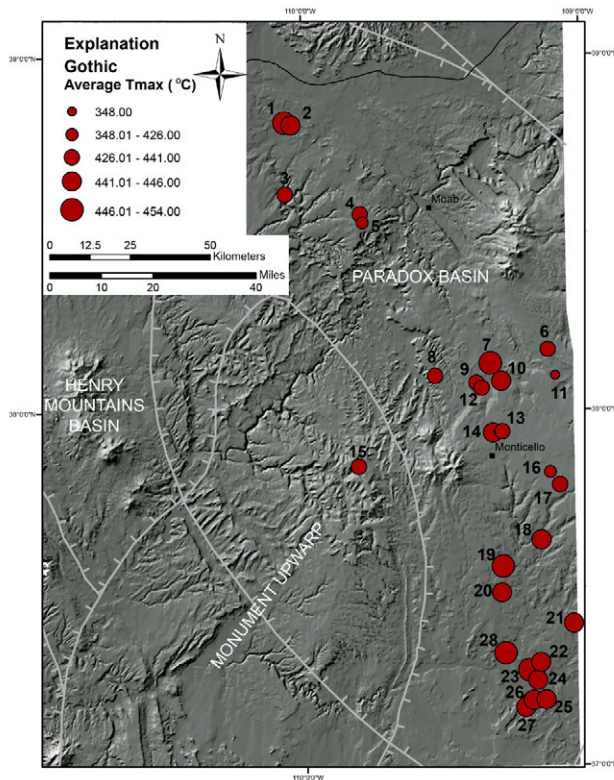


Figure 6.30. Averaged Tmax for wells penetrating the Gothic shale of the Paradox Formation, Paradox Basin, Utah. See appendix C for source of data; wells are listed on figure 6.29.

Hovenweep Shale

Data for the Hovenweep shale arises from 16 wells throughout the Utah part of the Paradox Basin. Bubble maps image values for PI, Tmax, R_o, and TOC are compiled from well data. Production index ratios range from 0.11 to 0.79 (figure 6.36) with seven of the 16 wells in the beginning oil to peak oil maturation levels; Tmax vary from 759 to 847°F (404–453°C) (figure 6.37). Total organic carbon values, from 0.41 to 3.0% (figure 6.38), are modest with some wells in the good to very good generative potential categories. Average calculated and visual vitrinite reflectance values are between 0.11 and 0.99% (figure 6.39) and alone suggest seven wells may be at oil-prone maturation. The pseudo-van Krevelen plot shows the majority of wells are in oil-prone levels (type II; figure 6.40). Several wells in the HI versus TOC chart display very good source rock potential with possible hydrocarbon generation (figure 6.41), but the chart for TOC versus S2 shows only a few wells have higher amounts of organic matter and associated hydrogen (figure 6.42).

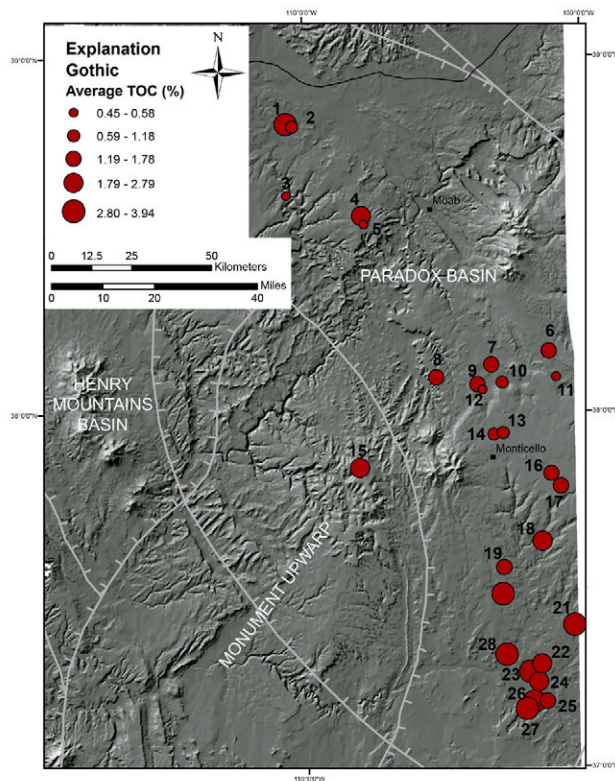
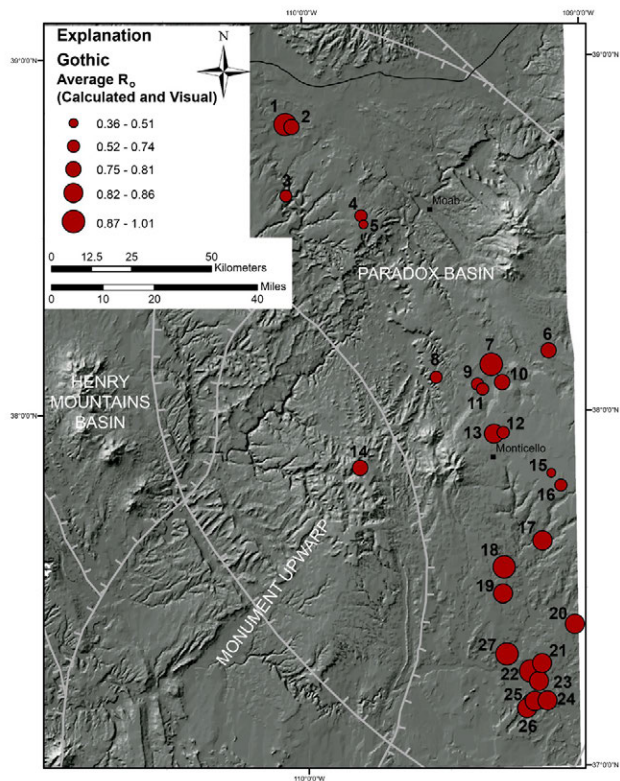


Figure 6.31. Averaged vitrinite reflectance for wells penetrating the Gothic shale of the Paradox Formation, Paradox Basin, Utah. See appendix C for source of data. Well names: 1 = Government Smoot 1; 2 = Salt Wash Unit 1; 3 = Bowknot Unit 43-20; 4 = Tidewater Oil Co 74-11; 5 = Big Flat Unit 3; 6 = Big Indian 6; 7 = Federal 1-31; 8 = Hart Point Federal 1; 9 = Marie Ogden State 1; 10 = Winchester 21-1H; 11 = Church Rock Unit 1; 12 = Jefferson 4-1; 13 = Morris Nelson 6-11; 14 = Elk Ridge Unit 1; 15 = S.P. Meyer 1; 17 = Lake Canyon Federal 1-27; 18 = Deadman Canyon Unit 1; 19 = Alkali Point 17-22; 20 = Federal G-G1; 21 = McElmo Creek Unit T-04; 22 = Aneth K-231; 23 = McElmo Creek Unit R-18; 24 = Navajo Tribal 34-31; 25 = Clay Canyon 32-11; 26 = Lone Mountain Canyon 1-33; 27 = Aneth Unit H-117.

Figure 6.32. Averaged total organic carbon for wells penetrating the Gothic shale of the Paradox Formation, Paradox Basin, Utah. See appendix C for source of data; wells are listed on figure 6.29.

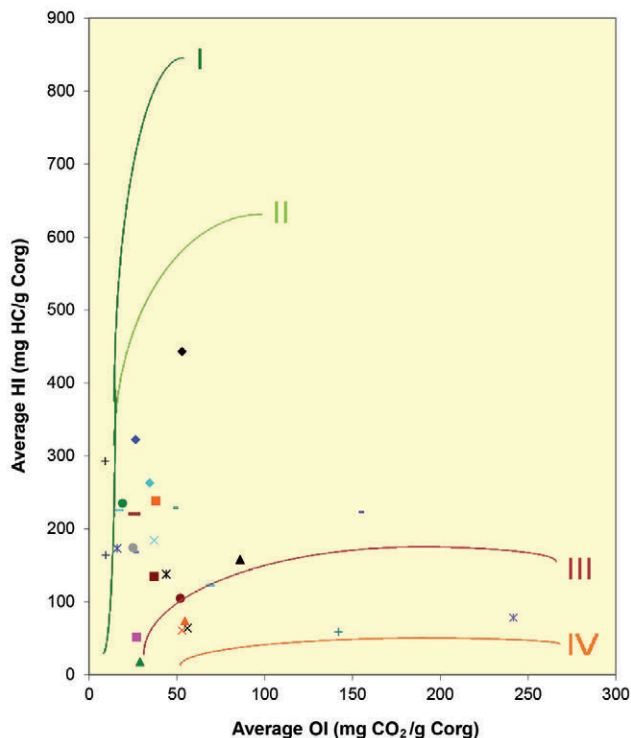


Figure 6.33. Pseudo-van Krevelen plot of wells through the Gothic shale, Paradox Formation, Utah. Most of the wells are in the type II gas-prone window, with a few in the type III immature kerogen zone.

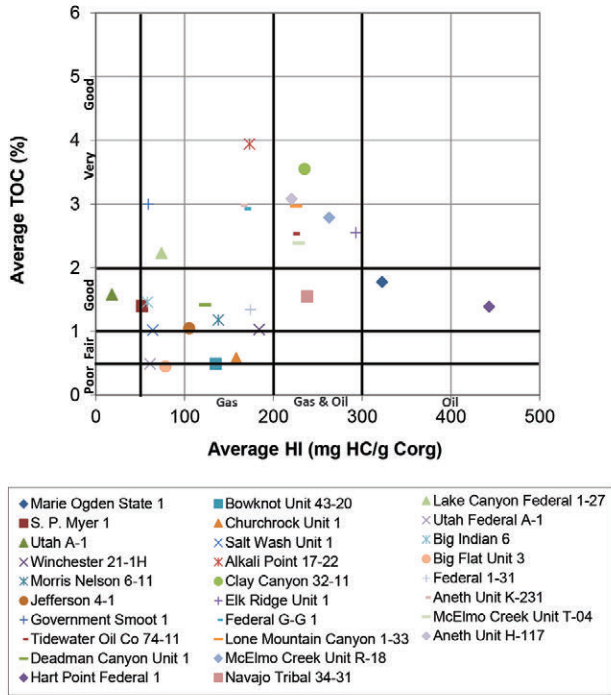


Figure 6.34. Plot comparing the average hydrogen index and amount of total organic carbon for wells through the Gothic shale, Paradox Formation, Utah.

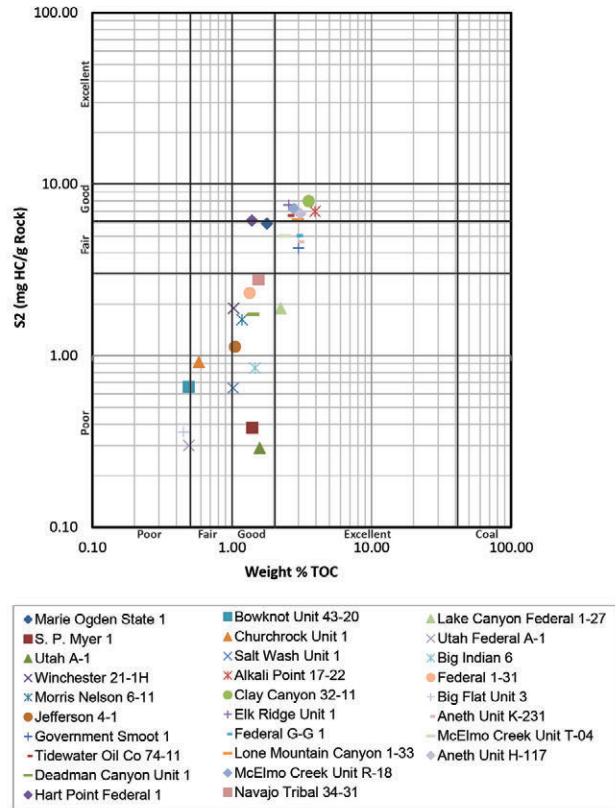


Figure 6.35. Logarithmic cross plot comparing amount of total organic carbon (TOC) with the amount of generated hydrocarbons from the decomposition of kerogen (S2) for the Gothic shale, Paradox Formation, Utah.

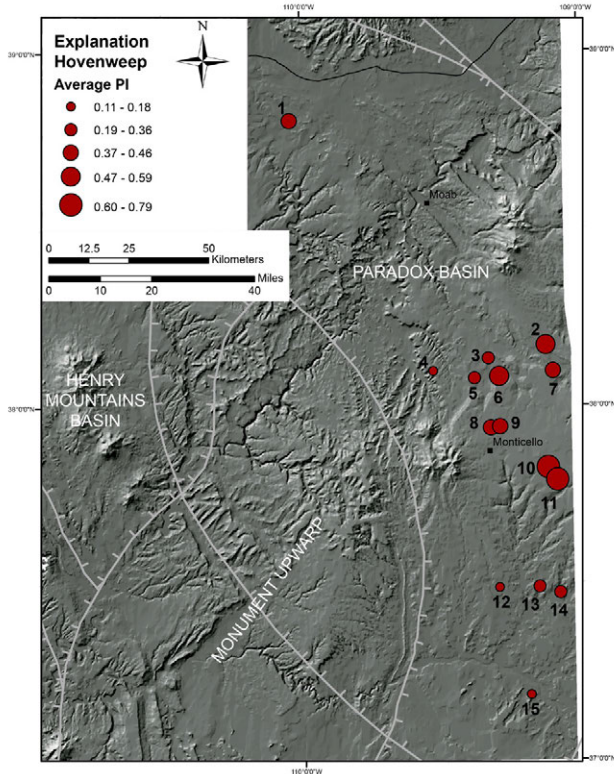


Figure 6.36. Averaged production index for wells penetrating the Hovenweep shale of the Paradox Formation, Paradox Basin, Utah. See appendix C for source of data. Well names: 1 = Salt Wash Unit 1; 2 = Big Indian 6; 3 = Federal 1-31; 4 = Hart Point Federal 1; 5 = Marie Ogden State 1; 6 = Winchester 21-1H; 7 = Utah Federal A-1; 8 = Morris Nelson 6-11; 9 = Jefferson 4-1; 10 = Utah A-1; 11 = S.P. Meyer 1; 12 = Alkali Point 17-22; 13 = Cliffhouse Buttes Federal 1-15; 14 = Federal 20-2; 15 = Clay Canyon 32-11.

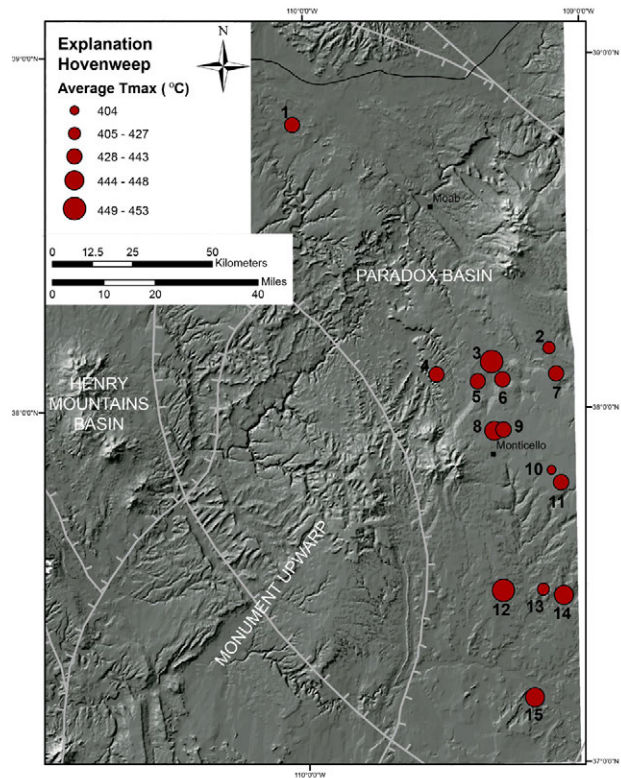


Figure 6.37. Averaged Tmax for wells penetrating the Hovenweep shale of the Paradox Formation, Paradox Basin, Utah. See appendix C for source of data; wells are listed on figure 6.36.

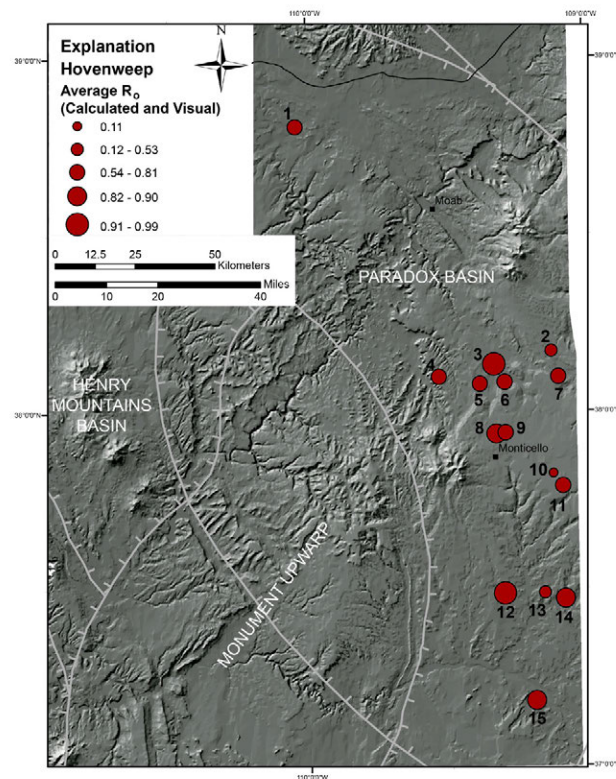
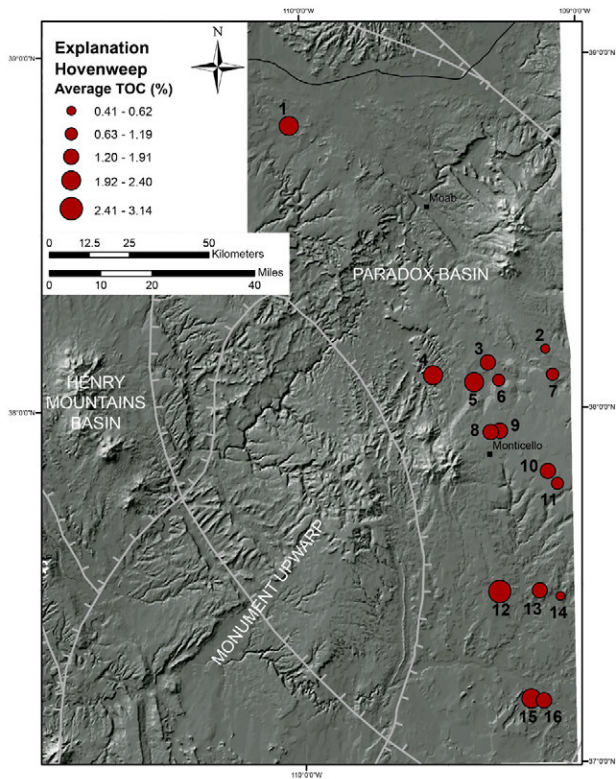


Figure 6.38. Averaged total organic carbon for wells penetrating the Hovenweep shale of the Paradox Formation, Paradox Basin, Utah. See appendix C for source of data. Well names: 1 = Salt Wash Unit 1; 2 = Big Indian 6; 3 = Federal 1-31; 4 = Hart Point Federal 1; 5 = Marie Ogden State 1; 6 = Winchester 21-1H; 7 = Utah Federal A-1; 8 = Morris Nelson 6-11; 9 = Jefferson 4-1; 10 = Utah A-1; 11 = S.P. Meyer 1; 12 = Alkali Point 17-22; 13 = Cliffhouse Buttes Federal 1-15; 14 = Federal 20-2; 15 = Clay Canyon 32-11; 16 = Navajo Tribal 34-33.

Figure 6.39. Averaged vitrinite reflectance for wells penetrating the Hovenweep shale of the Paradox Formation, Paradox Basin, Utah. See appendix C for source of data; wells are listed on figure 6.36.

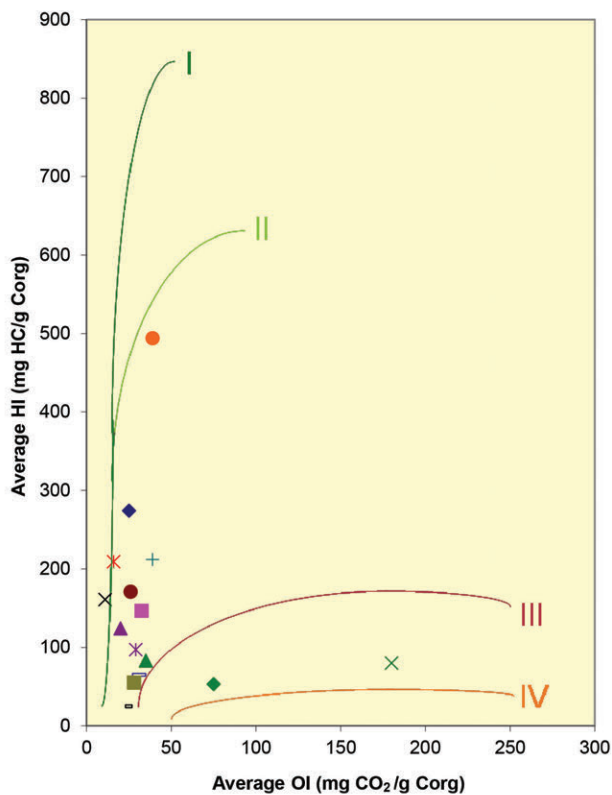


Figure 6.40. Pseudo-van Krevelen plot of wells through the Hovenweep shale, Paradox Formation, Utah. The majority of the wells are in the type II gas-prone window, with two wells in the type III immature kerogen zone.

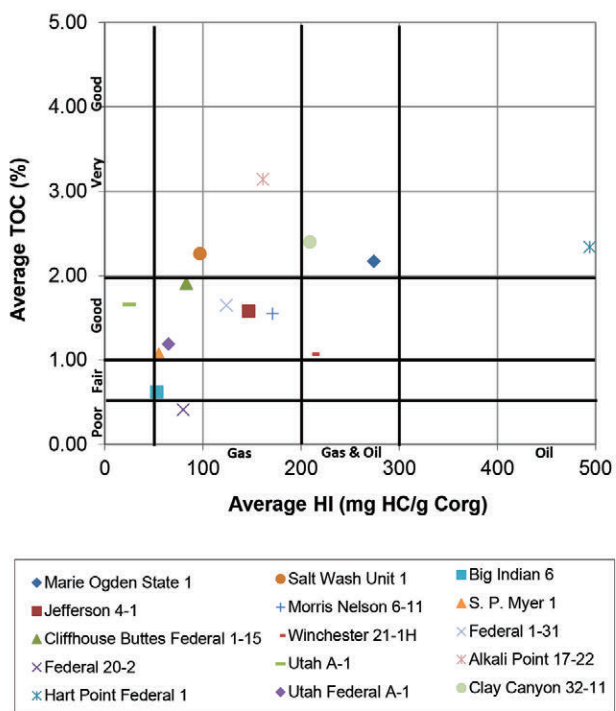


Figure 6.41. Plot comparing the average hydrogen index and amount of total organic carbon for wells through the Hovenweep shale, Paradox Formation, Utah.

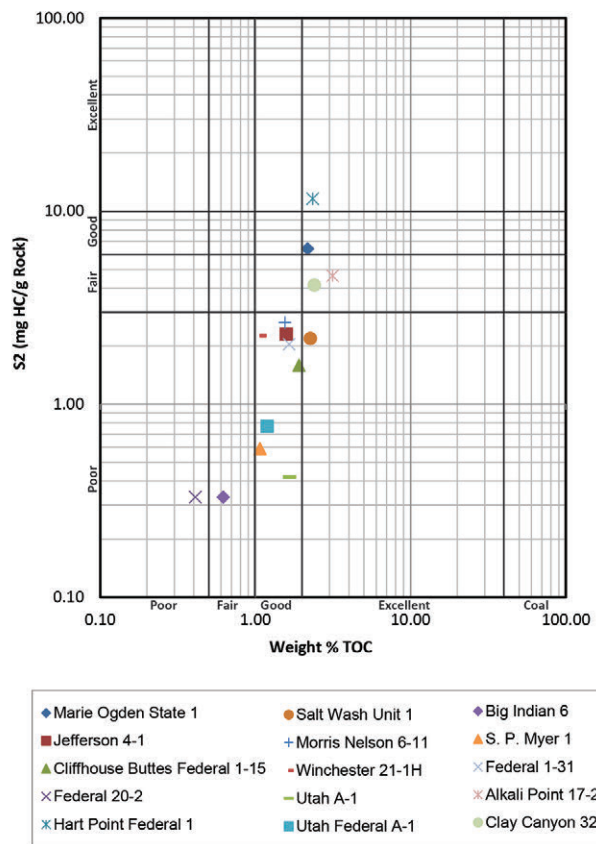


Figure 6.42. Logarithmic cross plot comparing amount of total organic carbon (TOC) with the amount of generated hydrocarbons from the decomposition of kerogen (S2) for the Hovenweep shale, Paradox Formation, Utah.

CHAPTER 7: PETROPHYSICS AND ROCK MECHANICS

BY

Thomas C. Chidsey, Jr., *Utah Geological Survey*;
S. Robert Bereskin, *Bereskin and Associates, Inc.*;
Steven Schamel, *GeoX Consulting, Inc.*

CONTENTS

INTRODUCTION	119
YOUNG'S MODULUS AND POISSON'S RATIO	119
METHODS	119
Core Plugs.....	119
Petrophysical Measurements	119
Porosity and Grain Density	120
Matrix Permeability.....	120
Fluid Saturations	120
Geomechanical Measurements	120
DOUGHNUT FORMATION.....	121
Petrophysical Analysis.....	121
Results	121
Interpretation	124
Geomechanical Analysis.....	126
Young's Modulus and Poisson's Ratio.....	126
Compressional Testing	126
PARADOX FORMATION	127
Petrophysical Analysis.....	127
Results	127
Interpretation	133
Geomechanical Analysis.....	135
Young's Modulus and Poisson's Ratio.....	135
Compressional Testing	138

FIGURES

Figure 7.1. Petrophysical properties of the Carbon Canal 5-12 core samples	122
Figure 7.2. Fluid saturation profiles measured in the Carbon Canal 5-12 core	124
Figure 7.3. Cleaned plug porosity/permeability cross plot by Doughnut lithofacies, Carbon Canal 5-12 core.....	125
Figure 7.4. Crushed shale porosity/permeability cross plot by Doughnut lithofacies, Carbon Canal 5-12 core.....	125
Figure 7.5. Porosity/grain density (crushed shale and plug data) cross plot by Doughnut lithofacies, Carbon Canal 5-12 core.....	126
Figure 7.6. Deviatoric stress versus radial and axial strain based on triaxial testing, Doughnut Formation, Carbon Canal 5-12 core.....	128
Figure 7.7. Porosity and permeability plots for the Marie Ogden State 1 core samples	129
Figure 7.8. Density and saturation plots for the Marie Ogden State 1 core samples.....	129
Figure 7.9. Bound clay water versus water saturation, Marie Ogden State 1 core samples	130
Figure 7.10. Porosity and permeability plots for the Jefferson State 4-1 core samples.....	131
Figure 7.11. Gas-filled porosity versus pressure decay permeability, Jefferson State 4-1 core samples.....	131
Figure 7.12. Density and saturation plots for the Jefferson State 4-1 core samples	132
Figure 7.13. Bound clay water versus water saturation, Jefferson State 4-1 core samples	132
Figure 7.14. Porosity and permeability plots for the Aneth Unit H-117 core samples.....	133
Figure 7.15. Gas-filled porosity versus pressure decay permeability, Aneth Unit H-117 core samples.....	133
Figure 7.16. Density and saturation plots for the Aneth Unit H-117 core samples	134
Figure 7.17. Bound clay water versus water saturation, Aneth Unit H-117 core samples	134
Figure 7.18. Porosity/permeability plots from Paradox Formation shale beds examined from three study wells	134
Figure 7.19. Variation of laboratory and logging-predicted values for Poisson's ratio, Jefferson State 4-1 well	138
Figure 7.20. Synthesized values of static and dynamic Young's modulus, Jefferson State 4-1.....	138
Figure 7.21. Vertical and horizontal dynamic Young's modulus as a function of vertical and horizontal static Young's modulus, Aneth Unit H-117 well.....	140
Figure 7.22. Vertical and horizontal dynamic Poisson's ratio as a function of vertical and horizontal static Poisson's ratio, Aneth Unit H-117 well.....	140
Figure 7.23. Plot of axial stress difference versus radial and axial strains for the Gothic and Hovenweep shales, and the lower and upper Ismay zones, Marie Ogden State 1 well	140
Figure 7.24. In-situ compressive strength and the stress drop at failure plotted against the sonic porosity, Jefferson State 4-1 core	141

Figure 7.25. Logging inference of in-situ strength based on the sonic porosity, Jefferson State 4-1 core	141
Figure 7.26. Logging inference of brittleness based on estimates of stored energy, Jefferson State 4-1 core	141
Figure 7.27. Results of unconfined compression testing, Aneth Unit H-117 core.....	142
Figure 7.28. Continuous unconfined compressive strength profile of the Gothic shale core, Aneth Unit H-117 well.....	143

TABLES

Table 7.1. Summary of petrophysical measurements (conventional plug analysis – Dean-Stark fluid saturations), Doughnut Formation, Carbon Canal 5-12 core	122
Table 7.2. Summary of petrophysical measurements (gas shale core analysis), Doughnut Formation, Carbon Canal 5-12 core	123
Table 7.3. Triaxial static Young’s modulus, Poisson’s ratio, and compressive strength measurements from the Doughnut Formation, Carbon Canal 5-12 core	126
Table 7.4. Acoustic velocities and dynamic moduli at triaxial conditions from the Doughnut Formation, Carbon Canal 5-12 core	127
Table 7.5. Summary of petrophysical measurements of core samples from three wells in the Paradox Formation, Paradox Basin	130
Table 7.6. Triaxial static Young’s modulus, Poisson’s ratio, and compressive strength measurements from the Paradox Formation, Marie Ogden State 1 core	135
Table 7.7. Triaxial static Young’s modulus, Poisson’s ratio, and compressive strength measurements from the Paradox Formation, Jefferson State 4-1 core.....	136
Table 7.8. Acoustic velocities and dynamic moduli at triaxial conditions from the Paradox Formation, Jefferson State 4-1 core	136
Table 7.9. Triaxial static Young’s modulus, Poisson’s ratio, and compressive strength measurements from the Gothic shale, Paradox Formation, Aneth Unit H-117 core.....	138
Table 7.10. Acoustic velocities and dynamic moduli at triaxial conditions from the Gothic shale, Paradox Formation, Aneth Unit H-117 core	139

CHAPTER 7:

PETROPHYSICS AND ROCK MECHANICS

INTRODUCTION

Shales are heterogeneous and strongly anisotropic. Thus analysis of the heterogeneity is a necessary component of shale reservoir evaluations, and has subsequent utility for stimulation and completion design (hydraulic fracturing, log calibration, horizontal well stability, etc.). One of the most significant observations in shale analysis is the poor differentiation of rock properties by individual geophysical log measurements. Thus logs alone do not provide reliable information for analysis and evaluation of shale. Comprehensive laboratory testing can relate laboratory-measured properties to log responses. Once these relationships are established, geophysical well logs are highly valuable tools for exploration, development, and well engineering.

Shale analysis included a thorough description of fundamental reservoir properties (basic reservoir parameters), mechanical properties, and in-situ stress. Laboratory measurements on core and data analysis had the specific goal of comprehensively characterizing the petrophysical and mechanical properties of the potential Paleozoic shale-gas reservoirs. The study results can be used to determine the geologic controls on reservoir quality, locating field development wells, and planning engineering best completion practices.

YOUNG'S MODULUS AND POISSON'S RATIO

Young's modulus is a measure of the stiffness of an isotropic elastic material. It is defined as the ratio of the uniaxial stress over the uniaxial strain in the range of stress in which Hooke's Law (a linear relationship between stress and strain) holds. Young's modulus is the ratio of stress, which has units of pressure (typically in 10^6 psi or gigapascal [GPa]), to strain, which is dimensionless; therefore Young's modulus itself has units of pressure. It can be expressed as:

$$E = \sigma / e \quad \text{Eq. 7-1}$$

where σ = stress, e = extension (one dimensional strain), and E = Young's modulus. It is a measurement of the difficulty of deforming a rock (Fossen, 2010). Rocks with low E values are weak and easily deformed. For example, the E values for shale have a wide range of 0.7 to 10×10^6 psi (5–70 GPa). Limestone has an E value of 12×10^6 psi (80 GPa), whereas sandstone E values range from 1.5 to 3×10^6 psi (10 to 20 GPa), (Fossen, 2010).

Poisson's ratio is the ratio between strain on a rock (or core sample) in one direction and the resulting strain perpendicular to that direction (Fossen, 2010). In other words, Poisson's ratio compares the contraction or transverse strain (normal to the applied load), to the extension or axial strain (in the direction of the applied load). It can be written as:

$$\nu = -e_x / e_z \quad \text{Eq. 7-2}$$

where e_x = perpendicular elongation, e_z = parallel elongation, and ν = Poisson's ratio (the minus is omitted when referring to rocks). It is a measure of compressibility perpendicular to an applied stress. The closer to $\nu = 0.5$, the less compressible the substance is; ν is almost 0.5 for rubber. Poisson's ratio values for shale, like Young's modulus, range widely from 0.03 to 0.4. Limestone can have ν values from 0.15 to 0.4, while sandstone ν values may be from 0.21 to 0.38 (Fossen, 2010).

METHODS

Core Plugs

Core-plug sampling was used for additional measurements along the whole core. Core-plug sampling requires a sufficient number of carefully selected sample locations to facilitate a representative description of reservoir quality in shale. Because slight changes in mineralogy, texture, or fluid content may result in significant differences in mechanical properties of shale, the selection of core-plug samples for laboratory characterization is of critical importance for subsequent analysis and the ability to predict reservoir properties. In heterogeneous and/or thinly inter-bedded shale, poor sampling may result in a poor or biased representation. Samples are used to identify patterns in the geophysical log responses and discriminate small but consistent variations in the combined log responses along the length of the shale. The principal goals of well-selected core plugs were to (1) develop a clear definition of the potential shale-gas reservoirs, (2) identify their petrophysical and geomechanical properties, and (3) construct a core to well log integration model that honors all the laboratory-measured properties and relates them to their corresponding log responses.

Petrophysical Measurements

Petrophysical measurements (Tight Rock Analysis [TRA] performed by TerraTek Schlumberger and Core Laboratories) were conducted to determine the density, porosity, permeabil-

ity, saturations (gas, oil, and water), and bound water of potential Utah shale-gas reservoirs. These petrophysical data are presented in appendix M. These measurements are fundamental for gas-in-place and gas productivity evaluations of potential shale gas reservoirs. The tests characterize the gas-filled and the effective porosities, the fluid saturations including mobile hydrocarbons (such as condensates), and the “as received” matrix permeability to gas. Pressure decay permeability measures to 10 nanodarcies accurately under reservoir net confining stress conditions and permits effective permeability to be measured at residual fluid pressure without moving fluid in the pore system. The methods described below represent Core Laboratories procedures found in Grover (2008).

Approximately 300 g of sample was removed from each preserved core section. Each sample was weighed and the bulk volume was measured by mercury immersion. These initial measurements were performed to determine natural sample density (bulk density). Each sample was processed using a mechanical rock crusher and sieved through 20 and 35 U.S. standard mesh sieve screens. The material retained on the 35-mesh screen was separated into a Dean-Stark sub-sample (~100 g), a permeability sub-sample (~30 g), and an atmospheric distillation sub-sample (~70 g). These procedures were performed while minimizing exposure time and evaporative losses. These sample splits were sealed in airtight vials.

Porosity and Grain Density

Porosity was determined by measuring grain volume at ambient conditions using the Boyle’s Law double-cell technique with helium as the expansion gas. Sample bulk volume was calculated using the weight of the sample before extraction and the bulk density of the original core piece. Grain density values were calculated by direct measurement of grain volume and weight on dried crushed samples.

Matrix Permeability

Matrix permeability was determined by monitoring pressure decay. The permeability sub-sample was placed into a sealed sample chamber and approximate 30 cc of helium gas at ~200 pounds force per square inch gauge (psig) was injected into the sample chamber system. Pressure decay was recorded in 0.25-second increments to a maximum time of 2000 seconds. Pressure versus time data were used to calculate matrix permeability.

Fluid Saturations

The Dean-Stark sub-samples were placed in glass thimbles to eliminate grain loss and weighed. The samples were loaded into the Dean-Stark apparatus and refluxed for seven days. Water volumes were recorded twice daily to ensure complete water extraction. The extraction solvent discoloration was noted to validate removal of trace quantities of mobile hy-

drocarbon. The retort sub-sample was sealed in a retort cup for atmospheric distillation. Distilled fluids were recovered in calibrated receiving tubes. These fluid volumes were used to calculate values for bound hydrocarbon saturation and bound water saturation.

Geomechanical Measurements

Rock mechanics tests (triaxial compression testing) were performed to assess the variability of elastic properties and in-situ stresses. They simulate in-situ reservoir stress conditions. As stated earlier, shales, in particular, are strongly heterogeneous and anisotropic, and thus their elastic properties differ in the vertical and horizontal directions. This contrast in elastic properties is not directly measured by geophysical well logs, but can have a dominant impact on predictions of in-situ stress. Therefore, the evaluation of anisotropic material properties and the in-situ stress throughout the core (for example, in-situ stress variations with respect to reservoir units and seals) is of fundamental importance. In-situ stress analysis of potential gas-shale reservoirs was conducted to obtain a reasonable profile of the in-situ stress tensor (magnitude and orientation). In-situ stress analysis and mechanical property measurements provide fundamental data for evaluation of fracture containment. All geomechanical data and graphs produced from the study are included in appendix N. The methods described below represent TerraTek procedures presented in their various lab reports.

Triaxial compression testing was performed: (1) to provide data points for determining a failure locus (Mohr envelope), (2) for parameters needed in constitutive modeling for numerical stability calculations, and (3) to provide parameters for hydraulic fracturing design. In a conventional triaxial compression test, a cylindrical core sample is loaded axially to the point of failure, at constant confining pressure. Conceptually, the peak value of the axial stress is taken as the confined compressive strength of the sample. In addition to axial stress, axial and radial strains may be monitored during this test to determine basic elastic constants (Young’s modulus [E] and Poisson’s ratio [ν]). In view of the variability of rock properties, when adequate samples are available, repeat testing may be merited to determine average values. If triaxial testing is performed at several confining pressures, and preferably if unconfined compression and tensile test data are available, a representative failure locus can be constructed. The selected confining pressures for triaxial testing are generally spread over a range from very low to beyond the maximum anticipated in-situ effective stress conditions. Measurements performed at in-situ temperature and pore pressure can be applied.

Axial load is applied with a servo-controlled actuator. Confining pressure and pore pressure are hydraulically generated. Axial force up to 1.5×10^6 psi can be applied to samples up to ten inches in diameter. Axial stress is monitored with a load cell. Confining pressure and pore pressure are monitored with

conventional pressure transducers. Axial and radial strains are measured using cantilever type strain transducers. Tests can be conducted at temperatures up to 500°F (260°C). In-flow or outflow of pore fluid is measured with accumulators (or burettes with pressure transducers, if the test is drained to atmosphere).

The sample preparation steps are listed below:

- A cylindrical sample with a length-to-diameter ratio of two (common diameters are 1, 1.5, and 2 inches—although numerous others can be tested) was cut with an inert fluid and the ends ground flat and parallel, in accordance to International Society for Rock Mechanics (ISRM) standards (recommended tolerance in end parallelism is ± 0.001 inches).
- The sample was pre-saturated with an appropriate native fluid (or other desired fluids).
- The sample was installed between hardened-steel end caps and this assembly was sealed with a thin, deformable, heat shrink jacketing material. The jacket prevents confining fluid from penetrating the sample and allows independent control and monitoring of the confining and pore pressures during testing. The end caps are ported to allow application of pore pressure and/or flow if permeability is measured.

The assembled sample and instrumentation fixtures were installed in a pressure vessel.

- The pressure vessel was filled with hydraulic confining fluid. The confining pressure (σ_3) was raised to a nominal value (100 psi) at a servo-controlled rate (3 psi/s for example). This initial confining pressure was applied so that there will always be at least a small difference between confining pressure acting outside of the jacket and pore pressure in the rock (inside the jacket). Otherwise leakage will occur.
- The confining pressure (σ_3) and the pore pressure (P_p) were simultaneously increased at a controlled rate (for example, 1 psi/s) until the pore pressure reached a target value.
- The pore pressure was maintained constant and the confining pressure was increased at a controlled rate until σ_3 reached a specified value.
- The axial stress difference ($\sigma_1 - \sigma_3$) was increased at a rate corresponding to an axial strain rate of $10^{-5}/s$. Alternatively, rather than controlling the axial strain rate, the axial stress rate can be controlled. Loading is continued until the sample fails. If behavior was not brittle, loading was continued so that the post-peak regime was adequately defined.
- The sample was unloaded slowly, the pressure vessel was emptied and the sample assembly was disassembled.

- The sample was examined, documented, and archived in a specified manner.

Experimental results are represented as stress-strain curves, and tabulated values of elastic constants and strength. The stress-strain data were used to determine the compressive strength and elastic constants. Typical stress-strain curves show axial and radial strains (radial strains are measured at 90° to each other) as a function of the axial stress difference.

The equations used to obtain the elastic constants and the compressive strength are:

$$E = \frac{\Delta(\sigma_1 - \sigma_3)}{\Delta\varepsilon_a} \quad \text{Eq. 7-3}$$

$$\nu = \frac{\Delta\varepsilon_r}{\Delta\varepsilon_a} \quad \text{Eq. 7-4}$$

$$C(\sigma'_3) = \sigma'_1{}^{\max} \quad \text{Eq. 7-5}$$

where:

E	=	Young's modulus (psi),
ν	=	Poisson's ratio (dimensionless),
$C(\sigma'_3)$	=	compressive strength (psi),
σ_1	=	total axial stress (psi),
$\sigma_1{}^{\max}$	=	maximum (peak) total axial stress (psi),
$\sigma'_1{}^{\max}$	=	maximum (peak) effective axial stress (psi),
ε_a	=	axial strain (inch/inch),
ε_r	=	radial strain (inch/inch), and
Δ	=	change in the relevant quantity.

DOUGHNUT FORMATION

The 544.4 feet (165.9 m) of Doughnut Formation core in the Carbon Canal 5-12 well provides a wealth of material to conduct petrophysical and rock mechanics analyses. Most of these data were donated to the UGS by the operator, Shell Western Exploration & Production, Inc., and are included in appendices M and N. A suite of rock samples from the Carbon Canal 5-12 core was analyzed from the full length of the core. The samples represent the range of lithotypes in the Doughnut—a mix of carbonaceous, argillaceous, silty limestone to calcareous shale beds.

Petrophysical Analysis

Results

Two types of porosity-permeability measurements are reported (figure 7.1 and tables 7.1 and 7.2). The conventional plug analysis (table 7.1) is an unsteady-state, pressure-transient measurement under in-situ stress conditions. In this case,

the Klinkenberg permeability is determined at a net confining stress of 2900 psig. The porosities are in the range 1 to 5% and the permeabilities are on the order of 0.1 microdarcy (μD) to 1.0 millidarcy (mD). Gas shale core analysis measures the effective matrix permeability as determined from pressure decay from fresh crushed dry 20/35 mesh size rock samples. The crushed shale data have two porosity measurements, one on uncleaned crushed samples (gas-filled porosity) and a second porosity measurement after Dean-Stark cleaning (table 7.2). Because the samples have fairly high organic matter and the cleaning process is more effective on crushed samples, the porosity values for the cleaned crushed shale samples are relatively high and somewhat close to what is measured on the downhole porosity logs. Porosity is relative to the total interconnected pore space rather than the total pore space as with conventional plug analysis. The resulting permeability (K_g) values for the same rock samples are many orders of magnitude lower than the conventional plug analyses, in the nanodarcy range, and the porosity values extend over a somewhat broader range (figure 7.1 and tables 7.1 and 7.2). Typical gas shale has K_g of 0.00001 to 0.1 mD (10^{-8} to 10^{-4} Darcy)

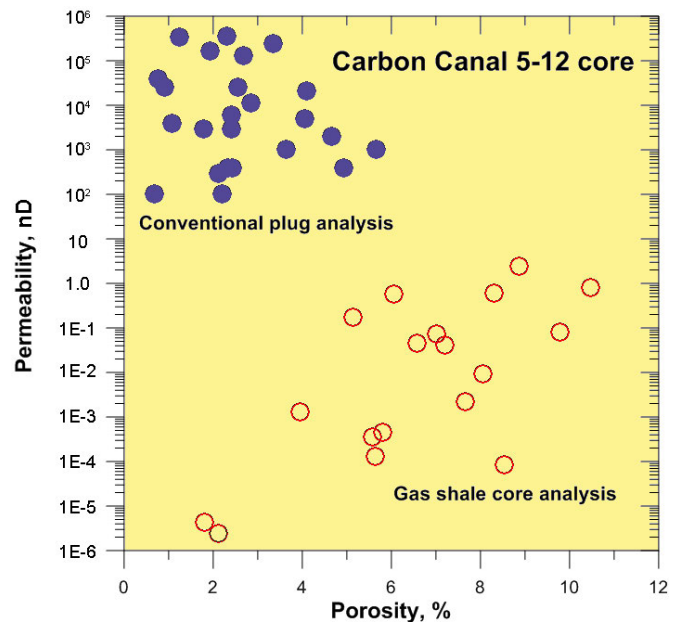


Figure 7.1. Petrophysical properties of the Carbon Canal 5-12 core samples. Data from Core Laboratories as reported in Grover (2008).

Table 7.1. Summary of petrophysical measurements (conventional plug analysis – Dean-Stark fluid saturations), Doughnut Formation, Carbon Canal 5-12 core. Modified from Grover (2008).

Depositional Environment	Depth (ft)	Porosity (%)	Permeability		Saturation		Grain Density (g/cm ³)	Description
			Klinkenberg (mD)	Kair (mD)	Oil %	Water %		
Lagoon?	8190.00	2.40	0.006	0.013	0.00	61.8	2.695	Limestone, brown-gray, very fine crystalline, shaly to silty
Middle Shoreface	8360.00	1.82	NA	NA	0.00	27.7	2.681	Siltstone, gray, shaly to limey
Shoal?	8632.00	0.91	0.025	0.026	0.00	81.0	2.702	Limestone, dark gray, very fine crystalline, shaly
Distal Shoal	8827.30	1.35	NA	NA	0.00	62.4	2.717	Shale, dark gray, limey
Shoreface	8859.00	4.93	0.0004	0.001	0.00	19.5	2.680	Sandstone, gray, very fine grained, shaly to silty
Shoreface	8882.90	3.64	0.001	0.002	0.00	75.7	2.697	Sandstone, gray, very fine grained, shaly to silty
Algal Flat	8901.00	2.38	NA	NA	0.00	34.2	2.765	Limestone, gray, very fine crystalline, shaly w/filled fractures
Bay/Shelf	8951.30	1.94	0.165	0.184	0.00	60.4	2.640	Limestone, black, very fine crystalline, shaly & carbonaceous
Bay/Shelf	8955.00	2.68	0.127	0.136	0.00	60.6	2.650	Limestone, black, very fine crystalline, shaly & carbonaceous
Bay/Shelf	8958.10	1.24	0.335	0.485	0.00	41.8	2.717	Limestone, dark gray, very fine crystalline, shaly
Bay/Shelf	8959.90	2.84	0.011	0.013	0.00	42.4	2.656	Limestone, black, very fine crystalline, shaly & carbonaceous
Bay/Shelf	8962.60	4.10	0.021	0.022	0.00	91.5	2.682	Limestone, black, very fine crystalline, shaly & carbonaceous
Algal Flat	8972.40	1.79	0.003	0.006	0.00	31.0	2.710	Limestone, gray, very fine crystalline, shaly
Restricted Bay	9012.00	4.05	0.005	0.011	0.00	83.6	2.670	Limestone, black, very fine crystalline, shaly & carbonaceous
Distal Shoal	9079.50	2.21	0.0001	0.0005	0.00	82.2	2.708	Limestone, gray, very fine crystalline, shaly
Restricted Bay	9090.90	2.11	0.0003	0.001	0.00	74.4	2.730	Limestone, gray, very fine crystalline, shaly
Distal Shoal	9108.50	3.34	0.244	0.250	0.00	90.2	2.720	Limestone, gray, very fine crystalline, shaly

Table 7.1. Continued.

Depositional Environment	Depth (ft)	Porosity (%)	Permeability		Saturation		Grain Density (g/cm ³)	Description
			Klinkenberg	Kair	Oil	Water		
			(mD)	(mD)	% Pore Volume			
Bay/Shelf	9120.15	4.66	0.002	0.006	0.00	83.5	2.633	Siltstone, black, shaly & carbonaceous w/ shaly silt laminations
Middle Shoreface	9153.80	5.65	0.001	0.003	0.00	86.1	2.701	Limestone, gray, very fine crystalline, shaly w/filled fractures
Restricted Bay	9198.00	2.43	0.0004	0.001	0.00	67.5	2.696	Limestone, black, very fine crystalline, shaly & carbonaceous
Restricted Bay	9246.00	2.40	0.003	0.006	0.00	86.8	2.653	Limestone, black, very fine crystalline, shaly & carbonaceous
Shoal	9276.00	1.08	0.004	0.009	0.00	79.9	2.700	Limestone, gray, very fine crystalline, shaly
Shoal	9280.15	0.69	0.0001	0.0002	0.00	71.0	2.810	Dolomite, gray, shaly & limey
Shoal	9292.20	2.33	0.0004	0.001	0.00	89.4	2.832	Dolomite, gray, shaly & limey
Shoal	9296	0.76	0.04	0.045	0.00	88.2	2.782	Dolomite, gray, shaly & limey
Shoreface	9324	2.3	0.352	0.369	0.00	30.6	2.900	Siltstone, light gray, very shaly, laminated, limey, pyrite
Distal Shoal	9342	2.56	0.025	0.028	0.00	64.1	2.762	Limestone, dark gray, very fine crystalline, shaly

Table 7.2. Summary of petrophysical measurements (gas shale core analysis), Doughnut Formation, Carbon Canal 5-12 core. Modified from Grover (2008).

Depositional Environment	Depth (ft)	As received				Dry & Dean-Stark Extracted Conditions ²			
		Bulk Density (g/cc)	Matrix Permeability ¹ (mD)	Gas-filled Porosity (%)	Gas Saturation (%)	Grain Density (g/cc)	Porosity (%)	Oil Saturation ³ (%)	Water Saturation ⁴ (%)
Restricted Bay	8840.60	2.683	4.37E-12	0.19	10.5	2.716	1.80	0.0	89.5
Lagoon	8872.30	2.643	3.60E-10	0.88	15.8	2.748	5.57	0.0	84.2
Lagoon	8891.70	2.679	2.43E-12	0.24	11.1	2.717	2.12	0.0	88.9
Bay/Shelf	8930.90	2.407	2.42E-06	7.00	79.0	2.620	8.86	2.1	18.9
Bay	8984.50	2.627	1.28E-09	0.98	24.6	2.704	3.96	0.0	75.4
Restricted Bay	9063.00	2.602	1.33E-10	0.84	14.8	2.706	5.64	0.0	85.2
Restricted Bay	9092.45	2.565	9.22E-09	1.86	23.1	2.721	8.05	0.0	76.9
Bay/Shelf	9115.30	2.539	2.20E-09	1.66	21.7	2.683	7.66	0.0	78.3
Bay/Shelf	9143.30	2.535	8.49E-11	0.73	8.6	2.685	8.53	0.0	91.4
Restricted Bay	9167.20	2.524	3.91E-07	4.00	53.0	2.691	7.55	0.0	47.0
Restricted Bay	9193.15	2.533	8.20E-08	3.30	33.7	2.734	9.79	0.0	66.3
Restricted Bay	9208.20	2.454	5.86E-07	2.79	46.0	2.577	6.06	0.0	54.0
Distal Shoal	9215.40	2.403	6.14E-07	3.65	44.0	2.569	8.31	0.0	56.0
Restricted Bay	9237.10	2.613	1.75E-07	1.92	37.3	2.720	5.13	0.0	62.7
Restricted Bay	9250.00	2.503	1.21E-07	1.64	32.3	2.600	5.07	0.0	67.7
Restricted Bay	9266.20	2.609	4.54E-10	0.57	9.8	2.713	5.81	0.0	90.2
Shoal	9284.30	2.612	4.47E-08	2.22	33.8	2.749	6.58	0.0	66.2
Restricted Bay	9302.30	2.529	8.12E-07	4.33	41.3	2.755	10.48	0.0	58.7
Restricted Bay	9316.20	2.779	4.12E-08	1.86	25.8	2.937	7.21	0.0	74.2
Middle Shoreface	9332.90	2.543	7.22E-08	1.94	27.6	2.680	7.02	0.0	72.4

¹ Matrix Permeability is an effective K_g determined from pressure decay results on the fresh, crushed, 20/35 mesh size sample.² Dean-Stark extracted sample (20/35 mesh size) dried at 110 °C. Porosity and saturations are relative to total interconnected pore space.³ Oil volume computed assuming an oil density of 0.8 g/cc.⁴ Water volume corrected assuming a brine concentration of 30,000 ppm NaCl with an ambient density of 1.018 g/cc.

and porosity of 4 to 6 porosity units (Lewis and others, 2004). Compared to commercial gas shale, such as the Barnett and Marcellus Shales, the Doughnut Formation samples have typical to better porosity and about half of the samples have typical matrix permeabilities. Unfortunately, the Doughnut water saturations are very large.

Fluid saturations (figure 7.2 and tables 7.1 and 7.2) are relative to the total interconnected pore space in the rock. No oil saturation was observed in the Carbon Canal well samples and the gas saturation is generally in the 10 to 50% range, somewhat higher below a depth of 9160 feet (2792 m) in the core. Consequently, the water saturations are large, 50 to 90% of pore space.

In examining the core, it was noted that 36 samples, each about one foot long (0.3 m), had been removed for gas desorption tests. The results of the tests were not provided to the UGS with the core and other rock analyses. However, most of the samples removed for measuring gas content had a reserve sample of similar size sealed in Mylar pouches. Whereas most of the pouches were deflated, in the interval from 9104 to 9248 feet (2775–2818 m) in the core the pouches were inflated, some to the point of near bursting. We interpret this phenomena to indicate the gas-rich portion of the Doughnut Formation in the core. The locations of inflated pouches are indicated in figure 5.7.

Interpretation

To determine the reservoir potential of the Doughnut Formation in the Carbon Canal 5-12 well, Grover (2008) subdivided

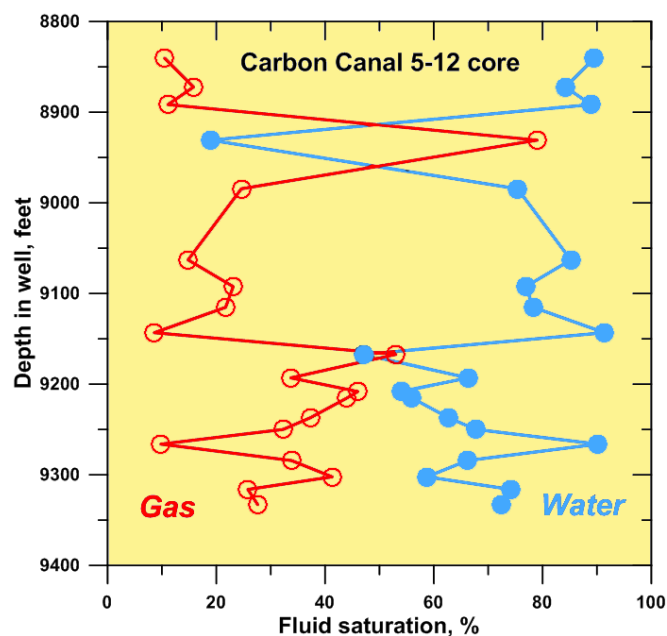


Figure 7.2. Doughnut Formation fluid saturation profiles measured in the Carbon Canal 5-12 core. Data are from Core Laboratories as reported in Grover (2008).

the core analysis data into different lithofacies and averaged various petrophysical properties (figures 7.3 through 7.5). No porosity/permeability measurements were made in the coastal-plain deposits judged to have poor reservoir potential.

The restricted lagoon and algal flat limestone beds have some of the lower porosity and permeability values (figures 7.3 and 7.4) and have very poor reservoir potential. The lagoonal limestones may have better reservoir potential if they were extensively dolomitized. The shoreface deposits have the best reservoir potential with the highest average porosity, due to intergranular pores, and the second highest average permeability (figures 7.3 and 7.4). However, clay-filled pores and pore throats reduce permeability resulting in poor to possibly fair reservoir potential in some beds. The lack of oil saturation values also lowers reservoir potential. The limestone beds of the shoal lithofacies (figures 7.3 and 7.4) have the lowest average porosity, the third lowest average permeability, and highest water saturation values. These limestone beds have very poor reservoir potential unless they are fractured or dolomitized. The pore system of the restricted marine bay lithofacies has an average (conventional plug) porosity of 2.7%, consisting of poorly developed micropores in the argillaceous matrix, and the lowest permeability (figures 7.3 and 7.4).

The bay/shelf shale beds have the second highest average porosity, dominated by micropores in micritic matrix, and the highest average permeability in the sample set (figures 7.3 and 7.4). According to Grover (2008) the amount of microporosity in clay and organic matter can be estimated by examining the difference between gas-filled porosity (measured on uncleaned samples) and total porosity on cleaned samples. The greater the difference between porosity values, the larger the volume of organic matter, bound water, and microporous clay (figure 7.4).

Grover (2008) also reports that in the cleaned plug data set a porosity/permeability cross plot by lithofacies (figure 7.3) indicates the shales show slightly higher permeability in samples with lower porosity. Cleaning of grain-poor, organic-rich shale may increase porosity but leave the non-permeable micropore system intact. The higher energy, grain-rich shale does not have much organic matter so the porosity does not increase with cleaning, but the more intergranular matrix will yield higher permeability values. For example, as grain density in the bay/shelf shale samples decreases (more organic-rich?) the porosity increases (figure 7.5).

In summary, the pore systems in most of the Doughnut Formation shale beds in the Carbon Canal 5-12 core consist of poorly interconnected micropores that result in very low permeability. Brittle silty shale beds could be susceptible to fracturing (both hydraulically induced and natural). Without natural or artificially induced fractures, the Doughnut, at least in the immediate Carbon Canal well area, has very poor inherent reservoir potential (Grover, 2008).

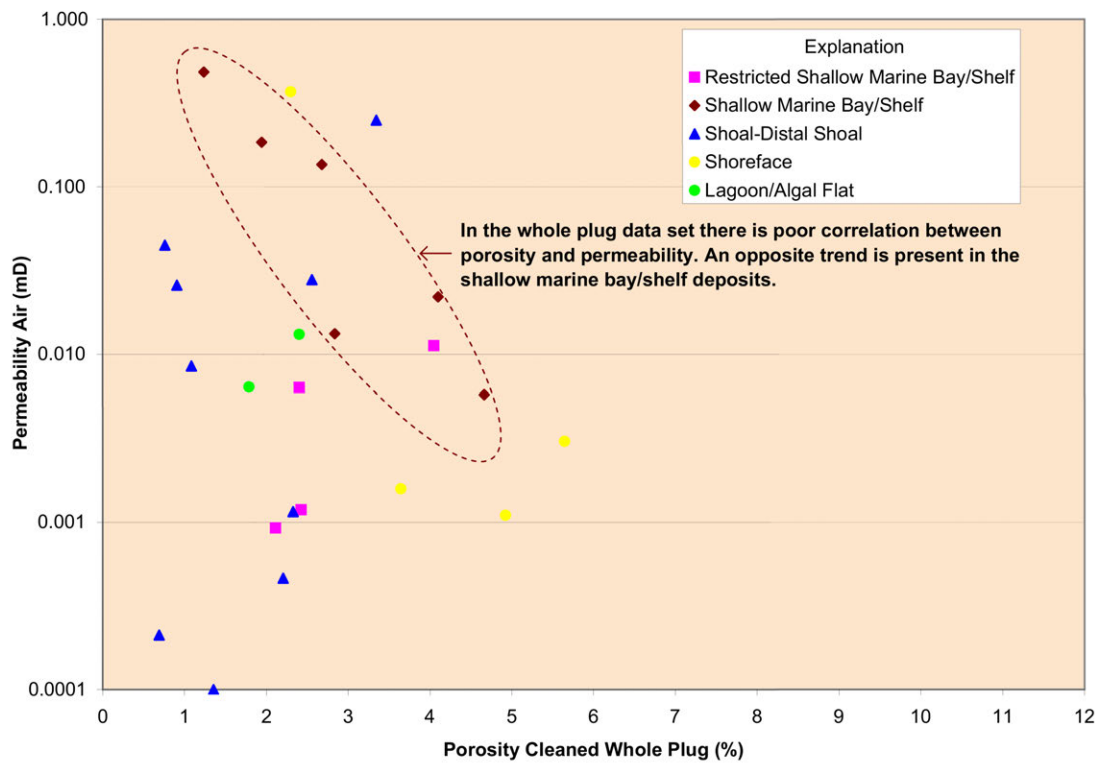


Figure 7.3. Cleaned plug porosity/permeability cross plot by Doughnut lithofacies, Carbon Canal 5-12 core. Modified from Grover (2008).

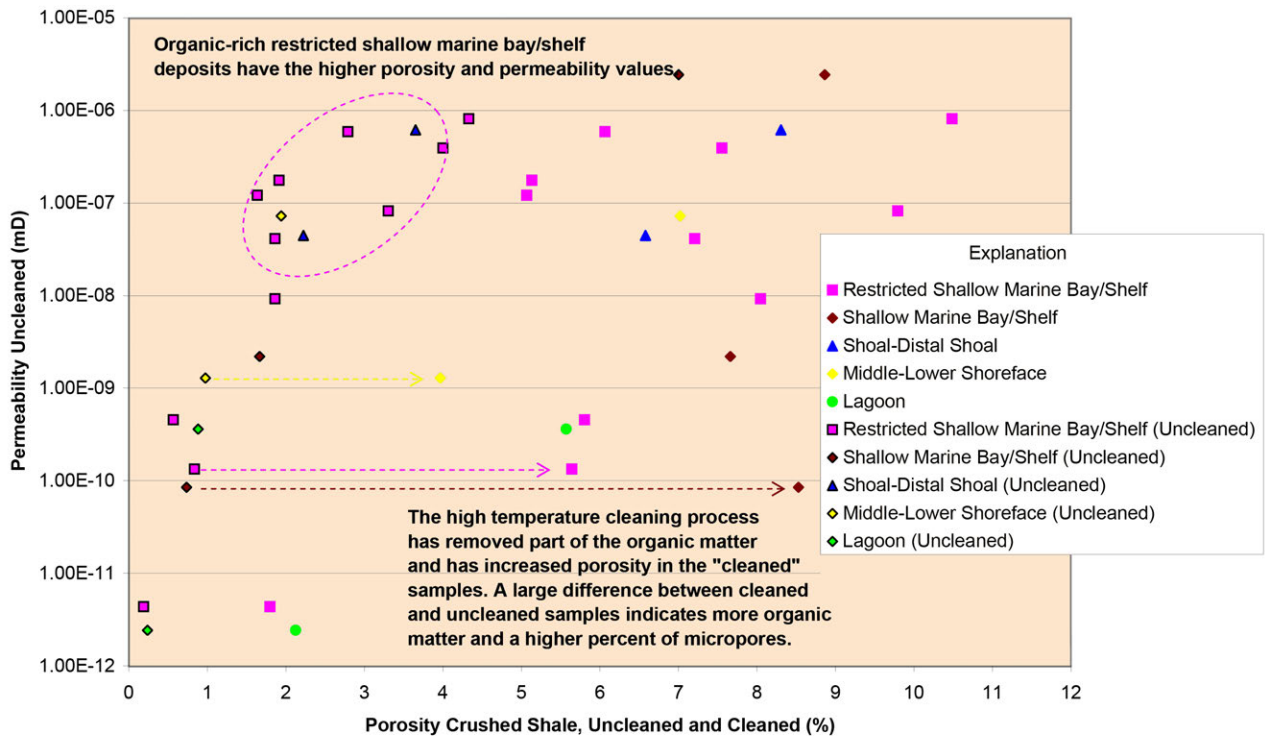


Figure 7.4. Crushed shale porosity/permeability cross plot by Doughnut lithofacies, Carbon Canal 5-12 core. Modified from Grover (2008).

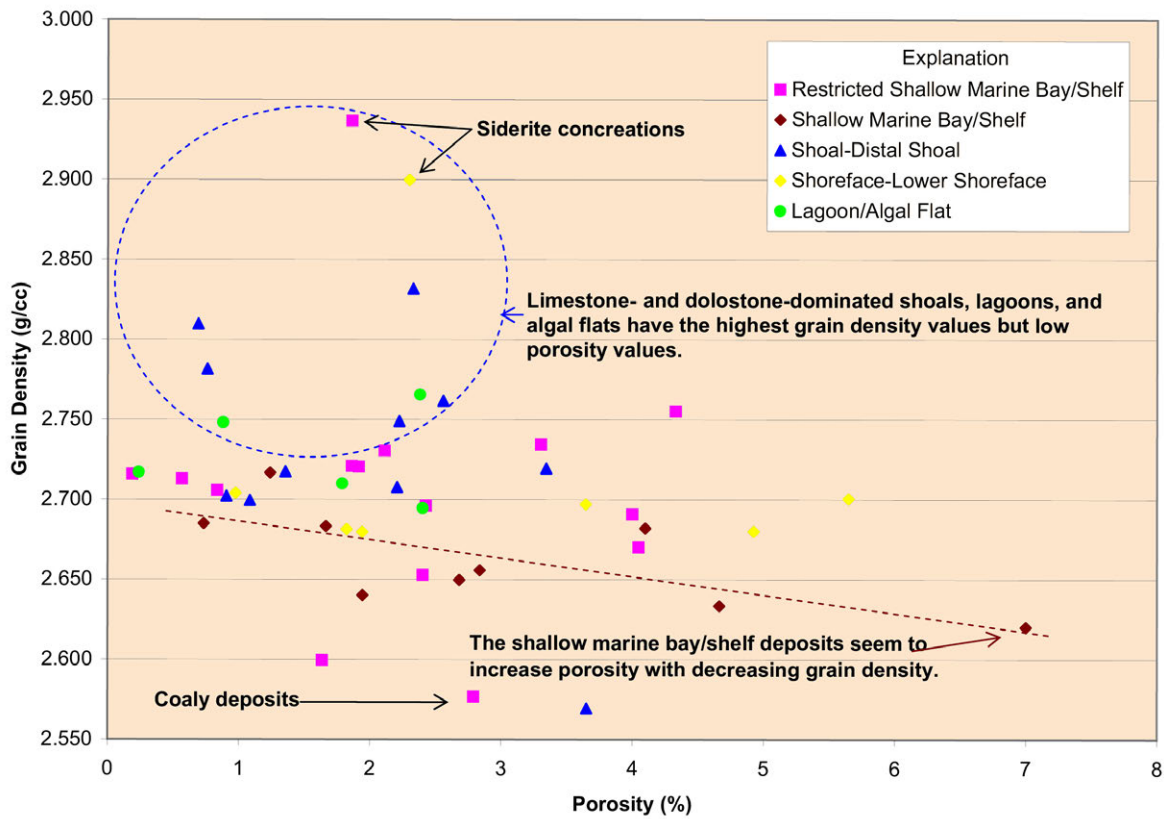


Figure 7.5. Porosity/grain density (crushed shale and plug data) cross plot by Doughnut lithofacies, Carbon Canal 5-12 core. Modified from Grover (2008).

Geomechanical Analysis

Triaxial compression measurements from the Carbon Canal 5-12 core were taken at multiple vertical locations through both potential productive zones and barriers. In addition to the static mechanical properties (table 7.3), ultrasonic wave velocities were measured using standard transmission techniques. Elastic formulae were further used to calculate the dynamic mechanical properties (table 7.4). These laboratory data can be used to calibrate logging data and optimize hydraulic fracture designs. However, for Young’s modulus dynamic values of the modulus are overestimates. Static values are required for completion design (Bereskin and McLennan, 2008).

Young’s Modulus and Poisson’s Ratio

At a confining pressure of 2040 psi for six sample depths, the static Young’s modulus values ranged from 4.32 to 10.59 x 10⁶ psi (table 7.3); the dynamic elastic Young’s modulus values range from 3.97 to 11.27 x 10⁶ psi (table 7.4). The static Poisson’s ratio values show little variation, ranging from 0.21 to 0.25; the dynamic elastic Poisson’s ratio values range from 0.12 to 0.30 (table 7.4). Compressional acoustical velocities range from 11,147 to 20,399 ft/sec; shear acoustical velocities range from 7129 to 11,347 ft/sec. The sample with the highest velocity, taken at 9276 feet (2827 m), is an argillaceous

dolomitic limestone. It has a static Young’s modulus value of 10.59 x 10⁶ psi and a Poisson’s ratio of 0.24. These values are fairly typical for limestone. The other samples are from a variety of shale beds, including calcareous/carbonaceous to silty shale, and have static Young’s modulus and Poisson’s ratio values that suggest generally non-brittle rocks.

Compressional Testing

At a confining pressure of 2040 psi for six sample depths, the compressional strength values range from 16,150 to 42,268 psi (table 7.3). The argillaceous dolomitic limestone has the

Table 7.3. Triaxial static Young’s modulus, Poisson’s ratio, and compressive strength measurements from the Doughnut Formation, Carbon Canal 5-12 core samples..

Depth (ft)	Confining Pressure (psi)	Bulk Density (gm/cm ³)	Compressive Strength (psi)	Young's Modulus (10 ⁶ psi)	Poisson's Ratio
8891.90	2040	2.69	28,543	9.85	0.25
8930.70		2.42	36,851	7.23	0.21
9276.15		2.62	42,268	10.59	0.24
9284.10		2.65	16,150	4.69	0.24
9321.35		2.49	19,614	4.32	0.21
9342.85		2.72	22,084	4.55	0.24

Table 7.4. Acoustic velocities and dynamic moduli at triaxial conditions from the Doughnut Formation, Carbon Canal 5-12 core samples.

Depth (ft)	Confining Pressure (psi)	Axial Pressure (psi)	Bulk Density (g/cc)	Acoustic Velocity				Dynamic Elastic Parameters			
				Compressional		Shear		Bulk Modulus (x10 ⁶ psi)	Young's Modulus (x10 ⁶ psi)	Shear Modulus (x10 ⁶ psi)	Poisson's Ratio
				ft/sec	μs/ft	ft/sec	μs/ft				
8891.9	2040	2040	2.71	19,642	50.91	10,725	93.24	8.48	10.80	4.20	0.29
8891.9	2040	12,000	2.71	20,399	49.02	10,898	91.76	9.40	11.27	4.33	0.30
8930.7	2040	2040	2.42	15,486	64.58	10,146	98.56	3.35	7.55	3.36	0.12
8930.7	2040	13,000	2.42	16,497	60.62	10,504	95.20	4.08	8.34	3.60	0.16
9276.2	2040	1000	2.65	18,400	54.35	11,160	89.60	6.16	10.75	4.45	0.21
9276.2	2040	12,000	2.65	18,949	52.77	11,347	88.13	6.69	11.22	4.60	0.22
9284.1	2040	2040	2.65	13,119	76.22	8160	122.54	2.98	5.64	2.38	0.18
9284.1	2040	8000	2.65	14,727	67.90	8577	116.60	4.25	6.54	2.63	0.24
9321.8	2040	2040	2.49	14,344	69.71	9175	109.00	3.14	6.52	2.83	0.15
9321.8	2040	8000	2.49	15,337	65.20	9416	106.20	3.93	7.13	2.98	0.20
9342.9	2040	2040	2.49	14,170	70.57	8810	113.51	3.27	6.18	2.61	0.18
9342.9	2040	12,000	2.49	16,655	60.04	9303	107.49	5.44	7.40	2.91	0.27
9103.0	2040	2040	2.51	11,147	89.71	7129	140.26	1.91	3.97	1.72	0.15
9103.0	3000	3000	2.51	11,621	86.05	7198	138.93	2.23	4.17	1.75	0.19

highest compressive strength whereas the non-silty shale samples have the lowest. Figure 7.6 displays plots of deviatoric stress versus radial and axial strains measured during compression triaxial testing. The figure describes the evolution of rock deformation (i.e., axial and radial strains) and failure (i.e., yield stress, peak stress, and residual strength—when available) during confined compression loading.

PARADOX FORMATION

The Gothic and Hovenweep shales of the Paradox Formation were selected for detailed petrophysical and rock mechanic analysis. Core samples were analyzed from three wells extending north to south across the Paradox Basin: Marie Ogden State 1, Jefferson State 1-4, and Aneth Unit H-117 (figure 4.2). All data, graphs, and figures generated from these analyses are included in appendices M and N.

Petrophysical Analysis

Results

In northern Blanding sub-basin, one sample was selected from the Gothic shale and two samples from the Hovenweep shale in the Marie Ogden State 1 core. The results are summarized in table 7.5. Porosity varies only slightly between the two shales and averages 2.3% (figure 7.7A); permeability shows little variation with depth (figure 7.7B) and averages 0.116 μD. Bulk and grain density increase slightly with depth (figure 7.8A) and are 2.62 and 2.67 g/cc, respectively, for the Gothic, and average 2.59 and 2.65 g/cc, respectively, for the

Hovenweep. Water saturations show a small increase with depth (figure 7.8B) ranging from 14.7 to 20.8%. Figure 7.9 is a cross-plot of bound clay water versus water saturation. Bound clay water is less in the Gothic (5.1% based on the one sample) than in the Hovenweep (6.1 to 6.5%).

In the Jefferson State 4-1 core, two samples were selected from both the Gothic and Hovenweep shales (table 7.5). Porosity varies in both zones, 2.4% in the Gothic and 3.4% in the Hovenweep (figure 7.10A). The permeability is lower than that found in these same shales in the Marie Ogden State 1 core to the north, averaging 0.06 μD (figure 7.10B). Figure 7.11 is a cross-plot of pressure-decay permeability versus gas-filled porosity and reflects the variations of porosity whereas the permeabilities show minor differences among the samples. Bulk and grain density vary slightly through the samples with depth (figure 7.12A), averaging 2.64 and 2.69 g/cc, respectively, for the Gothic and average 2.62 and 2.68 g/cc, respectively, for the Hovenweep. Water saturations (figure 7.12B) are less in the Gothic than in the Hovenweep (averaging 6% versus 12%). Bound clay water is less in the Gothic (3.0 to 4.1%) than in the Hovenweep (4.3 to 4.4%) (figure 7.13). This suggests that the Hovenweep is more clay rich than the Gothic. The lower water saturations in the Gothic imply a higher hydrocarbon saturation. Thus, the plot shown on figure 7.13 shows the Gothic to have the greater reservoir potential.

On the Aneth platform in the southern part of the basin, four samples from the Gothic shale were selected from the Aneth Unit H-117 core (table 7.5). Porosity varies just over a percentage point from 2.72 to 4.30% (figure 7.14A); permeability does not vary significantly with depth (figure 7.14B), averag-

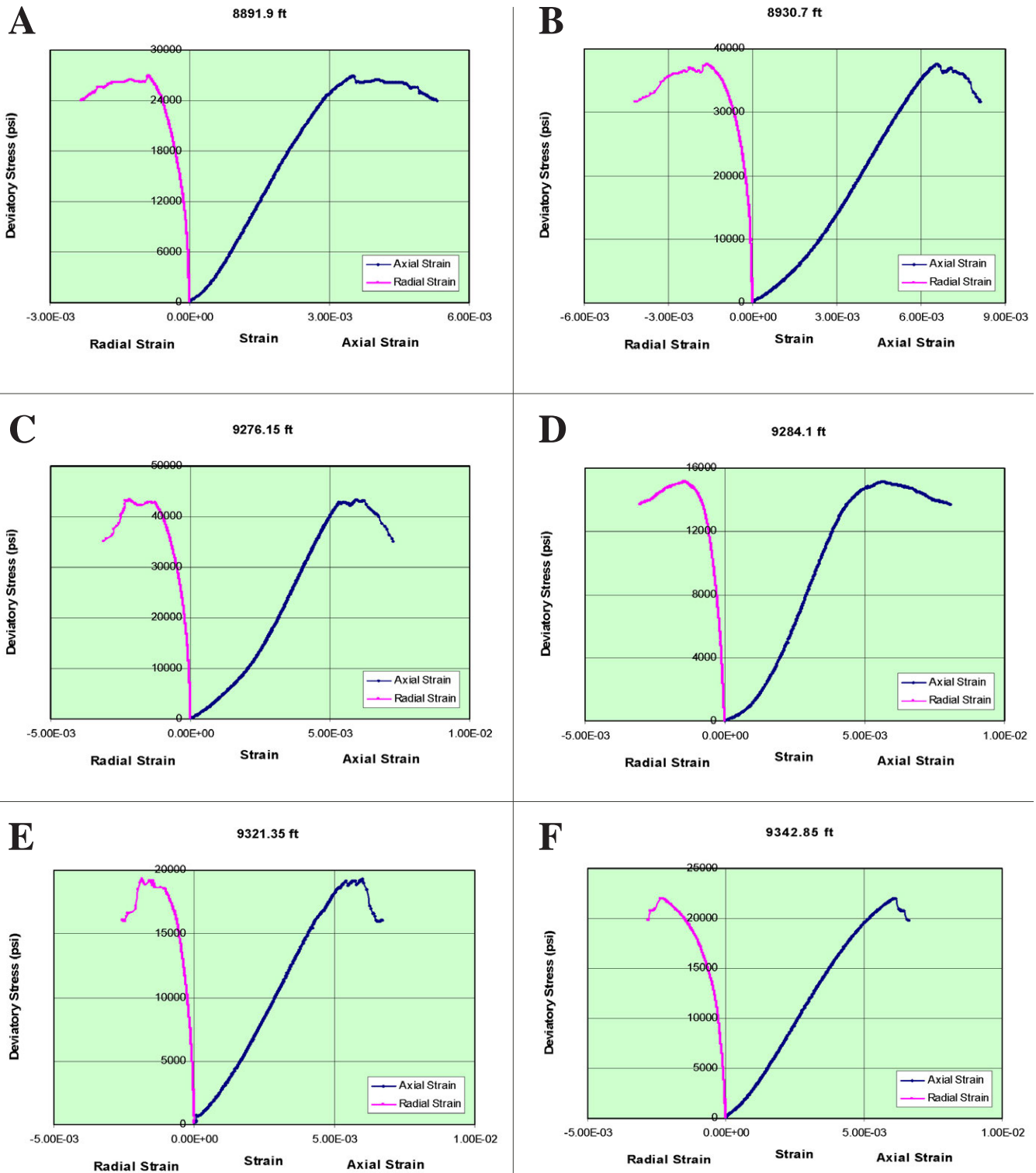


Figure 7.6. Deviatory stress versus radial and axial strain at six depths (A through F) based on triaxial testing, Doughnut Formation, Carbon Canal 5-12 core. Modified from Grover (2008).

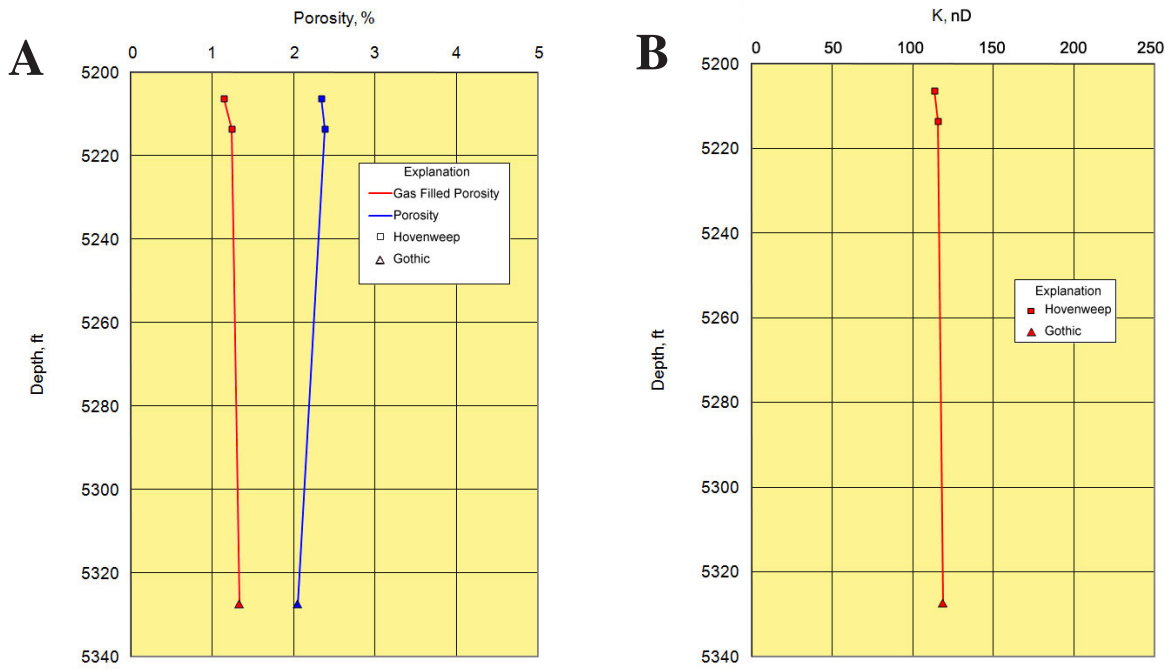


Figure 7.7. Porosity and permeability plots for the Marie Ogden State 1 core samples. **A.** Porosity versus depth. **B.** Permeability versus depth.

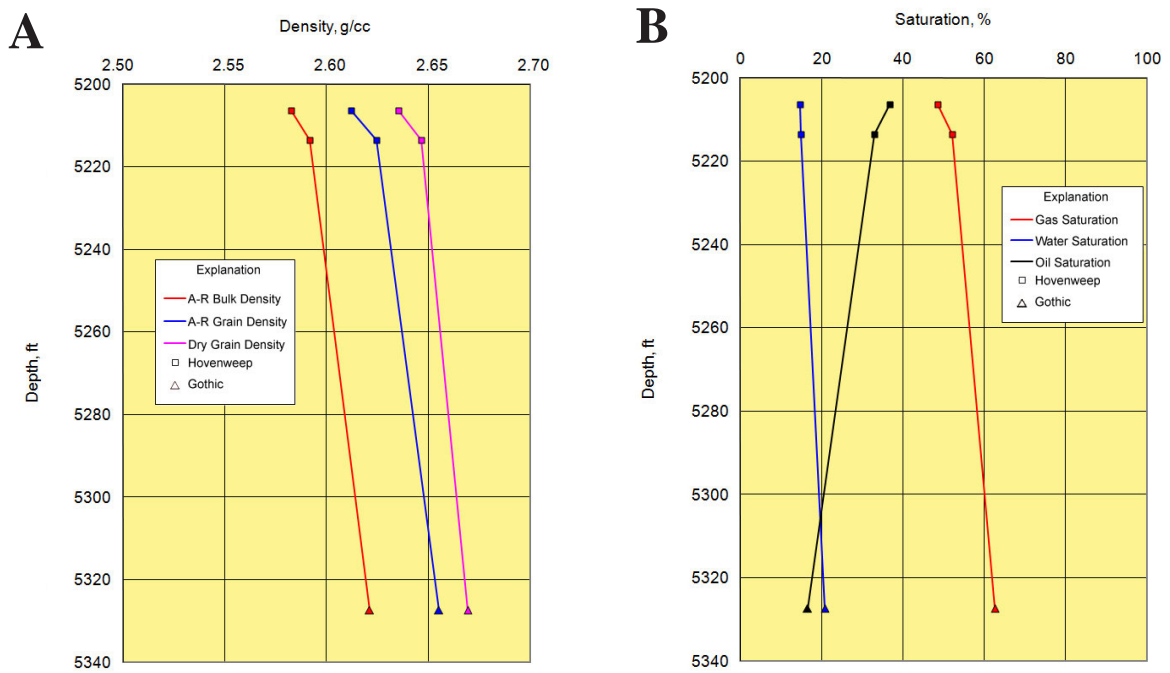


Figure 7.8. Density and saturation plots for the Marie Ogden State 1 core samples. **A.** Density versus depth. **B.** Saturation versus depth.

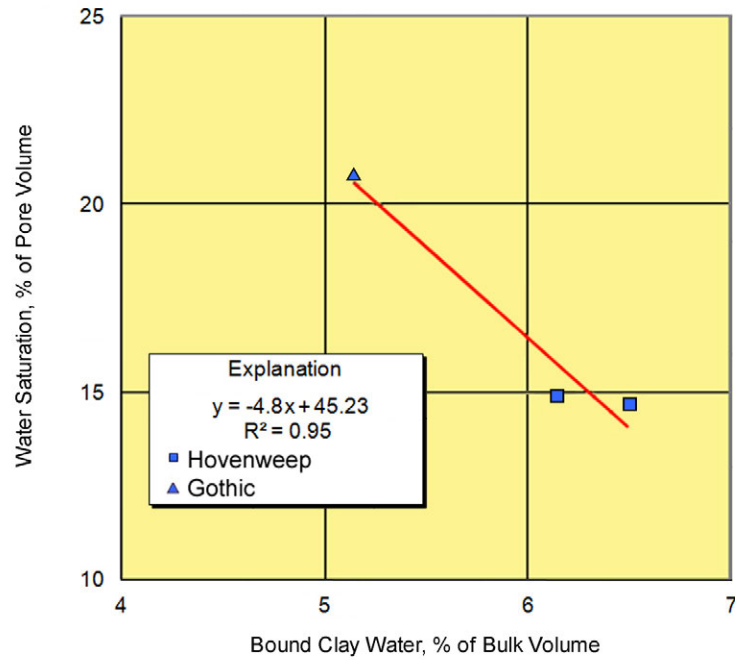


Figure 7.9. Bound clay water versus water saturation, Marie Ogden State 1 core samples.

Table 7.5. Summary of petrophysical measurements of core samples from three wells in the Paradox Formation, Paradox Basin.

Zone	Depth (ft)	As Received Bulk Density (g/cc)	As Received Grain Density (g/cc)	Dry Grain Density (g/cc)	Porosity (% of Bulk Volume)	Water Saturation (% of Pore Volume)	Gas Saturation (% of Pore Volume)	Mobile Oil Saturation (% of Pore Volume)	Gas-Filled Porosity (% of Bulk Volume)	Bound Hydrocarbon Saturation (% of Bulk Volume)	Bound Clay Water (% of Bulk Volume)	Pressure Decay Permeability (mD)
Marie Ogden State 1												
Hovenweep	5206.30	2.582	2.612	2.635	2.33	14.73	48.44	36.83	1.14	1.72	6.50	113
	5213.50	2.592	2.624	2.646	2.38	14.91	52.04	33.05	1.24	1.13	6.14	115
Gothic	5327.40	2.621	2.655	2.669	2.05	20.82	62.61	16.56	1.33	1.21	5.14	119
Jefferson State 4-1												
Hovenweep	5904.70	2.616	2.693	2.716	4.05	11.97	71.28	16.75	2.88	0.68	4.26	70
	5929.70	2.624	2.676	2.691	2.69	12.48	71.91	15.60	1.94	0.56	4.44	64
Gothic	6029.80	2.656	2.690	2.697	1.61	7.31	77.45	15.24	1.25	0.44	3.04	57
	6030.60	2.624	2.698	2.706	3.16	4.61	87.71	7.68	2.77	0.55	4.08	65
Aneth Unit H-117												
Gothic	5379.40	2.570	2.623	2.648	3.35	19.55	60.61	19.84	2.03	1.14	6.56	146
	5382.80	2.561	2.597	2.621	2.72	24.73	50.88	24.39	1.38	1.33	7.01	133
	5386.90	2.572	2.615	2.649	3.51	30.07	47.71	22.22	1.67	0.90	7.42	138
	5390.80	2.522	2.573	2.614	4.30	36.18	46.05	17.77	1.98	1.47	7.46	141

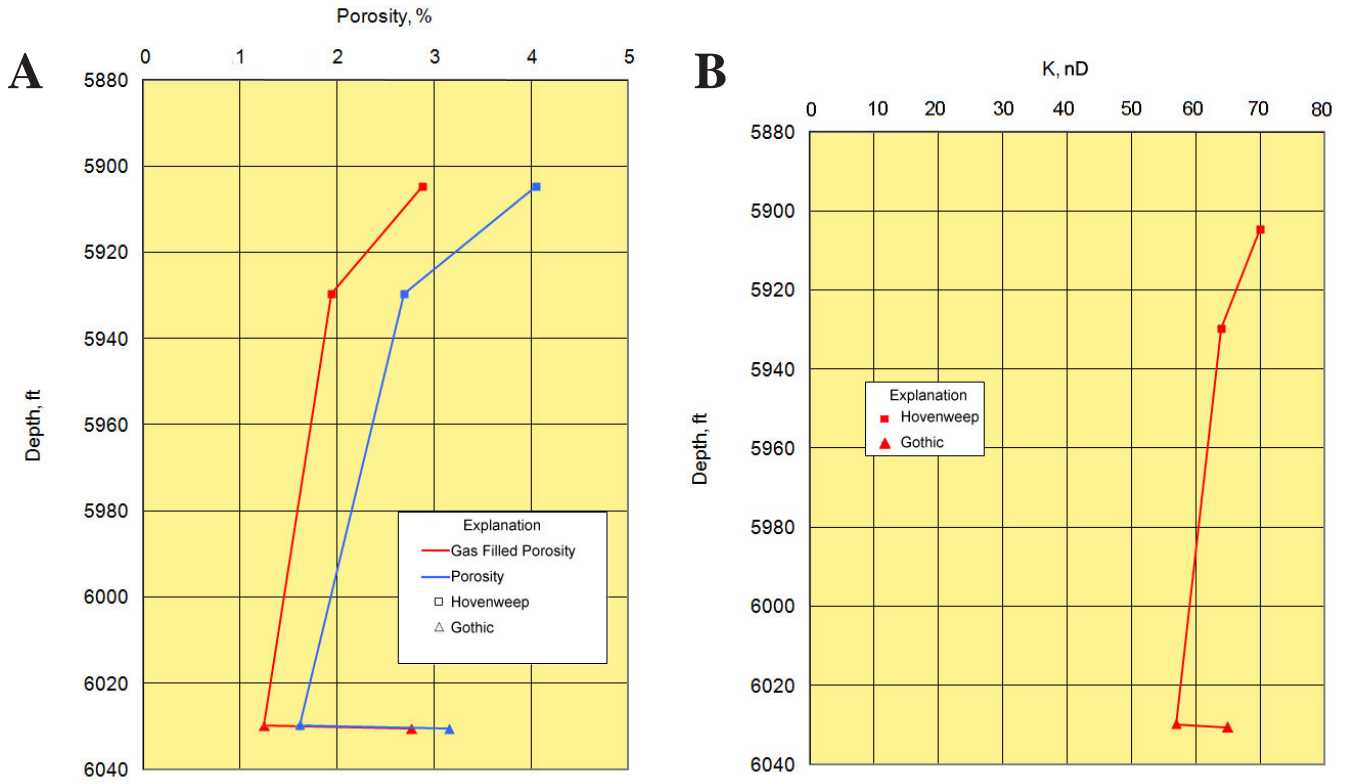


Figure 7.10. Porosity and permeability plots for the Jefferson State 4-1 core samples. **A.** Porosity versus depth. **B.** Permeability versus depth.

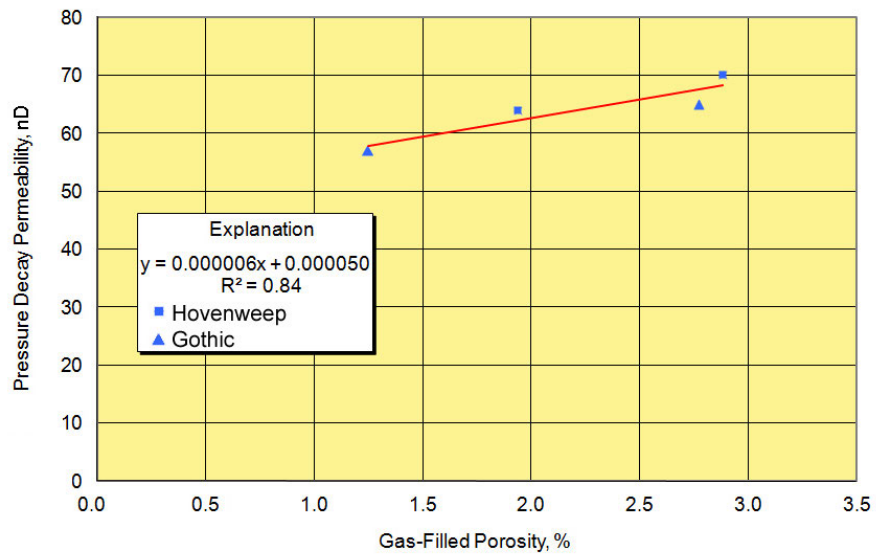


Figure 7.11. Gas-filled porosity versus pressure-decay permeability, Jefferson State 4-1 core samples.

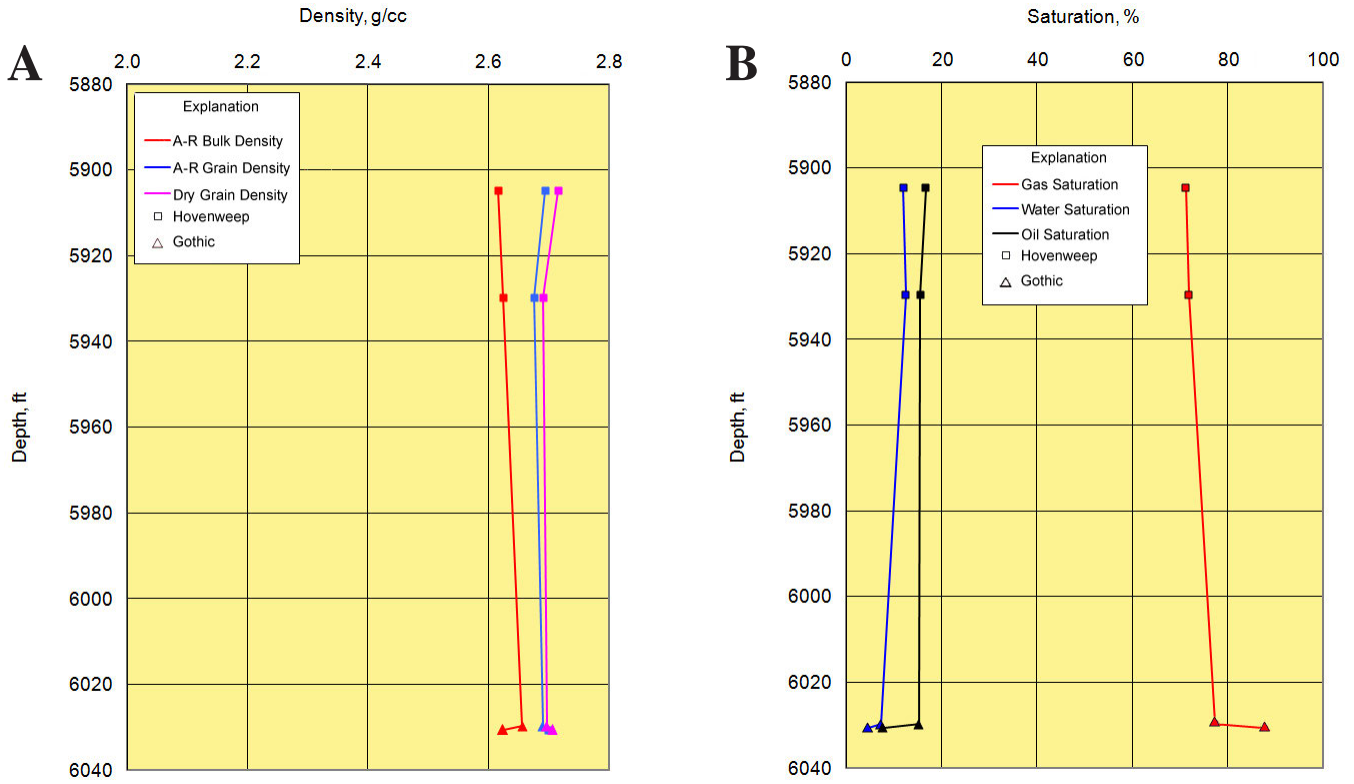


Figure 7.12. Density and saturation plots for the Jefferson State 4-1 core samples. **A.** Density versus depth. **B.** Saturation versus depth.

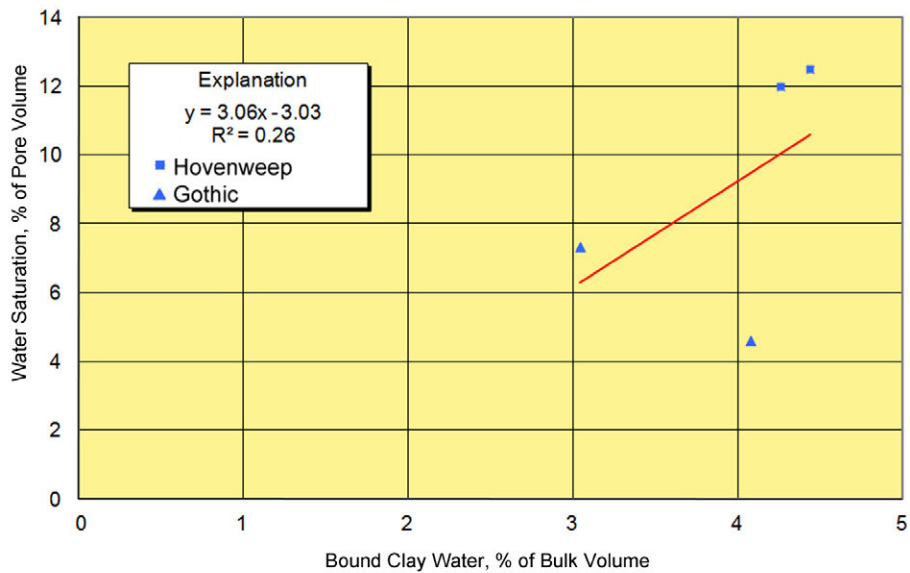


Figure 7.13. Bound clay water versus water saturation, Jefferson State 4-1 core samples.

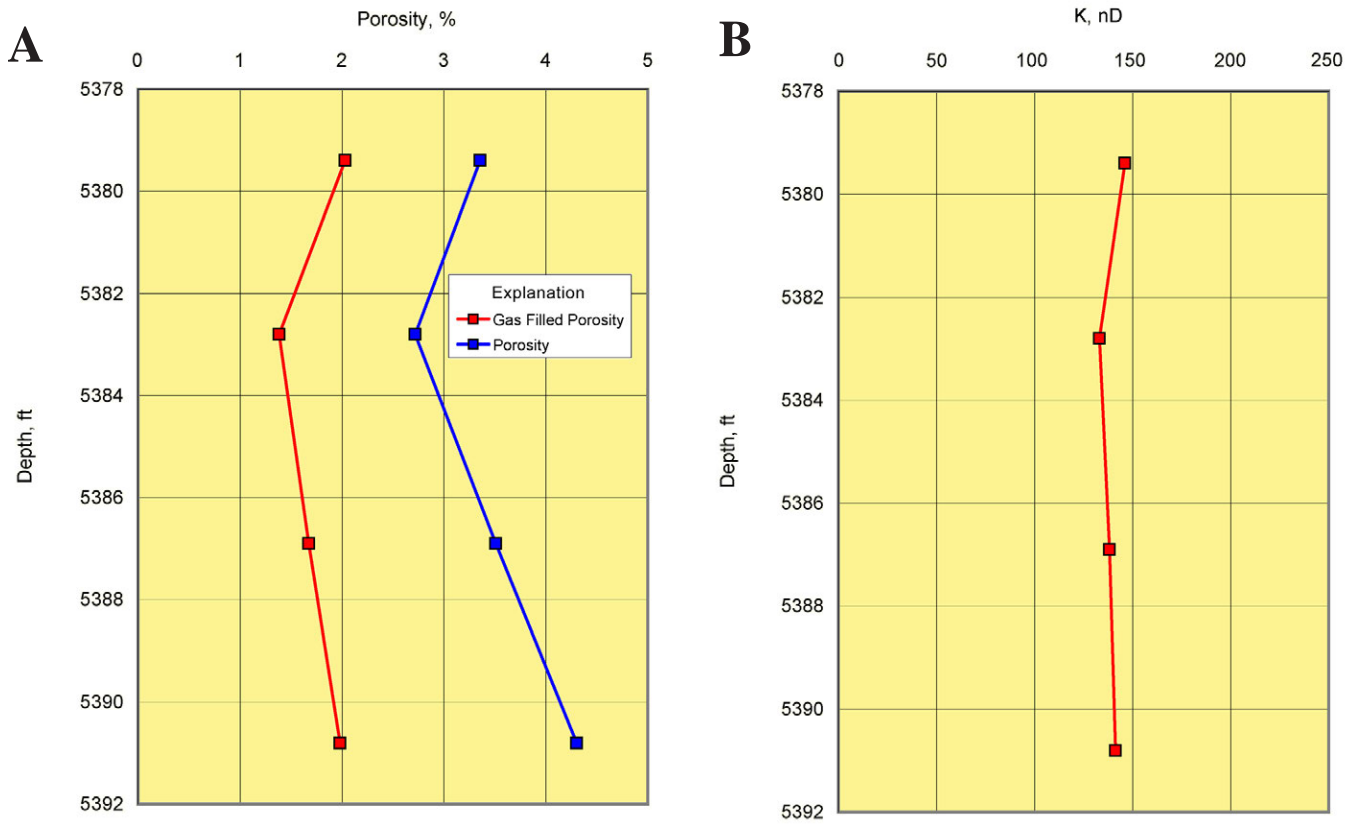


Figure 7.14. Porosity and permeability plots for the Aneth Unit H-117 core samples. A. Porosity versus depth. B. Permeability versus depth.

ing 0.14 μ D. Figure 7.15 shows that the pressure-decay permeability increases about 10% for every 50% increase in gas-filled porosity. Bulk and grain density decrease slightly with depth (figure 7.16A) and average 2.56 and 2.63 g/cc, respectively. Water saturations increase with depth (figure 7.16B) ranging from 19.6 to 36.2%. Figure 7.17 is a cross-plot of bound clay water versus water saturation. Bound clay water increases with depth (6.6 to 7.5%) corresponding to increased water saturation.

Interpretation

Petrophysical data from the Hovenweep and Gothic shales, presented in table 7.5, all have porosities less than 4% with gas-filled porosities between 1 and 3%; permeabilities using tight rock analysis are all below 150 nD. Most of the matrix porosity is attributable to clay micropores in shale and to microintercrystalline porosity in the dolomite interbeds. Compared to acceptable porosity/permeability levels from the same type of analysis of other Paleozoic shale-gas reservoirs in North America (figure 7.18) (e.g., Barnett Shale of central Texas and Fayetteville Shale of Arkansas), these numbers are minimally acceptable for economic gas production. Most

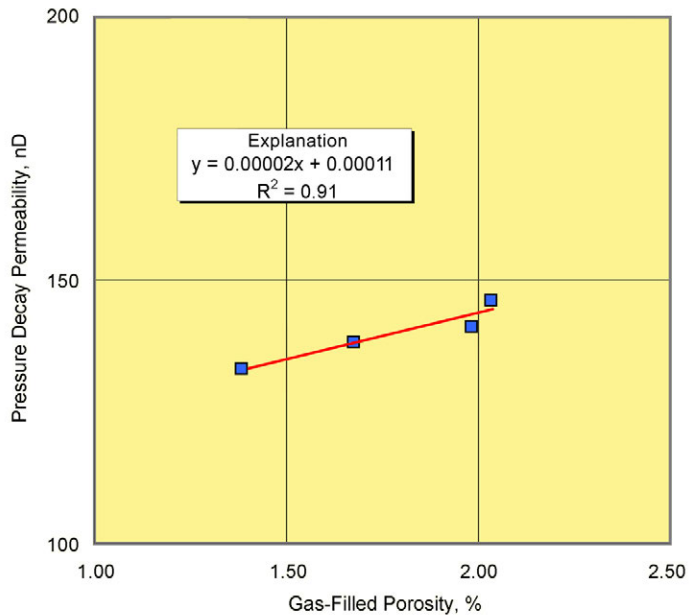


Figure 7.15. Gas-filled porosity versus pressure decay permeability, Aneth Unit H-117 core samples.

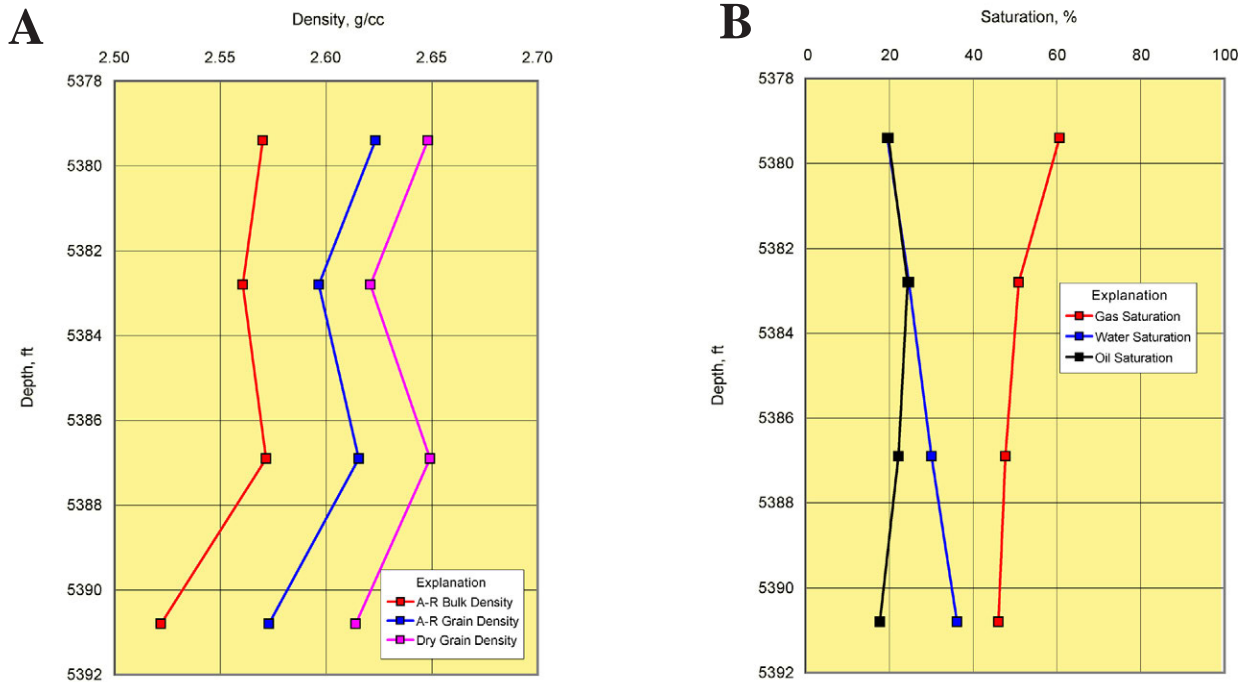


Figure 7.16. Density and saturation plots for the Aneth Unit H-117 core samples. A. Density versus depth. B. Saturation versus depth.

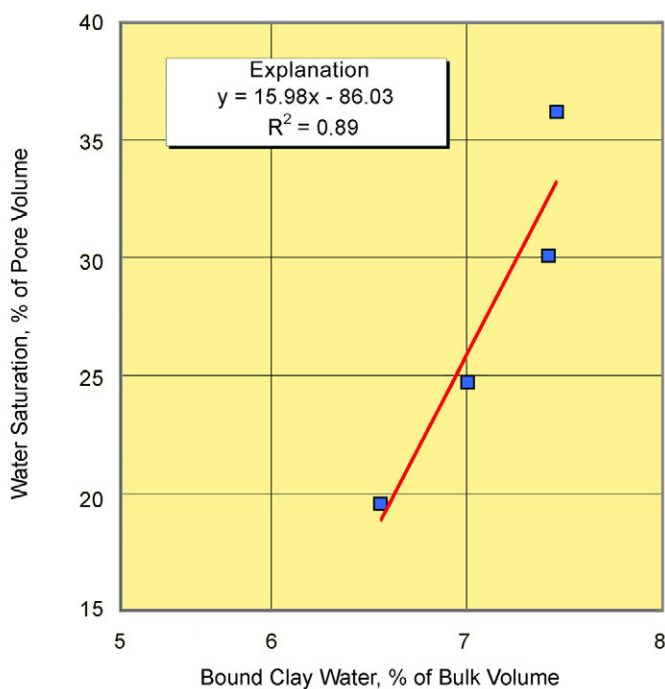


Figure 7.17. Bound clay water versus water saturation, Aneth Unit H-117 core samples.

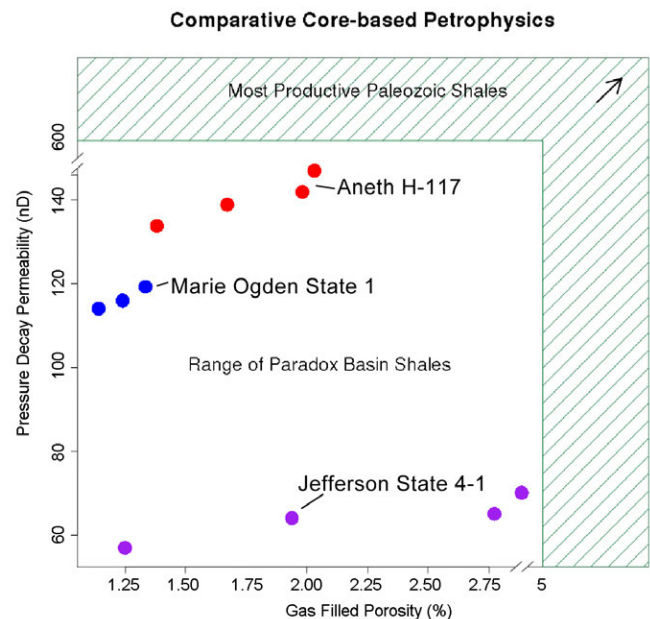


Figure 7.18. This graph reveals the matrix porosity/permeability plots from 11 organic-rich Gothic and Hovenweep shales from the Paradox Formation wells examined. All gas-filled porosity values plot below 3%, and all permeabilities fall beneath 150 nD. Most prolifically productive Paleozoic mudstones studied to-date in North America commonly plot above 5% gas filled porosity and above 500 nD of permeability (shaded region of figure). Thus, reservoir quality of the Paradox Basin mudstones appear below favorable values.

good producers approach 5% gas-filled porosity or above, and permeabilities attain values near 500 nD and above. The low Paradox porosity/permeability values suggest the natural fractures common to the Gothic may be largely responsible for production in the Colorado part of the Paradox Basin (Bereskin and McLennan, 2008).

The associated dolomite porosities and permeabilities range widely, but many numbers for the Marie Ogden State 1 carbonate rocks (appendix M), described erroneously in part as limestone, are very good for any conventional reservoir. However, some of these carbonates will likely be affected by any stimulation protocol in nearby mudstone. Moreover, these acceptable numbers are taken from just one well of the numerous wells studied—the only data of this kind available to the study.

At Greater Aneth field, the fact that porosity ranges from 2.7 to 3.4% and pressure-decay permeability is no greater than 146 nD is significant. These and other basic matrix petrophysical parameters indicate the Gothic shale is a highly effective reservoir seal for the oil in the underlying grainstone units of the Desert Creek zone, but may not necessarily produce hydrocarbons.

We emphasize that the shale beds themselves have some gas-filled porosity (see table 7.5) that would contribute to the production as well. The shale beds will be instrumental in sustaining any hydrocarbon production in Utah, both in terms of interstitial gas as well as desorbed gas from the organic material (Bereskin and McLennan, 2008). Hydraulic fracturing of the shale beds will enhance reservoir quality produced by natural fractures.

Geomechanical Analysis

Triaxial compression measurements from the Paradox Formation in the Marie Ogden State 1, the Jefferson State 1-4, and the Aneth Unit H-117 (figure 4.2) were taken at selected representative potential shale-gas zones. Like the geomechanical analyses from the Doughnut Formation on the Carbon Canal 5-12, in addition to the static mechanical properties, ultrasonic wave velocities were

measured using standard transmission techniques in two of the wells. Elastic formulae were used again to calculate the dynamic mechanical properties.

Young's Modulus and Poisson's Ratio

In northern Blanding sub-basin the Marie Ogden State 1 core samples (one each zone) were selected from the Gothic and Hovenweep shales and the lower and upper Ismay zone carbonate units that separate and overlie them. Understanding the bounding Ismay intervals is crucial for planning any hydraulic fracturing programs. The results of the testing are summarized in table 7.6. The values for Young's modulus and Poisson's ratio from the Gothic and Hovenweep are very similar. At a confining pressure of 2000 psi for the four sample depths, the static Young's modulus values for the Gothic and Hovenweep averaged 4.99×10^6 psi; the average static Poisson's ratio was 0.27 (table 7.6). The values for Young's modulus and Poisson's ratio from the adjacent bounding dolomite units in the upper and lower Ismay were significantly higher from the Gothic and Hovenweep. The static Young's modulus values averaged 8.64×10^6 psi; the average static Poisson's ratio was 0.37 (table 7.6). These values are fairly typical for dolomite or limestone. The upper Ismay sample contained a fair amount of detrital silt and therefore would be expected to have some brittle characteristics. The lower Ismay sample contained natural fractures and Young's modulus and Poisson's ratio values are typical for a carbonate. The Gothic and Hovenweep samples are from beds that have dispersed silt and contain dolomite crystals as reflected in the Young's modulus and Poisson's ratio values, suggesting some brittleness.

In the Jefferson State 4-1 core, samples were also selected from the Gothic (two samples) and Hovenweep shales (two samples) and the lower and upper Ismay zone carbonate units (two and one samples, respectively). The results of triaxial compression measurements on horizontal samples and dynamic mechanical properties from the core are shown on tables 7.7 and 7.8, respectively. These laboratory data were used by Bereskin and McLennan (2008) to calibrate logging data (figures 7.19 and 7.20). In this well, the values for Young's modulus from the Gothic and

Table 7.6. Triaxial static Young's modulus, Poisson's ratio, and compressive strength measurements from the Paradox Formation, Marie Ogden State 1 core samples.

Zone	Depth (ft)	As-Tested Bulk Density (g/cm ³)	Effective Confining Pressure* (psi)	Effective Compressive Strength (psi)	Effective Residual Compressive Strength (psi)	Quasi-Static Young's Modulus (10 ⁶ psi)	Quasi-Static Poisson's Ratio
Upper Ismay	5184.45	2.658	2000	43,470	36,840	9.3	0.38
Hovenweep	5205.5	2.581		21,355	12,200	4.8	0.26
Lower Ismay	5320	2.679		43,815	-	8.0	0.35
Gothic	5327.2	2.627		21,755	16,430	5.2	0.28

*All tests conducted with pore pressure = 0 psi.

Hovenweep are somewhat different. The average static Young's modulus value for the Gothic was 7.46×10^6 psi; the average static Poisson's ratio was 0.25 (table 7.7). The average static Young's modulus value for the Hovenweep was 5.77×10^6 psi; the average static Poisson's ratio was 0.25 (table 7.7). The values for Young's modulus from the bounding dolomite in the lower Ismay were surprisingly lower than the Gothic. The static Young's modulus value for the lower Ismay averaged 6.68×10^6 psi; the average static Poisson's ratio was 0.32 (table 7.7). These values indicate that the Gothic likely contains a fair amount of silt and is therefore more brittle than the overlying lower Ismay and Hovenweep; units in the Hovenweep also contain some silt, however. The upper Ismay sample also probably contains some silt near the boundary with the Hovenweep and therefore would be expected to have brittle characteristics.

On the Aneth platform, six samples from the Gothic shale were selected from the Aneth Unit H-117 core at multiple vertical locations through various changes in shale facies. The static Young's modulus values range from 2.897 to 5.766×10^6 psi, averaging 3.68×10^6 psi (table 7.9);

the dynamic elastic Young's modulus values range from 4.37 to 7.97×10^6 psi, averaging 4.49×10^6 psi (table 7.10). The static Poisson's ratio values range from 0.18 to 0.3 (table 7.9); the dynamic elastic Poisson's ratio values range from 0.23 to 0.31 (table 7.10). Compressional acoustical velocities increase with depth from 12,647 to 16,593 ft/sec; shear acoustical velocities range from 7018 to 9640 ft/sec (table 7.10). Figure 7.21 displays vertical dynamic Young's modulus as a function of vertical static Young's modulus (A) and horizontal dynamic Young's modulus as a function of horizontal static Young's modulus (B). Figure 7.22 displays vertical dynamic Poisson's ratio as a function of vertical static Poisson's ratio (A) and horizontal dynamic Poisson's ratio as a function of horizontal static Poisson's ratio (B). These graphs and analysis from Young's modulus and Poisson's ratio suggest that the Gothic shale in Greater Aneth field is not brittle, in contrast to areas in the eastern Paradox Basin (the Colorado part) where it produces gas (Peter Moreland, formerly with Bill Barrett Corporation, verbal communication, 2009). Therefore, the Gothic is less likely to respond to hydraulic fracturing of the underlying Desert Creek zone.

Table 7.7. Triaxial static Young's modulus, Poisson's ratio, and compressive strength measurements from the Paradox Formation, Jefferson State 4-1 core samples.

Zone	Depth (ft)	As-Received Bulk Density (g/cm ³)	Effective Confining Pressure* (psi)	Effective Compressive Strength (psi)	Effective Residual Compressive Strength (psi)	Quasi-Static Young's Modulus (10 ⁶ psi)	Quasi-Static Poisson's Ratio
Upper Ismay	5876.2	2.672	3526	38,546	15,891	8.211	0.29
Hovenweep	5903.7	2.613	3610	24,130	18,435	5.945	0.24
	5930.0	2.636	3558	25,783	19,563	5.593	0.25
Lower Ismay	6009.6	2.656	3606	38,181	17,976	6.402	0.31
	6017.3	2.720	3610	36,350	22,075	6.962	0.33
Gothic	6030.0	2.652	3618	42,263	20,543	7.592	0.25
	6036.5	2.663	3622	45,092	26,227	7.332	0.24

*Pore pressure = 0 psi in all tests.

Table 7.8. Acoustic velocities and dynamic moduli at triaxial conditions from the Paradox Formation, Jefferson State 4-1 core samples.

Zone	Depth (ft)	Axial Stress Difference (psi)	Effective Confining Pressure* (psi)	Effective Mean Stress (psi)	Test Bulk Density (g/cm ³)	Acoustic Velocity		Dynamic Elastic Parameters			
						Compressional-Wave Velocity (ft/s)	Shear-Wave Velocity (ft/s)	Bulk Modulus (10 ⁶ psi)	Young's Modulus (10 ⁶ psi)	Shear Modulus (10 ⁶ psi)	Poisson's Ratio
Upper Ismay	5876.2	5	3526	3528	2.678	19,363	10,515	8.208	10.300	3.989	0.29
		5753		5445	2.679	19,566	10,551	8.461	10.406	4.018	0.30
		14,518		8366	2.680	19,779	10,601	8.717	10.538	4.058	0.30
		20,906		10,495	2.681	19,904	10,627	8.871	10.611	4.079	0.30
		27,808		12,796	2.681	19,930	10,626	8.912	10.618	4.079	0.30
		33,565		14,714	2.682	19,862	10,600	8.843	10.565	4.061	0.30
		12,348		7642	2.668	18,790	10,003	7.896	9.369	3.597	0.30

Table 7.8. Continued.

Zone	Depth (ft)	Axial Stress Difference (psi)	Effective Confining Pressure* (psi)	Effective Mean Stress (psi)	Test Bulk Density (g/cm ³)	Acoustic Velocity		Dynamic Elastic Parameters			
						Compressional-Wave Velocity (ft/s)	Shear-Wave Velocity (ft/s)	Bulk Modulus (10 ⁶ psi)	Young's Modulus (10 ⁶ psi)	Shear Modulus (10 ⁶ psi)	Poisson's Ratio
Hovenweep	5903.7	0	3610	3609	2.622	17,062	10,067	5.512	8.830	3.581	0.23
		5647		5493	2.624	17,077	10,070	5.529	8.843	3.585	0.23
		12,094		7642	2.625	17,162	10,068	5.637	8.873	3.585	0.24
		18,054		9628	2.626	17,211	10,062	5.704	8.887	3.582	0.24
		20,458		10,429	2.625	17,231	10,050	5.738	8.876	3.573	0.24
		14,818		8549	2.645	16,731	9837	5.379	8.526	3.450	0.24
	5930.0	3	3558	3559	2.647	17,232	10,039	5.800	8.938	3.595	0.24
		4291		4988	2.648	17,293	10,053	5.863	8.978	3.606	0.24
		16,071		8915	2.651	17,400	10,060	5.994	9.029	3.614	0.25
		18,774		9816	2.651	17,426	10,058	6.029	9.036	3.614	0.25
		21,193		10,622	2.651	17,450	10,055	6.063	9.039	3.611	0.25
		15,893		8855	2.634	17,162	9928	5.791	8.736	3.499	0.25
		15,279		8651	2.633	17,175	9923	5.807	8.730	3.494	0.25
		Lower Ismay		6009.6	4	3606	3607	2.676	19,142	10,538	7.872
4295	5037		2.677		19,575		10,693	8.322	10.618	4.124	0.29
12,996	7938		2.678		19,598		10,720	8.333	10.671	4.147	0.29
20,631	10,483		2.679		19,620		10,679	8.407	10.618	4.117	0.29
30,428	13,748		2.679		19,493		10,568	8.339	10.414	4.030	0.29
34,438	15,085		2.676		19,692		10,568	8.613	10.452	4.027	0.30
6017.3	2		3610		3610		2.809	20,577	11,013	9.905	11.930
	6003			5611	2.810	20,874	11,139	10.235	12.226	4.699	0.30
	11,198			7342	2.811	20,961	11,223	10.282	12.397	4.772	0.30
	18,968			9932	2.812	21,146	11,298	10.494	12.578	4.837	0.30
	25,340			12,056	2.812	21,122	11,286	10.470	12.550	4.826	0.30
	28,411			13,080	2.811	21,050	11,205	10.442	12.386	4.756	0.30
	18,462			9764	2.733	18,975	9725	8.615	9.206	3.482	0.32
Gothic	6030		4	3618	3,619	2.656	18,501	10,874	6.608	10.462	4.232
		7,033	5,962		2.658	18,567	10,878	6.694	10.497	4.237	0.24
		15,070	8,641		2.659	18,631	10,869	6.794	10.513	4.232	0.24
		21,185	10,680		2.660	18,615	10,869	6.774	10.512	4.234	0.24
		29,055	13,303		2.661	18,676	10,856	6.873	10.522	4.226	0.24
		37,430	16,094		2.663	18,644	10,823	6.870	10.474	4.203	0.25
		16,816	9223		2.655	18,065	10,270	6.644	9.519	3.774	0.26
	6036.5	4	3622	3624	2.668	18,420	10,165	7.245	9.519	3.715	0.28
		4,918		5,262	2.669	18,546	10,181	7.401	9.576	3.728	0.28
		10,928		7265	2.671	18,622	10,189	7.497	9.610	3.735	0.29
		18,831		9899	2.672	18,648	10,190	7.536	9.624	3.738	0.29
		26,802		12,556	2.673	18,719	10,180	7.644	9.632	3.733	0.29
		35,244		15,371	2.675	18,539	9845	7.730	9.110	3.494	0.30
		23,016		11,295	2.645	18,194	9650	7.373	8.657	3.319	0.30

*Pore pressure = 0 psi in all tests.

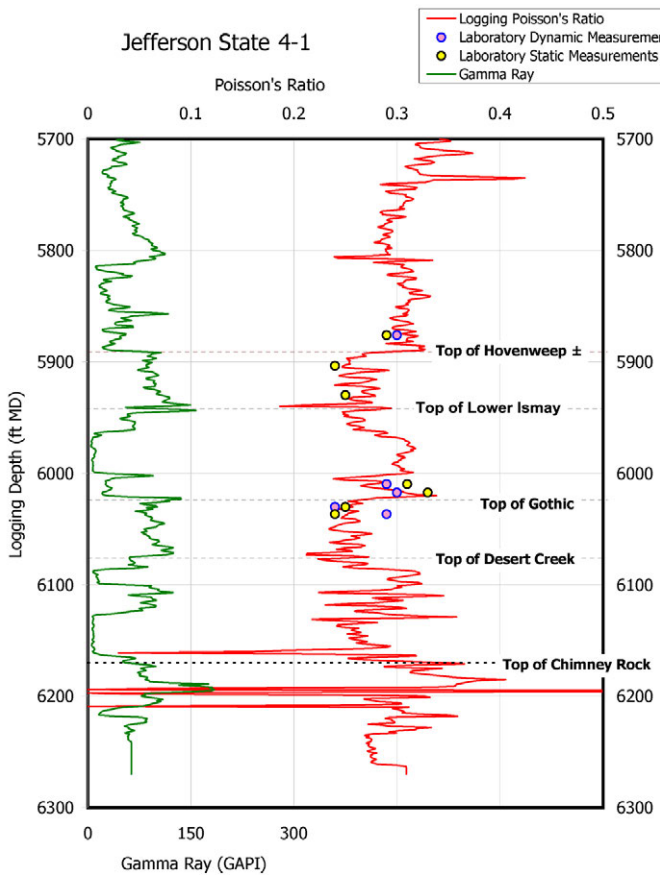


Figure 7.19. Variation of laboratory and logging-predicted values for Poisson's ratio, Jefferson State 4-1 well (from Bereskin and McLennan, 2008).

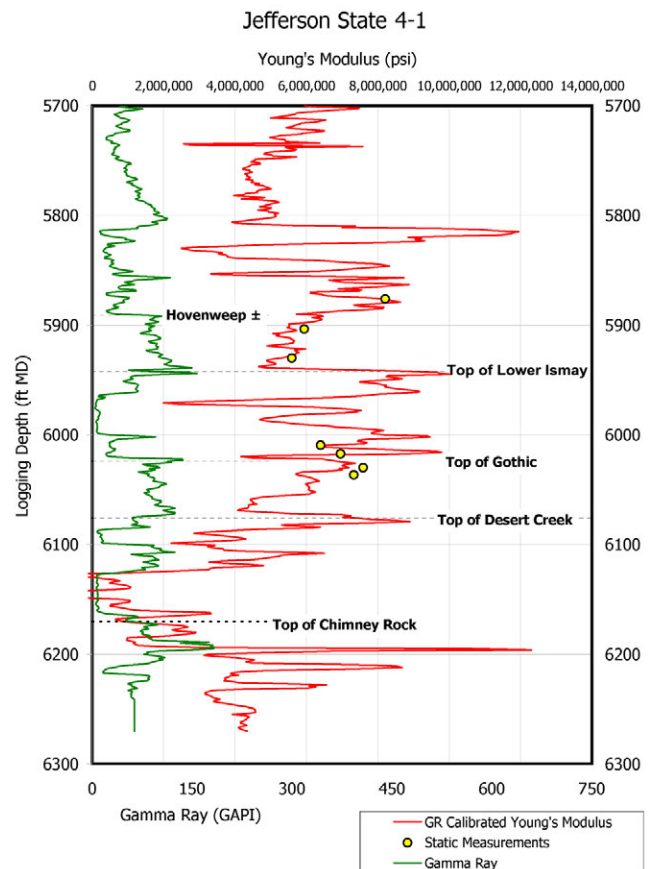


Figure 7.20. Synthesized values of static Young's modulus and the laboratory measurements used to correct the raw dynamic values, Jefferson State 4-1 well (from Bereskin and McLennan, 2008).

Compressional Testing

In the Marie Ogden State 1 core, the compressive strength for the Gothic and Hovenweep shales and the upper and lower Ismay zone carbonate units was determined (table 7.6). At a confining pressure of 2000 psi, the compressional strengths for the Gothic and Hovenweep were very similar and averaged 21,555 psi. Likewise, the compressional strengths for the bounding upper and lower Ismay carbonate samples were similar and averaged 43,643 psi. Figure 7.23 is a plot of axial stress difference versus radi-

al and axial strains, measured during confined compression testing. Like figure 7.6, figure 7.23 describes the evolution of axial and radial strains and failure (yield stress, peak stress, and residual strength) during compression loading. Note the lower axial stress differences between the Gothic and Hovenweep shales and the lower and upper Ismay carbonate test samples.

In the Jefferson State 4-1 core, the compressive strength for the Gothic and Hovenweep shales and the upper and

Table 7.9. Triaxial static Young's modulus, Poisson's ratio, and compressive strength measurements from the Gothic shale in the Paradox Formation, Aneth Unit H-117 core samples.

Depth (ft)	Orientation (deg)	Bulk Density (g/cm ³)	Effective Confining Stress (psi)	Volumetric Yield Stress Compressive (psi)	Peak Compressive Strength (psi)	Residual Compressive Strength (psi)	Young's Modulus (10 ⁶ psi)	Poisson's Ratio
5381.15	H	2.574	1994	18,235	18,383	0	5.766	0.303
5381.20	V	2.569	1994	19,364	19,364	0	2.897	0.175
5381.20	45	2.569	1994	8874	9752	0	2.952	0.278
5398.75	H	2.258	2004	10,586	11,532	0	3.334	0.242
5398.80	V	2.283	1994	10,808	11,888	0	3.552	0.249
5399.00	45	2.316	1994	10,648	12,587	0	3.608	0.193

Table 7.10. Acoustic velocities and dynamic moduli at triaxial conditions from the Gothic shale in the Paradox Formation, Aneth Unit H-117 core samples.

Depth (ft)	Orientation (deg.)					Acoustic Velocity		Dynamic Elastic Parameters			
		Axial Stress Difference (psi)	Effective Confining Pressure (psi)	Effective Mean Stress (psi)	Bulk Density (g/cm ³)	Compressional P-Wave Velocity (ft/s)	Shear S-Wave Velocity (ft/s)	Apparent Bulk Modulus (10 ⁶ psi)	Apparent Young's Modulus (10 ⁶ psi)	Apparent Shear Modulus (10 ⁶ psi)	Apparent Poisson's Ratio
5381.20	V	207	1994	2063	2.576	12,647	7018	3.273	4.368	1.709	0.280
		2099	2004	2704	2.577	12,885	7042	3.469	4.432	1.722	0.290
		4205	1994	3396	2.578	12,805	7066	3.383	4.444	1.735	0.280
		7232	2004	4415	2.580	12,885	7090	3.441	4.484	1.748	0.280
		10,851	2004	5621	2.582	13,048	7115	3.575	4.539	1.761	0.290
		14,618	1994	6867	2.585	13,216	7164	3.699	4.619	1.788	0.290
		17,004	2004	7672	2.587	13,301	7189	3.765	4.661	1.802	0.290
		9338	1994	5117	2.622	13,475	7215	3.964	4.778	1.839	0.300
5381.20	45	224	2004	2079	2.580	13,542	7977	3.426	5.461	2.212	0.230
		2264	1994	2749	2.581	13,587	8008	3.446	5.503	2.230	0.230
		4057	1994	3346	2.582	13,632	8039	3.466	5.546	2.248	0.230
		5982	2004	3998	2.582	13,723	8039	3.554	5.571	2.249	0.240
		7758	1994	4580	2.582	13,723	8055	3.542	5.586	2.257	0.240
		6113	1994	4032	2.568	13,723	8055	3.522	5.555	2.245	0.240
5381.15	H	191	1994	2068	2.583	16,273	9618	4.925	7.931	3.220	0.230
		2066	1994	2683	2.584	16,403	9618	5.074	7.974	3.220	0.240
		4633	2004	3549	2.584	16,338	9618	5.000	7.955	3.221	0.230
		4633	2004	3549	2.584	16,273	9640	4.907	7.959	3.236	0.230
		7775	2004	4596	2.585	16,338	9640	4.981	7.981	3.237	0.230
		8071	1994	4684	2.585	16,469	9618	5.151	7.998	3.222	0.240
		14,947	2004	6987	2.586	16,403	9595	5.098	7.956	3.208	0.240
		16,346	1994	7443	2.587	16,469	9618	5.155	8.004	3.224	0.240
5398.80	V	225	1994	2069	2.297	15,827	8625	4.683	5.934	2.302	0.290
		1645	1994	2532	2.298	16,138	8698	4.939	6.067	2.342	0.300
		3644	1994	3209	2.298	16,395	8753	5.160	6.172	2.373	0.300
		5609	1994	3864	2.299	16,461	8791	5.201	6.226	2.394	0.300
		7674	1994	4552	2.299	16,461	8810	5.188	6.248	2.405	0.300
		9342	1984	5098	2.299	16,527	8772	5.284	6.218	2.384	0.300
		8318	1994	4767	2.311	16,201	8311	5.306	5.685	2.151	0.320
5399.00	45	191	2004	2058	2.329	15,412	8465	4.455	5.775	2.249	0.280
		1576	2004	2530	2.330	15,706	8607	4.643	5.978	2.325	0.290
		3867	1994	3273	2.331	15,888	8680	4.773	6.091	2.366	0.290
		5895	2004	3949	2.332	16,012	8680	4.900	6.116	2.367	0.290
		6274	2004	4086	2.332	16,201	8625	5.132	6.089	2.338	0.300
		7494	1994	4482	2.334	16,138	8607	5.085	6.064	2.330	0.300
		8746	2004	4910	2.339	16,012	8553	5.006	5.996	2.306	0.300
		9884	1994	5279	2.379	15,950	8067	5.373	5.540	2.086	0.330
5398.75	H	208	2004	2074	2.271	15,950	8643	4.737	5.908	2.286	0.290
		1840	2004	2618	2.272	16,138	8735	4.858	6.039	2.336	0.290
		3373	2004	3129	2.272	16,461	8791	5.141	6.155	2.366	0.300
		4988	1994	3657	2.273	16,593	8829	5.250	6.219	2.387	0.300
		7345	1994	4443	2.274	16,593	8848	5.238	6.243	2.398	0.300
		8697	2004	4903	2.275	16,527	8829	5.186	6.213	2.389	0.300
		8499	2004	4837	2.276	15,827	8228	4.913	5.459	2.076	0.310

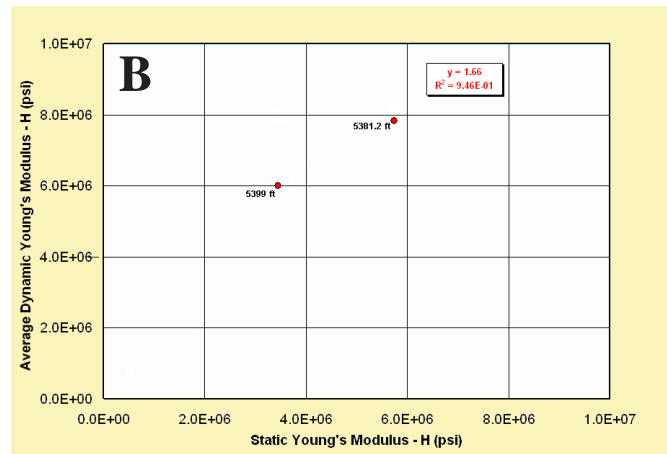
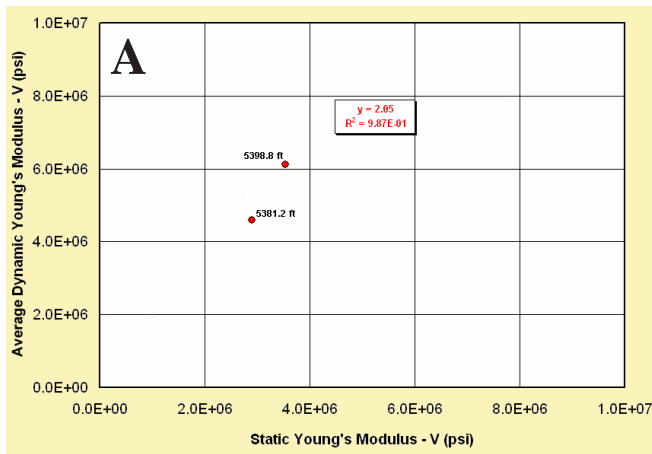


Figure 7.21. A. Vertical dynamic Young's modulus as a function of vertical static Young's modulus. B. Horizontal dynamic Young's modulus as a function of horizontal static Young's modulus; Aneth Unit H-117 well, depth 5381.18 to 5398.85 feet.

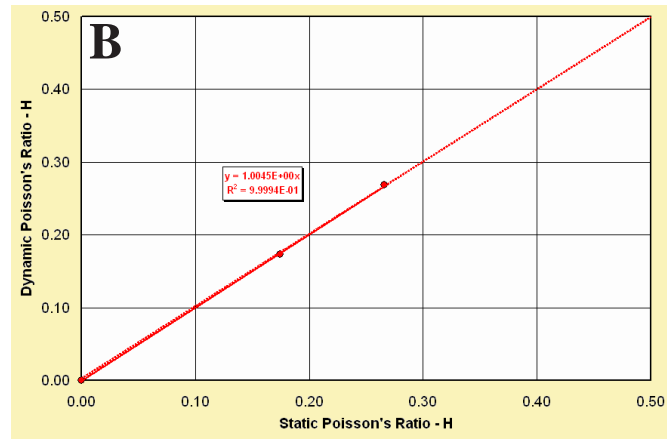
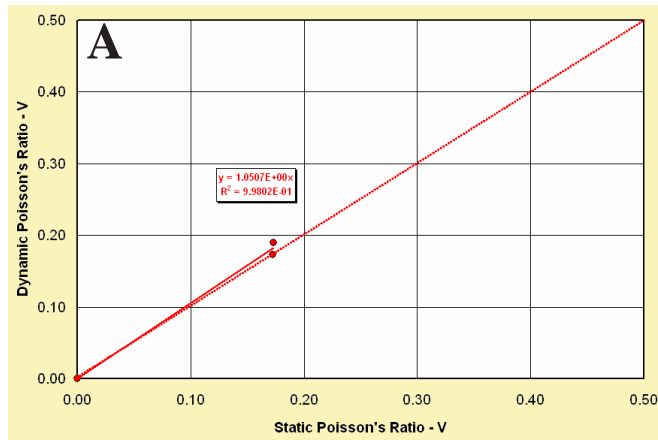


Figure 7.22. A. Vertical dynamic Poisson's ratio as a function of vertical static Poisson's ratio. B. Horizontal dynamic Poisson's ratio as a function of horizontal static Poisson's ratio; Aneth Unit H-117 well, depth 5381.18 to 5398.85 feet.

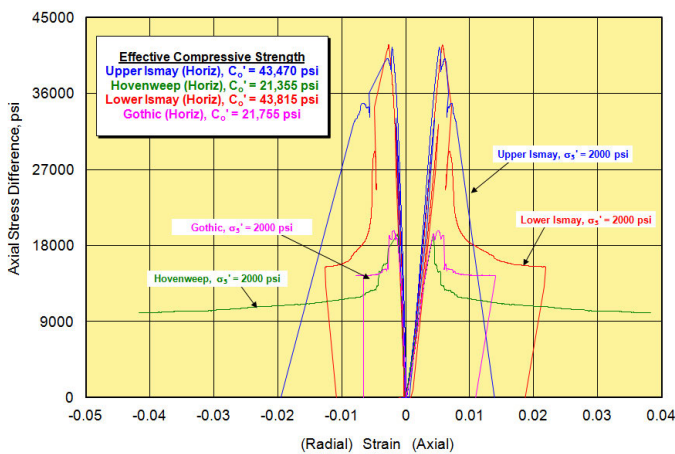


Figure 7.23. Plot of axial stress difference versus radial and axial strains for the Gothic and Hovenweep shales, and the lower and upper Ismay zones, Marie Ogden State 1 well.

lower Ismay zone carbonate units was also determined (table 7.7). The compressive strength for the Gothic is considerably higher than that of the Hovenweep—an average of 43,678 versus 24,957 psi, respectively. The compressive strength values for the bounding carbonate beds of the upper and lower Ismay zones are relatively consistent with each other and average 37,692 psi. Forecasting in-situ strength is usually conducted strictly on the basis of correlations with existing logging data (Bereskin and McLennan, 2008). A common approach is to use relationships shown by Deere and Miller (1966) where the measured strength data are compared with various linear combinations of logging data. The relationship between in-situ strength and sonic porosity was the best match (Bereskin and McLennan, 2008). The strength-porosity relationship used from the Jefferson State 4-1 Gothic, Hovenweep, and Ismay samples is shown in figure 7.24 and the vertical profile of in-situ strength is shown in fig-

ure 7.25. Bereskin and McLennan (2008) determined that the best calibration relationship for an estimate of in-situ strength used the sonic porosity (figure 7.24A). Similarly, figure 7.24B shows a prediction of how much stress drop occurs at failure (part of a relationship showing energy stored in the rock)—an indicator of the degree of brittleness (Bereskin and McLennan, 2008). The analysis suggests these are very strong rocks. A measure of the potential for fracturing and brittleness is the amount of energy released when failure occurs (Bereskin and McLennan, 2008). An energy analog based on the data from the Jefferson State 4-1 core is plotted in figure 7.26. Bereskin and McLennan (2008) speculate that the greatest fracture potential is where the stored energy is highest.

On the Aneth platform, the six samples from the Aneth Unit H-117 core were taken at vertical, horizontal, and 45° orientations (two each) for compressive strength analysis of the Gothic shale only (table 7.9). The confining stress was variable with depth and orientation. Closely spaced vertical, horizontal, and 45° oriented samples between 5398.75 and 5399.0 feet (1645.46 and 1645.53 m) had similar confining stress values with an average of 10,681 psi. The horizontal and 45° oriented samples from 5381.15 and 5381.20 feet (1640.09 and 1640.10 m) had compressive strength values of 18,235 and 8874 psi, respectively. Figure 7.27A is a plot of axial stress difference versus radial and axial strains, measured during unconfined compression testing, again describing the evolution of rock deformation and failure during unconfined com-

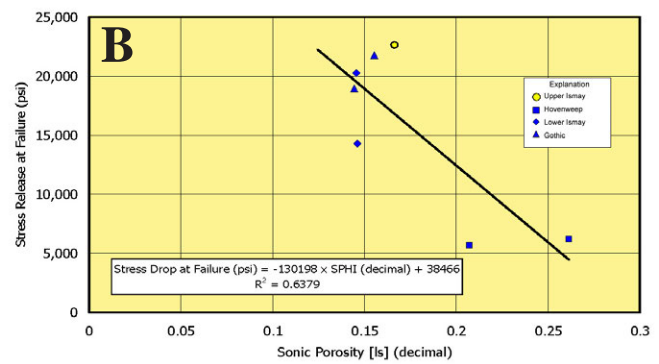
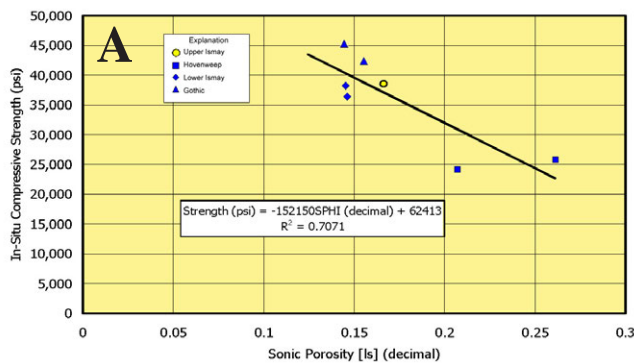


Figure 7.24. Laboratory measured data (the in-situ compressive strength – A) and the stress drop at failure – B) plotted against the sonic porosity with an annotation of linear regression fits, Jefferson State 4-1 core. After Bereskin and McLennan, 2008.

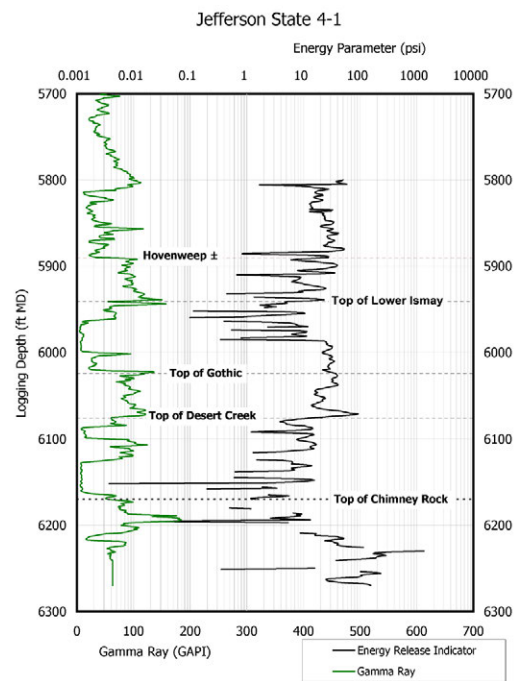
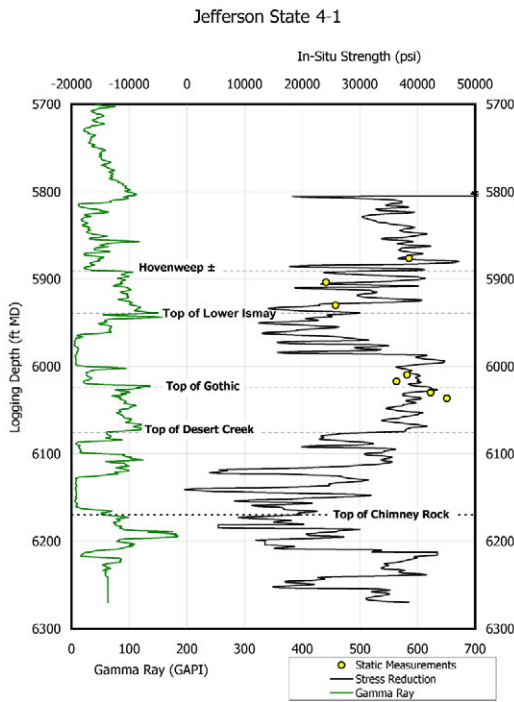


Figure 7.25. Logging inference of in-situ strength, Jefferson State 4-1 core. Calibration was based on the sonic porosity. From Bereskin and McLennan, 2008.

Figure 7.26. Logging inference of brittleness based on estimates of stored energy, Jefferson State 4-1 core. From Bereskin and McLennan, 2008.

pression loading. Figure 7.27B is plot of axial stress difference versus volumetric strain, measured during unconfined compression testing. The figure describes the evolution of the rock deformation (dilation versus compaction) and the yield stress during unconfined compression loading. Axial stress difference versus axial strain, measured during unconfined compression testing, is displayed on figure 7.27C. The figure describes the evolution of the axial modulus (Young's modulus) during unconfined compression loading. The averaged radial strain versus axial strain, measured during unconfined compression testing, is shown on figure 7.27D. The figure describes the evolution of the transverse modulus (Poisson's ratio) during unconfined compression loading. Continuous unconfined compressive strength profiles show a relatively uniform homogenous Gothic shale package—20,000 psi (figure 7.28) (Chidsey and others, 2009). Compressional testing suggests some degree of hydraulic fracture containment.

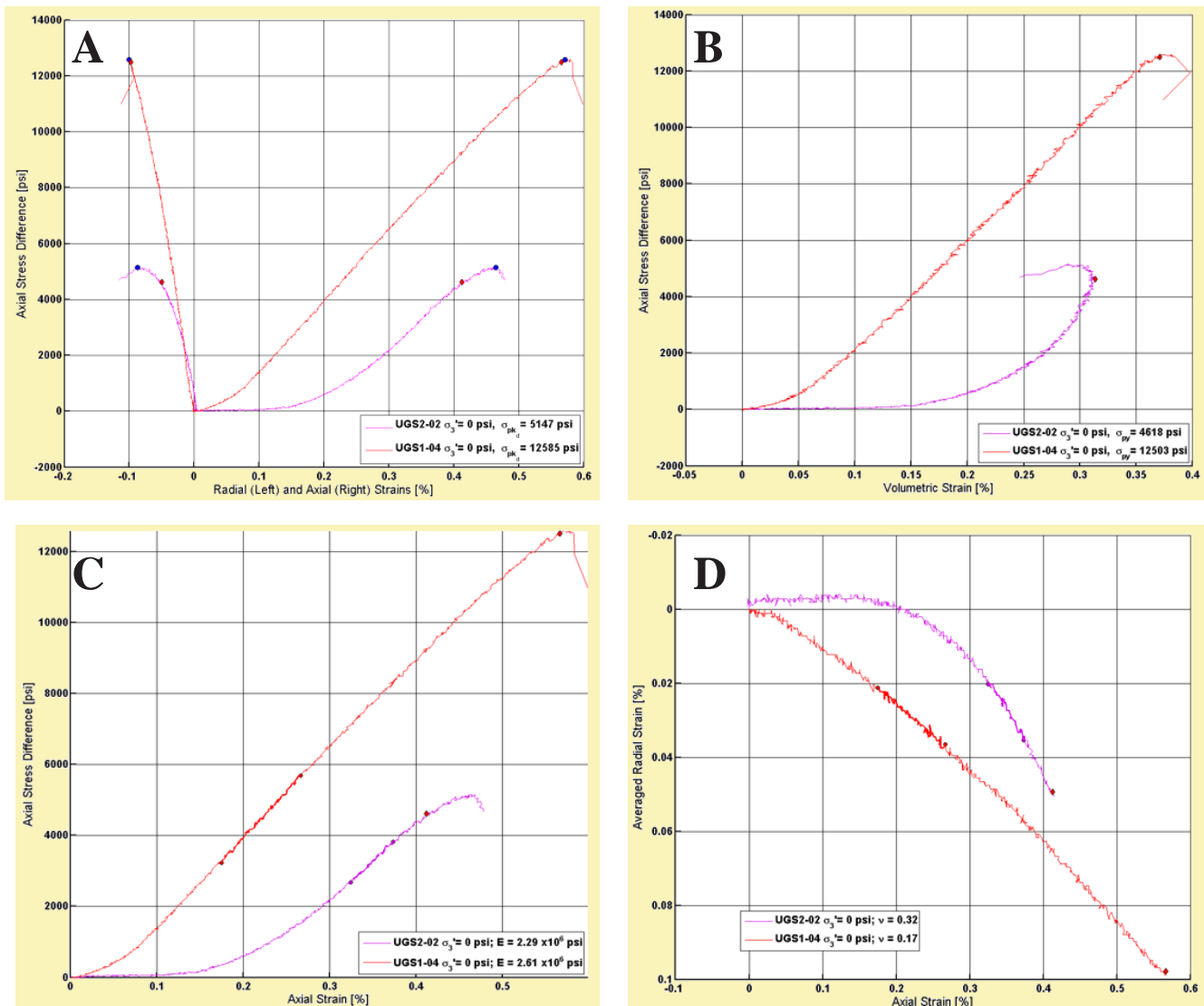


Figure 7.27. Results of unconfined compression testing, Aneth Unit H-117 core. **A.** Axial stress difference versus radial and axial strains. **B.** Axial stress difference versus volumetric strain. **C.** Axial stress difference versus axial strain. **D.** Averaged radial strain versus axial strain.

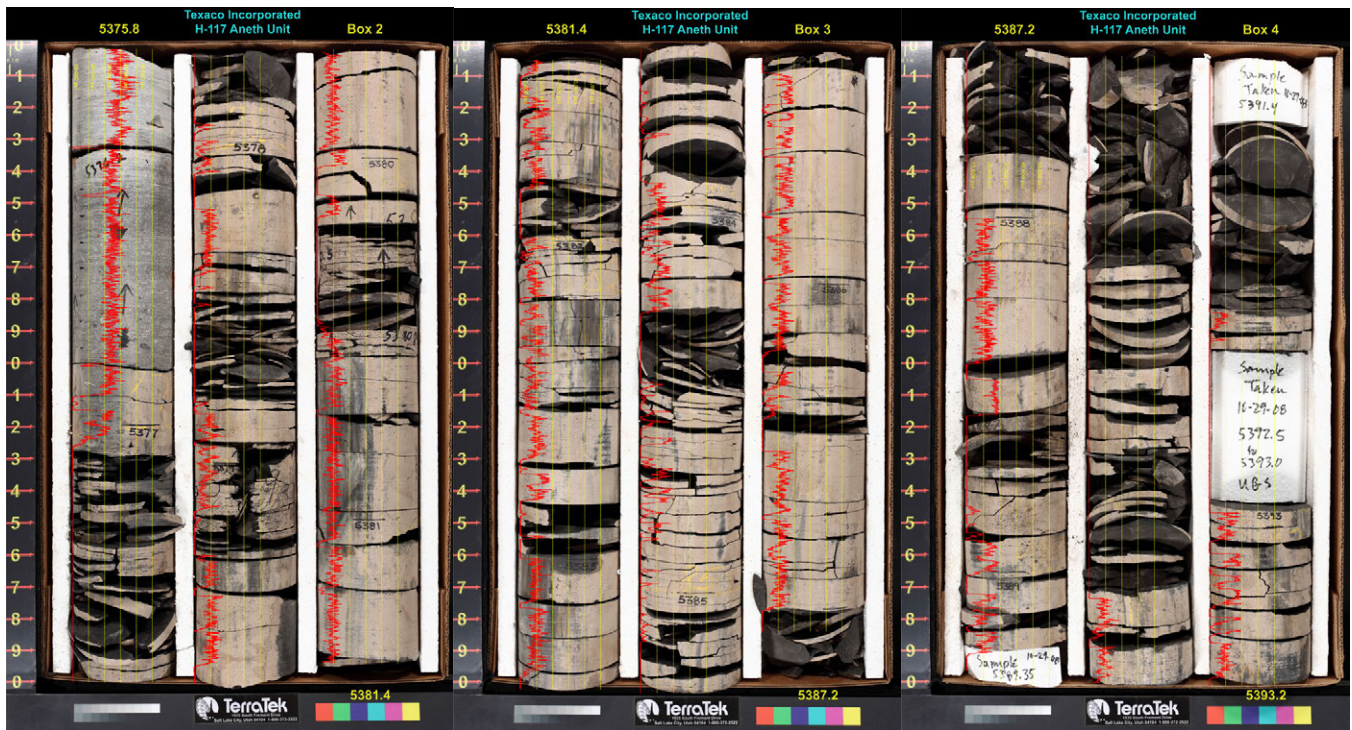


Figure 7.28. Continuous unconfined compressive strength profile of the Gothic shale core from the Aneth Unit H-117 well. From Chidsey and others, 2009.

CHAPTER 8: REGIONAL CORRELATIONS AND OUTCROP ANALOGS

BY

Craig D. Morgan, Stephanie Carney, Thomas C. Chidsey, Jr.,
Douglas A. Sprinkel, and Steve Herbst, *Utah Geological Survey*;
Gerald Waanders, *Consulting Palynologist*;
David E. Eby, *Eby Petrography & Consulting, Inc.*;
Steven Schamel, *GeoX Consulting, Inc.*;
Gary L. Gianniny, *Fort Lewis College*

CONTENTS

INVESTIGATION OF THE MISSISSIPPIAN MANNING CANYON SHALE AND DOUGHNUT FORMATION IN NORTHERN UTAH.....	149
Purpose and Methodology	149
Stratigraphic Nomenclature	152
Manning Canyon Shale.....	152
Doughnut Formation.....	153
Soldier Canyon Measured Section.....	154
Thermal Maturity of the Manning Canyon Shale and Doughnut Formation	156
Well Log Correlation of the Manning Canyon Shale and Doughnut Formation.....	158
LOWER MISSISSIPPIAN NOMENCLATURE IN NORTHEASTERN UTAH	159
Background.....	159
Historical Interpretations	159
Delle Phosphatic Member, Deseret Limestone.....	159
Summary.....	164
CHIMNEY ROCK, GOTHIC, AND HOVENWEEP SHALES IN OUTCROP, SAN JUAN RIVER CANYON.....	165
Geologic Setting	165
Sequence Stratigraphy	166
Raplee Anticline Measured Section.....	166

FIGURES

Figure 8.1. Location map showing area of Doughnut Formation and Manning Canyon/Great Blue Limestone.....	149
Figure 8.2. Typical Manning Canyon Shale outcrops.....	150
Figure 8.3. Geologic map of Soldier Canyon, Tooele County, Utah	150
Figure 8.4. Outcrop of the Manning Canyon Shale in Soldier Canyon.....	150
Figure 8.5. Examples of Manning Canyon and Doughnut palynomorphs collected from outcrop and well cuttings.....	151
Figure 8.6. Stratigraphic column for the Doughnut Formation and Manning Canyon Shale/Great Blue Limestone, and overlying and underlying formations	152
Figure 8.7. Thickness of the upper Middle to Upper Mississippian shallow marine deposits of the Manning Canyon Shale and Doughnut Formation.....	153
Figure 8.8. Thickness of the Manning Canyon Shale plus Great Blue Limestone and the Doughnut Formation.....	153
Figure 8.9. Late Meramecian to Early Chesterian deposition of the lower Doughnut Formation and Great Blue Limestone	154
Figure 8.10. Late Chesterian deposition of the upper Doughnut Formation and Manning Canyon Shale.....	155
Figure 8.11. View west showing folding and faulting in the Manning Canyon Shale, Soldier Canyon	156
Figure 8.12. Basal portion of the Soldier Canyon stratigraphic section showing surface gamma-ray data, palynomorph types, and photomicrographs of the basal shale and limestone.....	156
Figure 8.13. Portion of the Soldier Canyon stratigraphic section showing surface gamma-ray data, palynomorph types, TOC, and photomicrographs of the Medial limestone and overlying shale	157
Figure 8.14. Vitrinite reflectance of upper Mississippian	157
Figure 8.15. Cross section illustrating untested Sevier thrust structures that could have Manning Canyon Shale gas potential.....	158
Figure 8.16. Index map to the location of significant wells and outcrops used to correlate the Lower Mississippian section from central to northeastern Utah.....	160
Figure 8.17. Stratigraphic cross section showing the correlation of the Mississippian section, from central to northeastern Utah	161
Figure 8.18. Formations exposed in Whiterocks Canyon, South Flank, Uinta Mountains	165
Figure 8.19. Geologic map of the Raplee anticline-Goosenecks area, southeastern Utah	166
Figure 8.20. Stratigraphic column for the Pennsylvanian and Permian section, Raplee anticline-Goosenecks area, southeastern Utah	166
Figure 8.21. Stratigraphic profile of the Chimney Rock shale, Raplee anticline section, showing sequence stratigraphic interpretations, TOC, and gamma-ray data.....	167
Figure 8.22. The west-dipping flank of Raplee anticline on the north side of the San Juan River showing Paradox Formation and location of the measure section and gamma-ray profile.....	168
Figure 8.23. Stratigraphic and gamma-ray profile of the upper Akah zone, Chimney Rock shale, and lower Desert Creek zone in the Raplee anticline section	169

Figure 8.24. Stratigraphic and gamma-ray profile of the Gothic shale, lower Desert Creek zone, and Hovenweep shale in the Raplee anticline section..... 169

Figure 8.25. Correlation of the Chimney Rock, Gothic, and Hovenweep gamma-ray profile from the Raplee anticline measured section to the Mexican Hat 1 well..... 171

TABLES

Table 8.1. Paleozoic formation tops and thicknesses from the wells in central and northeastern Utah 162

Table 8.2. Paleozoic formation thicknesses from the measured sections in northeastern Utah..... 164

CHAPTER 8: REGIONAL CORRELATIONS AND OUTCROP ANALOGS

INVESTIGATION OF THE MISSISSIPPIAN MANNING CANYON SHALES AND DOUGHNUT FORMATION IN NORTHERN UTAH

Outcrop and well data of the Manning Canyon Shale and Doughnut Formation were investigated to determine the shale gas potential of the formations through improved geologic characterization (figure 8.1). Geologic characterization included a detailed stratigraphic measured section of the Manning Canyon where we described the lithology and dep-

ositional features, sampled key beds for thin section analyses and age dating, and collected spectral gamma-ray data. Other outcrops of the Manning Canyon and the Doughnut were sampled throughout northern Utah. Sample analyses consisted of palynomorph age dating and equivalent R_o (based on the thermal alteration of the palynomorphs), XRF, XRD, and description of thin sections.

Purpose and Methodology

The shales within the Manning Canyon Shale and the Doughnut Formation contain sufficient organic content to have been

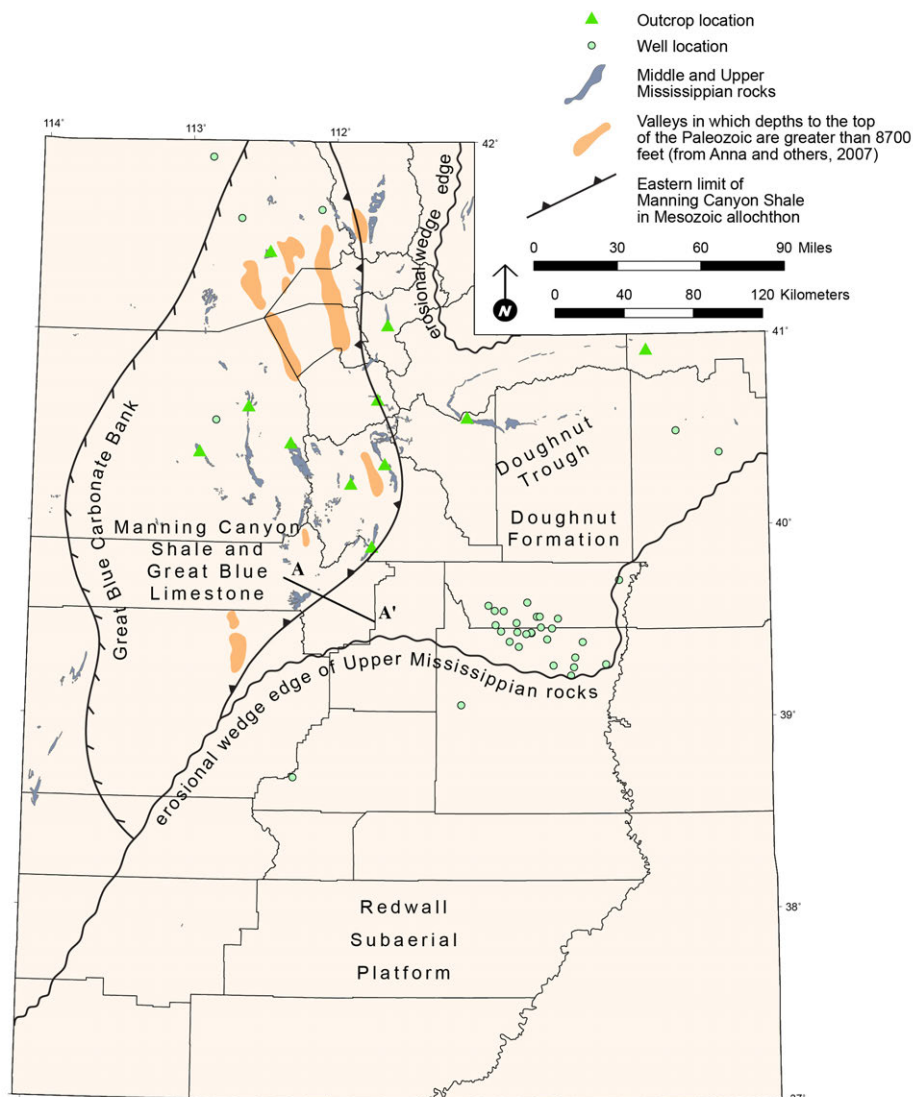


Figure 8.1. Location map showing area of Doughnut Formation and Manning Canyon/Great Blue Limestone. Data used in this study includes wells (circles) and outcrop samples (triangles). See figure 8.15 for cross section A–A'.

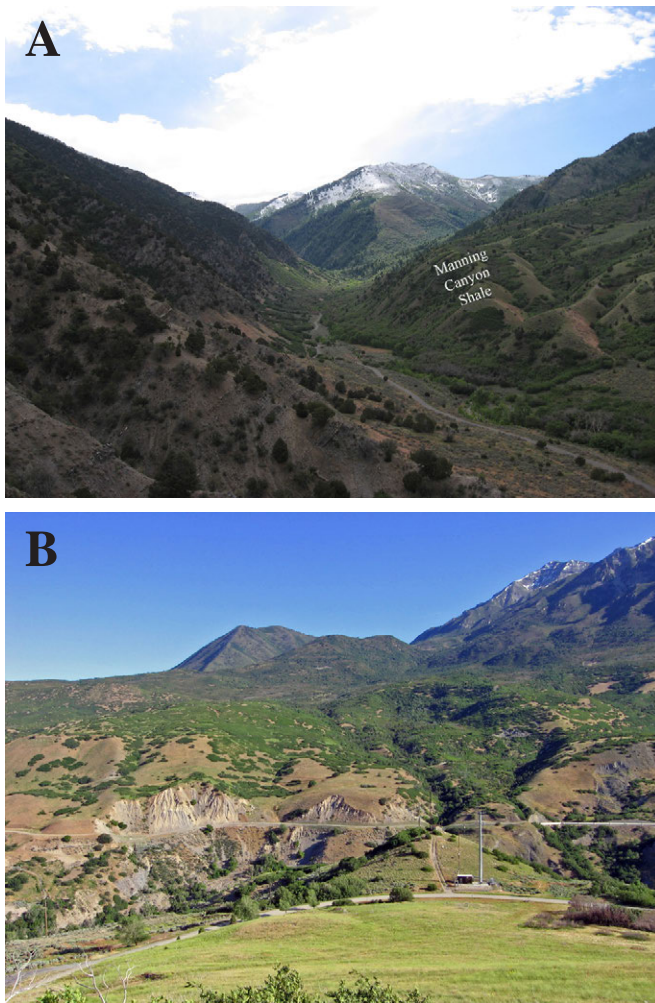


Figure 8.2. Typical Manning Canyon Shale outcrop; abundant landslides and high vegetation. **A** – view east up Soldier Canyon and **B** – view north along the strike valley formed in the Manning Canyon in Provo Canyon

a source of hydrocarbons and to have the potential for in-situ gas production, commonly referred to as shale gas. A study of the outcrops provided knowledge about the depositional environments and related organic content of each formation, regional thermal history of the formations, and regional distribution of potentially gas productive facies.

Surface exposures of the Manning Canyon Shale and Doughnut Formation are very poor. The abundant shale in the formations results in extensive slide surfaces and heavy vegetation cover (figure 8.2). Soldier Canyon in Tooele County at the southern end of the Oquirrh Mountains has the most complete exposure of the Manning Canyon (figures 8.3 and 8.4). The stratigraphic section at Soldier Canyon was selected for detailed measurement and description due to the easy access and nearly complete exposure. The only complete exposure of the Doughnut is in Dinosaur National Monument’s Whirlpool Canyon. Due to the remoteness and difficult access of the area we were unable to visit the Whirlpool Canyon outcrop.

Samples of most of the shale beds were collected and analyzed for palynomorphs to determine age and thermal alteration (figure 8.5 and appendix O). Shale, sandstone, and carbonate beds were sampled and thin sections made to determine detailed petrology and depositional environments. Appendix P consists of photomicrographs and descriptions of thin sections from the Manning Canyon Shale field samples. Outcrop samples and well cuttings were collected throughout the Basin and Range Province and analyzed by Gerald Waanders to assist with the regional correlation and thermal history (burial history models are described in chapter 9). Palynomorph analysis was selected because the small amount of sample needed allowed us to sample well cuttings and core.

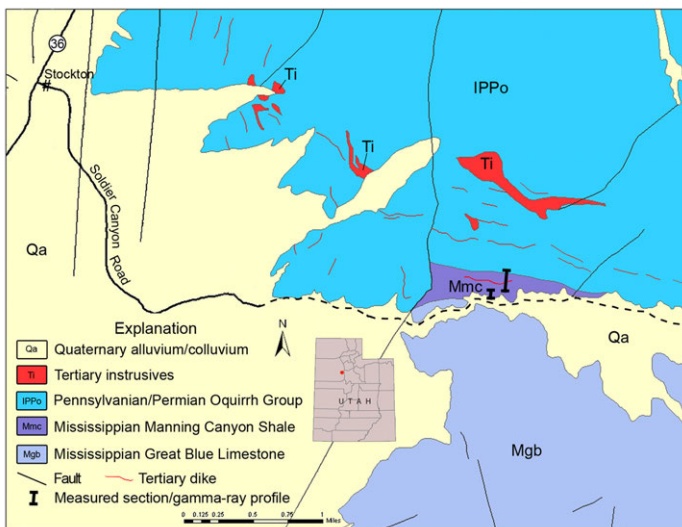


Figure 8.3. Geologic map of Soldier Canyon, Tooele County, Utah (modified from Clark and others, 2012).



Figure 8.4. Outcrop of the Manning Canyon Shale in Soldier Canyon, view west towards the mouth of the canyon.

*Lycospora pusilla**Patoniesporites sp.**Densosporites spinifer**Discernisporites micromanifestus**Triparitites vetustus*

Figure 8.5. Examples of Manning Canyon and Doughnut palynomorphs collected from outcrop and well cuttings.

The Soldier Canyon stratigraphic section was measured using a Jacob staff and steel tape. We used a portable Radiation Solutions Inc. RS-230 BGO Super-Spec scintillometer, which uses a bismuth-germanate-oxide detector, to collect gamma-ray spectrometer data every 3 feet (1 m). The spectrometer detects gamma radiation emitted by naturally occurring radioactive elements present in the rock. After properly stabilizing the instrument, a sampling time of one minute was used for each measurement. We took measurements in assay mode to determine the concentration of thorium (Th), uranium (U), and potassium (K). Readings are expressed as weight % K and parts per million (ppm) for U and Th. For covered sections we dug small trenches to an adequate depth for stable reading. Data from the reading were converted into API units using the equation

um (U), and potassium (K). Readings are expressed as weight % K and parts per million (ppm) for U and Th. For covered sections we dug small trenches to an adequate depth for stable reading. Data from the reading were converted into API units using the equation

$$\text{API unit} = (\%K * 16) + (U \text{ ppm} * 8) + (\text{Th ppm} * 4)$$

The final gamma-ray log was created with the converted API units (appendix Q).

Stratigraphic Nomenclature

The Manning Canyon Shale was called the upper shale of the Great Blue Limestone by Spurr (1895 [cited in Gilluly, 1932]). Gilluly (1932) described the exposures in Manning Canyon of the Oquirrh Mountains as the Manning Canyon Shale, a distinct and mappable formation, but stated the “section in Soldier Canyon is believed to represent the formation better than any of the others.” Moyle (1959) referred to the Manning Canyon section as the type locality and the Soldier Canyon section as the type section. The Manning Canyon was considered upper Chesterian to lower Morrowan by earlier workers, but Tooker and Roberts (1970) and Davis and others (1994) have dated the overlying Oquirrh Group in Soldier Canyon and elsewhere as upper Chesterian to Atokan, making the underlying Manning Canyon entirely Mississippian (Figure 8.6). Palynomorphs that we collected from the Manning Canyon and Doughnut Formation were all Mississippian (appendix O). The age discrepancy between previous workers may be due, in part, to the highly gradational contact of the Manning Canyon and Oquirrh, which can be difficult to identify with confidence. The Manning Canyon is underlain by the lower Chesterian and Meramecian Great Blue Limestone (Hintze and Kowallis, 2009).

The Doughnut Formation was defined by Granger and others (1952) for Mississippian-aged black shale and limestone exposed in the cliffs near Doughnut Falls in Big Cottonwood Canyon, east of Salt Lake City. The Doughnut is Chesterian and Meramecian and is overlain by the Pennsylvanian Round Valley Limestone and underlain by the Meramecian Humbug Formation. The Doughnut is equivalent to the Great Blue Limestone and the Manning Canyon Shale (figure 8.6).

The records of many of the wells drilled in the Colorado Plateau that penetrate the Upper Mississippian reported the Doughnut Formation as Manning Canyon Shale. Although the lithology of the Manning Canyon and the Doughnut are similar, and they are partially equivalent in age, we recognize sufficient differences between them to warrant separating out the two formations. Also, using Manning Canyon in central Utah implies a direct correlation between the Manning Canyon and Doughnut, whereas the Doughnut is equivalent to the Manning Canyon and the Great Blue Limestone, which is typically 1000 to 2000 feet (300–600 m) thick. In this report the Manning Canyon generally represents allochthonous rocks of the Basin and Range Province in western Utah. The Doughnut represents autochthonous rocks beneath the Wasatch Range, and rocks in the Uinta Mountains and the Colorado Plateau in eastern Utah.

Manning Canyon Shale

The Manning Canyon Shale is dominantly a marine shale to shaley mudstone with some interbedded limestone and thin sandstone beds. Organic matter is dominantly of terrestrial origin (Schamel and Quick, 2010; appendix L) and was prob-

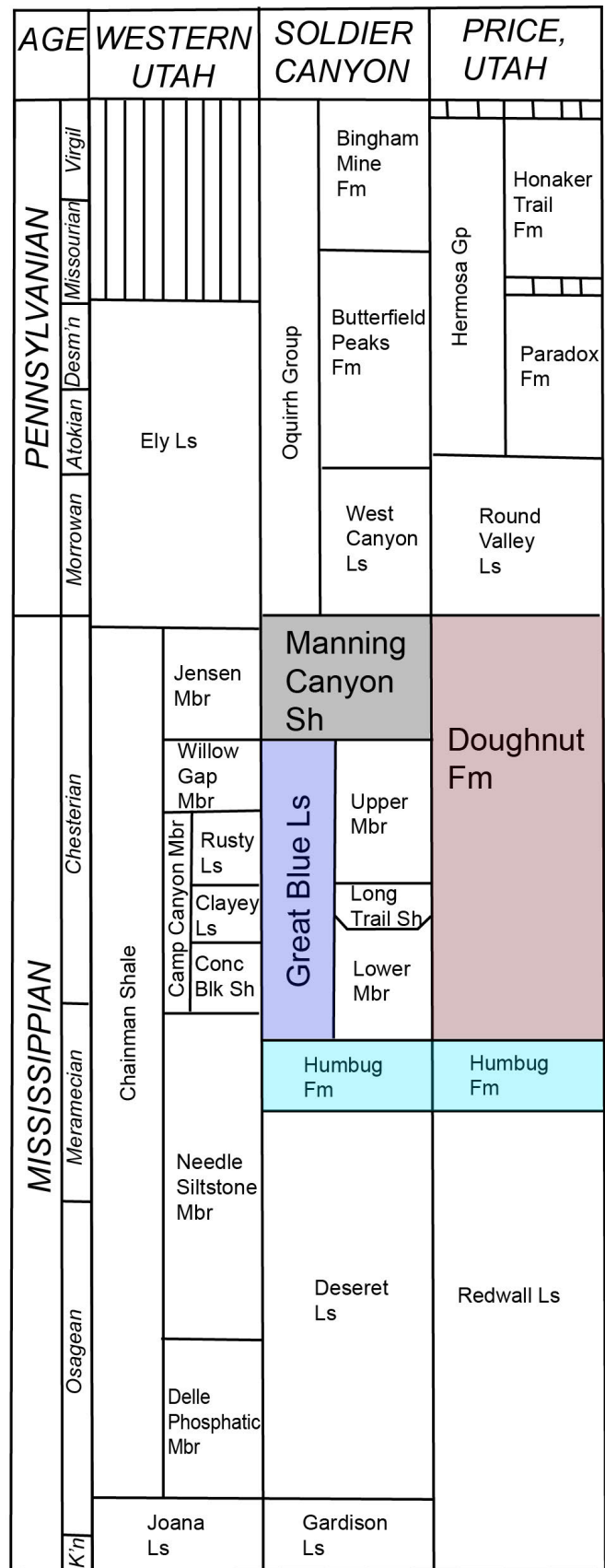


Figure 8.6. Stratigraphic column for the Doughnut Formation and Manning Canyon Shale/Great Blue Limestone, and overlying and underlying formations. Modified from Hintze and Kowallis (2009).

ably transported into the low energy environment through the proximal Doughnut trough. Well to moderately preserved leaf impressions have been described at several locations indicating little to no transportation or quiescent deposition. Although Prince (1964) described coal in the Manning Canyon at Soldier Creek, we did not find any; nor was coal found in the Soldier Canyon section or any of the other Manning Canyon measured sections described by Moyle (1959).

The soft and impervious shales form very unstable slopes and are typically highly vegetated. The shales are often the glide plane for thrusts, as in Provo Canyon. In Box Elder County, reverse faulting may have resulted in attenuation of the shales and repetition of the more competent sandstone beds. As a result, the true thickness of any stratigraphic section measured on outcrop or penetrated by a well is highly suspect as to whether it represents a true Manning Canyon thickness.

Moyle (1959) measured and described the Manning Canyon Shale at several localities—Manning Canyon, Soldier Canyon, Ophir Pass, West Canyon, and Lake Mountains—and concluded that Soldier Canyon was the most complete and best exposed section. Moyle (1959) measured 1910 feet (582 m) at Lake Mountain, but Biek and others (2009) measured only 1176 feet (359 m) in the Soldiers Pass quadrangle. Biek

(2004) mapped 1121 to 1419 feet (342–433 m) in the northern portion of the Lake Mountains. Moyle’s (1959) isopach map shows the greatest thickness of Manning Canyon at 2600 feet (800 m) in Provo Canyon where the Manning Canyon forms a north-south strike valley in the Wasatch Range and is bisected by the canyon. The area is highly vegetated with few rock exposures, consisting of abundant covered landslides. The Charleston-Nebo thrust is believed to be located within the Manning Canyon at this location. As a result, we believe the true stratigraphic thickness is probably far less than the 1645 feet (500 m) that Baker (1947) measured in Rock Canyon 4.5 miles (7.2 km) southeast of the mouth of Provo Canyon. Moyle (1959, figure 13) shows 2500 feet (750 m) of Manning Canyon south of Utah Lake, citing Bissell (1950), but we were unable to find such a thickness in any of Bissell’s publications. Possibly the maximum true stratigraphic thickness of the Manning Canyon is in the Oquirrh Mountains Soldier Canyon and Manning Canyon sections (figures 8.7 and 8.8).

Doughnut Formation

The Doughnut Formation is underlain by the Humbug Formation and overlain by the Round Valley Formation. The Doughnut is dominantly a marine shale to shaley mudstone with some interbedded limestone and thin sandstone beds. It

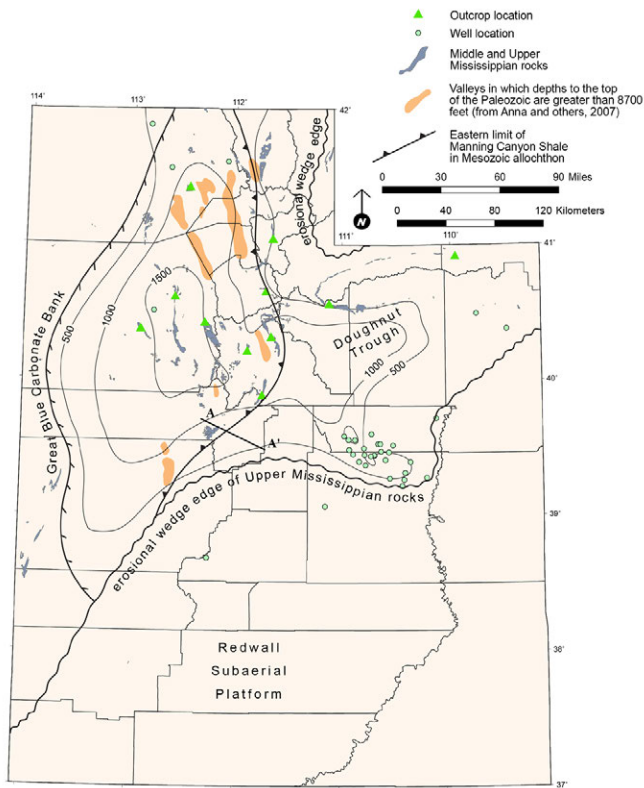


Figure 8.7. Thickness (in feet) of the upper Middle to Upper Mississippian shallow marine deposits of the Manning Canyon Shale and Doughnut Formation. The Manning Canyon is equivalent to only the upper portion of the Doughnut. Contour interval is 500 feet. See figure 8.15 for cross section A–A’.

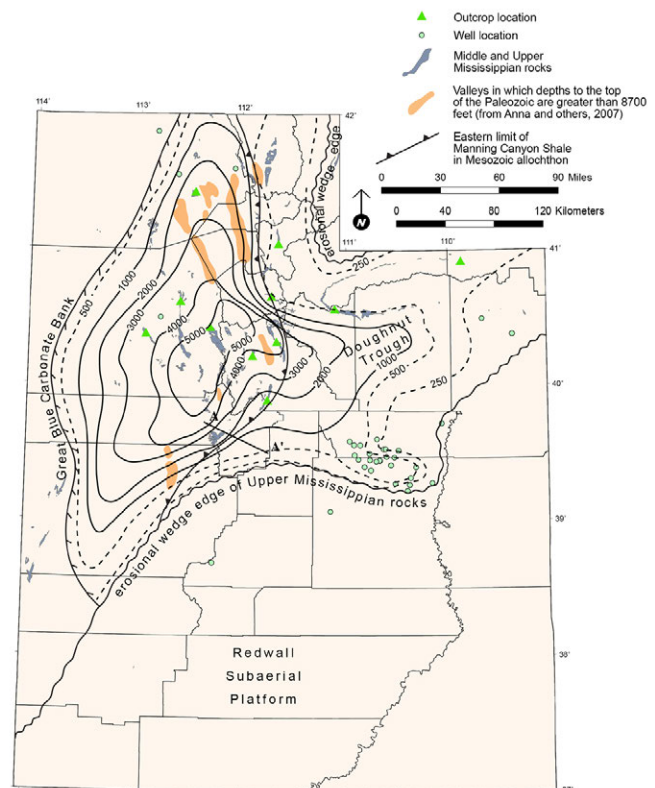


Figure 8.8. Thickness (in feet) of the Manning Canyon Shale plus Great Blue Limestone and the Doughnut Formation. Contour interval is 1000 feet with some 500-foot contours (dashed). See figure 8.15 for cross section A–A’.

also contains thin coals, carbonaceous shale, and thin red beds of sandstone and shale. Schamel and Quick (2010) describe the Doughnut depositional environment as shallow, restricted marine to brackish to freshwater, similar to the modern Everglades and Florida Bay (figures 5.18 and 5.19). A complex mix of environments from coastal plain, lagoon, and bay to offshore marine was identified in cores (appendix D). Organic matter is dominantly of terrestrial origin (appendix O) transported into the Doughnut trough from the neighboring lowlands. The Doughnut is generally a more proximal facies than the Manning Canyon Shale.

The Doughnut Formation is Chesterian and Meramecian age (figure 8.6). The lower portion of the Doughnut is equivalent to the Great Blue Limestone and was deposited while the Great Blue carbonate bank was being constructed to the west. Initially the slope was probably steep, but leveled and shallowed over time as the carbonate bank was built (figures 8.9 and 8.10). The steep slope may have caused upwelling currents and the deposition of phosphate nodules that are observed in the Doughnut core (appendix D). The Great Blue carbonate bank reached its maximum construction in the late Chesterian, resulting in the extensive coastal plain and shal-

low lagoon to restricted-bay deposits that comprise the upper Doughnut and Manning Canyon Shale.

Samples of the Doughnut Formation were collected from three locations (Mill Creek Canyon, Morgan Valley, and Sols Canyon) and from four wells in Carbon County (State 1-16, North Springs 1, Miller Creek 1, and Carbon Canal 5-12) (appendix O and appendix Q, plate Q-1). The age of most palynomorphs from the Doughnut are Chesterian, but some lower Doughnut samples contain Meramecian taxa. The kerogen distribution from the wells in Carbon County averaged 50% amorphous, 17% cuticular, and 33% woody/inertinite and had an average thermal alteration index (TAI) of 0.7. The kerogen from outcrop samples averaged 45% amorphous, 17% cuticular, and 38% woody/inertinite.

Soldier Canyon Measured Section

We measured and described 1535 feet (467 m) of Manning Canyon Shale along three traverses on the south-facing slope in Soldier Canyon (Figure 8.3 and appendix Q, plates Q-2 and Q-3.). The area is along the north-plunging axis of an anticline with numerous faults and folds complicating measurement (fig-

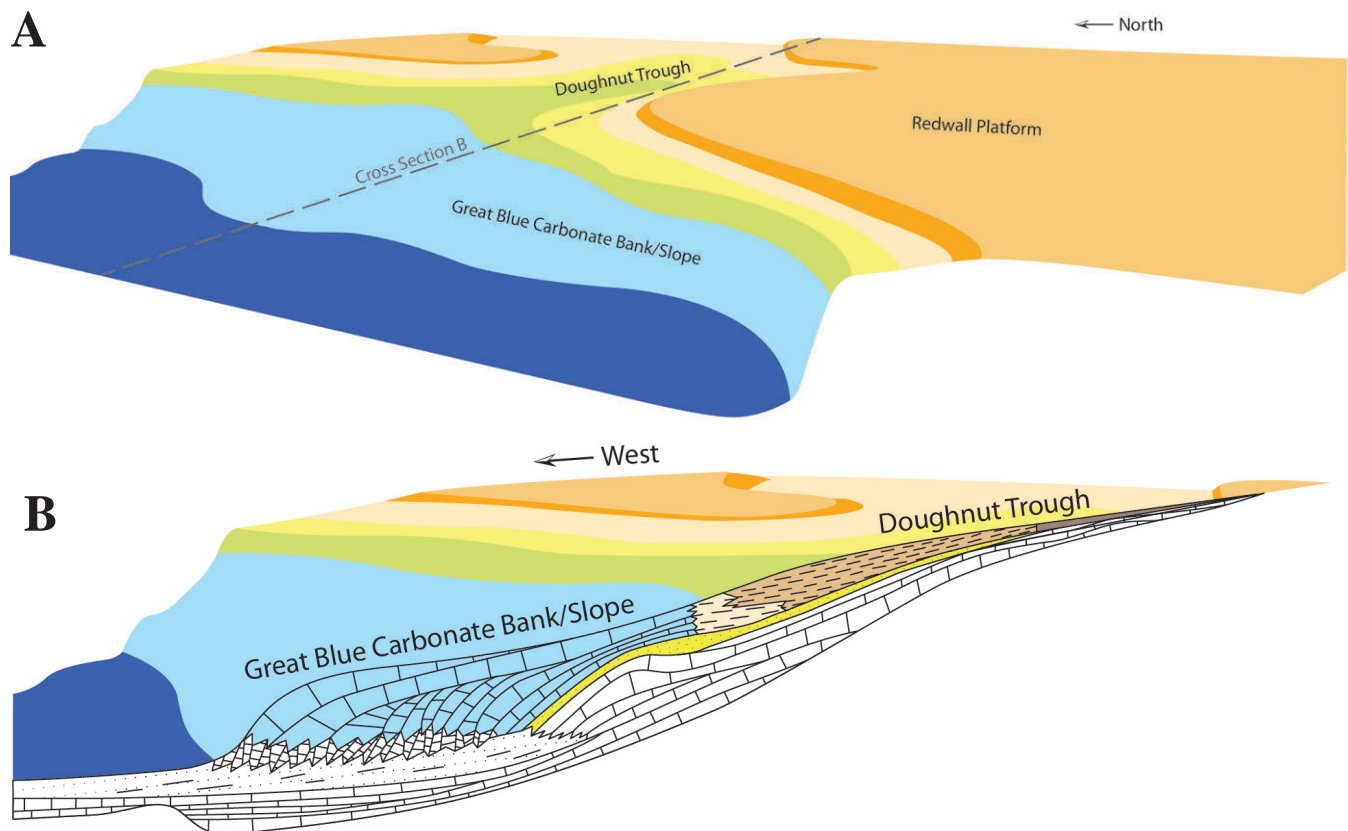


Figure 8.9. **A.** Oblique three-dimensional view to the north-northeast showing late Meramecian to early Chesterian deposition of the lower Doughnut Formation and Great Blue Limestone. **B.** Cut-away cross sectional view of block A showing lithologies. This represents an early constructional phase of the Great Blue carbonate bank. Block A is about 100 miles by 100 miles at maximum north-to-south and east-to-west directions. Cross sectional view B about 100 miles maximum length.

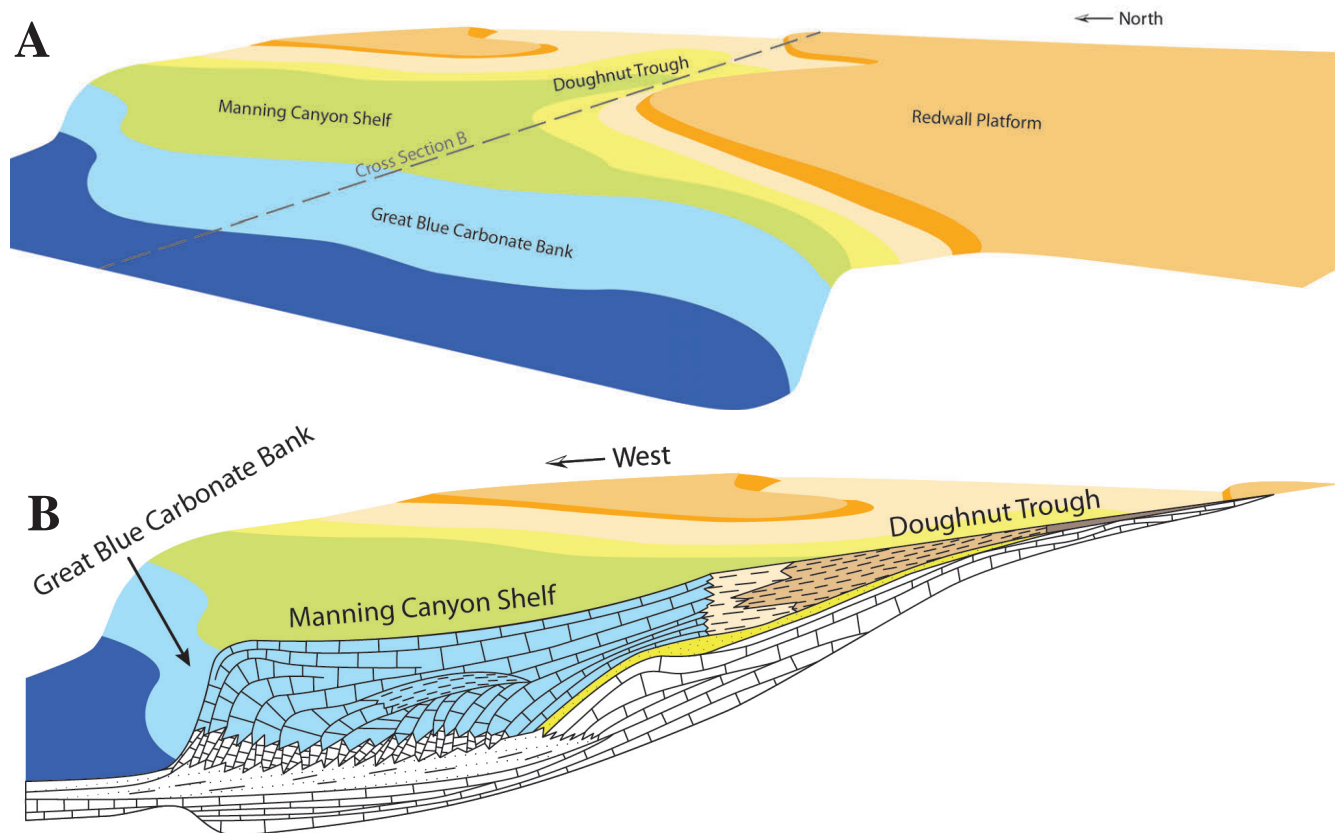


Figure 8.10. **A.** Oblique three-dimensional view to the north-northeast showing late Chesterian deposition of the upper Doughnut Formation and Manning Canyon Shale. **B.** Cut-away cross sectional view of block A showing lithologies. The Great Blue carbonate bank is fully developed providing a shallow water depositional environment. Block A is about 100 miles by 100 miles at maximum north-to-south and east-to-west directions. Cross sectional view B about 100 miles maximum length.

ure 8.11). We referred to Moyle's (1959) Soldier Canyon measured section and found close correlation except in two portions of the section. We believe Moyle followed a different traverse and may have crossed a fault that we may have crossed in a different portion of the section. The overall thickness we measured is very similar to the 1559 feet (475 m) of Manning Canyon measured by Moyle. No unconformities or sequence boundaries were identified in the Manning Canyon, and both upper and lower contacts are conformable and gradational.

The section consists of 945 feet (288 m) of shale/claystone (61%), 424 feet (129 m) of limestone (28%), 45 feet (13 m) of sandstone (3%), and 121 feet (36 m) of covered slope (8%). The shale/claystone beds are (appendix P): (1) black to shades of gray (some thin red beds are present), (2) calcareous or non-calcareous, and (3) non-fossiliferous or contain plant and other fossil fragments (brachiopods). These units are often interbedded with thin, non-fossiliferous limestone beds (figures 8.12 and 8.13).

Limestone beds are calcareous to shaley or silty (quartz) micrite and vary from thinly laminated to thick bedded or massive; some display cross-bedding whereas others are bioturbated. Carbonate fabrics include skeletal grainstone through packstone (figures 8.12 and 8.13), and microbial (stromat-

olitic and thrombolitic) lime mudstone (appendix P). These carbonates commonly contain a variety of marine fossils, such as abundant crinoids, brachiopods, bryozoans, benthic forams, corals, trilobite carapaces, bivalve mollusks, sponge spicules, and ostracodes, whereas some units are non-fossiliferous. Non skeletal grains consist of intraclasts, coated grains, detrital quartz, and peloids.

Sandstone beds are light gray to tan-brown to maroon and consist of fine-grained to coarse-grained, subangular to sub-rounded quartz grains with mild metamorphic overprints (appendix P). They vary from poor to well sorted, contain clay, and are thin to medium bedded with cross-beds.

The shale beds were deposited in (1) lower coastal plain, (2) marsh to backshore, (3) lagoon/restricted bay, and (4) open shelf environments. Carbonate depositional environments include: (1) shallow, low to moderate energy subtidal, (2) salinity-restricted platform interior, (3) moderate energy, open marine platform, (4) quiet (below wave and storm base), deep, poorly oxygenated water, and (5) high energy, near-shore terrigenous settings. Sandstone beds represent an upper shoreface environment. The modern analog for the Manning Canyon Shale depositional system is the Florida Bay and Everglades area of south Florida (figures 5.18 and 5.19).

Seven of nine samples from the Soldier Canyon Manning Canyon Shale measured section yielded palynomorphs of middle to late Chesterian age (appendix O). The kerogen distribution in the nine samples was 42% amorphous, 10% cuticular, and 48% woody/inertinite; no marine taxa were identified. Four

of the samples ranged from 70 to 90% woody/inertinite. The alteration index ranged from 1.0 to 1.5 TAI.

Thermal Maturity of the Manning Canyon Shale and Doughnut Formation

The equivalent R_o values and published R_o values (Sandberg and Gutschick, 1984) for Upper Mississippian rocks were contoured (figure 8.14). The generalized R_o map shows a high heat flow in northwest Utah related to the Raft River intrusion, and in west-central Utah possibly due to deep burial in the Oquirrh basin. A high R_o is assumed along the deep axis of the Uinta Basin due to the depth of burial (>30,000 feet [9000 m]) of the Mississippian rocks. Sandberg and Gutschick (1984) mapped the Conodont Alteration Index (CAI) of their samples. We collected palynomorph samples and identified the TAI. Both data sets are presented as equivalent R_o (figure 8.14). The Sandberg and Gutschick (1984) data generally have higher R_o values than our data.

Most of the Manning Canyon Shale outcrop samples are estimated to have reached temperatures by the end of the Permian that placed the formation in the gas-generative window (see chapter 9). The Doughnut Formation did not enter the main

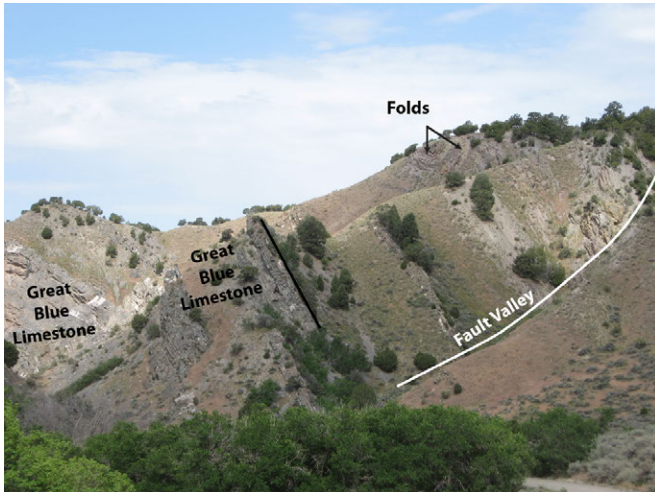


Figure 8.11. View west showing folding and faulting that are common in the Manning Canyon Shale in Soldier Canyon.

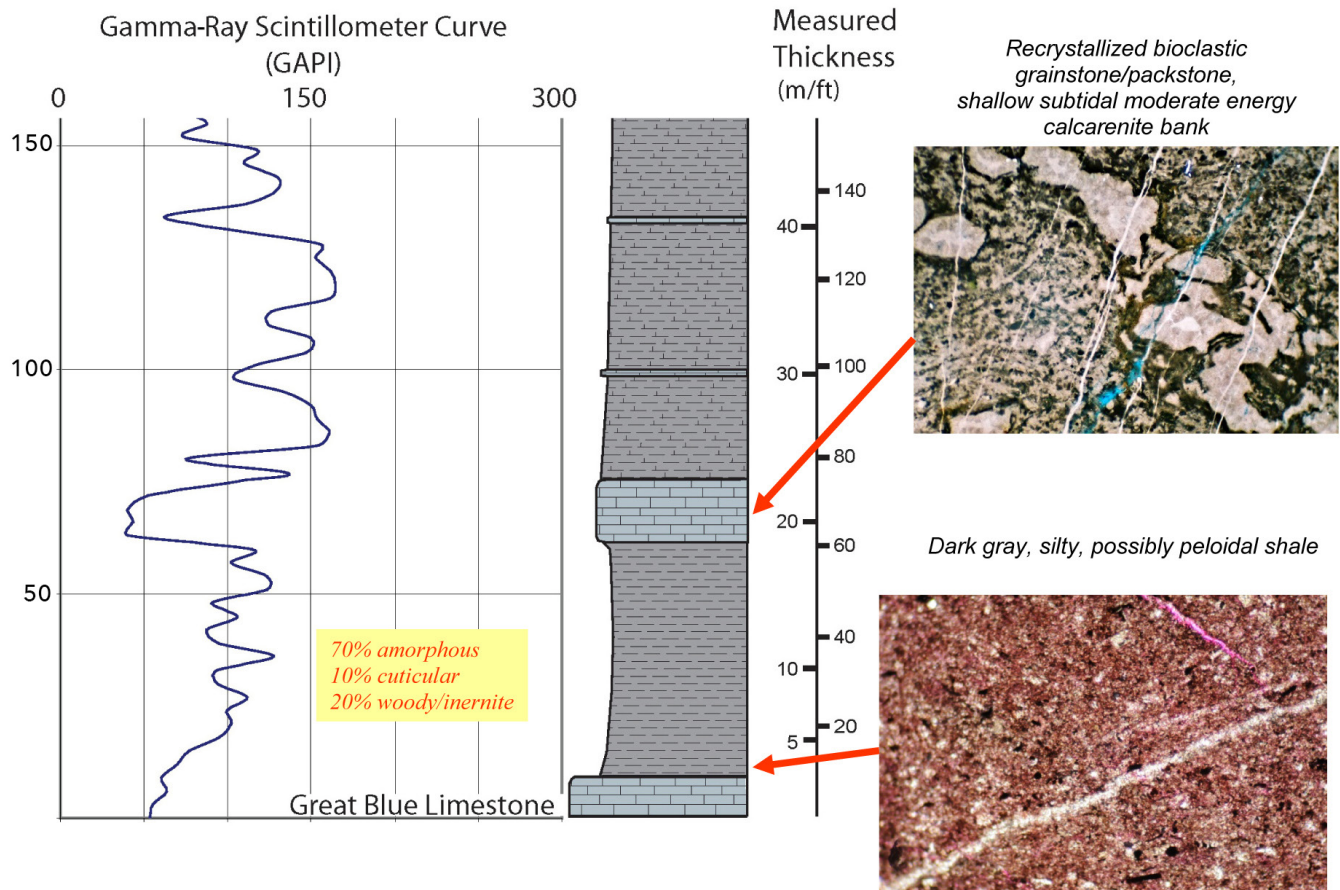


Figure 8.12. Basal portion of the Soldier Canyon stratigraphic section showing surface gamma-ray data, kerogen types, and photomicrographs of the basal shale and limestone. See plate 2, appendix Q for complete section and appendix P for additional photomicrographs.

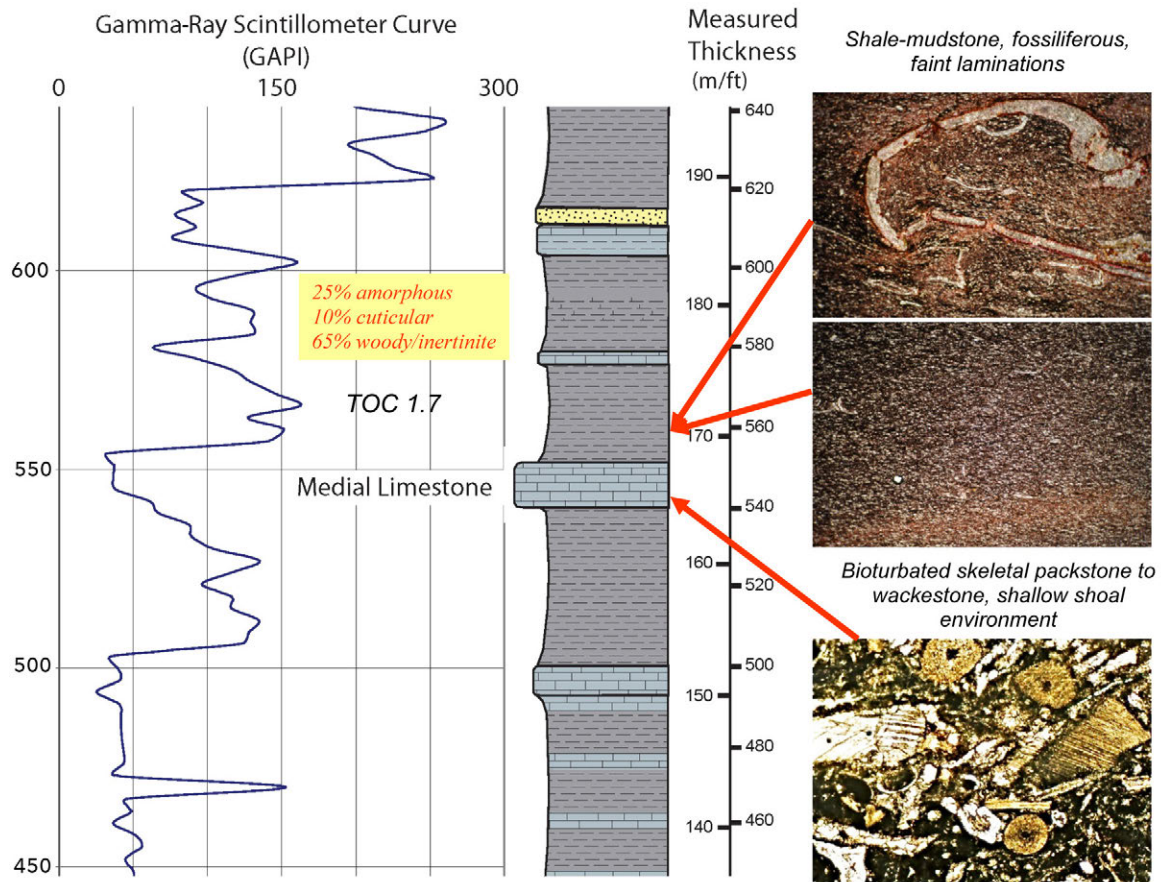


Figure 8.13. Portion of the Soldier Canyon stratigraphic section showing surface gamma-ray data, kerogen types, total organic carbon (TOC), and photomicrographs of the Medial limestone and overlying shale. See plate 2, appendix Q for complete section and appendix P for additional photomicrographs.

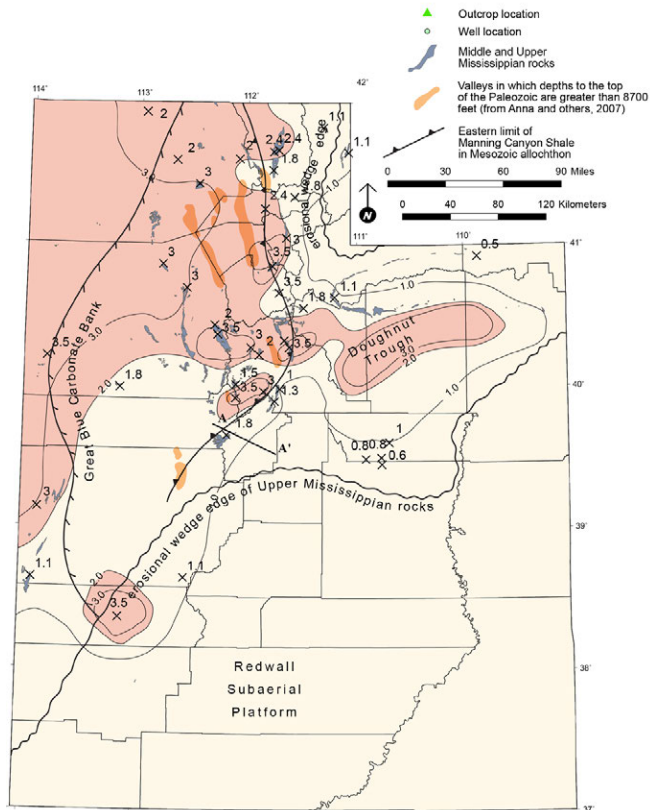


Figure 8.14. Vitrinite reflectance (R_v) of Upper Mississippian. Data are from Sandberg and Gutschick (1984) and appendix O. The colored area is $R_v \geq 2.0$, which means the rocks are well within the dry gas window. See figure 8.15 for cross section A-A'.

drilled the Manning Canyon in 1994 about 29 miles (47 km) west to northwest of Soldier Canyon. The well has good-quality logs, sample description, and palynomorph age dates in the DOGM well records. The correlation of the Manning Canyon section in the well to our measured section is reasonably good (appendix Q, plate Q-4). There were no shows of oil and gas in the well and it was plugged and abandoned.

Numerous wells (about 25) have penetrated the Doughnut Formation in the Carbon County area, but correlation between them is difficult due to the complex heterogeneity of the formation and the many faults in the area. Reliable correlation of beds within the Doughnut was not possible. The correlation of the top and bottom of the formation is often questionable due to the gradational nature of the contacts and is largely based on age dates where available (appendix Q, plate Q-1). The Doughnut, along with many of the Mississippian-aged and Pennsylvanian-aged formations, is missing on the Emery High south of Carbon County due to erosion and/or nondeposition (appendix Q, plate Q-5).

LOWER MISSISSIPPIAN NOMENCLATURE IN NORTHEASTERN UTAH

Background

The Lower Mississippian nomenclature in northeastern Utah was examined as part of this study due to the correlation of the Delle Phosphatic Member of the Deseret Limestone from the central Utah thrust belt to the eastern Uinta Mountains. The Delle is an important marker bed that provides a better understanding of the regional Mississippian section in northeastern Utah and where the Doughnut with its potential shale-gas facies can be found. The Delle itself may have some shale-gas potential. Recent geologic mapping of Mississippian strata in the eastern Uinta Mountains (Sprinkel, 2006, 2007) has followed previous mapping in the region (Hansen and Bonilla, 1956; Hansen, 1965, 1977; Hansen and others, 1981, 1983; Rowley and others, 1985; Hansen and Rowley, 1991). On these geologic maps the Mississippian section, in ascending order, includes the Madison Limestone, Humbug Formation, and Doughnut Formation. Preliminary reviews of geologic maps of the Dutch John and Vernal 30' x 60' quadrangles (Sprinkel, 2006, 2007) questioned the use of Madison Limestone for the Mississippian map unit that underlies the Humbug Formation. The reviewers felt that identification of the Delle in the Uinta Mountains necessitated subdividing the Madison Limestone into two map units, which provided a more accurate approach to mapping this section, and reflected earlier stratigraphic work. Thus, the following discussion is an attempt to resolve the issue of Mississippian nomenclature in the Uinta Mountains to assist with shale-gas exploration efforts in the region.

Historical Interpretations

The Mississippian section exposed along the flanks of the Uinta Mountains includes the Madison Limestone, Humbug Formation, and Doughnut Formation. Identification of the Humbug and Doughnut Formations in the Uinta Mountains seems unquestioned, but the interval currently mapped as Madison Limestone has long been controversial. Huddle and McCann (1947) and Baker and others (1949) considered the interval below the Humbug Formation as Madison Limestone overlain by the Deseret Limestone in the western Uinta Mountains. Kinney (1955) indicated the Mississippian section in the eastern Uinta Mountains was likely equivalent to the Madison, Deseret, and Humbug Formations as exposed along the Wasatch Range and western Uinta Mountains, but the subdivisions were tentatively recognized only as far east as Buck Ridge above the Whiterocks River in the eastern Uinta Mountains. East of the Whiterocks River, Kinney (1955) indicated the section was too indistinct to map at a scale of 1:63,360. Thus, Kinney (1955) mapped the section as informal units: a lower limestone unit that represented the Madison, Deseret, and Humbug Formations and an upper shale unit that represented the Doughnut Formation.

Sadlick (1957) identified the Madison, Deseret, and Humbug Formations, but called the upper shale the Manning Canyon Shale. Crittenden (1959) continued Madison, Deseret, and Humbug nomenclature for the western Uintas, but used Doughnut Formation instead of Manning Canyon in the eastern Uinta Mountains based on fossil evidence. Welsh and Bissell (1979) also recognized the upper part of the questionable interval as Deseret Limestone, but used Lodgepole Limestone for the lower dark-gray limestone after the work of Holland (1952). The use of Madison Limestone for the entire interval to the base of the Humbug Formation in the eastern Uinta Mountains was adopted by Hansen (1965) because fossil evidence reported in Crittenden (1959) suggested the interval referred to as the Humbug was pre-Deseret age, and that paradigm has been followed by mapping geologists ever since.

Delle Phosphatic Member, Deseret Limestone

Some of the geologists who worked on Mississippian stratigraphic relations recognized a twofold aspect to the Madison Limestone in the Uinta Mountains: a lower mostly dark-gray cherty and fossiliferous limestone (with some dolomite) and an upper medium- to light-gray limestone and dolomite (Huddle and McCann, 1947; Baker and others, 1949; Sadlick, 1957; Crittenden, 1959; Welsh and Bissell, 1979). The contact between the two units was generally placed at the base of a phosphatic unit, black shale, or a tripolitic chert bed (Baker and others, 1949; Sadlick, 1957; Crittenden, 1959; Sandberg and Gutschick, 1984). The lower part was generally like the lower Madison of Montana and the upper part was like the Deseret Limestone of the Wasatch Range area because of lithologic similarities and fossil content. The phosphatic interval at the base of the Deseret Limestone is the Delle Phosphatic

Member, and it is preserved in several formations in Utah, southeastern Idaho, southeastern Nevada, and southwestern Wyoming. It represents a large starved basin that developed during Early Mississippian (Osagean) time (Sandberg and Gutschick, 1984). However, Siberling and Nichols (1992) interpreted the Delle as a shelf deposit, influenced by upwelling.

It seems reasonable to subdivide the Madison Limestone, as currently mapped, into two formations. It also seems reasonable to apply the name Deseret Limestone to the upper medium- to light-gray limestone and dolomite part, particularly where the Delle Phosphatic Member is present. There is less certainty about what name to use for the lower dark-gray cherty limestone; Madison Limestone or Lodgepole Limestone are reasonable candidates as they both have been used in the past and contain a fossil assemblage consistent with those formations (Baker and others, 1949; Sadlick, 1957;

Crittenden, 1959; Welsh and Bissell, 1979). Thus, we believe redefining the Lower Mississippian stratigraphy of the Uinta Mountains can be justified if it can be correlated with confidence to the Delle Phosphatic Member from central Utah.

We used a series of petroleum exploration wells extending from the central Utah thrust belt to the eastern Uinta Mountains to identify and correlate the Delle Phosphatic Member, and determine its eastern limit of deposition (figures 8.16 and 8.17). Published measured sections, located mostly on the south flank of the Uinta Mountains, were studied to identify the Delle. Formation tops and thicknesses from the wells and measured sections are listed in tables 8.1 and 8.2. The Delle Phosphatic Member is fairly easy to identify in the central Utah thrust belt sector of the cross section. The thickness of the Delle and other Mississippian formations are reasonably consistent with nearby surface measurements (Sandberg and Gutschick, 1984).



Figure 8.16. Index map to the location of significant wells and outcrops used to correlate the Lower Mississippian section from central to northeastern Utah. Cross section A–A' is shown on figure 8.17. See tables 8.1 and 8.2 for well and section data.

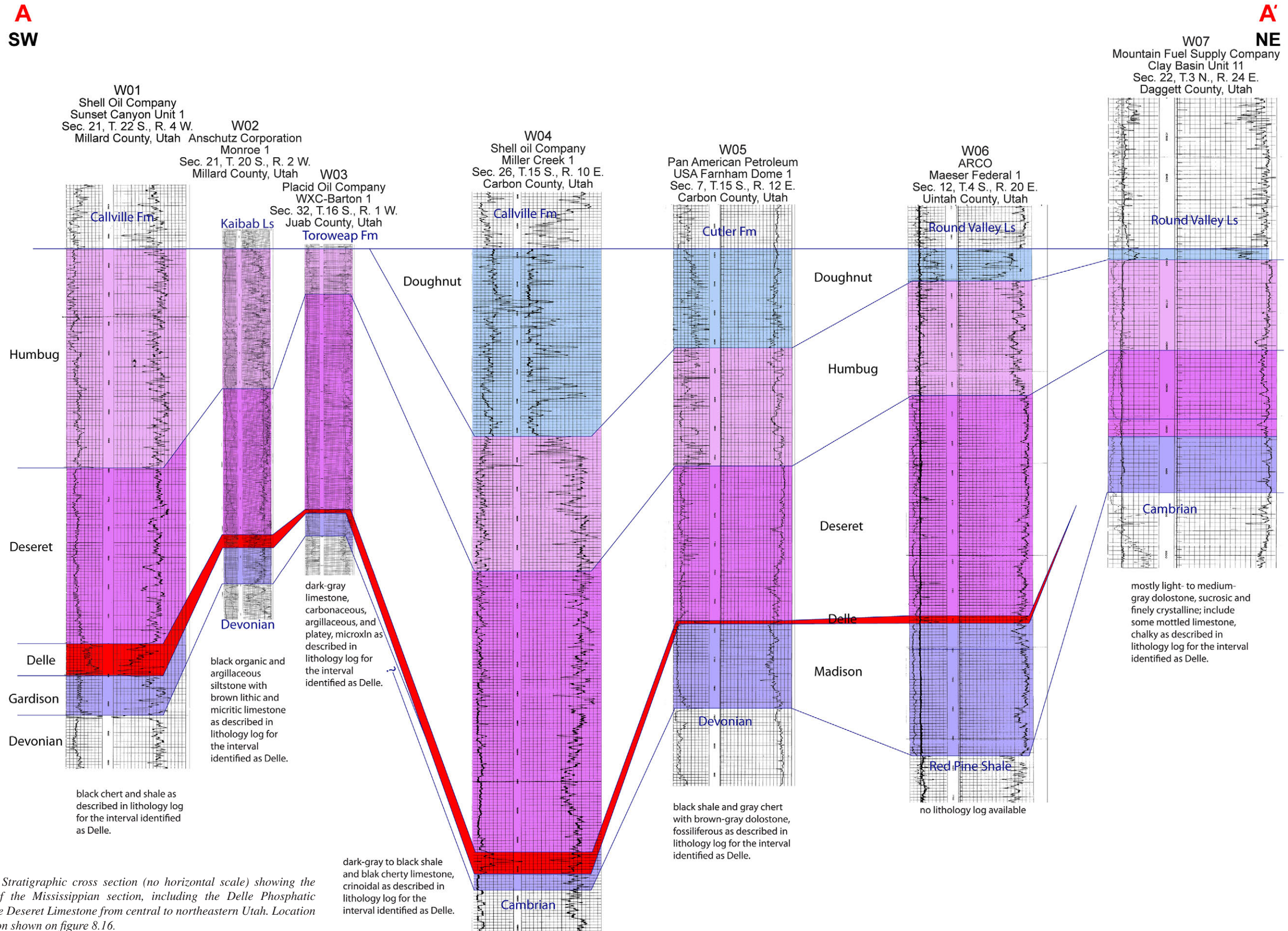


Figure 8.17. Stratigraphic cross section (no horizontal scale) showing the correlation of the Mississippian section, including the Delle Phosphatic Member of the Deseret Limestone from central to northeastern Utah. Location of cross section shown on figure 8.16.

Table 8.1. Paleozoic formation tops and thicknesses from the wells in central and northeastern Utah shown on figure 8.16.

ID	Cross Section	Well Information	Formation	Top (feet)	Thickness (feet)	Comments
W-01	A-A'	Shell Oil Company	Callville Formation			Doughnut missing; Pennsylvanian on Humbug.
		Sunset Canyon Unit 1	Humbug Formation	4845	750	
		SW1/4 SE1/4 Section 21, T. 22 S., R. 4 W.	Deseret Limestone	5595	601	
		Salt Lake Base Line & Meridian	Delle Phosphatic Member	6196	109	
		Millard County, Utah	Gardison Limestone	6305	90	
		API: 43-027-11038	Devonian	6395		
		Wildcat				
W-02	A-A'	Anschutz Corporation	Kaibab Formation			Doughnut missing; Permian on Humbug.
		Monroe 1	Humbug Formation	13,740	482	
		SW1/4 SE1/4 Section 21, T. 20 S., R. 2 W.	Deseret Limestone	14,222	501	
		Salt Lake Base Line & Meridian	Delle Phosphatic Member	14,723	45	
		Millard County, Utah	Gardison Limestone	14,768	126	
		API: 43-027-30008	Devonian	14,894		
		Wildcat				
W-03	A-A'	Placid Oil Company	Toroweap Formation			Doughnut missing; Permian on Humbug.
		WXC-Barton 1	Humbug Formation	18,905	157	
		NW1/4 SE1/4 Section 32, T.16 S., R. 1 W.	Deseret Limestone	19,062	722	
		Salt Lake Base Line & Meridian	Delle Phosphatic Member	19,784	34	
		Juab County, Utah	Gardison Limestone	19,818	78	
		API: 43-023-30004	Devonian	19,896		
		Wildcat				
W-04	A-A'	Shell Oil Company	Callville Formation			Pennsylvanian reported by Welsh, 1979.
		Miller Creek 1	Doughnut Formation	8278	642	
		NE1/4 NE1/4 Section 26, T.15 S., R. 10 E.	Humbug Formation	8920	360	
		Salt Lake Base Line & Meridian	Deseret Limestone	9280	1060	
		Carbon County, Utah	Delle Phosphatic Member	10,340	75	
		API: 43-007-11029	Madison Limestone	10,415	55	
		Wildcat	Cambrian	10,470		
W-05	A-A'	Pan American Petroleum	Cutler Formation(?)			Arkosic bed on Mississippian; reported by operator.
		USA Farnham Dome 1	Doughnut Formation	6280	341	
		SW1/4SW1/4 Section 7, T.15 S., R. 12 E.	Humbug Formation	6621	410	

Table 8.1. Continued.

ID	Cross Section	Well Information	Formation	Top (feet)	Thickness (feet)	Comments
W-05	A-A'	Salt Lake Base Line & Meridian	Deseret Limestone	7031	534	
		Carbon County, Utah	Delle Phosphatic Member	7565	15	
		API: 43-007-10819	Madison Limestone	7580	251	
		Wildcat	Devonian	7831		
W-06	A-A'	ARCO	Round Valley Limestone	5400	440	normal section
		Maeser Federal 1	Doughnut Formation	5840	110	
		SE1/4SE1/4 Section 12, T.4 S., R. 20 E.	Humbug Formation	5950	385	
		Salt Lake Base Line & Meridian	Deseret Limestone	6335	750	
		Uintah County, Utah	Delle Phosphatic Member	7085	25	
		API: 43-047-30090	Madison Limestone	7110	450	
		Wildcat	Red Pine Shale	7560		noted as Morgan Formation by operator.
W-07	A-A'	Mountain Fuel Supply Company	Round Valley Limestone	10,270	295	normal section
		Clay Basin Unit 11	Doughnut Formation	10,565	28	
		NE1/4NW1/4 Section 22, T.3 N., R. 24 E.	Humbug Formation	10,593	212	
		Salt Lake Base Line & Meridian	Deseret Limestone	10,805	168	
		Daggett County, Utah	Delle Phosphatic Member?	10,973	47	
		API: 43-009-15635	Madison Limestone	11,020	130	
		Clay Basin field	Gros Ventre (Death Canyon Limestone Member)	11,150	329	
			Gros Ventre (Wolsey Shale Member)	11,479	146	
			Lodore	11,625	153	
	TD	11,778				

Table 8.2. Paleozoic formation thicknesses from the measured sections in northeastern Utah shown on figure 8.16.

ID	Location	Formation	Thickness (feet) from Huddle and McCann (1947); Baker and others (1949)	Thickness (feet) from Kinney (1955)	Thickness (feet) from Sadlick (1957)	Comment
S-1	Duchesne River	Doughnut Formation	±200		300	
		Humbug Formation	359		359	
		Deseret Limestone	631		632	Baker and others (1949) and Sadlick (1957) described phosphatic beds but did not give thickness.
		Delle Phosphatic Member	20			Black chert and shale beds in top 20 feet of Madison (Huddle and McCann, 1947).
		Gardison Limestone	226		247	
S-2	Whiterocks	Doughnut Formation	279	279	259	
		Humbug Formation	400	252	252	
		Deseret Limestone	600	750	744	Baker and others (1949) and Sadlick (1957) described phosphatic beds but did not give thickness
		Delle Phosphatic Member		25		Included at top of Kinney's (1955) lower limestone interval (Madison).
		Madison Limestone	231	190	215	
S-3	Diamond Gulch	Doughnut Formation	80	25		
		Humbug Formation	281	268	359	
		Deseret Limestone	496	475	496	
		Delle Phosphatic Member		29		Baker and others (1949) and Sadlick (1957) described phosphatic beds but did not give thickness.
		Madison Limestone	188	193	188	
S-4	Sols Canyon	Doughnut Formation			545	
		Humbug Formation			359	
		Deseret Limestone			612	Sadlick (1957) described phosphatic beds but did not give thickness.
		Madison Limestone			297	

The Delle Phosphatic Member was correlated northeastward based on lithology log descriptions and petrophysical log responses. The Delle was likely drilled in ARCO Maeser Federal 1 well (section 12, T. 4 S., R. 20 E., SLBL&M, Uintah County [figures 8.16 and 8.17, table 8.1), although a lithology log was not available to confirm the petrophysical log response. Sadlick (1955a, 1955b) had noted beds of dark-gray shale or tripolitic chert that separated the Madison and Deseret in wells in eastern Utah and western Colorado. Correlation of the dark-gray shale with the Delle seems reasonable, but the significance of the tripolitic chert and its correlation with the Delle to the west seem uncertain. Figure 8.18 is an annotated photograph showing the formations exposed on the west side of Buck Ridge above the Whiterocks River. The cliff-forming Madison Limestone (or Lodgepole Limestone) and Deseret Lime-

stone can be seen with a prominent topographic recess that represents the Delle Phosphatic Member. This lithologic and topographic expression of the Mississippian section below the Humbug Formation can be seen on the ground and on aerial photographs east of the Whiterocks River to the western part of the Diamond Mountain Plateau. The topographic expression becomes more difficult to see in the eastern part of the Diamond Mountain Plateau, particularly in the Jones Hole area.

Summary

In northeastern Utah, the lower part of the Mississippian section can be subdivided and mapped as two map units: a lower Madison Limestone (or Lodgepole Limestone) and upper Deseret Limestone, based on correlation of the Delle Phosphatic

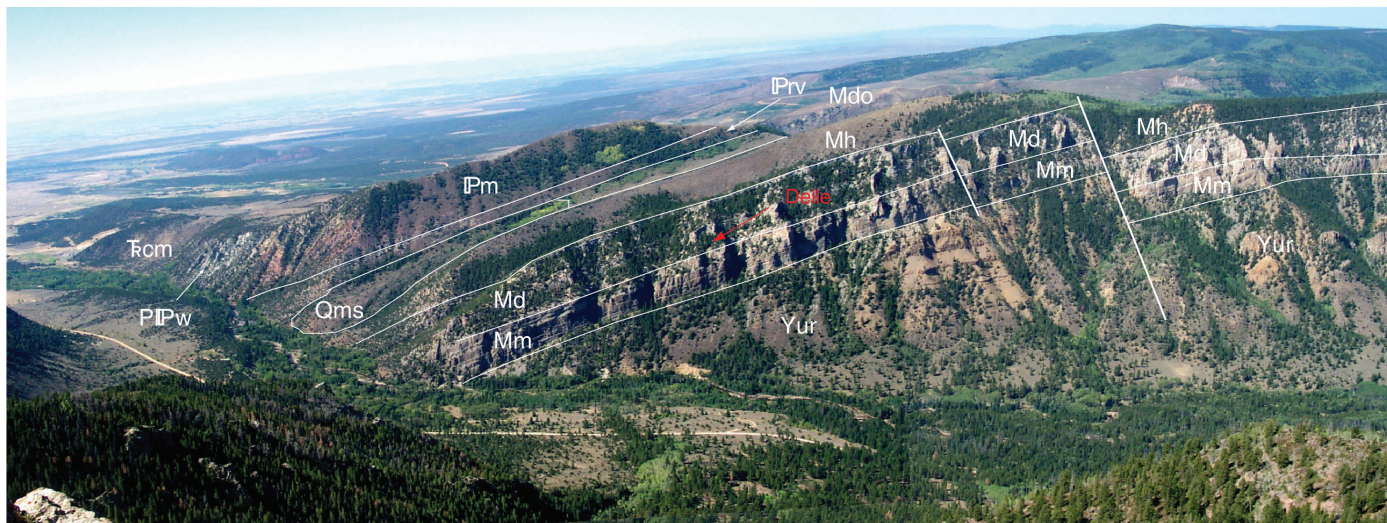


Figure 8.18. Formations exposed in Buck Ridge west of Whiterocks River, South Flank of the Uinta Mountains (view to the west from a point near Ice Cave Peak). Yur – Red Pine Shale, Mm – Madison Limestone, Md – Deseret Limestone, Mh – Humbug Formation, Mdo – Doughnut Formation, IPrv – Round Valley Limestone, IPm – Morgan Formation, PIPw – Weber Sandstone, Trcm – Moenkopi-Chinle Formations, Qms – landslide deposit.

Member from the central Utah thrust belt. The key findings derived from this correlation are listed below.

1. The Mississippian section in central Utah consists of the upper Fitchville, Gardison, Deseret, Humbug, and Doughnut Formations.
2. The Delle Phosphatic Member of the Deseret Limestone is a good stratigraphic marker and easily identified on petrophysical and mud logs.
3. The Delle Phosphatic Member was correlated in wells from central Utah to the northern Uinta Basin near Vernal, Utah.
4. Correlation of the Delle Phosphatic Member and identification of Deseret lithofacies in the Uinta Mountains redefines the Mississippian section to Madison, Deseret, Humbug, and Doughnut Formations.
5. The Madison Limestone (Kinderhookian) is dark gray cherty limestone; the Deseret Limestone (Osagean) is medium to light gray limestone and dolomite with a basal dark gray shale and chert (Delle Phosphatic Member).

CHIMNEY ROCK, GOTHIC, AND HOVENWEEP SHALES IN OUTCROP, SAN JUAN RIVER CANYON

Geologic Setting

The Chimney Rock, Gothic, and Hovenweep shales and the oil-producing zones (the Desert Creek and Ismay) of the Par-

adox Formation are only exposed along a few parts of the San Juan River canyon near Mexican Hat in southeasternmost Utah (figures 8.19 and 8.20). Nearly the entire Paradox section crops out west of Mexican Hat in the famous Goosenecks area (see Stevenson, 2010, for a complete geological description of Goosenecks State Park), where it can be spectacularly viewed from the canyon rim and accessed up close along the Honaker Trail, which traverses the overlying Pennsylvanian Honaker Trail Formation to the river 1220 feet (372 m) below. East of Mexican Hat, most of the Paradox (Barker Creek zone) through the Permian Halgaito Formation is exposed along the west-dipping flank of the Raplee anticline (figures 8.19 and 8.20). Though mainly found in the subsurface of the Paradox Basin, these formations were uplifted by the large, north-south-trending, Laramide-age Monument upwarp. Raplee anticline and the Goosenecks area are subsidiary structures on the upwarp separated by the Mexican Hat syncline.

When the Colorado Plateau rose in the late Cenozoic, the ancestral Colorado River and its tributaries, such as the San Juan River, flowed possibly northeast through meandering channels in wide valleys on easily eroded rocks such as the now-removed Cretaceous Tropic Shale. About 5.5 million years ago, capture of the ancestral Colorado River by lower drainages west of the Grand Wash fault near the Utah-Nevada border dramatically changed the flow to the Gulf of California (Lucchitta, 1989). Rapid headward erosion and continued regional uplift caused the established river channels to quickly erode soft strata and carve deep narrow canyons in resistant strata. They become superimposed and entrenched into buried structures, such as the Raplee anticline, thereby exposing Jurassic and older rocks throughout the Colorado Plateau, including the Paradox Formation along the San Juan River canyon.

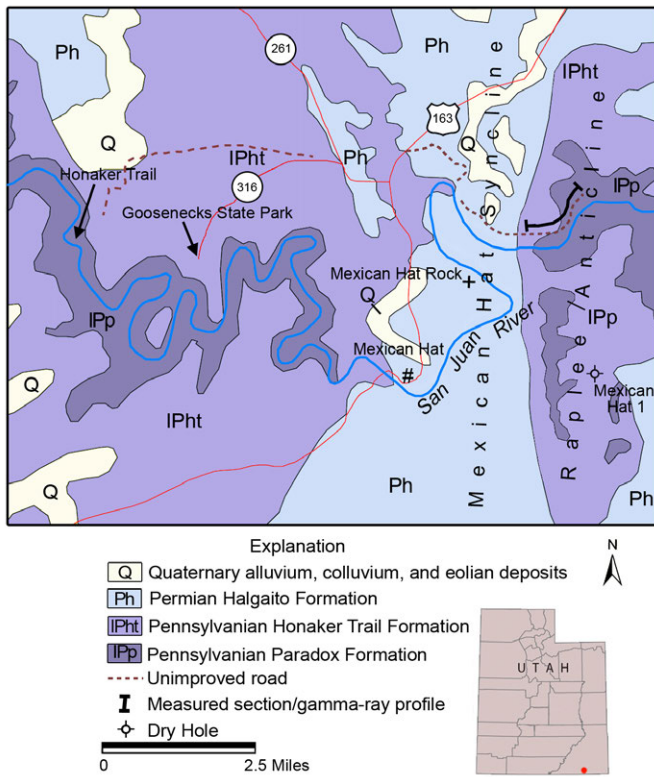


Figure 8.19. Geologic map of the Raplee anticline-Gooseheads area along the San Juan River, southeastern Utah (modified from Hintze, 1980).

Sequence Stratigraphy

Numerous classic sequence stratigraphic studies have been conducted on the Pennsylvanian section in the Gooseheads area: Goldhammer and others (1991, 1994), Weber and others (1995), Gianniny and Simo (1996), Grammer and others (1996, 2000), Sarg and others (1999), and Rasmussen and Rasmussen (2009) to name a few. Goldhammer and others (1991), Sarg and others (1999), Ritter and others (2002), and Ritter and Gianniny (2012) subdivided the Pennsylvanian section in the Gooseheads area into eight depositional sequences based on exposure surfaces and systems tracts. The Chimney Rock shale is included with the lower Desert Creek zone, the Gothic shale with the lower Ismay zone, and the Hovenweep shale with the upper Ismay zone and lower Honaker Trail Formation depositional sequences. Ritter and Gianniny (2012) determined that these represent fourth-order cycles (50,000 to 500,000 years) with an average duration of 93,750 years. They also concluded that the fourth-order cycles contain an average of 5.2 high-frequency fifth-order cycles, each with a duration of around 18,000 years. Finally, Guthrie and Bohacs (2009) identified two or more parasequences in the Chimney Rock and Gothic in the area.

The Paradox and Honaker Trail Formations were deposited during Desmoinesian and Missourian time under icehouse

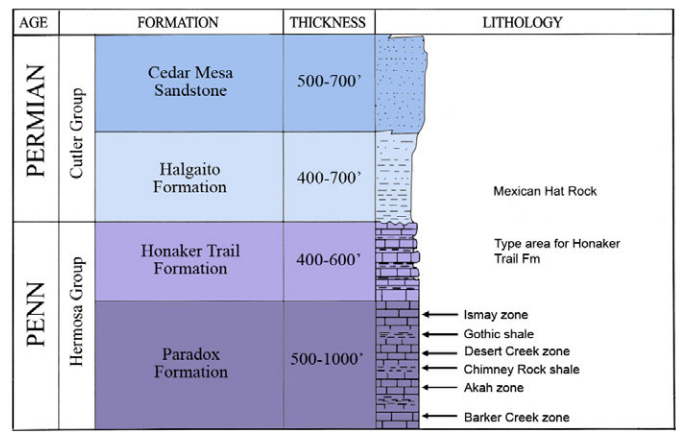


Figure 8.20. Stratigraphic column for the Pennsylvanian and Permian section, Raplee anticline-Gooseheads area along the San Juan River, southeastern Utah. Modified from Hintze and Kowallis (2009).

conditions, during which high-frequency and high-amplitude sea-level oscillations occurred (Ritter and Gianniny, 2012). The Chimney Rock, Gothic, and Hovenweep shales and thick carbonates were deposited during fourth-order high stands on the Aneth platform (including the Gooseheads/Raplee anticline area) near the landward edge of the Paradox Basin. Guthrie and Bohacs (2009) and Ritter and Gianniny (2012) recognized maximum flooding surfaces (MFS) within the Chimney Rock (figure 8.21) and Gothic. The MFS represents the period between the maximum rate of relative sea-level rise and the maximum relative sea level (Coe and Church, 2005). Thus, the presence of the deeper water, black argillaceous, organic-rich dolomitic mudstone (typical of the Chimney Rock and Gothic) on the Aneth platform would be expected during the widest landward extent of marine conditions as indicated by the MFS. Although carbonate deposition dominated the platform area, the distal basin center was sediment starved in terms of carbonate production. However, the thin shale/mudstone of the Chimney Rock, Gothic, and Hovenweep correlate with the basin-center evaporite-black shale cycles (Rasmussen and Rasmussen, 2009; Rasmussen, 2010).

Raplee Anticline Measured Section

The Paradox Formation section at Raplee anticline was selected for measurement, description, and gamma-ray data collection. This section was chosen because of easy access to the west-dipping beds on the north side of the San Juan River along an old "road" (figure 8.22) that once led to an exploratory well drillsite, in contrast to the vertical cliffs at the Honaker Trail. In addition, Weber and others (1995) published an excellent measured section at the road site. Our goals were not to redescribe their section but to modify it based on our own observations and, more importantly, to create a gamma-ray profile that could be used to correlate the Chimney Rock, Gothic, and Hovenweep shales from the outcrop section to well logs in the basin (appendix Q, plates Q-6 and Q-7).

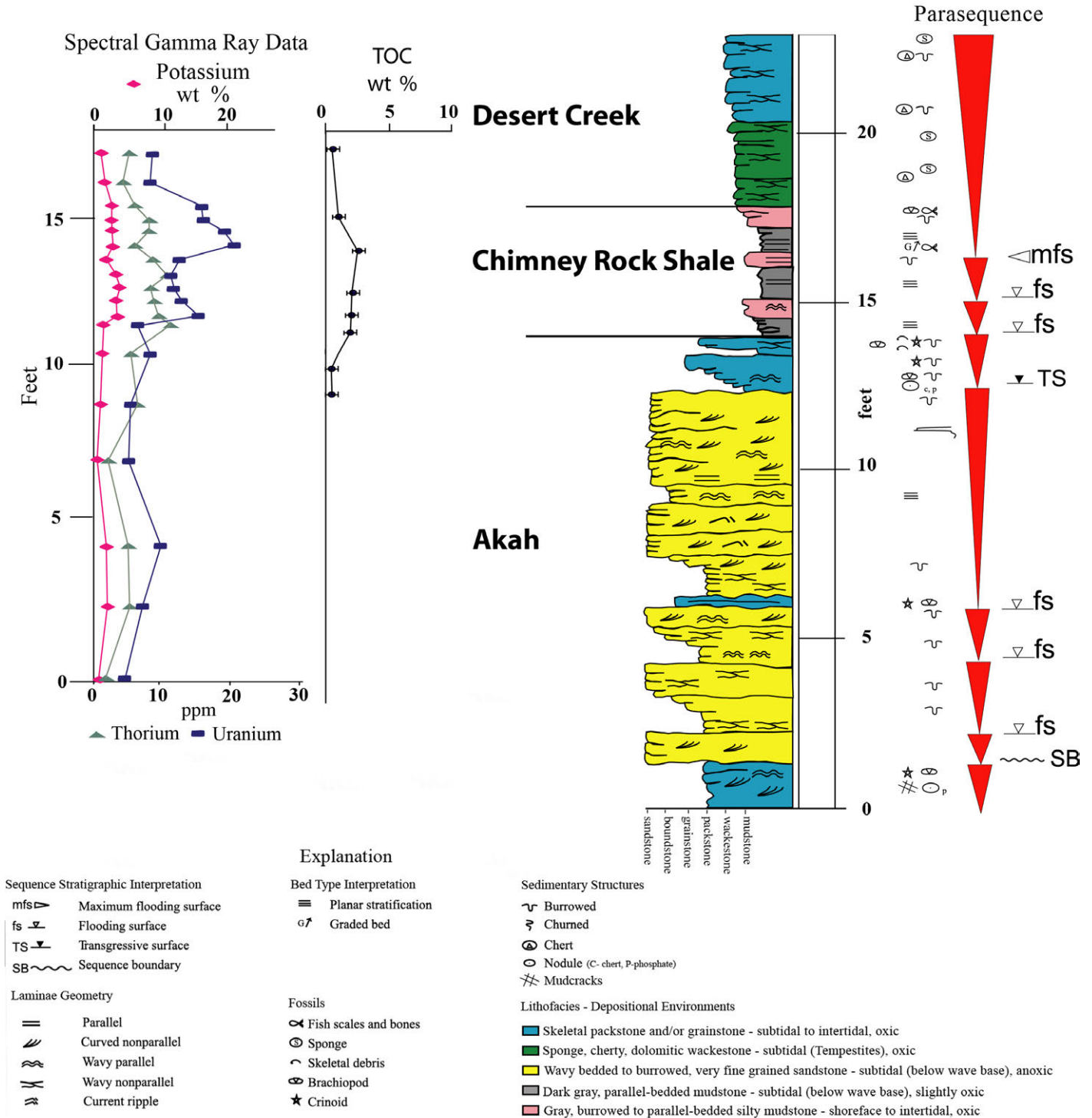


Figure 8.21. Stratigraphic profile of the Chimney Rock shale in the Raplee anticline section showing sequence stratigraphic interpretations, total organic carbon (TOC), and spectral gamma-ray data. Modified from Guthrie and Bohacs (2009).

The Chimney Rock shale consists of a maximum flooding facies, about 25 feet (7.6 m) thick (figure 8.23). Beds consist of (1) dark gray to black argillaceous, organic-rich fissile dolomitic mudstone and shale, (2) gray, burrowed silty mudstone, and (3) gray skeletal wackestone. Bedding is mostly planar with some upward grading in the upper part; laminae are parallel to wavy parallel (Guthrie and Bohacs,

2009). Anoxic conditions existed during Chimney Rock deposition so only pelagic fossils are found, consisting of fish scales and bones and open-marine conodonts (Ritter and Gianniny, 2012). The Chimney Rock is underlain by a cross-bedded sandstone as part of a transgressive systems tract, and overlain by thin-bedded shaley dolomite of a highstand systems tract.

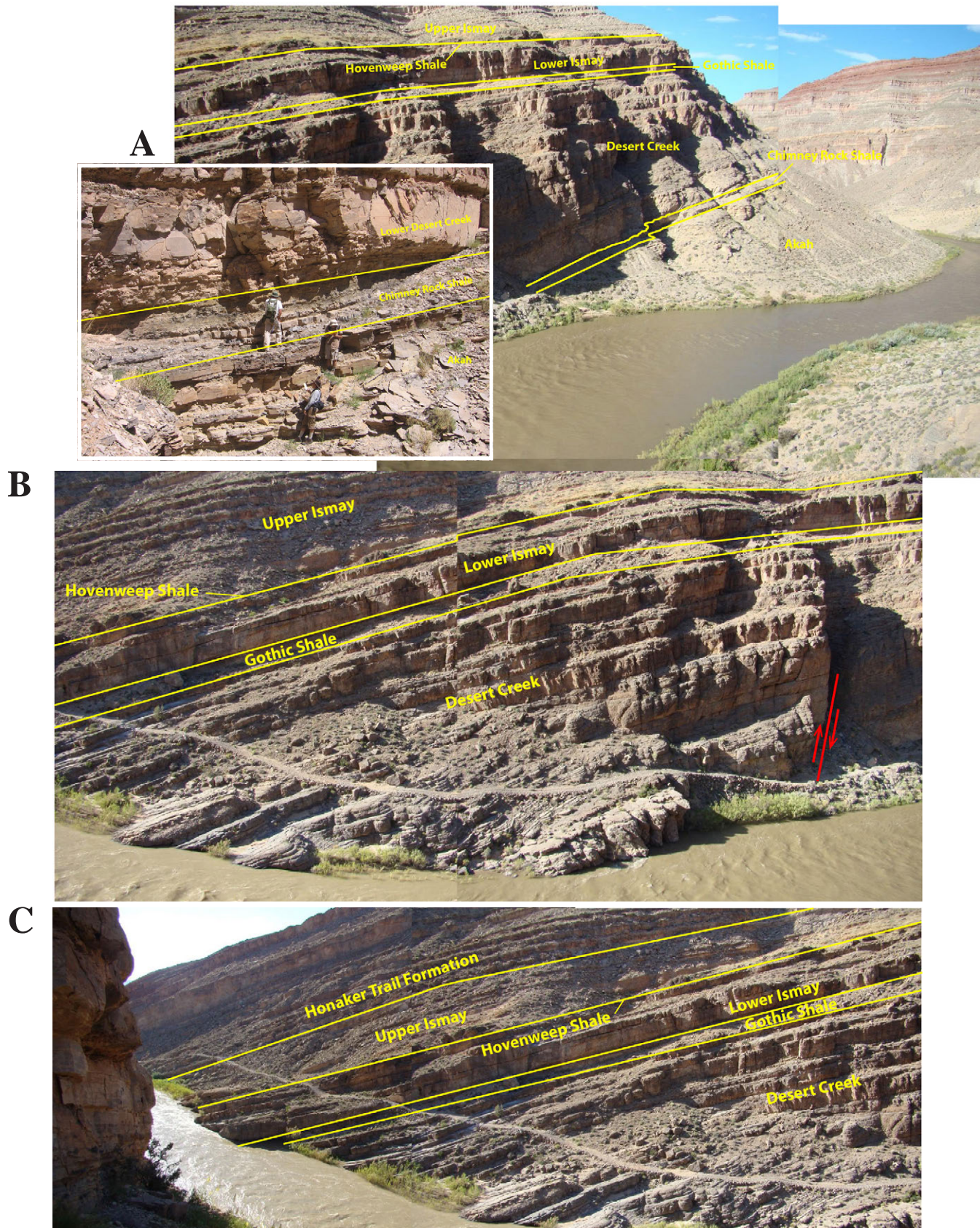


Figure 8.22. The west-dipping flank of Raplee anticline on the north side of the San Juan River showing Paradox Formation and location of the measured section and gamma-ray profile. **A.** View to the northeast up river displaying the Akah through Desert Creek zones including the Chimney Rock shale (inset shows close up of the Chimney Rock section). **B.** View north of the Desert Creek through the lower Ismay zones including the Gothic shale. **C.** View to the west down river of the upper Desert Creek through the Ismay zones, including the Gothic and Hovenweep shales, to the Honaker Trail Formation.

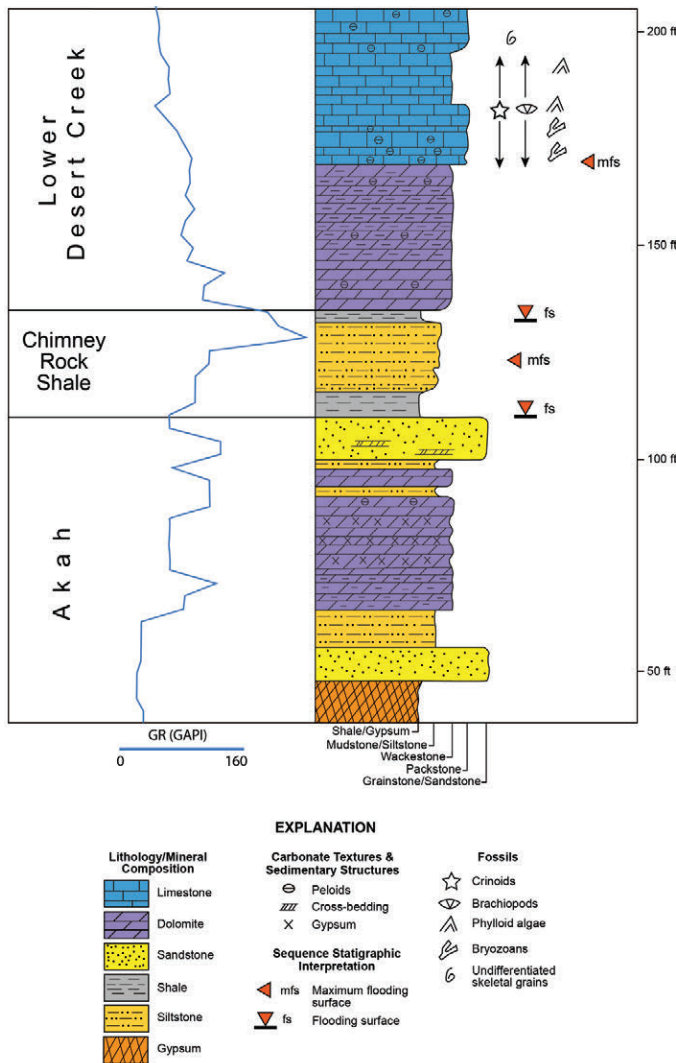


Figure 8.23. Stratigraphic and gamma-ray profile of the upper Akah zone, Chimney Rock shale, and lower Desert Creek zone in the Raplee anticline section; datum is the base of measured section, plate 6, appendix Q. Modified from Weber and others (1995).

The Gothic shale is also a maximum flooding facies. The Gothic is poorly exposed and thin—about 12 feet (3.7 m) thick (figure 8.24). Beds are similar to the Chimney Rock shale, consisting of (1) dark gray to black, argillaceous, organic-rich, fissile dolomitic shale, mudstone, and wackestone, and (2) gray, burrowed silty mudstone. Ritter and Gianniny (2012) reported a concentration of quartz silt and phosphatic and skeletal grains at the base of the Gothic in the Honaker Trail section. Bedding is planar with upward grading; laminae are parallel (Guthrie and Bohacs, 2009). Fossils consist of brachiopods, crinoids, and foraminifera (Weber and other, 1995). The Gothic also contains an *Idiognathodus* conodont fauna that correlates to the Lower Fort Scott cycle in the Midcontinent (Ritter and others, 2002). The Gothic is underlain by a transgressive systems tract consisting of thin-bedded skeletal packstone, and overlain by a thin- to medium-bedded, skeletal to algal grainstone/bafflestone of a highstand systems tract.

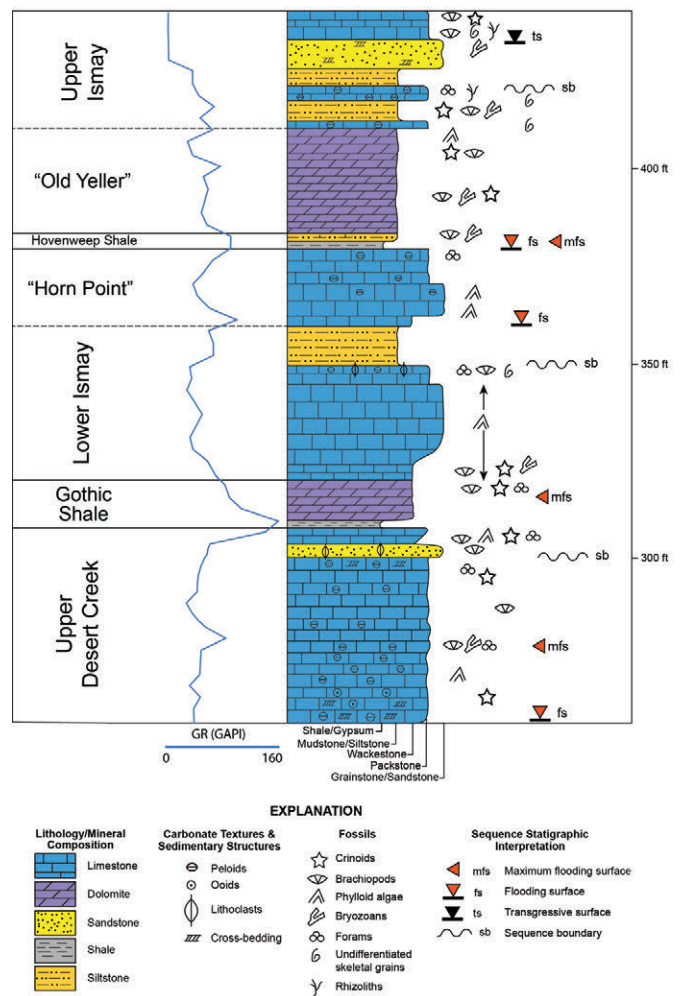


Figure 8.24. Stratigraphic and gamma-ray profile of the Gothic shale, lower Ismay zone, and Hovenweep shale in the Raplee anticline section; datum is the base of measured section, plate 6, appendix Q. Modified from Weber and others (1995).

The Hovenweep shale is a maximum flooding facies that is very thin—only 5 feet (1.5 m) thick (figure 8.24). In outcrop, both at the Raplee anticline and Honaker Trail sections, the Hovenweep is a relatively poor outcrop analog to the potential shale-gas targets seen in cores and well logs in the deeper Paradox Basin. The character of the rocks in cores and outcrops differs as well, suggesting to us that a good Hovenweep outcrop analog simply does not exist. A thin bed of dark gray to black dolomitic shale and mudstone is found at the base, overlain by a tan- to yellowish-weathering limey siltstone. The Hovenweep is underlain by a transgressive systems tract of medium-bedded skeletal/peloidal packstone, and overlain by a highstand systems tract of thin- to medium-bedded, dolomitic, skeletal to algal mudstone/wackestone; these units are locally referred to as the “Horn Point” and “Old Yeller,” respectively.

Gamma-ray measurements followed the same 3-foot (1 m) sampling procedure as used for the Soldier Canyon section of the Manning Canyon Shale. Pits were dug in the Gothic

shale in an attempt to reach unweathered bedrock as well as to better describe the various units. The gamma-ray profile shows distinct increases in API units in the Chimney Rock, Gothic, and Hovenweep shales, confirming its use as a correlation tool to the subsurface (figure 8.25 and appendix Q, plate Q-7). Guthrie and Bohacs (2009) determined that the uranium measurement (in parts per million) can also be an indicator of the MFS. They demonstrated the MFS is characterized by relatively higher uranium content (20 to 40 ppm) in the Gothic section measured at Eight Foot Rapids, farther east on Raplee anticline, and the Chimney Rock section at the Honaker Trail. The increase in uranium content was observed by our measurements in the Chimney Rock, Gothic, and even the Hovenweep at Raplee anticline (figure 8.21). The high uranium content in the Hovenweep was unexpected because there are only a few thin shale and mudstone beds exposed. Finally, Guthrie and Bohacs (2009) showed the TOC was highest in the upper parasequence.

North

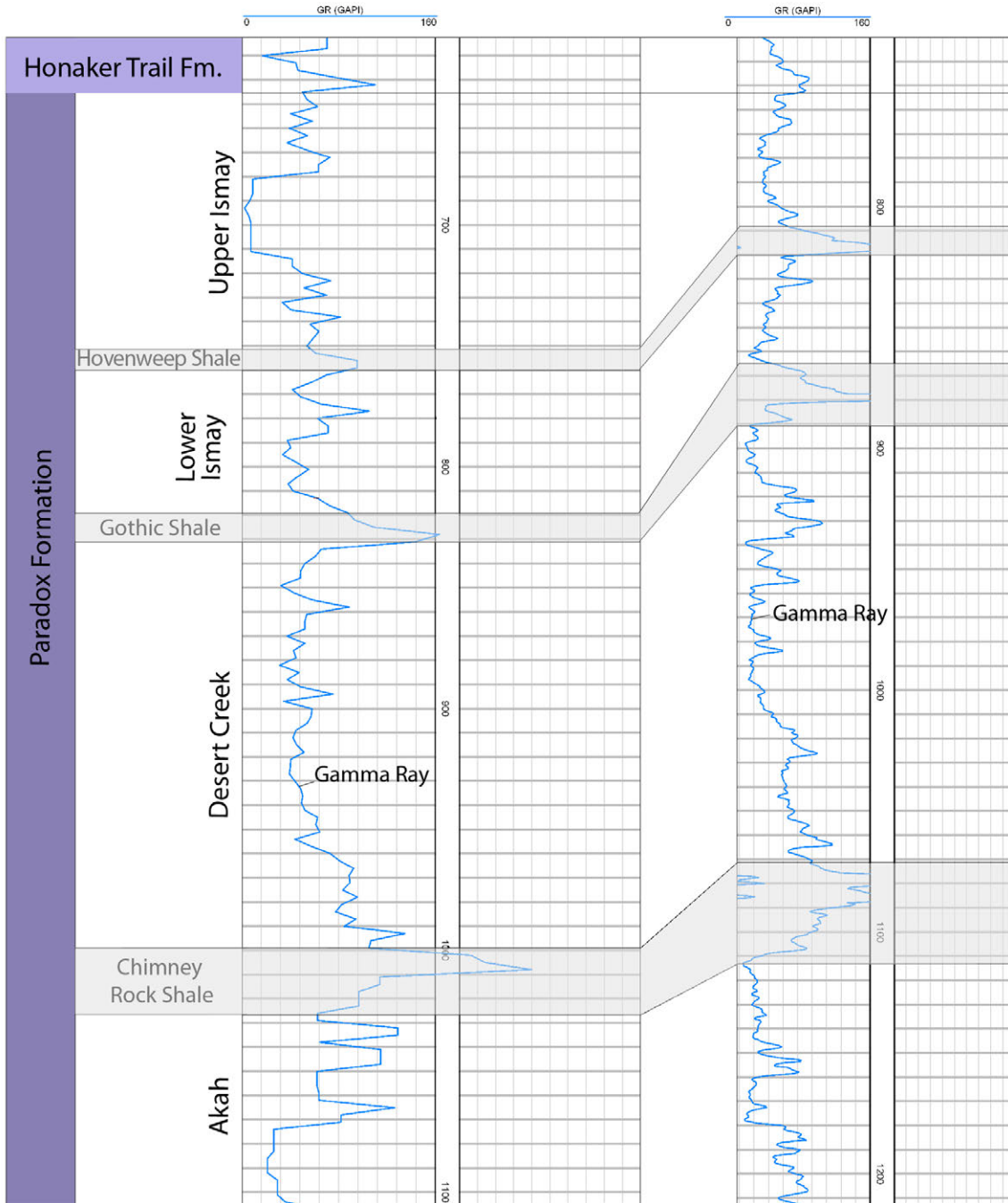
2.5 miles

South

Utah Geological Survey
 Raplee Anticline Measured Section
 Gamma-Ray Profile
 Sec. 33 & 34, T. 41 S., R. 19 E.,
 San Juan County, Utah

Skelly Oil Company
 Mexican Hat 1
 SWSE Sec. 10, T. 42 S., R. 19 E.,
 San Juan County, Utah

 G.L.: 5254 ft



Thickness (ft)
 from top of section

T.D.: 3228 ft
 Completed: June 4, 1964

*No horizontal scale

Figure 8.25. Correlation of the Chimney Rock, Gothic, and Hovenweep gamma-ray profile from the Raplee anticline measured section to the Mexican Hat 1 well (about 2 miles [3 km] south). See figure 8.19 for well and measured section locations.

CHAPTER 9: REGIONAL MAPPING AND BURIAL HISTORIES

BY

Robert Ressetar, *Utah Geological Survey*
Sonja Heuscher, *formerly with Utah Geological Survey*

CONTENTS

INTRODUCTION	175
REGIONAL MAPPING METHODS	175
Data Used to Create Maps	175
Creating Maps	175
MAPPING RESULTS	175
Thickness Maps	175
Doughnut Formation	175
Paradox Formation Shale Units	175
Structure Maps	180
Doughnut Formation	180
Paradox Formation Shale Units	180
BURIAL AND ORGANIC MATURATION MODELS OF POTENTIAL SOURCE AND MISSISSIPPIAN SHALE-GAS RESERVOIR ROCKS	180
Burial History Methods	180
Results of Burial and Maturation Models	188
Oquirrh Basin Sites	188
Sevier Thrust Belt Sites	188
Uinta Basin Sites	191
San Rafael Swell Sites	192
Wasatch Plateau Sites	192
Burial History Conclusions	194

FIGURES

Figure 9.1. Thickness map of the Doughnut Formation, San Rafael Swell	176
Figure 9.2. Thickness map of the Chimney Rock shale, Paradox Formation, Paradox Basin, Utah	177
Figure 9.3. Thickness map of the Gothic shale, Paradox Formation, Paradox Basin, Utah	178
Figure 9.4. Thickness map of the Hovenweep shale, Paradox Formation, Paradox Basin, Utah	179
Figure 9.5. Structure contour map of the top of the Doughnut Formation, San Rafael Swell	181
Figure 9.6. Structure contour map of the top of the Mississippian Redwall Limestone, San Rafael Swell	182
Figure 9.7. Structure contour map of the top of the Permian Kaibab Limestone, San Rafael Swell	183
Figure 9.8. Structure contour map of the top of the Chimney Rock shale, Paradox Formation, Paradox Basin, Utah	184
Figure 9.9. Structure contour map of the top of the Gothic shale, Paradox Formation, Paradox Basin, Utah	185
Figure 9.10. Structure contour map of the top of the Hovenweep shale, Paradox Formation, Paradox Basin, Utah	186
Figure 9.11. Site locations for burial and maturation models	187
Figure 9.12. Sample calculation of age and thickness of missing section	187
Figure 9.13. Oquirrh basin type maturation model, site 13, Hogup Mountains	190
Figure 9.14. Sevier thrust belt type maturation model, site 29, Weber Canyon	190
Figure 9.15. Uinta Basin type maturation model, site 48, Federal 22-1 well	191
Figure 9.16. San Rafael Swell type maturation model, site 52, Carbon Canal 5-12 well	193
Figure 9.17. Wasatch Plateau type maturation model, site 64, USA E-1 well	193
Figure 9.18. Time the Manning Canyon/Doughnut entered the oil window	194
Figure 9.19. Time the Manning Canyon/Doughnut entered the wet gas window	195
Figure 9.20. Modeled versus measured vitrinite reflectance with depth, site 51, State 1-16 well	196
Figure 9.21. Modeled versus measured vitrinite reflectance with depth, site 52, Carbon Canal 5-12 well	196
Figure 9.22. Modeled versus measured vitrinite reflectance with depth, site 54, North Springs 1 well	196

TABLE

Table 9.1. Locations and summary results of burial and maturation models	189
--------------------------------------------------------------------------------	-----

CHAPTER 9:

REGIONAL MAPPING AND BURIAL HISTORIES

INTRODUCTION

The distribution, thickness, and structural configuration of the Mississippian/Pennsylvanian Doughnut Formation (Manning Canyon Shale) and Pennsylvanian Paradox Formation are critical to determining areas to explore and locating “sweet spots” for shale-gas potential. We provide new, updated thickness and structure maps for the Doughnut and the Chimney Rock, Gothic, and Hovenweep shales of the Paradox Formation. These maps indicate that the organic-rich Paleozoic shale beds described in previous chapters are widely distributed and thick enough to have shale-gas potential.

Burial and thermal histories are complex and vary regionally for these formations, especially the Doughnut Formation (Manning Canyon Shale). Burial histories of the Doughnut and its equivalents in central and western Utah were constructed as an aid to both modeling their thermal maturation histories and understanding their reservoir properties. This study indicates the organic-rich shale beds of the Doughnut/Manning Canyon were buried deep enough to enter the dry gas window. The burial and thermal history of the Paradox Basin has been described in detail by Nuccio and Condon (1996a, 1996b). Their work, along with similar conclusions from our study (see chapter 6), suggests that the Paradox shale units have both gas and oil potential.

REGIONAL MAPPING METHODS

Data Used to Create Maps

Geographic and stratigraphic spatial data were used to create shale thickness and structure maps. Shale units include the Gothic, Chimney Rock, and Hovenweep shales of the Paradox Formation, and the Doughnut Formation (Manning Canyon Shale). We used data from UGS files, the Utah Division of Oil, Gas, and Mining (2010), Environmental Systems Research Institute (2009), and the Utah Automated Geographic Reference Center (2010). Our database includes the American Petroleum Institute (API) drill-hole number, surface elevations, and Universal Transverse Mercator (UTM) coordinates as well as the depth of geologic units. We assigned zero or blank thickness values for drill-hole locations where shale units are known to be absent or faulted, respectively. Additional drilling is needed to determine shale thickness and structure in several areas where drill-hole data are sparse.

Creating Maps

The shale thickness and structure maps were created from drill-hole data using the Spatial Analyst extension for ArcGIS 10 software. The calculations are based on identically registered, 10 x 10-meter grid cells (0.0247 acre [0.01 ha]) using zone 12, NAD83, UTM coordinates. The thickness maps were made using a second-order, six nearest neighbor, inverse-distance mapping function. The structure maps were made using a tension, six nearest neighbor, spline mapping function. For data sets that were sparse, interpolation results were confined to a circular buffer surrounding the data points. Some inaccuracies may exist in the Doughnut Formation maps due to the Doughnut top being difficult to pick in well logs and the presence of faults in the study area.

MAPPING RESULTS

Thickness Maps

Doughnut Formation

Figure 9.1 shows the thickness of the Doughnut Formation in the northern San Rafael Swell. A very thick area of shale (918 feet [280 m]) exists northeast of Huntington; from here, the Doughnut rapidly thins (down to zero feet) in a southeast direction, and more gradually (down to 250 feet [76 m]) thins in a northwest direction.

Paradox Formation Shale Units

Figures 9.2, 9.3, and 9.4 show the thickness of the Chimney Rock, Gothic, and Hovenweep shale units of the Paradox Formation by 5- or 10-foot (1.5 or 3 m) thickness intervals. The Chimney Rock thickness map (figure 9.2) shows a thick area of shale (30 to 35 feet [9–11 m]) extending northwest of the town of Bluff, Utah, thinning to the east, northeast, and southwest to 0 to 10 feet (0–3 m) thick. The Gothic thickness map (figure 9.3) shows thick (50 to 70 feet [15–21 m]) areas of shale near the Four Corners area and north of the town of Monticello, Utah, in what was the deepest part of the Paradox Basin. In other areas of the basin the Gothic is less than 40 feet (12 m) thick. The Gothic thickness map covers a much greater area than the Chimney Rock or Hovenweep maps because of greater availability of well penetration data. The Hovenweep shale thickness map (figure 9.4) shows a northwestward thickening from 0 to 10 feet (0–3 m) near Bluff to 100 feet (30 m) near the Utah-Colorado border. Thickening in this direction

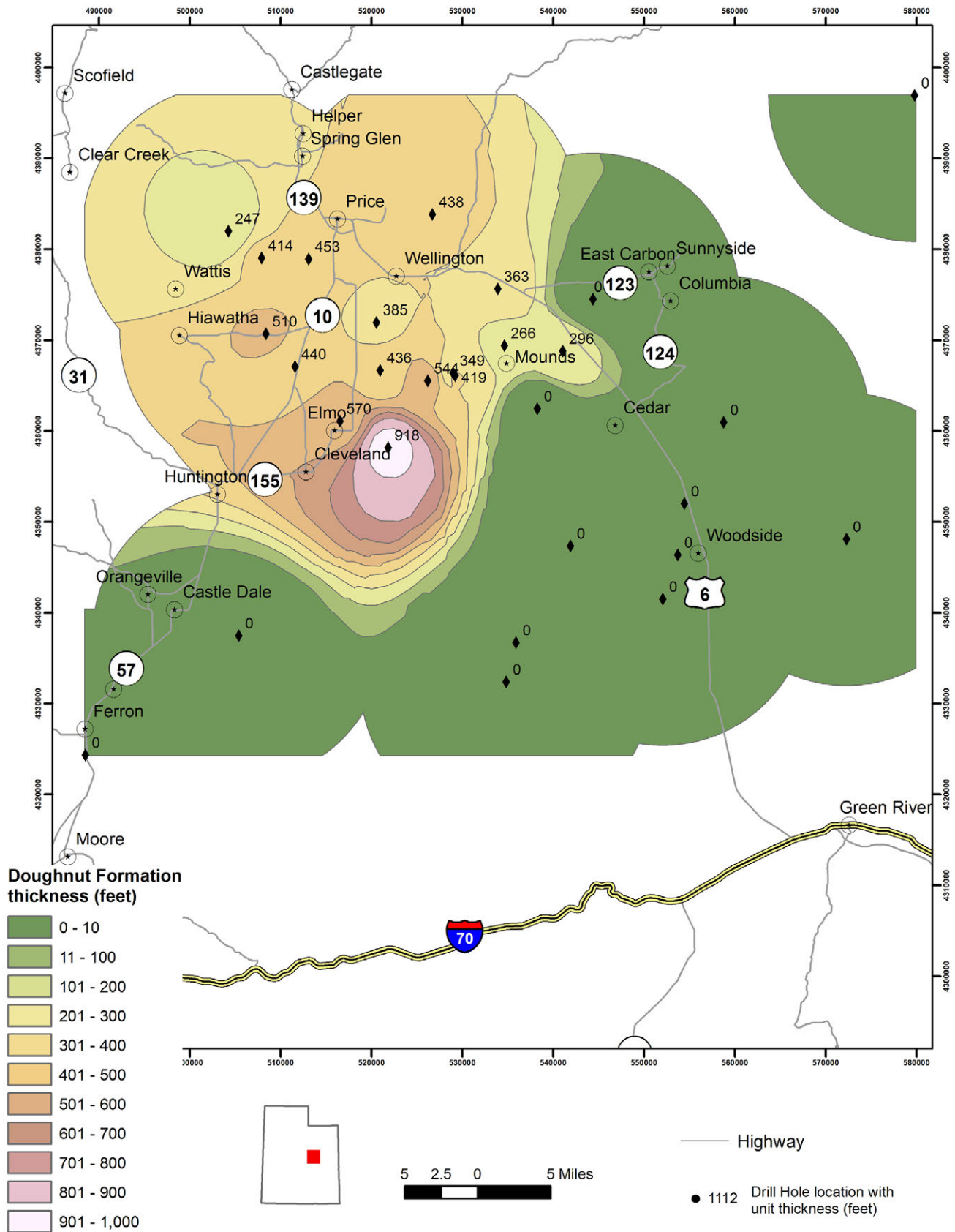


Figure 9.1. Thickness map of the Doughnut Formation in the northern San Rafael Swell.

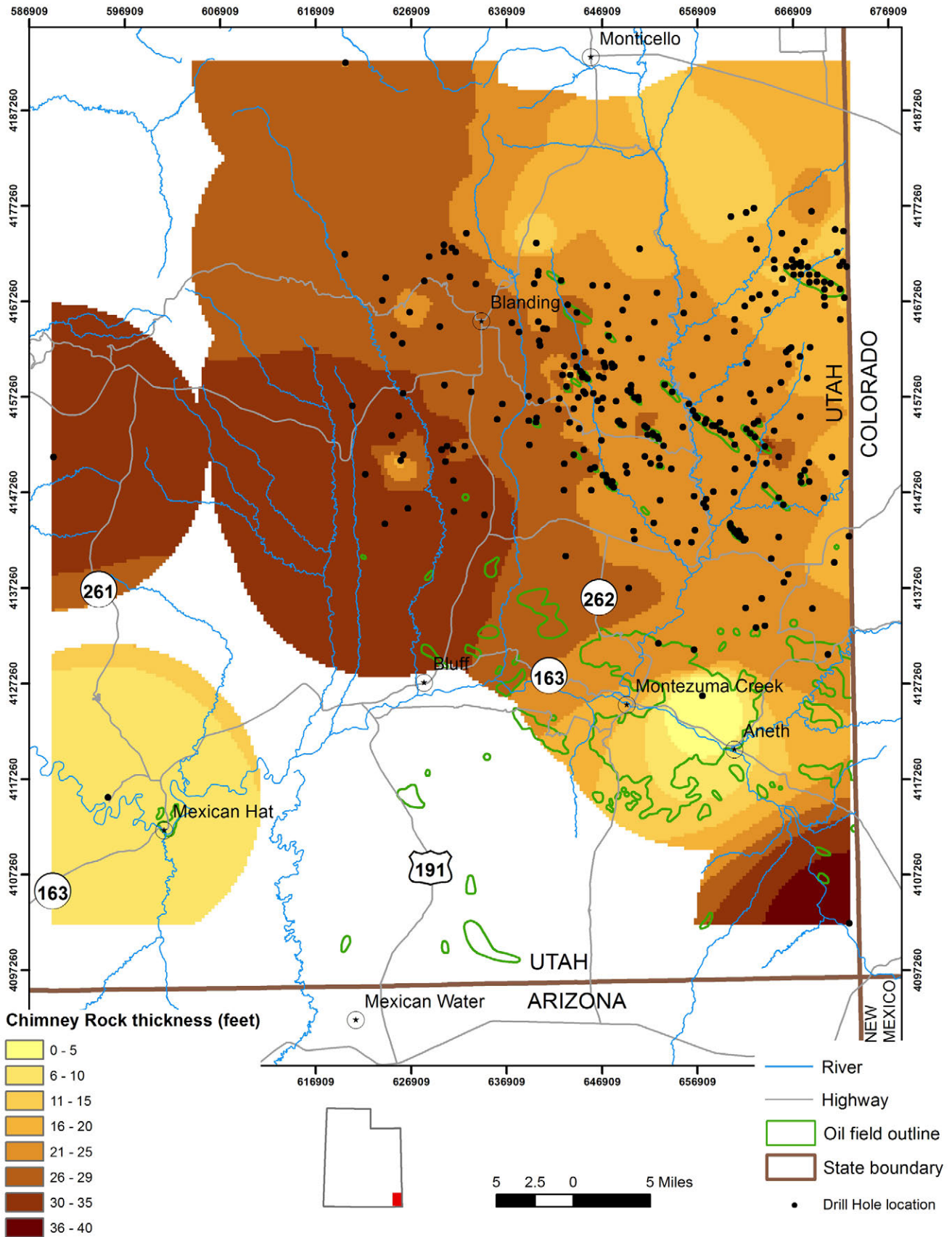


Figure 9.2. Thickness map of the Chimney Rock shale of the Paradox Formation, southwestern Paradox Basin, Utah.

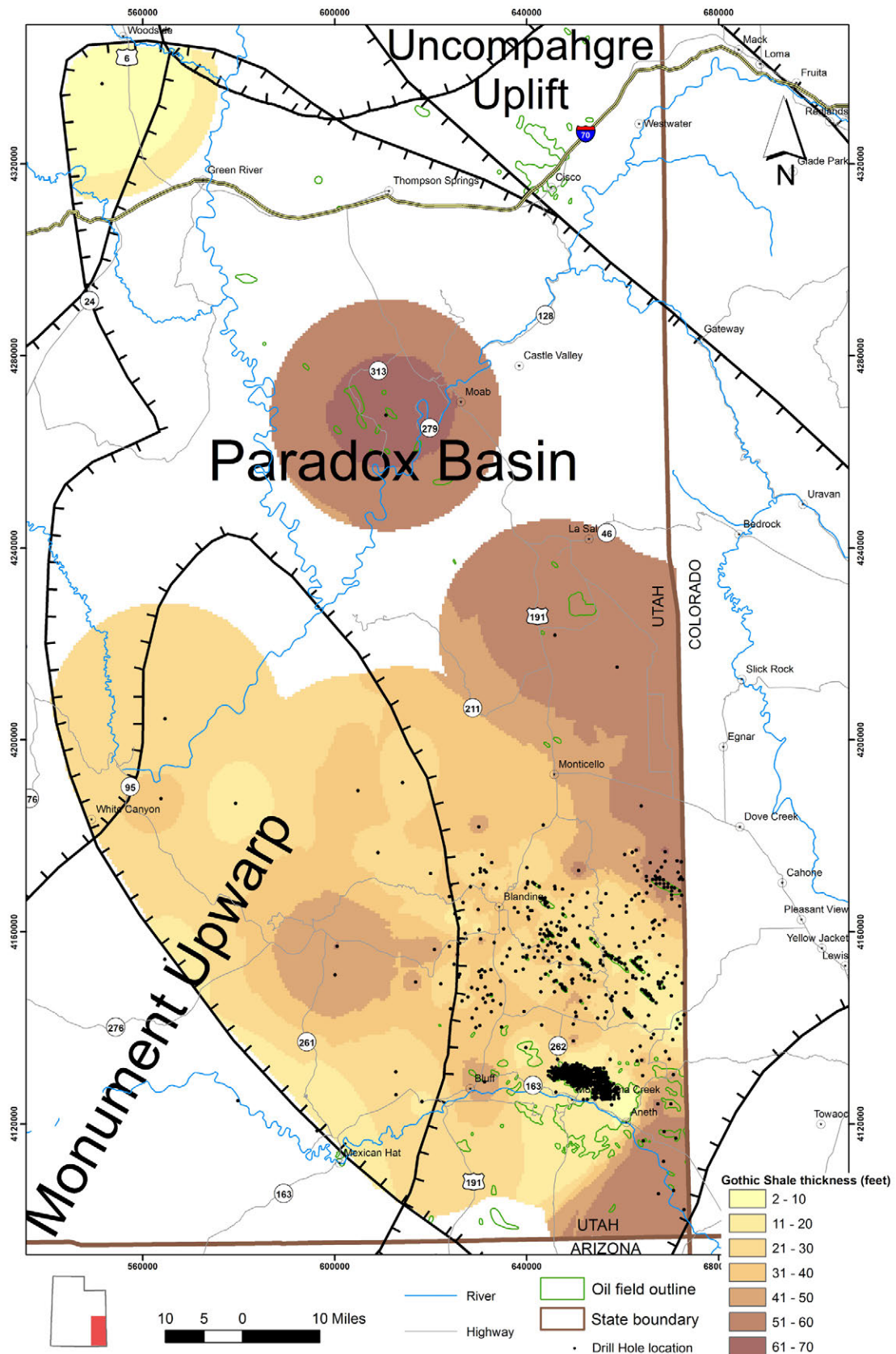


Figure 9.3. Thickness map of the Gothic shale of the Paradox Formation, southwestern Paradox Basin, Utah.

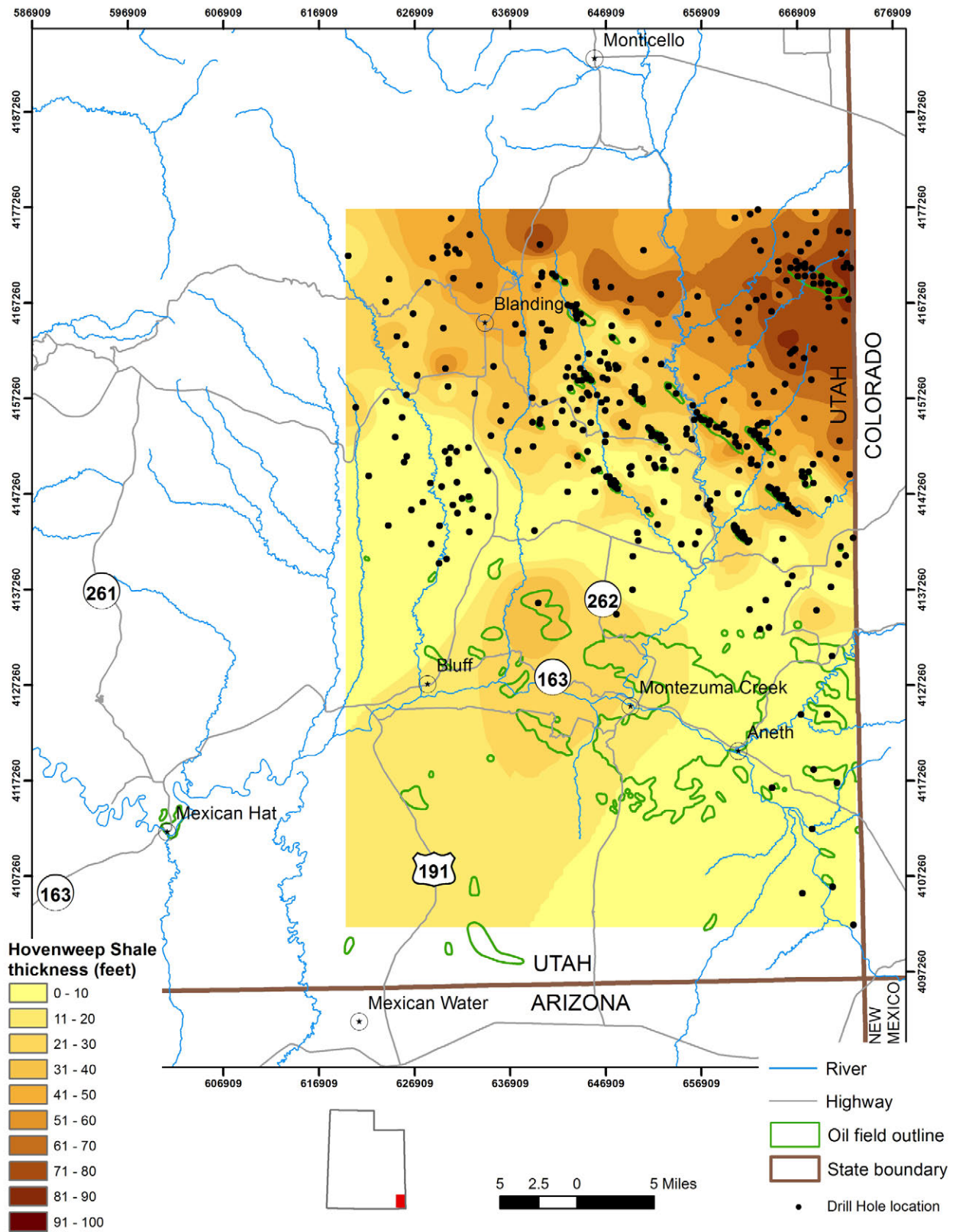


Figure 9.4. Thickness map of the Hovenweep shale of the Paradox Formation, southwestern Paradox Basin, Utah.

is consistent with thickening toward the deepest part of the Paradox Basin.

Of the three Paradox Formation shale units in Utah, the Hovenweep is the thickest, approaching 100 feet (30 m) thick. The Gothic is the second thickest shale unit, approaching 70 feet (21 m) thick. The maximum thickness of the Chimney Rock shale is 40 feet (12 m). The Gothic and Hovenweep show similar locations of thicker shale with the exception of the southernmost part of the basin, where the Gothic thickens but the Hovenweep does not. Unlike the Gothic and Hovenweep, the Chimney Rock thins toward the deepest part of the Paradox Basin.

Structure Maps

Doughnut Formation

The structure map of the top of the Doughnut Formation (figure 9.5) shows a north plunging syncline in the northwest corner of the map area, and a north plunging anticline in the southwest corner of the map area. The north-plunging anticline is the northernmost part of the San Rafael Swell (see chapter 2 for general description). Figures 9.6 and 9.7 show structure maps of the Mississippian Redwall and Permian Kaibab Limestones. Both maps cover a larger area and thus show a greater extent of the San Rafael Swell.

Paradox Formation Shale Units

Figures 9.8 through 9.10 show structure contour maps of the Paradox Formation shale units. The Chimney Rock shale structure map (figure 9.8) shows an uplifted area west of Bluff and Blanding. This area is called the Monument upwarp (Stokes, 1986). The Gothic shale structure contour map also shows the Monument upwarp (figure 9.9), and an uplifted area near the junction of La Sal shows the influence of the Uncompahgre uplift. The Chimney Rock shale structure map does not show the Uncompahgre uplift due to a lack of data points. The Hovenweep shale structure contour map (figure 9.10) does not show either the Monument upwarp or the Uncompahgre uplift due to a lack of data points. Where there is a high concentration of data, in the vicinity of Blanding and Greater Aneth oil field (figures 2.7 and 9.10), the maps show a slight dip to the south.

BURIAL AND ORGANIC MATURATION MODELS OF POTENTIAL SOURCE AND MISSISSIPPIAN SHALE-GAS RESERVOIR ROCKS

The burial and maturation histories in this section focus on the Late Mississippian (late Chesterian) to earliest Pennsylvanian Manning Canyon Shale and correlative rocks (collectively, the MCS) in northern Utah. Deposition of the Upper

Mississippian and Lower Pennsylvanian rocks of northern Utah occurred on a low-relief marine shelf that graded westward into the successor foreland basin of the Antler Orogeny (Blakey, 1997; Trexler and others, 2004). The thickness of the MCS ranges between 500 and 1500 feet (150–460 m) in much of northern Utah, and exceeds 3000 feet (900 m) in the Blue Spring Hills (appendix R, site 6). Accurate thicknesses are scarce, however, owing to the unit acting as a detachment surface for Mesozoic thrust sheets and to its susceptibility to weathering and slumping in modern outcrops (Hintze and Kowallis, 2009). In north-central Utah the Manning Canyon grades into the Doughnut Formation, which represents a greater time range (late Meramecian to end Mississippian), but is generally thinner than 500 feet (150 m). Total organic content of the MCS ranges from 1% to greater than 8%, and is probably mostly type III kerogen (Laine and others, 2008; see chapter 6 of this report).

The sites for the burial histories stretch across northern and central Utah, and include locations in the Basin and Range Province, Sevier thrust belt, Uinta Basin, northern San Rafael Swell, and Wasatch Plateau (figure 9.11). Depending on location, the MCS has been affected to various degrees by late Paleozoic subsidence of the Oquirrh basin, the Jurassic Nevadan Orogeny, the Cretaceous to Paleogene Sevier and Laramide Orogenies, and late Cenozoic Basin and Range extension.

Burial History Methods

The stratigraphic and lithologic data for the burial and maturation models are from published descriptions of petroleum exploration wells, well logs from the Utah Division of Oil, Gas, and Mining website, and measured stratigraphic sections (modeled as pseudo wells). The burial and maturation histories were calculated using ZetaWare Inc.'s Genesis 5.1™ software. To calculate the burial histories, we usually entered the stratigraphic thicknesses of the MCS and overlying units as presented in the source of the data, but in a few cases we adjusted the thickness of the Phosphoria Formation and Arapien Shale to reflect post-depositional structural thickening (see Sprinkel, 1994).

The amounts of section missing across unconformities were estimated by classifying two types of intervals of missing strata:

1. Depositional unconformities (type-1) that occurred when relative base-level fall led to relatively brief (~5 to 25 million year) intervals of non-deposition and erosion.
2. Tectonic unroofing (type-2) that occurred when structural uplift of the sedimentary section resulted in erosion of the upper plates of thrust sheets. Erosion may have removed anywhere from insignificant amounts to the greater part of the sedimentary section.

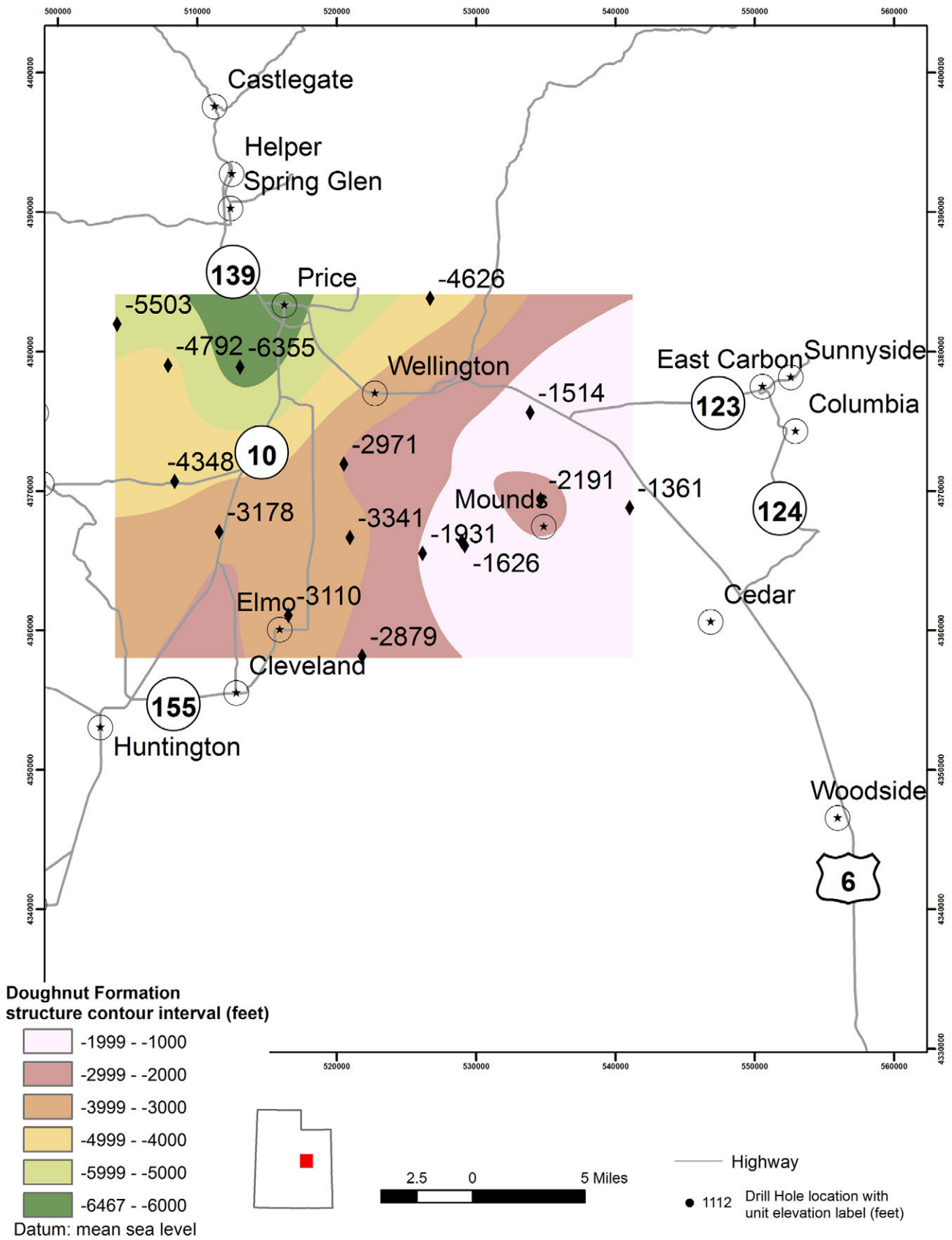


Figure 9.5. Structure contour map of the top of the Doughnut Formation in the northern San Rafael Swell.

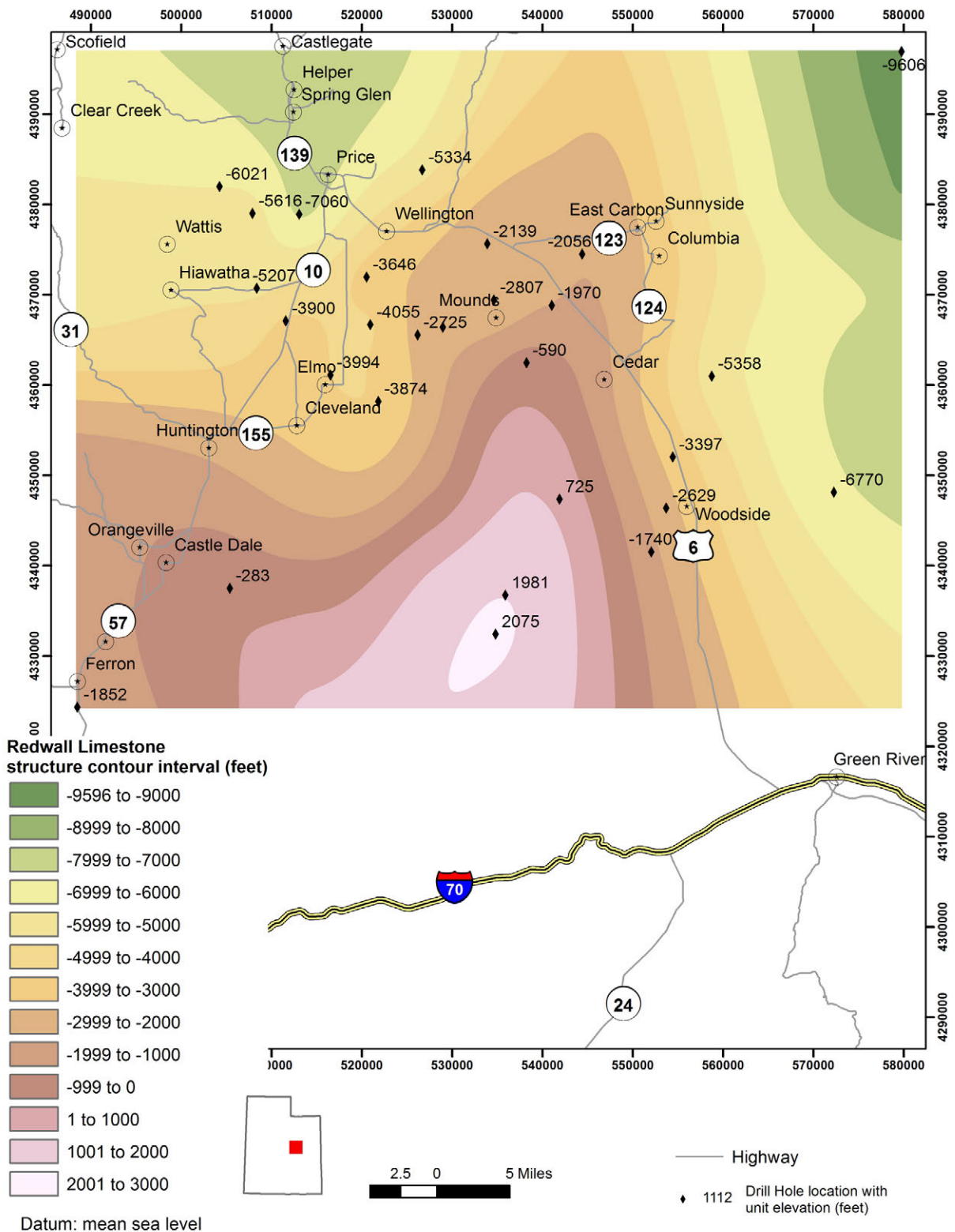


Figure 9.6. Structure contour map of the top of the Mississippian Redwall Limestone in the northern San Rafael Swell.

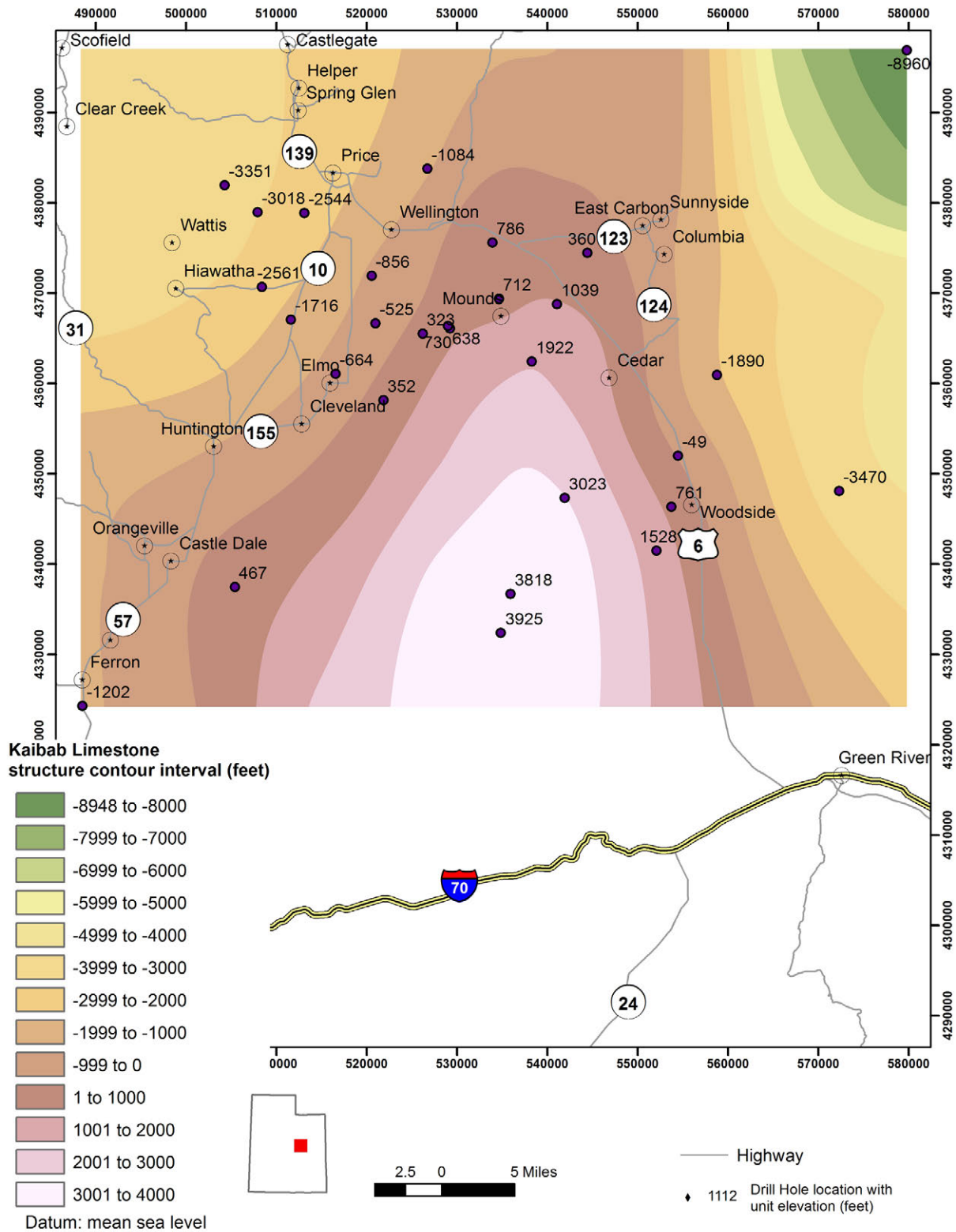


Figure 9.7. Structure contour map of the top of the Permian Kaibab Limestone in the northern San Rafael Swell.

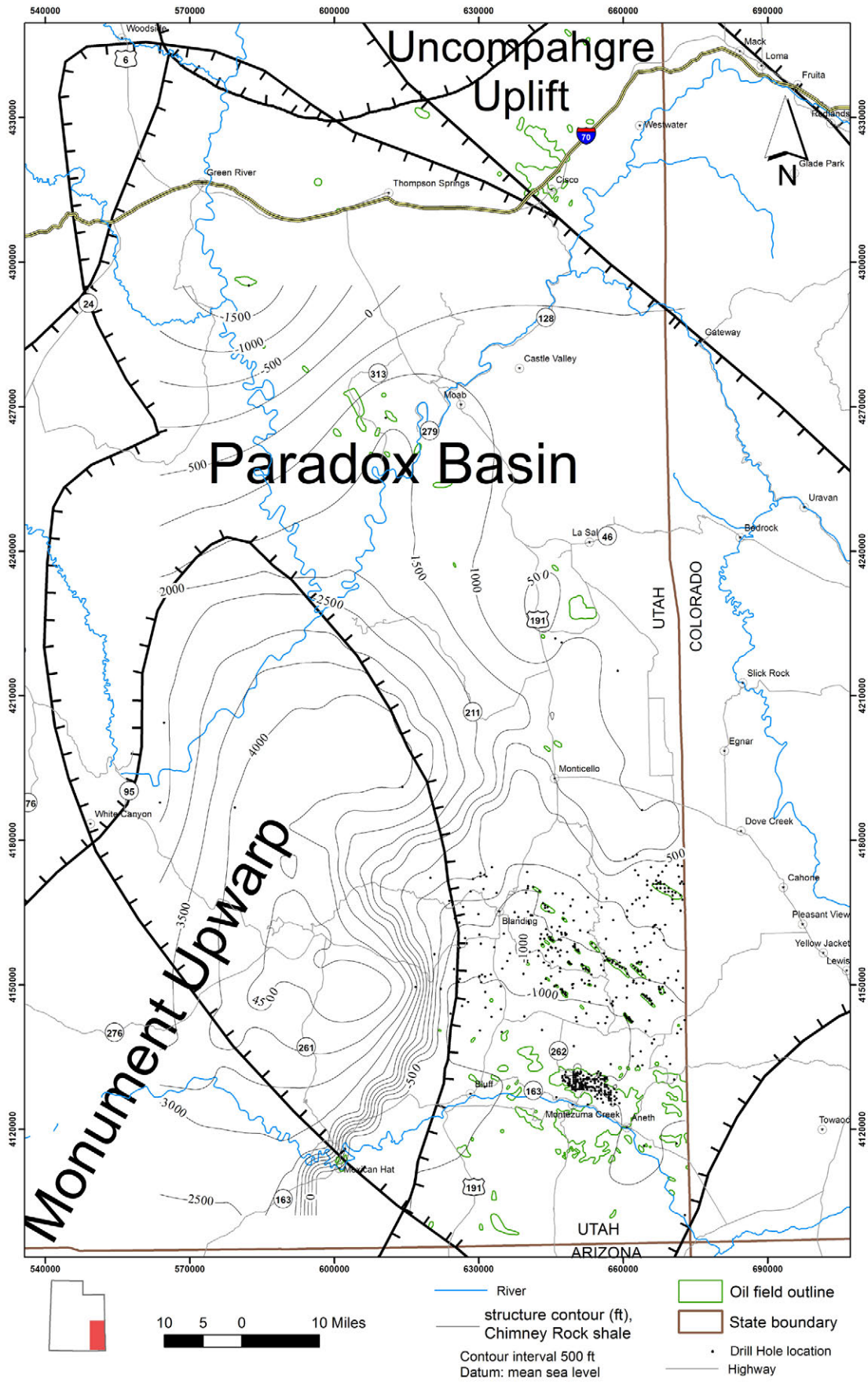


Figure 9.8. Structure contour map of the top of the Chimney Rock shale, Paradox Formation, southwestern Paradox Basin, Utah.

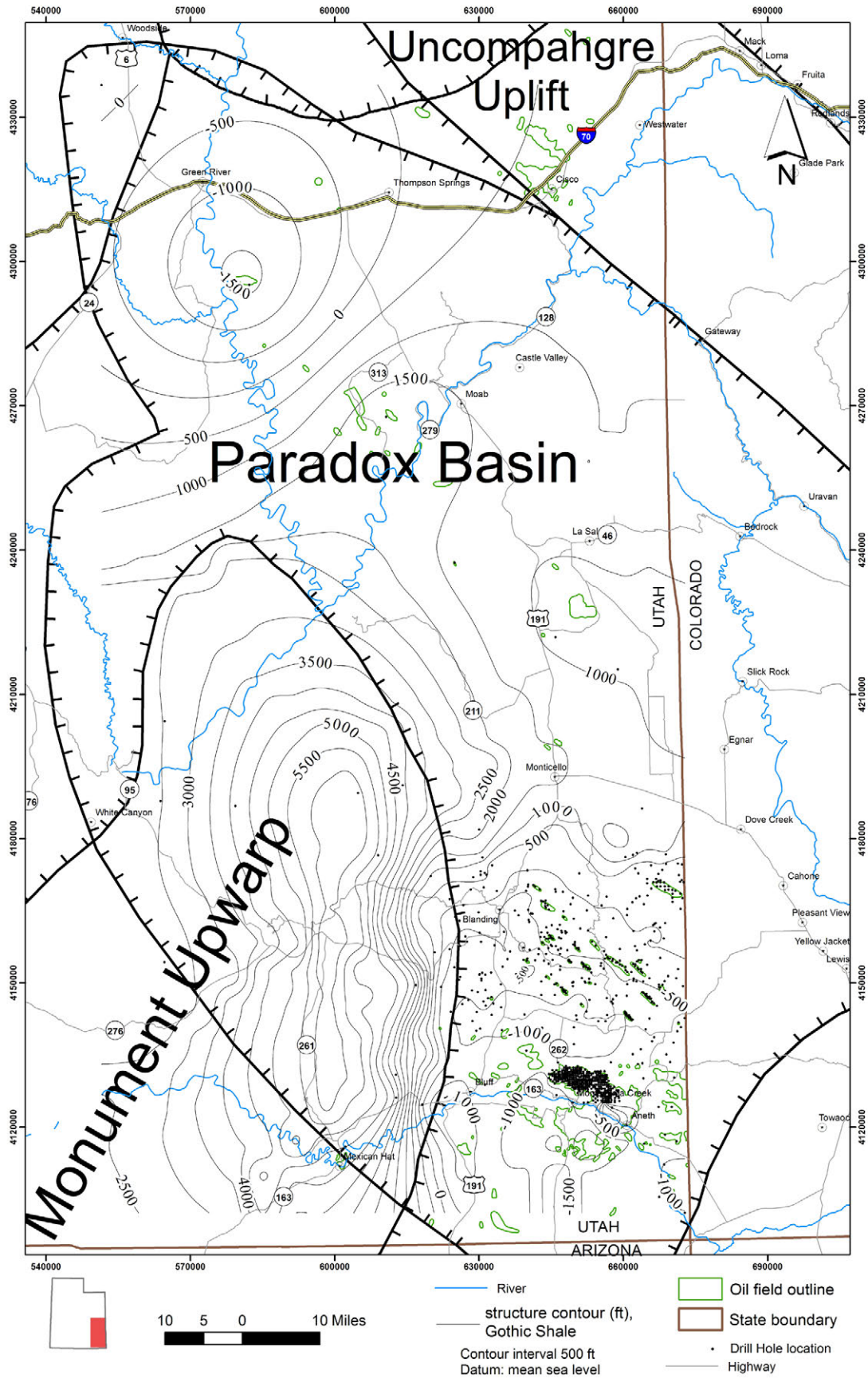


Figure 9.9. Structure contour map of the top of the Gothic shale, Paradox Formation, southwestern Paradox Basin, Utah.

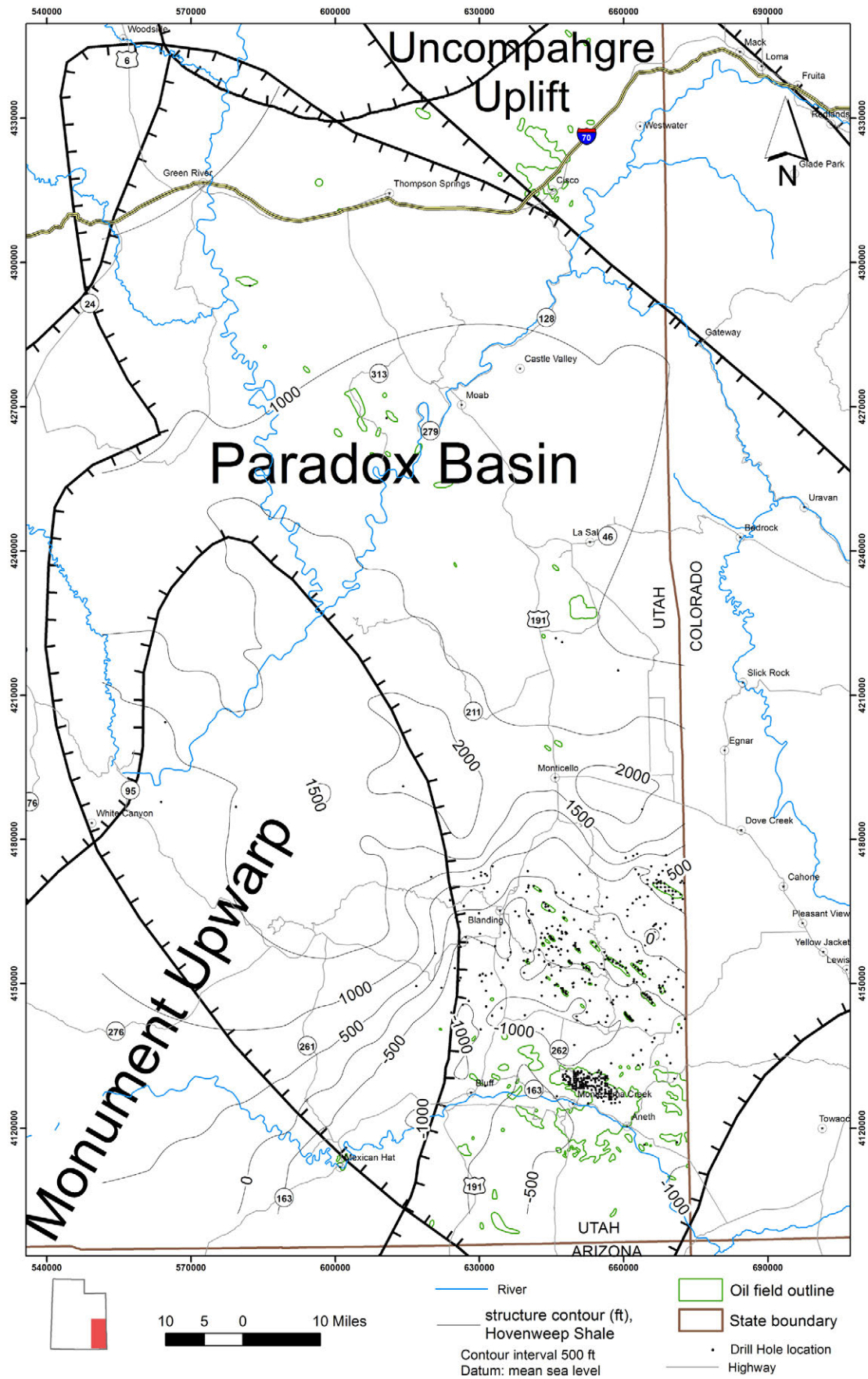


Figure 9.10. Structure contour map of the top of the Hovenweep shale, Paradox Formation, southwestern Paradox Basin, Utah.

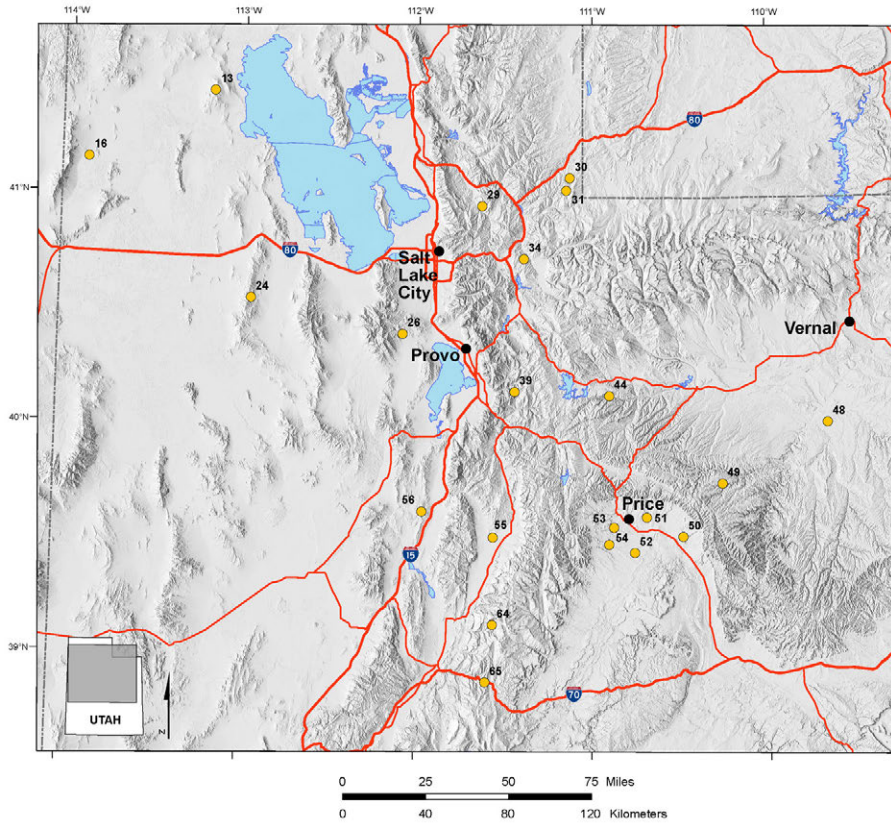


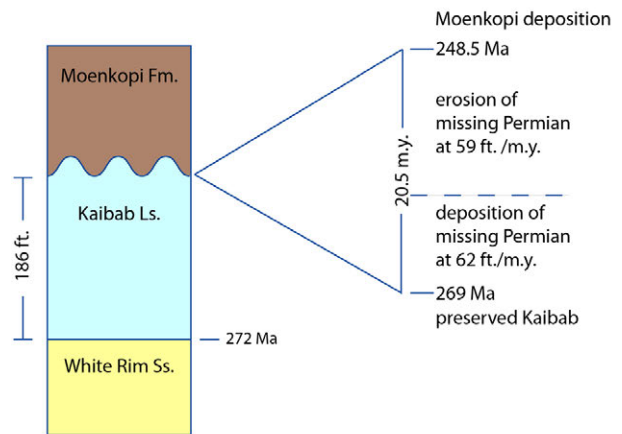
Figure 9.11. Site locations for burial and maturation models. Numbers correspond to sites in table 9.1 and Appendices R through U.

We calculated thicknesses of rocks removed during type-1 unconformities using the simplifying assumption that deposition of the unit underlying the unconformity continued for some time at the same rate as that of the portion that was preserved. We determined those rates using the thickness of the preserved units and the ages in the Mississippian through Cenozoic correlation tables of Hintze and Kowallis (2009). An erosion rate of 59 feet (18 m)/million years for the Mississippian to the mid-Cretaceous was calculated by averaging modern denudation rates in major drainage basins of Africa (Summerfield, 1991), which is a reasonable analog to the low paleorelief and low paleolatitude of Utah. For the Cenozoic, we used the denudation rate for the modern Colorado River drainage basin of 275 feet (84 m)/m.y. (Summerfield, 1991), on the assumption that after the Sevier Orogeny, Utah’s topography and climate were similar to the modern Rocky Mountains and Colorado Plateau. For the mid- through Late Cretaceous, an intermediate rate of 150 feet (46 m)/m.y. was used. Figure 9.12 shows an example of the calculation of the amount of section deposited and eroded, and the results of all the calculations used in the burial histories are in appendix S.

Tectonic unroofing was most significant at sites on thrust sheets of the Sevier Orogeny and at the northern San Rafael Swell. We calculated the amount of section removed during type-2 unconformities from the regional isopachs constructed for this project from the stratigraphic data in appendix R.

Sample calculation of thickness deposited and eroded.

Hunt State 1-16 (# 51)
Upper Permian unconformity



$$\begin{aligned}
 x &= \text{time of missing Permian deposition} \\
 20.5 - x &= \text{time of missing Permian erosion} \\
 62x &= 59(20.5 - x) \\
 62x &= 1210 - 59x \\
 121x &= 1210 \\
 x &= 10 \text{ m.y.} \\
 10 \text{ m.y.:} & \text{ deposit } 620 \text{ ft. of missing Permian} \\
 10.5 \text{ m.y.:} & \text{ erode } 620 \text{ ft. of missing Permian}
 \end{aligned}$$

Figure 9.12. Sample calculation of age and thickness of missing section.

To model organic maturation we used a modern passive margin average heat flow of 50 mW/m² (Allen and Allen, 2005) for the interval from the Late Mississippian until the onset of the earliest igneous activity in the area being modeled. From that time to the present, the heat flow was increased to reach the modern heat flows reported by Henrikson and Chapman (2002) and by Henrikson (written communication, 2008). The timing of initial igneous activity varies from Late Jurassic in northwest Utah to late Cenozoic in the thrust belt and eastern Basin and Range. We determined surface temperatures from the late Paleozoic through the Cretaceous from paleolatitudes as described by Barker (2000). The Genesis 5.1™ program calculates vitrinite reflectance (R_o) values based on the ages, burial depths, and thermal regimes of the modeled rock column, and these values predict if and when the potential source rocks may have generated hydrocarbons. Tables in appendix T present the stratigraphic, chronologic, lithologic, and thermal data in the format used to enter them into the Genesis 5.1™ software.

Results of Burial and Maturation Models

Maximum burial depths of the MCS and its equivalents in the models range from about 14,000 to 34,000 feet (4300–10,400 m) (table 9.1). However, more deeply buried MCS strata undoubtedly exist beneath thrust sheets of the Sevier Orogeny. No attempt was made to model these, as results from models of the hanging walls of the thrusts show that the MCS is overmature at these deeper levels.

The models show that the MCS is everywhere mature to overmature for hydrocarbon generation. Hydrocarbon generation occurred earliest in northwestern and north-central Utah, where the MCS was rapidly buried in the Oquirrh basin, and occurred latest in the southeast part of the study area, where the MCS typically was at relatively shallow burial depths until the mid-Cretaceous development of the Sevier foreland basin. The earliest entry of the MCS into the oil window occurred about 305 to 310 Ma (Middle and Late Pennsylvanian), and the latest occurred approximately 130 Ma (Early Cretaceous). Entries into the wet gas window range from 293 to 53 Ma (Early Permian to early Eocene), and generation of dry gas began as early as 285 Ma (Early Permian) and as late as 40 Ma (middle Eocene).

Although the models display considerable variety of burial and maturation styles, they fall into regional patterns that reflect the diverse geologic history of northern Utah. The remainder of this section describes examples of these patterns. For more complete descriptions of individual models, see appendix U.

Oquirrh Basin Sites

The Oquirrh basin was a Pennsylvanian-Permian, northwest-trending depocenter in northern Utah that accumulated

up to 25,000 feet (7600 m) of siliciclastic and carbonate sediment (the Oquirrh Group) in a remarkably short time (Jordan, 1979). Most of the basin is now in the Basin and Range Province (e.g., sites 13, 24, and 26), but the southeastern part of the Oquirrh basin is preserved in the Wasatch Range (site 39). Site 13 in the Hogup Mountains presents what is likely a typical burial history for the Oquirrh basin (figure 9.13). The dominant event in the history is the burial of the MCS to ~25,000 feet (~7600 m) by the end of the Permian. Except for relatively thin remnants of Triassic rocks, Mesozoic strata are mostly absent in this part of the Basin and Range, so the amounts of section deposited and eroded are estimated from regional isopachs and paleogeographic reconstructions (e.g., Blakey, 1997; Hintze and Kowallis, 2009). However, the estimates of post-Paleozoic burial probably have little effect on the maturation model since the MCS was already in the dry gas window by 270 Ma.

Sites 24 and 39 show similar burial histories and time of organic maturation. Site 26, Cedar Valley, is a variation of the Oquirrh basin history in which most of the Pennsylvanian-Permian section was eroded following uplift on a Sevier thrust fault. Site 16, Lemay Island, is located on the southwest rim of the Oquirrh basin and represents a second variant on the Oquirrh basin style. Here, Pennsylvanian to Early Permian tectonics, variously attributed to the C3 to P1 unconformities of Trexler and others (2004), and to periodic exposure of the West Central Utah Highlands (Ritter and Robinson, 2009) and the Lucin high (Hintze and Kowallis, 2009), likely prevented significant deposition of the Oquirrh Group. Consequently, if MCS strata are preserved in this area, they may still be in the early stages of gas generation.

Sevier Thrust Belt Sites

Sites 29, 30, 31, 34, 55, and 56 are distributed in the Sevier thrust belt from near the southwestern corner of Wyoming to Sanpete County, Utah, a distance of about 110 miles (180 km). Site 39, Hobble Creek, is also in the thrust belt, on the upper sheet of the Charleston thrust, but since that section contains a very thick Oquirrh Group, it has more in common with the Oquirrh basin sites than it does with the thrust belt. Despite the distance spanned by the thrust-belt sites and the fact that they are on different thrust sheets, they display rather similar burial histories. Site 29, Weber Canyon, is representative of the thrust belt burial models, and recent geologic mapping there (Coogan and others, in preparation) allows modeling the Late Cretaceous in some detail (figure 9.14).

In contrast to the Oquirrh basin histories, those from the thrust belt show relatively constant and more gradual subsidence in the late Paleozoic, typically burying the MCS to depths of 5000 to 7000 feet (1500–2100 m) by the beginning of the Triassic. Sedimentation rates remained nearly constant until about 170 Ma when they increased during deposition of the Middle Jurassic Twin Creek and Preuss Formations in the northern sites, and the Arapien Formation at sites 55 and 56.

Table 9.1. Locations and summary results of burial and maturation models of the Manning Canyon Shale and its equivalents (MCS).

Site Number	Name	Section Type	API Number	Latitude	Longitude	Maximum MCS Burial Depth (ft)	Time MCS Entered Oil Window (Ma)	Time MCS Entered Wet Gas Window (Ma)	Time MCS Entered Dry Gas Window (Ma)
13	Hogup Mountains	Pseudo well	—	41.45	-113.18	33,800	295	273	270
16	Lemay Island	Pseudo well	—	41.15	-113.90	16,000	257	139	not reached
24	Southern Cedar Mountains	Pseudo well	—	40.55	-112.95	24,400	308	273	249
26	Cedar Valley	Pseudo well	—	40.40	-112.08	33,200	305	289	272
29	Weber Canyon (Devils Slide)	Pseudo well	—	40.96	-111.63	28,600	247	201	162
30	Amoco Island Ranching D-1	Well	43-043-30161	41.0838	-111.1279	23,100	238	153	122
31	Anschutz Ranch 3-1	Well	43-043-30058	41.0285	-111.1483	20,200	234	137	100
34	Heber	Pseudo well	—	40.73	-111.39	21,700	234	113	90
39	Hobble Creek	Pseudo well	—	40.15	-111.44	31,500	305	293	285
44	Shell 1-16 D9 Ute	Well/pseudo well	43-051-30003	40.1326	-110.9012	33,100	227	88	81
48	Conoco-Federal 22-1	Well	43-047-30111	40.0157	-109.6601	23,500	131	53	50
49	Chevron Stone Cabin U-1	Well	43-007-20286	39.7505	-110.2603	22,300	128	68	52
50	Mountain Fuel Sunnyside U-1	Well	43-007-30012	39.5189	-110.4835	14,400	164	56	40
51	Hunt State 1-16	Well	43-007-30071	39.6036	-110.6890	14,300	214	84	75
52	Shell Carbon Canal 5-12	Well	43-015-30709	39.4493	-110.7564	13,200	204	82	40
53	Conoco Phillips Drunkards Wash 31-1	Well	43-007-30040	39.5596	-110.8742	16,100	243	110	79
54	Pacific North Springs 1	Well	43-007-10791	39.4858	-110.9019	14,200	196	82	49
55	Moroni – 1AX	Well	43-039-30006	39.5157	-111.5588	25,000	224	88	75
56	Placid WXC Howard 1A	Well	43-023-30007	39.6268	-111.9623	21,300	240	153	91
64	Phillips USA E-1	Well	43-039-30004	39.1340	-111.5609	19,500	153	80	71
65	Phillips USA D-1	Well	43-041-30004	38.8836	-111.6009	17,600	164	77	45

Entries into oil, wet gas, and dry gas windows correspond to R_o values of 0.6%, 1.0%, and 1.3%, respectively.

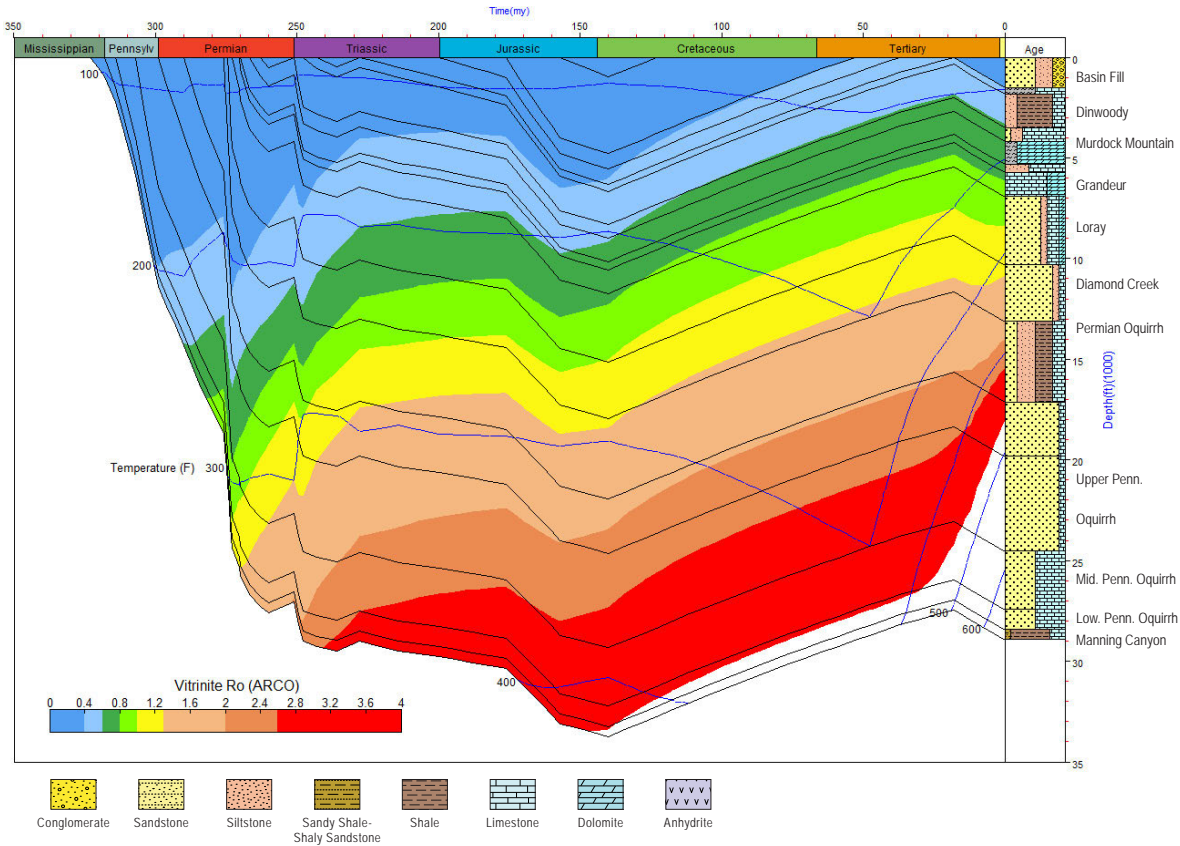


Figure 9.13. Oquirrh basin type maturation model, site 13, Hogup Mountains. The vertical axis shows the thickness of the stratigraphic section (in thousands of feet); the horizontal axis shows the time before the present (in millions of years) during which sediments were deposited or eroded. The fill colors show the level of organic maturation (in percent vitrinite reflectance [R_o]) calculated by the model, and the isotherms show the depths and times at which strata were at temperatures indicated. Lithologic column shows major stratigraphic units; see appendix R for full details.

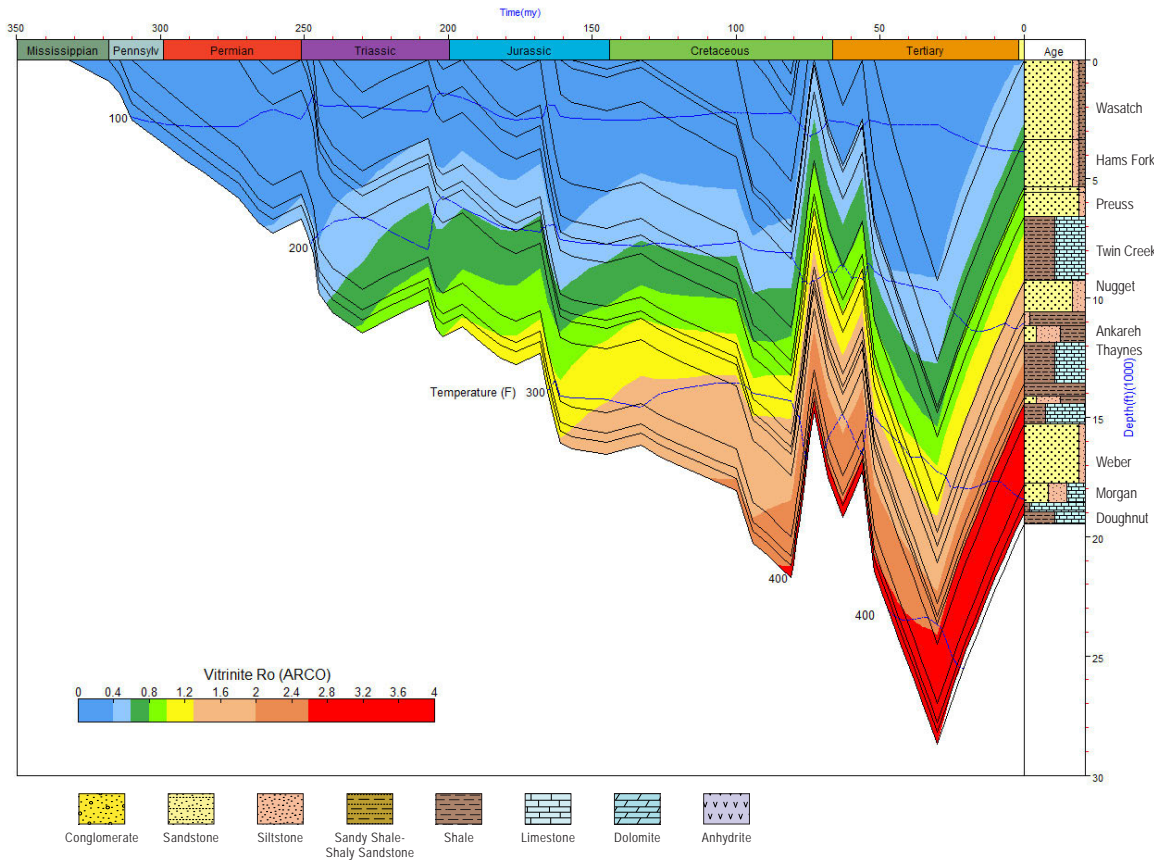


Figure 9.14. Sevier thrust belt type maturation model, site 29, Weber Canyon. See figure 9.13 for explanation.

Hintze and Kowallis (2009) suggested the increase in subsidence and sedimentation resulted from development of a back-bulge basin during the Nevadan Orogeny. Uplift and erosion occurred during the Late Jurassic and Early Cretaceous, until deposition of the Kelvin and Cedar Mountain Formations at ~120 Ma. At Weber Canyon, however, the Hams Fork Member of the Evanston Formation (Maastrichtian, ~70 Ma) unconformably overlies the Jurassic, suggesting that the Lower Cretaceous through Campanian strata were eroded during the Sevier Orogeny following movement of the Crawford thrust, which underlies the site.

Maximum burial of the MCS at all the thrust-belt sites, at depths ranging from 21,000 to 28,000 feet (6400–8500 m), followed the Sevier and Laramide Orogenies in the early Tertiary. The onset of oil generation from the MCS in the thrust belt seems to have occurred in a fairly narrow time range between 247 and 224 Ma. Entries into the wet and dry gas windows, however, are more dispersed, ranging from 201 to 88 Ma for wet gas, and from 162 to 75 Ma for dry. In general, the modeled ages become younger from north to south, and probably reflect different thicknesses of the Mesozoic sections.

Uinta Basin Sites

Sites 44, 48, and 49 represent burial histories in the western, eastern, and southern Uinta Basin, respectively. Sites 48 and 49 are two of the relatively few wells in the basin that penetrated the Paleozoic. However, site 44 (Shell 1-16D9 Ute well), like the great majority of wells in the eastern basin, did not drill into lower Mesozoic or Paleozoic strata, having reached total depth in the Upper Cretaceous Price River Formation. The thicknesses of lower units used in the site 44 model, from Sprinkel (1994), have therefore not been confirmed.

All three sites have very similar burial patterns, beginning with gradual and uniform subsidence from the Mississippian to the Early Cretaceous, which brought the MCS to a depth of about 6000 feet (1800 m) (figure 9.15). This subdued pattern, in contrast to burial during the same time range at sites farther west, probably reflects the absence of tectonism in the more cratonward region of the Uinta Basin. The pattern changed abruptly, however, at about 95 Ma (Cenomanian-Turonian boundary) with the onset of rapid deposition in the Sevier foreland basin. The clastic wedge shed from the Sevier highlands to the west buried the MCS to about 15,000 feet (4600 m) by the end of the Cretaceous. A short episode of nondeposition and erosion

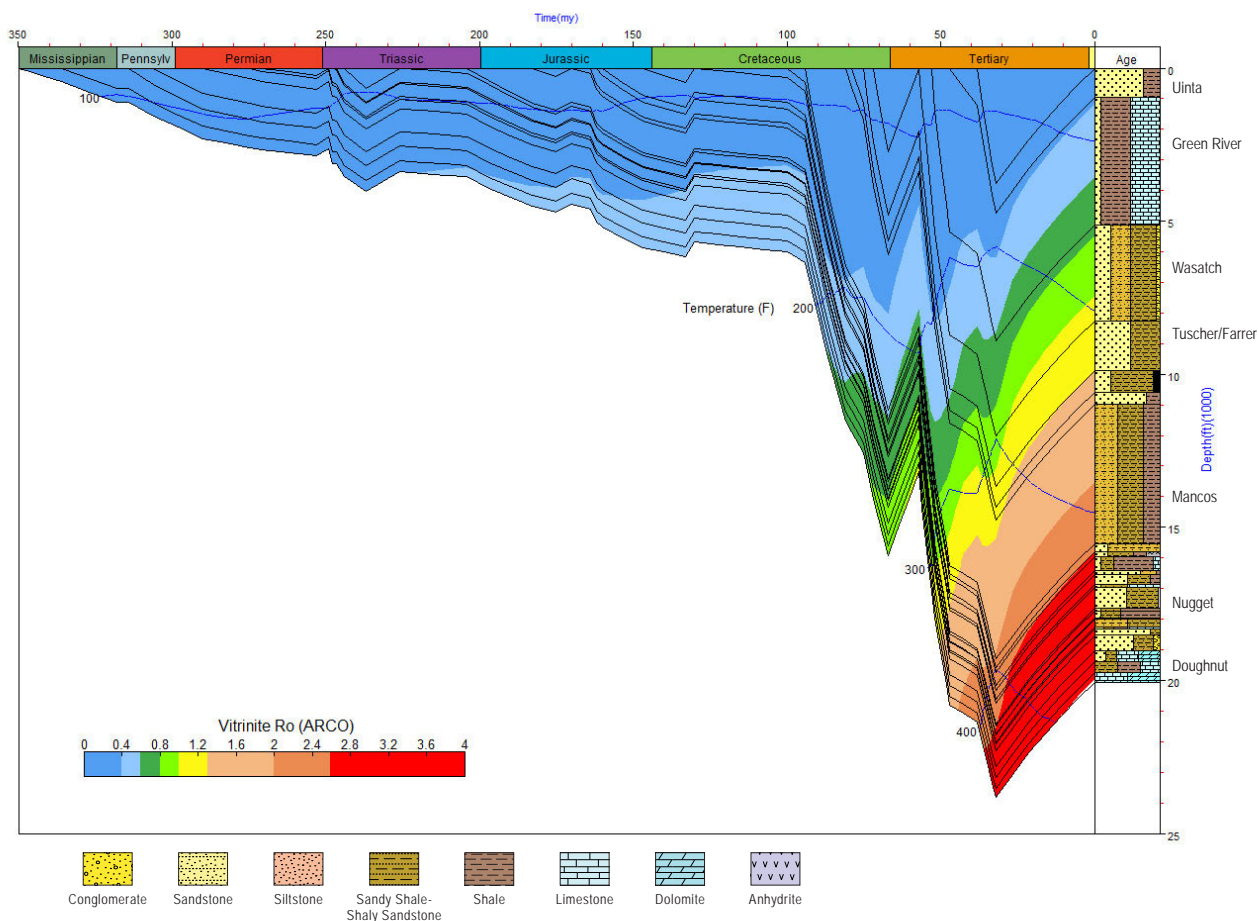


Figure 9.15. Uinta Basin type maturation model, site 48, Federal 22-1 well. See figure 9.13 for explanation.

in the Paleocene, which probably reflects the Laramide Orogeny, is evidenced by the Eocene Wasatch Formation unconformably overlying the Maastrichtian Tuscher/Farrer Formations. An additional ~7000 feet (2100 m) of burial occurred in the Eocene to early Oligocene during deposition of the lacustrine and fluvial strata of the Uinta Basin, which lasted until about 32 Ma at this location (Franczyk and others, 1992).

As a result of the gradual and modest amount of burial from the late Paleozoic to the Late Cretaceous, the MCS remained thermally immature, only reaching the top of the oil window at the beginning of the Cretaceous. Once foreland basin subsidence began, however, maturation accelerated; the wet gas window was reached at 53 Ma, and the dry gas window was reached at 50 Ma. By 40 Ma the MCS was probably post-mature.

San Rafael Swell Sites

Approximately 30 exploration wells penetrate the upper Paleozoic around the margins of the northern San Rafael Swell. The reports on these wells in the Utah Division of Oil, Gas, and Mining files, however, use conflicting or incomplete stratigraphic terms for the upper Paleozoic. In part, this is because the area is at the junction of the Oquirrh basin (to the northwest), the Paradox Basin (to the southeast), and the Callville shelf (to the southwest), and the reports use stratigraphic nomenclature from all three areas. Other reports simply omit the stratigraphic units between the Permian White Rim Sandstone and the Mississippian Redwall Limestone. The stratigraphic correlations used for this study are provided in chapter 8, which assigns Paradox Basin names to the Pennsylvanian and Lower Permian.

Five wells on the northern San Rafael Swell (sites 50–54) were modeled, including four in a relatively small area on the northwest flank of the swell. This area received detailed attention because a core through the Upper Mississippian Doughnut Formation was donated to the UGS for this project (the Carbon Canal 5-12 well) and a number of vitrinite reflectance analyses were either donated or made by the UGS (see chapters 4 through 7).

The Carbon Canal 5-12 well was spudded in the Blue Gate Shale Member of the Upper Cretaceous Mancos Shale (figure 9.16). Subsidence was relatively constant through the late Paleozoic and led to burial of the MCS to about 5000 feet (1500 m) at the beginning of the Triassic. Mississippian and Lower Pennsylvanian strata are mostly shallow-marine carbonates and fine-grained siliciclastics. In the Middle Pennsylvanian the Uncompahgre uplift emerged as a source of coarser clastics, which accumulated into the Middle Permian. From the Early Triassic through the Early Cretaceous, subsidence was again fairly constant, but less rapid than in the Paleozoic. Like sites to the west, the San

Rafael Swell area experienced a brief, but less pronounced, episode of enhanced subsidence in the Middle Jurassic.

The most rapid subsidence occurred in the Late Cretaceous as deltaic to marine-shelf clastics were deposited in the Sevier foreland basin. However, since the youngest rocks preserved in this area are Cenomanian, the Late Cretaceous and Tertiary burial histories derive from paleogeographic reconstructions, and the thicknesses of the missing units were extrapolated from outcrops in the Wasatch Plateau and Book Cliffs. Late Cretaceous deposition probably ended about 72 Ma, and non-marine Tertiary deposition began around 55 Ma (Franczyk and others, 1992). The depositional break coincides with the Laramide Orogeny and uplift of the San Rafael Swell, and it resulted in erosion of about 1500 feet (450 m) of Upper Cretaceous deposits.

The MCS around the northern San Rafael Swell entered the oil window between 243 and 164 Ma, the earliest entries recorded in the wells having the thickest Pennsylvanian and Lower Permian rocks. The MCS in most wells reached the wet gas window in the Late Cretaceous during the time of burial beneath the Sevier Orogeny clastic wedge. The erosional event at the Cretaceous-Tertiary boundary imparted a double-dip pattern to the burial model, resulting in most wells having two intervals of maximum burial. Those wells that did not enter the dry gas window during the first interval did so during the second.

Wasatch Plateau Sites

Although outside the depositional area of the MCS, two sites were modeled in the Wasatch Plateau because of their proximity to the Covenant and Providence oil fields. Sites 64 and 65 are east of the surface exposures of the Sevier thrust faults, but otherwise have burial and maturation histories similar to those in the thrust belt. The main differences are absence of the MCS and nearly constant deposition across the Cretaceous-Cenozoic boundary.

Site 64, the Phillips Petroleum USA E-1 well, was spudded in the Upper Cretaceous to Paleocene North Horn Formation and reached total depth in the Cambrian Tintic Quartzite. The unconformity separating the Lower Permian Toroweap/White Rim Sandstone from the Mississippian Redwall Limestone in the well represents 61 m.y., from 335 Ma to 274 Ma. The unconformity developed on the Emery uplift, which may have formed as a forebulge of the Uncompahgre uplift (Johnson and others, 1992). The Emery uplift probably had low relief and may have been periodically flooded during transgressions; consequently it was not deeply eroded (Johnson and others, 1992) and is modeled as a hiatus (figure 9.17). Platform carbonate deposition occurred in the Early Permian and Early Triassic, followed by non-marine deposition in the Late Triassic. Like the sites in the Sevier thrust belt, subsidence increased

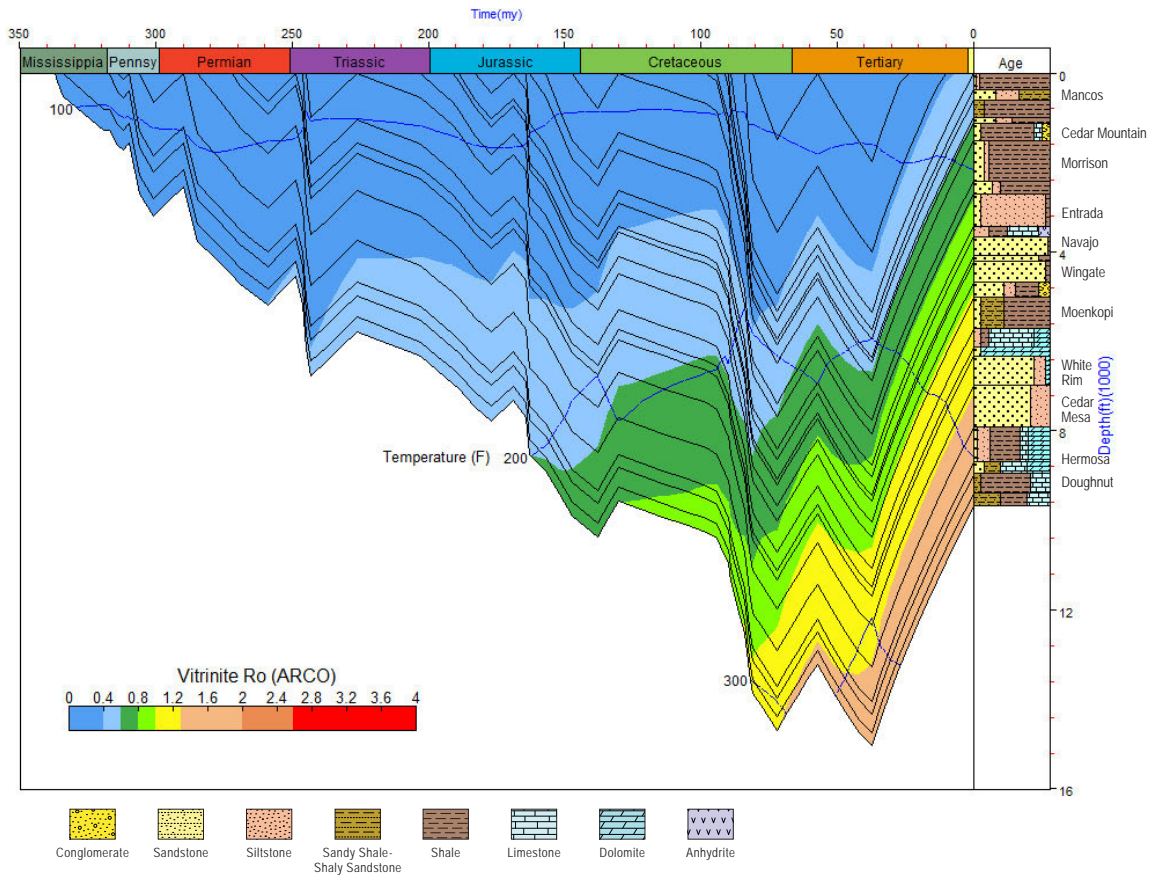


Figure 9.16. San Rafael Swell type maturation model, site 52, Carbon Canal 5-12 well. See figure 9.13 for explanation.

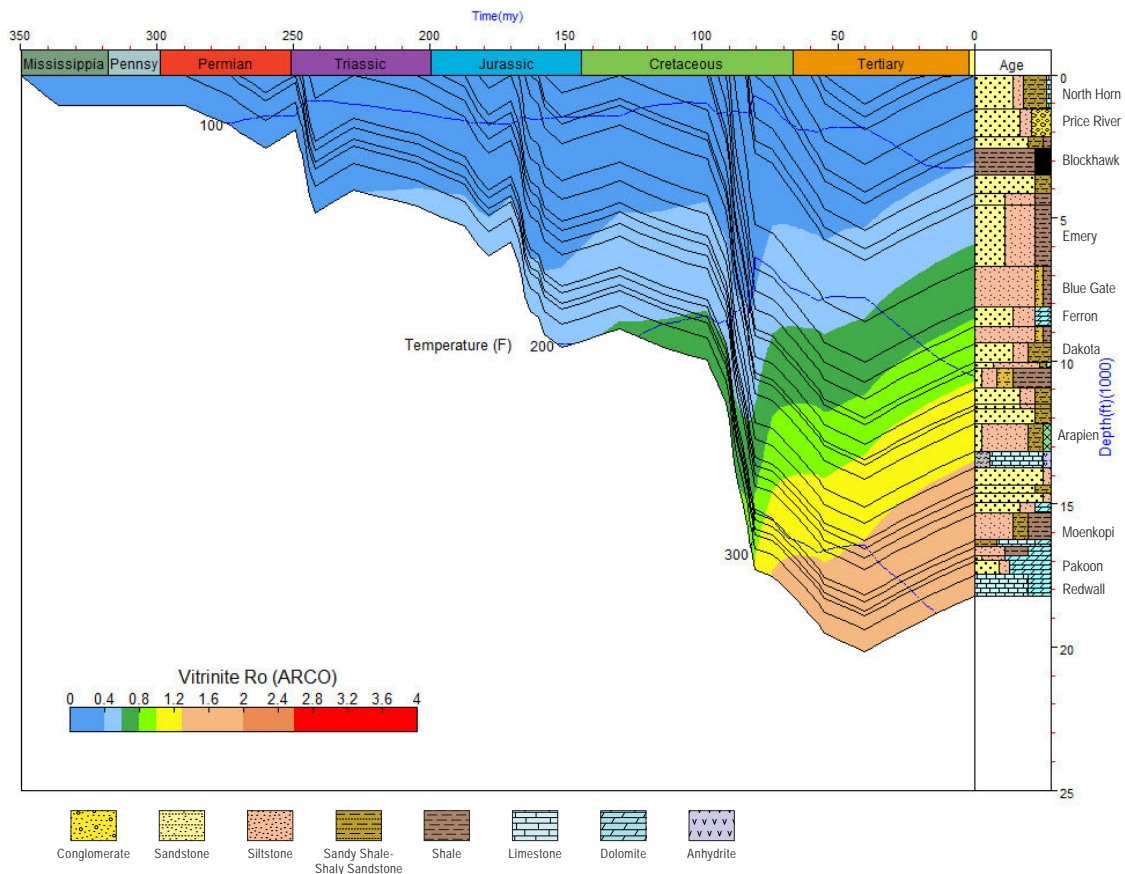


Figure 9.17. Wasatch Plateau type maturation model, site 64, USA E-1 well. See figure 9.13 for explanation.

in the Middle Jurassic in the back-bulge basin of the Nevada Orogeny. Following Late Jurassic and Early Cretaceous uplift and erosion (possibly representing a Sevier Orogeny forebulge), deposition resumed in the Barremian and continued to the Paleocene. Maximum subsidence rates from the Turonian to the Campanian represent deltaic to marine sedimentation in the Sevier foreland basin. Subsidence rates declined until deposition ended at about 40 Ma (Franczyk and others, 1992). The thicknesses of the eroded North Horn, Flagstaff, Colton, Green River, and Crazy Hollow Formations are based on the preserved units at the Hanson Moroni 1-AX well (site 55).

Times of organic maturation at the Wasatch Plateau sites are generally younger than those in the Sevier thrust belt, reflecting the near absence of Pennsylvanian and Permian strata, and

the thinner Triassic section. The oil window was entered at about 160 Ma, and the dry gas window from 45 to 70 Ma.

Burial History Conclusions

The burial histories and models of organic maturation for the MCS at 21 sites in northern Utah show that the MCS is thermally mature to postmature at all of them. At only one site (16) has the MCS not reached the dry gas window, and this site is in an area that saw little late Paleozoic sedimentation. The times at which the MCS was mature for oil and gas vary widely: from 308 Ma to 128 Ma (Middle Pennsylvanian to Early Cretaceous) for entry into the oil window, to 293 Ma to 53 Ma (Early Permian to Eocene) for entry into the wet gas window.

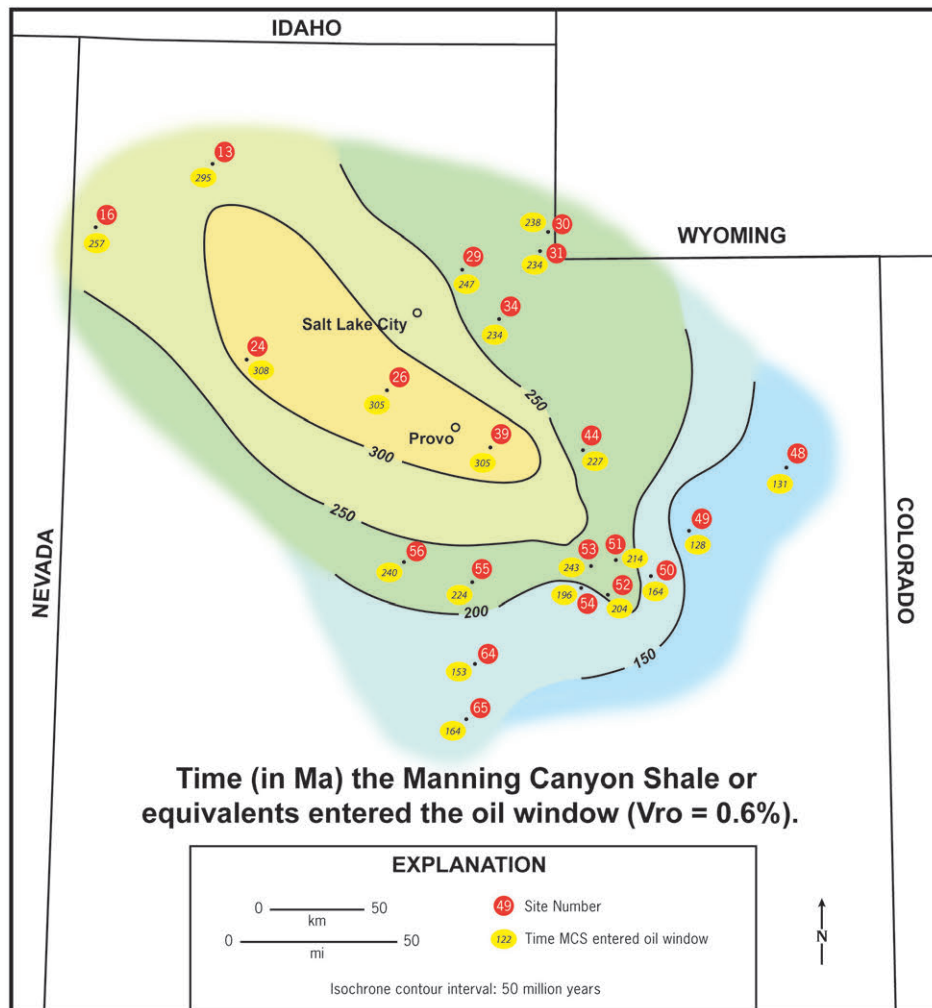


Figure 9.18. Time the Manning Canyon Shale/Doughnut Formation entered the oil window.

Figures 9.18 and 9.19 show that the MCS is most mature in a northwest-trending zone that coincides with the late Paleozoic Oquirrh basin. Away from this zone the MCS reached organic maturity at progressively later times, the most recent being in the Uinta Basin, the northern San Rafael Swell, and the south-central Sevier thrust belt. The distribution of maturation ages in the various tectonic settings indicates that in most areas hydrocarbon generation predated events that may have created structural traps. However, at the northern San Rafael Swell and the south-central thrust belt gas generation coincided with or post-dated formation of Sevier structures.

The accuracy of the organic maturation predicted by the models in this study can be gauged by comparing modeled and

measured vitrinite reflectances. Figures 9.20 through 9.22 plot modeled and measured vitrinite reflectances (R_o) against depth for three wells at the northern San Rafael Swell. The Genesis 5.1™ program calculates R_o using two algorithms, one developed by the Atlantic Richfield Company (ARCO) and the other by the Lawrence-Livermore National Laboratory (LL). Both algorithms produce similar results, but the ARCO model calculates lower R_o at shallower depths (<2000 to 3000 feet [600–900 m]) and higher ones at greater depths. The ARCO model seems to agree better with the R_o measured at the UGS, and was used in the maturation history plots presented here. Deviations between the measured and modeled R_o probably indicate that the paleo-heat-flow values used in the model were set too low.

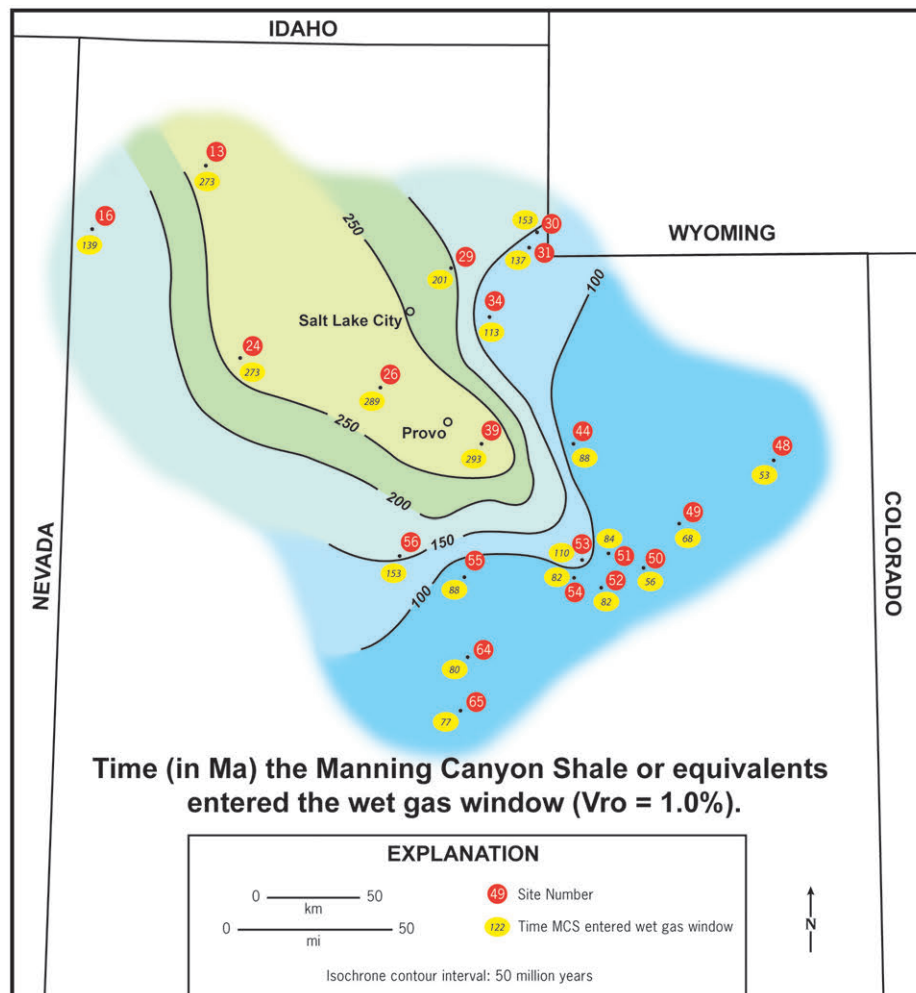


Figure 9.19. Time the Manning Canyon Shale/Doughnut Formation entered the wet gas window.

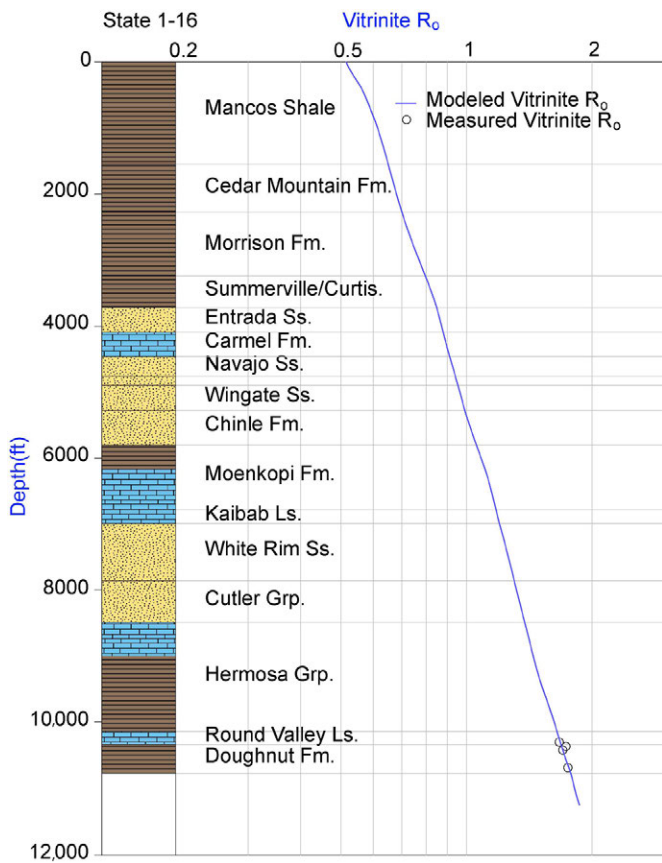


Figure 9.20. Modeled versus measured vitrinite reflectance (R_o) with depth, site 51, State 1-16 well.

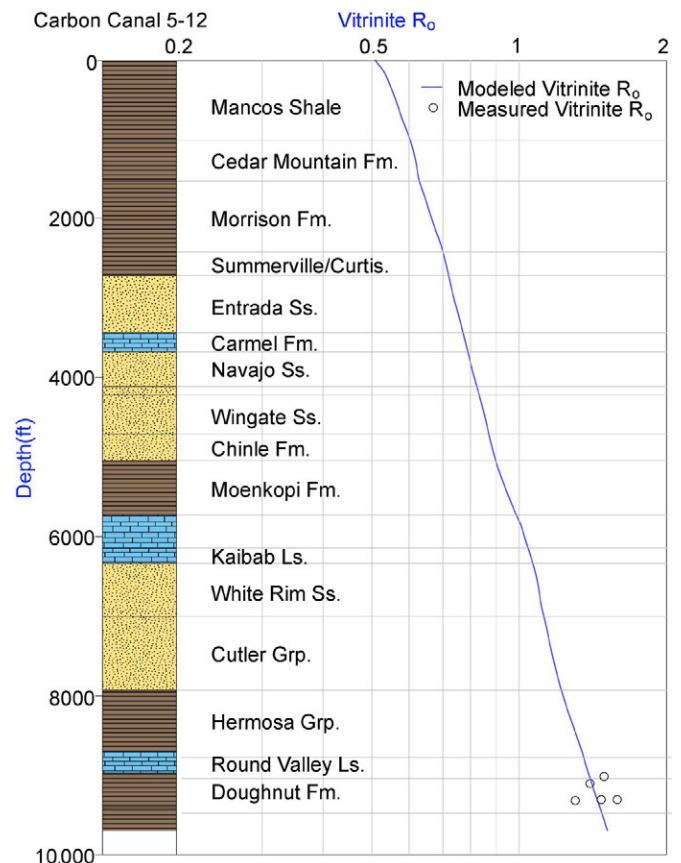


Figure 9.21. Modeled versus measured vitrinite reflectance (R_o) with depth, site 52, Carbon Canal 5-12 well.

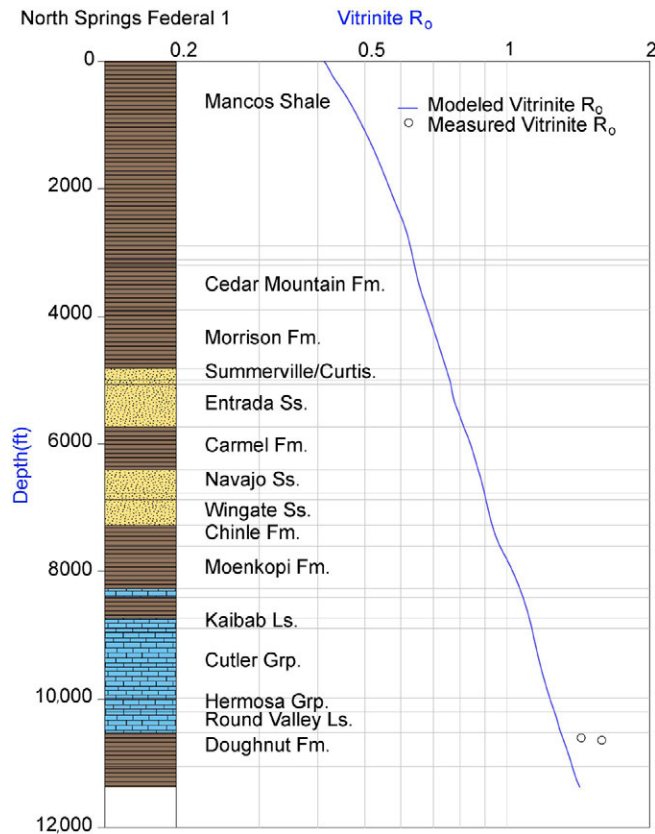


Figure 9.22. Modeled versus measured vitrinite reflectance (R_o) with depth, site 54, North Springs 1 well.

CHAPTER 10:
GENERALIZED BEST
COMPLETION PRACTICES
FOR DEVELOPING PALEOZOIC
SHALE GAS PLAYS IN UTAH

BY

Richard Curtice, *Halliburton Energy Services*;
Stephanie Carney and Thomas C. Chidsey, Jr., *Utah Geological Survey*

CONTENTS

INTRODUCTION	201
HISTORY OF HYDROCARBON PRODUCTION FROM SHALE.....	201
GETTING STARTED.....	202
Planning the Well.....	203
Gathering Geologic Reservoir Data.....	205
Petrophysical Log Model.....	206
HYDRAULIC STIMULATION	207
Completion Methods	207
Perforations.....	208
Stimulations Fluids	208
Fluid Volumes	209
Diagnostic Fracture-Injection Test.....	210
Post-Stimulation Follow Up	211
CASE STUDIES.....	211
Doughnut Formation (Manning Canyon Shale).....	211
State 15-32-15-12 and State 16H-32-15-12 Wells	211
Carbon Canal 5-12 Well	214
Gothic Shale, Paradox Formation.....	214
Frack Fluids and Proppants	215
Pumping Conditions	215
Job Design	215
SUMMARY	215

FIGURES

Figure 10.1. Liner hanger comparison.....	204
Figure 10.2. Horizontal interventionless completion string consisting of ball-drop actuated sliding sleeves, swellable isolation packers, and an expandable liner hanger	204
Figure 10.3. Example of compiling open-hole data with core data for petrophysical log model.....	207
Figure 10.4. Typical frack spread during stimulation treatments in shale	209
Figure 10.5. Ownership/leasehold status and well locations for Bill Barrett Corporation, Carbon and Emery Counties, Utah	212
Figure 10.6. Proposed horizontal wells targeting shale in the Doughnut Formation by Bill Barrett Corporation	212
Figure 10.7. Doughnut Formation landing point for the Bill Barrett Corporation State 16H-32-15-12 wells based on 3-D seismic	213

TABLES

Table 10.1. Generalized characteristics used to help identify a productive shale gas	202
Table 10.2. Kerogen types and classification.....	202
Table 10.3. Thermal maturity classification.....	203
Table 10.4. Various average frack gradients for shale formations	205
Table 10.5. General guide for stimulation fluid selections	209
Table 10.6. Example of a typical slick water stimulation treatment.....	210
Table 10.7. Pumping schedule for Gothic shale completion.....	216

CHAPTER 10:

GENERALIZED BEST COMPLETION PRACTICES FOR DEVELOPING PALEOZOIC SHALE GAS PLAYS IN UTAH

INTRODUCTION

The purpose of this report is to develop a best practice for producing hydrocarbons from the Paleozoic shale zones located primarily in central Utah and the Paradox Basin of southeastern Utah. The shale zones of primary interest are the Mississippian/Pennsylvanian Doughnut Formation (Manning Canyon Shale) and the Chimney Rock, Gothic, and Hovenweep shales in the Pennsylvanian Paradox Formation. An extensive search into the Utah Division of Oil, Gas, and Mining database revealed a total of 712 wells which had at least one of these intervals in them. However, reviewing the production data from each of these wells showed only two had limited production from any of the shale zones of interest. Therefore, it is extremely difficult to make a specific case for best practice on a particular shale for this study. Thus, the best practices described in this document may be better described as current practices used when completing a well for production from a shale reservoir. As operators develop more experience with the effective completion of these wells best practices will be developed for each

HISTORY OF HYDROCARBON PRODUCTION FROM SHALE

The beginning of the modern oil industry in North America is commonly credited as August 27, 1859, the date of oil discovery in a well drilled to a depth of 70 feet (21 m) in Titusville, Pennsylvania, by “Colonel” Edwin Drake. However, the modern natural gas industry in North America can trace its beginnings as far back as November 25, 1825, when gas produced from the Devonian Marcellus Shale was first used as an energy source to light street lamps in Fredonia, New York. There are reports of this occurring as early as 1821, but the first documentation of wells being drilled in the area appeared in the local paper, the Fredonia Censor, dated August 25, 1825. On November 30, 1825, a contemporary newspaper account was published in the Fredonia Censor declared that the “hole was drilled 27 feet into a slaty rock,” which was actually Marcellus Shale (Lash and Lash, 2010). The Marcellus Shale is currently one of the hottest shale prospects in North America.

Oil was also produced from the Upper Cretaceous Pierre Shale in Fremont County, Colorado, in Florence field as early as 1862. Over 13,000,000 barrels (2,100,000 m³) of oil has been produced out of this area since oil was first discovered. Also, in 1902 oil was produced from the Upper Cretaceous Mancos Shale in Rio Blanco County, Colorado, in Rangely field prior to the discovery of oil in the Pennsylvanian Weber Sandstone (Pickering and Dorn, 1948). Drilling in the Michigan Basin’s Devonian Antrim Shale began in 1936 and has been producing gas since the early 1940s. So producing hydrocarbons from shale is not entirely new to the industry. However, historical production from shale wells was not consistently economic. The development of modern drilling and completion methods has allowed for the possibility of economic production, which has led to the current interest in producing from shale gas and oil reservoirs.

The discovery of gas in the Mississippian Barnett Shale occurred on September 15, 1981, in the Newark East field of the Fort Worth Basin, north-central Texas. Initial development of the play was limited; however, in the mid to late 1990s, with the introduction of horizontal drilling, both exploration and production took off. Production from the Barnett accounted for 25% of the gas produced in Texas during 2009. However, drilling permits plummeted from a high of 2065 in 2008 to just 184 in 2015 due to continued low gas prices. Yet, the Barnett production was over 4.3 million (0.1 million m³) cubic feet per day in 2015 (Texas Railroad Commission, 2016).

Another major shale play is the Upper Devonian–Lower Mississippian Bakken Formation in the Williston Basin of North Dakota. The discovery well for the Bakken was drilled in April, 1951 on the Clarence Iverson farm south of Tioga, North Dakota, at a depth of approximately 10,500 feet (3200 m). This marked the beginning of the oil and gas industry in North Dakota (Key, 2010). Since then other formations have been discovered as oil producers throughout the Williston Basin. Some early attempts to use horizontal well technology to develop the Bakken shale occurred in the late 1980s and early 1990s. A second wave of horizontal drilling began in 2000 with the successful Lyco Burning Tree State well, and this has resulted in a dramatic increase in production from the play. Until the collapse in oil prices beginning in 2014, the Williston Basin was one of the hottest spots in North America

to drill for oil. This increased production was primarily due to targeting the middle Bakken, coupled with advanced technology in horizontal drilling and hydraulic fracturing.

There are 29 basins with potential hydrocarbon production in shale in North America. The successful operations in the Barnett Shale and the Bakken Formation have demonstrated the feasibility of economic production of natural gas and oil from shale, respectively. The general outlook for hydrocarbon production in shale is very encouraging once prices rise to economic levels for exploratory and development drilling, but producing from these reservoirs can be challenging. Both the reservoirs themselves, and the drilling and completion technologies are complex, and expert application of geosciences and engineering are required for the development of a potentially successful play. Shale is a rock that has extremely low permeability and low porosity. The hydrocarbons reside in the organic content of the rock and within the limited rock and fracture porosity. It is not uncommon to have porosities less than 4% with permeability in the nanodarcy range. Shale can be considered a source rock, a barrier, and in some cases a producing reservoir. Each shale is unique in lithology, geological setting, and production mechanism (Chong and others, 2010).

GETTING STARTED

A good understanding of the shale rock fabric is required in order to plan the best well paths and completion design. It is important to understand the existing stress fields immediate to the well location and the distribution of the natural fractures within the reservoir. Also, rock properties of the shale that will

dictate the response of the reservoir to the hydraulic fracturing process need to be understood. The basin-level geologic descriptions of the Paleozoic shales found in this report provide good starting values for petrophysical, geomechanical, and geochemical parameters of each of the shales: Manning Canyon/Doughnut, Chimney Rock, Gothic, and Hovenweep.

Other sources for such information, including information about other shale plays, can be found in both public and private databases. Most states currently have some type of website with electronic databases that are easy to access. Some of these are free to the general public; however, a few states charge a modest service fee to get the desired information. Geological and reservoir evaluations of an area can also provide good information about the extent of formations, depths, thickness, etc. Table 10.1 lists general shale screening aspects to help determine if a shale has the characteristics to be economically producible. The depositional environment and the thermal maturity are also critical pieces of the reservoir puzzle needed to determine if the shale of interest has economic potential (tables 10.2 and 10.3). It is important to obtain data that pertains as specifically as possible to the planned well location to ensure adequate technical basis for the decisions that will need to be made during the play discovery and development stages (Chong and others, 2010).

Much of the generalized information from tables 10.1, 10.2, and 10.3 can be found in most state's geological databases. Gathering this general type of data typically requires little monetary investment, but does require some time for evaluation. Most states also have some type of core storage (the UGS's Core Research Center in Salt Lake City for example),

Table 10.1. Generalized characteristics used to help identify a productive shale gas compared to Utah shale reservoirs.

	Zone thickness (ft)	Gas-in-place (Bcf/mi ²)	Gas content (scf/ton)	R _o (%)	TOC (%)	Poisson's Ratio	Young's Modulus (psi 10 ⁶)	Kerogen type
Favorable	≥50	≥50	≥50	1.1–2.1	≥2.0	≤0.25	≥4.5	I-III
Doughnut	0–1000	NA	NA	1.2–1.9	4.43	0.12–0.3	3.97–11.27	III
Chimney Rock	0–40	NA	NA	0.6–1.7	2.2	NA	NA	I-III
Gothic	2–70	50	NA	0.6–1.7	2.1	0.18–0.3	4.42–7.46	I-III
Hovenweep	1–100	50	NA	0.6–1.7	2.1	0.25–0.27	4.99–5.77	I-III

NA = not available

Table 10.2. Kerogen types and classification.

Kerogen Type	Depositional Environment	Organic Precursors	Hydrocarbon Product
I	Lacustrine	Algal bodies or structural debris of algal origin	Very H-Rich; very good for oil
II	Marine, reducing conditions	Skins of spores and pollen, cuticle of leaves and herbaceous plants	H-rich; precursors for oil and gas
III	Marine, oxidizing conditions	Fibrous and woody plant fragments and structure less colloidal humic matter	H-poor; mainly precursors for gas
IV	Marine, oxidizing conditions	Oxidized, recycled woody debris	Very H-poor; largely inert, but may produce gas at very late stages of maturation

Table 10.3. Thermal maturity classification.

Vitrinite Reflection (R_o %)	Potential Hydrocarbon Type
0–0.55%	Onset of oil generation
0.55–0.9%	Peak oil production
0.9–1.1%	Wet gas
1.1–1.4%	Dry and wet gas
1.4–2.1%	Dry gas only
> 2.1%	CO ₂

and analyses of cores in such collections can provide some valuable information. Other information that can help reduce the risk of pursuing shale reservoirs includes the shale mineralogy, regional stress regime, distribution of natural fractures, and comparisons to analog reservoirs.

Planning the Well

Most of the current economical shale plays began with vertical wellbores, but field development has since proven that horizontal wellbores are by far more economically efficient. The use of a single drill pad from which several horizontal wells are drilled minimizes the required footprint. For these reasons, a horizontal wellbore may be preferable to a vertical wellbore regardless of the thickness of the shale. The drilling of a vertical pilot hole can be done prior to kick-off of a horizontal well. This allows for the logging and coring of the full vertical section of the shale interval so that well path and completion can be better planned. Identification of local stress patterns is of critical importance in the planning of the hydraulic fracture completion. The horizontal well path is planned to take advantage of the natural fracture pattern of the shale and to align the well path such that the hydraulic fractures will be generated perpendicular to the well. Continuous improvement in horizontal drilling techniques to reduce the time and cost to complete such a well has allowed shale gas (and oil) development to advance.

The beginning of horizontal drilling can be traced back as far as September 8, 1891, when John Smalley Campbell issued the first U.S. patent (No. 459,152) for using flexible shafts for rotating drill bits. The first documented true horizontal well was drilled near Texon, Texas, in the Austin Chalk in 1929 (King and Morehouse, 1993). Commercialization of horizontal drilling began in the 1980s. Most early horizontal wells had horizontal sections that measured in the hundreds of feet (several tens of m); as the technology has grown, horizontal sections are typically drilled in the thousands of feet (several hundreds of m) and in some cases reach out for several miles. The longer the horizontal section, the more challenging the drilling and completion of the well will be.

When considering the overall length of the horizontal section of the wellbore, one needs to consider the feasibility of suc-

cessfully completing the well. A 10,000-foot horizontal (3000 m) section that is drilled but cannot be effectively stimulated wastes time and money. Another thing to consider is the ability to do future well repairs or recompletions as the reservoir is developed. Also, the limitations of the materials and tools that are planned for the drilling and completion of the well need to be considered. Stick tubing, coiled tubing, and wireline all have limitations on their practical reach in a horizontal wellbore.

Shale wells are completed using hydraulic fracturing as the preferred stimulation treatment. Because of the very low permeability of shales, a good fracture design is crucial to the success of the well. The horizontal section of the well may be completed (1) as an open hole, (2) with a slotted liner, (3) as a cased hole, or (4) by using swellable packers with mechanical sleeves. The most common sizes of casing used are 4.5 and 5.5 inch (11 and 14 cm). The predominant completions in the Rocky Mountains are cased hole with swellable packers and mechanical sleeves. The choice of completion type will depend, in part, on the overall length of the horizontal section of the wellbore.

Horizontal wells in shale normally have at least three strings of pipe: surface casing, intermediate, and the liner, which is set in the horizontal portion of the well. Mechanical and expandable liner hangers are both dependable ways to hang off the liner in the intermediate casing. The mechanical liner hanger has been used longer, but it contains moving parts that can malfunction and prematurely set. The expandable liner hanger is a fairly recent innovation that has no moving parts and has proven to be very dependable. Either of these types of liner hangers can be used whether the casing is cemented in place or swell packers and mechanical sleeves are employed.

Once a decision has been made to cement the liner in place, some risks arise in a horizontal well that are typically absent in a vertical wellbore. It is more difficult to get a cement sheath placed completely around the casing in a horizontal wellbore than in a vertical because the casing tends to lie flat in the horizontal section, making it more difficult to achieve adequate cement coverage. Without adequate centralization it is virtually impossible to get a competent cement job, making zonal isolation extremely difficult during well stimulation.

Poor casing centralization can also lead to casing problems over the life of the well. Although, the type of cement to be used varies from region to region, a competent cement with adequate centralization is of utmost importance for the completion of the well, in addition to providing required wellbore integrity. Good fluid-loss control in the slurry will minimize any damage to the shale due to cement filtrate. Since shales are extremely low in porosity and permeability, all steps should be taken to minimize any damage that can be caused by cement filtrate.

If it is decided not to cement the liner in place, it will be extremely difficult to get a good, tight seat upon anchoring the liner system at the top. Another risk when using a conventional mechanical liner is that of presetting the liner hanger and/or the liner hanger packer. Using an expandable liner hanger (ELH) greatly reduces these risks due to its design (figure 10.1) (Vargus and others, 2008). The benefits of using an expandable liner hanger over a mechanical hanger are:

- no risk of pre-setting the liner hanger:
 - no external slips,
 - pressure balanced,
 - washing/circulating operation;
- less tortuous flow path directly around the hanger, reducing surge and equivalent circulating density;
- liner lap integrity:
 - hydraulically energized elements,
 - gas-tight seal,
 - does not require cement to effect the seal;

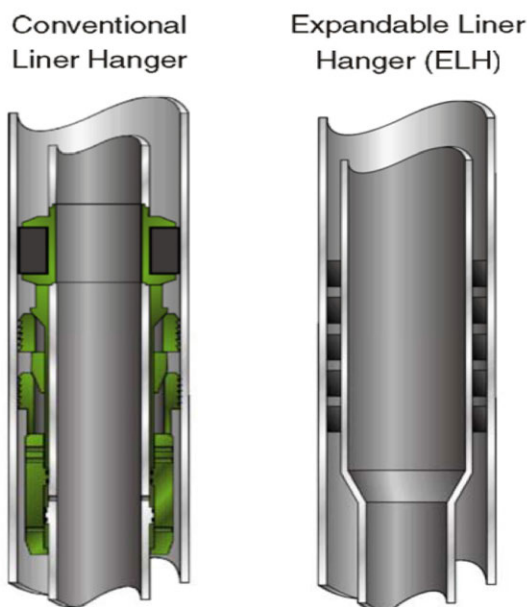


Figure 10.1. Liner hanger comparison.

- optional tie-back seal anchor threads:
 - some designs come with a latching thread and seal bore to allow a frack string to be anchored below the tieback receptacle, allowing for retrieval of frack seal in favor of running production seals tied in the upper tieback receptacle (Vargus and others, 2008).

A completion technique that is becoming more popular is the use of swell packers with mechanical sliding sleeves. This technique allows the operator to effectively isolate and treat fairly long horizontal sections of the wellbore from the toe to the heel. A swell packer is an oilfield tubular that has a long section of rubber as a packer element, which is chemically bonded to the casing. It is installed as just another joint of casing. The packer element is then allowed to swell in hydrocarbon, typically diesel, and can expand up to 200% of the original size by volume of rubber. The swelling forms a positive seal, allowing for zonal isolation without the use of cement. Sliding sleeves are placed between the swell packers so that pinpoint stimulation along the horizontal portion of the wellbore can be accomplished. This provides the operator with a good opportunity to treat the entire horizontal section.

There are several variations in the type of sliding sleeve that can be used. The most common type uses various sizes of dropped balls, which activate the sliding sleeves. This is done by positioning the smallest inside diameter (ID) tubing nearest the toe and progressively larger IDs near the heel. These sleeves can be designed to be used more than once, via hydraulic control lines that have been run during the installation of the system. Some sliding sleeves have been designed to open and close, using a mechanical means such as standard tubing or coiled tubing. Figure 10.2 illustrates the installation of an ELH and a series of swell packers with sliding sleeves (Vargus and others, 2008).

Appropriate choice of drilling fluid, whether oil- or water-based, is another critical element in drilling a well. Drill-



Figure 10.2. The horizontal interventionless completion string consisting of ball-drop actuated sliding sleeves, swellable isolation packers, and an expandable liner hanger.

Table 10.4. Various average frack gradients for shale formations.

Formation/ Zone	Basin	Depth (ft)	Well Type	Average Frack Gradient (psi/ft)
Bakken	Williston	6000–9500	Horizontal	0.69–0.80
Baxter	Vermillion	9500–13,000	Vertical/Horizontal	0.90–0.95
Gothic	Paradox	4500–6000	Vertical/Horizontal	1.0–1.2
Lewis	San Juan	4500–6000	Vertical	0.55–0.70
Mancos	Uinta	9000–15,000	Vertical	0.89–1.10
Pierre	Raton	4000–6000	Vertical/Horizontal	0.55–0.65

ing fluid choice will depend primarily on the specific shale being completed and can vary from area to area. Shales fall apart, swell up, slough in, etc., if the incorrect drilling fluid is used. The type, size, and grade of casing are other important aspects to consider when drilling a well. For the most part, shales tend to have fairly high frack gradients, so depending on the depth of well, the operator might be faced with fairly high treating pressures during the stimulation phase of a well (table 10.4) (Kundert and Mullen, 2009). When stimulating shale reservoirs, most treatments are pumped down casing because high pump rates are needed to effectively treat the multiple intervals over long horizontal lengths or thick shale sections. Therefore, depending on the depth of the formation, wellhead-treating pressures on deep shales can easily be over 10,000 pounds per square inch (psi) (69,000 kPa). A good casing string is needed to handle the high pressures required to effectively stimulate the numerous intervals typically treated for a shale formation.

Gathering Geologic Reservoir Data

Gathering geologic reservoir data is one of the most critical pieces needed in the earliest part of the shale gas or exploration phase. Depending on the depth and overall thickness of the shale this can be a very costly part of the program, but a very necessary one. Without good information, an operator could spend \$100 million on ten wells using the hit or miss method, and get little or no return on this investment. Or an operator could spend the same amount on five wells, gathering key data that allow more intelligent drilling decisions over the life of the field, including well placement. The drilling of a vertical pilot hole that penetrates the entire geologic section of interest can allow access to the shale for the collection of the site-specific data needed for proper placement of the horizontal section in the best portion of the shale.

The two primary methods of gathering the necessary data are geophysical well logging and core samples. The types of information needed are geochemical, geomechanical, and petrophysical, as described in previous chapters. The geochemical properties needed to effectively build a good petrophysical model are:

- TOC,
- maturity, % R_o (Tmax),
- kerogen type,
- gas content,
- free and adsorbed gas,
- mineralogy (X-ray diffraction [XRD], scanning electron microscopy [SEM], chemostratigraphy),
- acid solubility/sensitivity, and
- fluid sensitivity (capillary suction time [CST] tests, SEM, roller oven stability tests, shale fracture flow, and ultra-low-permeability testing apparatus [ULPTA®]).

The geomechanical data needed to build the petrophysical model are:

- Young's modulus of elasticity,
- Poisson's ratio,
- Brinell hardness,
- compressive strength, and
- proppant embedment.

Certain log characteristics are common to organic-rich shale plays. Shale beds with high organic content typically have elevated gamma-ray measurements in comparison to surrounding shale. The organic material, possibly in combination with thinly laminated sandstone and carbonate, imparts a higher electric resistivity than occurs in organic-poor shale. In addition, organic-rich shale beds have a lower bulk density than the surrounding shale (Kundert and Mullen, 2009).

A comprehensive logging program will assist the operator from the beginning of the exploration phase through the declining phase of the project. Information obtained through the logging program that can be used throughout the entire life of the reservoir includes:

- fracture identification and orientation,
- total organic content and organic maturity,

- rock strength and brittleness/ductility, and
- shale gas-in-place conventional analysis.

The recommended suite of logs is:

- exploration phase—
 - triple combo, spectral gamma ray (GR), microLog (shale evaluation),
 - WaveSonic®, water-based mud imaging (XRMI™) (mechanical properties, fracture identification and orientation),
 - magnetic resonance imaging log (MRIL) (free porosity identification),
 - mud log, LaserStrat® (mineralogy horizontal or deviated wellbores),
 - pulsed neutron for cased hole interpretation (CHI) training, and
 - production logging;
- development phase if vertical—
 - triple combo – spectral GR, micolog,
 - pulsed neutron technology run cased hole, and
 - production logging;
- development phase if horizontal—
 - logging while drilling (LWD) GR, mud log,
 - LaserStrat®, pulsed neutron,
 - Azimuthal Focused Resistivity™, and
 - production logging .

Coring of the shale is also a critical step in gathering data in the early stages of development or exploration, and can provide information which cannot be obtained from logging. There are several ways to obtain formation samples for analysis, the choice of which is somewhat dependent on the stage of field development. Drill cuttings are quick and easy to gather. Cuttings can provide some geochemical properties, but this process is best used in the latter stages of development once a full-scale drilling program has been put into place. Sidewall coring is the next option; it is more expensive and time consuming but can provide both geochemical and geomechanical properties. However, the best process is the drilling of full-diameter cores, especially in the very beginning of developing the play. This is by far the most time consuming and expensive process, but it allows the operator to complete all the testing needed (Kundert and Mullen, 2009). A comprehensive coring program and analysis can provide the following information:

- TOC,
- shale maturity,
- gas content,

- matrix permeability,
- rock mechanics,
- chemostratigraphy,
- X-ray analysis,
- SEM,
- immersion tests,
- fluid sensitivity, and
- rock strength.

Petrophysical Log Model

Once all of the log data, along with the core analysis, have been obtained it is then possible to develop a good representation of the shale resources. Figure 10.3 shows what type of petrophysical log model can be developed using open-hole-log and core data. The curves on the left of the depth track are the original open-hole-log data, and the information on the right is a calculated visual representation of rock properties, gas content, gas-in-place, TOC, kerogen, stress, and shale porosity. Once this model has been built, it can be used to choose the best completion intervals, and can be reviewed for organic content, brittleness, hydrocarbon shows in mud, etc. The log data in this example have been calibrated by supportive laboratory data, which was obtained from core (Kundert and Mullen, 2009).

Constructing a petrophysical log model of this nature allows the operator to have all of the necessary data in one location, and it is a very useful tool when determining what parts of the reservoir are the best to complete. This is particularly useful in very thick zones found in vertical wells. A model of this type can be used to readily identify the following (Kundert and Mullen, 2009):

- organic-rich portion of the shale—
 - organic material in the mineralogy track is shaded light green,
 - kerogen content is shaded black in the kerogen/organic track, and
 - shale porosity is shown in pink on the shale-porosity track;
- brittle part of the reservoir rock—
 - the more red, the more brittle the rock on the brittleness track, and
 - green represents more ductile rock;
- gas shows—
 - gas shows on the mud-log track appear red;
- natural fractures on the full-core samples and imaging log;
- intervals to be treated, which should have similar calculated stresses—

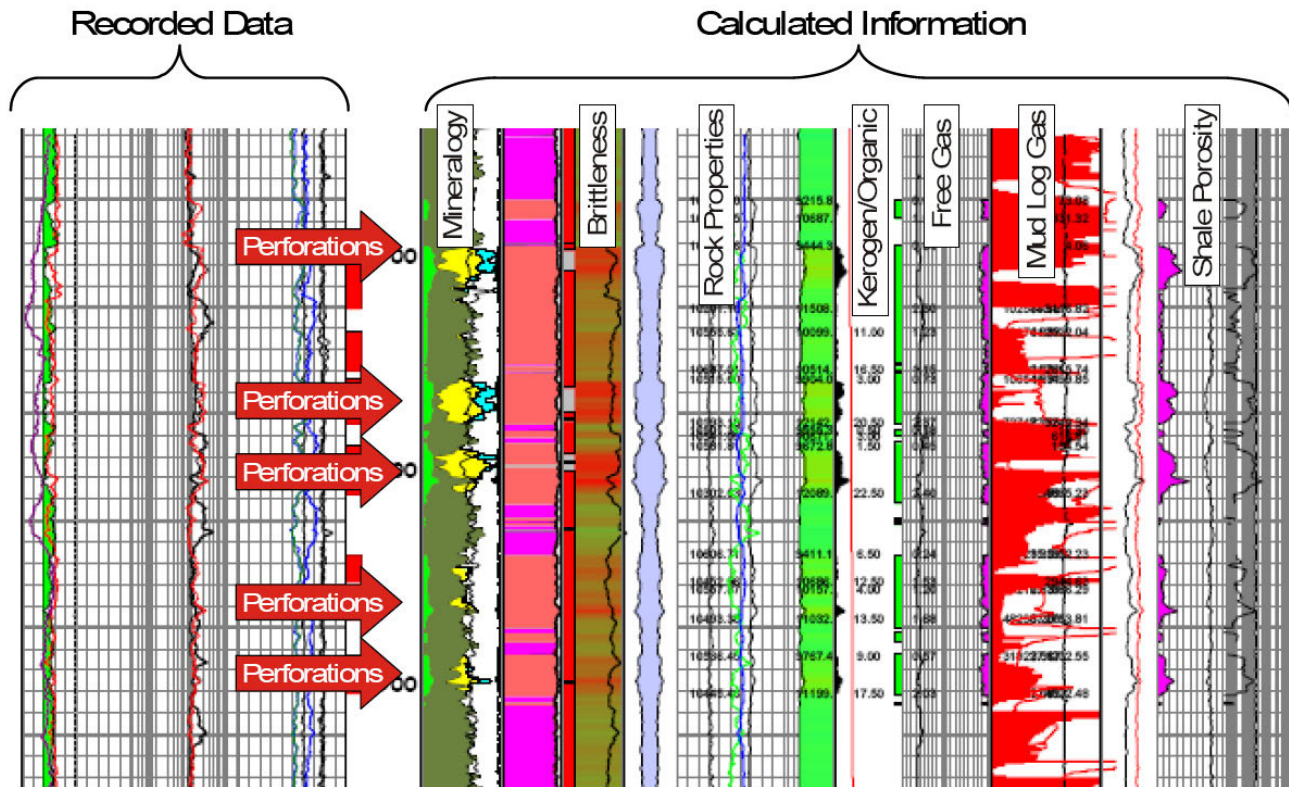


Figure 10.3. Example of compiling open-hole data with core data for a petrophysical log model (from Kundert and Mullen, 2009; ShaleLOG®). Courtesy of Halliburton.

- make the stage length 200 to 300 feet (60–90 m), if possible, and
- in areas using swell packers and sliding sleeve, intervals should be compartmentalized in 500-foot (150 m) sections.

HYDRAULIC STIMULATION

As stated earlier, how the well was drilled and completed directly affects how it is hydraulically fractured. Vertical wells might be a good choice if the shale section is very thick. However, shale plays around the country have demonstrated that drilling horizontal legs results in the most economical wells in most areas. The biggest advantages that a vertical well has over a horizontal well are that intervals can be isolated more easily, problems with logging tools or perforating guns are reduced, workovers are easier to accomplish throughout the life of the well, and getting a good primary cement job is easier. Horizontal wells expose more shale to the stimulation treatment and have a much better chance of connecting to a large natural fracture network. Effective treatment of the entire lateral interval is therefore important.

However, some aspects of a horizontal well may be more challenging when compared with those of a vertical well. Torque and drag restrictions may limit the ability to work over ar-

eas of the wellbore, either with conventional tubing or coiled tubing. Also, it is harder to get conventional tools to work in long horizontal legs. Inflatable packers can be run, to reduce sticking risk, but eventually the ability to reach the end of the lateral will reach a limit with either conventional tubing or coiled tubing.

Completion Methods

How the well is completed will have a dramatic impact on how effective the stimulation treatment will be and whether all of the shale will be treated. The four major methods for completing wells are:

1. open hole,
2. slotted or pre-perforated liners,
3. cased hole that is cemented, and
4. uncemented casing with swell packers with sliding sleeves (figure 10.2).

All of these completion techniques are viable options regardless of whether the well is vertical or horizontal. Each method has its unique shortcomings. A slotted or pre-perforated liner presents the most difficulty for treatment of the entire shale section because there is little or no control over the placement of the stimulation fluid. Diversion techniques can be used to

direct the stimulation treatment to specific locations along the wellbore, but once the fluid is displaced behind the liner, there is little control over where it goes into the formation. Open hole completions also make it difficult to effectively treat over all of the shale drilled. Relative to the slotted or pre-perforated liner, open holes offer a better chance of diverting fluid from one part of the reservoir to another because the pumping is directly into the formation. However, both the slotted or pre-perforated liner and the open-hole completion make attempting to treat a large interval impractical. The biggest advantage of using a slotted liner or pre-perforated liner over an open-hole completion is that the slotted liner will help prevent the wellbore from filling in with formation should it begin to slough.

The best completion options are cased hole cemented in place, or un-cemented casing using swell packers with sliding sleeves. Completing the well by running casing requires that a good primary cement job on the liner is obtained. The type of cement will vary from area to area. Casing centralization is key in a horizontal wellbore because the pipe has a tendency to lie on the low side of the wellbore. Fluid loss is another problem that must be controlled to minimize production zone damage. It is also important to minimize filling natural fractures, which can be critical to production, with cement.

Once the liner is cemented in a vertical or horizontal wellbore, the well can be completed with what is commonly referred to as a “stack and frack” in the industry. In this technique, the deepest interval to be treated is perforated and the first stimulation treatment is pumped. Then a wireline is run in the well to set a frack plug and the second interval can be treated. This process is repeated until all of the desired intervals have been treated. Drillable frack plugs are designed as check valves to provide wellbore zonal isolation. These tools are used primarily between zones in multistage stimulation treatments. The frack plug isolates the lower zone during stimulation but allows flow from below once the stimulation is over to aid in well cleanup. Once all of the intervals have been treated, the bridge plugs are drilled out and the well is placed on production. In horizontal wells the bridge plugs and perforating guns are pumped down and typically take longer to get in place than when run in a vertical well using wireline. This can take several days, in some cases weeks, to complete in a horizontal well, depending on the number of intervals to be treated.

One of the more popular methods being used today, especially in horizontal wells, is the use of swellable packers with sliding sleeves, along with an expandable liner hanger (see figure 10.2). The swellable packers eliminate the need for a primary cement job and provide isolation for a specific interval. The sliding sleeves eliminate the need to perforate and allow for pinpoint stimulation of a particular interval. The sleeves are typically activated by dropping a ball that opens up the sliding sleeve for the upper interval and acts as a barrier to prevent fluid from entering the lower zone, which was just treated. This allows for a continuous stimulation treatment of the en-

tire interval. Typically, all of the intervals to be treated can be done without stopping operations. Therefore, by using this technique an entire stimulation process can be completed in two to three days (in a best case scenario) instead of one to three weeks, depending on the number of intervals to be stimulated. Based on the size of casing and supplier of the packers and sleeves, one can treat up to 20 to 30 separate intervals in a wellbore. Again, once all of the intervals are stimulated the balls and the baffles are typically drilled out and the well is placed on production. The greatest advantage this process has over the other completion techniques is that each targeted interval is successfully treated. The stimulation process does not need to shut down until all of the intervals are treated, which greatly reduces the time necessary to complete the entire lateral. This is by far the most efficient method for treating long horizontal intervals.

In some cases, where the number of intervals to be treated are greater than the number of sleeves, the stimulation process can be run by cementing the lower portion of the liner, combined with using sleeves on the upper part of the lateral. Sleeves can also be designed to open and close throughout the life of the well. However, if this approach is taken, the individual sleeves have to be mechanically opened and closed during the entire stimulation process, which will increase the time needed to treat all of the intervals. The advantage is that it gives the operator better options throughout the life of the well for isolating potential problems such as thief zones or water production. This is something that the operator needs to evaluate prior to running the swellable packers and sleeve system.

Perforations

In the event the liner is cemented into place, it is necessary to perforate the intervals to be treated. Some general rules of thumb can be applied. Perforate the most brittle portion of the rock. Experience has shown that the more ductile portion of the formation is the most difficult to treat and typically does not take a significant (or any) portion of the hydraulic stimulation treatment. It is recommended that 2-foot intervals at each location be perforated using three shots per foot and 120° phasing, unless experience in the area has shown poor results. It is also recommended that the perforations be low-gram charges that will penetrate the casing, the cement, and a few inches into the formation (Kundert and Mullen, 2009).

Stimulations Fluids

The sensitivity of shale to particular fluids is critical information to ensure that the base fluid used for the stimulation treatment is compatible with the shale being treated. It may be possible to use fairly fresh water, or in some cases a particular brine may be necessary to minimize damaging the formation being treated. Usually hydraulic fracturing of shale uses extremely large volumes of fluids in order to contact a large sur-

face area of the formation. Fluid sensitivity tests can indicate whether or not a reactive fluid, such as acid, can help initiate the frack into the desired interval. Such tests are usually cheap insurance for proper fracture initiation and can make the difference between pumping a stimulation treatment or shutting down the entire treatment.

Since the permeability and porosity of shale are very low, the simpler the stimulation fluid the better. The overall goal is to minimize the risk of damaging the formation with stimulation fluids. The first choice of stimulation fluid is referred to as slick water with as few additives as possible, particularly gelling agents. For a slick water frack the primary additives are a friction reducer, breaker for the friction reducer, surfactant, biocide, and clay control if necessary. If possible, a microemulsion surfactant should be used if laboratory testing shows it is compatible. The brittleness of the shale plays an important part in selection of the stimulation fluid (table 10.5). In some cases it may be necessary to run gelled fluid, with or without a crosslinking agent, but one should use the least amount of gelling agent as possible. Also, a gelled fluid of any type should include plenty of breakers to minimize any potential gel damage. Typically, the addition of breakers to a gelled system is based on 80 to 90% of the bottom hole static temperature, and the final tank temperature plus 20°F (11°C). This usually gives adequate break to gelled fluid systems (Kundert and Mullen, 2009). The initial base fluid should be from a clean, reliable water source.

Another fluid system beneficial to hydrocarbon production in shale is a weak acid, commonly referred to as surface reactive fluid. This has been valuable even when the carbonate content in the shale is low because the surface reactive fluid can etch the face of the shale, providing a conduit for hydrocarbon production. It can also reduce high process zonal stress in the shale, which can lower the overall surface treating pressure (Kundert and Mullen, 2009).

Proppants are another essential element regardless of what type of fluid system is used. It is not uncommon to use very small proppant sizes such as 30/50 mesh, 40/70 mesh, or a combination of the several small-size proppants in very low proppant concentration. This is especially true when pumping slick water treatments because of the inability of slick water to transport large-size or highly concentrated proppants. However, when comparing the initial permeability of shale to

the fracture conductivity provided by the small and very low proppant concentration, the fractured shale has by far a higher permeability than the in-situ shale itself.

The results are still inconclusive on the use of high-strength proppant in slick water shale fracks, but closure stress on proppant should be considered when the stimulation fluid is gelled or crosslinked fluid. Gelled and crosslinked fluids carry larger size proppants and in higher concentrations than slick waters. In some areas 100 mesh sand is needed for fracking shales that exhibit an extensive fracture network; thus it is a good practice to have 100 mesh sand available while stimulating the initial exploration wells. Field experience will then dictate whether this is needed for full-scale development of the field.

Fluid Volumes

Shale fracks typically require very large volumes of fluid, especially when using slick water, which is the most common fluid system currently in use. The primary frack goal is to contact as much surface area as possible to create the largest fracture network. The recommendation is to begin with the larger end of the injection volume scale initially and then increase or decrease fluid volumes during the development stage. Fracture treatments typically are conducted at fairly high pump rates, in the 50 to 100 barrels per minute (BPM) (8–16 CPM) range, and can have fairly high treatment pressures, in some cases over 10,000 psi (69,000 kPa). These treatments typically require large pad sites (figure 10.4) and in some cases can take considerable up front planning to accomplish the stimulation portion in the shortest amount of time.

Table 10.5. General guide for stimulation fluid selections.

Rock Properties	Stimulation Fluid	Fluid Volume	Prop Concentration
Brittle	Slick Water	High	Low
Laminated	Hybrid		
Ductile	Liner or Cross-linked Gel	Low	High



Figure 10.4. Typical frack spread during stimulation treatments in shale. Note pit in the upper right used to store frack water.

Some general guidelines on determining how large a slick water treatment to pump are listed below (see also table 10.6).

- Fluid volume: ≈ 2000 gallons/foot (gals/ft) (24,840 L/m) in the brittle portion of the formation (e.g., 110 feet [34 m] of brittle shale $\times 2000$ gals/ft = 220,000 gals [845,000 L] of fluid).
- Proppant volume: ≈ 1000 pounds/foot (lbs/ft) (1490 kg/m) of the brittle portion of the formation (e.g., 110 feet [34 m] of brittle shale $\times 1000$ lb/ft = 110,000 lbs [50,700 kg] of proppant).
- Injection rates: 10 BPM (1.6 CMPM) minimum per injection point or 2 BPM (0.3 CMPM) per perforation (e.g., 5 entry points $\times 10$ BPM = 50 BPM [8 CMPM]; 30 perforations $\times 2$ BPM = 60 BPM [9.5 CMPM]); use 60 BPM (9.5 CMPM) as the designed pump rate.

The pumping injection rate is commonly stepped up over time to help pressure up the shale and the natural fracture system, should one exist. In some areas treatments have been known to prematurely pressure out well before pumping any proppant when the designed pump rate is reached immediately. Note that a volume for displacement is not listed above; this will depend on each well and should be determined for each individual interval prior to pumping the treatment. Spacers have also proven beneficial, since they appear to keep the

proppant from building up in the wellbore, in perforations, near the fracture face, and within the fracture itself.

Diagnostic Fracture-Injection Test

Prior to moving in all of the frack equipment and completing the first interval on the well, a diagnostic fracture-injection test (DFIT) can provide valuable information to further calibrate the petrophysical log model (Barree and others, 2007). Typically, the first interval is perforated, then a pump in test is conducted using fairly small volumes of fluid. The data are recorded in 1-second intervals for the pump-in and the fall-off. An electronic memory gauge is typically used because it provides the best accuracy during the test, and fall-off data are compiled for a minimum of 48 hours so that after closure the complete data are obtained. A successful DFIT test should provide the following information:

- bottom-hole treating pressure,
- bottom-hole closure pressure,
- process-zone stress,
- leak-off type,
- reservoir-pressure estimate, and
- permeability or permeability thickness (kH) estimates.

This test can provide invaluable information about the formation that can be used to calibrate stress and reservoir pressures

Table 10.6. Example of a typical slick water stimulation treatment.

Stage	Fluid	Pump Rate (BPM)	Fluid Volume (gals)	Proppant (#/gal)	Total Proppant (lbs)
Acid	7 ½% Acid	10	2000	-0-	-0-
Pad	Slick Water	20	10,000	-0-	-0-
Reactive Fluid	Weak Acid	20	10,000	-0-	-0-
Spacer	Slick Water	30	4000	-0-	-0-
0.5 #/gal 100 M	Slick Water	40	4400	0.50	2200
Spacer	Slick Water	50	6000	-0-	-0-
1.0 #/gal 100 M	Slick Water	60	8800	1.00	8800
Spacer	Slick Water	60	6000	-0-	-0-
0.5 #/gal 40/70	Slick Water	60	22,000	0.50	11,000
Spacer	Slick Water	60	8000	-0-	-0-
0.5 #/gal 40/70	Slick Water	60	22,000	0.50	11,000
Spacer	Slick Water	60	8000	-0-	-0-
0.75 #/gal 40/70	Slick Water	60	22,000	0.75	16,500
Spacer	Slick Water	60	8000	-0-	-0-
0.75 #/gal 40/70	Slick Water	60	22,000	0.75	16,500
Spacer	Slick Water	60	8000	-0-	-0-
1.0 #/gal 40/70	Slick Water	60	22,000	1.00	22,000
Spacer	Slick Water	60	6000	-0-	-0-
1.0 #/gal 40/70	Slick Water	60	22,000	1.00	22,000
Totals			221,200		110,000

in the petrophysical log model. The pressure dependent leak off can also indicate the presence of natural fractures within the reservoir.

Post-Stimulation Follow Up

Post-stimulation follow up is one of the most critical steps that must be taken to effectively evaluate the stimulation treatments and production results to determine if all of the intervals have been effectively treated. There are several approaches to evaluate the effectiveness of the stimulation treatment. One technique that has been used for many years is the radioactive tracer survey. Many different tracers can be used to tag various stages of the stimulation treatments and help identify what perforations accepted fluid and/or proppant and to some degree quantify the variations. Radioactive tracers are typically pumped inexpensively during the actual stimulation treatments. Once the well has been allowed to flow and is cleaned up, a tracer survey can be run to identify where the various tracers went, which aids in determining the effectiveness of the stimulation treatments.

Microseismic mapping is another invaluable tool especially in the early exploration phase of the process. Mapping is done in real time by running geophones into another well near the one to be treated. The fracture development can be monitored while the individual zones are being treated. The overall objective when fracturing a shale bed is to contact as much surface area as possible and to create a large, complex fracture network. The vertical and horizontal geometry of the fractures can be mapped, confirming the presence or lack of vertical barriers and giving an idea of the lateral extent away from the wellbore. An empirical relationship can be observed between fluid slurry volume used for the treatments and the overall extent of the microseismic events.

Finally, production logs are crucial in determining which intervals are contributing to the overall hydrocarbon production, and how much is being produced or not being produced from each interval. Tracer surveys and microseismic mapping along with production logs can help provide the information needed to determine why certain intervals are better than others. Production logs can also be related back to the organic richness and brittleness within the reservoir and to the associated fracture network that has been created. Routinely running production logs in all wells is recommended, both during the development stage and later as the field matures. This practice helps give a picture of how the reservoir is producing throughout the life of the field. Production logs can help identify problem zones before they become a field-wide problem, which can be costly to fix. A thorough post-stimulation evaluation allows lessons learned to be incorporated as early as possible to improve the overall stimulation process and production throughout the life of the field.

CASE STUDIES

Doughnut Formation (Manning Canyon Shale)

State 15-32-15-12 and State 16H-32-15-12 Wells

Bill Barrett State 15-32-15-12 (API No. 43-007-31366) was a pilot well drilled to test shale beds in the Doughnut Formation for natural gas. Information presented here was gathered from a public hearing held before the State of Utah, Department of Natural Resources, Board of Oil, Gas, and Mining on July 29, 2009 (Docket No. 2009-10, Cause No. 267-001). The State 15-32-15-12 well is located in SW1/4 SE1/4 section 32, T. 15 S., R. 12 E., SLB&M, Carbon County (see chapter 3 for details) (figure 10.5). The well is vertical and reached a total drilling depth of ~8550 feet (2606 m) in the Mississippian Humbug Formation. The top of the Doughnut is reported at 7585 feet (2312 m) and the top of Humbug is 8401 feet (2561 m). A core taken from the Doughnut from approximately 7550 to 7950 feet (2301–2423 m) contained total organic carbon up to 5% maximum. The natural fracture orientation within the shale is north to south. Gas shows are documented, but exact volumes were not revealed.

In the fall of 2008, Bill Barrett Corporation submitted an Application for Permit to Drill (APD) for a horizontal well with a drill pad located in the same section, east of the State 15-32-15-12 pilot well. The APD was approved January 22, 2009, for the State 16H-32-15-12 well (API No. 43-007-31482) located in the SE1/4 SE1/4 section 32, T. 15 S., R. 12 E., SLBL&M (figure 10.5). The well was spud on March 23, 2009, and completed November 2, 2009. Total drilling depth is 10,565 feet (3220 m) measured depth (MD) and 7923 feet (2415 m) true vertical depth (TVD). The well was plugged back to 10,499 feet (3200 m) MD. The formation at total depth is the Doughnut Formation, the top of which is at 7600 feet (2317 m) MD. The horizontal kickoff point is at 7168 feet (2185 m) MD and the total length of the horizontal section is approximately 3397 feet (1035 m). The well was drilled in a westerly direction and runs perpendicular to the natural fracture orientation (north-south) in the Doughnut (figures 10.6 and 10.7).

The State 16H-32-15-12 well was completed with 9-5/8 inch (24.5 cm) surface casing set at 1029 feet (314 m) MD using 560 sacks of cement, 7 inch (17.8 cm) intermediate casing set at 7066 feet (2154 m) MD using 560 sacks of cement, and 4-1/2 inch (11.4 cm) production casing set to 10,537 feet (3212 m) MD using 1050 sacks of cement. Logs run include composite resistivity, neutron-density, sonic, and mud log.

The production casing was perforated in 48 intervals of the Doughnut Formation from 8251 to 10,436 feet (2515–3181

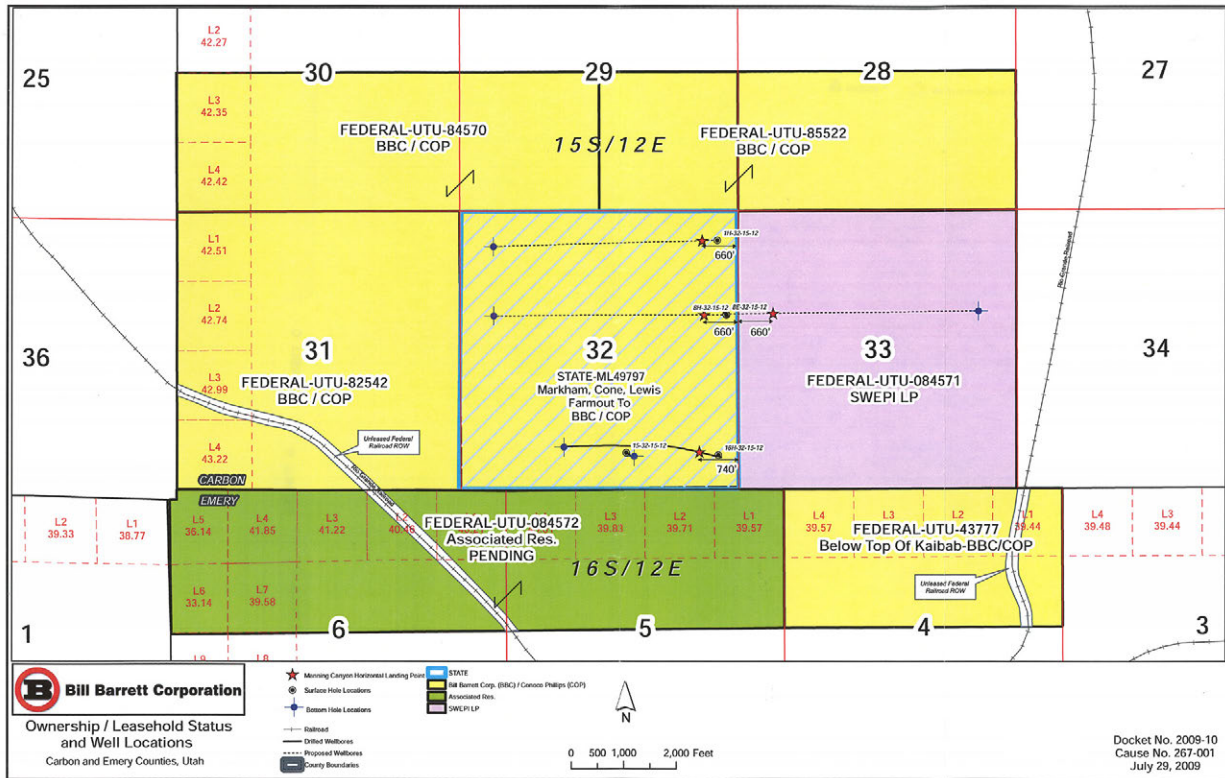


Figure 10.5. Ownership/leasehold status and well locations in 2009 for Bill Barrett Corporation, Carbon and Emery Counties, Utah (Utah Division of Oil, Gas, and Mining, 2009a).

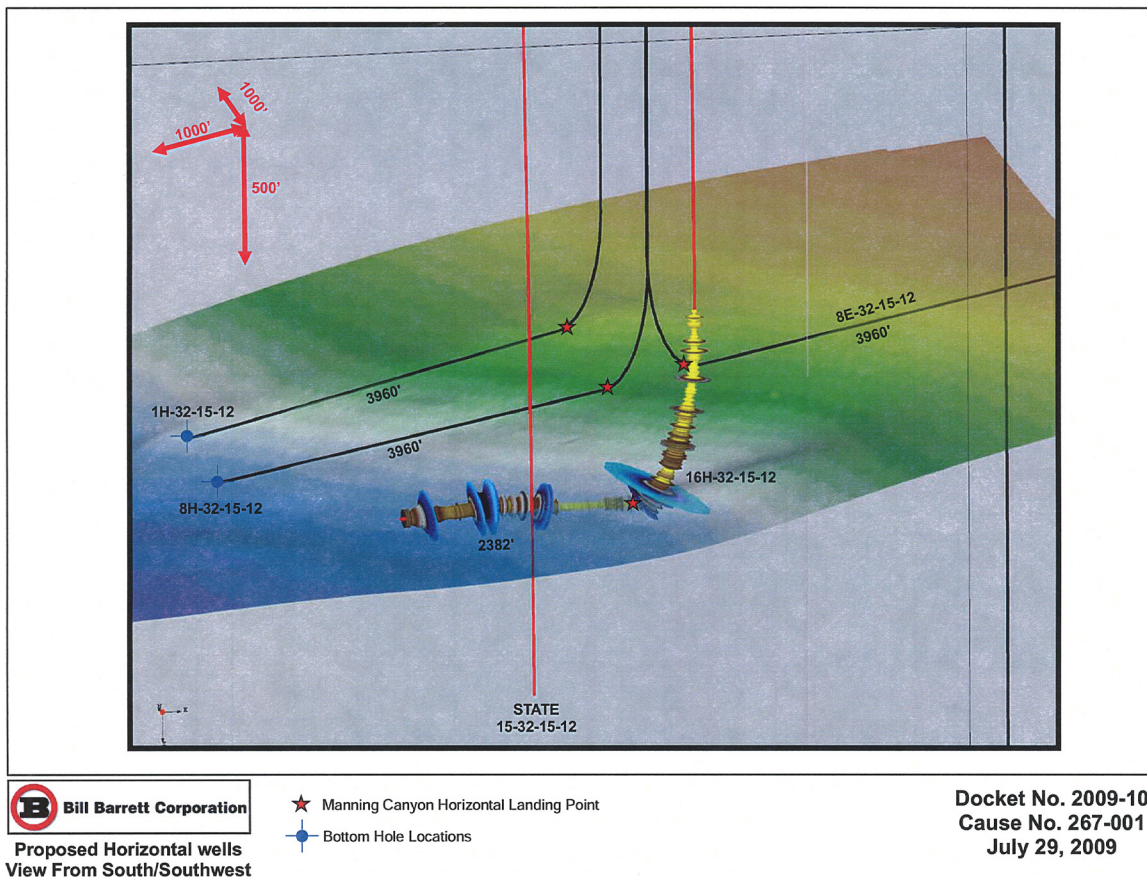


Figure 10.6. Proposed horizontal wells targeting shale in the Doughnut Formation (Manning Canyon Shale) by Bill Barrett Corporation in 2009; view from the south-southwest (Utah Division of Oil, Gas, and Mining, 2009b).

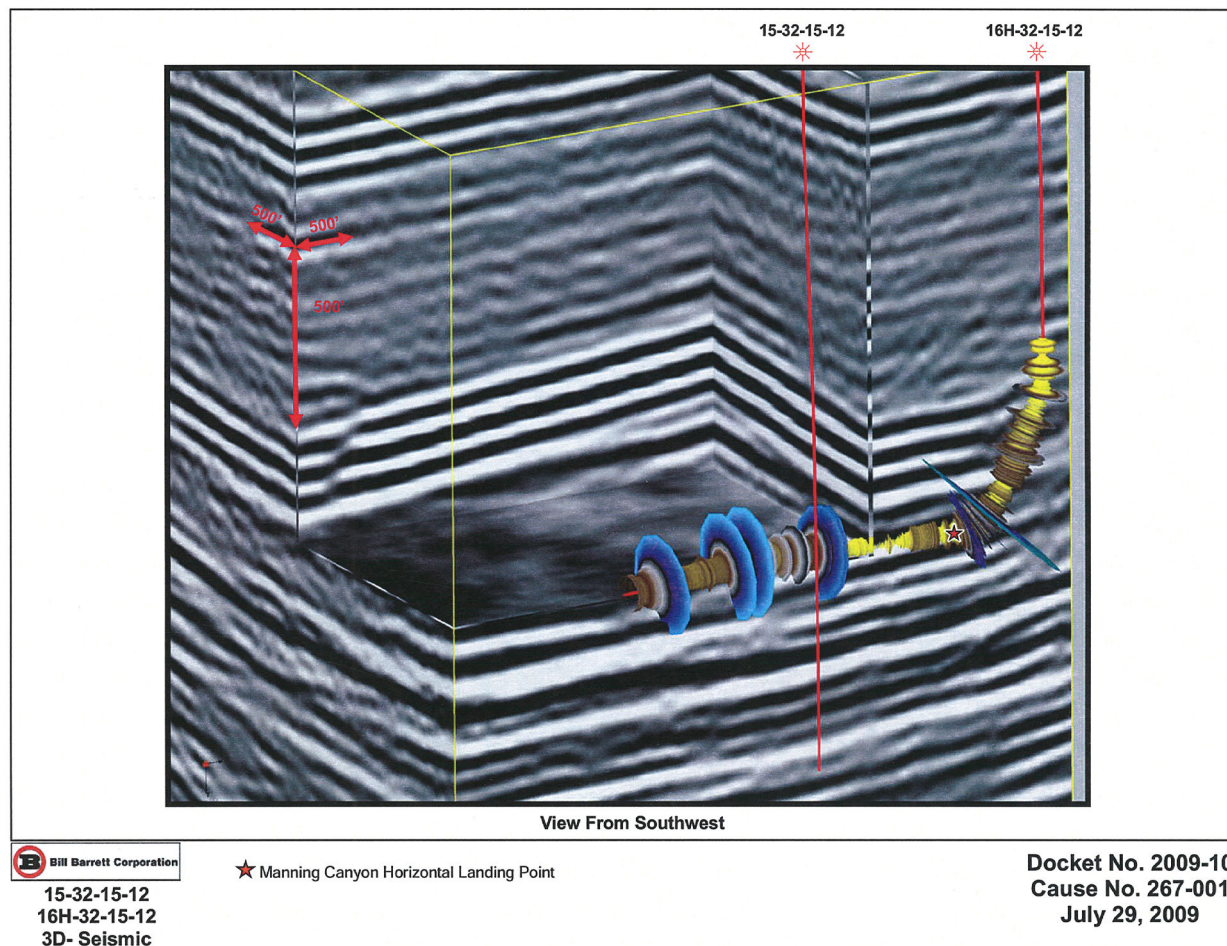


Figure 10.7. Doughnut Formation (Manning Canyon Shale) horizontal landing point for the Bill Barrett Corporation State 16H-32-15-12 well based on 3-D seismic (Utah Division of Oil, Gas, and Mining, 2009c).

m) MD using six jet shots per foot. The 48 intervals were grouped into eight stages and fracture stimulated.

- Stage 1, 10,166 to 10,436 feet (3099–3181 m) MD, was treated with 2500 gallons (9463 L) of 15% hydrochloric acid (HCl) and fracture stimulated with 110,740 gallons (419,151 L) of 3% potassium chloride (KCl) brine using 97,000 pounds (44,038 kg) of 100-mesh sand as a proppant.
- Stage 2, 9870 to 10,139 feet (3008–3090 m) MD, was treated with 2500 gallons (9463 L) of 15% HCl and fracture stimulated with 180,293 gallons (682,409 L) of 3% KCl brine using 40,700 pounds (18,478 kg) of 100-mesh sand and 43,800 pounds (19,885 kg) of 40/70-mesh sand as a proppant.
- Stage 3, 9575 to 9844 feet (2919–3000 m) MD, was treated with 2500 gallons (9463 L) of 15% HCl and fracture stimulated with 208,545 gallons (789,343 L) of 3% KCl brine using 41,900 pounds (19,023 kg) of 100-mesh sand and 44,300 pounds (20,112 kg) of 40/70-mesh sand as a proppant.
- Stage 4, 9280 to 9548 feet (2829–2910 m) MD, was treated with 2500 gallons (9463 L) of 15% HCl and fracture stimulated with 214,713 gallons (812,689 L) of 3% KCl brine using 44,500 pounds (20,203 kg) of 100-mesh sand and 62,700 pounds (28,466 kg) of 40/70-mesh sand as a proppant.
- Stage 5, 8985 to 9254 feet (2739–2821 m) MD, was treated with 2500 gallons (9463 L) of 15% HCl and fracture stimulated with 214,527 gallons (811,985 L) of 3% KCl brine using 42,500 pounds (19,295 kg) of 100-mesh sand and 52,000 pounds (23,608 kg) of 40/70-mesh sand as a proppant.
- Stage 6, 8690 to 8959 feet (2649–2731 m) MD, was treated with 2500 gallons (9463 L) of 15% HCl and fracture stimulated with 206,155 gallons (780,297 L) of 3% KCl brine using 55,000 pounds (24,970 kg) of 100-mesh sand and 73,300 pounds (33,278 kg) of 40/70-mesh sand as a proppant.
- Stage 7, 8395 to 8664 feet (2559–2641 m) MD, was treated with 2500 gallons (9463 L) of 15% HCl and fracture

stimulated with 220,057 gallons (832,916 L) of 3% KCl brine using 55,000 pounds (24,970 kg) of 100-mesh sand and 72,300 pounds (32,824 kg) of 40/70-mesh sand as a proppant.

- Stage 8, 8251 to 8369 feet (2515–2551 m) MD, was treated with 2900 gallons (109,765 L) of 15% HCl and fracture stimulated with 123,580 gallons (467,750 L) of 3% KCl brine using 53,120 pounds (24,117 kg) of 100-mesh sand and 36,500 pounds (16,571 kg) of 40/70-mesh sand as a proppant.

All stages tested were commingled over a 24-hour period and produced at a daily rate of 275 MCFG (7.79 MCMG) and 235 BW (37 CMW) through an 18/64-inch (0.7 cm) choke. The well, now owned by Whiting Oil & Gas Corporation, was shut-in upon completion and remains still shut-in.

Carbon Canal 5-12 Well

The Shell Western Exploration & Production, Inc. Carbon Canal 5-12 well (API No. 43-015-30709) is a wildcat drilled to explore and test the Doughnut Formation. The well is located in section 12, T. 16 S., R. 10 E., SLBL&M, Emery County and is a vertical well that was spud on August 8, 2007. Surface casing of 13-3/8 inch (34 cm) was set at 930 feet (284 m) using 990 sacks cement. Due to drilling problems, the well was plugged back to 1100 feet (335 m) and a vertical sidetrack was drilled from beneath the surface casing to the northeast. The well reached a total drilling depth of 9731 feet (2966 m) in the Humbug Formation. Core was taken from 8046 to 9352 feet (2452–2851 m) and extensively evaluated as part of this study (see chapters 4 through 7). According to the well completion report in DOGM files, the top of Doughnut is at 8573 feet (2613 m), but correlations as part of this project put the Doughnut between 8955 and 9378 feet (2729–2858 m) (see chapter 8). Open-hole wireline logs were run to a depth of 3400 feet (1036 m), but could go no farther. So the well was completed with a 9-5/8 inch (24.5 cm) intermediate casing set at 2170 feet (661 m) using 440 sacks cement, and 5-1/2 inch (14 cm) production casing set to 9682 feet (2951 m) using 1193 sacks cement. Casing-specific logs were run the length of the well and include resistivity, neutron-density, gamma-ray neutron, gamma-ray spectralog, sonic, and cement bond.

Shale beds in the Doughnut Formation were fracture stimulated and completed in four stages.

- Stage 1, from 9465 to 9514 feet (2885–2900 m), was perforated with 32 squeezed holes and fracture stimulated with 2175 barrels (346 m³) of high-rate water frack fluid (HRWF) and 102,000 pounds (46,308 kg) of 100 mesh and 40/70 mesh sand as a proppant.

- Stage 2, from 9315 to 9351 feet (2839–2850 m), was perforated with 28 open holes and fracture stimulated with 5720 barrels (910 m³) of HRWF and 43,000 pounds (19,522 kg) of 40/70 mesh sand.
- Stage 3, from 9125 to 9242 feet (2781–2817 m), was perforated with 36 open holes and fracture stimulated with 1846 barrels (294 m³) of HRWF and 346,000 pounds (157,084 kg) of 40/70 mesh sand.
- Stage 4, from 9030 to 9061 feet (2752–2762 m), was perforated with 40 open holes and fracture stimulated with 3369 barrels (536 m³) of HRWF and 64,000 pounds (29,056 kg) of 40/70 mesh sand.

Stage 1 was tested for 30 hours and flowed back a total of 644 BW (102 CMW) and no gas. The zone lost pressure and was plugged and abandoned. Stages 2, 3, and 4 were tested, commingled, and had an initial gas flow of 320 MCFGPD (9.06 MCMGPD). These zones were tested for 63 hours with a total of 468 MCFG (13.3 MCMG) and 1750 BW (278 CMW) produced through chokes ranging from 16/64 to 64/64 inch (0.6–2.5 cm). After a decline in pressure and cessation of flow, the stages were unsuccessfully stimulated with a coil tubing nitrogen lift to try to re-establish flow. Initial gas composition is reported as 93% methane, 4% ethane, 1.4% nitrogen, and 0.5% carbon dioxide. The well was completed on April 6, 2008, and has been shut-in since; Whiting is also the current operator.

Gothic Shale, Paradox Formation

In the Colorado side of the Paradox Basin, Bill Barrett Corporation conducted an extensive horizontal drilling exploration and development program for the Gothic and Hovenweep shales beginning in 2008. The total organic carbon of the Gothic ranges from 1 to 2%, maturity (as R_o) is from 1.0 to 1.5%, and gas content is about 50 standard cubic feet per ton (1.6 m³/Mg); these data yield a gas in place estimate of 50 BCF (1.4 BCM) per section. The reservoir pressure and average fracture gradient ranged from 0.5 to 0.59 and 1.0 to 1.2 psi/ft (11–13 and 23–27 kPa/m), respectively. The bottom-hole temperatures ranged from 130 to 150°F (54–66°C). The principle fracture orientation was east-west.

Wells targeted a single zone, ranging in thickness from 80 to 160 feet (24–48 m) at a TVD of about 5000 to 7000 feet (1500–2100 m). The average horizontal length drilled was 4000 feet (1200 m). These wells are generally completed using un-cemented swell packers and require an average of 10 frack stages. For perforating, both Delta Stim Sleeves™ and “plug and perf” methods have been used. Well problems include high process-zone stress (PZS) and saturated saltwater production. Rapid production declines also proved disappointing in the Bill Barrett wells in Colorado.

Frack Fluids and Proppants

A variety of frack fluids are preferred in the treatments of the Gothic shale, including iron sequestering agents, corrosion inhibitors, surfactants, friction reducers, and bactericides. These are outlined below.

1. 15% HCl acid spearhead of approximately 1000 gallons (3785 L) volume:
 - a. 20 gal/1000 gal (20 L/1000 L) FE-1A™ iron sequestering agent,
 - b. 100 lb/1000 gal (12.0 kg/1000 L) FE-2™ iron sequestering agent,
 - c. 10 gal/1000 gal (10 L/1000 L) Musol® A solvent,
 - d. 2 gal/1000 gal (2 L/1000 L) HAI-404 M™ corrosion inhibitor, and
 - e. 2 gal/1000 gal (2 L/1000 L) LoSurf-300™ surfactant.
2. ShaleFrac RF™ reactive fluid of approximately 10,000 gallons (37,850 L) per stage:
 - a. formulate the ShaleFrac RF™ by diluting one part of the 15% HCl spearhead acid with four parts freshwater,
 - b. 1 gal/1000 gal (1 L/1000 L) FR-48W™ for friction reduction, and
 - c. 0.5 gal/1000 gal (0.5 L/1000 L) SuperFlo 2000™ microemulsion surfactant.
3. Friction-reducer (FR) water for main frack fluid:
 - a. freshwater base fluid,
 - b. 0.5 gal/1000 gal (0.5 L/1000 L) FR-66™ friction reducer,
 - c. 0.5 gal/1000 gal (0.5 L/1000 L) SuperFlo™ 2000 microemulsion surfactant,
 - d. 0.25 gal/1000 gal (0.25 L/1000 L) LoSurf-300™ surfactant, and
 - e. 0.5 gal/1000 gal (0.5 L/1000 L) BE-7™ bactericide.

It is important to be prepared for worst-case conditions by having chemicals for linear gel formulation on location. Some well conditions may require switching from FR water to linear gel to overcome PZS or other injection problems.

The preferred proppants for treatments of the Gothic shale are (1) 100 mesh sand for leakoff control and propping/wedging of natural fissures, and (2) 40/70 or 30/50 mesh White Jordan™.

Pumping Conditions

The frack treatment is pumped down the casing, typically 4-1/2 inch (11.4 cm). The average pumping rate is 50 to 70

BPM (8–11 MCPM). The average wellhead tubing pressure is 6000 psi (41,000 kPa), with pressure sometimes as high as 7500 psi (52,000 kPa). Table 10.7 is a typical pumping schedule for a Gothic shale frack treatment.

Job Design

The horizontal lateral is divided into segments or compartments using swelling packers. Maximum compartment lengths are about 500 feet (150 m) with 300-foot (90 m) compartments recommended. A single Delta Stim Sleeve™ is centered in each compartment interval.

The proppant weight is determined by multiplying the compartment length times shale thickness times a factor of 5. For example, a 300-foot (90-m) compartment length times a 100-foot-thick (30 m) shale times 5 = 150,000 pounds (68,000 kg) of proppant. All proppants including 100 mesh sand are included in the proppant total weight. The fluid volume is based on an approximate overall proppant concentration of 0.5 pound/gallon (0.06 kg/L). For example, 150,000 pounds (68,000 kg) of proppant requires about 300,000 gallons (1,140,000 L) of fluid.

SUMMARY

Although gas production from shale predates commercially drilled oil production by approximately 35 years, the commercialization of producing hydrocarbons from shale did not begin on a very large scale until the mid 1990s. Shale occurs in most oil and gas fields that have been producing from conventional wells. These shale beds hold great potential for producing both natural gas and oil, but all shale beds are not the same. Successful and effective drilling and completion of shale wells requires a good understanding of the formation that is to be completed. A comprehensive development plan is required. This plan must include a step by step, systematic procedure for evaluation and stimulation of the shale reservoir, while gathering data to refine the process so that commercial production is obtained. The methods discussed in this chapter are designed to provide an operator a general idea of what needs to be done in order to develop shale into a productive asset. Some of the major elements of a successful shale reservoir program are:

- plan the shale well (horizontal laterals appear to give the best results),
- gather reservoir data,
- build a petrophysical model,
- calibrate the model,
- plan and execute the stimulation treatment,
- conduct post-stimulation follow up, and
- refine the program.

The potential Paleozoic shale gas reservoirs include the Mississippian/Pennsylvanian Doughnut Formation and the Chimney Rock, Gothic, and Hovenweep shales in the Pennsylvanian Paradox Formation. Even though numerous wells penetrate these units, very few attempts to produce from them have been made. In spite of limited shale gas drilling in Utah,

the information provided here is offered as preliminary best practices for operators to use in exploring and developing the potential of Utah's Paleozoic shale reservoirs.

*Note: the Utah Geological Survey does not endorse or promote any particular product or service.

Table 10.7. Pumping schedule for Gothic shale completion.

Event	Stage Description	Stage Volume (gal)	Slurry Rate (BPM)	Prop Conc (gal)	Stage Prop (lbs)	Prop Type	Prop Mesh Size
1	15% Double Strength FE	2000	10		0		
2	Water Flush	15,000	20		0		
3	ShaleFrac RF	10,000	25		0		
4	Fresh Water - Step Up	15,000	30		0		
5	Fresh Water - Step Up	15,000	35		0		
6	Fresh Water - Step Up	15,000	40		0		
7	Fresh Water - Step Up	15,000	45		0		
8	FW 100 Mesh Sand Slug	8000	50	0.25	2000	Sand	100
9	Fresh Water Sweep	10,000	55		0		
10	FW 100 Mesh Sand Slug	15,000	60	0.5	7500	Sand	100
11	Fresh Water Sweep	10,000	65		0		
12	FW 100 Mesh Sand Slug	15,000	65	1	15,000	Sand	100
13	Fresh Water Sweep	10,000	65		0		
14	FW 40/70 Mesh Sand	30,000	65	0.25	7500	Sand	40/70
15	FW 40/70 Mesh Sand	30,000	65	0.5	15,000	Sand	40/70
16	Fresh Water Sweep	10,000	65		0		
17	FW 40/70 Mesh Sand	30,000	65	0.5	15,000	Sand	40/70
18	FW 40/70 Mesh Sand	30,000	65	0.6	18,000	Sand	40/70
19	Fresh Water Sweep	10,000	65		0		
20	FW 40/70 Mesh Sand	25,000	65	0.7	17,500	Sand	40/70
21	FW 40/70 Mesh Sand	20,000	65	0.8	16,000	Sand	40/70
22	Fresh Water Sweep	10,000	65		0		
23	FW 40/70 Mesh Sand	20,000	65	1	20,000	Sand	40/70
24	FW 40/70 Mesh Sand	20,000	65	1.25	25,000	Sand	40/70
25	Fresh Water Sweep	10,000	65		0		
26	FW 40/70 Mesh Sand	15,000	65	1.25	18,750	Sand	40/70
27	FW 40/70 Mesh Sand	15,000	65	1.5	22,500	Sand	40/70
28	Fresh Water Flush	6000	65		0		
	Totals	436,000			199,750		
	Repeat Schedule for each Frack Stage						

CHAPTER 11: CONCLUSIONS AND PLAY AREA "SWEET SPOTS"

BY

S. Robert Bereskin, *Bereskin and Associates, Inc.*;
Steven Schamel, *GeoX Consulting, Inc.*;
Thomas C. Chidsey, Jr., *Utah Geological Survey*

CONTENTS

MANNING CANYON SHALE/DOUGHNUT FORMATION	221
PARADOX FORMATION	221
BEST COMPLETION PRACTICES	222

CHAPTER 11:

CONCLUSIONS AND PLAY AREA "SWEET SPOTS"

Paleozoic shales in Utah have significant untapped gas potential. The shales include the Mississippian/Pennsylvanian Manning Canyon/Doughnut and Pennsylvanian Paradox Formations of central and southeastern Utah (Paradox Basin), respectively. Shale beds within these formations are widespread, thick, buried deep enough to generate dry gas (or oil in some areas of the Paradox Basin), and sufficiently rich in organic material and fractures to hold significant recoverable gas reserves. "Sweet spots" are areas identified in central Utah and the Paradox Basin that have the greatest shale-gas potential and should be targeted for exploration (figure 1.2).

MANNING CANYON SHALE/ DOUGHNUT FORMATION

- The greatest Manning Canyon Shale/Doughnut Formation potential is a 600-square-mile (1600 km²) area at the north end of the San Rafael Swell in central Utah. Gas tests and shows are reported from many of the exploration wells in this area.
- The Doughnut Formation is 400 to 1200 feet (130–400 m) thick; average depth to the top of the formation is 7470 feet (2280 m) at the north end of the San Rafael Swell. Four major lithotypes are (1) carbonate, (2) fine-grained quartz sand and silt, (3) illite, smectite, and chlorite clays, and (4) organic matter composed dominantly of degraded fragments of terrestrial plants. This organic matter has good to excellent richness (TOC up to 15%) distributed throughout the shale, limestone, and even siltstone. Vitrinite reflectance indicates that the kerogen is in the dry gas thermal maturity window.
- The pore systems in most of the Doughnut Formation shale consist of poorly interconnected micropores that contribute to very low permeability. Brittle silty shale beds could be susceptible to fracturing (both hydraulically induced and natural). Without natural or artificially induced fractures, the Doughnut in the northern San Rafael Swell area has very poor reservoir potential.
- The Manning Canyon/Doughnut lacks the cyclicity and lateral continuity found in many Carboniferous cyclothems units. It may have been deposited in a shallow, organic-rich, restricted-marine, brackish, and freshwater setting not unlike the modern Everglades and Florida Bay.
- The burial histories and models of organic maturation for the Manning Canyon/Doughnut at 21 sites in northern Utah show that it is thermally mature to post-mature at all of them. The times at which the Manning Canyon was mature for oil and gas vary widely, from Middle Pennsylvanian to Early Cretaceous for entry into the oil window, to Early Permian to Eocene for entry into the wet gas window. The Manning Canyon is most mature in a northwest-trending zone that coincides with the late Paleozoic Oquirrh basin. Away from this zone the Manning Canyon (Doughnut) reached organic maturity at progressively later times, most recently in the Uinta Basin, the south-central Sevier thrust belt, and the northern San Rafael Swell. The distribution of maturation ages in the various tectonic settings indicates that in most areas hydrocarbon generation predated events that may have created structural traps. However, at the northern San Rafael Swell and the south-central thrust belt gas generation coincided with or post-dated structuring.
- The Doughnut Formation is often referred to as Manning Canyon Shale, but significant differences exist. We restrict the Manning Canyon to the allochthonous rocks of the eastern Basin and Range Province and central Utah thrust belt, and the Doughnut to the autochthonous rocks of central and eastern Utah. Based on palynomorphs extracted from samples of the limited outcrops and from well cuttings, the Manning Canyon is middle to late Chesterian (possibly as young as Morrowan). The Doughnut is late Meramecian through late Chesterian, equivalent to the Manning Canyon and underlying Great Blue Limestone in the Basin and Range Province.

PARADOX FORMATION

- Within the Paradox Formation, the Chimney Rock, Gothic, and Hovenweep shales have the greatest shale-gas potential and are the principal targets of exploration. The Colorado part of the Paradox Basin has seen some moderate success, particularly for the Gothic shale zone, using horizontal drilling.
- Two unconventional assessment units (AU) in the Paradox Formation, defined by the U.S. Geological Survey (2012), consist of potential shale gas zones: the Gothic, Chimney Rock, Hovenweep Shale Gas AU and the Gothic, Chimney Rock, Hovenweep Shale Oil AU. The oil and gas AUs are separated by a maturation boundary where $R_o = 1.1\%$. The more mature gas-prone shale zones are located in the deep-

er northeast part of the basin (Paradox fold and fault belt) parallel to the Uncompahgre uplift. The Gothic, Chimney Rock, Hovenweep Shale Gas AU was assessed to contain a mean of 6490 BCFG (184 BCMG); the Gothic, Chimney Rock, Hovenweep Shale Oil AU was assessed to contain a mean of 256 million barrels of oil (40.7 MMCM) and 205 BCF (5.8 BCM) of associated gas (U.S. Geological Survey, 2012).

- Within the Paradox fold and fault belt, in structurally low areas beyond the salt walls or synclines parallel to the anticlines, one can expect less deformation, thicker deposits, and shale zones possibly in the gas generation window and retained natural gas (Schamel, 2005, 2006). Thus, structurally low or synclinal areas remain untested over a significant area.
- Individual shale units generally range in thickness between 25 and 50 feet (8 and 15 m); the cumulative shale thickness is typically 100 to 200 feet (30–60 m). The average depths to these units range from 5800 to 6500 feet (1900–2200 m). These dark-colored shale (mudrock) beds contain organic matter, but their overall organic content is diluted by significant percentages of numerous minerals, including quartz, feldspar, calcite, dolomite, pyrite, phosphate, and clays. As a result, TOC levels usually are modest (1.5 to 3%) in spite of the carbonate maceration associated with the TOC process. For the most part, the maturation levels of the organic carbon fall in the oil or oil-gas windows according to pyrolysis and vitrinite reflectance measurements.
- Compared to other productive North American Paleozoic “shale” reservoirs, the Pennsylvanian Paradox Basin mudrocks possess limited reservoir quality in terms of matrix characteristics. In the Hovenweep and Gothic shales, porosities are all less than 4%, and gas-filled porosities range from 1 to 3%; permeabilities using tight rock analysis usually fall at 100 nD or below. Most of the matrix porosity is attributable to clay micropores in shale and to microintercrystalline porosity in the dolomite interbeds. Production from the Gothic and Hovenweep shales is possibly related to both interstitial and desorbed gas.
- Some natural fractures (usually on the crest of anticlinal closures) in Chimney Rock, Gothic, and Hovenweep shales and related carbonate beds (mostly dolomite) may serve to enhance permeability, but most fractures are healed by calcite. More importantly, these fractures likely represent zones of weakness and could probably re-open during any stimulation procedure, as suggested from triaxial testing.
- The interbedded dolomite may be the key to economic production levels, as it commonly possesses acceptable porosity/permeability levels. Many carbonate units were apparently not recognized as porous dolomite because

open-hole logging in this region commonly involved using a density tool calibrated on a 2.71 g/cm (limestone) matrix density, erroneously revealing very low matrix porosities. If the density logging had used proper calibration (2.80 g/cm, or somewhat less), the resulting porosities would have been more encouraging, ranging from 4 to 11%.

- Vertical wells already produce modestly from the Gothic shale within southeastern Utah. Some gas and occasional slugs of oil come from these few wells; no horizontal wells have yet been drilled, due mostly to recent low natural gas prices. Where these hydrocarbons come from is somewhat conjectural at this point, but one production log, run after hydraulic fracturing, strongly suggests that the uppermost perforations within the mudstone probably represent the major source. Not surprisingly, these perforations are immediately below a series of overlying dolomites. Alternatively, these largely gaseous recoveries in oil-prone rocks could originate from a complex pressure-volume-temperature relationship downhole. Thus, this shale play is likely an intermixed series of reservoir types, all of which could produce upon successful stimulation.

BEST COMPLETION PRACTICES

- Although numerous wells penetrate the Manning Canyon/Doughnut and the Chimney Rock, Gothic, and Hovenweep shales, there have been very few attempts to produce any of them. These shale beds are not the same and a comprehensive completion plan is needed for each. This plan must include a step-by-step, systematic procedure for development, evaluation, and stimulation of the shale reservoir while gathering data to refine the process so that commercial production is obtained economically. Some of the major focuses are as follows: plan the well (horizontal laterals appear to give the best results), gather the reservoir data, build a petrophysical model, calibrate the model, plan and execute the stimulation treatment, conduct post-stimulation follow-up, and refine the process.
- Horizontal wellbores are recommended instead of vertical wellbores regardless of the thickness of the shale. However, in extremely thick shale intervals it might be necessary to drill vertically through the entire shale section to gather the necessary geochemical and geomechanical properties to determine where best to drill the horizontal section of the well.
- An expandable liner hanger should be used to hang off the liner in the intermediate casing. Swell packers with mechanical sliding sleeves effectively isolate and treat fairly long horizontal sections of the wellbore from the toe to the heel.

- Perforate the most brittle part of the section at 2-foot (0.6 m) intervals at each location using three shots per foot and 120° phasing. The perforations should be low-gram charges that will penetrate the casing, cement, and a few inches into the formation.
- The first choice of stimulation fluid is slick water with as few additives as possible, particularly gelling agents. For a slick water frack the primary additives are a friction reducer, breaker for the friction reducer, surfactant, biocide, and clay control if necessary. If possible, the stimulation should employ a microemulsion surfactant if laboratory testing shows it is compatible. The frack job should use very small proppant sizes, such as 30/50 mesh, 40/70 mesh, or a combination of the several small-size proppants, in very low proppant concentration. This is especially the case when pumping slick water treatments because of the inability for slick water to transport large-sized proppants and higher proppant concentrations. In terms of fluid volumes, the recommendation is to begin with the larger end of the injection volume scale initially and then increase or decrease fluid volumes during the development stage. Successful treatments typically are at fairly high pump rates in the 50 to 100 BPM (8–16 CPM) range and can have fairly high treating pressures, in some cases over 10,000 psi (69,000 kPa).
- For post-stimulation follow-up, radioactive tracers, microseismic mapping, and production logs are recommended to effectively evaluate the stimulation and production results.

ACKNOWLEDGMENTS & REFERENCES

CONTENTS

ACKNOWLEDGMENTS	227
REFERENCES	227

ACKNOWLEDGMENTS

Funding for this project was provided by the Research Partnership to Secure Energy for America (RPSEA) through the “Ultra-Deepwater and Unconventional Natural Gas and Other Petroleum Resources” program authorized by the U.S. Energy Policy Act of 2005. RPSEA (www.rpsea.org) is a nonprofit corporation whose mission is to provide a stewardship role in ensuring the focused research, development, and deployment of safe and environmentally responsible technology that can effectively deliver hydrocarbons from domestic resources to the citizens of the United States. RPSEA, operating as a consortium of premier U.S. energy research universities, industry, and independent research organizations, manages the program under a contract with the U.S. Department of Energy’s National Energy Technology Laboratory.

The research for the *Paleozoic Shale-Gas Resources of the Colorado Plateau and Eastern Great Basin, Utah*, project was performed under the direction of the Utah Geological Survey (UGS), Thomas C. Chidsey, Jr., Principal Investigator. Partial funding was also provided by the UGS. Other partners and contributors for this project include Bereskin and Associates, Inc., GeoX Consulting, Inc., and Halliburton Energy Services. Shell Exploration and Production and ST Oil Company generously donated core and data for this project. Andrew Henriksen, University of Utah, kindly provided geothermal well data for use in maturation models.

Vicky Clarke, Cheryl Gustin, Jim Parker (deceased), Jay Hill, Richard Austin, Stevie Emerson, Lori Steadman, and Jeremy Gleason of the UGS, drafted figures. Michael D. Laine, Thomas Dempster, Brad Wolverton, Ammon McDonald, and Chad Lyman of the Utah Core Research Center prepared samples for thin-section and geochemical analysis and photographed core. Peter Nielsen and Steve Herbst of the UGS conducted X-ray diffraction and X-ray fluorescence analyses. Nikki Simon of the UGS prepared the layout and design of this publication.

This report was reviewed by Richard D. Fritz and Daniel Bassett, SM Energy, Tulsa, Oklahoma; Charlotte Schroeder, RPSEA, Sugar Land, Texas; and David Tabet, Mike Hylland, Robert Resselar (retired), Kimm Harty (retired), and Richard G. Allis, UGS. Their careful reviews and constructive criticism greatly improved the manuscript.

REFERENCES

- Allen, P.A., and Allen, J.R., 2005, Basin analysis—principles and applications (second edition): Malden, Massachusetts, Blackwell Publishing Ltd., 549 p.
- Allmendinger, R.W., and Jordan, T.E., 1989, Geologic map of the Newfoundland Mountains, northwestern Utah: U.S. Geological Survey, Miscellaneous Field Studies Map MF-2087, scale 1:31,680.
- Allmendinger, R.W., and Platt, L.B., 1983, Stratigraphic variation and low-angle faulting in the North Hansel Mountains and Samaria Mountain, southern Idaho, in Miller, D.M., Todd, V.R., and Howard, K.A., editors, Tectonic and stratigraphic studies in the eastern Great Basin, Geological Society of America Memoir 157, p. 149–163.
- Anderson, P.B., Willis, G.C., Chidsey, T.C., Jr., and Sprinkel, D.A., 2010, Geology of Glen Canyon National Recreation Area, Utah-Arizona, in Sprinkel, D.A., Chidsey, T.C., Jr., and Anderson, P.B., editors, Geology of Utah’s parks and monuments (3rd edition): Utah Geological Association Publication 28, p. 309–347.
- Anna, L.O., Roberts, N.R., and Potter, C.J., 2007, Geologic assessment of undiscovered oil and gas in the Paleozoic-Tertiary composite total petroleum system of eastern Great Basin, Nevada and Utah, in U.S. Geological Survey Eastern Great Basin Province Assessment Team, Geologic assessment of undiscovered oil and gas resources of the eastern Great Basin Province, Nevada, Idaho, and Arizona: U.S. Geological Survey Digital Data Series DDS-69-L, version 1.0, 79 p.
- Asquith, G., and Krygowski, D., 2004, Basic well log analysis: American Association of Petroleum Geologists Methods in Exploration Series, No. 16, 244 p.
- Armstrong, R.L., 1968, Sevier orogenic belt in Nevada and Utah: Geological Society of America Bulletin, v. 79, p. 429–458.
- Baars, D.L., Parker, J.W., and Chronic, J., 1967, Revised stratigraphic nomenclature of Pennsylvanian System, Paradox Basin: American Association of Petroleum Geologists Bulletin, v. 51, no. 3, p. 393–403.
- Baars, D.L., and Stevenson, G.M., 1981, Tectonic evolution of the Paradox Basin, Utah and Colorado, in Wiegand, D.L., editor, Geology of the Paradox Basin: Rocky Mountain Association of Geologists Guidebook, p. 23–31.
- Baer, J.L., and Rigby, J.K., 1980, Geologic guide to Provo Canyon and Weber Canyon, central Wasatch Mountains, Utah: Brigham Young University Geology Studies, v. 27, pt. 3, 24 p.
- Bahlburg, H., and Dobrzinski, N., 2009, A review of the chemical index of alteration (CIA) and its application to the study of Neoproterozoic glacial deposits and climate transitions, in Arnaud, E., Halverson, G.P., and Shields, G.A., editors, The geological record of Neoproterozoic glaciations: London, Geological Society Memoir 36, p. 81–92.
- Baker, A.A., 1947, Stratigraphy of the Wasatch Mountains in the vicinity of Provo, Utah: U.S. Geological Survey Oil and Gas Investigations preliminary Chart 30.
- Baker, A.A., Dane, C.H., and Reeside, J.B., Jr., 1933, Paradox Formation of eastern Utah and western Colorado: American Association of Petroleum Geologists Bulletin, v. 17, p. 963–980.

- Baker, A.A., Huddle, J.W., and Kinney, D.M., 1949, Paleozoic geology of the north and west sides of Uinta Basin, Utah: *American Association of Petroleum Geologists Bulletin*, v. 33, no. 7, p. 1161–1197.
- Barker, C.E., 2000, A paleolatitude approach to assessing surface temperature history for use in burial heating models: *International Journal of Coal Geology*, v. 43, p. 121–135.
- Barker, K.S., and Barker, S.W., 1993, Interim geologic map of the Wellsville quadrangle, Cache County, Utah: Utah Geological Survey Contract Report 93-2, 17 p., 2 plates, scale 1:24,000.
- Barree, R., Barree, V., and Craig, D., 2007, Holistic fracture diagnostics: Society of Petroleum Engineers, Rocky Mountain Oil & Gas Technology Symposium, Denver, Colorado, SPE Paper 107877.
- Bebout, D.G., and Loucks, R.G., 1984, Handbook for logging carbonate rocks: Bureau of Economic Geology, University of Texas at Austin, Handbook 5, 43 p.
- Beck, T., 2010, Sediment characteristics and distribution along the west-central Florida inner shelf, *in* west Florida shelf—a natural laboratory for the study of ocean acidification: U.S. Geological Survey Open-File Report 2010-1134, p. 9–14.
- Bereskin, S.R., and McLennan, J., 2008, Hydrocarbon potential of Pennsylvanian black shale reservoirs, Paradox Basin, southeastern Utah: Utah Geological Survey Open-File Report 534, 53 p.
- Berner, R.A., 1971, Principles of chemical sedimentology: New York, McGraw-Hill, 240 p.
- Berner, R.A., 1981, A new geochemical classification of sedimentary environments: *Journal of Sedimentary Petrology*, v. 51, p. 359–365.
- Biek, R.F., 1991, Provisional geologic map of the Nephi quadrangle, Juab County, Utah: Utah Geological Survey Map 137, 21 p., 2 plates, scale 1:24,000.
- Biek, R.F., 2004, Geologic map of the Saratoga Springs quadrangle, Utah County, Utah: Utah Geological Survey Map 201, 2 plates, scale 1:24,000.
- Biek, R.F., Clark, D.L., and Christiansen, E.R., 2009, Geologic map of the Soldiers Pass quadrangle, Utah County, Utah: Utah Geological Survey Map 235, 3 plates, scale 1:24,000.
- Biek, R.F., Solomon, B.J., Keith, J.D., and Smith, T.W., 2005, Geologic map of the Tickville Spring quadrangle, Salt Lake and Utah Counties, Utah: Utah Geological Survey Map 214, 2 plates, scale 1:24,000.
- Bissell, H.J., 1950, Carboniferous and Permian stratigraphy of the Uintah Basin area, *in* Guidebook to the geology of Utah No. 5, petroleum geology of the Uinta Basin: Intermountain Association of Petroleum Geologists, p. 71–96.
- Bissell, H.J., 1952, Stratigraphy and structure of northeast Strawberry Valley quadrangle, Utah: *American Association of Petroleum Geologists Bulletin*, v. 36, p. 575–634.
- Bissell, H.J., and Barker, H.K., 1977, Deep-water limestones of the Great Blue Formation (Mississippian) in the eastern part of the Cordilleran miogeosyncline in Utah, *in* Cook, H.E., and Enos, P., editors, Deep-water carbonate environments: Society for Sedimentary Geology (SEPM) Special Publication 25, p. 171–186.
- Blakey, R.C., 1997, Paleogeographic evolution of the passive-margin to active-margin transition, early Mesozoic, western North America [abs.]: Geological Society of America Abstracts with Programs, v. 29, no. 6, p. 202, accessed May 10, 2010, at <http://jan.ucc.nau.edu/rcb7/paleogeogwus.html>.
- Blakey, R.C., 2005, Paleogeography and tectonic evolution of late Paleozoic sedimentary basins, southwestern North America [abs.]: Geological Society of America Abstracts with Programs v. 37, no. 7, p. 442: Online at <http://jan.ucc.nau.edu/rcb7/garm.html>, last accessed March 17, 2008.
- Blakey, R.C., 2009, Paleogeography and geologic history of the western Ancestral Rocky Mountains, Pennsylvanian-Permian, southern Rocky Mountains and Colorado Plateau, *in* Houston, W.S., Wray, L.L., and Moreland, P.G., editors, The Paradox Basin revisited—New developments in petroleum systems and basin analysis: Rocky Mountain Association of Geologists Special Publication, p. 222–264.
- Bosence, D.W.J., 1995, Anatomy of a Recent biodetrital mud-mound, Florida Bay, USA, *in* Monty, C.L.V., Bosence, D.W.J., Bridges, P.H., and Pratt, B.R., editors, Carbonate mud-mounds: their origin and evolution: Oxford, Blackwell Science, p. 475–493.
- Bonelli, J.R., Jr., and Patzkowsky, M.E., 2011, Taxonomic and ecologic persistence across the onset of the late Paleozoic ice age: evidence from the Upper Mississippian (Chesterian Series), Illinois basin, United States: *PALAIOS*, v. 26, p. 5–17.
- Burchfiel, B.C., Lipman, P.W., and Zoback, M.L., editors, 1992, The Cordilleran orogen—conterminous U.S.: Geological Society of America, Decade of North American Geology, 734 p.
- Bryant, B., 1990, Geologic map of the Salt Lake City 30' x 60' quadrangle, north-central Utah, and Uinta County, Wyoming: U.S. Geological Survey Miscellaneous Investigations Series Map I-1944, 2 plates, scale 1:100,000.
- Bryant, B., 1992, Geologic and structure maps of the Salt Lake City 1° x 2° quadrangle, Utah and Wyoming: U.S. Geological Survey Miscellaneous Investigations Series Map I-1997, 3 plates, scale 1:125,000.
- Butkus, T.A., 1975, Sedimentary and depositional environments of the Great Blue Limestone (Late Mississippian), north central Utah: Salt Lake City, University of Utah, M.S. thesis, 142 p.

- Butts, S.H., 2005, Latest Chesterian (Carboniferous) initiation of Gondwanan glaciation recorded in facies stacking patterns and brachiopod paleocommunities of the Antler foreland basin, Idaho: *Paleogeography, Paleoclimatology, Paleoecology*, v. 223, p. 275–289.
- Carroll, A.R., Stephens, N.P., Hendrix, M.S., and Glenn, C.R., 1998, Eolian-derived siltstone in the Upper Permian Phosphoria Formation—implications for marine upwelling: *Geology*, v. 26, p. 1023–1026.
- Chidsey, T.C., Jr., DeHamer, J.S., Hartwick, E.E., Johnson, K.R., Schelling, D.D., Sprinkel, D.A., Strickland, D.K., Vrona, J.P., and Wavrek, D.A., 2007, Petroleum geology of Covenant oil field, central Utah thrust belt, *in* Willis, G.C., Hylland, M.D., Clark, D.L., and Chidsey, T.C., Jr., editors, Central Utah—diverse geology of a dynamic landscape: Utah Geological Association Publication 36, p. 273–296.
- Chidsey, T.C., Jr., Hartwick, E.E., Johnson, K.R., Schelling, D.D., Sbarra, R., Sprinkel, D.A., Vrona, J.P., and Wavrek, D.A., 2011, Petroleum geology of Providence oil field, central Utah thrust belt, *in* Sprinkel, D.A., Yonkee, W.A., and Chidsey, T.C., Jr., editors, The Sevier thrust belt—northern and central Utah and adjacent areas: Utah Geological Association Publication 40, p. 213–231.
- Chidsey, T.C., Jr., Carney, S.M., Heath, J., and Dewers, T., 2009, The Gothic shale from Greater Aneth oil field, Paradox Basin, southeastern Utah—seal for hydrocarbons and carbon dioxide geologic sequestration [abs.]: American Association of Petroleum Geologists Annual Convention Abstracts, v. 18, p. 42.
- Choquette, P.W., and Pray, L.C., 1970, Geologic nomenclature and classification of porosity in sedimentary carbonates: American Association of Petroleum Geologists Bulletin, v. 54, no. 2, p. 207–250.
- Christensen, O.D., 1975, Metamorphism of the Manning Canyon and Chainman Formations: Palo Alto, California, Stanford University, Ph.D. dissertation, 166 p.
- Chong, K.K., Grieser, B., Jaripake, O., and Passman, A., 2010, A completion roadmap to shale-play development—a review of successful approaching toward shale-play stimulation in the last two decades: Society of Petroleum Engineers, presented at the CPS/SPE International Oil & Gas Conference, Beijing, China, SPE Paper 130369.
- Clark, D.L., Kirby, S.M., and Oviatt, C.G., 2012, Interim geologic map of the Rush Valley 30' x 60' quadrangle, Tooele, Utah, and Salt Lake Counties, Utah: Utah Geological Survey Open-File Report 593, 1 plate, scale 1:62,500.
- Clarke, F.W., 1924, The data of geochemistry: U.S. Geological Survey Bulletin 770, 841 p.
- Cline, E.J., and Bartley, J.M., 2007, Nature of the Cenozoic-Mesozoic contact in Sevier Valley and tectonic implications, *in* Willis, G.C., Hylland, M.D., Clark, D.L., and Chidsey, T.C., Jr., editors, Central Utah—diverse geology of a dynamic landscape: Utah Geological Association Publication 36, p. 31–45.
- Coe, A.L., and Church, K.D., 2005, Sequence stratigraphy, *in* Coe, A.L., editor, The sedimentary record of sea-level change: Cambridge University Press, p. 57–98.
- Cole, R.D., White, H., and Kirschbaum, M., 2008, Stops 1–4 through 1–10, Thompson Canyon–Sego Canyon, *in* Longman, M.W., and Morgan, C.D., editors, Hydrocarbon systems and production in the Uinta Basin, Utah: Rocky Mountain Association of Geologists, Utah Geological Association Publication 37, p. 417–437.
- Constenius, K.N., Clark, D.L., King, J.K., and Ehler, J.B., 2011, Interim geologic map of the Provo 30' x 60' quadrangle, Utah, Wasatch, and Salt Lake Counties, Utah: Utah Geological Survey Open-File Report 586DM, 42 p., 2 plates, scale 1:62,500, compact disk.
- Coogan, J.C., and King, J.K., 2006, Interim geologic map of the Durst Mountain quadrangle, Morgan and Weber Counties, Utah: Utah Geological Survey Open-File Report 498, 29 p., 1 plate, scale 1:24,000.
- Coogan, J.C., King, J.K., and McDonald, G., in preparation, Geologic map of the Devils Slide quadrangle, Morgan and Summit Counties, Utah: Utah Geological Survey Open-File Report, scale 1:24,000.
- Covington, R.E., and Young, K.J., 1985, Brief history and recent developments in tar sand deposits of Uinta Basin, *in* Picard, M.D., editor, Geology and energy resources, Uinta Basin of Utah: Utah Geological Association Publication 12, p. 227–241.
- Crittenden, M.D., Jr., 1959, Mississippian stratigraphy of the central Wasatch and western Uinta Mountains transition area: Intermountain Association of Petroleum Geologists Guidebook, 19th Annual Field Conference, p. 63–74.
- Crittenden, M.D., Jr., 1988, Bedrock geologic map of the Promontory Mountains, Box Elder County, Utah: U.S. Geological Survey Open-File Report 88-646, 1 plate, scale 1:100,000.
- Crittenden, M.D., Sharp, B.J., and Calkins, F.C., 1952, Geology of the Wasatch Mountains east of Salt Lake City—Parleys Canyon to the Traverse Range, *in* Marsell, R.E., editor, Geology of the central Wasatch Mountains, Utah: Utah Geological Society Guidebook to the Geology of Utah, No. 8, p. 1–37.
- Currie, B.S., 2002, Structural configuration of the Early Cretaceous Cordilleran foreland-basin system and Sevier thrust belt, Utah and Colorado: *The Journal of Geology*, v. 110, p. 697–718.
- Dahlstrom, C.D.A., 1970, Structural geology in the eastern margin of the Canadian Rocky Mountains: *Bulletin of Canadian Petroleum Geology*, v. 18, no. 3, p. 332–406.

- Davis, L.E., Webster, G.D., and Dyman, T.S., 1994, Correlation of the West Canyon, Lake Point, and Bannock Peak Limestones (Upper Mississippian to Middle Pennsylvanian), Basal Formations of the Oquirrh Group, northern Utah and southeastern Idaho: U.S. Geological Survey Bulletin 2088, 50 p.
- Davis, S.W., Davis, M.E., Lucchitta, I., Hanks, T.C., Finkel, R.C., and Caffee, M., 2001, Erosional history of the Colorado River through Glen and Grand Canyons, *in* Young, R.A., and Spamer, E.E., editors, Colorado River origin and evolution—proceedings of a symposium held at Grand Canyon National Park in June, 2000: Grand Canyon Association, p. 135–139.
- DeCelles, P.G., 2004, Late Jurassic to Eocene evolution of the Cordilleran thrust belt and foreland basin system, western U.S.A.: *American Journal of Science*, v. 304, p. 105–168.
- DeCelles, P.G., and Coogan, J.C., 2006, Regional structure and kinematic history of the Sevier fold-and-thrust belt, central Utah: *Geologic Society of America Bulletin*, v. 118, no. 7/8, p. 841–864.
- Deere, D.U., and Miller, R.P., 1966, Engineering classification and index properties for intact rock: Air Force Weapons Laboratory Technical Report AFWLTR-65-116, 277 p.
- De Voto, R.H., 1988, Late Mississippian paleokarst and related mineral deposits, Leadville Formation, central Colorado, *in* James, N.P., and Choquette, P.W., editors, Paleokarst: New York, Springer-Verlag, p. 278–305.
- Dickinson, W.R., Fiorello, A.R., Hall, D.L., Monreal, R., Pottochnik, A.R., and Swift, P.N., 1989, Cretaceous strata of southern Arizona, *in* Jenney, J.P., and Reynolds, S.J., editors, Geologic evolution of Arizona: Tucson, Arizona Geological Society Digest 17, p. 447–461.
- Diessel, C.F.K., 2010, The stratigraphic distribution of inertinite: *International Journal of Coal Geology*, v. 81, p. 251–268.
- Doelling, H.H., 1988, Geology of Salt Valley anticline and Arches National Park, Grand County, Utah, *in* Doelling, H.H., Oviatt, C.G., and Huntoon, P.W., editors, Salt deformation in the Paradox Basin, Utah: Utah Geological and Mineral Survey Bulletin 122, p. 1–58.
- Doelling, H.H., 2003, Geology of Arches National Park, Grand County, Utah, *in* Sprinkel, D.A., Chidsey, T.C., Jr., and Anderson, P.B., editors, Geology of Utah's parks and monuments: Utah Geological Association Publication 28, p. 11–36.
- Doelling, H.H., Chidsey, T.C., Jr., and Benson, B.J., 2010, Geology of Dead Horse Point State Park, Grand and San Juan Counties, Utah, *in* Sprinkel, D.A., Chidsey, T.C., Jr., and Anderson, P.B., editors, Geology of Utah's parks and monuments (3rd edition): Utah Geological Association Publication 28, p. 409–428.
- Doelling, H.H., and Hyland, M.D., 2002, San Rafael Swell proposed as site of new national monument: Utah Geological Survey, Survey Notes, v. 34, no. 2, p. 9–11.
- Doelling, H.H., and Kuehne, P.A., in preparation, Geologic map of the Yogo Creek 7.5-minute quadrangle: Utah Geological Survey.
- Doelling, H.H., Solomon, B.J., and Davies, S.F., 1994, Geologic map of the Grayback Hills quadrangle, Tooele County, Utah: Utah Geological Survey Map 166, 22 p., 2 plates, scale 1:24,000.
- Dunham, R.J., 1962, Classification of carbonate rocks according to depositional texture, *in* Ham, W.E., editor, Classification of carbonate rocks: American Association of Petroleum Geologists Memoir 1, p. 108–121.
- Eardley, A.J., 1939, Structure of the Wasatch-Great Basin region: *Geological Society of America Bulletin*, v. 50, p. 1277–1310.
- Ellis, D.V., and Singer, J.M., 2008, Well logging for earth scientists: Dordrecht, Springer, 692 p.
- Embry, A.R., and Klovan, J.E., 1971, A Late Devonian reef tract on northeastern Banks Island, Northwest Territories: *Canadian Petroleum Geologists Bulletin*, v. 19, p. 730–781.
- Enos, P., and Perkins, R.D., 1979, Evolution of Florida Bay from island stratigraphy: *Geological Society of America Bulletin*, Part I, v. 90, p. 59–83.
- Environmental Systems Research Institute, 2009, ESRI Data and Maps 9.3, ArcGIS 9 Media Kit: Media Kit, DVD.
- Evans, J.E., and Reed, J.M., 2007, Integrated loessite-paleokarst depositional system, early Pennsylvanian Molas Formation, Paradox Basin, southwestern Colorado, U.S.A.: *Sedimentary Geology*, v. 195, p. 161–181.
- Fielding, C.R., Frank, T.D., and Isbell, J.L., 2008, The late Paleozoic ice age—a review of current understanding and synthesis of global climate patterns, *in* Fielding, C.R., Frank, T.D., and Isbell, J.L., editors, Resolving the Late Paleozoic ice age in time and space: *Geological Society of America Special Paper 244*, p. 343–354.
- Finkl, C.W., Benedet, L., Andrews, J.L., Suthard, B., and Locker, S.D., 2007, Sediment ridges on the west Florida inner continental shelf—sand resources for beach nourishment: *Journal of Coastal Research*, v. 23, p. 143–159.
- Fleming, R.F., 1994, Cretaceous pollen in Pliocene rocks—implications for Pliocene climate in the southwestern United States: *Geology*, v. 22, p. 787–790.
- Fossen, H., 2010, Structural geology: New York, Cambridge University Press, 463 p.
- Frahme, C.W., and Vaughn, E.B., 1983, Paleozoic geology and seismic stratigraphy of the northern Uncompahgre front, Grand County, Utah, *in* Lowell, J.D., editor, Rocky Mountain foreland basins and uplifts: Rocky Mountain Association of Geologists Guidebook, p. 201–211.

- Franczyk, K.J., Fouch, T.D., Johnson, R.C., Molenaar, C.M., and Cobban, W.A., 1992, Cretaceous to Tertiary paleogeographic reconstructions for the Uinta-Piceance basin study area, Colorado and Utah: U.S. Geological Survey Bulletin 1787Q, 37 p.
- Franczyk, K.J., Pitman, J.K., and Nichols, D.J., 1990, Sedimentology, mineralogy, palynology, and depositional history of some uppermost Cretaceous and lowermost Tertiary rocks along the Utah Book and Roan Cliffs east of the Green River: U.S. Geological Survey Bulletin 1787-N, 27 p.
- Gianniny, G.L., and Simo, J.A.T., 1996, Implications of unfilled accommodation space for sequence stratigraphy on mixed carbonate-siliciclastic platforms—an example from the lower Desmoinesian (Middle Pennsylvanian), southwestern Paradox Basin, Utah, *in* Longman, M.W., and Sonnenfeld, M.D., editors, Paleozoic systems of the Rocky Mountain region: Rocky Mountain Section, SEPM (Society for Sedimentary Geology), p. 213–234.
- Gibson, R.I., 1987, Basement tectonic controls on structural style of the Laramide thrust belt interpreted from gravity and magnetic data, *in* Miller, W.R., editor, The thrust belt revisited: Wyoming Geological Association 38th Field Conference Guidebook, p. 27–35.
- Gillette, D.D., 1999, Vertebrate paleontology in Utah: Utah Geological Survey Miscellaneous Publication 99-1, 554 p.
- Gilluly, J., 1932, Geology and ore deposits of the Stockton and Fairfield quadrangles, Utah: U.S. Geological Survey Professional Paper 173, 171 p., 32 plates.
- Goldberg, K., and Humayun, M., 2010, The applicability of the chemical index of alternation as a paleoclimatic indicator—an example from the Permian of the Paraná Basin, Brazil: *Paleogeography, Paleoclimatology, Paleoecology*, v. 293, p. 175–183.
- Goldhammer, R.K., Oswald, E.J., and Dunn, P.A., 1991, Hierarchy of stratigraphic forcing—example from Middle Pennsylvanian shelf carbonates of the Paradox Basin, *in* Franseen, E.K., Watney, W.L., Kendall, C.G., and Ross, W., editors, Sedimentary modeling: Kansas Geological Survey Bulletin 233, p. 361–413.
- Goldhammer, R.K., Oswald, E.J., and Dunn, P.A., 1994, High frequency, glacio-eustatic cyclicity in Middle Pennsylvanian of the Paradox Basin—an evaluation of Milankovitch forcing, *in* deBoer, P.L., and Smith, D.G., editors, Orbital forcing and cyclic sequences: Special Publication of the International Association of Sedimentologists 19, p. 243–283.
- Gordon, M., Jr., Tooker, W.W., and Dutrom J.T., 2000, Type locality for the Great Blue Limestone in the Bingham nappe, Oquirrh Mountains, Utah: U.S. Geological Survey Open-File Report OF 00-012, 61 p.
- Gorman, D.R., 1962, A study of the Amsden Formation: Urbana-Champaign, University of Illinois, Ph.D. dissertation, 167 p.
- Gradstein, F., Ogg, J., and Smith, A., 2004, A geologic time scale 2004: New York, Cambridge University Press, 589 p.
- Graf, W.L., Hereford R., Laity, J., and Young, R.A., 1987, Colorado Plateau, *in* Graf, W.L., editor, Geomorphic systems of North America: Geological Society of America Centennial Special Volume 2, p. 259–302.
- Grammar, G.M., Eberli, G.P., Van Buchem, F.S.P., Stevenson, G.M., and Homewood, P.W., 1996, Application of high-resolution sequence stratigraphy to evaluate lateral variability in outcrop and subsurface—Desert Creek and Ismay intervals, Paradox Basin, *in* Longman, M.W., and Sonnenfeld, M.D., editors, Paleozoic systems of the Rocky Mountain region: Rocky Mountain Section, SEPM (Society for Sedimentary Geology), p. 235–266.
- Grammar, G.M., Eberli, G.P., Van Buchem, F.S.P., Stevenson, G.M., and Homewood, P.W., 2000, Application of high resolution sequence stratigraphy in developing an exploration and production strategy for a mixed carbonate/siliciclastic system (Carboniferous), Paradox Basin, USA, *in* Homewood, P.W., and Eberli, G.P., editors, Genetic stratigraphy on the exploration and production scales: Elf EP Editions, Memoir 24, p. 29–69.
- Granger, A.E., Calkins, F.C., Crittenden, M.D., Jr., and Sharp, B.J., 1952, Geology of the Wasatch Mountains east of Salt Lake City, *in* Marcel, R.E., editor, Geology of the central Wasatch Mountains, Utah: Utah Geological Society, Guidebook to the Geology of Utah, no. 8, p. 1–37.
- Gromet, L.P., Dymek, R.F., Haskin, L.A., and Korotev, R.L., 1984, The 'North America shale composite'—its compilation, major and trace element characteristics: *Geochimica et Cosmochimica Acta*, v. 48, p. 2469–2482.
- Grove, K.W., Horgan, C.C., Flores, F.E., and Bayne, R.C., 1993, Bartlett Flat Big Flat (Kane Springs Unit), *in* Hill, B.G., and Bereskin, S.R., editors, Oil and gas fields of Utah: Utah Geological Association Publication 22, non-paginated.
- Grover, P.W., 2008, Geological and fracture evaluation of conventional core from the Shell Exploration and Production Carbon Canal 5-12 well, Emery County, Utah: Houston, Texas, unpublished consultant's report, Core Laboratories Job #071154G, p. 18.
- Guthrie, J.M., and Bohacs, K.M., 2009, Spatial variability of source rocks: a critical element for defining the petroleum system of Pennsylvanian carbonate reservoirs of the Paradox Basin, SE Utah, *in* Houston, W.S., Wray, L.L., and Moreland, P.G., editors, The Paradox Basin revisited—new developments in petroleum systems and basin analysis: Rocky Mountain Association of Geologists Special Publication, p. 95–130.

- Hanks, T.C., Lucchitta, I., Davis, S.W., Davis, M.E., Finkel, R.C., Lefton, S.A., Garvin, C.D., 2001, The Colorado River and the age of Glen Canyon, *in* Young, R.A., and Spamer, E.E., editors, Colorado River origin and evolution—proceedings of a symposium held at Grand Canyon National Park in June, 2000: Grand Canyon Association, p. 129–133.
- Hansen, W.R., 1965, Geology of the Flaming Gorge area, Utah–Colorado–Wyoming: U.S. Geological Survey Professional Paper 490, 196 p.
- Hansen, W.R., 1977, Geologic map of the Jones Hole quadrangle, Uintah County, Utah, and Moffat County, Colorado: U.S. Geological Survey Geologic Quadrangle Map GQ-1401, scale 1:24,000.
- Hansen, W.R., and Bonilla, M.G., 1956, Geology of the Manila quadrangle, Utah–Wyoming: U.S. Geological Survey Miscellaneous Geologic Investigations Map I-156, scale 1:24,000.
- Hansen, W.R., Carrara, P.E., and Rowley, P.D., 1981, Geologic map of the Crouse Reservoir quadrangle, Uintah and Daggett Counties, Utah: U.S. Geological Survey Geologic Quadrangle Map GQ-1554, scale 1:24,000.
- Hansen, W.R., and Rowley, P.D., 1991, Geologic map of the Hoy Mountain quadrangle, Daggett and Uintah Counties, Utah, and Moffat County, Colorado: U.S. Geological Survey Geologic Quadrangle Map GQ-1695, scale 1:24,000.
- Hansen, W.R., Rowley, P.D., and Carrara, P.E., 1983, Geologic map of Dinosaur National Monument and vicinity, Utah and Colorado: U.S. Geological Survey Miscellaneous Investigations Series Map I-1407, scale 1:50,000.
- Harr, C.L., 1996, Paradox oil and gas potential of the Ute Mountain Ute Indian Reservation, *in* Huffman, A.C., Jr., Lund, W.R., and Godwin, L.H., editors, Geology and resources of the Paradox Basin: Utah Geological Association Publication 25, p. 13–28.
- Harry, D.L., and Mickus, K.L., 1998, Gravity constraints on lithospheric flexure and the structure of the late Paleozoic Ouachita orogen in Arkansas and Oklahoma, south-central North America: *Tectonics*, v. 17, no. 2, p. 187–202.
- Heath, J., McPherson, B., Dewers, T., Chidsey, T.C., Jr., Petrusak, R., Siriwardane, H., Bromhal, G., Grigg, R., and Esposito, R., 2009, Seal analysis of geologic CO₂ storage sites [abs.]: American Association of Petroleum Geologists Annual Convention Abstracts, v. 18, p. 90–91.
- Henderson, G.V., 1970, The origin of pyrophyllite rectorite in shales of north-central Utah: *Clays and Clay Minerals*, v. 18, p. 239–246.
- Henrikson, A., and Chapman, D.S., 2002, Terrestrial heat flow in Utah: Salt Lake City, University of Utah, Department of Geology and Geophysics, accessed December 29, 2005, at <http://geology.utah.gov/emp/geothermal/pdf/terrestrialhf.pdf>.
- Hintze, L.F., 1980, Geologic map of Utah: Utah Geological Survey Map M-A-1, 2 plates, scale 1:500,000.
- Hintze, L.F., and Davis, F.D., 2003, Geology of Millard County, Utah: Utah Geological Survey Bulletin 133, 305 p.
- Hintze, L.F., and Kowallis, B.J., 2009, Geologic history of Utah: Brigham Young University Geology Studies Special Publication 9, 225 p.
- Hite, R.J., 1960, Stratigraphy of the saline facies of the Paradox Member of the Hermosa Formation of southeastern Utah and southwestern Colorado, *in* Smith, K.G., editor, Geology of the Paradox Basin fold and fault belt: Four Corners Geological Society, Third Field Conference Guidebook, p. 86–89.
- Hite, R.J., and Cater, F.W., 1972, Pennsylvanian rocks and salt anticlines, Paradox Basin, Utah and Colorado, *in* Malloy, W.W., editor, Geologic atlas of the Rocky Mountain region: Rocky Mountain Association of Geologists Guidebook, p. 133–138.
- Hite, R.J., Anders, D.E., and Ging, T.G., 1984, Organic-rich source rocks of Pennsylvanian age in the Paradox Basin of Utah and Colorado, *in* Woodward, J., Meissner, F.F., and Clayton, J.L., editors, Hydrocarbon source rocks of the greater Rocky Mountain region: Rocky Mountain Association of Geologists Guidebook, p. 255–274.
- Holland, F.D., 1952, Stratigraphic details of Lower Mississippian rocks of northeastern Utah and southwestern Montana: *American Association of Petroleum Geologists Bulletin*, v. 36, no. 9, p. 1697–1734.
- Houlik, C.W., Jr., 1973, Interpretation of carbonate-detrital silicate transitions in the Carboniferous of western Wyoming: *American Association of Petroleum Geologists Bulletin*, v. 57, p. 498–509.
- Huddle, J.W., and McCann, F.T., 1947, Geologic map of Duchesne River area, Wasatch and Duchesne Counties, Utah: U.S. Geological Survey Circular 16.
- Hunt, C.B., 1956, Cenozoic geology of the Colorado Plateau: U.S. Geological Survey Professional Paper 279, 99 p.
- Hurlow, H.A., and Burk, N., 2008, Geology and ground-water chemistry, Curlew Valley, northwestern Utah and south-central Idaho—implications for hydrogeology: Utah Geological Survey Special Study 126, 185 p., 2 plates, scale 1:100,000.
- International Commission on Stratigraphy, 2009, International chronostratigraphic chart: Online, www.stratigraphy.org/column.php?id=Chart/Time%20Scale, accessed January 2012.
- James, N.P., 1997, The cool-water carbonate depositional realm, *in* James, N.P., and Clarke, J.A.D., editors, Cool-water carbonates: Society for Sedimentary Geology (SEPM) Special Publication 56, p. 1–20.
- Jensen, M.E., and King, J.K., 1999, Geologic map of the Brigham City quadrangle, Box Elder and Cache Coun-

- ties, Utah: Utah Geological Survey Map 173, 2 plates, scale 1:24,000.
- Johnson, R.C., 2003, Northwest to southeast cross section of Cretaceous and lower Tertiary rocks across the eastern part of the Uinta Basin, Utah, *in* USGS Uinta-Piceance Assessment Team, compilers, Petroleum systems and geologic assessment of oil and gas in the Uinta-Piceance Province, Utah and Colorado: U.S. Geological Survey Digital Data Series DDS-69-B, compact disk.
- Johnson, S.Y., 1989, Significance of loessite in the Maroon Formation (Middle Pennsylvanian to Lower Permian), Eagle Basin, northwest Colorado: *Journal of Sedimentary Petrology*, v. 59, p. 782–791.
- Johnson, R.C., and Johnson, S.Y., 1991a, Stratigraphic and time-stratigraphic cross sections of Phanerozoic rocks along line B–B', Uinta and Piceance Basin area, west-central Uinta Basin, Utah to eastern Piceance Basin, Colorado: U.S. Geological Survey Miscellaneous Investigation Series 2184-B, 2 plates.
- Johnson, S.Y., and Johnson, R.C., 1991b, Stratigraphic and time-stratigraphic cross sections of Phanerozoic rocks along line A–A', Uinta and Piceance Basin area-Eagle Basin, Colorado, to eastern Basin and Range area, Utah: U.S. Geological Survey Miscellaneous Investigation Series 2184-A, 2 plates.
- Johnson, S.Y., Chan, M.A., and Konopka, E.A., 1992, Pennsylvanian and Early Permian paleogeography of the Uinta-Piceance Basin, northwestern Colorado and northeastern Utah: U.S. Geological Survey Bulletin 1787-CC, 35 p.
- Jordan, T.E., 1979, Lithofacies of the Upper Pennsylvanian and Lower Permian western Oquirrh Group, northwest Utah: *Utah Geology*, v. 6, no. 2, p. 41–56.
- Jordan, T.E., 1983, Structural geometry and sequence, Bovine Mountain, northwestern Utah, *in* Miller, D.M., Todd, V.R., and Howard, K.A., editors, Tectonic and stratigraphic studies in the eastern Great Basin, *Geological Society of America Memoir* 157, p. 215–227.
- Jordan, T.E., Crittenden, M.D., Jr., Allmendinger, R.W., and Miller, D.M., 1988, Geologic map of the Thatcher Mountain quadrangle, Box Elder County, Utah: Utah Geological and Mineral Survey Map 109, 10 p. pamphlet, scale 1:24,000.
- Jordan, T.E., and Douglas, R.C., 1980, Paleogeography and structural development of the Late Pennsylvanian to Early Permian Oquirrh Basin, northwestern Utah, *in* Fouch, T.D., and Magathan, E.R., editors, Paleozoic paleogeography of the west-central United States, Rocky Mountain Paleogeography Symposium I: Denver, Rocky Mountain Section, Society of Economic Paleontologists and Mineralogists, p. 217–238.
- Judge, S.A., 2007, The origin and evolution of the Wasatch monocline, central Utah: Columbus, The Ohio State University, Ph.D. dissertation, 396 p.
- Judge, S.A., Wilson, T., and Elliot, D., 2011, Kinematics of the Sevier backthrusting, central Utah, *in* Sprinkel, D.A., Yonkee, W.A., and Chidsey, T.C., Jr., editors, The Sevier thrust belt—northern and central Utah and adjacent areas: Utah Geological Association Publication 40, p. 73–87.
- Kapp, P., Pelletier, J.D., Rohrmann, A., Heermance, R., Russell, J., and Ding, L., 2011, Wind erosion in the Qaidam basin, central Asia—implications for tectonics, paleoclimate, and the source of the Loess Plateau: *GSA Today*, v. 21, p. 4–10.
- Kay, M., 1951, North American geosynclines: *Geological Society of America Memoir* 48, 143 p.
- Key, J., 2010, Rockin the Bakken—oil in Williston, The history of oil in the Williston Basin: Online, <www.rockin-thebakken.com>, accessed in June 2010.
- King, R., and Morehouse, D., 1993, Drilling sideways—a review of horizontal well technology and its domestic applications: U.S. Department of Energy Technology Report, DOE/EIA-TR-0565.
- Kinney, D.M., 1955, Geology of the Uinta River-Brush Creek area, Duchesne and Uintah Counties, Utah: U.S. Geological Survey Bulletin 1007, 185 p.
- Kirschbaum, M.A., Lillis, P.G., and Roberts, L.N.R., 2007, Geologic assessment of undiscovered oil and gas resources in the Phosphoria total petroleum system of the Wind River Basin province, Wyoming, *in* Wind River Basin Province Assessment Team, editors, Petroleum Systems and Geologic Assessment of Oil and Gas in the Wind River Basin Province, Wyoming: U.S. Geological Survey Digital Data Series DDS-69-J, p. 1–27.
- Kluth, C.F., 1986, Plate tectonics of the Ancestral Rocky Mountains, *in* Peterson, J.A., editor, Paleotectonics and sedimentation: American Association of Petroleum Geologists Memoir 41, p. 353–369.
- Kluth, C.F., and Coney, P.J., 1981, Plate tectonics of the Ancestral Rocky Mountains: *Geology*, v. 9, p. 10–15.
- Kundert, D., and Mullen, M., 2009, Proper evaluation of shale gas reservoirs leads to more effective hydraulic-fracture stimulation: Society of Petroleum Engineers, Rocky Mountain Petroleum Technology Conference, SPE Paper 123586.
- Laine, M.D., Chidsey, T.C., Jr., and Morgan, C.D., 2008, Potential shale-gas resources in Utah [abs.]: American Association of Petroleum Geologists Annual Convention Abstracts, v. 17, p. 115; accessed May 10, 2010, at http://geology.utah.gov/emp/shalegas/pdf/shalegas_poster0408.pdf.
- Lamerson, P.R., 1982, The Fossil Basin and its relationship to the Absaroka thrust system, Wyoming and Utah, *in* Powers, R.B., editor, Geologic studies of the Cordilleran thrust belt: Denver, Rocky Mountain Association of Geologists, v.1, p. 279–340.

- Lash, E., and Lash, G., 2010, Kicking down the well, *in* The early history of natural gas: The SUNY Fredonia Shale Research Institute.
- Lewis, R., Ingraham, D., Percy, M., Williamson, J., Sawyer, W., and Frantz, J., 2004, New evaluation techniques for gas shale reservoirs: Schlumberger Reservoir Symposium, 11 p.
- Li, C., and Yang, S., 2010, Is chemical index of alteration (CIA) a reliable proxy for chemical weathering in global drainage basins?: *American Journal of Science*, v. 310, p. 111–127.
- Lucchitta, I., 1979, Late Cenozoic uplift of the southwestern Colorado Plateau and adjacent Colorado River region: *Tectonophysics*, v. 61, p. 63–95.
- Lucchitta, I., 1989, History of the Grand Canyon and of the Colorado River in Arizona, *in* Jenney, J.P., and Reynolds, S.J., editors, *Geologic evolution of Arizona*: *Arizona Geological Society Digest* 17, p. 701–715.
- Mallory, W.W., 1967, Pennsylvanian and associated rocks in Wyoming: *U.S. Geological Survey Professional Paper* 554-G, 31 p.
- Marchetti, D.W., and Cerling, T.E., 2001, Bedrock incision rates for the Fremont River tributary of the Colorado River, 2001, *in* Young, R.A., and Spamer, E.E., editors, *Colorado River origin and evolution—Proceedings of a symposium held at Grand Canyon National Park in June, 2000*: *Grand Canyon Association*, p. 125–127.
- Maurer, R.E., 1970, *Geology of the Cedar Mountains, Tooele County, Utah*: Salt Lake City, University of Utah, Ph.D. dissertation, 184 p.
- McCarthy, P.T., and Miller, D.M., 2002, *Geologic map of the Terrace Mountain East quadrangle, Box Elder County, Utah*: *Utah Geological Survey Miscellaneous Publication* 02-2, 14 p., 2 plates, scale 1:24,000.
- McDougald, W.D., 1953, *Geology of Beaver Creek and adjacent areas, Utah*: Salt Lake City, Utah, University of Utah, M.S. thesis, 54 p.
- Merritt, W.M., and Winar, R.M., 1958, Molas and associated formations in San Juan Basin-Needle Mountains area, southwestern Colorado: *American Association of Petroleum Geologists Bulletin*, v. 42, p. 2107–2132.
- Mickle, K., 2009, The lower Actinopterygian fauna of the Manning Canyon Shale Formation (Upper Mississippian-Lower Pennsylvanian) of Utah: *Tenth Annual Kansas Academy of Science Paleontology Symposium*, March 27–28, 2009, Topeka, Kansas.
- Miller, D.M., 1985, *Geologic map of the Lucin quadrangle, Box Elder County, Utah*: *Utah Geological Survey Map* 78, 10 p., 2 plates, scale 1:24,000.
- Miller, D.M., Crittenden, M.D., Jr., and Jordan, T.E., 1991, *Geologic map of the Lampo Junction quadrangle, Box Elder County, Utah*: *Utah Geological Survey Map* 136, 17 p., 2 plates, scale 1:24,000.
- Miller, D.M., and Glick, L.L., 1986, *Geologic map of the Lemay Island quadrangle, Box Elder County, Utah*: *Utah Geological Survey Map* 96, 9 p., 2 plates, scale 1:24,000.
- Miller, D.M., Jordan, T.E., and Allmendinger, R.W., 1990, *Geologic map of the Crater Island quadrangle, Box Elder County, Utah*: *Utah Geological Survey Map* 128, 16 p., 2 plates, scale 1:24,000.
- Miller, D.M., Lush, A.P., and Schneyer, J.D., 1993, *Geologic map of the Patterson Pass quadrangle, Box Elder County, Utah, and Elko County, Nevada*: *Utah Geological Survey Map* 144, 20 p., 2 plates, scale 1:24,000.
- Miller, D.M., and Oviatt, C.G., 1994, *Geologic map of the Lucin NW quadrangle, Box Elder County, Utah*: *Utah Geological Survey Map* 158, 13 p., 2 plates, scale 1:24,000.
- Miller, D.M., and Schneyer, J.D., 1985, *Geologic map of the Tecoma quadrangle, Box Elder County, Utah, and Elko County, Nevada*: *Utah Geological Survey Map* 77, 8 p., 2 plates, scale 1:24,000.
- Miller, S.T., Martindale, S.G., and Fedewa, W.T., 1984, Permian stratigraphy of the Leach Mountains, Elko County, Nevada, *in* Kearns, G.J., and Kearns, R.L., Jr., editors, *Geology of northwest Utah, southern Idaho and northeast Nevada*: *Utah Geological Association Publication* 13, p. 65–78.
- Molenaar, C.M., and Cobban, W.A., 1991, Middle Cretaceous stratigraphy on the south and east sides of the Uinta Basin, northeastern Utah and northwestern Colorado: *U.S. Geological Survey Bulletin* 1787, p. P1–P34.
- Montgomery, S., 1992, Paradox Basin—Cane Creek play: *Petroleum Frontiers*, v. 9, 66 p.
- Morgan, C.D., 1992, Horizontal drilling potential of the Cane Creek shale, Paradox Formation, Utah, *in* Schmoker, J.W., Coalson, E.B., and Brown, C.A., editors, *Geological studies relevant to horizontal drilling—examples from western North America*: *Rocky Mountain Association of Geologists*, p. 257–265.
- Morgan, C.D., 2007, Structure, reservoir characterization, and carbon dioxide resources of Farnham Dome field, *in* Willis, G.C., Hylland, M.D., Clark, D.L., and Chidsey, T.C., Jr., editors, 2007, *Central Utah—diverse geology of a dynamic landscape*: *Utah Geological Association Publication* 36, p. 297–310.
- Morris, H.T., Douglass, R.C., and Kopf, R.W., 1977, Stratigraphy and microfaunas of the Oquirrh Group in the southern East Tintic Mountains, Utah: *U.S. Geological Survey Professional Paper* 1025, 22 p.
- Moulton, F.C., 1976, Lower Mesozoic and upper Paleozoic petroleum potential of the Hingeline area, central Utah, *in* Hill, J.G., editor, *Symposium on geology of the Cordilleran Hingeline*: *Rocky Mountain Association of Geologists Guidebook*, p. 219–229.

- Moyle, R.W., 1958, Paleocology of the Manning Canyon Shale in central Utah: Brigham Young University Research Studies, v. 5, no. 7, 86 p.
- Moyle, R.W., 1959, Mississippian and Pennsylvanian rocks, Manning Canyon Shale, in Bissell, H.J., editor, Geology of the southern Oquirrh Mountains and Fivemile Pass—northern Boulter Mountain area, Tooele and Utah Counties, Utah: Utah Geological Society Guidebook to the Geology of Utah, no. 14, p. 59–92.
- Mytton, J.W., Morgan, W.A., and Wardlaw, B.R., 1983, Stratigraphic relations of Permian units, Cassia Mountains, Idaho, in Miller, D.M., Todd, V.R., and Howard, K.A., editors, Tectonic and stratigraphic studies in the eastern Great Basin: Geological Society of America Memoir 157, p. 281–303.
- Nelson, C.R., and Tidwell, W.D., 1987, *Brodioptera stricklandi* n. sp. (Megaseoptera: Brodiopteridae), a new fossil insect from the upper Manning Canyon Shale Formation, Utah (lowermost Namurian B): Psyche, v. 9, p. 309–316.
- Nesbitt, H.W., and Young, G.M., 1982, Early Proterozoic climates and plate motions inferred from major element chemistry of lutiles: Nature, v. 299, p. 715–717.
- Nettleton, W.D., and Chadwick, O.A., 1996, Late Quaternary redeposited loess-soil development sequences, South Yemen: Geoderma, v. 70, p. 21–36.
- Neuhauser, K.R., 1988, Sevier-age ramp-style thrust faults at Cedar Mountain, northwestern San Rafael Swell (Colorado Plateau), Emery County, Utah: Geology, v. 16, p. 299–302.
- Nichols, K.M., and Silberling, N.J., 1993, Upper Devonian to Upper Mississippian strata of the Antler foreland in the Leppy Hills, easternmost northern Nevada: U.S. Geological Survey Bulletin 1988-G, 13 p.
- Nohara, T., 1966, Microfauna of the Upper Mississippian Great Blue Limestone near Morgan, Utah: Salt Lake City, University of Utah, M.S. thesis, 88 p.
- Nuccio, V.F., and Condon, S.M., 1996a, Burial and thermal history of the Paradox Basin, Utah and Colorado, and petroleum potential of the Middle Pennsylvanian Paradox Formation, in Huffman, A.C., Jr., Lund, W.R., and Godwin, L.H., editors, Geology of the Paradox Basin: Utah Geological Association Publication 25, p. 57–76.
- Nuccio, V.F., and Condon, S.M., 1996b, Burial and thermal history of the Paradox Basin, Utah and Colorado, and petroleum potential of the Middle Pennsylvanian Paradox Formation: U.S. Geological Survey Bulletin 2000-O, 41 p., 2 plates.
- Nuccio, V.F., and Roberts, L.N.R., 2003, Chapter 4—Thermal maturity and oil and gas generation history of petroleum systems in the Uinta—Piceance province, Utah and Colorado, in Petroleum systems and geologic assessment of oil and gas in the Uinta—Piceance province, Utah and Colorado: U.S. Geological Survey Digital Data Series, DDS-69-B, 39 p.
- Parrish, J.T., 1982, Upwelling and petroleum source beds, with reference to Paleozoic: American Association of Petroleum Geologists Bulletin, v. 66, p. 750–774.
- Pederson, J., Karlstrom, K., Sharp, W., and McIntosh, W., 2002, Differential incision of the Grand Canyon related to Quaternary faulting—constraints from U-series and Ar/Ar dating: Geology, v. 30, p. 739–742.
- Peters, K.E., and Cassa, M.R., 1994, Applied source rock geochemistry, in Magoon, L.B., and Dow, W.G., editors, The petroleum system—from source to trap: American Association of Petroleum Geologists Memoir 60, p. 93–120.
- Peterson, J.A., 2001 (updated 2003), Carboniferous–Permian (late Paleozoic) hydrocarbon system, Rocky Mountains and Great Basin U.S. region—major historic exploration objective: Rocky Mountain Association of Geologists Open-File Report, 54 p.
- Peterson, J.A., and Hite, R.J., 1969, Pennsylvanian evaporite-carbonate cycles and their relation to petroleum occurrence, southern Rocky Mountains: American Association of Petroleum Geologists Bulletin, v. 53, p. 884–908.
- Pickering, W., and Dorn, C., 1948, Rangely oil field, Rio Blanco County, Colorado, in Howell, J.V., editor, Structure of typical American oil fields—a symposium on the relation of oil accumulation to structure, Volume III: American Association of Petroleum Geologists Special Publication 14, p. 134.
- Porter, S.C., 2007, Loess records—China, in Elias, S.A. editor, Encyclopedia of Quaternary science, v. 2: Oxford, Elsevier, p. 1429–1440.
- Potochnik, A.R., and Faulds, J.E., 1998, A tale of two rivers—Tertiary structural inversion and drainage reversal across the southern boundary of the Colorado Plateau, in Duebendorfer, E.M., editor, Geologic excursions in northern and central Arizona: Field Trip Guidebook for Geological Society of America Rocky Mountain Section Meeting.
- Potter, C.J., Tang, R., and Hainsworth, T.J., 1992, Late Paleozoic structure of the southern part of the Uinta Basin, Utah, from seismic reflection data, in Thorman, C.H., editor, Application of structural geology to mineral and energy resources of the central and western United States: U.S. Geological Survey Bulletin 2012, p. J1–J8.
- Potter, P.E., Maynard, J.B., and Depetris, P.J., 2005, Mud and mudstones—introduction and overview: Berlin, London, Springer, 297 p.
- Powell, M.G., 2008, Timing and selectivity of the Late Mississippian mass extinction of brachiopod genera from the central Appalachian basin: PALAIOS, v. 23, p. 525–534.
- Power, P.E., 1969, Clay mineralogy and paleoclimatic significance of some red regoliths and associated rocks in

- western Colorado: *Journal of Sedimentary Research*, v. 39, p. 876–890.
- Prince, D., 1964, Mississippian coal cyclothems in the Manning Canyon Shale of central Utah: *Brigham Young University Geology Studies*, v. 10, p. 83–104.
- Pye, K., 1987, *Aeolian dust and dust deposits*: London, Academic Press, 334 p.
- Rasmussen, D.L., 2010, Halokinesis features related to flowage and dissolution of Pennsylvanian Hermosa salt in the Paradox Basin, Colorado and Utah [abs]: American Association of Petroleum Geologists, Rocky Mountain Section Meeting Program with Abstracts, p. 59.
- Rasmussen, L., and Rasmussen, D.L., 2009, Burial history analysis of the Pennsylvanian petroleum system in the deep Paradox Basin fold and fault belt, Colorado and Utah, *in* Houston, W.S., Wray, L.L., and Moreland, P.G., editors, *The Paradox Basin revisited—new developments in petroleum systems and basin analysis*: Rocky Mountain Association of Geologists Special Publication, p. 24–94.
- Reid, F.S., and Berghorn, C.E., 1981, Facies recognition and hydrocarbon potential of the Pennsylvanian Paradox Formation, *in* Wiegand, D.L., editor, *Geology of the Paradox Basin*: Rocky Mountain Association of Geologists Guidebook, p. 111–117.
- Rhoads, D.C., and Morse, J.W., 1971, Evolutionary and ecologic significance of oxygen-deficient marine basins: *Lethaia*, v. 4, p. 413–428.
- Rider, M., 1996, *The geological interpretation of well logs*: Houston, Gulf Publishing Company, 280 p.
- Ritter, S.M., and Gianniny, G.L., 2012, Geological guide to Honaker Trail, San Juan River gorge (near Goose-necks State Park), southeastern Utah, *in* Anderson, P.B., and Sprinkel, D.A., editors, *Geologic road, trail, and Lake guides to Utah's parks and monuments* (3rd edition): Utah Geological Association Publication 29, 32 p.
- Ritter, S.M., and Robinson, T.S., 2009, Sequence stratigraphy and biostratigraphy of Carboniferous-Permian boundary strata in western Utah, *in* Tripp, B.T., Krahulec, K., and Jordan, J.L., editors, *Geology and geologic resources and issues of western Utah*: Utah Geological Association Publication 38, p. 27–42.
- Ritter, S.M., Barrick, J.E., and Skinner, M.R., 2002, Conodont sequence biostratigraphy of the Hermosa Group (Pennsylvanian) at Honaker Trail, Paradox Basin, Utah: *Journal of Paleontology*, v. 76, no. 3, p. 495–517.
- Roberts, L.N.R., and Kirschbaum, M.A., 1995, Paleogeography of the Late Cretaceous of the western interior of North America—coal distribution and sediment accumulation: U.S. Geological Survey Professional Paper 1561, 115 p.
- Rose, P.R., 1976, Mississippian carbonate shelf margins, western United States, *in* Hill, J.G., editor, *Geology of the Cordilleran Hingeline*: Rocky Mountain Association of Geologists, p. 135–151.
- Rouse, F., Jr., 1996, Detachment fold train, Reed Wash area, west flank, San Rafael Swell, Utah—an example of a limb-lengthening roll-through folding process on the eastern margin of the Sevier thrust belt: *The Mountain Geologist*, v. 33, p. 45–64.
- Rowley, P.D., Hansen, W.R., Tweto, O., and Carrara, P.E., 1985, Geologic map of the Vernal 1° x 2° quadrangle, Colorado, Utah, and Wyoming: U.S. Geological Survey Miscellaneous Investigations Series Map I-1526, scale 1:250,000.
- Royse, F., Jr., 1993, Case of the phantom foredeep—Early Cretaceous in west-central Utah: *Geology*, v. 21, no. 2, p. 133–136.
- Sadlick, W., 1955a, Carboniferous formation of northeastern Uinta Mountains: Wyoming Geological Association Guidebook, Tenth Field Conference, p. 49–59.
- Sadlick, W., 1955b, The Mississippian-Pennsylvanian boundary in northeastern Utah: Salt Lake City, University of Utah, M.S. thesis, 77 p.
- Sadlick, W., 1956, Some Upper Devonian-Mississippian problems in eastern Utah, *in* Peterson, J.A., editor, *Geology and economic deposits, east-central Utah*: Intermountain Association of Petroleum Geologists Guidebook, 7th Annual Field Conference, p. 65–76.
- Sadlick, W., 1957, Regional relations of Carboniferous rocks of northeastern Utah, *in* Seal, O.G., editor, *Guidebook to the geology of the Uinta Basin*: Intermountain Association of Petroleum Geologist 8th Annual Field Conference, p. 57–77.
- Sandberg, C.A., and Gutschick, R.C., 1984, Distribution, microfauna, and source-rock potential of Mississippian Delle Phosphatic Member of Woodman Formation and equivalents, Utah and adjacent states, *in* Woodward, J., Meissner, F.F., and Clayton, J.L., editors, *Hydrocarbon source rocks of the greater Rocky Mountain region*: Rocky Mountain Association of Geologists, p. 135–178.
- Sandberg, C.A., Gutschick, R.C., Johnson, J.G., Poole, F.G., and Sando, W.J., 1982, Middle Devonian to Late Mississippian geologic history of the overthrust belt region, western United States, *in* Powers, R.B., editors, *Geologic studies of the Cordilleran thrust belt, v. II*: Rocky Mountain Association of Geologists, p. 691–719.
- Sando, W.J., 1988, Madison Limestone (Mississippian) paleokarst: a geologic synthesis, *in* James, N.P., and Choquette, P.W., editors, *Paleokarst*: New York, Springer-Verlag, p. 256–277.
- Sando, W.J., Gordon, M., Jr., and Dutro, J.T., Jr., 1975, Stratigraphy and geologic history of the Amsden Formation (Mississippian and Pennsylvanian) of Wyoming: U.S. Geological Survey Professional Paper 848-A, 83 p.

- Sarg, J.F., Markello, J.R., and Weber, L.J., 1999, The second-order cycle, carbonate platform growth, and reservoir, source, and trap prediction, *in* Harris, P.M., Saller, A.H., and Simo, J.A., editors, *Advances in carbonate sequence stratigraphy—applications to reservoirs, outcrops, and models: SEPM (Society for Sedimentary Geology) Special Publication 63*, p. 451–465.
- Schaeffer, F.E., 1960, Stratigraphy of the Silver Island Mountains, *in* Schaeffer, F.E., editor, *Guidebook to the geology of Utah: Utah Geological Society Bulletin 15*, p. 15–113.
- Schamel, S., 2005, Shale gas reservoirs of Utah—survey of an unexploited potential energy resource: *Utah Geological Survey Open-File Report 461*, 114 p.
- Schamel, S., 2006, Shale gas resources of Utah—assessment of previously undeveloped gas discoveries: *Utah Geological Survey Open-File Report 499*, 85 p.
- Schamel, S., and Quick, J., 2010, Manning Canyon Shale—Utah’s newest shale gas resource [abs.]: *American Association of Petroleum Geologists Annual Convention Abstracts volume on CD ROM*.
- Schamel, S., Pilifossov, V.M., and Votsalevsky, E.S., 1995, Geologic controls on style of salt piercements in the Pricaspian basin, Kazakhstan—contrasts with the Gulf of Mexico, *in* Salt, sediment and hydrocarbons: Gulf Coast Section, Society for Sedimentary Geology (SEPM), 16th Annual Research Conference, p. 253–255.
- Schelling, D.D., Strickland, D., Johnson, K.R., Vrona, J.P., Wavrek, D.A., and Reuter, J., 2005, Structural architecture and evolution of the central Utah thrust belt—implications for hydrocarbon exploration [abs.]: *American Association of Petroleum Geologists Annual Convention, Official Program with Abstracts*, v. 14, non-paginated.
- Schelling, D.D., Strickland, D.K., Johnson, K.R., and Vrona, J.P., 2007, Structural geology of the central Utah thrust belt, *in* Willis, G.C., Hylland, M.D., Clark, D.L., and Chidsey, T.C., Jr., editors, *Central Utah—diverse geology of a dynamic landscape: Utah Geological Association Publication 36*, p. 1–29.
- Schneyer, J.D., 1984, Structural and stratigraphic complexities within an extensional terrain—examples from the Leppy Hills area, southern Silver Island Mountains, near Wendover, Utah, *in* Kearns, G.J., and Kearns, R.L., Jr., editors, *Geology of northwest Utah, southern Idaho and northeast Nevada: Utah Geological Association Publication 13*, p. 93–116.
- Schneyer, J.D., 1990, Geologic map of the Leppy Peak quadrangle and adjacent area, Elko County, Nevada, and Tooele County, Utah: *U.S. Geological Survey Miscellaneous Investigations Series Map I-1938*, 1 plate, scale 1:24,000.
- Schwing, P., 2010, Assessing carbonate and total organic content trends in sediments of the west Florida shelf, *in* West Florida shelf—a natural laboratory for the study of ocean acidification: *U.S. Geological Survey Open-File Report 2010-1134*, p. 9–14.
- Scott, A.C., and Glasspool, I.J., 2006, The diversification of Paleozoic fire systems and fluctuations in atmospheric oxygen concentration: *Proceedings of the National Academy of Sciences*, v. 103, p. 10861–10865.
- Sheldon, R.P., 1964, Paleolatitudinal and paleogeographic distribution of phosphorite: *U.S. Geological Survey Professional Paper 501-C*, p. C106–C113.
- Shoore, D.J., and Ritter, S.M., 2007, Sequence stratigraphy of the Bridal Veil Limestone Member of the Oquirrh Formation (Lower Pennsylvanian) in the central Wasatch Range, Utah—towards a Bashkirian cyclostratigraphy for the Oquirrh basin, *in* Willis, G.C., Hylland, M.D., Clark, D.L., and Chidsey, T.C., Jr., editors, *Central Utah—diverse geology of a dynamic landscape: Utah Geological Association Publication 36*, p. 57–74.
- Silberling, N.J., and Nichols, K.M., 1992, Depositional cycles of the Upper Devonian-Lower Mississippian limestone succession in the southern Lakeside Mountains, Utah, *in* Wilson, R.J., editor, *Field guide to geological excursions in Utah and adjacent areas of Nevada, Idaho, and Wyoming: Utah Geological Survey Miscellaneous Publication 92-3*, p. 131–145.
- Smith, J.F., Jr., 1983, Paleozoic rocks in the Black Pine Mountains, Cassia County, Idaho: *U.S. Geological Survey Bulletin 1536*, 36 p.
- Smith, M.E., Carroll, A.R., and Singer, B.S., 2008, Synoptic reconstruction of a major ancient lake system—Eocene Green River Formation, western United States: *Geological Society of America Bulletin*, v. 120, no. 1/2, p. 54–84, doi: 10.1130/B26073.1.
- Solomon, B.J., Biek, R.F., and Smith, T.W., 2007, Geologic map of the Magna quadrangle, Salt Lake County, Utah: *Utah Geological Survey Map 216*, 2 plates, scale 1:24,000.
- Soreghan, G.S., 1992, Preservation and paleoclimatic significance of eolian dust in the Ancestral Rocky Mountains province: *Geology*, v. 20, p. 1111–1114.
- Soreghan, G.S., and Soreghan, M.J., 2002, Atmospheric dust and algal dominance in the Late Paleozoic—a hypothesis: *Journal of Sedimentary Research*, v. 72, p. 457–461.
- Sprinkel, D.A., 1994, Stratigraphic and time-stratigraphic cross sections—a north-south transect from near the Uinta Mountain axis across the Basin and Range transition zone to the western margin of the San Rafael Swell, Utah: *U.S. Geological Survey Miscellaneous Investigation Series 2184-D*, 31 p., 2 plates.
- Sprinkel, D.A., 2006, Interim geologic map of the Dutch John 30' x 60' quadrangle, Daggett and Uintah Counties, Utah,

- Moffat County, Colorado, and Sweetwater County, Wyoming: Utah Geological Survey Open-File Report 491DM, compact disc, GIS data, 3 plates, scale 1:100,000.
- Sprinkel, D.A., 2007, Interim geological map of the Vernal 30' x 60' quadrangle, Uintah and Duchesne Counties, Utah, Moffat and Rio Blanco Counties, Colorado: Utah Geological Survey Open-File Report 506DM, compact disc, GIS data, 3 plates, scale 1:100,000.
- Sprinkel, D.A., and Chidsey, T.C., Jr., 1993, Jurassic Twin Creek Limestone, *in* Hjellming, C.A., editor, Atlas of major Rocky Mountain gas reservoirs: New Mexico Bureau of Mines and Mineral Resources, p. 76.
- Sprinkel, D.A., and Chidsey, T.C., Jr., 2006, Exploration history and petroleum geology of the central Utah thrust belt [abs.]: Online, American Association of Petroleum Geologists Search and Discovery Article No. 10103, <<http://www.searchanddiscovery.net/documents/2006/06028sprinkel/index.htm>>, posted May 13, 2006.
- Stevenson, G.M., 2010, Geology of Goosenecks State Park, Utah, *in* Sprinkel, D.A., Chidsey, T.C., Jr., and Anderson, P.B., editors, Geology of Utah's parks and monuments: Utah Geological Association Publication 28 (3rd edition), p. 451–465.
- Stevenson, G.M., and Baars, D.L., 1986, The Paradox—a pull-apart basin of Pennsylvanian age, *in* Peterson, J.A., editor, Paleotectonics and sedimentation in the Rocky Mountain region: American Association of Petroleum Geologists Memoir 41, p. 513–539.
- Stevenson, G.M., and Baars, D.L., 1987, The Paradox—a pull-apart basin of Pennsylvanian age, *in* Campbell, J.A., editor, Geology of Cataract Canyon and vicinity: Four Corners Geological Society, 10th Field Conference, p. 31–55.
- Stokes, W.L., 1976, What is the Wasatch Line?, *in* Hill, J.G., editor, Symposium on geology of the Cordilleran Hinge-line: Rocky Mountain Association of Geologists Guidebook, p. 11–25.
- Stokes, W.L., 1979, Stratigraphy of the Great Basin region, *in* Newman, G.W., and Goode, H.D., editors, Basin and Range symposium: Rocky Mountain Association of Geologists and Utah Geological Association, p. 195–219.
- Stokes, W.L., 1986, Geology of Utah: Utah Museum of Natural History and Utah Geological and Mineral Survey, Occasional Paper No. 6, 280 p.
- Stonecipher, S.A., 1999, Genetic characteristics of glauconite and siderite—implications for the origin of ambiguous isolated marine sandbodies, *in* Bergman, K.M., and Snedden, J.W., editors, Isolated shallow marine sand bodies—sequence stratigraphic analysis and sedimentologic interpretation: Society for Sedimentary Geology (SEPM) Special Publication No. 64, p. 191–204.
- Summerfield, M.A., 1991, Global geomorphology—an introduction to the study of landforms: Harlow, England, 537 p.
- Swart, P.K., and Kramer, P.A., 1997, Geology of mud islands in Florida Bay, *in* Vacher, L., and Quinn, T., editors, Geology and hydrogeology of carbonate islands: Developments in Sedimentology 54, Elsevier, p. 249–274.
- Swetland, P.J., Claton, J.L., and Sable, E.G., 1978, Petroleum source-bed potential of Mississippian-Pennsylvanian rocks in parts of Montana, Idaho, Utah, and Colorado: Rocky Mountain Association of Geologists, The Mountain Geologist, v. 14, p. 79–87.
- Texas Railroad Commission, 2016, Barnett Shale information: Online, www.rrc.state.tx.us/oil-gas/major-oil-gas-formations/barnett-shale-information, accessed March 8, 2016.
- Tidwell, W.D., 1966, A Lower Pennsylvanian flora from Utah and its significance: East Lansing, Michigan State University, Ph.D. dissertation.
- Tidwell, W.D., 1998, Common fossil plants of western North America: Washington D.C., Smithsonian Institution Press, 299 p.
- Tooker, E.W., and Roberts, R.J., 1970, Paleozoic rocks in the Oquirrh Mountains and Bingham mining districts, Utah: U.S. Geological Survey Professional Paper 629-A, 76 p.
- Trexler, J.H., Jr., Cashman, P.H., Snyder, W.S., and Davydov, V.I., 2004, Late Paleozoic tectonism in Nevada—timing, kinematics, and tectonic significance: Geological Society of America Bulletin, v. 116, p. 525–538.
- Trudgill, B.D., and Paz, M., 2009, Restoration of mountain front and salt structures in the northern Paradox Basin, SE Utah, *in* Houston, W.S., Wray, L.L., and Moreland, P.G., editors, The Paradox Basin revisited—new developments in petroleum systems and basin analysis: Rocky Mountain Association of Geologists Special Publication, p. 132–177.
- U.S. Geological Survey, 2012, Assessment of undiscovered oil and gas resources in the Paradox Basin province, Utah, Colorado, New Mexico, and Arizona, 2011: U.S. Geological Survey Fact Sheet 2012-3021, March 2012, 4 p.: Online, <http://pubs.usgs.gov/fs/2012/3031/FS12-3031.pdf>, accessed July 25, 2012.
- U.S. National Oceanic and Atmospheric Administration, 2002, Climatology of the United States No. 81, 42 Utah: Asheville, N.C., National Climatic Data Center, 38 p.
- Utah Automated Geographic Reference Center, 2010, Utah GIS Portal: Online, agrc.its.state.ut.us, accessed December 2010.
- Utah Division of Oil, Gas, and Mining, 2009a, Ownership/leasehold status and well locations: Cause No. 267-001, Exhibit C.
- Utah Division of Oil, Gas, and Mining, 2009b, Proposed horizontal wells: Cause No. 267-001, Exhibit I.
- Utah Division of Oil, Gas, and Mining, 2009c, 15-32-15-12, 16H-32-15-12, 3D seismic: Cause No. 267-001, Exhibit H.

- Utah Division of Oil, Gas, and Mining, 2010, Utah oil and gas information center, Utah Department of Natural Resources: Online, ogm.utah.gov/oilgas/default, accessed December 2010.
- Utah Division of Oil, Gas, and Mining, 2016a, Oil and gas summary report by field, December 2015: Online, ogm.utah.gov/pub/Publications/Reports/Prod/Field/Fld_Dec_2015.pdf, accessed March 8, 2016.
- Utah Division of Oil, Gas, and Mining, 2016b, Oil and gas summary production report by well, December 2015: Online, https://oilgas.ogm.utah.gov/pub/Publications/Reports/Prod/Well/Wel_Dec_2015.pdf, accessed March 7, 2016.
- Vargus, G., Howell, M., Hinkie, R., Williford, J., and Bozeman, T., 2008, Completion system allows for interventionless stimulation treatments in horizontal wells with multiple shale pay zones: Society of Petroleum Engineers, SPE Paper 115476.
- Villien, A., and Kligfield, R.M., 1986, Thrusting and synorogenic sedimentation in central Utah, *in* Peterson, J.A., editor, Paleotectonics and sedimentation in the Rocky Mountain region: American Association of Petroleum Geologists Memoir 41, p. 281–306.
- Wanless, H.R., and Tagett, M.G., 1989, Origin, growth and evolution of carbonate mud banks in Florida Bay: *Bulletin of Marine Science*, v. 44, p. 454–489.
- Wanless, H.R., Cottrell, D.J., Tagett, M.G., Tedescot, L.P., and Warzeski, J.E.R., 1995, Origin and growth of carbonate banks in south Florida, *in* Monty, C.L.V., Bosence, D.W.J., Bridges, P.H., and Pratt, B.R., editors, Carbonate mud-mounds: their origin and evolution: Oxford, Blackwell Science, p. 439–473.
- Wardlaw, B.R., Collinson, J.W., and Ketner, K.B., 1979a, Regional relations of middle Permian rocks in Idaho, Nevada, and Utah, *in* Newman, G.W., and Goode, H.D., editors, 1979 Basin and Range symposium: Denver, Rocky Mountain Association of Geologists and Utah Geological Association, p. 277–283.
- Wardlaw, B.R., Collinson, J.W., and Maughan, E.K., 1979b, Stratigraphy of Park City Group equivalents (Permian) in southern Idaho, northeastern Nevada, and northwestern Utah, *in* Wardlaw, B.R., editor, Studies of the Permian Phosphoria Formation and related rocks, Great Basin–Rocky Mountain region: U.S. Geological Survey Professional Paper 1163-C, p. 9–16.
- Wavrek, D.A., Ali-Adeeb, J., Chao, J.C., Santon, L.E., Hardwick, E.E., Strickland, D.K., and Schelling, D.D., 2007, Paleozoic source rocks in the central Utah thrust belt—organic facies response to tectonic and paleoclimatic variables [abs.]: American Association of Petroleum Geologists, Rocky Mountain Section Meeting, Official Program with Abstracts, p. 58–59.
- Wavrek, D.A., Schelling, D.D., Sbarra, R., Vrona, J.P., and Johnson, K.R., 2010, Central Utah thrust belt discoveries—a tale of two hydrocarbon charges [abs.]: American Association of Petroleum Geologists, Rocky Mountain Section Meeting, Official Program with Abstracts, p. 72–73.
- Wavrek, D.A., Strickland, D., Schelling, D.D., Johnson, K.R., and Vrona, J.P., 2005, A major paradigm shift—Carboniferous versus Permian petroleum systems in the central Rocky Mountains, U.S.A. [abs.]: American Association of Petroleum Geologists Annual Convention, Official Program with Abstracts, v. 14, non-paginated.
- Weber, L.J., Sarg, J.F., and Wright, F.M., 1995, Sequence stratigraphy and reservoir delineation of the Middle Pennsylvanian (Desmoinesian), Paradox Basin and Aneth field, southwestern UDS, *in* Read, J.F., Kerans, C., and Weber, F.M., editors, Milankovitch sea level changes, cycles, and reservoirs on carbonate platforms in greenhouse and ice-house worlds: SEPM (Society for Sedimentary Geology) Short Course No. 35, p. 1–81.
- Weiss, M.P., and Sprinkel, D.A., 2002, Geologic map of the Manti quadrangle, Sanpete County, Utah: Utah Geological Survey Map 188, 22 p., 2 plates, scale 1:24,000.
- Wells, M.L., 2009, Geologic map of the Kelton Pass quadrangle, Box Elder County, Utah, and Cassia County, Idaho: Utah Geological Survey Miscellaneous Publication 09-3, 22 p., 3 plates, scale 1:24,000 and 1:12,000.
- Welsh, J.L., 1979, Paleogeography and tectonic implications of the Mississippian and Pennsylvanian in Utah, *in* Newman, G.W., and Goode, H.D., editors, Basin and Range symposium: Rocky Mountain Association of Geologists and Utah Geological Association, p. 93–106.
- Welsh, J.E., and Bissell, H.J., 1979, The Mississippian and Pennsylvanian (Carboniferous) Systems in the United States—Utah: U.S. Geological Survey Professional Paper 1110-Y, 35 p.
- Wenger, L.M., and Baker, D.R., 1986, Variations in organic geochemistry of anoxic-oxic black shale-carbonate sequences in the Pennsylvanian of the Midcontinent, U.S.A.: *Organic Geochemistry*, v. 10, p. 85–92.
- Wengerd, S.A., and Matheny, M.L., 1958, Pennsylvanian System of the Four Corners region: American Association of Petroleum Geologists Bulletin, v. 42, p. 2048–2106.
- White, H., Cole, R., Stancel, S., Lee, C., and MacMillan, L., 2008, “Window” outcrop analogues for Greater Natural Buttes Field, *in* Longman, M.W., and Morgan, C., editors, Hydrocarbon systems and production in the Uinta Basin, Utah: Rocky Mountain Association of Geologists–Utah Geological Association Publication 37, p. 209–235.
- Wignall, P.B., 1994, Black shales: Oxford, Clarendon Press, 127 p.
- Willard, D.A., 1989, Source plants for carboniferous microspores—lycospores from permineralized *Lepidostrobus*: *American Journal of Botany*, v. 76, p. 820–827.

- Williams, R.M.E., Chidsey, T.C., Jr., and Eby, D.E., 2007, Exhumed paleochannels in central Utah—analogs for raised curvilinear features on Mars, *in* Willis, G.C., Hylland, M.D., Clark, D.L., and Chidsey, T.C., Jr., editors, *Central Utah—diverse geology of a dynamic landscape*: Utah Geological Association Publication 36, p. 221–235.
- Willis, G.C., 1999, The Utah thrust system—an overview, *in* Spangler, L.E., editor, *Geology of northern Utah and vicinity*: Utah Geological Association Publication 27, p. 1–9.
- Willis, G.C., and Biek, R.F., 2001, Quaternary incision rates of the Colorado River and major tributaries in the Colorado Plateau, Utah, *in* Young, R.A., and Spamer, E.E., editors, *Colorado River origin and evolution—proceedings of a symposium held at Grand Canyon National Park in June, 2000*: Grand Canyon Association, p. 119–123.
- Wilson, J.L., 1975, *Carbonate facies in geologic history*: New York, Springer-Verlag, 471 p.
- Witkind, I.J., 1982, Salt diapirism in central Utah, *in* Nielson, D.L., editor, *Overthrust belt of central Utah*: Utah Geological Association Publication 10, p. 13–30.
- Witkind, I.J., 1988, Geologic map of the Huntington 30' x 60' quadrangle, Carbon, Emery, Grand, and Uintah Counties, Utah: U.S. Geological Survey Miscellaneous Investigation Map I-1764, 1 plate, 1:100,000.
- Witkind, I.J., 1991, Implications of distinctive fault sets in the San Rafael Swell and adjacent areas, east-central Utah, *in* Chidsey, T.C., Jr., editor, *Geology of east-central Utah*: Utah Geological Association Publication 19, p. 141–148.
- Witkind, I.J., Weiss, M.P., and Brown, T.L., 1987, Geologic map of the Manti 30' x 60' quadrangle, Carbon, Emery, Juab, Sanpete, and Sevier Counties, Utah: U.S. Geological Survey Miscellaneous Investigation Map I-1631, 1 plate, 1:100,000.
- Xu, Y., Mead, R.N., and Jaffé, R., 2006, A molecular marker-based assessment of sedimentary organic matter sources and distributions in Florida Bay: *Hydrobiologia*, v. 569, no. 1, p. 179–192.
- Yonkee, W.A., DeCelles, P.G., and Coogan, J., 1997, Kinematics and synorogenic sedimentation of the eastern frontal part of the Sevier orogenic wedge, northern Utah, *in* Link, P.K., and Kowallis, B.J., editors, *Proterozoic to recent stratigraphy, tectonics, and volcanology—Utah, Nevada, southern Idaho, and central Mexico*: Brigham Young University Geology Studies, v. 42, part 1, p. 355–380.
- Young, R.A., and Spamer, E.E., editors, 2001, *Colorado River, origin and evolution*: Grand Canyon Natural History Association, symposium volume, 280 p.
- Zhang, J.Z., Fisher, C.J., and Ortner, P.B., 2004, Potential availability of sedimentary phosphorus to sediment resuspension in Florida Bay: *Global Biogeochemical Cycles*, American Geophysical Union, v. 18, GB4008, 14 p.

APPENDICES A-U: ON CD